Phy Sci
& Engr

QE
89
A1
C32
no.122
c.1

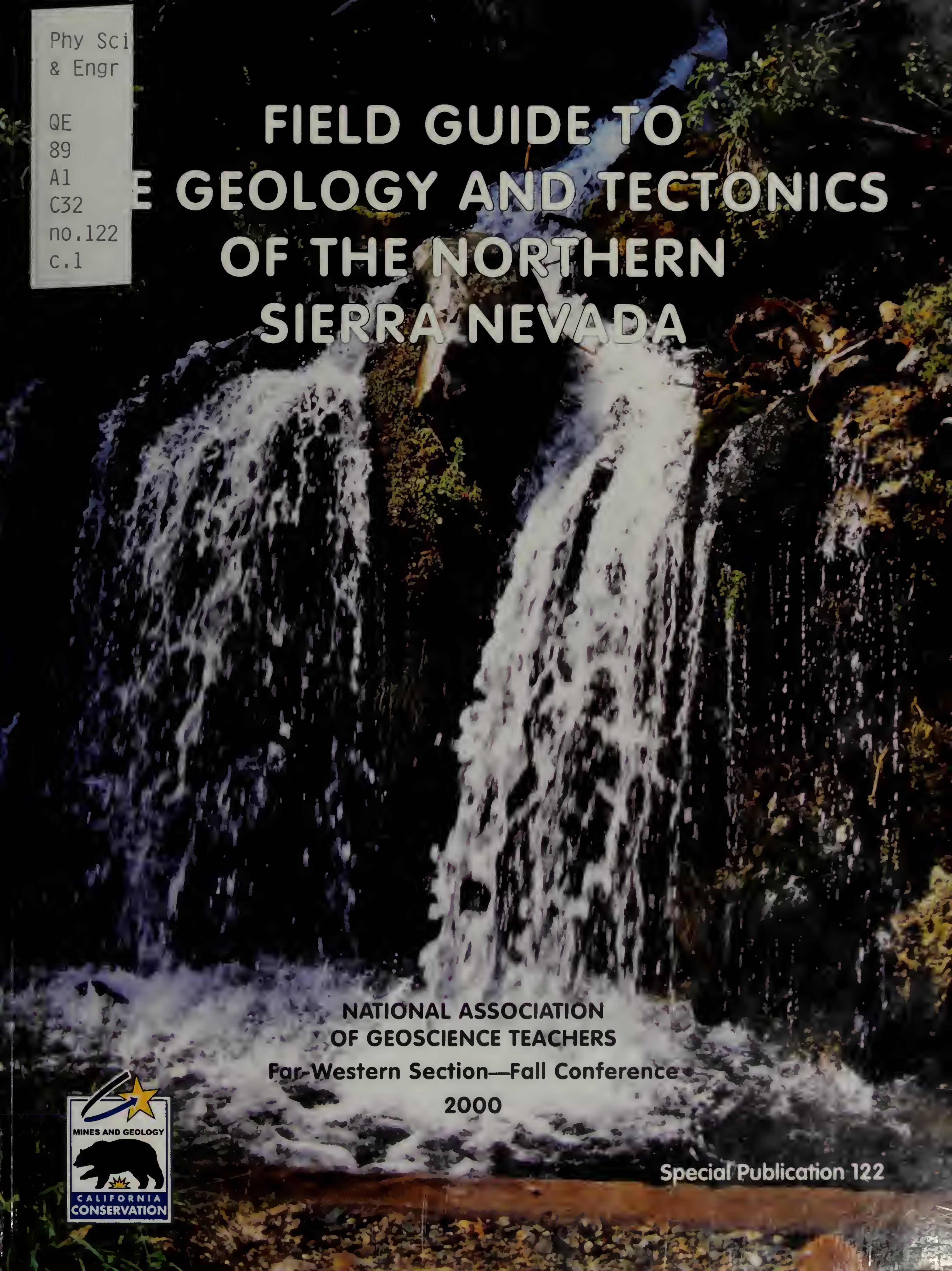

FIELD GUIDE TO
E GEOLOGY AND TECTONICS
OF THE NORTHERN
SIERRA NEVADA

NATIONAL ASSOCIATION
OF GEOSCIENCE TEACHERS

Far-Western Section—Fall Conference

2000

MINES AND GEOLOGY
CALIFORNIA
CONSERVATION

Special Publication 122

Digitized by the Internet Archive
in 2012 with funding from
University of California, Davis Libraries

http://archive.org/details/fieldguidetogeol122nati

Special Publication 122

FIELD GUIDE TO THE GEOLOGY AND TECTONICS OF THE NORTHERN SIERRA NEVADA

National Association of Geoscience Teachers
Far-Western Section

Fall Conference—2000

Editors

Elwood R. Brooks
California State University, Hayward

and

Lena Tabilio Dida
Division of Mines and Geology

MINES AND GEOLOGY
CALIFORNIA
CONSERVATION

UNIVERSITY LIBRARY
U.C. DAVIS
NOV 0 6 2000
CALIF. DEPOS.
GOV. INFO. DEPT.

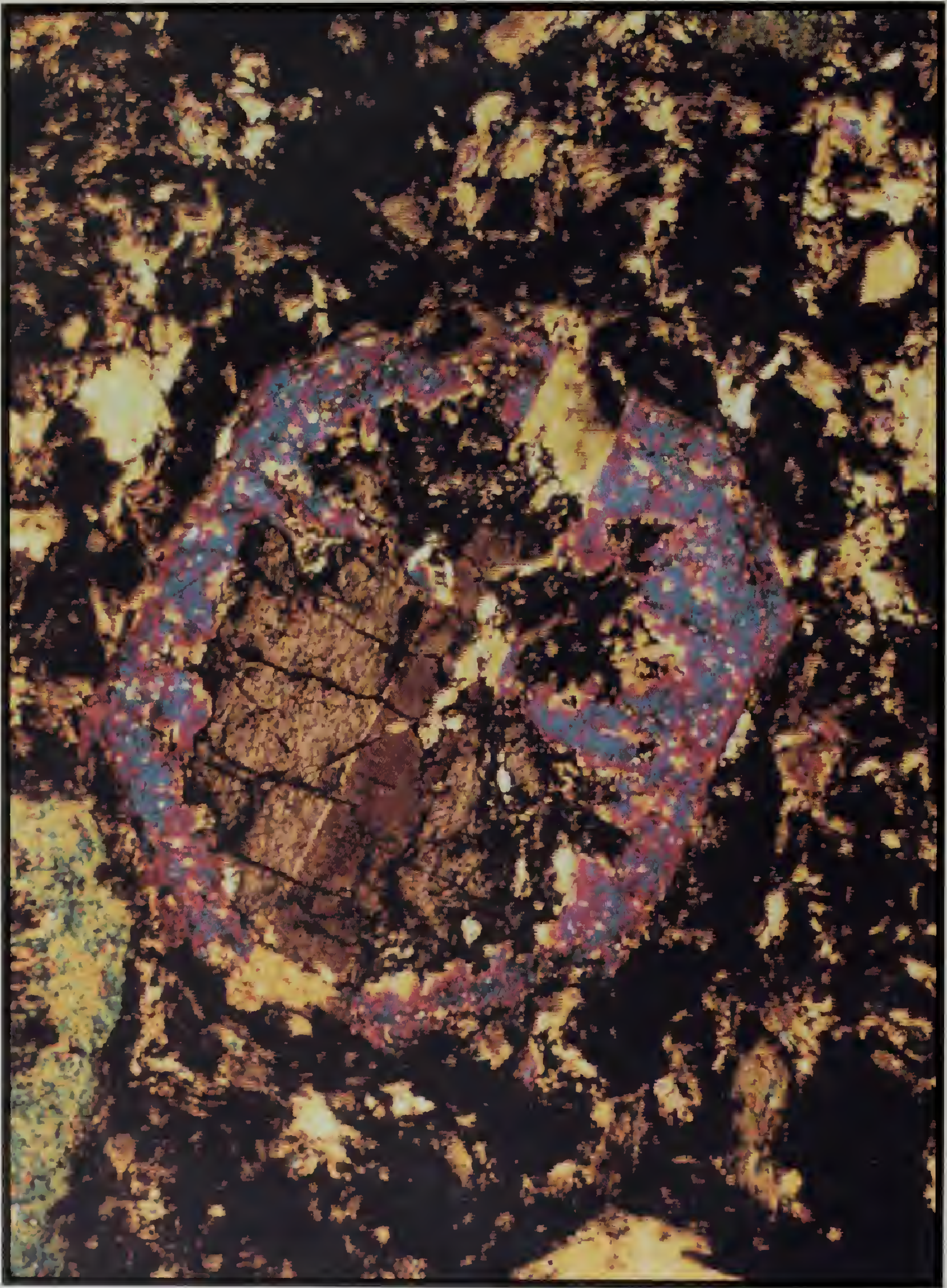

Euhedral augite phenocryst (gray) replaced along its edges by actinolite (red and blue) during Jurassic greenschist-facies metamorphism. A twin lamella runs down the middle of the phenocryst, through both augite and actinolite. The phenocryst is 1.5 mm long, and was collected from a Devonian basalt sill in the Lakes Basin, Plumas County. *Photomicrograph by E.R. Brooks.*

Cordell Durrell
1908-1986

This memorial to Cordell Durrell is an abridged version of one written by Eldridge Moores for the Geological Society of America. Permission to reproduce it was kindly granted by Faith Rogers, Managing Editor, *Geological Society of America.*

Born in 1908 in San Francisco, Cordell Durrell received his A.B. and Ph.D. degrees in geology from the University of California, Berkeley, in 1931 and 1936. He was an instructor in geology at U.C. Berkeley in 1936-37. In 1938, he became an instructor in geology at the University of California, Los Angeles, beginning an association that lasted for 25 years. In 1943 he received a two-year leave of absence from UCLA, during which he worked with the U.S. Geological Survey helping to assess U.S. resources in barite and optical-quality calcite. He returned to UCLA in 1945 as assistant professor, receiving promotions to associate professor in 1946 and professor in 1951.

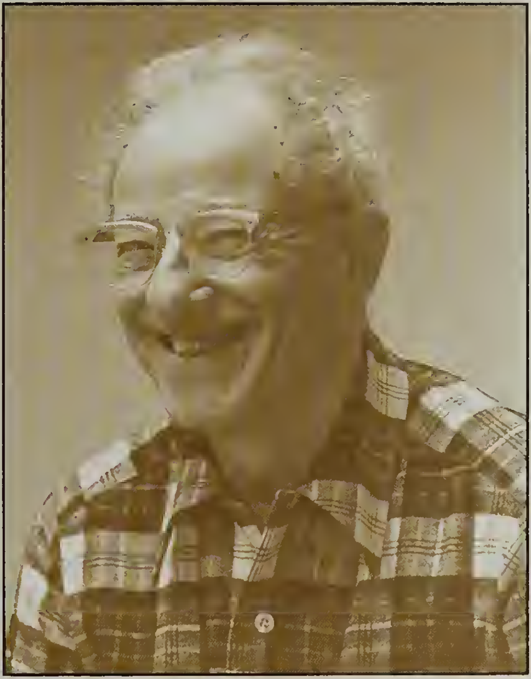

In 1963, Durrell went to the University of California, Davis, as professor and chairman of the Geology Department to oversee the growth of the then-small department into a first-rank research and teaching group. During his chairmanship (1963-67), he laid the foundation for departmental expansion and planned a new building, occupied in 1971.

Durrell was principally known as an outstanding and dedicated educator and an expert in Sierra Nevada geology. As an educator he inspired hundreds of graduate and undergraduate students at both UCLA and UC Davis, many of whom went on to distinguished geological careers in industry, government and academia. Two courses were standouts. One was an undergraduate course in hand specimen petrology, in which he spent hours on a one-to-one basis with each student. Many students remember facing their conferences with Durrell with a great deal of apprehension; afterward they recalled the experience as one of the most memorable of their college careers. Durrell's other famous course was a graduate seminar in the geology of California. This course involved thoroughly analyzing, and usually demolishing, selected primary references on field geology of California. For most students, this sort of critical analysis of an individual author's arguments was a real eye-opener. A measure of his memorable qualities as a teacher was demonstrated in 1974 when Durrell became one of the very few professors in the history of the University of California ever to receive a promotion to over-scale professor based upon his lifelong effectiveness as a teacher, rather than his research.

Durrell began work on the Blairsden Quadrangle in the northeastern Sierra Nevada in 1938, a study that continued throughout his career. During the course of this work, he became the principal authority on the Cenozoic geology of the northern Sierra Nevada and surrounding regions. He wrote *Geologic History of the Feather River Country, California*, documenting his lifelong Sierran work. The University of California Press published the book in 1987. Cord was a tireless and indefatigable field geologist. Even after his first heart attack in 1966, he would set a pace on a field traverse that left much younger geologists panting in his dust. He remained an active and influential member of the Geology Department at UC Davis even after his retirement in 1976.

Cover Photo: Stream runoff or surface springs form waterfalls in several locations visible from Highway 49 near Downieville. *Photo by Max Flanery, DMG.*

PREFACE

This collection of somewhat disparate papers and accompanying field-trip guides reflects the extremely varied geology of the northern Sierra Nevada. All contributions do have one thing in common, however. Each includes a 1-day (or less) field trip that conveniently originates at the Feather River Inn in Blairsden, California, site of the 2000 Fall Conference of the Far-Western Section of the National Association of Geoscience Teachers. Also, most of the contributing authors are current or former students or faculty members of the Department of Geological Sciences, California State University, Hayward, host of the conference.

Papers deal with rocks as old as pre-early Devonian and as young as Quaternary; one paper focuses on neotectonics, most on paleotectonics. The emphasis is on volcanic and volcaniclastic rocks, reflecting the writer's bias and the dominant character of rocks cropping out in the northern Sierra, but other igneous rocks are considered too. Of course, many rocks also have been subjected to at least one episode of metamorphism. I wish to stress that readers of this volume will find much that is new. For the most part, data and interpretations have not been published elsewhere. Indeed, some studies currently are in progress, and others, mine included, have been in gestation for many years.

All contributions include detailed guides to field trips designed to be taken without a leader. In fact, several trips include more stops than are possible to visit in a single day; it is intended that interested persons will complete these trips as time permits. Lacking any more rational approach, the papers are presented in order of age of the rocks considered, from oldest to youngest.

The Feather River Belt, largely consisting of variably serpentinized mantle peridotite, is being investigated on a regional scale by Jason Mayfield for his Ph.D. dissertation at UC, Davis. Accordingly, the contribution by *Mayfield and Day* contains a number of brand-new geologic maps of portions of this important northern California suture. The peridotite comprises harzburgite and dunite tectonites representing deformed mantle restites, and Wehrlite and olivine clinopyroxenite cumulates that perhaps formed in the uppermost mantle; discordant dunites may represent melts that rose through the mantle. The field trip visits serpentinized dunite, harzburgite, diabase, and serpentinite in the northernmost area mapped by Mayfield, on the North Fork Feather River. Additional field trip stops are described in the three southern mapped areas for those wishing to learn more about the Feather River Belt on another day.

Silva, Bullen and Brooks use trace-element and isotopic data to attempt to ascertain the petrogenetic processes that resulted in compositionally varied lavas that comprise the Sierra Buttes Formation, the relatively silicic basal unit of the oldest, late Devonian-early Mississippian island arc in the Northern Sierra terrane. Nd isotopic ratios require substantial involvement of ancient continental crust in the formation of the first-erupted, dacitic lavas, and Silva and others turn to continentally derived sedimentary rocks in the underlying Shoo Fly Complex as a source of isotopically correct, crustal, partial melts. Indeed, Nd concentrations and isotopic ratios make it possible to calculate the degree of partial melting of Shoo Fly sandstones (22%) and the proportions of Shoo Fly (21%) and mantle-derived mafic (79%) components necessary to produce the dacitic lavas (assuming no fractionation). For those more interested in seeing what the Sierra Buttes rocks look like, Steve Silva has prepared an off-trail tour of the formation in the Jamison Lake-Wades Lake area. The earliest, dacitic lava flows are found to be autobrecciated and flow-laminated. These are overlain by a pyroclastic breccia rich in more mafic highly vesicular lapilli and blocks, which is in turn overlain by an unusual subaqueous pyroclastic-flow deposit. The youngest map unit consists of columnar-jointed sill-like intrusions of quartz porphyry.

My contribution, which deals with the petrology of the lowest of three stacked Paleozoic and Mesozoic island arcs in the Northern Sierra terrane, summarizes large amounts of mostly unpublished chemical data acquired from 1978 to 1998. A major goal has been to use these data—concentrations of immobile trace elements and rare earth elements, and clinopyroxene phenocryst compositions—to determine the tectonic setting of eruption of these once-, twice-, and thrice-metamorphosed volcanic rocks. Tholeiitic, calcalkaline, and transitional magmas are identified. Many chemical analyses of pillow lavas in the Devonian-Mississippian(?) Taylor Formation show that REE, Th, and U were added to them by hydrothermal fluids emanating from ing from an early Cretaceous tonalite stock. Also, I expand considerably on two other studies previously treated only in abstracts. One describes a subaqueous pyroclastic-flow deposit in the Sierra Buttes Formation thought by another worker to be isolated-pillow breccia, and the other characterizes cumulate augite phenocrysts in early Taylor hypabyssal intrusions. My walking tour of the upper, andesitic to basaltic part of the island arc focuses on pillow lava, isolated- pillow breccia, epiclastic and pyroclastic turbidites and debris-flow deposits, augite-phyric hypabyssal intrusions, phosphatic chert, and two kinds of peperite.

The contribution by *Bruce Pauly* on the Verdi Range represents M.S. thesis work in progress at CSU, Hayward, when this was written in January, 2000. These Jurassic(?) island-arc deposits are separated from probable correlatives (Tuttle Lake Formation) to the west by nearly 25 miles of mostly Cenozoic rocks. Bruce is using a multifaceted approach—mineral and trace-element chemistry, optical petrography, volcaniclastic facies analysis, etc.—to attempt to discern the paleogeographic and paleotectonic significance of the Verdi Range rocks. He tentatively concludes that the Verdi Range island arc marks the western edge of Middle Jurassic North America. The field trip emphasizes relationships among the metamorphosed island-arc rocks, interpreted as subaqueous, cohesive, debris-flow deposits interbedded with volcanogenic sandstones, the whole cut by mafic dikes and a granitic pluton.

John Lull describes a radial swarm of andesite and dacite dikes and related tonalite stock present in the Lakes Basin. The early Cretaceous dikes and stock (120-122 Ma) have been extensively deuterically altered. Lull feels that both dikes and stock are higher level manifestations of a larger, unexposed pluton beneath the Lakes Basin. He has designed an easy walking tour to show off this splendid swarm of prominently plagioclase- and hornblende-phyric dikes; such interesting features of the dikes as magmatic inclusions and flow differentiation and flow lineation of phenocrysts are discussed. The field trip concludes with examination of the tonalite stock.

Wagner, Saucedo, and Grose review our present understanding of Miocene andesitic and basaltic volcanic rocks in the Blairsden Quadrangle, revising and updating the pioneering work of Cordell Durrell. The problems involved in trying to reconcile traditional field mapping methods and K/Ar and Ar/Ar ages of mafic volcanic rocks are emphasized. The Lovejoy Basalt is of particular interest. Durrell considered it Eocene, but the most recent Ar/Ar age is 16 Ma. The field trip visits Red Clover Creek, type locality of the Lovejoy, to review less-than-straightforward field relationships among the Lovejoy, andesite breccias, and rhyolite tuff. It then proceeds to the probable source of the Lovejoy at Thompson Peak, on the Honey Lake escarpment to the north. Wagner and others speculate that the very fluid Lovejoy Basalt erupted from a fissure opened during inception of Basin and Range faulting in the region, and flowed in paleovalleys down the west slope of the Sierra Nevada into the Middle Miocene Sacramento Valley, eventually reaching present-day Putnam Peak north of Vacaville. Wagner and others point out the similarities in age and character of the Lovejoy and flood basalts of the Columbia River Plateau, Steens Mountain, and northern Nevada.

Wakabayashi and Sawyer find the late Cenozoic volcanic deposits of the northern Sierra Nevada much to their liking, as they serve as strain gages and time markers necessary to analyze late Cenozoic faulting along the eastern margin of the Sierra. These authors synthesize a great deal of new and old data on uplift estimates and stream incision rates to attempt to determine amount and time of onset of Sierran uplift and tilting. The Lovejoy Basalt again plays an important role in estimating the amount of post-16 Ma uplift of the Sierra Nevada. Wakabayashi and Sawyer argue that the Sierra Basin and Range boundary has migrated westward since late Cenozoic inception of faulting along the Sierra Nevada Frontal fault system. A field trip in the northernmost part of the Sierra (Quincy-Lake Almanor area) investigates the neotectonics of the Sierra Basin and Range boundary, which broadens northward from the narrow Mohawk Valley graben to a zone of distributed Quaternary faulting ca. 35 km wide along the North Fork Feather River.

Elwood R. Brooks, Sierra City, California.

CONTENTS

ULTRAMAFIC ROCKS IN THE FEATHER RIVER BELT, NORTHERN SIERRA NEVADA, CALIFORNIA
Jason D. Mayfield, Howard W. Day 1

DEVONIAN SIERRA BUTTES FORMATION IN THE JAMISON LAKE AREA: INVOLVEMENT OF ANCIENT CONTINENTAL CRUST IN MAGMA GENESIS
Steven R. Silva, Thomas D. Bullen, Elwood R. Brooks 16

GEOLOGY OF A LATE PALEOZOIC ISLAND ARC IN THE NORTHERN SIERRA TERRANE
Elwood R. Brooks 53

THE BEACON POINT FORMATION, SIERRA COUNTY, CALIFORNIA: A JURASSIC TECTONIC BOUNDARY
Bruce D. Pauly 111

CHARACTERISTICS AND EMPLACEMENT OF AN EARLY CRETACEOUS DIKE SWARM AND STOCK IN THE LAKES BASIN, NORTHERN SIERRA NEVADA
John S. Lull 136

TERTIARY VOLCANIC ROCKS OF THE BLAIRSDEN AREA, NORTHERN SIERRA NEVADA, CALIFORNIA
David L. Wagner, George J. Saucedo, Thomas L.T. Grose 155

NEOTECTONICS OF THE SIERRA NEVADA AND THE SIERRA NEVADA-BASIN AND RANGE TRANSITION, CALIFORNIA, WITH FIELD TRIP STOP DESCRIPTIONS FOR THE NORTHEASTERN SIERRA NEVADA
John Wakabayashi, Thomas L. Sawyer 173

Graphic design by Peggy Walker, assisted by Debbie Maldonado, Ed Foster and Jim Williams of the California Department of Conservation, Division of Mines and Geology in digitally recreating many graphic figures.

ULTRAMAFIC ROCKS IN THE FEATHER RIVER BELT, NORTHERN SIERRA NEVADA, CALIFORNIA

Jason D. Mayfield[1], Howard W. Day[2]

INTRODUCTION

Subsequent to the fashioning of plate tectonics in the late 1960s, it has become generally accepted that continental crustal growth can occur by way of lateral accretion of oceanic material to the edge of a continent. This process may take place in one of two ways: 1) either through the underplating or offscraping of material from the down-going plate onto a continent margin in an Andean style subduction zone (Coleman, 1971) or; 2) by the subduction of a continental margin, subsequent uplift, and rearrangement of plate motions (Moores, 1970). Oceanic material is added to the continental margin in either case, but different plate margin configurations are required for each of the two methods of accretion. Although most cases may be more complicated than these generalizations, the presence of ophiolites within an orogen indicates the location of these fossil subduction zones (i.e., a suture) (Moores, 1987).

The Feather River Belt (Figure 1) is composed primarily of ultramafic rocks and extends for approximately 150 kilometers (km) within the orogen of the Western Sierra Nevada Metamorphic Belt of California (Day and others, 1985). The Feather River Belt separates widely disparate Mesozoic and Paleozoic near-continental rocks on the east from Mesozoic oceanic and island arc rocks on the west. As such, it represents the scar of a now disappeared ocean basin and marks a major tectonic suture in northern California. New evidence suggests that the Western

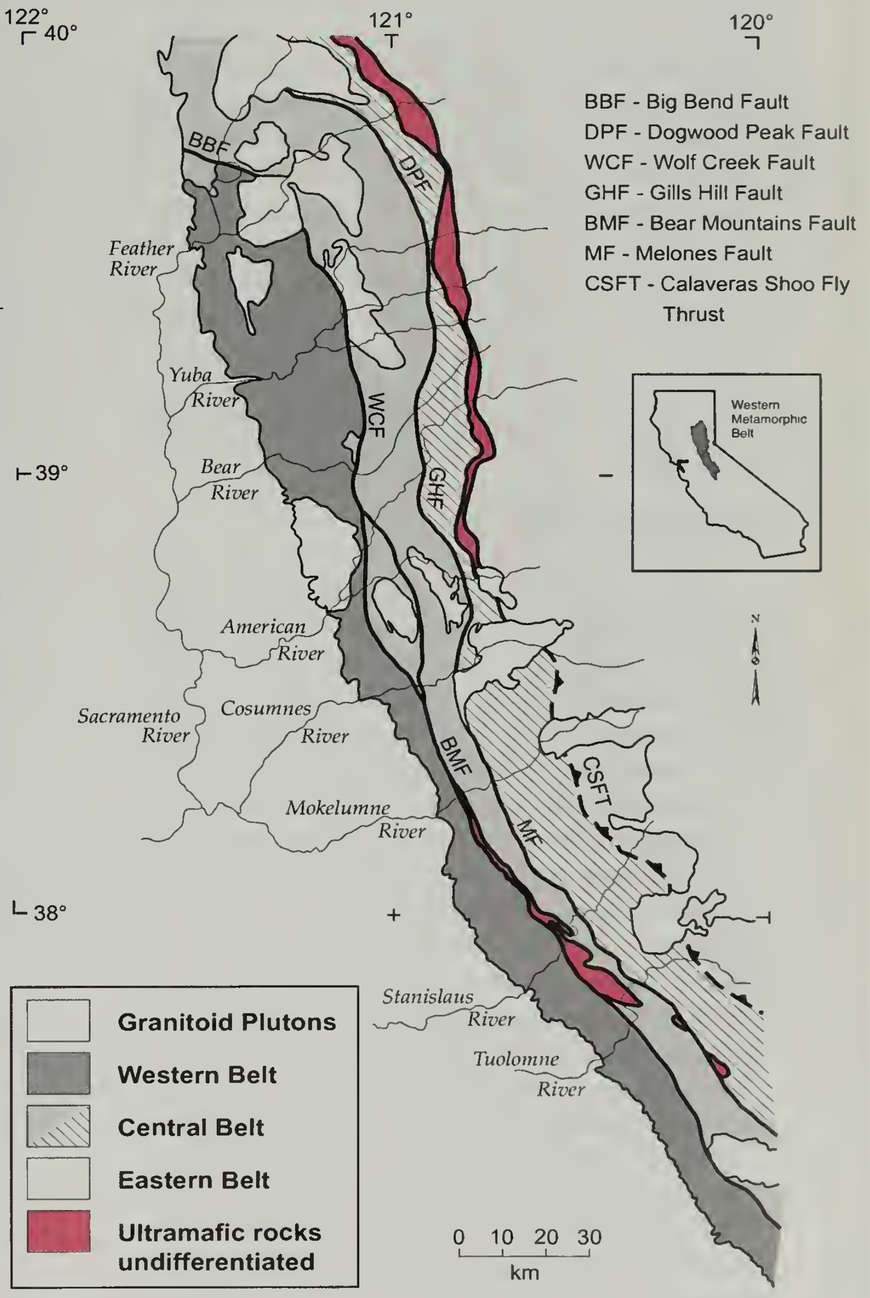

Figure 1. Lithotectonic belts of the Western Sierra Nevada Metamorphic Belt (from Day, 1992). The prominent body of ultramafic rocks on the boundary between the Central and Eastern belts marks the location of the Feather River Belt.

---

[1] Department of Geology, University of California, Davis, CA 95616; mayfield@geology.ucdavis.edu

[2] Department of Geology, University of California, Davis, CA 95616

Belt arc was constructed atop a basement that included rocks of the Central Belt (Mayfield and Day, 1996). Therefore, other fault bounded ultramafic bodies in the northern Sierra Nevada (e.g., Wolf Creek Fault zone) may not be major sutures.

The most common rocks in the Feather River Belt are variably serpentinized mantle metaperidotite; however, metagabbro, mafic, pelitic, and talc schist, as well as crosscutting mafic and felsic dikes are not uncommon. The proportion and distribution of these lithologies within the Feather River Belt have remained relatively unknown due to the lack of detailed mapping. In this guide, we summarize the regional setting and age of the Feather River Belt, followed by five new geologic maps and descriptions of some of the important lithologic units in the Feather River Belt. We outline a road log to nine selected stops within the Feather River Belt. Only the first five stops will be visited on this trip. We encourage readers to visit the other stops to see additional features of the Feather River Belt.

REGIONAL SETTING

Rocks of the Western Sierra Nevada Metamorphic Belt (Figure 1) represent a long and complex Paleozoic and Mesozoic history of sedimentation at a continental margin, construction of magmatic arcs across this margin, and subsequent accretion of oceanic terranes to the margin. These metamorphic rocks are intruded on the east and south by granitic rocks of the Sierra Nevada Batholith, unconformably overlain to the north by Tertiary and Quaternary volcanic rocks of the Cascade Mountains and to the west by Cretaceous and Tertiary sediments of the Great Valley Sequence. The Western Sierra Nevada Metamorphic Belt comprises four N-S trending regional belts (Figure 1): the Western Belt, Central Belt, Feather River Belt, and Eastern Belt (Northern Sierra Terrane of Harwood, 1988), from west to east respectively (Schweickert and Cowan, 1975; Day and others, 1985). These four internal belts are separated by steep faults collectively termed the Foothills Fault system (Clark, 1960; Clark and Huber, 1975).

The Eastern Belt comprises early Paleozoic siliciclastic Shoo Fly Complex overlain unconformably by Devonian-Mississippian, Permo-Triassic, and Early Jurassic arc volcanic rocks (D'Allura and others, 1977; Hannah and Moores, 1986; Harwood, 1988). The Central and Western belts are composed of a collage of Paleozoic and Mesozoic mafic volcanic sequences (ophiolites?) structurally overlying deformed metasedimentary rocks. Rocks of the Eastern Belt are generally accepted as *near-continental* (Paleozoic) to *continental* (Jurassic) arcs. Rocks west of the Feather River Belt, the Western and Central belts, clearly represent *oceanic* terranes that may or may not have been amalgamated by the time of their addition to the continental margin. The Feather River Belt, therefore, represents a major Mesozoic suture between continental rocks on the east and oceanic arc rocks on the west (termed the "Foothill suture" by Saleeby and others, 1978). Farther south, this suture between continental and oceanic rocks is marked by a major thrust fault (Calaveras-Shoo Fly Thrust of Schweickert, 1981) and lacks appreciable ultramafic or mafic rocks.

The general Paleozoic and Mesozoic tectonic history of the continental margin is well known (Burchfiel and Davis, 1972; Dickinson, 1981). The early Paleozoic sequence recorded in the Eastern Belt of the Sierra Nevada likely represents an accretionary complex at the edge of the passive "Atlantic type" continental margin. Arcs were intermittently active above the deformed early Paleozoic basement throughout the late Paleozoic and early Mesozoic. The continentally derived sediments and arc volcanic rocks of the Eastern Belt were variably deformed and amalgamated to the continent during the late Paleozoic-early Mesozoic Sonoma orogeny. This newly constructed continental margin was subsequently truncated by strike-slip faulting during the Triassic. Subsequent to the truncation of the margin, oceanic rocks of the Western and Central were added to the continental margin.

New evidence suggests that the two western oceanic terranes (Western and Central belts) were amalgamated at the time of their addition to the continental margin and that the Western Belt arc was built on a basement that included, in part, Central Belt lithologies (Bickford and Day, 1988; Edelman and others, 1989; Souter and Day, 1991; Mayfield and Day, 1996). Whether or not this is the case, a question remains unanswered (Day, 1992): Do the oceanic rocks of the Western and Central belts represent far traveled terranes or were they built more or less in situ with respect to the continental margin? (Burchfiel and Davis, 1972; Schweickert and Cowan, 1975; Moores and Day, 1984). An obvious place to look for an answer is in the suture that separates these oceanic rocks from the continental margin.

AGE RELATIONSHIPS

Middle Paleozoic, late Paleozoic and Mesozoic dates have been reported for rocks within the Feather River Belt (Standlee, 1978; Schweickert and others, 1980; Saleeby and others, 1989). Felsic igneous rocks that crosscut mafic lithologies associated with the ultramafic rocks have yielded multiple middle Paleozoic ages (387±7 Ma, ^{40}Ar/^{39}Ar hornblende age, Standlee, 1978; 388±17 Ma, U-Pb zircon age, Saleeby and Moores, 1979). Amphiboles from mafic rocks, associated with the ultramafic rocks, have yielded K-Ar ages ranging from 345 to 236 Ma (Weisenberg and Ave' Lallemant, 1977; Standlee, 1978; Hietanen, 1981; Bohlke and McKee, 1984; Saleeby and others, 1989). K-Ar analyses of white mica from blueschists in the Feather River Belt give Early Jurassic (174 Ma) and older ages (Schweickert and others, 1980).

Three important conclusions can be derived from these data. First, cross cutting dikes show that at least part of the Feather River Belt ultramafic suite is older than Early Devonian (~388 Ma). Second, amphibolite facies metamorphism affected portions of the Feather River Belt ultramafic rocks during the middle to late Paleozoic (345 to 236 Ma) and may be responsible for resetting some older ages. Last, the presence of blueschist facies rocks suggests that portions of the Feather River Belt may have been associated with a subduction zone during the Jurassic.

NEW GEOLOGIC MAPPING

Many workers have previously defined the boundaries of the Feather River Belt (Saucedo and Wagner, 1992; references in this paper). However, little is known about the details of the distribution of the ultramafic lithologies, even though peridotites, and their serpentinized equivalents, comprise more than 95% of the rocks within the Feather River Belt. In this section, we present five new geologic maps of selected localities in the Feather River Belt (1:48,000) and discuss their main features (Figure 2).

Peridotite

Approximately 50% of the Feather River Belt consists of unserpentinized peridotite bodies that may be 2-6 km long. These bodies generally are elongate in a north-south direction and have gradational boundaries with surrounding massive serpentinite. Fresh peridotite can be distinguished from strongly serpentinized counterparts by the characteristic red to brown weathering. Both tectonite and cumulate peridotite have been mapped.

Harzburgite (Pzfh) is the dominant tectonite lithology and, although present in various amounts in all areas, is best exposed in the Red Hill area (Figure 3). Dunite (Pzfd) is the next most abundant peridotite tectonite and is present as sizable bodies in the Red Hill and Middle Fork Feather River areas (Figure 4). In addition, small pods of chromite-bearing dunite (not shown on the maps) are common in harzburgite of the Sugar Pine Reservoir and South Yuba River areas (Figure 2). Lherzolite is present in only minor amounts. Harzburgite, dunite, and the minor amounts of lherzolite have granoblastic textures and may contain a pyroxene and/or spinel foliation readily seen in outcrop. Spinel and pyroxene foliations, specifically, are not parallel to the regional N-NW trends present in the surrounding metasedimentary rock of the northern Sierra Nevada. Harzburgite has a characteristic "warty" surface texture due to differential weathering of the olivines and pyroxenes. Dunite (Pzfd), in contrast, is devoid of pyroxene, lacks a pronounced foliation, commonly has smooth surfaces, and displays no warty texture. Although Ehrenberg (1975) suggested that the dunite and harzburgite occur exclusively of one another, pods of harzburgite, 2 to 20 meters (m) in size, are fully enclosed within dunite on the west and south slopes of Red Hill. The various ultramafic tectonites represent deformed restites from the mantle.

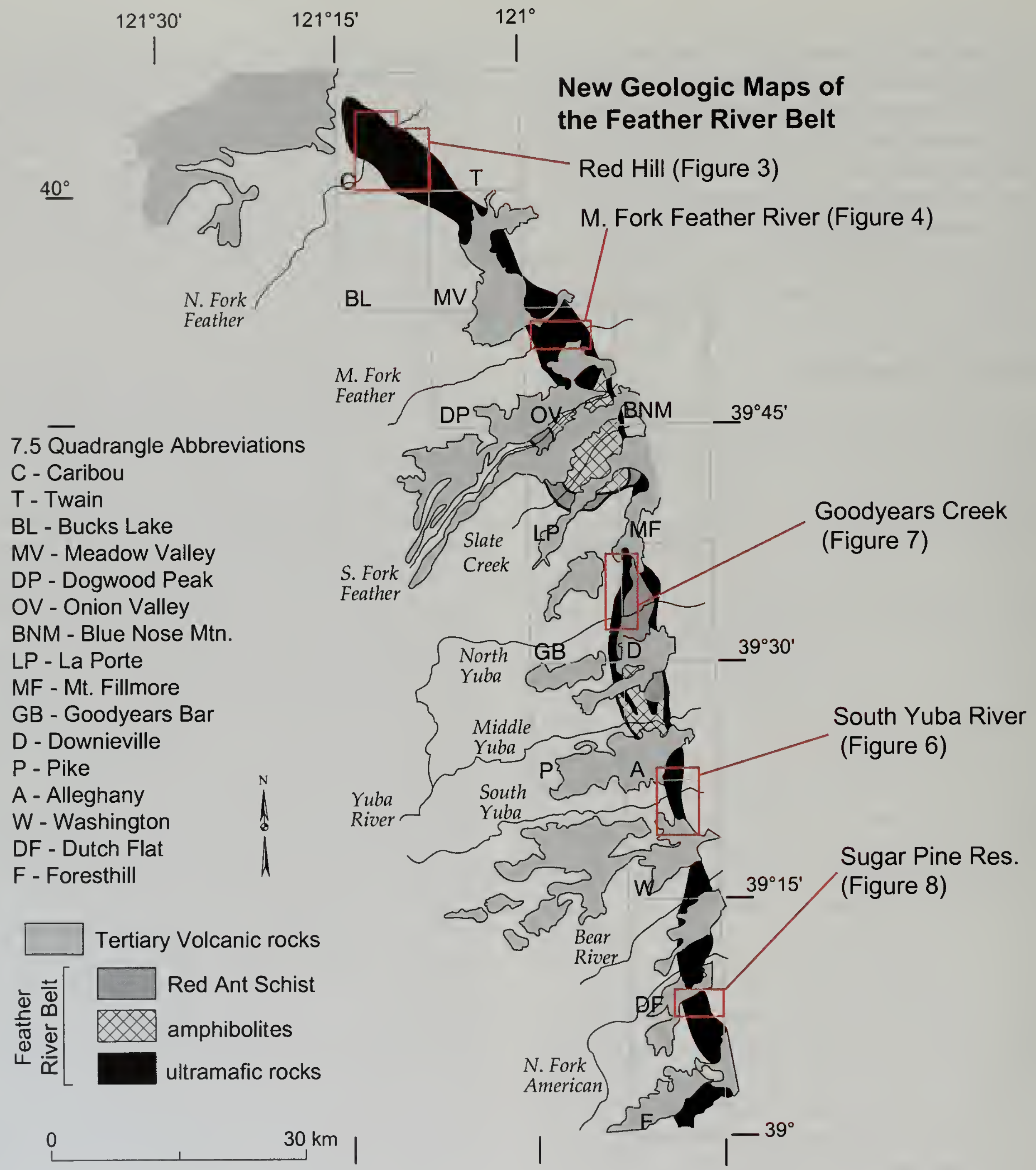

Figure 2. Geologic map of the Feather River Belt. Tertiary (superjacent) volcanic and sedimentary rocks are shown with a light gray pattern. Locations of five new geologic maps are outlined in red.

Relationships along the contacts between dunite and harzburgite suggest that at least some dunite bodies may be melt migration pathways. The contacts are typically gradational and characterized by discordant dunite apophyses extending into the harzburgite. These dunite apophyses penetrate across the regional pyroxene foliation and may contain a relict spinel foliation that mimics the local trends. These observations suggest that the discordant dunite bodies are created as high-pressure melts percolate upward through the mantle. The percolating melts, saturated with olivine by their depressurization, dissolve pyroxene and precipitate olivine during their ascent (Figure 5). The

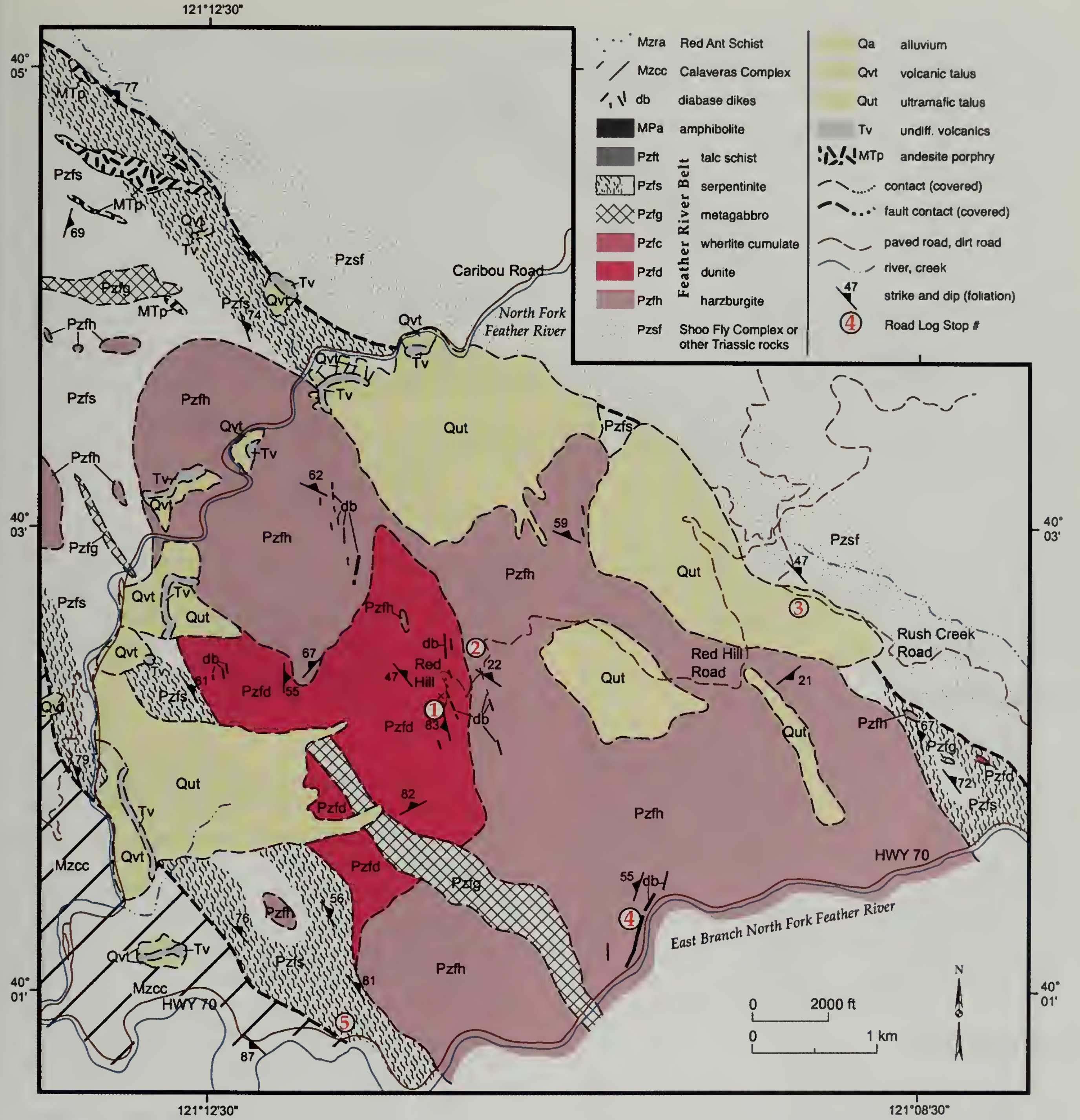

Figure 3. Geologic map of the Feather River Belt in the Red Hill area. See Figure 2 for location. Scale is approximately 1:48,000.

features left behind have been termed "melt migration pathways" or "discordant dunites" as summarized in Ceuleneer and Rabinowicz (1992) and Keleman (1990).

Wehrlite and olivine clinopyroxenite (Pzfc) occur only in the South Yuba River area (Figure 6) where they occur as a 0.5 by 2 km body. These clinopyroxene-rich ultramafic rocks (Pzfc) have *cumulate* textures that are distinct from the other (tectonite) peridotites. Warty surface texture is also common in both tectonite and cumulate rocks, but cumulate rock contains distinctive euhedral clinopyroxene grains. Within the cumulate body, igneous layering

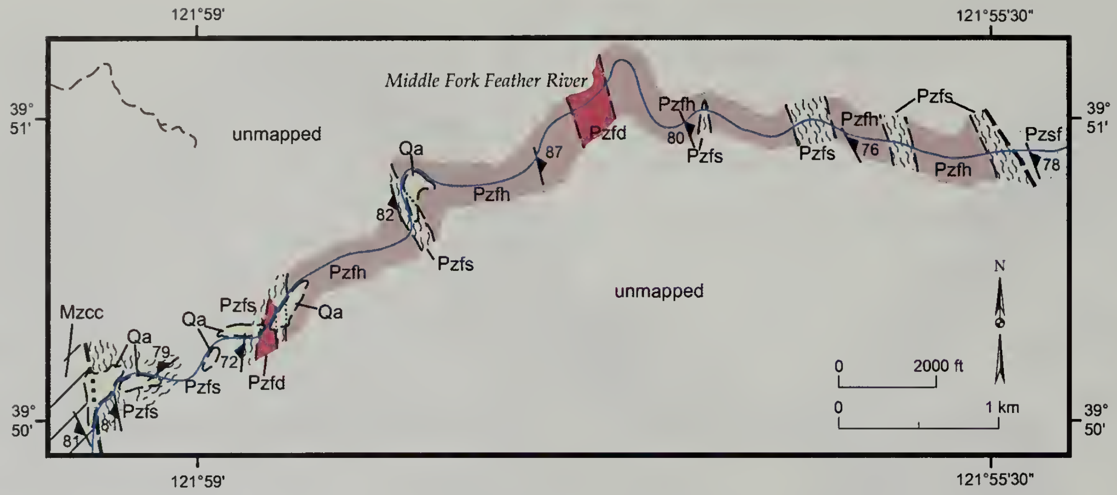

Figure 4. Geologic map of the Feather River Belt in the Middle Fork Feather River area. See Figures 2 and 3 for location and legend respectively. Scale is approximately 1:48,000.

is difficult to characterize due to poor exposure. These clinopyroxene-rich rocks may represent igneous accumulations from basalts that ponded at the base of the crust.

Metagabbro

Metagabbro (Pzfg) is only common in the Red Hill area (Figure 3). It forms elongate bodies that crop out poorly, are densely vegetated, and commonly are foliated along their margins. Contacts between the metagabbro and ultramafic rock are typically sharp but poorly exposed. The common mineral assemblage of the metagabbro is plagioclase, hornblende and minor clinopyroxene. However, much of the green amphibole appears to be alteration of original clinopyroxene grains.

Serpentinite

Three textural varieties of serpentinite (Pzfs) can be distinguished in the field: massive and scaly serpentinite, as well as serpentine schist. These three types are shown on the geologic maps either with no pattern (massive), a wavy line pattern (scaly), or a straight line pattern (serpentine schist). Some of the regions with no pattern lack sufficient outcrop to determine the textural variety.

Massive serpentinite is present in various amounts in each area and typically occurs around the margins of fresh peridotite bodies. It is also present as large (up to 0.4 km) blocks within scaly serpentinite, for example in the regions north and south of the South Yuba River, west of the town of Washington (Figure 6). Massive varieties weather to light green and gray hues and commonly display relict textures such as the "warty" surface of harzburgite.

Scaly serpentinite comprises most of the serpentinite outcrop and is especially abundant in the Goodyears Creek (Figure 7) and Sugar Pine Reservoir areas (Figure 8). At the Goodyears Creek location, over 90% of the ultramafic outcrop is scaly serpentinite. Scaly serpentinite consists of lenticular fragments of ultramafic rock (phacoids) bounded by an anastomosing cleavage. Phacoids range from 1 to 40 centimeter (cm) and commonly contain a mineral lineation (slickenfibers?) on the bounding cleavage surfaces. Cores of the phacoids are typically composed of serpentine and magnetite but rarely contain weakly serpentinized peridotite. Thin-section textures (mesh and hourglass) suggest that lizardite and/or chrysotile are the dominant varieties of serpentine mineral in the scaly serpentinite. Due to the irregular nature of the cleavage, attitudes of foliations in the scaly serpentinite may vary ±10° from the values shown on the maps.

At present, serpentine schist has only been found in the Goodyears Creek area. It occurs

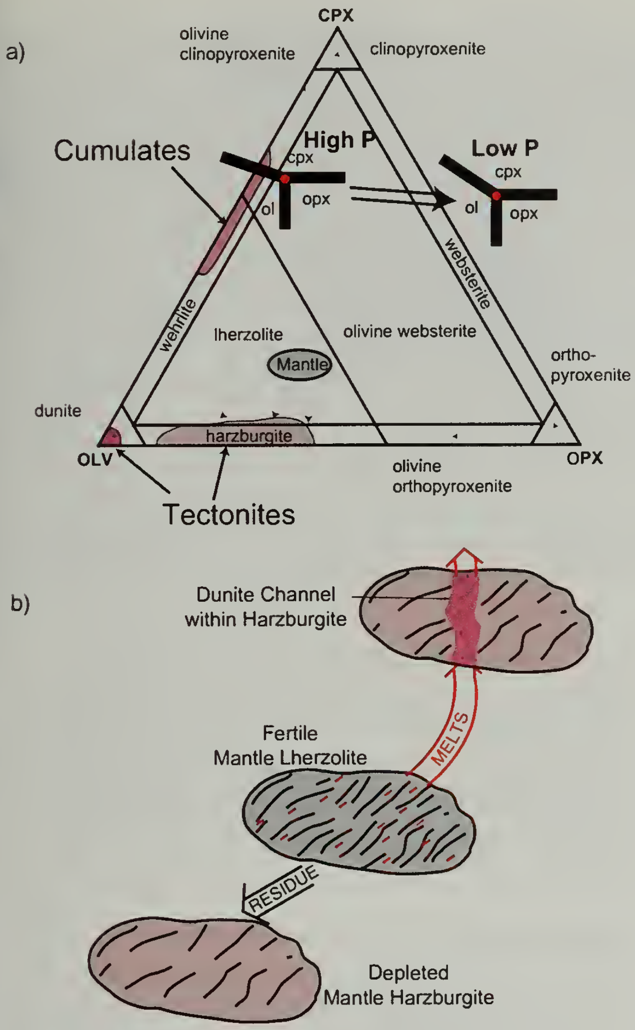

Figure 5. Modal composition and petrogenesis of the unserpentinized periotites. a) Composition of tectonic and cumulate periotites from the Feather River Belt shown on the IUGS classification for ultramafic rocks. Overlain on this diagram is a generalized field for fertile mantle lherzolites and positions for two basaltic liquids in equilibrium with olivine-cpx-opx. The arrow shows the direction of change of this composition with decreasing pressure. Note that the high and low-pressure positions on this diagram are highly schematic and were converted from the "Walker" projection shown in Figure 2 of Stolper (1980). They are only intended to illustrate the relative positions of the invariant points. The extraction of such melts from mantle lherzolite causes the composition of the residue to shift radically away from the melt compositioin. Therefore, mantle rocks that started as lherzolites could be progressively depleted of a basaltic component to form harzburgites. b) Schematic representation of the formation of dunite channels. As the higher pressure melts percolate upward through any overlying mantle, they are constrained by lower pressure phase equilibria. Thus, a melt composition formed at high pressure lies in the olivine field of stability at low pressure, where it would ascent to the surface. This process causes the "zone refining" of pyroxene-bearing peridotites into dunites that commonly occur as channels or tabular bodies.

along a 2 km stretch of the eastern bounding fault contact with the Red Ant Schist and along internal faults bounding slivers of Shoo Fly Complex (Figure 7). Penetratively schistose serpentinite occurs as narrow zones up to 15 m across and is commonly discontinuous along strike. This textural variety of serpentinite is composed of very fine-grained, "pseudo-fibrous" (or platy) grains of

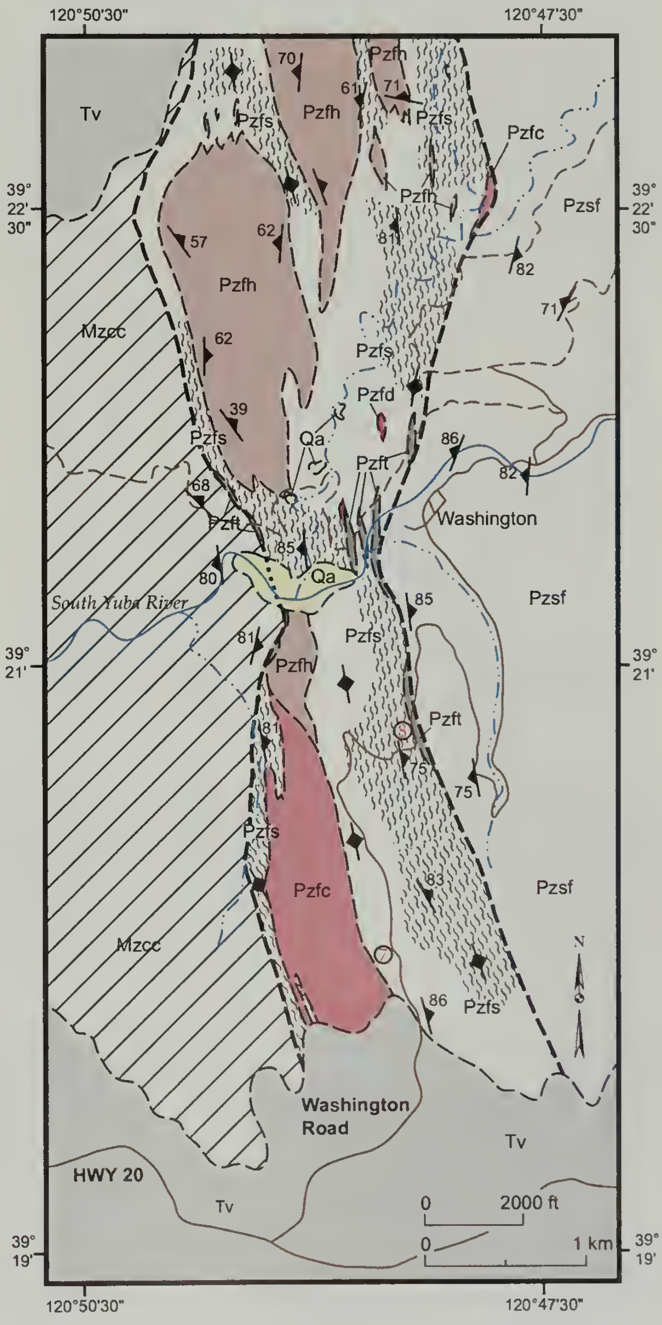

Figure 6. Geologic map of the Feather River Belt in the South Yuba River area. See Figures 2 and 3 for location and legend respectively. Scale is approximately 1:48,000.

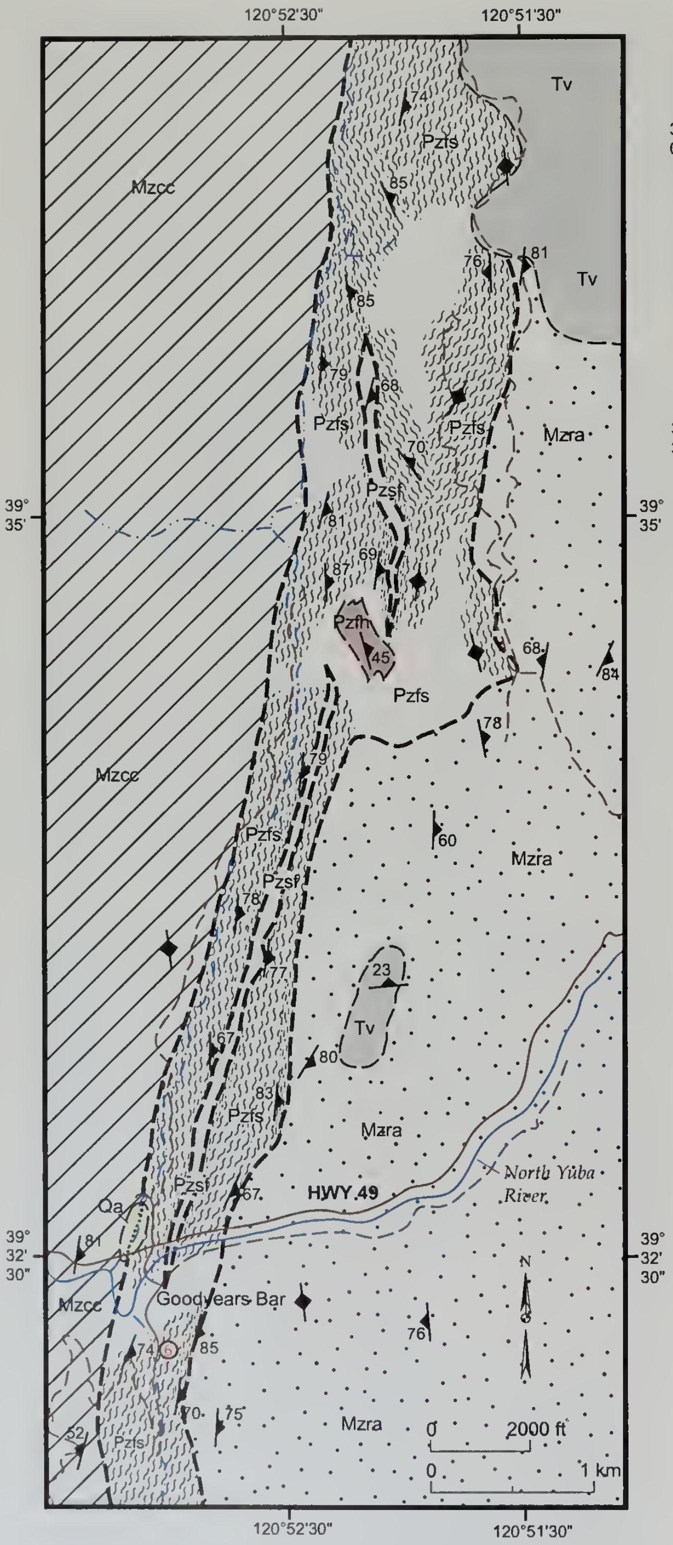

Figure 7. Geologic map of the Feather River Belt in the Goodyears Creek area. See Figures 2 and 3 for location and legend respectively. Scale is approximately 1:48,000.

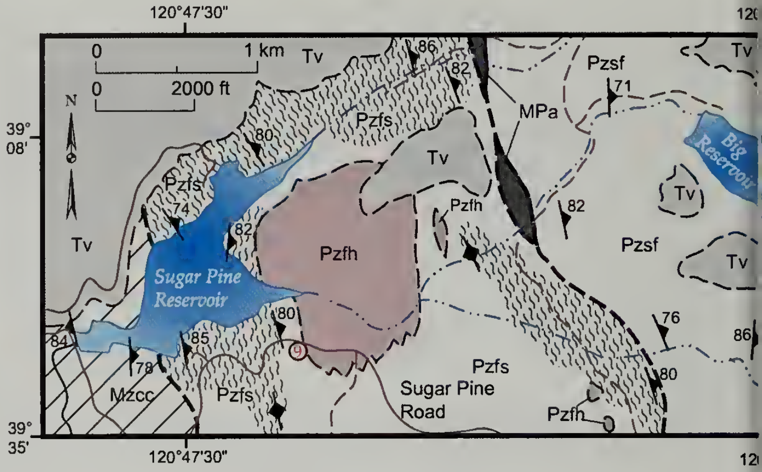

Figure 8. Geologic map of the Feather River Belt in the Sugar Pine Reservoir area. See Figures 2 and 3 for location and legend respectively. Scale is approximately 1:48,000.

serpentine and fine-grained, equant grains of magnetite. In addition, the length-slow character of the pseudo-fibrous serpentine suggests these serpentinites may be composed of the antigorite variety. However, preliminary x-ray diffraction work has only encountered the chrysolite variety of serpentine.

Talc schist

Talc schist has been observed only in the South Yuba River area (Figure 6) where it is present along both margins and within the interior of the Feather River Belt. Most bodies of talc schist are highly foliated, with fabrics parallel to the regional trends. Others are massive bodies of deep green talc and are commonly associated with silica-carbonate rocks. This assemblage has been reported in the Sierra Nevada near many Mother Lode type quartz veins where the veins cross ultramafic rocks (Ferguson and Gannett, 1932).

ACKNOWLEDGMENTS

We thank Robert Coleman and Robert Springer for prompt yet thorough reviews that resulted in considerable revision and improvement of the manuscript. Financial support was provided by the Educational Mapping Program (EDMAP) at the U.S. Geological Survey, the Geological Society of America, and the Cordell Durrell Fund, Department of Geology, University of California, Davis.

ROAD LOG

This road log begins at the Feather River Inn, which is northwest of the junction of Highway 70 and southbound Highway 89 near Blairsden, California.

0.0 Leave Feather River Inn. Set your mileage trip meter as you turn west onto Highway 70. Pass through Quincy and stay on Highway 70. West of the junction with north-bound Highway 89, the predominant rock type exposed in the canyon is the Early Paleozoic Shoo Fly Complex. Although the Feather River Belt is bounded on the east by rocks of the Shoo Fly Complex for much its length, we will not be stopping to look at the Shoo Fly on this trip. Excellent exposures are along Indian Creek at the Highway 70-89 junction. In the mile and half before the turn onto Rush Creek Road, you can catch brief glimpses of the top of Red Hill, the location of the first stop on this trip.

42.0 Turn right on Rush Creek Road. Beyond here the road is relatively narrow, so stay alert around turns and watch for people or debris in the road.

43.4 The paved road turns to a well maintained gravel road at this point.

45.9 Turn left at Deadwood saddle. Note there are two roads to the left; take the first, more extreme left turn.

46.3 Beyond here the road gets quite rough and rocky. Four wheel drive vehicles are not necessary, but are recommended for safety. Good tires are essential.

48.7 Past this small saddle, the road is very rough. Be very careful and watch for large rocks in the road. Rocks can really take a heavy toll on tires in the next mile or so.

50.2 **Stop 1** *Dunite*. At the top of Red Hill, park near the small building next to the wooden outhouse. If the weather is nice and no fires are burning nearby, this site affords excellent views to the south (Photo 1) and may be one of the most beautiful spots in the northern Sierra Nevada. Next to the outhouse and all around the summit of Red Hill are excellent exposures of Feather River Belt dunite (Photo 2).

The fresh dunite (Pzfd) weathers to shades of red and orange, has a smooth surface

Photo 1. Panorama looking south-southeast from Red Hill (Stop 1). *Photo by Jason Mayfield.*

texture, and is only weakly serpentinized. Primary anhydrous phases present are olivine and spinel (partly altered to magnetite) whereas secondary (dominantly hydrous) phases comprise tremolite, talc, serpentine, and minor amounts of chlorite rimming spinel. Fine-grained olivine comprises approximately 80% of the rock with most grains between 0.2 and 1.5 millimeters (mm) in diameter; the spinel (< 2%) has approximately the same size range. Tremolite grains are typically prismatic, between 1 and 3 mm long, and constitute 4 to 7% of the rock. Talc occurs in small fibrous clumps no larger than 1 mm and commonly rims the colorless amphibole. Serpentine constitutes up to 15% of the dunite, whereas talc only accounts for 1 to 2%. Serpentine rims olivine grains and also occurs as cross-fiber veins throughout the dunite. Mesoscopic textures associated with the initial serpentinization of the dunite can be seen in outcrops only a few tens of meters to the north along the road. Serpentinization has enhanced the relict spinel foliation of N14°E/83°SE in the dunite and creates the blocky nature of the outcrop.

The contact between dunite and harzburgite occurs between Stops 1 and 2 and is mostly covered. Only in the outcrops on the steep slopes of the mountain is it well exposed. Fine to medium grained diabase dikes crop out along the road between Stops 1 and 2.

50.5 **Stop 2** *Harzburgite*. Return down the hill about 0.3 miles. Just before a sharp turn to the right, park near one side of the road. Outcrops of Feather River Belt harzburgite (Pzfh) are on the west side of the road. Time permitting, take the opportunity to walk 20 or 30 m north to the clearing in the trees and admire the spectacular view of Lake Almanor, Humbug Valley, and Mount Lassen (Photo 3).

Photo 2. The top of Red Hill with the outcrops for Stop 1 to the right of the outhouse. Rocks around this area are mostly dunites or their partly serpentinized equivalents. *Photo by Jason Mayfield.*

Photo 3. Panorama looking north from the saddle just below the summit of Red Hill (Stop 2). *Photo by Jason Mayfield.*

Similar to the dunite at the previous stop, the harzburgite weathers to red and orange shades and is also only weakly serpentinized. It is distinguished from dunite by its characteristic "warty" surface texture formed by the resistant orthopyroxene grains (Photo 4). In these harzburgites, orthopyroxene forms approximately 20 to 25% of the original anhydrous assemblage whereas olivine is 75 to 80% (Figure 8). Spinel is present in amounts up to 2%. Olivine grains are typically much larger (2 to 3 mm) in the harzburgite than in the dunite, and the orthopyroxene can be up to 3 to 7 mm; spinel is approximately 0.5 mm. Common in many of these outcrops is a pyroxene and spinel foliation, N56°W/22°NE.

53.8 Return to Deadwood saddle. Turn hard right back onto Rush Creek Road.

54.2 **Stop 3** *Quaternary ultramafic talus.* Just past a sharp left turn, look for room to park on the left (east) side of the road. The large talus fields (Qut) extend almost a mile west up the hillside and are composed, almost entirely, of fresh (unserpentinized) harzburgite. Five hundred blocks in this talus field resulted in 97% harzburgite, 0.2% dunite, 1.2% diabasic blocks, and 1.6% serpentinized blocks. The average block size at this locality is approximately 40 cm but clasts larger than 1 m are common. The harzburgite blocks are petrographically similar to harzburgites exposed in outcrop higher up on Red Hill. Regions shown as Quaternary ultramafic talus on the map of the Red Hill area (Figure 3) often contain more than one generation of talus slope. The multiple generations are distinguished by different amounts of organic accumulation and the amount of forest cover. The uniformity of organic debris accumulation as well as the commonly sharp boundary between different talus field generations indicate that talus deposition must be rapid and probably represents catastrophic rock falls. This conclusion, coupled with the large areal extent of the talus fields, suggests slope instability around the mountain that may prevent further development on Red Hill. In addition, because peridotite is easily weathered to form iron-rich laterite, the lack of these soils supports the idea of a rapid Quaternary uplift of the northern Sierra Nevada (Coleman, 1999 written communication).

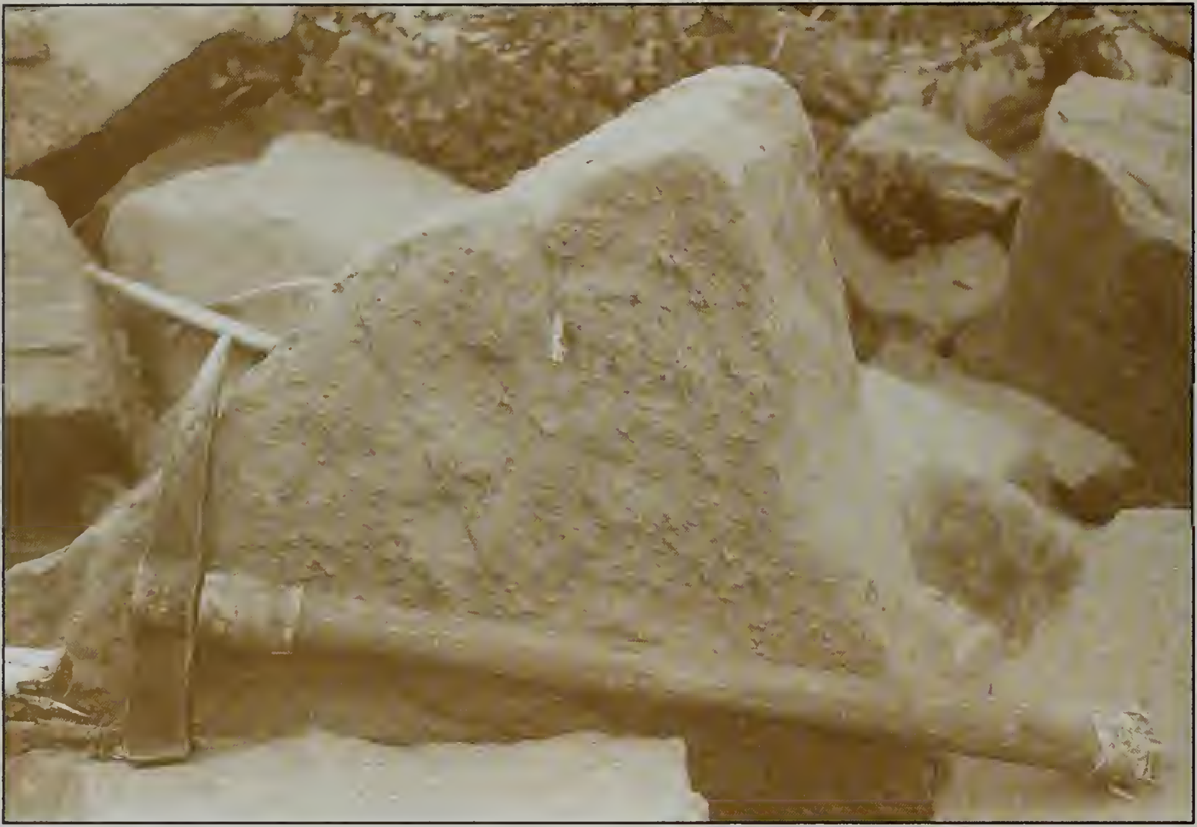

Photo 4. Fresh harzburgite from Stop 2. Note the "warty" surface texture of the more resistant pyroxenes. *Photo by Jason Mayfield.*

57.7 Turn west on Highway 70 at the end of Rush Creek Road. This is a blind turn for west-bound traffic, so be careful.

58.2 At this large turn to the left is the contact between the Feather River Belt serpentinite and metasedimentary rocks of the Eastern Belt.

59.3 At this point we return to the relatively unserpentinized portion of the Feather River Belt. Although most of the fresh exposure along the road west of here appears to be serpentinite, a quick look up at the slopes above the road reveals the red colors characteristic of the weathered surfaces of unserpentinized peridotites.

60.4 **Stop 4** *Diabase dike intruding harzburgite.* Use the large turnout on the south side of the road near the "falling rock" or "ICY" sign. Looking north up to Red Hill you can see the red and rocky landscape typical of the fresh peridotite that extends all the way down the mountain. Hike northwest up the small ravine nearest the "ICY" road sign. About 30 m up from the road is a medium- to fine-grained diabase dike (db) that cuts across the fresh peridotites. A 5-to-20 m halo of serpentinization commonly surrounds such dikes.

This 6-to-8 m wide diabase dike displays a beautiful chilled margin on both sides becoming almost aphanitic at the contacts. It is commonly gray and only rarely contains any appreciable phenocrysts. The plagioclase, amphibole, and clinopyroxene phases that constitute the majority of the rock are 1 to 2 mm near the core of these larger dikes. An important feature is the absence of a penetrative fabric within the dikes, suggesting post-orogenic emplacement. However, Ehrenberg (1975) noted the existence of scaly serpentinite along the margins of the dikes and suggested that the more rigid diabase resisted the foliation whereas the serpentinite did not.

62.2 **Stop 5** *Western fault contact with Calaveras Complex.* Proceed west on Highway 70 for 1.8 miles. Look for the large turnout on the right side of the road. The turnout is within scaly and massive serpentinite outcrops, and the fault contact is 40 m west along the road. When walking along the road, watch for traffic; logging trucks drive quite fast along Highway 70 and the shoulder here is very narrow.

The Feather River Belt serpentinite (Pzfs) weathers to shades of green, gray, and white and is dark gray to black on fresh surfaces. The degree of deformation within the serpentinite increases toward the fault as shown by the increase of scaly textures at the expense of massive serpentinite and by the decreasing size of phacoids adjacent to the contact.

The Calaveras Complex (Mzcc) is composed of highly deformed chert and argillite that is interbedded on a centimeter to decimeter scale. Argillites contain a slaty cleavage, and cherts are commonly boudined in the plane of the foliation. Foliations on either side of the fault average N47°W/87°SW.

END OF ROAD LOG

DIRECTIONS FOR ADDITIONAL STOPS

The following four stops are in different geographic regions of the northern Sierra Nevada. Accordingly, we do not maintain the mileage log throughout the four stops but do give detailed mileage and directions from certain landmarks.

Stop 6 *Serpentine schist.* Proceed to Downieville. From Downieville travel 4 miles west on Highway 49 to the small town of Goodyears Bar. Turn south and go across the bridge into the town. Note your trip meter at the Goodyears Bar Road-Highway 49 junction, Stop 6 is 0.7 miles to the south. At the "T" intersection turn right, continue past a few homes, and cross over a small bridge. Park on the left about 100 m past the bridge (Figure 7). The outcrops are up the slope to the east. From the car, cross the small creek and start up the hill. The first 200 m up the slope are sparse outcrops of scaly serpentinite, but as you approach, the deformation in the serpentinite is increasingly penetrative. The best serpentine schist outcrops are approximately 250 m east of the road.

The serpentinite weathers to black or green shades and is dark greenish-black where fresh. The penetrative foliation is the dominant fabric, but up to 10% scaly serpentinite phacoids may be present. The attitude of the foliation is approximately N9°E/70°SE, which is parallel to the orientation of the nearby contact with the Red Ant Schist. The rocks are composed of the assemblage antigorite, magnetite, ± chlorite and the foliation is defined by the preferred orientation of the antigorite grains.

Return to Highway 49 and follow it west 41 miles to the junction with Highway 20 just outside the town of Nevada City.

Stop 7 *Cumulate Wehrlite.* Note your mileage at the Highway 20-Highway 49 junction and then travel 13 miles east on Highway 20 to Washington Road. Turn left (north) on Washington Road and proceed 1.6 miles north. Park on the left side of the road; the outcrops are west of the road (Figure 6). Walk 100 m down the dirt road to the west. Take the left fork in the road at 100 m and proceed another 50 to 100 m onto the flat vegetated plain.

This is the only region within the Feather River Belt where ultramafic cumulates have been identified. The rocks weather red to brown and have the characteristic "warty" surface texture of a pyroxene-bearing peridotite. An important distinguishing feature of the Feather River cumulates is the large euhedral clinopyroxene grains that comprise approximately 40 to 70% of the rock. The remainder of the rock is composed of olivine or serpentinized olivine. These wehrlites are generally not foliated but rarely contain cryptic, possibly cumulate, layering, although none has been found in place. Return to the car.

Stop 8 *Talc schist.* Note your mileage and continue north on Washington Road. Travel 1.3 miles on Washington Road and park on the right side of the road just before a sharp bend to the left (north). You have parked in the scaly serpentinite unit (Figure 6); the talc schist is 50 to 100 m north along the road. The scaly serpentinite has relatively small phacoids at this site and a steep foliation at about N10°W/75°NE.

Walk 50 to 100 m north to the talc schist outcrops on the east side of the road. Be careful as you examine these outcrops; the cars go by fairly fast on this narrow road. At this site, there are both massive and schistose talc rocks with rare interleaved carbonates. Talc schists are typically gray and obviously very soft. The more massive variety of talc is pale green and lacks the strong foliation. The orientation of the dominant foliation is similar to the scaly serpentinite where the cars are parked. Unfortunately the contact between the talc schist and the scaly serpentinite is not exposed.

Stop 9 *Harzburgite—serpentinite transition.* Return to Highway 20 and return to Nevada City. From Nevada City continue 28 miles south on Highway 49 to Auburn and turn east onto Interstate 80. From Interstate 80, take the Foresthill exit and turn right onto Foresthill Road. Continue east 18 miles to the town of Foresthill. Drive 7 miles farther east on Foresthill Road, turn left (north) onto Sugar Pine Road. Follow the winding Sugar Pine Road 6.3 miles to the second junction with Finning Mill Road. Park at the junction and walk west along the paved Sugar Pine Road (Figure 8).

The outcrops on the north side of the road show an excellent example of the transition from fresh, unserpentinized harzburgite, through massive, wholly serpentinized rocks, to scaly serpentinite near the boat launch parking lot. Working from the east to west, the first 100 to 125 m of roadcut are composed of harzburgite, which has weathered to reds and browns. The characteristic warty surface texture can be seen as the fresh peridotites give way to massive serpentinite over the next 250 m toward the west. Here, the massive serpentinite weathers to shades of green and gray and contains only a weak foliation. Proceed west another 100+ m to the outcrops of scaly serpentinite near the boat launch parking lot. Rare blocks within the scaly serpentinite display relict harzburgite textures indicating the protolith. The general foliation of the scaly serpentinite is N16°W/80°NE, but the contact between the fresh and serpentinized harzburgite appears to have a more shallow dip.

REFERENCES

Bickford, M.E. and Day, H.W., 1988, Jurassic ages of arc-ophiolite complexes, northern Sierra Nevada: Implications for duration of the Nevadan "Orogeny": Geological Society of America Abstracts with Programs, v. 20, p. 274.

Bohlke, J.K. and McKee, E.H., 1984, K-Ar ages relating to metamorphism, plutonism, and gold-quartz vein mineralization near Allegheny, Sierra County, California: Isochron/West, v. 39, p. 3-7.

Burchfiel, B.C. and Davis, G.A., 1972, Structural framework and evolution of the southern part of the Cordilleran orogen, western United States: American Journal of Science, v. 272, p. 97-118.

Ceuleneer, G. and Rabinowicz, M., 1992, Mantle flow and melt migration beneath oceanic ridges: models derived from observations in ophiolites *in* Morgan, J.P., Blackman, D.K. and Sinton, J.M., editors, Mantle flow and melt generation at mid-ocean ridges: Geophysical Monograph 71, American Geophysical Union, p. 123-154.

Clark, L.D., 1960, Foothills Fault system, western Sierra Nevada, California: Geological Society of America Bulletin, v. 71, p. 483-496.

Clark, L.D. and Huber, N.K., 1975, Geologic observations and sections along selected stream travers, northern Sierra Nevada metamorphic belt, California: U.S. Geological Survey Miscellaneous Field Studies Map MF-690, scale 1:62,500.

Coleman, R.G., 1971, Plate tectonic emplacement of upper mantle peridotites along continental edges: Journal of Geophysical Research, v. 76, no. 5, p. 1212-1221.

D'Allura, J.A., Moores, E.M. and Robinson, 1977, Paleozoic rocks of the northern Sierra Nevada, their structural and paleogeographic implications *in* Stewart, J.H., Stevens, C.H. and Fritche, A.E., editors, Paleozoic Paleogeography of the Western United States: Pacific Coast Paleogeography Symposium 1: Pacific Section, Society of Economic Paleontologists and Mineralogists, p. 395-408.

Day, H.W., Moores, E.M. and Tuminas, A.C., 1985, Structure and tectonics of the northern Sierra Nevada: Geological Society of America Bulletin, v. 96, p. 436-450.

Day, H.W., 1992, Tectonic setting and metamorphism of the Sierra Nevada, California *in* Schiffman, P. and Wagner, D.L., editors, Special Publication 114: Field Guide to the Geology and Metamorphism of the Franciscan Complex and the Western Metamorphic Belt of Northern California: Sacramento, CA, California Department of Conservation, Division of Mines and Geology, p. 12-28.

Dickinson, W.R., 1981, Plate tectonics and the continental margin of California *in* Ernst, W.G., editor, The Geotectonic Development of California: Engelwood Cliffs, N.J., Prentice Hall, Inc, p. 1-28.

Edelman, S.H., Day, H.W., Moores, E.M., Zigan, S.M., Murphy, T.P. and Hacker, B.R., 1989, Structure across a Mesozoic ocean-continent suture zone in the northern Sierra Nevada, California: Geological Society of America Special Paper, v. 224, p. 1-56.

Ehrenberg, S.M., 1975, Feather River ultramafic body, northern Sierra Nevada, California: Geological Society of America Bulletin, v. 86, p. 1235-1243.

Ferguson, H.G. and Gannett, R.W., 1932, Gold quartz veins of the Alleghany district, California: U.S. Geological Survey Professional Paper, v. 172, p. 1-139.

Hannah, J.L. and Moores, E.M., 1986, Age relations and depositional environment of Paleozoic strata, northern Sierra Nevada, California: Geological Society of America Bulletin, v. 97, p. 787-797.

Harwood, D.S., 1988, Tectonism and metamorphism in the Northern Sierra Terrane, northern California *in* Ernst, W.G., editor, Metamorphism and Crustal Evolution of the Western United States: Engelwood Cliffs, N.J., Prentice Hall, Inc. p. 764-788.

Hietanen, A., 1981, Petrologic and structural studies in the northwestern Sierra Nevada, California: U.S. Geological Survey Professional Paper, v. 1226, p. 1-59.

Kelemen, P.B., 1990, Reaction between ultramafic rock and fractionating basaltic magma I. Phase relations, the origin of calc-alkaline magma series, and the formation of discordant dunite: Journal of Petrology, v. 31, no. 1, p. 51-98.

Mayfield, J.D. and Day, H.W., 1996, 200 Ma tonalitic basement in the eastern Smartville Complex: Implications for the emplacement of the Smartville arc: Geological Society of America Abstracts with Programs, v. 28, no. 7, p. 311.

Mayfield, J.D. and Day, H.W., 1999, New geologic mapping in the Feather River Belt of the northern Sierra Nevada, California: Geological Society of America Abstracts with Programs (Cordilleran Section), v. 31, no. 6, p. 78.

Moores, E.M., 1970, Ultramafics and orogeny, with models of the US Cordillera and the Tethys: Nature, v. 228, p. 837-842.

Moores, E.M., 1987, Suture zones: Memoirs Geological Society of India, v. 12, p. 25-28.

Moores, E.M. and Day, H.W., 1984, Overthrust model for the Sierra Nevada: Geology, v. 12, p. 416-419.

Peacock, S.M., 1987, Serpentinization and infiltration metasomatism in the Trinity peridotite, Klamath province, northern California; Implications for subduction zones: Contributions to Mineralogy and Petrology, v. 95, p. 55-70.

Saleeby, J.B., Goodin, S.E., Sharp, W.D. and Busby, C.J., 1978, Early Mesozoic paleotectonic-paleogeographic reconstruction of the southern Sierra Nevada region *in* Howell, D.G. and McDougall, K.A., editors, Mesozoic Paleogeography of the Western United States, Pacific Coast Paleogeography Symposium 2, Pacific Section, Society of Economic Paleontologists and Mineralogists, p. 311-336.

Saleeby, J.B. and Moores, E.M., 1979, Zircon ages on northern Sierra Nevadan ophiolite remnants and some possible regional correlations: Geological Society of America Abstracts with Programs, v. 11, p. 125.

Saleeby, J.B., Shaw, H.F., Niemeyer, S., Moores, E.M. and Edelman, S.H., 1989, U/Pb, Sm/Nd and Rb/Sr geochronological and isotopic study of northern Sierra Nevada ophiolitic assemblages, California: Contributions to Mineralogy and Petrology, v. 102, p. 205-220.

Saucedo, G.J. and Wagner, D.L., 1992, Geologic map of the Chico Quadrangle, California: Division of Mines and Geology Regional Map Series, no. 7A, scale 1:250,000.

Schweickert, R.A. and Cowan, D.S., 1975, Early Mesozoic tectonic evolution of the western Sierra Nevada, California: Geological Society of America Bulletin, v. 86, p. 1329-1336.

Schweickert, R.A. Armstrong, R.L. and Harakal, J.E., 1980, Lawsonite blueschist in the northern Sierra Nevada, California: Geological Society of America Bulletin, v. 8, p. 27-31.

Schweickert, R.A., 1981, Tectonic Evolution of the Sierra Nevada Range *in* Ernst, W.G., editor, The Geotectonic Development of California: Englewood Cliffs, N.J., Prentice Hall, p. 87-131.

Souter, B. and Day H.W., 1991, Arc basement of the Smartville Complex, northern Sierra Nevada, California: Geological Society of America Abstracts with Programs, v. 23, p. 99.

Standlee, L.A., 1978, Geology of the northern Sierra Nevada basement rocks, Quincy-Downieville area, California. [Ph.D. dissertation]: Houston, Texas, Rice University, 176 p.

Stolper, E.A., 1980, A phase diagram for mid-ocean ridge basalts: Contributions to Mineralogy and Petrology, v. 74, p. 13-27.

Weisenberg, C.W. and Ave Lallemant, H., 1977, Permo-Triassic emplacement of the Feather River ultramafic body, northern Sierra Nevada mountains, California: Geological Society of America Abstracts with Programs, v. 9, p. 525.

DEVONIAN SIERRA BUTTES FORMATION IN THE JAMISON LAKE AREA: INVOLVEMENT OF ANCIENT CONTINENTAL CRUST IN MAGMA GENESIS

Steven R. Silva,[1] Thomas D. Bullen,[2] Elwood R. Brooks[3]

INTRODUCTION

The Late Devonian Sierra Buttes Formation in the northern Sierra Nevada is the lowermost volcanic unit in a thick sequence of Late Devonian to Middle Jurassic island-arc volcanic and related rocks (D'Allura and others, 1977; Dickinson, 1977; Brooks and Coles, 1980; Dickinson, 1981; Schweickert, 1981; Schweickert and Snyder, 1981; Brooks and others; 1982 Harwood and Murchey, 1990). The island-arc rocks together with their basement, the pre-Late Devonian Shoo Fly Complex, constitute the northern Sierra terrane of Coney and others (1980). The Shoo Fly Complex is generally accepted as an accretionary assemblage upon which the volcanic rocks were deposited unconformably (Schweickert and Snyder, 1981; Schweickert and others, 1984; Harwood, 1988). The Shoo Fly Complex is composed predominantly of fine-grained metasedimentary rocks typical of continental- slope-and-rise deposits (Dickinson, 1981). It occupies four highly deformed, regionally extensive thrust sheets (Schweickert and others, 1984b). Middle to Late Ordovician conodonts are the oldest known fossils. An Early Silurian U-Pb zircon date from felsic tuff (Saleeby and others, 1987) is the youngest yet recorded, indicating that deformation of the Shoo Fly Complex occurred sometime between Early Silurian and deposition of the first arc rocks in the Late Devonian.

Speed (1979), Coney and others (1980), and Speed and Sleep (1982) have suggested that the northern Sierra terrane belongs to a far-traveled microplate. However, evidence based on comparative stratigraphy (Schweickert and Snyder, 1981; Harwood and Murchey, 1990), paleogeographic significance of phosphatic cherts (Varga, 1982; Coles and Varga, 1988), and U-Pb zircon analyses (Girty and Wardlaw, 1985) is consistent with the interpretation that the Shoo Fly Complex is the eugeoclinal counterpart of the miogeoclinal rocks deposited along the western margin of North America beginning about 850 Ma (Dickinson, 1977). If this interpretation is correct, the volcanic rocks of the northern Sierra terrane should provide important detail about the onset and development of active margin tectonism along the western North American continental margin.

The Sierra Buttes Formation is distinctive as the initial volcanic product in the northern Sierra terrane in that it erupted through an accretionary complex and represents a voluminous silicic phase of arc magmatism that contrasts with the overlying and equally extensive basaltic to andesitic Taylor Formation. These features relate to the early petrogenetic and tectonic evolution of the arc system and have been a subject of interest and speculation (Schweickert and Snyder, 1981; Rouer and others, 1989a). Previous geochemical and isotopic studies including analyses of U-Pb in zircon, Sr-Nd in whole rock, and $\delta^{18}O$ on quartz phenocrysts have indicated involvement of crustal material in the Sierra Buttes and Taylor magmas but have not determined the extent of crustal involvement or its

---

[1] U.S. Geological Survey, 345 Middlefield Road, M/S 434, Menlo Park, California, 94025
[2] U.S. Geological Survey, 345 Middlefield Road, M/S 420, Menlo Park, California, 94025
[3] California State University, Hayward, Department of Geological Sciences, Hayward, California, 94542

relation to the silicic nature of the Sierra Buttes magmas (Hanson and others, 1988; Rouer and others, 1989b).

This study presents new Sr-Nd isotopic and trace element data from a complete section of the Sierra Buttes Formation in the Jamison Lake area consisting of two silicic units that bound two relatively mafic units. The objectives of the study were to investigate the petrogenetic relationships among the four members and to draw inferences about the source of the Sierra Buttes magmas.

The Sierra Buttes Formation in the Jamison Lake Area

The extrusive rocks of the Sierra Buttes Formation in the Jamison Lake area were deposited in a subaqueous environment, as shown by lenses of intercalated chert and lesser coarse-grained marine sedimentary rock. They were subsequently regionally metamorphosed during the Late Jurassic Nevadan orogeny. Earlier metamorphic events associated with the Late Devonian to Early Mississippian Antler Orogeny and the Permian Sonoman Orogeny are probable, but as yet undocumented. Effects of metamorphism include a foliation and a lower greenschist facies mineral assemblage consisting principally of quartz, albite, calcite, epidote-clinozoisite, sphene-leucoxene, chlorite, and sericite. Despite the metamorphism, the stratigraphy and many primary igneous features including phenocrysts, flow-banding, perlitic cracks, spherulites, and vesicles are well preserved.

The Sierra Buttes Formation in the vicinity of Jamison Lake has been divided into four members, numbered 1 to 4 from oldest to youngest (Figures 1 and 2) on the basis of field mapping (Silva, 1990). Members 1 and 4 constitute most of the section and are composed of dacitic quartz porphyry lava flows and intrusive rocks, respectively. They are quite similar lithologically, consisting of relict phenocrysts of quartz and plagioclase in a light-colored, aphanitic, silicic groundmass. There is no evidence that any mafic silicate phases were present. Small grains of opaque oxides are

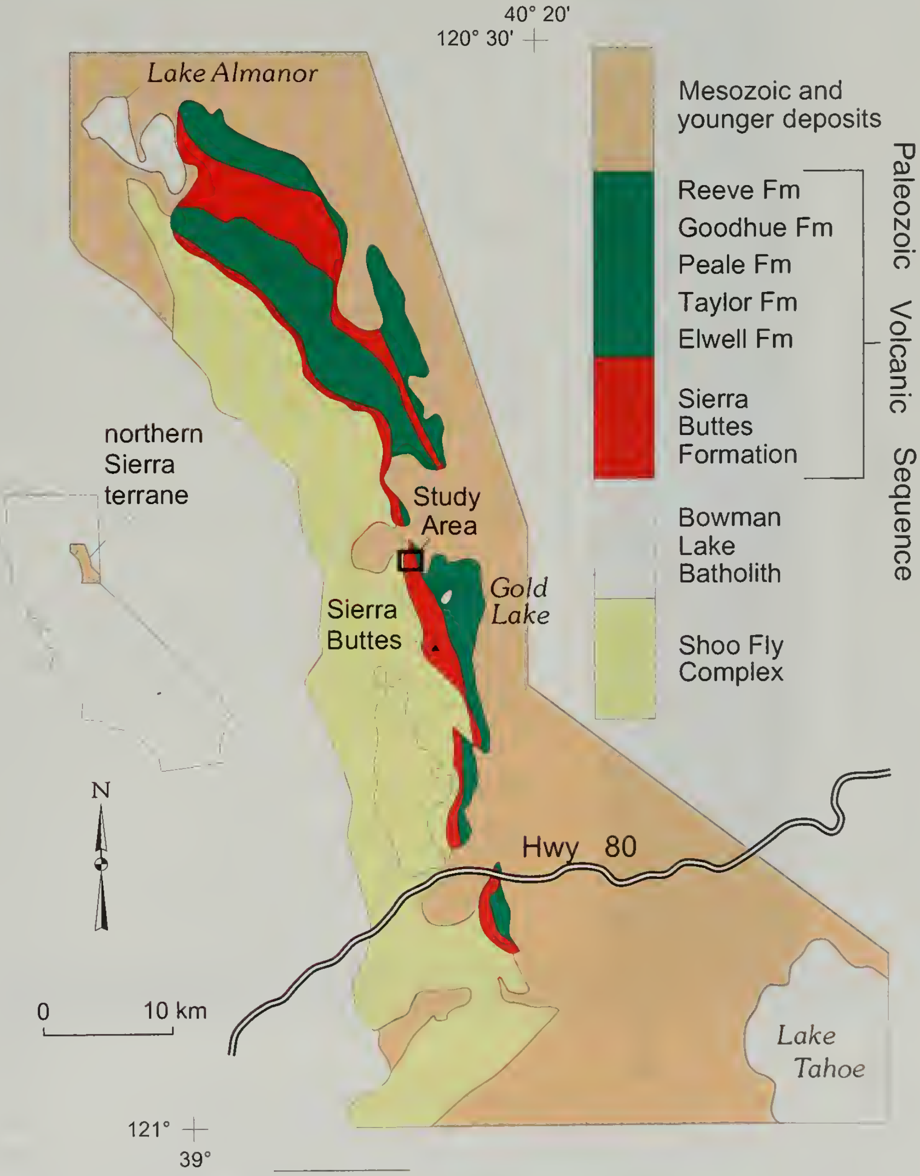

Figure 1. Location map of the Jamison Lake study area showing the approximate extent of the northern Sierra terrane, generalized from Harwood (1988).

rare. Members 2 and 3 are both relatively mafic pyroclastic deposits. Based on major element chemistry, compositons range from basalt to dacite; however, petrographic comparisons of Member 3 rocks suggest original compositions toward the mafic end of this range. The basal portion of Member 2 contains a high proportion of chert and occasional clasts of quartz porphyry and mafic pillow fragments apparently incorporated along the base of the flow. The primary components within Members 2 and 3 contain abundant relict plagioclase microlites, sparse relict phenocrysts of plagioclase, and rare fragments of quartz (xenocrysts?) in a dark, relict, aphanitic groundmass. The groundmass is composed of a secondary mineral assemblage including high proportions of chlorite, calcite, epidote-clinozoisite, leucoxene, and opaque oxides indicative of relatively mafic original compositions as compared to Members 1 and 4. Both Members 2 and 3 are variably vesicular, while silicic Members 1 and 4 are non-vesicular. All rocks within the study are sparsely phyric to nearly aphryic (≤5%) with the exception of Member 4, a small minority of which contains as much as 30% phenocrysts.

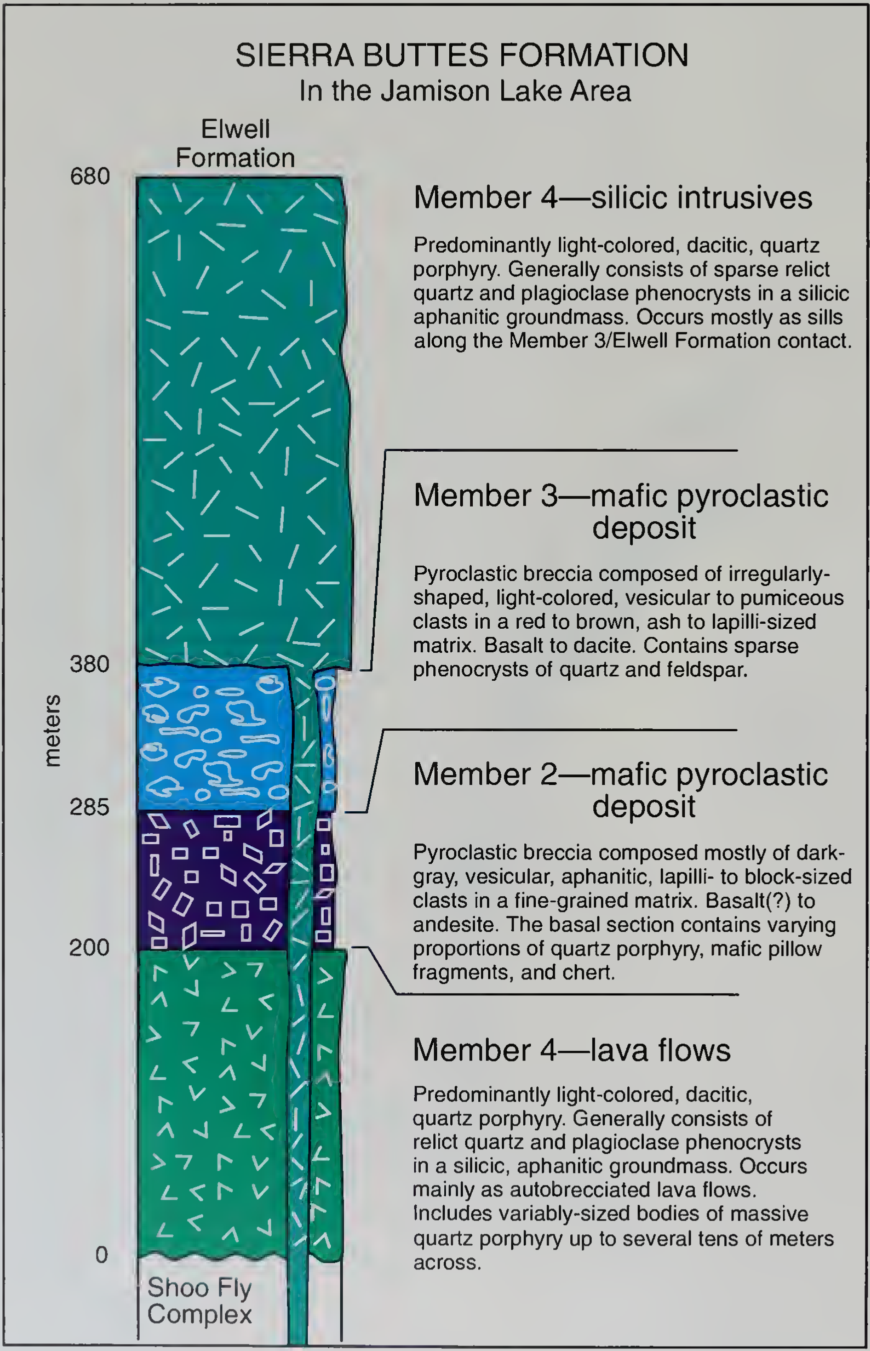

Predominantly light-colored, dacitic, quartz porphyry. Generally consists of sparse relict quartz and plagioclase phenocrysts in a silicic aphanitic groundmass. Occurs mostly as sills along the Member 3/Elwell Formation contact.

Pyroclastic breccia composed of irregularly-shaped, light-colored, vesicular to pumiceous clasts in a red to brown, ash to lapilli-sized matrix. Basalt to dacite. Contains sparse phenocrysts of quartz and feldspar.

Pyroclastic breccia composed mostly of dark-gray, vesicular, aphanitic, lapilli- to block-sized clasts in a fine-grained matrix. Basalt(?) to andesite. The basal section contains varying proportions of quartz porphyry, mafic pillow fragments, and chert.

Predominantly light-colored, dacitic, quartz porphyry. Generally consists of relict quartz and plagioclase phenocrysts in a silicic, aphanitic groundmass. Occurs mainly as autobrecciated lava flows. Includes variably-sized bodies of massive quartz porphyry up to several tens of meters across.

Figure 2. Generalized columnar section of the Sierra Buttes Formation in the Jamison Lake area (Note: Member 4 intrudes the Elwell Formation within the study area, as well as the older units of the Sierra Buttes Formation.) As noted by Hanson and Schweickert (1986) and Brooks and others (1982), the Elwell Formation should probably not have been accorded formational status.

Geochemistry

Samples were analyzed for selected major and trace elements: six samples each from Members 1 and 4, four samples from Member 3, one sample from a mafic pillow fragment in Member 2, and five samples of metasediments from the underlying Shoo Fly Complex. The Sierra Buttes rocks were also analyzed for Sr and Nd isotopes and the Shoo Fly rocks for Nd isotopes only. All samples were trimmed of weathered surfaces, veins, and inclusions before homogenization and analysis. Clasts within the matrix of Member 3 were selected to avoid secondary vesicle fillings of pumice fragments. Descriptions of the Sierra Buttes rocks are given in the field guide section of this paper and Shoo Fly rocks in Appendix A. All analyses were performed at the U.S. Geological Survey and are reported in the Table. Trace elements were analyzed on a Perkin Elmer* ICPMS and isotopic compositions were determined with a Finnigan* MAT 261 mass spectrometer. Analytical precisions are given in Appendix B.

Sr and Nd isotopes were used in this study to trace the involvement of a Proterozoic or older crustal component in the genesis of the rocks exposed in the Jamison Lake area. Rare-earth and other trace elements were used to investigate possible petrogenetic relations among the silicic and relatively mafic compositions sampled within the study area. Major elements are considered unreliable due to their relative mobility during metamorphism. Silica analyses in Members 1 and 4 are higher than the range normally seen in igneous rocks. Whether these actually reflect the compositions imparted by partial melts of sediment as discussed below or are the result of element mobility is unknown. In general, the major elements do reflect the relatively silicic and mafic natures of the four units but are not considered further in this study.

Sr-Nd Isotopes

Sr- and Nd-isotopic compositions trend toward the oceanic mantle array with decreasing relative age (Figure 3). Initial ε_{Nd} ranges from approximately -15 to -20 for Member 1, from 0 to -12 for Members 2 and 3, and from 0 to -5 for Member 4. Initial $^{87}Sr/^{86}Sr$ ranges from 0.7090 to 0.7180 for Member 1, from 0.7070 to 0.7120 for Members 2 and 3, and from 0.7060 to 0.7080 for Member 4. Epsilon Nd values between -15 and -20 for Member 1 lavas indicate the involvement of a Precambrian crustal component (DePaolo and Wasserburg, 1979).

Strontium isotopes show a much weaker age correlation than Nd isotopes due to highly variable Rb/Sr in crustal rocks (DePaolo and Wasserburg, 1979). In metamorphic rocks, Sr isotopic values are less reliable than those of Nd due to the relative mobility of Rb and Sr. The single Member 4 outlier that plots to the left of the mantle array (Figure 3) has very similar ε_{Nd} to the other Member 4 samples. This particular sample also has similar modern-day $^{87}Sr/^{86}Sr$, but about three times the

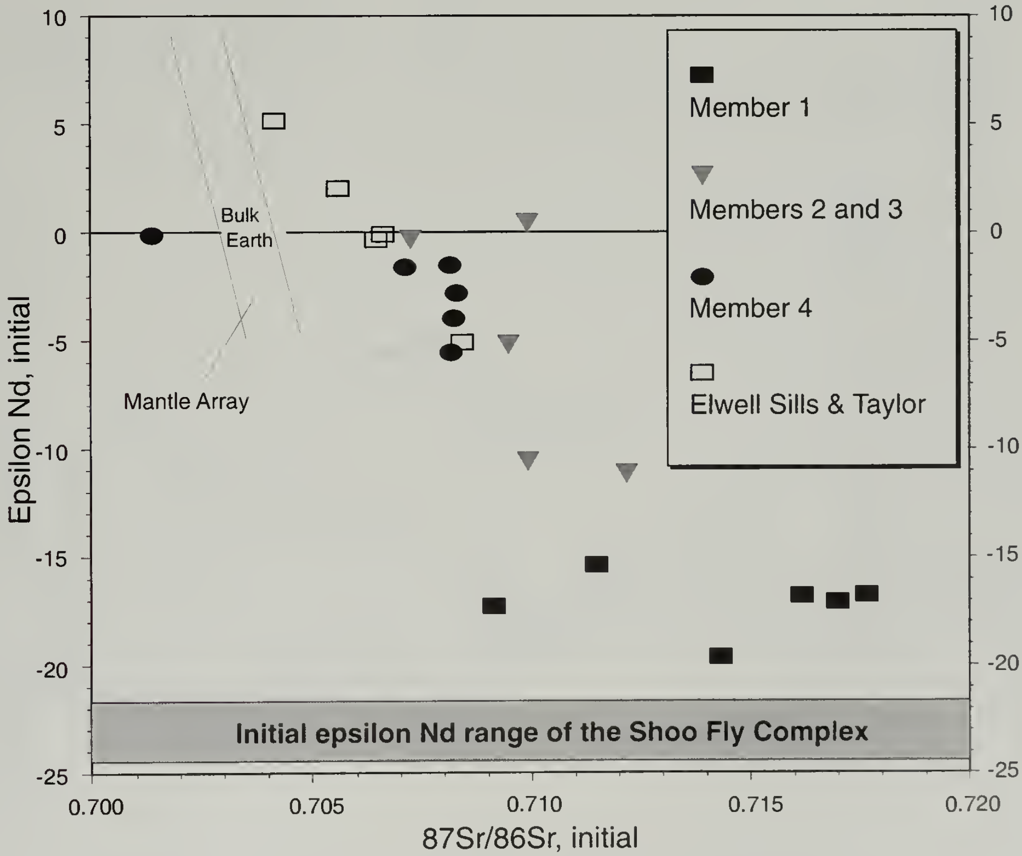

Figure 3. εNd vs initial $^{87}Sr/^{86}Sr$ (corrected to 360 Ma). Values used for the calculation of initial $^{87}Sr/^{86}Sr$ and εNd are: Half life of ^{87}Rb = 4.88 X 10^{10}; Half life of ^{147}Sm = 1.06 X 10^{11}; CHUR = 0.512638; ^{147}Sm = 0.14994 X Sm conc.; ^{144}Nd = 0.23793 X Nd conc.; ^{87}Rb = 0.27875 X Rb conc.; ^{86}Sr = 0.0986 X Sr conc.

---

* Use of trade names and trademarks in this paper is for descriptive purposes only and does not constitute endorsement by the U.S. Geological Survey.

Rb/Sr value of the other Member 4 samples, causing it to correct to an initial value, at 360 Ma, far to the left. Despite the variability of initial $^{87}Sr/^{86}Sr$ values in these rocks, the negative correlation between ε_{Nd} and $^{87}Sr/^{86}Sr$ is apparent (Figure 3). Additional analyses from the Elwell and overlying Taylor formations (E.R. Brooks, unpublished data) overlap the fields of Members 2, 3, and 4, and trend back toward the mantle array at an ε_{Nd} value of about +6.

The distinct fields for Members 1 and 4 eliminate the possibility of a single source for these silicic units. Member 4, however, lies within the ε_{Nd} range of Members 2 and 3, which is permissive of a related source. The general trend toward less negative values of ε_{Nd} upsection and toward the mantle array may suggest: 1) an increasing proportion of mantle-derived liquids into the magmatic system with time and/or 2) a decreasing influence of crustal contamination; and/or 3) a change in crustal source(s). The underlying Shoo Fly Complex was sampled as an obvious and accessible candidate for a crustal component in the Sierra Buttes rocks. Initial ε_{Nd} values from the Shoo Fly Complex range from -21.7 to -24.6 permissive of the crustal source.

Trace Elements

The chondrite-normalized REE patterns for Member 1 resemble those most common in calc-alkaline, island-arc compositions with (La/Yb)n values between about 4 and 10, (La)n abundances between about 50 and 100, prominent negative Eu anomalies, Eu/Eu* between about 0.4 and 0.5, and a slightly concave upward shape of the heavy rare-earth elements (HREE) in four of the six compositions (Figure 4). The relatively mafic Members 2 and 3 possess nearly flat MORB-like patterns with (La/Yb)n between about 1.0 and 3.0, (La)n between about 13 and 25, and slight to moderate negative Eu anomalies between about 1.0 and 0.6 (Figure 5). The REE patterns for Member 4 have similar (La/Yb)n and Eu anomalies to those of Members 2 and 3 but higher abundances of REE with (La)n between about 20 and 60 (Figure 6). The Shoo Fly samples have (La/Yb)n values between about 9 and 12 with (La)n between about 40 and 70 and Eu/Eu* between about 0.45 and 0.65 (Figure 7).

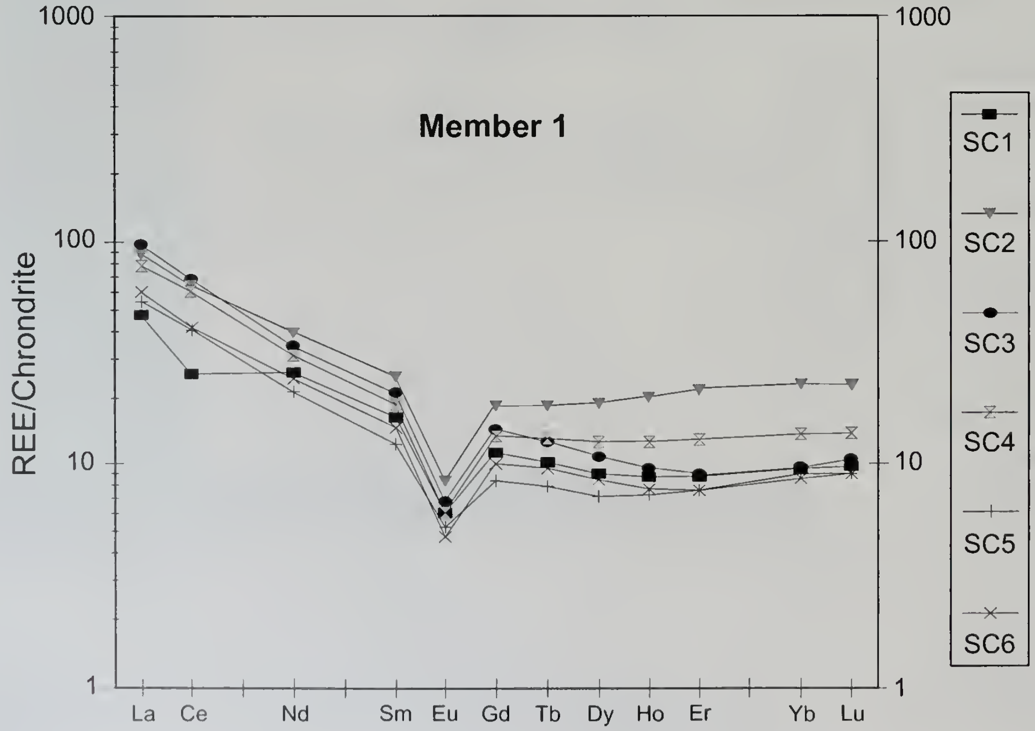

Figure 4. Chondrite-normalized REE diagram for Member 1.

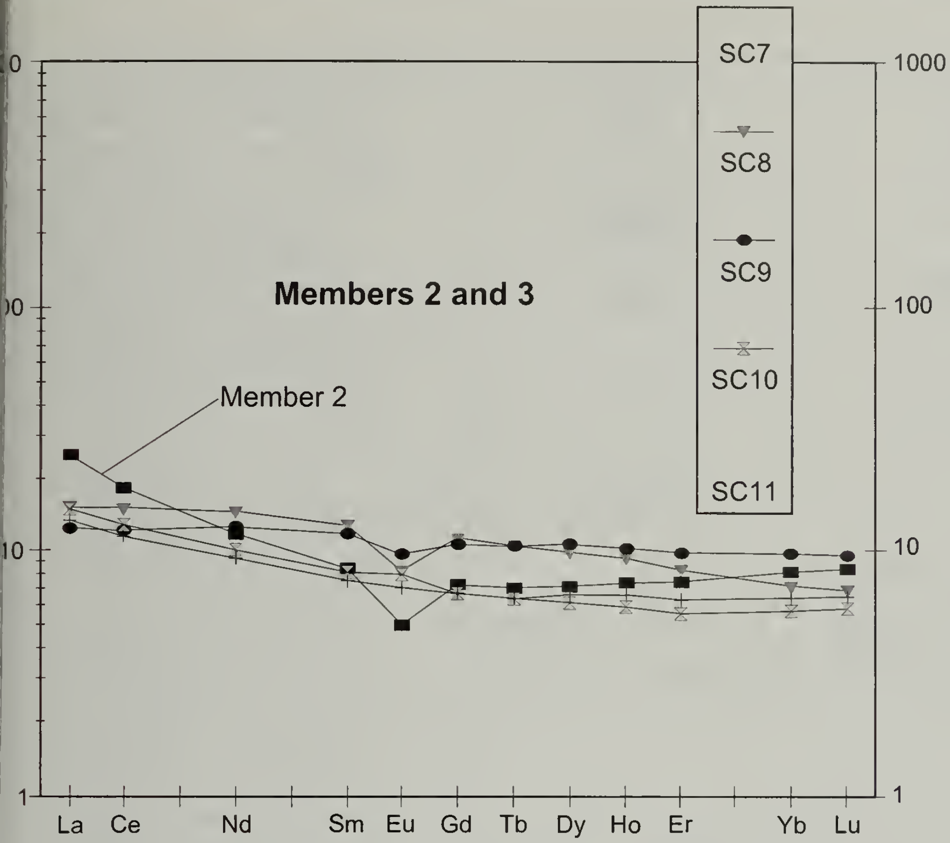

Figure 5. Chondrite-normalized REE diagram for Members 2 and 3

A plot of averaged chondrite normalized REE for the Sierra Buttes and Shoo Fly samples shows a parallel trend of Members 2 and 3 with Member 4, but with a deeper Eu anomaly for Member 4 consistent with the derivation of Member 4 primarily through crystal fractionation of plagioclase from a composition similar to that represented by Members 2 and 3 (Figure 10). The pattern for Member 1 on the averaged REE plot is quite similar to that of the Shoo Fly Complex for the light rare-earth elements (LREE) and significantly higher for the HREE. If the trace elements in Member 1 were derived in

On plots of (La/Yb)n vs (Yb)n and (La/Yb)n vs Eu/Eu* (the magnitude of the Eu anomaly) (Figures 8 and 9), arrows indicate the approximate trends produced by fractionation of some common minerals that have important influences on the plots (Hanson, 1980). On both plots the distinct fields for silicic Members 1 and 4 reflect their separate source, as required by the Sr and Nd isotopes, and/or separate evolutionary processes. Both plots show Member 4 lying essentially along a feldspar control line from Members 2 and 3, suggesting a relatively simple fractionation trend from compositions similar to the earlier and more mafic Members 2 and 3.

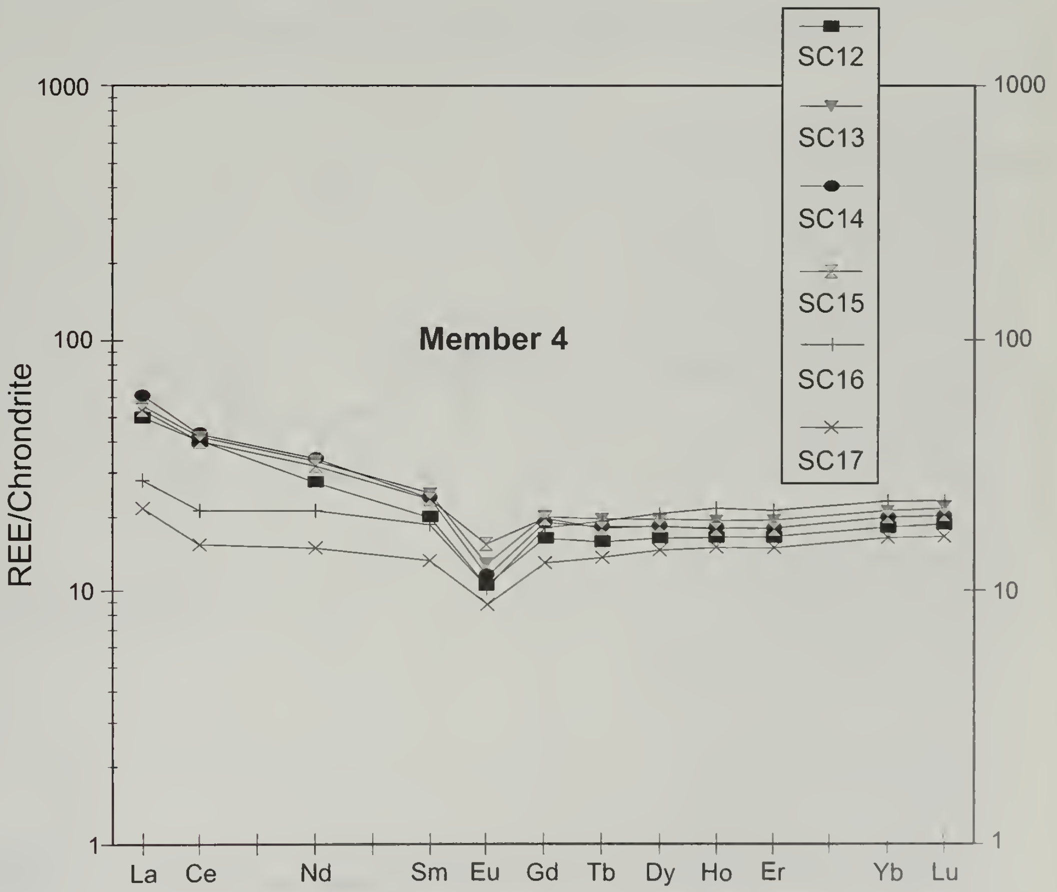

Figure 6. Chondrite-normalized REE diagram for Member 4.

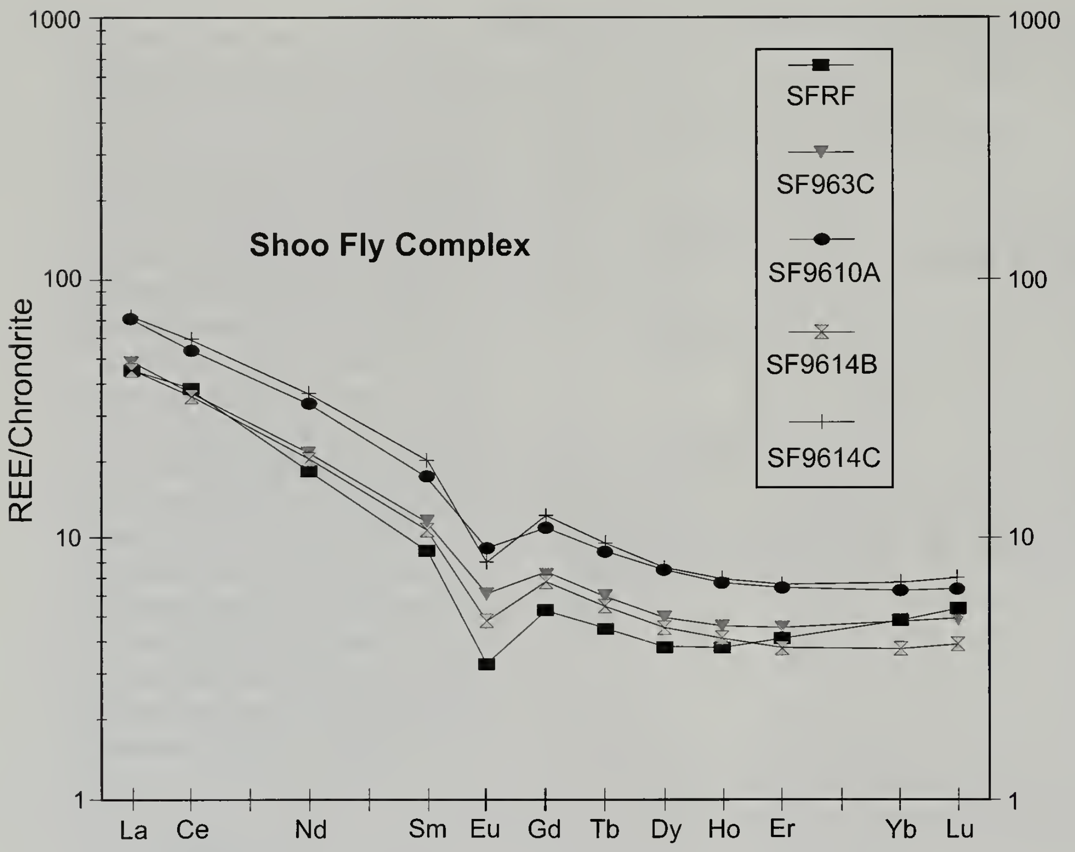

Figure 7. Chondrite-normalized REE diagram for the Shoo Fly Complex.

large part through partial melting of the Shoo Fly Complex, as allowed by the ε_{Nd} analyses, the REEs would require preferential melting of a HREE retentive phase(s) such as hornblende to elevate the HREE of Member 1 as compared to the LREE.

On Figures 11 and 12, the averaged compositions for Member 1, Members 2 and 3 combined, Member 4, and the Shoo Fly Complex were normalized to the most mafic composition sampled based on both its lowest overall REE concentrations and highest overall ε_{Nd} value (Member 3, sample SC11). The normalized trace elements were arranged generally in order of increasing incompatibility from right to left after Thompson and others (1984) to further investigate the possible petrogenetic relationships mentioned above.

Figure 11 compares analyses of Member 1 with those of the Shoo Fly Complex. The trace element patterns are nearly identical from Ba through Eu, but with disproportionally high concentrations for Member 1 at Ba. Member 1 is considerably lower than the Shoo Fly for Zr, Hf, and Ti, and higher for the

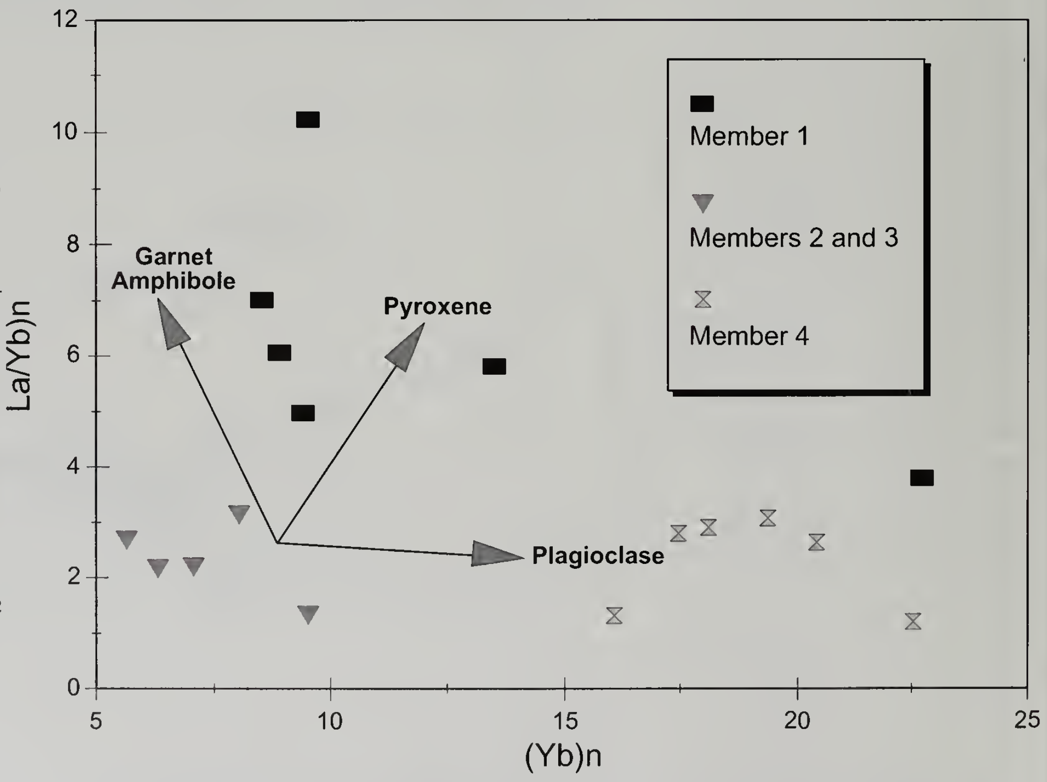

Figure 8. Chondrite-normalized La/Yb vs Yb as a measure of LREE enrichment relative to HREE abundances. Arrows indicate fractionation trends caused by the involvement of various minerals.

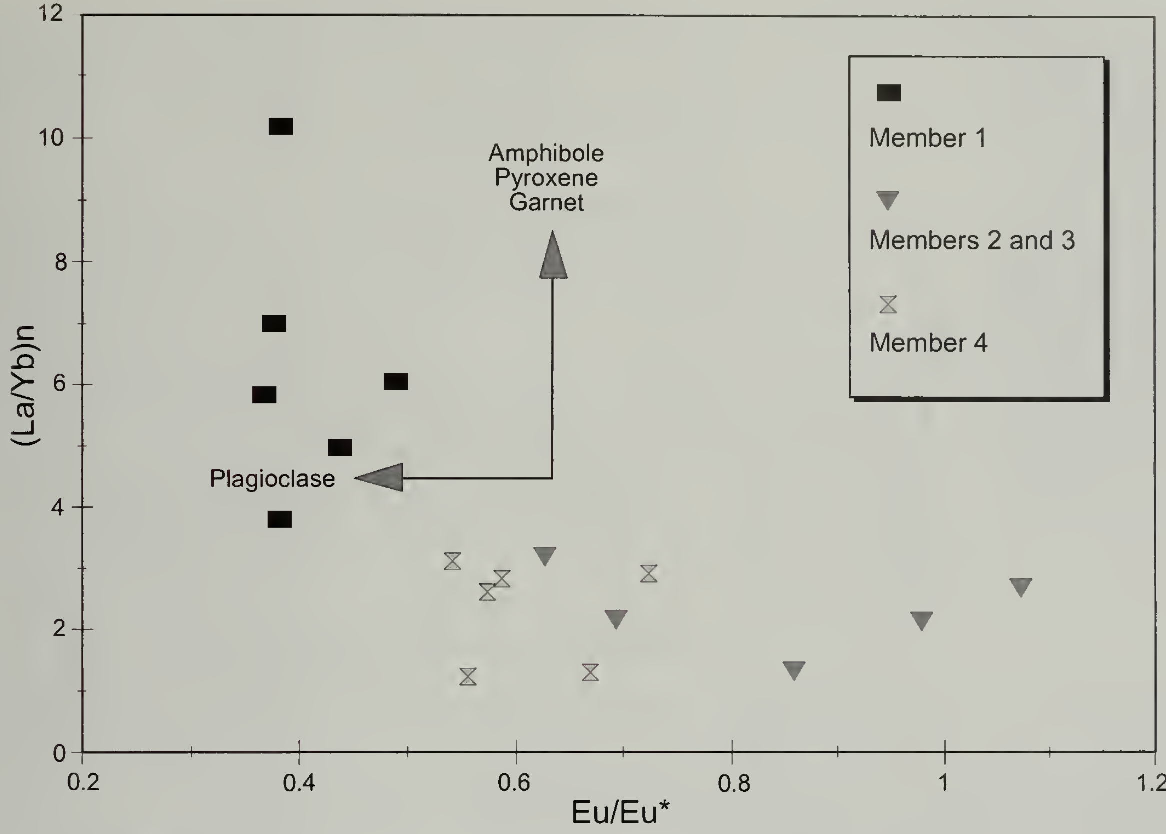

Figure 9. Chondrite normalized La/Yb vs Eu/Eu* as a measure of LREE enrichment relative to depth of Eu anomaly. Arrows indicate fractionation trends caused by the involvement of various minerals.

HREE plus Y. The similarity of the Member 1 and Shoo Fly trace element patterns along with the isotopic data suggest that Member 1 attained much of its trace element signature through partial melting of Shoo Fly rocks. The concentrations of the elements Rb through Sm are consistent with a mixture of a Shoo Fly partial melt, generally producing higher concentrations of incompatible elements in the melt, and a relatively mafic magma, which in turn lowers the concentrations of the elements that plot above 1.0, further elevating those that plot below 1.0, notably Sr. The relatively high values for Ba and the HREE plus Y again suggest disproportionate melting of a Ba and HREE retentive phase(s) such as hornblende. The relatively low values of Zr, Hf, and Ti, in Member 1

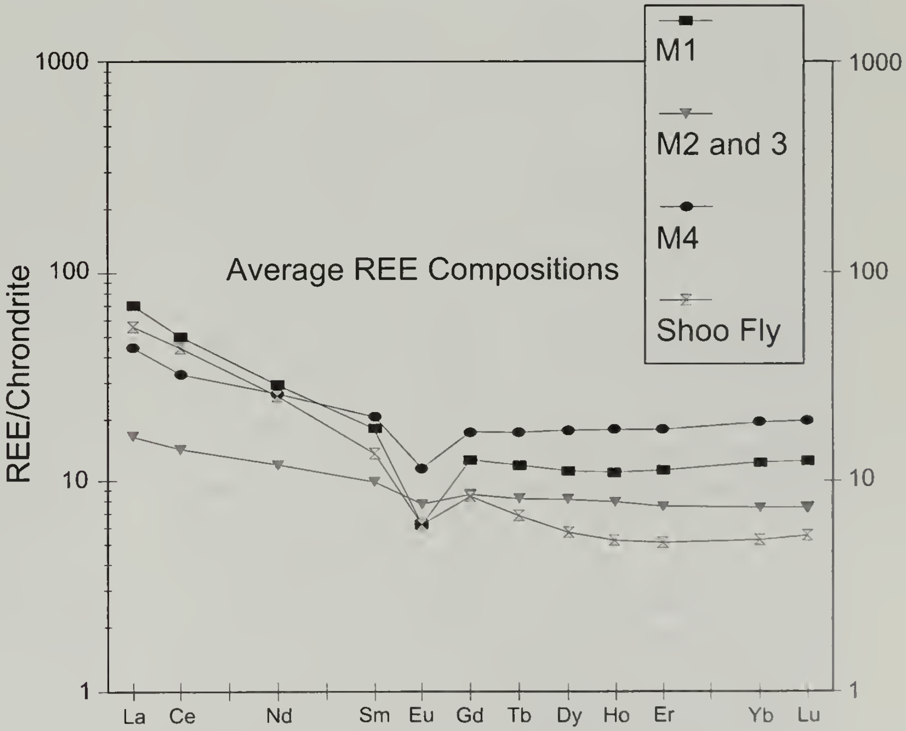

Figure 10. Chrondrite-normalized REE patterns for averaged compositions for Member 1, Members 2 and 3 combined, Member 4, and the Shoo Fly Complex.

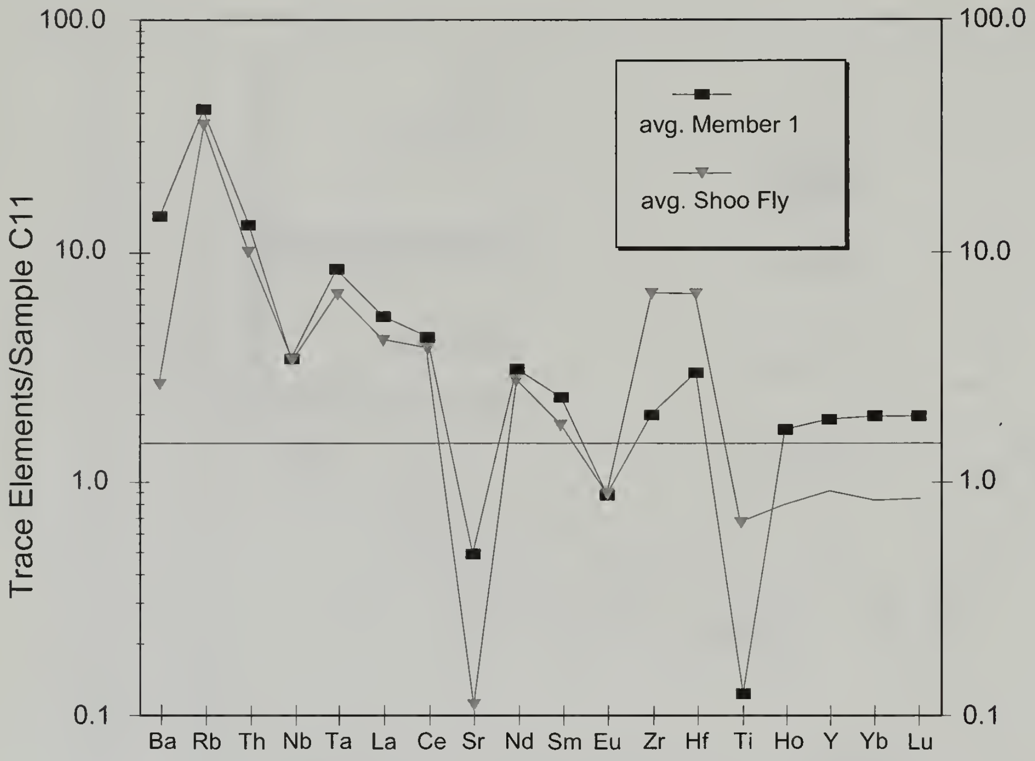

Figure 11. Spidergram (normalized to Member 3, sample C11) comparing the averaged trace element composition of Member 1 with that of the Shoo Fly Complex (modified after Thompson and others [1984]).

fractionation. A negative anomaly at Ti may be the result of fractionation of iron oxide.

Calculations of the degree of partial melting of Shoo Fly Complex and of the proportions of Shoo Fly and mafic components needed to produce Member 1 are highly model-dependent, but constrained to some degree by the Nd isotopic and concentration analyses of the Sierra Buttes and Shoo Fly rocks (Appendix C). Using the average ε_{Nd} and Nd concentrations from the Shoo Fly and Sierra Buttes Member 1 rocks plus the most mafic Member 3 composition (SC11), isotope mass balance requires that: 1) on average, 74% of the mass of

suggest retention of accessory phases, principally iron oxide sphene and/or rutile.

Figure 12 compares trace element analyses of Members 2 and 3 with Member 4. The pattern for Member 4 is generally parallel to that of Members 2 and 3 with an anomaly at Eu consistent with its derivation principally through plagioclase

Figure 12. Spidergram (normalized to Member 3, sample C11) comparing the averaged trace element composition of combined Members 2 and 3 with that of Member 4 (modified after Thompson and others [1984]).

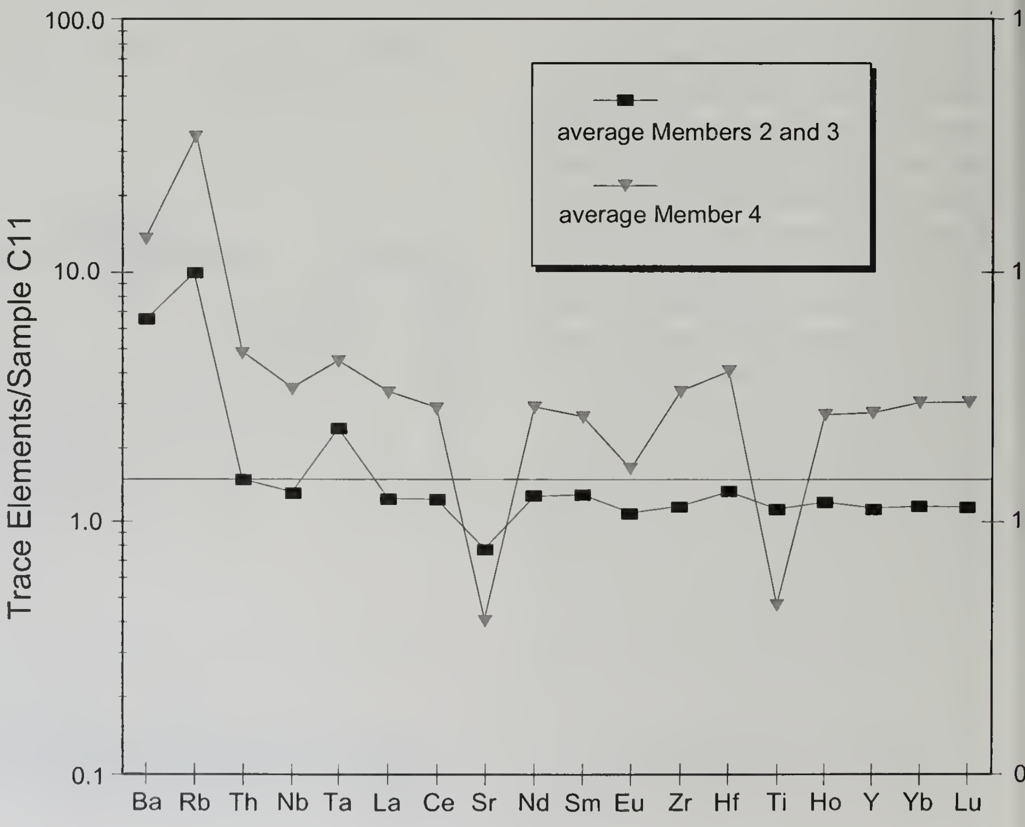

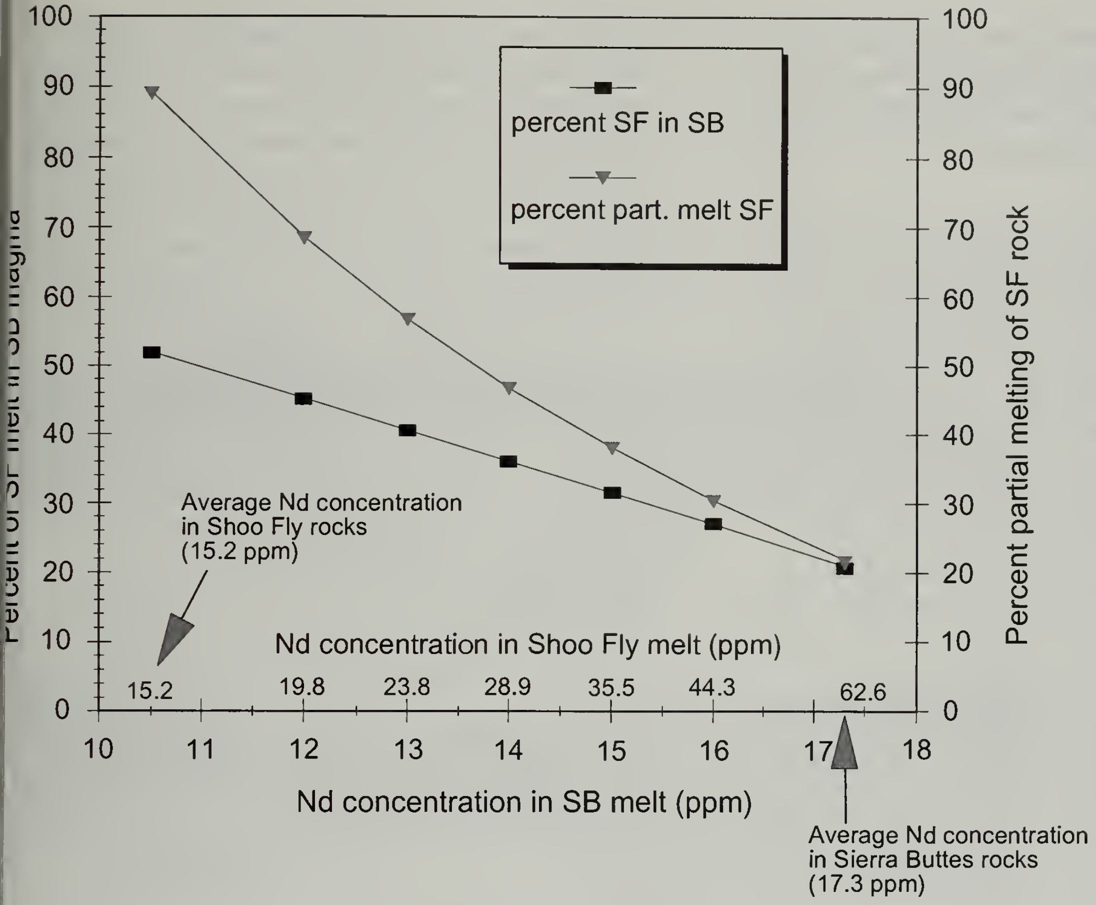

Figure 13. Variations in (1) the percent of Shoo Fly (SF) melt in the Sierra Buttes (SB) magma, (2) the percent of partial melting of Shoo Fly rock, and (3) Nd concentration in the Shoo Fly melt with Nd concentration in the Sierra Buttes melt prior to fractional crystallization. The probable bounding conditions are the Nd concentrations measured in the Shoo Fly and Sierra Buttes rocks (noted on graph). See Appendix C for calculations.

Nd in the Sierra Buttes rock was derived from the Shoo Fly Complex and 2) that 21% of the Sierra Buttes magma was derived from a Shoo Fly melt possessing about 63ppm Nd. Using the values stated above and a bulk partition coefficient for Nd of 0.1, and assuming batch melting, the degree of partial melting of Shoo Fly rocks is 22%. This is the limiting case assuming no fractional crystallization in the Member 1 melt. However, the trace element diagrams suggest some fractionation, particularly of plagioclase, which would increase the concentration of Nd in the melt before eruption. If, for instance, the concentration of Nd in the Sierra Buttes magma before fractionation is considered to be 15ppm rather than the average measured value in the rock of 17.4ppm, the calculated fraction of Shoo Fly melt in the Sierra Buttes magma increases from 21 to 31% and the degree of partial melting of Shoo Fly rocks increases from 22 to 38% (Figure 13). Other factors influencing the calculated effects of the Shoo Fly Complex on Sierra Buttes magma include the Nd concentration and ε_{Nd} of the mafic component and the bulk partition coefficient of Nd in the Shoo Fly rocks. Although the model is not unique, it serves to indicate that the Sierra Buttes Member 1 rocks contain a substantial proportion of melt generated from the Shoo Fly Complex.

Evidence of the involvement of the Shoo Fly Complex in the genesis of Sierra Buttes magmas is also presented by Hanson and others (1988) who suggest high level mixing of trondhjemitic and/or granodioritic magmas with partial melts of Shoo Fly rocks in the formation of the Bowman Lake Batholith. The Bowman Lake Batholith was emplaced within the Shoo Fly Complex and is thought to represent a high level magma chamber related to the Sierra Buttes volcanics. It is unknown, however, to what extent the Bowman Lake magma source contributed to the Sierra Buttes volcanics or to what extent melts from the Shoo Fly Complex are incorporated into the Bowman Lake Batholith.

Conclusion and Model for the Origin and Evolution of the Sierra Buttes Magmas Represented by the Stratigraphic Section in the Jamison Lake Area

The isotopic data presented above indicate the influence of an old crustal component in the genesis of the Sierra Buttes magmas and require a separate source for Member 1 than for Members 2, 3, and 4. Combined, isotopic and trace element data suggest that: 1) Member 1 was generated through mixing of mantle-derived compositions with partial melts from the Shoo Fly Complex sediments; 2) the Shoo Fly component progressively diminished through Members 2 and 3, and; 3) Member 4 was produced through fractionation of a composition similar to that of Members 2 and 3.

The tectonic environment during the deposition of the Sierra Buttes magmas is unknown, but an extensional setting best conforms to field observations and chemical data. Evidence for extension at the time of Sierra Buttes volcanism includes the presence of the correlative Havallah Basin to the east, and contemporaneous normal faulting in the northern Sierra terrane. The Havallah Basin has been widely interpreted as an extensional feature formed in an oceanic rift setting (Snyder, 1977; Snyder and Brueckner, 1983; Miller and others, 1984). Biostratigraphic and lithologic data link the Havallah Basin to both the northern Sierra terrane to the west and the Roberts Mountain allochthon to the east (Harwood and Murchey, 1990). Late Devonian to possibly early Mississippian normal faulting in the northern Sierra terrane, adjacent to and north of the Bowman Lake Batholith (Hanson and Schweickert, 1986), indicates extension contemporaneous with that in the Havallah Basin (Harwood and Murchey, 1990).

High eruption temperatures are commonly but not exclusively associated with extensional environments (Ewart, 1979). The lava flows in Member 1, which average about 200 meters (m) thick and extend along strike for at least 4 kilometers (km), suggest particularly fluid behavior and high extrusion rates for these submarine silicic lavas. Hanson (1983, 1991) also noted extremely fluid behavior of quartz porphyry forming intrusive hyaloclastite and pillows in the vicinity of the Sierra Buttes (Figure 1). High alkalinity, volatile content, and temperature are the factors most responsible for lowering viscosity in a silicic magma. There is no chemical evidence of particularly high alkalinity in the Sierra Buttes rocks at Jamison Lake (this text) or in the vicinity of the Sierra Buttes (Hanson, 1983, 1991). High volatile content is not indicated by the quartz porphyries of Members 1 and 4 that show no sign of vesiculation within the study area. Interlayered Members 2 and 3 show abundant vesiculation, indicating that hydrostatic pressure was not so great as to prohibit vesiculation in the more mafic compositions. Further, the presence of phosphatic chert throughout the Sierra Buttes Formation indicates a probable maximum water depth of 2,000 m, which equates to only about 200 bars of pressure (Coles and Varga, 1988). This is probably not enough to significantly reduce viscosity through volatile retention (Hanson, 1983). A high temperature environment seems a likely explanation for the substantial partial melting of sedimentary rock plus the fluid behavior and low phenocryst content of the silicic flows within the study area. The aforementioned relations are consistent with, but not proof of, magma generation in an extensional environment. The following conceptual model for generation of the Sierra Buttes magmas is intended to illustrate one possible interpretation of the data and ideas presented above.

After a period of west-facing subduction, thought to be responsible for creating the Shoo Fly accretionary complex and closing the arc-continent basin (Schweickert and Snyder, 1981; Schweickert and others, 1984), convergence may have slowed and subduction angle steepened, creating extension in the fore-arc similar to the situation in the modern Mariana-Izu system (Crawford and others, 1981). Alternatively, a subduction reversal may have placed the Shoo Fly Complex in a region of back-arc spreading similar to that of North Island, New Zealand, where volcanism is occurring through older accretionary rocks and producing a similar range of compositions (Kamp, 1984; Hamilton, 1988). The former scenario is depicted for simplicity and for lack of evidence for an older remnant arc fragment to the east of the northern Sierra terrane.

Panel A in Figure 14 depicts the tectonic situation just prior to generation of the Sierra Buttes magmas. The pre-Late Devonian arc (not present in the northern Sierra today) approaches the continental margin. A steepening subduction angle, perhaps in response to slowing convergence, causes asthenospheric upwelling and extension in the forearc. Panels B, C, and D are enlargements of the fore-arc area. In Figure 14B, increased temperature from upwelling asthenosphere generates mantle melts that rise and intrude the crust causing partial melting of sedimentary rocks of the accretionary Shoo Fly Complex. The mafic and silicic melts mix, fractionate, and rise through the crust as Member 1. Additional mafic melts are generated and undergo variable degrees of crustal assimilation and/or mixing with the previous melts to produce the relatively mafic Members 2 and 3 (Figure 14C). Finally, subsequent fractionation of a well mixed portion of a composition similar to Members 2 and 3 produces silicic Member 4 (Figure 14D).

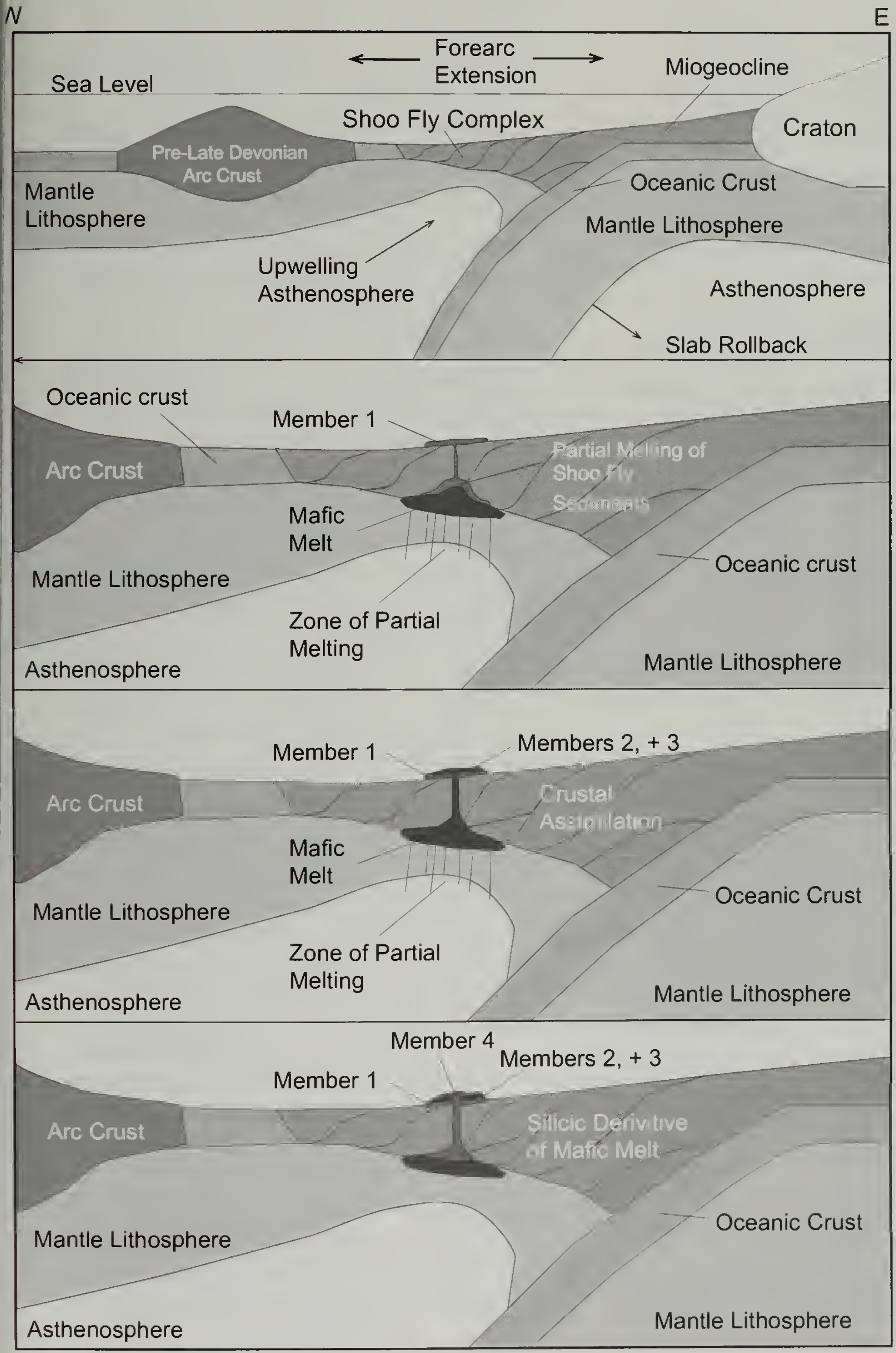

Figure 14. Model of generation and emplacement of the Sierra Buttes Formation in the study area. See text for explanation.

FIELD TRIP

Directions from Highway 89 at Graeagle to the Jamison Lake trailhead

Take County Route 506, which intersects Highway 89 approximately 0.4 miles north of Graeagle, toward Mohawk and Plumas Eureka State Park (Figure 15). Turn left onto the dirt road to Jamison Mine about 4.75 miles up Route 506. The park is less than 0.5 mile from the park entrance. Park in the designated area at the Jamison Mine site.

The field trip is a fairly rigorous 7 1/2 mile hike with about 1 1/2 miles off trail and an altitude gain of 1,300 feet from the parking area to the highest point. It requires a compass, adequate food, clothing, and especially water.

From the parking area to Stop 1

Member 1, at Jamison Lake

From the parking area, hike up the road past the gate and follow the signs toward Jamison Lake, about 3 miles. As you approach Jamison Lake, a trail sign reads *Jamison Lake, Elevation 6,260*. Stop 1, Member 1, is the planar outcrop dipping toward you approximately 50 m S45°W from the sign (Figure 16A).

Figure 16B illustrates the local geology and structure of the Sierra Buttes Formation along the field trip route. Stops 1, 2 and 3 are on the steeply dipping eastern limb of an asymmetric anticline where the first three members of the Sierra Buttes Formation are introduced. The route to Stops 4 through 8 crosses the anticline and an adjacent syncline where Member 4 is introduced and the first three members revisited. The anticline and syncline southwest of Wades Lake were first described by Durrell and Proctor (1948). In addition to the folding and minor faulting, the most obvious structural feature is the pervasive, steeply dipping, north-to-northwest striking foliation. The folding and foliation are both a result of the Late Jurassic Nevadan orogeny (Schweickert and others, 1984).

Within the Jamison Lake area, a continuous section of Member 1 is exposed

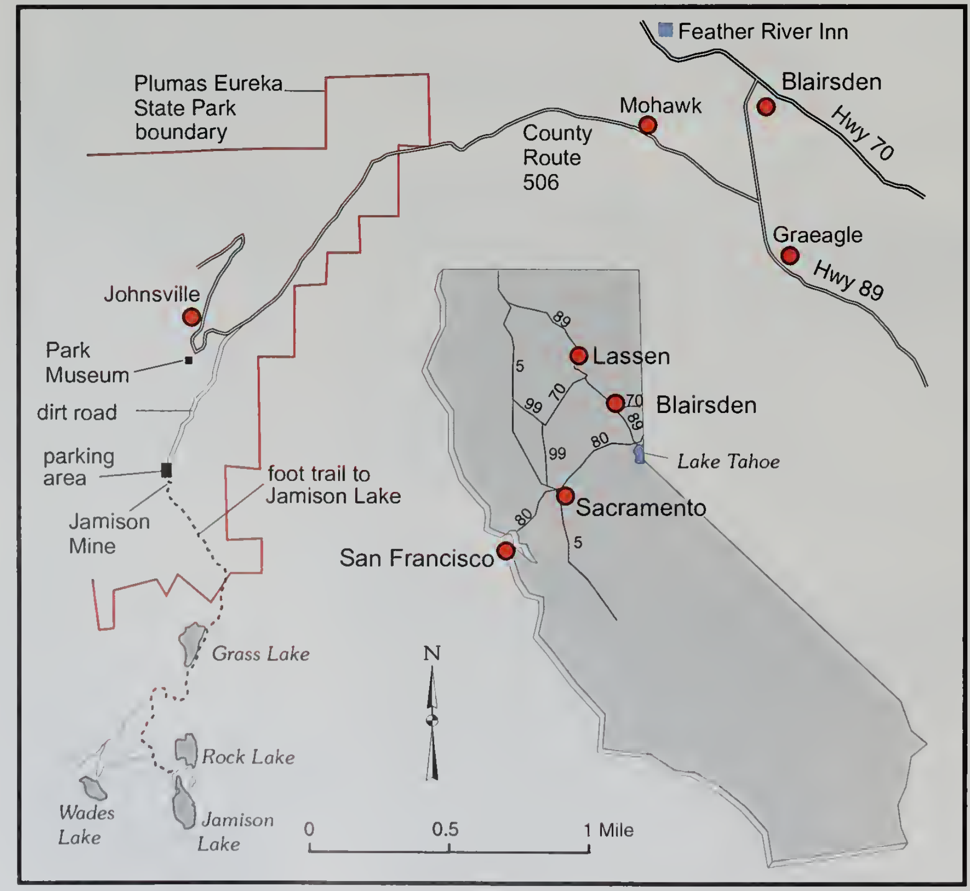

Figure 15. Location map showing route to Jamison Lake from the vicinity of Blairsden and Graeagel. Inset of California shows relationship of major highways to Blairsden.

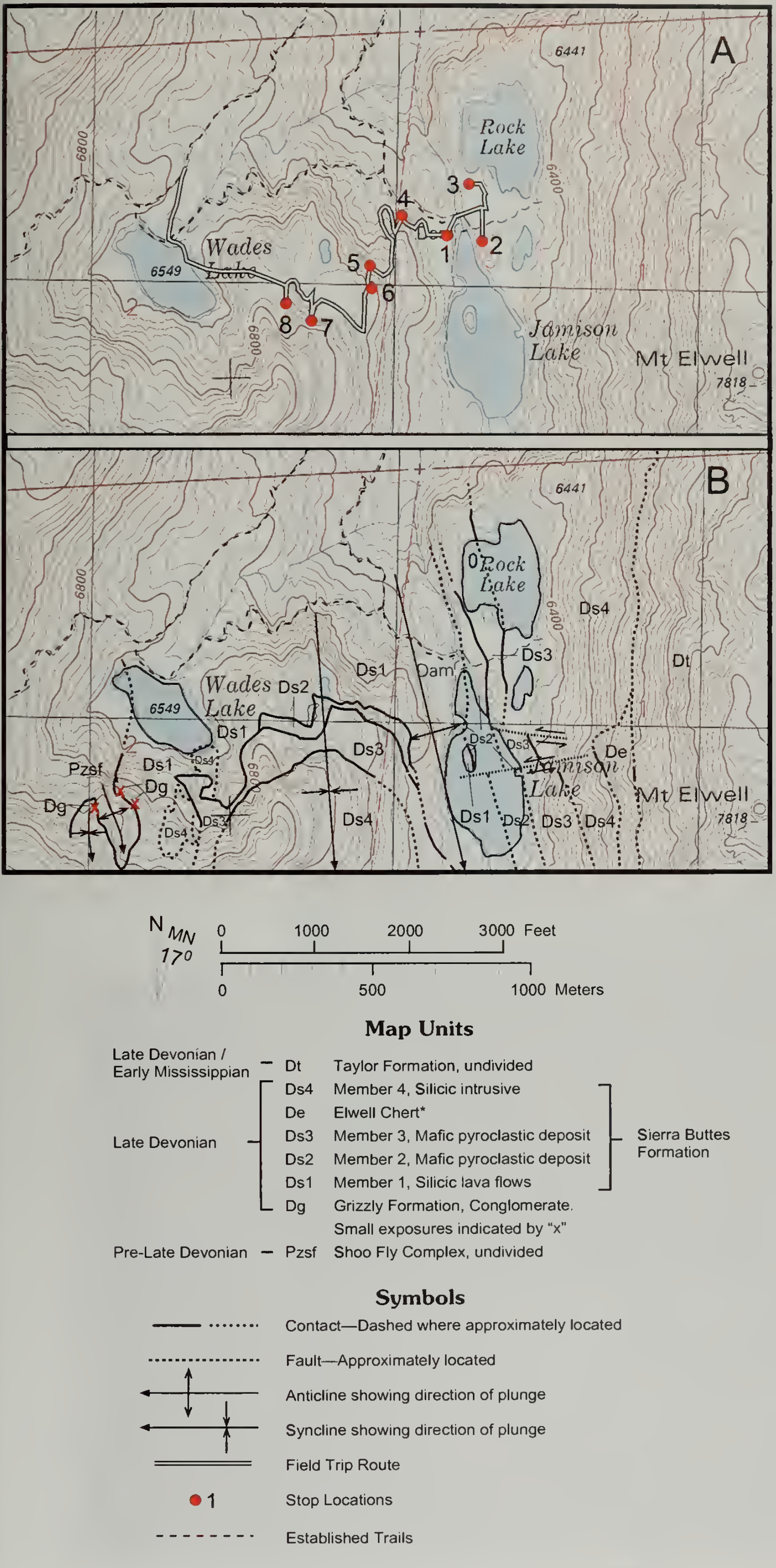
A
B
6441
Rock Lake
Wades Lake
Jamison Lake
Mt Elwell
7818
6549
6800
6400
6800
Dam
1
2
3
4
5
6
7
8
Dt
Ds4
Ds3
Ds2
Ds1
De
Dg
Pzsf
N
MN
17°
0
1000
2000
3000 Feet
0
500
1000 Meters
Map Units
Late Devonian / Early Mississippian
Dt Taylor Formation, undivided
Late Devonian
Ds4 Member 4, Silicic intrusive
De Elwell Chert*
Ds3 Member 3, Mafic pyroclastic deposit
Ds2 Member 2, Mafic pyroclastic deposit
Ds1 Member 1, Silicic lava flows
Sierra Buttes Formation
Dg Grizzly Formation, Conglomerate. Small exposures indicated by "x"
Pre-Late Devonian
Pzsf Shoo Fly Complex, undivided
Symbols
Contact—Dashed where approximately located
Fault—Approximately located
Anticline showing direction of plunge
Syncline showing direction of plunge
Field Trip Route
1
Stop Locations
Established Trails

*The Elwell Formation is included here within the Sierra Buttes Formation (see text).

Figure 16. (A) Topographic map of the Jamison Lake area showing field trip route and stops. (B) Generalized geologic map of the field trip area.

Base from U.S. Geological Survey's Gold Lake 7 1/2 minute Quadrangle.

along the cirque wall south of Wades Lake. It rests with angular unconformity on the Shoo Fly Complex and conformably on the discontinuous Grizzly Formation, which occurs south of Wades Lake as a thin conglomerate derived from the underlying Shoo Fly Complex. Member 1 at this location is approximately 200 m thick. With the exception of volumetrically minor chert, volcanogenic sediments, and mafic dikes, Member 1 is composed of autobrecciated silicic lava flows and subordinate bodies of unbrecciated quartz porphyry.

The exposure at Stop 1 displays some of the principal features that identify Member 1 as an autobrecciated lava flow. The majority of the outcrop consists of clasts that range from a few millimeters (mm) to about 20 centimeters (cm) with occasional large blocks set in an aphanitic matrix (Photo 1). Clasts are well defined on weathered surfaces but difficult to discern on fresh surfaces. Under a hand lens, sparse quartz phenocrysts, averaging about 0.8 mm across, are apparent in both clast and matrix. The Member 1 quartz porphyries are monolithologic, with the exception of rare clasts apparently derived from contemporaneous mafic dikes.

Relict pumice is absent in Member 1, unlike silicic tuffs occurring in the vicinity of the Sierra Buttes, where it is readily identifiable. Flow-banding is apparent in some of the clasts at Stop 1. Large bodies of massive, unbrecciated and locally flow-banded quartz porphyry occur elsewhere (Stop 5).

Locate the large block near the center of the outcrop (dimensions are approximately 6 x 1.3 m, Photo 2). Its long eastern boundary is sharp and distinct from the surrounding breccia. In contrast, its southern tip consists of several small lobes that are partially fragmented and nearly separated from the main block. Note also the small area of fragmentation within the block approximately 1.2 m from the block's southern tip. The large size of the block, the delicate lobate structure and patchy disaggregation evoke a raft or flow-lobe deforming and brecciating in a semi-ductile state within the flow and contributing fragmental material. Two beautifully flow-banded blocks, about 12 m to the north of the large block, display some of the same features as described above (Photo 3). Flow-banding in the blocks and smaller clasts suggests that both originated as part of a coherent flow prior to brecciation. Taken in total, the flow-banding, lack of pumice, monolithology, and the evidence of hot, but non-violent transport indicates that the exposure at Stop 1 represents a silicic lava flow that was in the process of brecciation. Stops 4 and 5 better illustrate earlier stages in the process of brecciation.

Descriptions of silicic submarine lava flows are rare in the literature, but one well-exposed Archean occurrence in Rouyn-Noranda, Quebec is described by De Rosen-Spence and others (1980); it may serve as a model for autobreccias in the Jamison Lake area. At the Rouyn-Noranda site, extensive Archean silicic submarine flows form domes and tabular bodies up to 10 km long. Most are mappable for 2 to 4 km. Thickness ranges from 30 to 400 m, averaging about 200 m. The principal brecciation mechanism envisioned for the bulk of silicic submarine

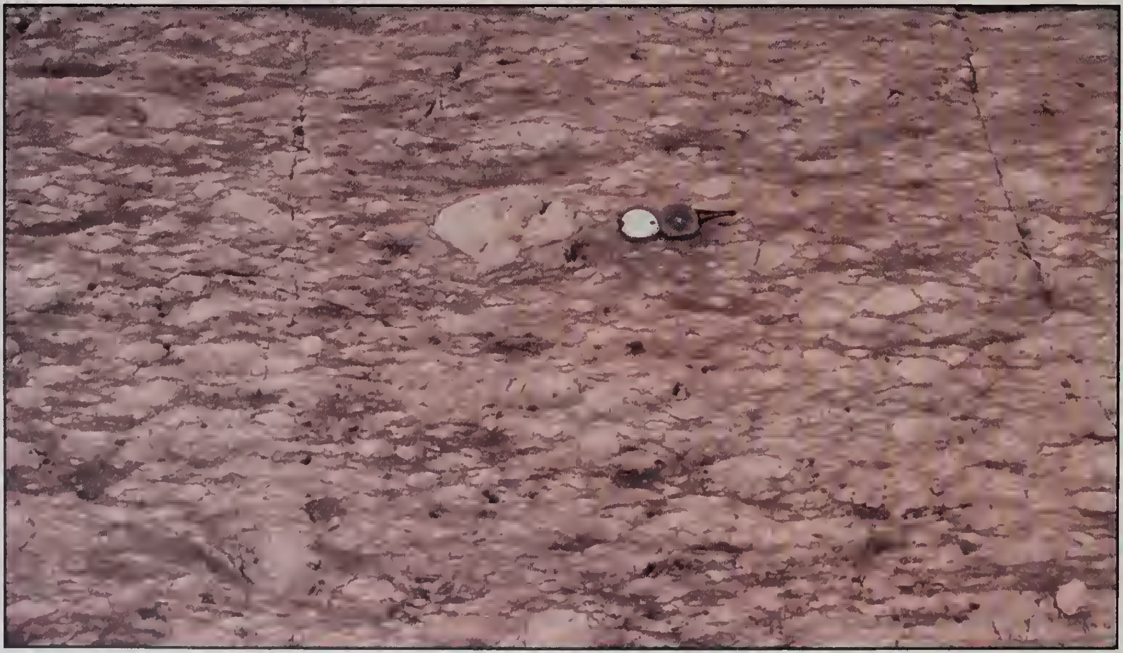

Photo 1. Member 1 silicic autobreccia at Stop 1. *Photo by Steven Silva.*

autobreccias is described in terms of thermally-induced stress, in situ fragmentation, and subsequent granulation. The flow front advances in the form of variably-sized lava lobes. The smaller lava lobes cool rapidly and fragment completely as the result of thermal stress (differential contraction caused by high thermal gradients). Hot fragments then cascade down the flow front, granulating as they go. This process of granulation leaves the larger fragments somewhat rounded. Facies changes from proximal to medial to distal, are defined generally in terms of the relative proportions of massive lava and breccia. The proximal facies is dominated by massive lava with a veneer of flow-breccia (autobreccia) at the top. In the medial facies, massive lava occurs in variably-shaped and -sized lobes with flow breccias occurring at the top and base. The distal facies is similar to the medial facies except that flow-breccia is more abundant, completely enveloping the lobes. Planar-to-cross-bedded epiclastic deposits, some of which are turbiditic, overlie the breccias and increase in abundance toward the distal facies.

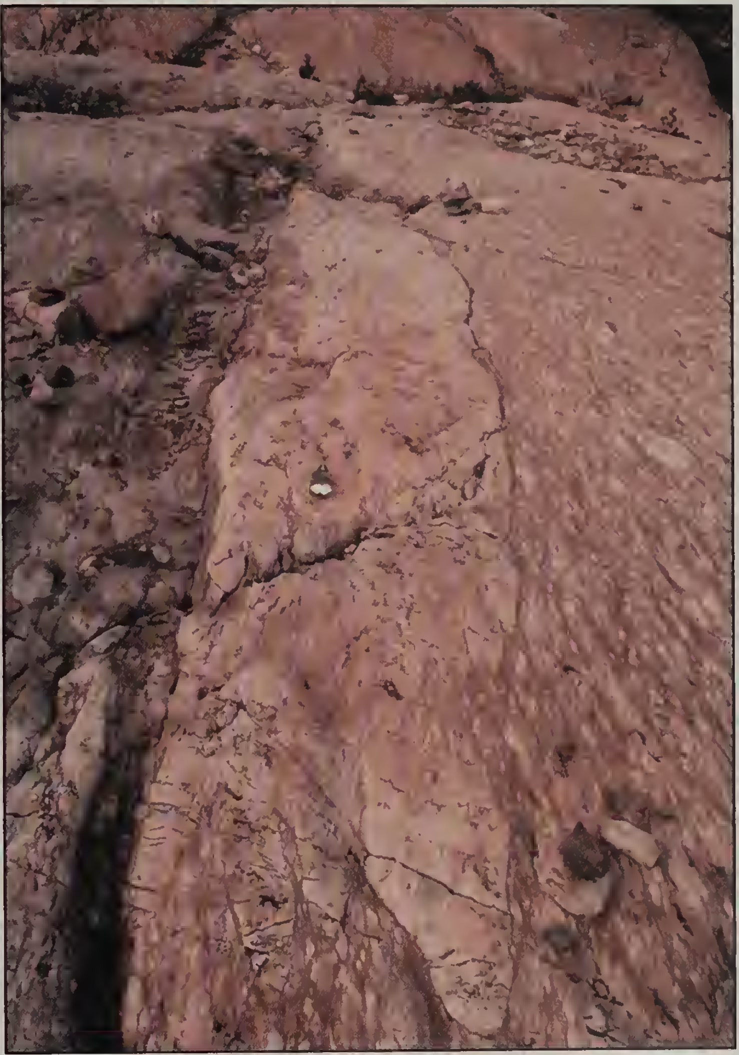

Photo 2. Large block within Member 1 autobreccia at Stop 1 (view to the north). Note sharp contact along the eastern margin; the western margin is bounded by a mafic dike. *Photo by Steven Silva.*

Individual flows and lobes have not been mapped in detail at Jamison Lake. However, the predominance of autobreccia over structureless lava and the rare occurrence of bedded and graded epiclastic deposits best conforms to a medial facies. In the examples presented by De Rosen-Spence and others, a location such as this occurs about 2 to 5 km from the source vent.

An additional feature to note before leaving this site is the mafic dike immediately to the west of the large block. The dike ends abruptly about 4 m to the north of the block, apparently truncated in the flow. The mafic dike is one of many that appears to have been disrupted by the Member 1 flows, indicating intrusion before the end of Member 1 deposition. There is similar evidence of the presence of mafic magma occurring contemporaneously with all

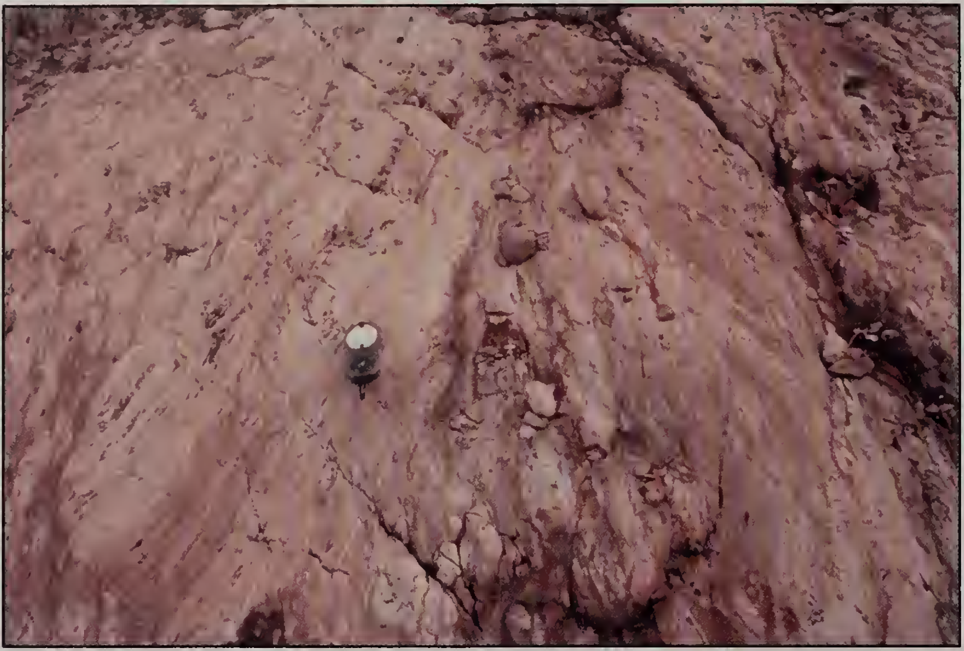

Photo 3. Flow-banded blocks within Member 1 autobreccia at Stop 1. *Photo by Steven Silva.*

of the silicic magmatism in the Jamison Lake area.

Thin-section petrography—Member 1

Quartz, plagioclase and magnetite occur as phenocrysts and are the only primary minerals observed in the Member 1 samples. The groundmass consists predominantly of a mosaic of microcrystalline quartz and albite(?), and volumetrically minor sericite, calcite, epidote, chlorite and sphene- leucoxene. Grain boundaries in the groundmass are typically not polygonal but generally are irregular and somewhat indistinct, typical of metamorphic recrystallization.

Quartz phenocrysts comprise from <0.1 to 2.4% of the rock, averaging 1.2%. Sizes range from 0.4 to 1.4 mm, averaging 0.8 mm. They are euhedral to anhedral, often rounded and highly embayed. Euhedral grains show rhombic and hexagonal outlines typical of β quartz. Quartz phenocrysts generally exhibit only slight strain (undulatory extinction); individuals rarely are recrystallized to aggregates and show little sign of distortion except within the most strongly foliated rocks.

Plagioclase phenocrysts vary in abundance from 0 to 4.1%, averaging 1.4%, and vary in size between 0.7 and 2.3 mm, averaging 1.1 mm. The majority are euhedral, typically with rectangular outlines; others are subhedral or anhedral and occasionally occur as glomerophenocrysts. Polysynthetic twinning is common, allowing determination of composition (Michel-Levy method) which is < An5. Albite is joined in the replacement of original plagioclase to a lesser degree by a variable combination of calcite, sericite, chlorite and rarely epidote. The degree of replacement by the latter minerals roughly corresponds to the intensity of foliation.

Magnetite occupies approximately 0.1% of the rock. It occurs as euhedral to anhedral grains that range in size from 0.05 to 0.3 mm. Yellow to red oxide staining often surrounds magnetite grains and follows fractures and foliation.

Several original fabric features are preserved by patterns of secondary minerals in thin sections. Due to the monolithology and pervasive recrystallization of the autobreccias, clast boundaries are difficult to see in thin section but may be revealed by concentrations of secondary minerals, chiefly sericite and to a lesser extent calcite. Perlitic cracks, now occupied by sericite, are revealed by a contrast in relief in plane polarized light. Relict spherulites, composed of radiating aggregates of albite(?), occur in several samples. These features are indicative of the original glassy nature of these rocks.

Stop 2.

Member 2

From Stop 1, walk back down the trail to the sign reading *Rock Lake 1/4 mi, Jamison Lake 50 yds* and take the trail toward Rock Lake. Cross Jamison Creek and continue up the trail about 75 m until you are adjacent to a small shallow pond (probably dry) on your right. Walk through the pond (about S30°E) and exit through the gap at the southwest corner. Walk about 40 m due south toward the tall dead tree. From the dead tree, locate the outcrop about 10 m directly ahead (a 6-inch wide dike runs diagonally through it) (Photo 4, inset). This is Stop 2, Member 2.

Member 2 is discontinuous within the Jamison Lake area and quite variable both vertically and laterally. It contains a very distinctive basal section (exposed here), characterized by the relatively mafic nature of the primary components, lapilli- to block- sized vesicular clasts (many with a spongy-looking texture), occasional clasts of quartz porphyry (apparently derived from Member 1), and fragments of chert in a black, chert-rich matrix (Photo 4). Occasional fragments of mafic pillow lava also occur in Member 2 at other locations. The heterolithology and abundance of chert comprising the matrix suggest an epiclastic deposit; however, the distinctive basal portion only comprises about 15 of the 50 m thickness of Member 2. It seems likely that the basal portion represents disruption and mixing of a pyroclastic flow with the cherty substrate over which it traveled, rather than a separate epiclastic deposit. A continuous section of Member 2 is exposed along the route between Stops 5 and 6 and is described later.

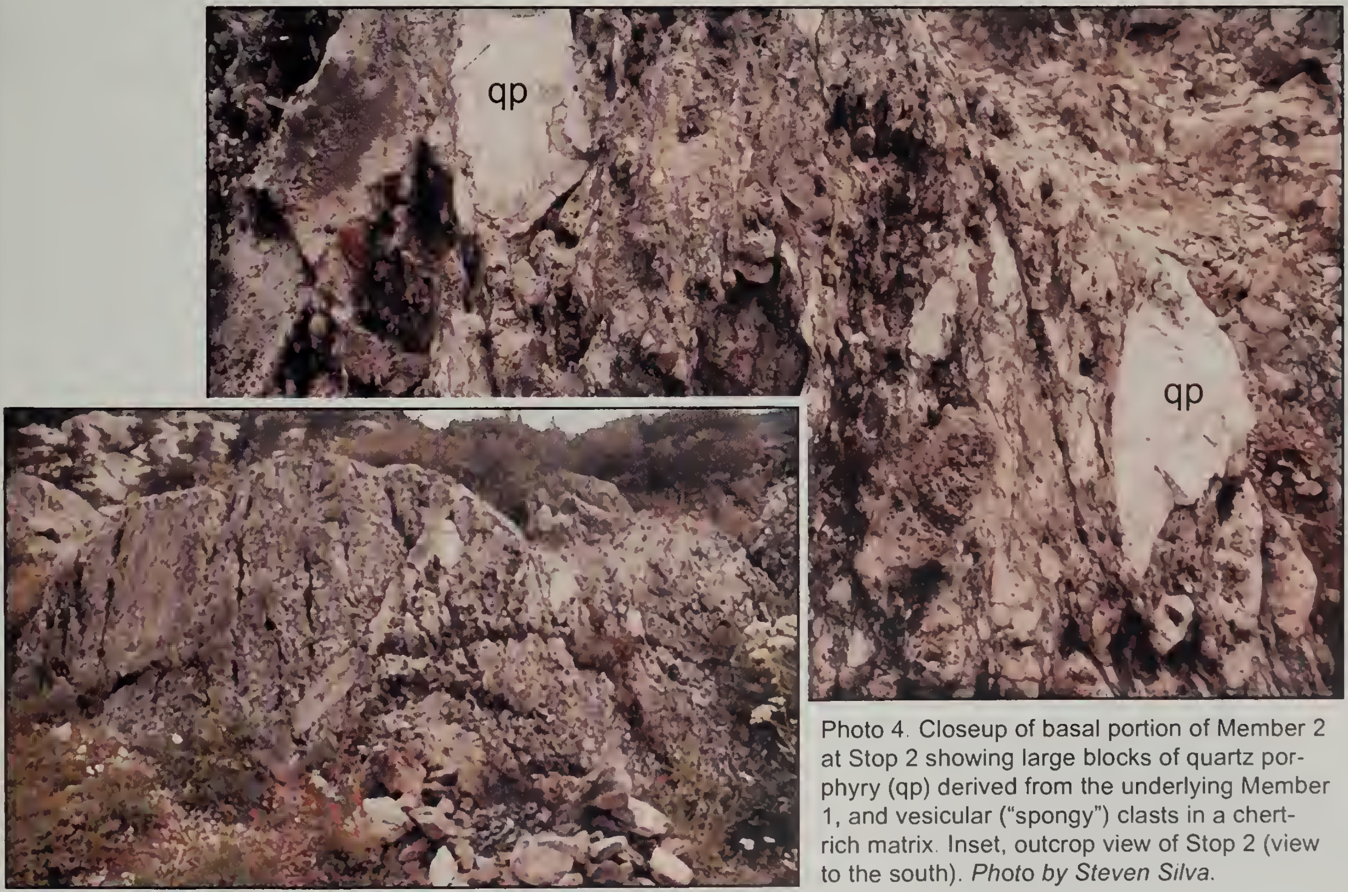

Photo 4. Closeup of basal portion of Member 2 at Stop 2 showing large blocks of quartz porphyry (qp) derived from the underlying Member 1, and vesicular ("spongy") clasts in a chert-rich matrix. Inset, outcrop view of Stop 2 (view to the south). *Photo by Steven Silva.*

Thin Section Petrography—Member 2

Volcanic components within Member 2 have in common an absence of any recognizable original ferromagnesian phases and a groundmass containing abundant plagioclase microlites. The material interstitial to the microlites is composed of varying proportions of chlorite and quartz, with minor, irregularly distributed patches of calcite. Quartz, calcite, chlorite, and, to a lesser extent, epidote occur as vesicle and fracture fillings. Assuming that the interstitial material was originally glassy, the original distribution of the microlites within the various clasts may be described as intersertal to hyalophitic, or trachytic where aligned. Pillow fragments are distinct from the other mafic fragments in possessing sparse quartz and plagioclase phenocrysts or perhaps xenocrysts.

Stop 3.

Member 3

Return where you left the trail to Rock Lake and continue up the trail toward Rock Lake another 10 to 15 m, then take the narrow path you see heading north. At the large pine tree about 50 m up the path, the trail jogs right for 10 or 12 m then left again to Rock Lake. At the lake, locate the pine tree with the deformed trunk growing at the southwest corner of the lake. Stop 3 is the exposure about 15 m S12°W from the base of the tree (Figure 16A). The contact between Members 2 and 3, exposed just west of the outcrop, is fairly sharp and nearly vertical.

Member 3 is continuously exposed in the northern half of the Jamison Lake area and intermittently exposed farther south, having been extensively intruded there by Member 4. Its maximum exposed thickness south of Rock Lake and east of Wades Lake is approximately 95 m. Based on its stratigraphic position and lithologic characteristics, it is most likely the northward extension of the Tamarack tuff, which has been mapped and described for approximately 11 km along the strike from Young America Lake northward to Long Lake (Brooks and Legler, 1989; Legler and others, 1991). The Tamarack tuff has a distinctive appearance on weathered surfaces, characterized by light-colored, highly vesicular to pumiceous blocks and coarse lapilli in a matrix of dark-colored, finer lapilli and ash. The blocks often occur in contorted, delicately shaped forms. In the Jamison Lake area, the "pumiceous" blocks in Member 3 are quite variable in size, shape, and abundance in no obvious pattern either laterally or vertically, and are generally less vesicular than those described in the Tamarack tuff to the south. The matrix composition is relatively consistent throughout the area.

The Member 3 exposed at Stop 3 is most similar to the Tamarack tuff. The clasts are generally equant to ovoid and comprise 10 to 15% of the rock volume (Photo 5). However, note the occasional clasts containing delicate embayments and peninsulas. The lighter colored lapilli are also highly vesicular to pumiceous. The vesicles are mostly microscopic and undetectable in hand sample. The matrix consists of reddish-brown, closely packed, angular lapilli and ash (Photo 6). In contrast to Member 3 at Stop 3, an exposure about 150 m to the southeast, near the top of the unit exhibits highly irregular to amoeboidal pumice blocks comprising approximately 25% of the outcrop.

The presence of pumice blocks set in a matrix of ash and lapilli characterizes the deposit as pyroclastic; however, the retention of the contorted and delicate shapes of the pumice blocks over a large lateral extent argues against the violence of eruption usually associated with subaerial pyroclastics. Member 3 is further described at

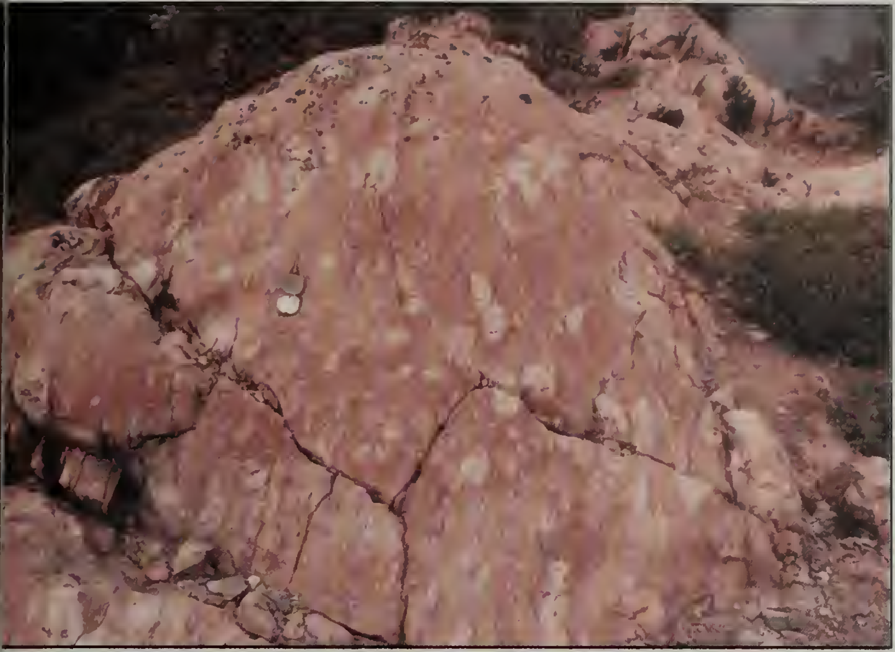

Photo 5. Outcrop view of Member 3 pyroclastic deposit showing light-colored pumiceous clasts (view to the north). *Photo by Steven Silva.*

Stop 8, where it exhibits a much lower-energy style of deposition.

Thin section petrography—Member 3

In general, Member 3 is composed of plastically deformed, highly vesicular to pumiceous clasts in a matrix consisting predominantly of finer angular fragments. Both components contain abundant plagioclase microlites and sparse phenocrysts of plagioclase and quartz. They are moderately to highly altered to a combination of albite, epidote-clinozoisite, quartz, calcite, chlorite, sericite, leucoxene, and opaque oxides(?). Quartz and plagioclase phenocrysts, and plagioclase and magnetite(?) microlites are the only recognizable primary minerals. Clasts differ from angular matrix fragments in being much more vesicular, having a lower concentration of microlites, and possessing a higher percentage of secondary minerals. The percentage of vesicles in the clasts varies from approximately 10-60%, averaging 25-30%. Vesicle size ranges from approximately 0.01 mm to 1 cm, averaging between 0.1 and 1 mm. Vesicles vary in shape from round to highly elliptical. Vesicles are much less common in the matrix fragments, averaging perhaps a few percent, and are filled with quartz, calcite, epidote- clinozoisite, and chlorite. Preferred fillings vary from area to area, with quartz, calcite or chlorite being dominant.

Relict plagioclase microlites throughout Member 3 range in length from 0.05 to 0.2 mm and commonly show a swallow-tail quench morphology. Within the matrix

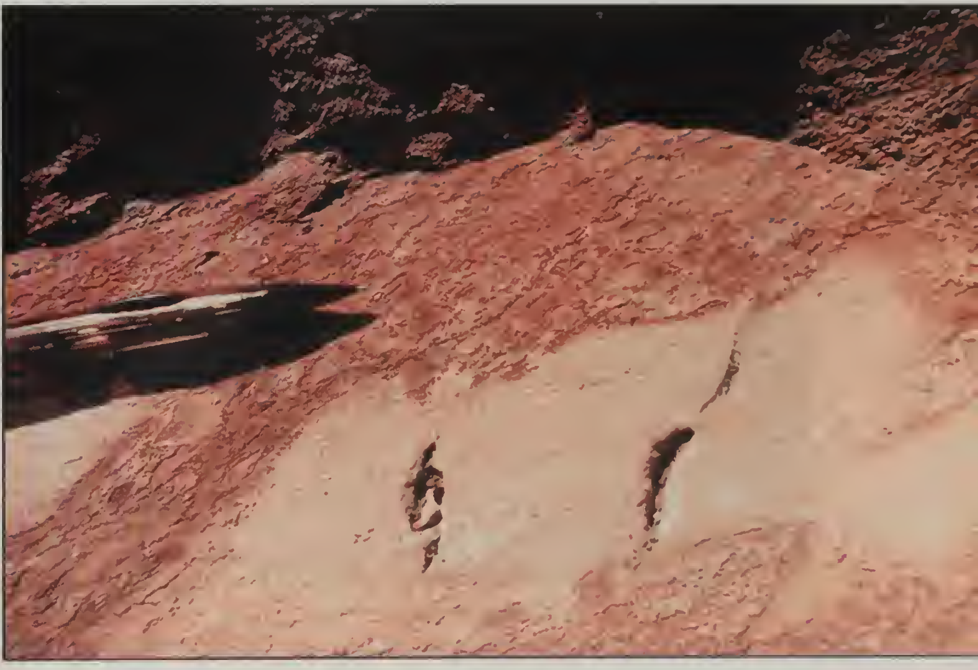

Photo 6. Closeup of Member 3 pumiceous clast and angular matrix material (Stop 3). *Photo by Steven Silva.*

fragments, the microlites are surrounded both by colorless, apparently optically isotropic material (chlorite?) and by an extremely fine- to fine-grained mosaic of quartz. Microlites within the clasts are often masked by patchy or spotty leucoxene (white in reflected light, dark brown and nearly opaque in transmitted light) and by epidote-clinozoisite.

Stop 4.

Member 1

Return to Stop 1. Starting from the large block (described at Stop 1) head about S75°W to near the bottom of the cliffy outcrops (you cross a small foot trail on the way). Walk parallel to the base of the cliffy outcrops toward the north about 40 m until you are adjacent to the north edge of the nearest cliffy outcrop. From here head west, skirting around the north end of the outcrop and across the southeast dipping (~15^0) planar exposure about 40 m ahead (Photo 7). As you cross the planar exposure, notice its general lack of primary structure except for flow-banding. This is typical of the unbrecciated quartz porphyry of Member 1. At the west edge of the planar outcrop is a small north-trending ravine. Stop 4 is the outcrop in the ravine about 25-30 m down to the north (Photo 8).

Stop 4 consists of autobrecciated Member 1 quartz porphyry. Unlike Stop 1, the majority of the exposure consists of large blocks, averaging 30 to 40 cm across, which are set in a sparse matrix of ash- to lapilli-sized fragments (Photo 9). You can easily imagine that the blocks were in the process of separation in the manner of puzzle fragments and then rafted away in the matrix material. The sparsity of the matrix material and the angularity of the

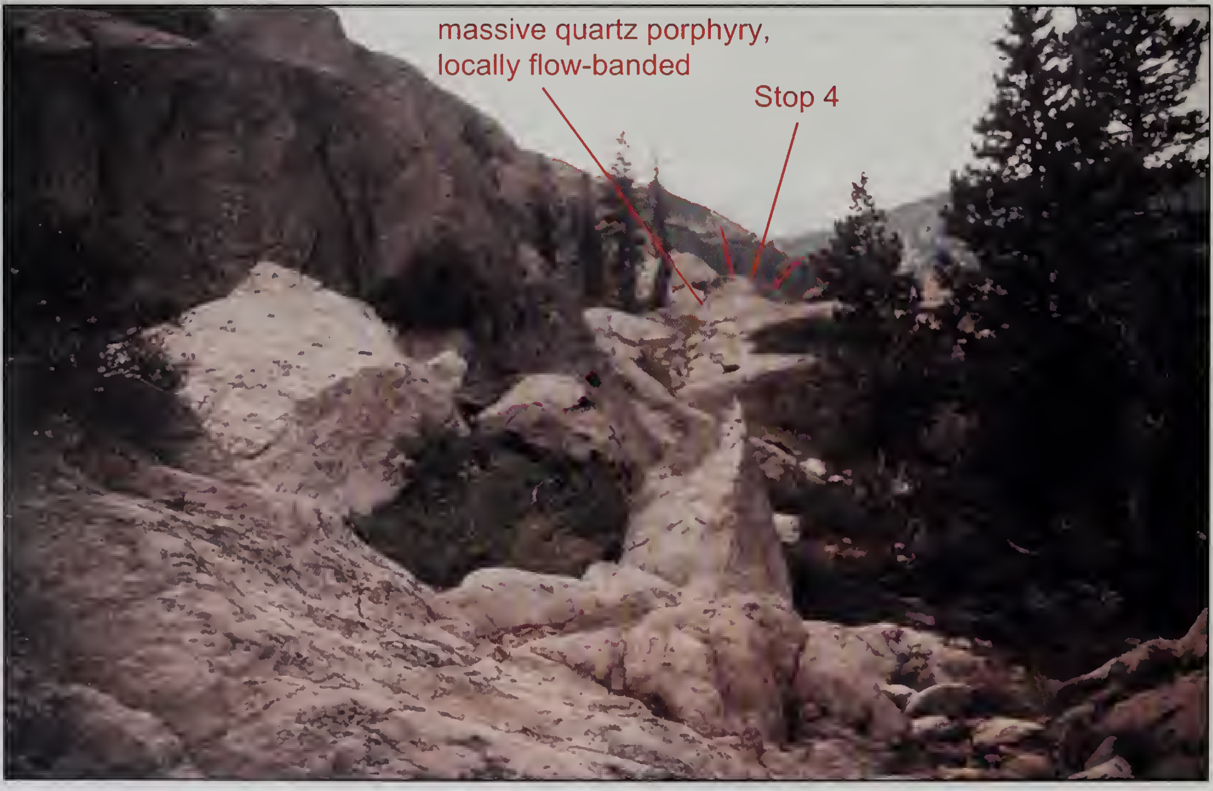

Photo 7. Orientation photo looking west toward Stop 4. Planar exposure, referred to in text, is labeled “massive quartz porphyry, locally flow-banded.” *Photo by Steven Silva.*

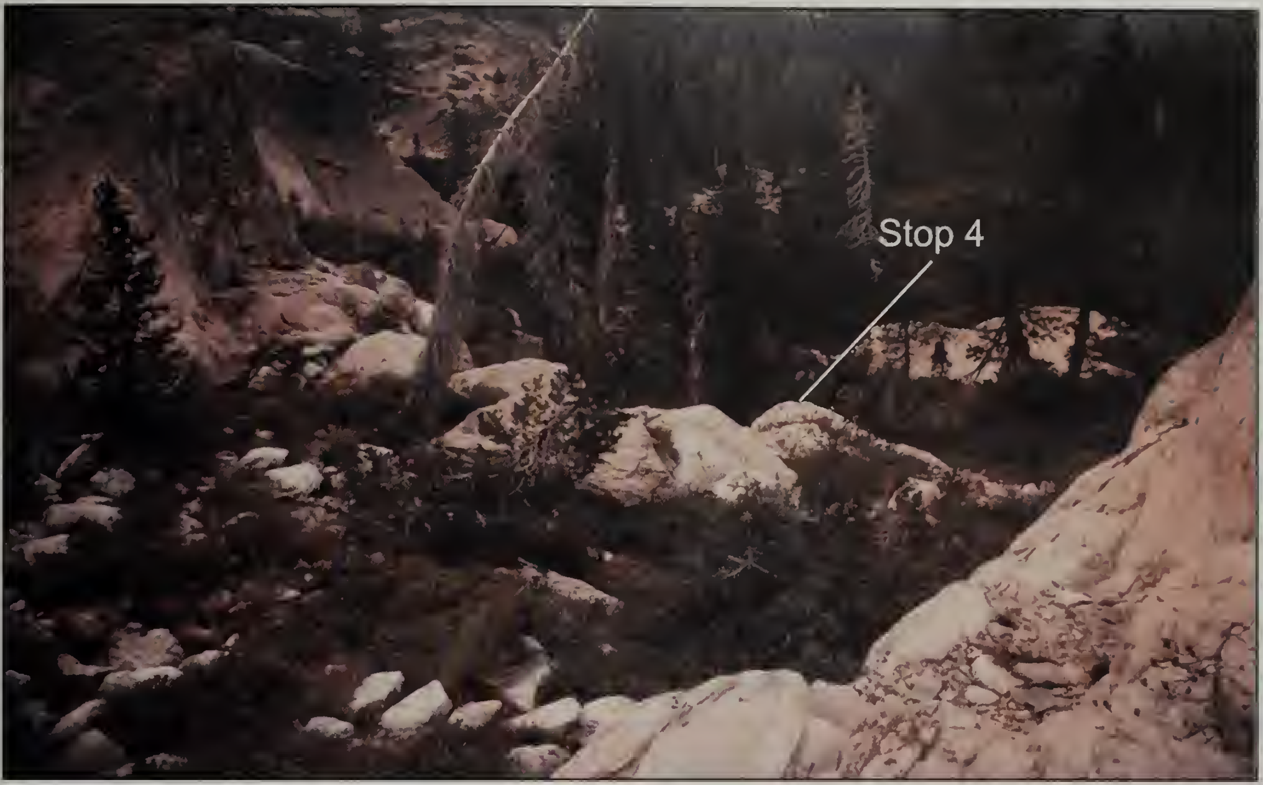

Photo 8. Orientation photo looking north and downhill at Stop 4 from western edge of planar exposure (see text). *Photo by Steven Silva.*

blocks suggest an earlier phase in the brecciation process and a more brittle mode of fragmentation than at Stop 1.

Stop 5.

Member 1

Continue walking to the west, skirting around the northern tip of the large cliffy outcrop that projects farthest to the north of any visible from the vantage of Stop 4. Just past the tip of this outcrop, turn south (steep uphill) and walk to the saddle, keeping the outcrop to your left and the tree line to your right. At the saddle, walk to the one conspicuously large pine tree. From the tree, walk due west about 15 m and look west at the exposure about 35 to 40 m immediately in front of you. Note, as you view the outcrop from north to south, the abrupt color change from very pale red to a medium gray. This is the contact between Member 1 to the north and Member 2 to the south (Photo 10). Stop 5 is in Member 1 on the planar portion of outcrop near its northern end just above the wide, north-trending mafic dike. Walk down to Stop 5 by the easiest route.

Locate the area of well-defined flow-banding near the center of the planar exposure. Note the contorted banding and the few isolated blocks with flow-bands slightly askew of the local pattern within the otherwise unbrecciated mass suggesting incipient transition from ductile to brittle behavior (Photo 11).

Flow-banding and brecciation may be related through a process where conductive heat loss creates zones of differing viscosities (Curtis, 1954). The cooler, more viscous zones, are slower in adjusting to movement than the adjacent less viscous zones causing a laminar flow. An incipient separation

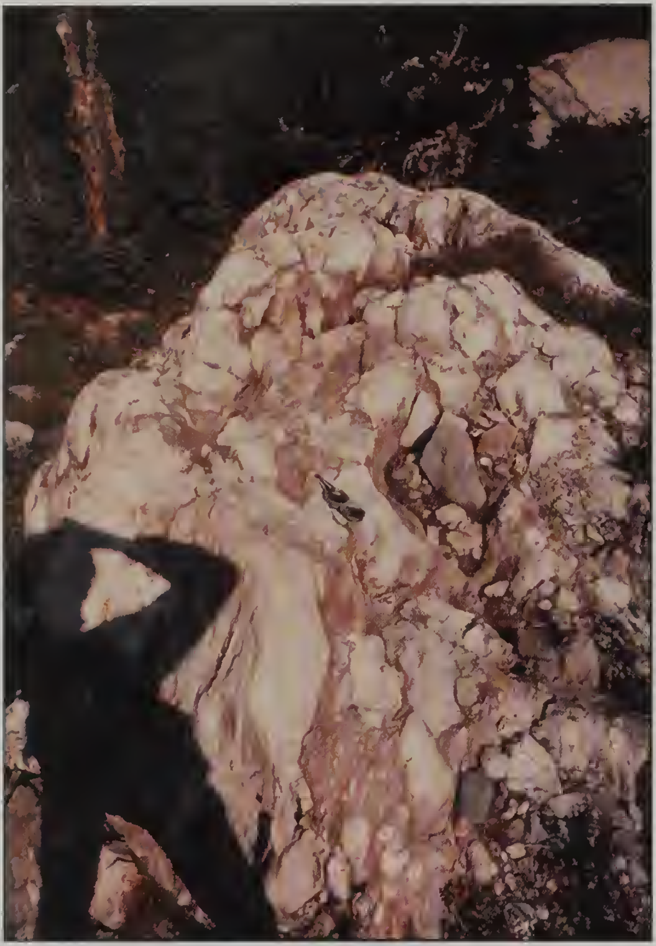

Photo 9. Member 1 autobreccia at Stop 4 showing large blocks separated by relatively thin zones and pockets of finer fragmental material. *Photo by Steven Silva.*

may occur along the planes of laminar flow, leading to a rapid drop in pressure and escape of volatiles, however minor, which create flow-banding and eventually initiate brecciation.

Stops 1, 4 and 5 exhibit different stages and/or styles of brecciation, but their positions relative to the source vent(s), as well as the geometry of flow lobes and breccia zones, is unknown. Interpretation of the flow morphology is complicated by a host of factors related to the style and extent of brecciation of a silicic submarine lava flow, including temperature, composition, extrusion rate and volume, topography, and proximity to the vent. Further study of the excellent exposures of Member 1 in this area offers an opportunity to decipher this interesting but little described phenomenon.

Stop 6.

Contact between Members 2 and 3

Stop 6 is at the top of Member 2. A complete section of Member 2 is exposed between Stops 5 and 6 and will be described on the way up. Begin walking up the steep ravine along the west side of the outcrop to the Member 1/Member 2 contact. Here a mafic dike obscures the contact relationship. Climbing on the outcrop above the dike is dangerous and not recommended. Continuing up the ravine from this point, the next 7.5 m are virtually identical to the exposure at Stop 2, consisting about 40% of the highly vesicular (spongy-looking), dark gray lapilli- to block-sized clasts, and a few percent each of quartz porphyry and chert clasts. Pillow fragments, recognized by their dark rims and radially-arranged amygdules, occur rarely. The matrix consists of an intimate mixture of fine-grained chert and ash- to lapilli-sized, dark gray volcanic material. The next 6 m consist of a coherent, ~2 m thick chert bed that has been folded nearly isoclinally (Photo 12). The next 20 m are composed of a gray, aphanitic, sparsely vesicular sill, partially brecciated and forming highly irregular contacts with the adjacent rocks above and below. The highly irregular contacts suggest penecontemporaneous intrusion. The next 12.5 m are composed 40% of highly vesicular clasts averaging 3 to 4 cm, most of which are lenticular to rounded. Angular red fragments (relict glass?) averaging 3 mm to 3 cm across, constitute another 30%. Blocks of quartz porphyry and chert are present, but in much lower abundance than in the basal portion of the section; they become

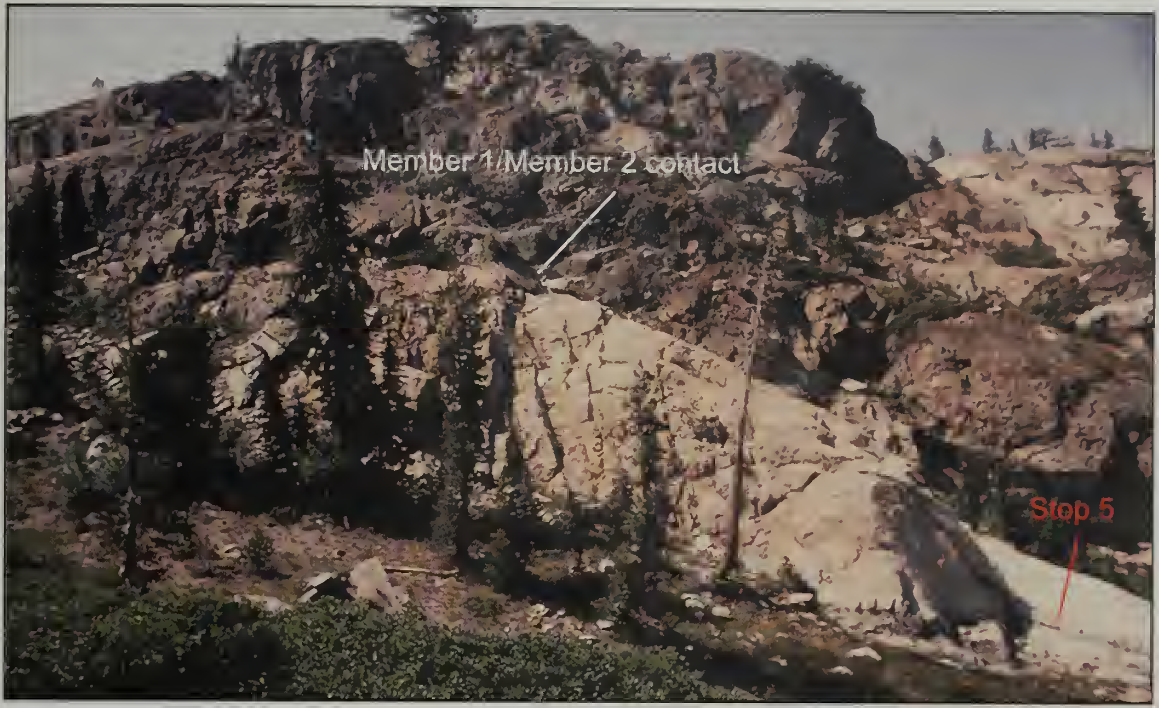

Photo 10. View to west showing contact between Members 2 and 3, and location of Stop 5. *Photo by Steven Silva.*

increasingly rare upsection. The remaining 30% is matrix consisting of red-weathered ash.

When you are about 20 m from the apparent top of the cut, you see a short pine tree. Walk up (to your left) on the outcrop at this point (Stop 6). This is the contact between Members 2 and 3. The top of Member 2 consists of a meter-thick bedded unit composed of ash- to lapilli-sized angular fragments that is capped by a 15-40 cm thick unit of coarser sediment (Photo 13). The bedded unit is composed predominantly if not entirely of the immediately underlying material of Member 2, consisting of about 50% vesicular clasts, 10% red angular fragments (glass?), and occasional clasts of quartz porphyry and chert, set in a fine-grained red-weathered matrix. At the top of the coarse layer is a disrupted and discontinuous band of gray phosphatic material (Photo 14). Phosphate commonly occurs as bands and nodules in chert within the northern Sierra terrane (Brooks and others, 1982) and is thought to have been derived from sea water. The contact with Member 3 occurs approximately 1 m above. The exact nature of the intervening material is not certain, although it appears to be pyroclastic at least in part and is most similar to the pyroclastic portion of Member 2. In all, the evidence suggests that Member 2 originated as an erosive pyroclastic flow that incorporated the underlying chert and quartz porphyry from Member 1.

On the west side of the ravine, Member 3 can be seen resting directly on the sediments of Member 2. Note here the irregularly-shaped, often elongate and delicate forms of the large light-colored blocks (pumice?) in Member 3. It is difficult to imagine that those forms could have been preserved as they traveled any great distance or by any violent transport mechanism.

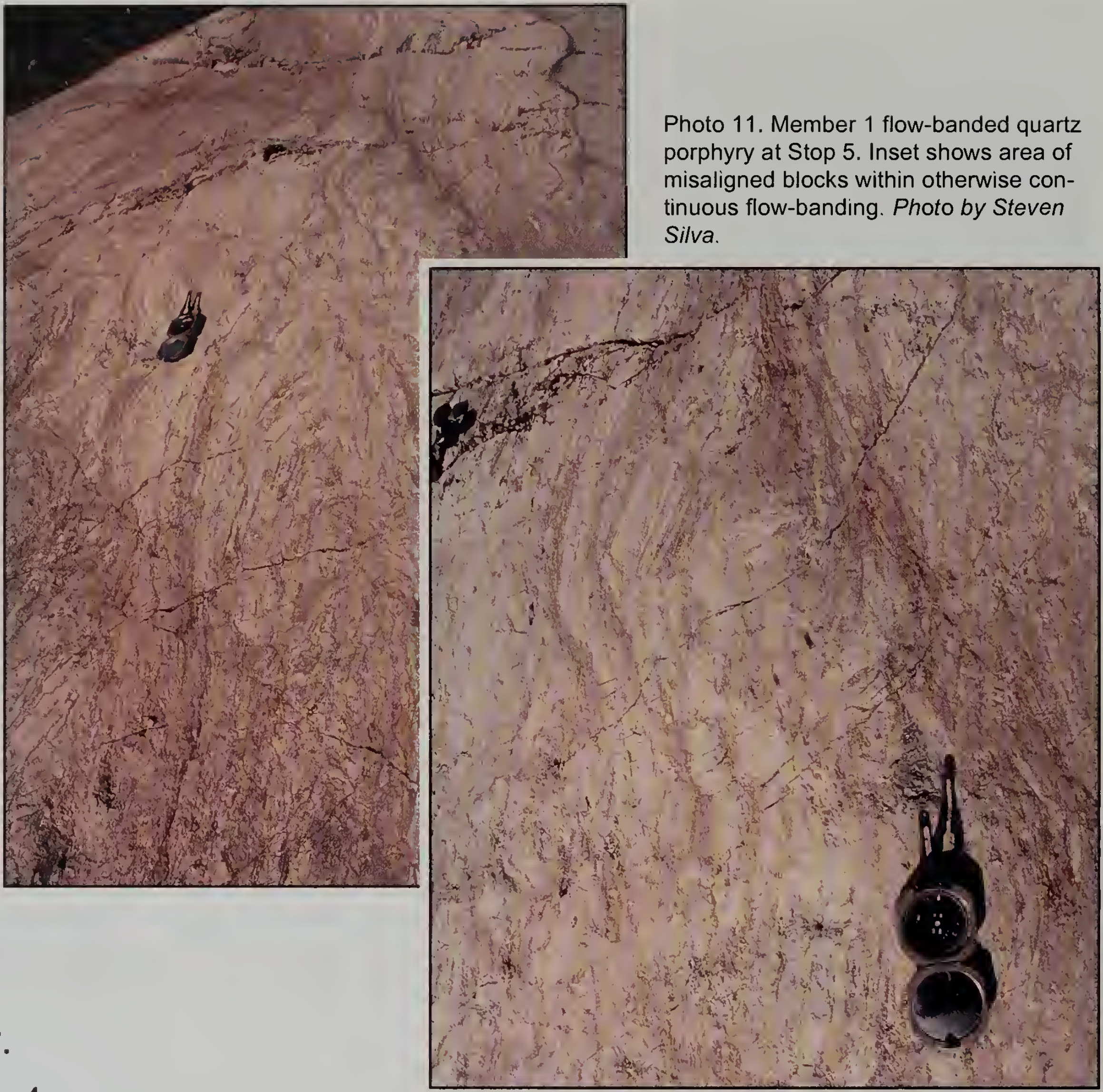

Photo 11. Member 1 flow-banded quartz porphyry at Stop 5. Inset shows area of misaligned blocks within otherwise continuous flow-banding. *Photo by Steven Silva.*

Stop 7.

Member 4

Walk up the ravine through about 10 m of low brush (ankle- to knee-deep at most). Continue walking straight, and when you are adjacent to a large pine on your left, take the path of least resistance (approximately S10°W) for another 100 m down to the shallow eastwest trending ravine. Just before reaching the small stand of trees, you will see a narrow path. Take this path west (uphill) through the saddle and toward the small pond indicated on the map (Figure 16A). Just southeast of the pond indicated on the map is a smaller pond that is probably dry. When you are adjacent to the smaller pond, head S25°E to the base of the cliffs, which is Stop 7 (Figure 16A).

Member 4 quartz porphyry consists of a number of sill-like intrusives that occur in the Jamison Lake area continuously and in greatest volume between Member 3 and the base of the Taylor Formation and to a lesser extent intruding the lower Members of the Sierra Buttes Formation. In the northern part of the Jamison Lake area, Member 4 intrudes in a sill-like fashion above Member 3 and extensively displaces Member 3 southward. Member 4 also intrudes the Elwell Formation of Durrell and D'Allura (1977) to the west of Long Lake and along the western flank of Mt. Elwell. The Elwell Formation is thus considered here to lie within the Sierra Buttes Formation. The validity of the formational status of the Elwell Formation has been questioned in earlier publications (Brooks and others, 1982; Hanson, 1983; Harwood, 1983; Hanson and Schweickert, 1986).

Stop 7 lies at the contact between Members 3 and 4. Small exposures of the sharp but irregular contact can be found toward the northwest. Member 4 is very similar in outcrop appearance to non-brecciated portions of Member 1 but is distinguished from Member 1 by its relatively large and abundant quartz phenocrysts and lack of flow-banding and brecciation. The base of Member 4 in many locations can be recognized at a distance by the presence of columnar joints as here, although Stop 7 displays the best columnar structure in the area (Photo 15). Look along the base of the cliffs and particularly up at the overhanging exposures to see the true size and shape of the cells (Photo 16). Note the columnar structure in the talus blocks, as they display various sections across the columns as may be encountered elsewhere in the field.

Thin section petrography—Member 4

As with the Member 1 quartz porphyries, the only recognizable relict primary phases are quartz, plagioclase and magnetite. The groundmass is composed of microgranular quartz and albite(?). Other secondary minerals are albite, calcite, sericite, chlorite, epidote-clinozoisite, and sphene- leucoxene. The secondary minerals occur throughout the groundmass and as replacements of plagioclase. Unlike Member 1, no perlitic cracks or spherulites were observed in Member 4.

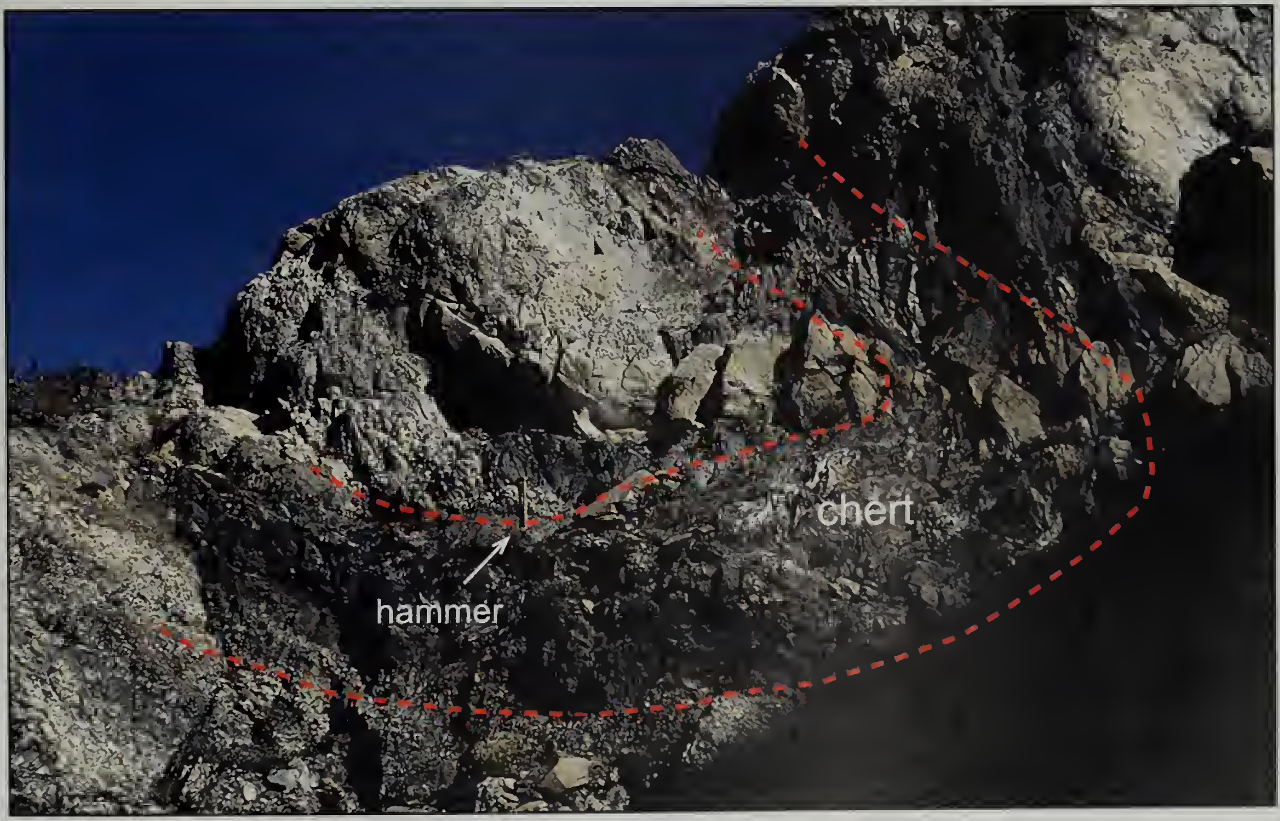

Photo 12. V-Folded chert bed within Member 2 between Stops 5 and 6 (view to the east). *Photo by Steven Silva.*

Photo 13. Sedimentary deposit at top of Member 2 at Stop 6, view to the south. *Photo by Steven Silva.*

may be solitary or occur in glomerocrysts. Individuals vary from 1.3 to 3.6 mm, averaging 1.9 mm, and vary in abundance from 0.5 to 17%. Replacement of plagioclase by secondary minerals is essentially identical to that in Member 1.

Stop 8.

Directions to Member 3

Walk back near the south end of the pond indicated on the map (Figure 16A). In general, you will be traveling due west by the path of least resistance, through the saddle on the ridge that overlooks Wades Lake, and visiting Stop 8 along the way. From the south end of the pond, start by walking west and around the brush and toward the east-facing, steeply-dipping, light-colored outcrops. Next, walk up the talus, keeping the light-colored outcrops to your left. When you reach the flattish area just above the height of the light-colored outcrops, stand just west of the brush line and look southward. Notice the series of planar exposures all dipping about 30 to 35° northeast. Stop 8 is the surface about 40 m S18°W from where you stand.

Quartz phenocrysts vary from 0.7 to 4.5 mm, average 2.0 mm, and vary in abundance from 1 to 10%. They are euhedral to rounded, with a greater percentage of rounded and embayed individuals than in the Member 1 quartz porphyries. Plagioclase occurs as euhedral phenocrysts, which

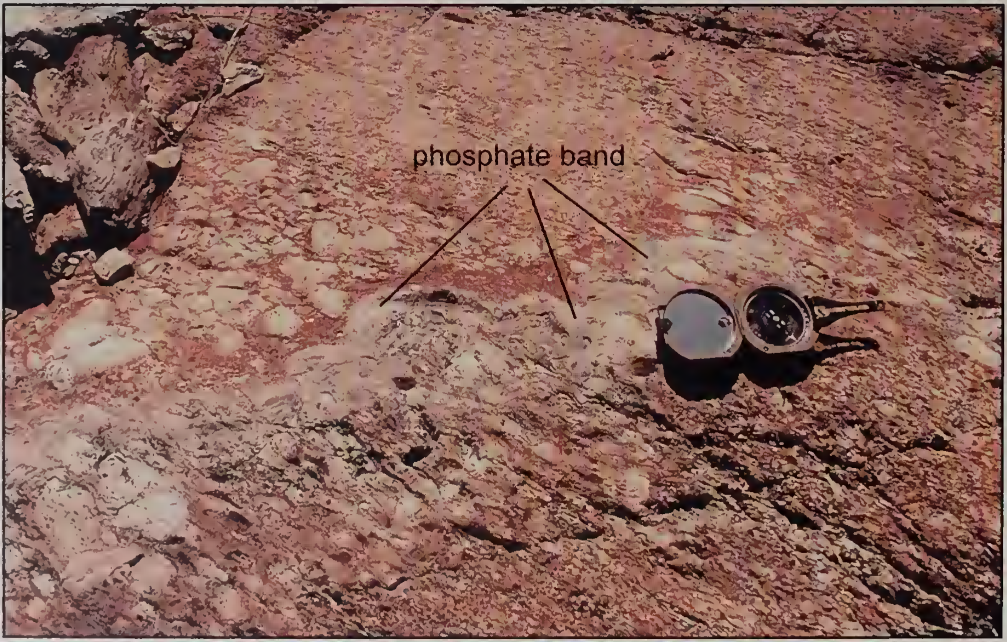

Photo 14. Closeup of the coarse upper layer and phosphate band at the top of the sedimentary deposit in Member 2 at Stop 6. *Photo by Steven Silva.*

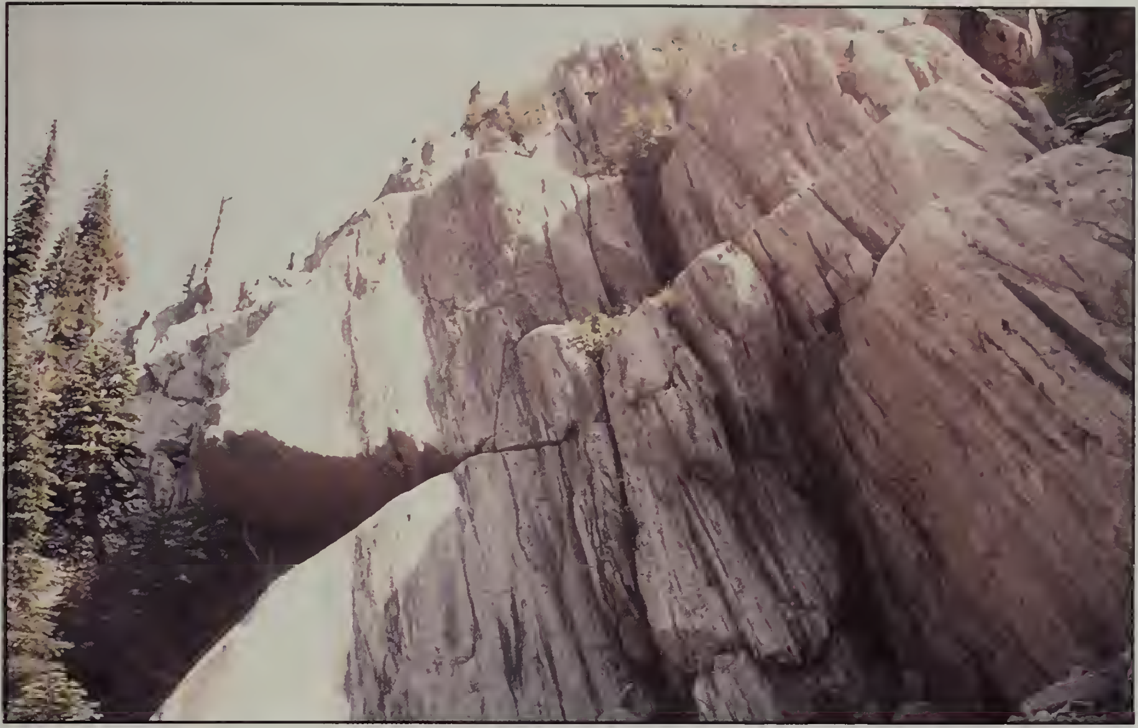

Photo 15. Columnar joints at the base of Member 4 quartz porphyry sill at Stop 7 (view towards the south). *Photo by Steven Silva.*

The exposure here is complex but exhibits several interesting features of Member 3 (Photo 17). Along the western margin of the outcrop about 6 m from the northwest corner is an area of light colored highly irregularly-shaped (taffy-like) clasts in a lapilli and ash matrix (Photo 17). The clasts here are vesicular but not pumiceous and comprise a greater proportion of the volume (perhaps 50%) than at Stops 3 and 6. Many appear rimmed or partially rimmed and the matrix is partially but not entirely composed of rim spall. Its characteristics superficially resemble an isolated-pillow breccia (Carlisle, 1963) but probably more correctly fall between that and a tuff. The progression of pillow lava to isolated-pillow breccia to broken-pillow breccia as described by Carlisle on Quadra Island is absent here. The stringy, taffy-like clasts would not have survived violent eruption and transport. As stated in Fisher and Schmincke (1984, p. 284), "A vertical eruption column entirely beneath water probably cannot develop into a hot pyroclastic flow because turbulent mixing with water would tend to destroy the column. There is a pos-

Photo 16. Closeup of overhanging ledge (at left of Photo 15) showing end view of columnar joints. *Photo by Steven Silva.*

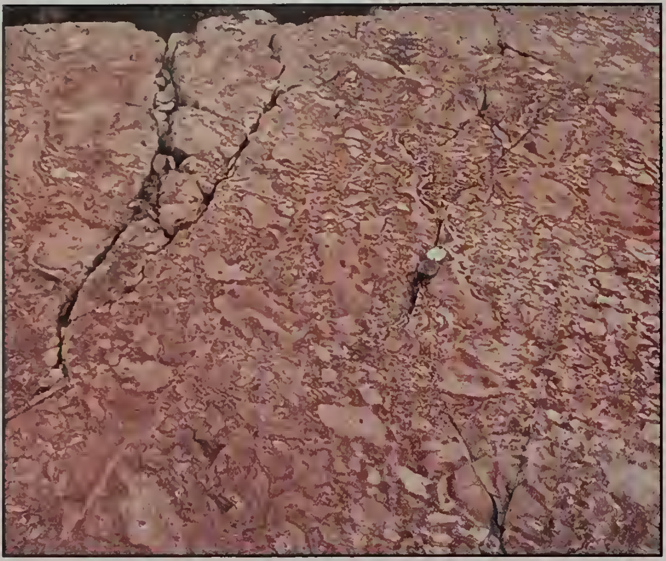

Photo 17. Member 3 volcanic breccia at Stop 8 (view towards the west). *Photo by Steven Silva.*

sibility, however, that a voluminous 'boiling-over' type of eruption may be extruded at rates great enough to produce a flow protected from the water by a carapace of steam and retain enough heat to become welded." The issue in the case of Member 3 is not welding but rather to retain enough heat to deform and preserve the often delicately-shaped clasts. The origin of the variably vesicular clasts, in an eruption of this type, may be a vesicular zone at the roof of the magma chamber that becomes entrained in an erupting magma column. A low-energy, high-volume eruption of this type could explain the great areal extent, and preservation of the relatively large and delicately-shaped vesicular to pumiceous clasts.

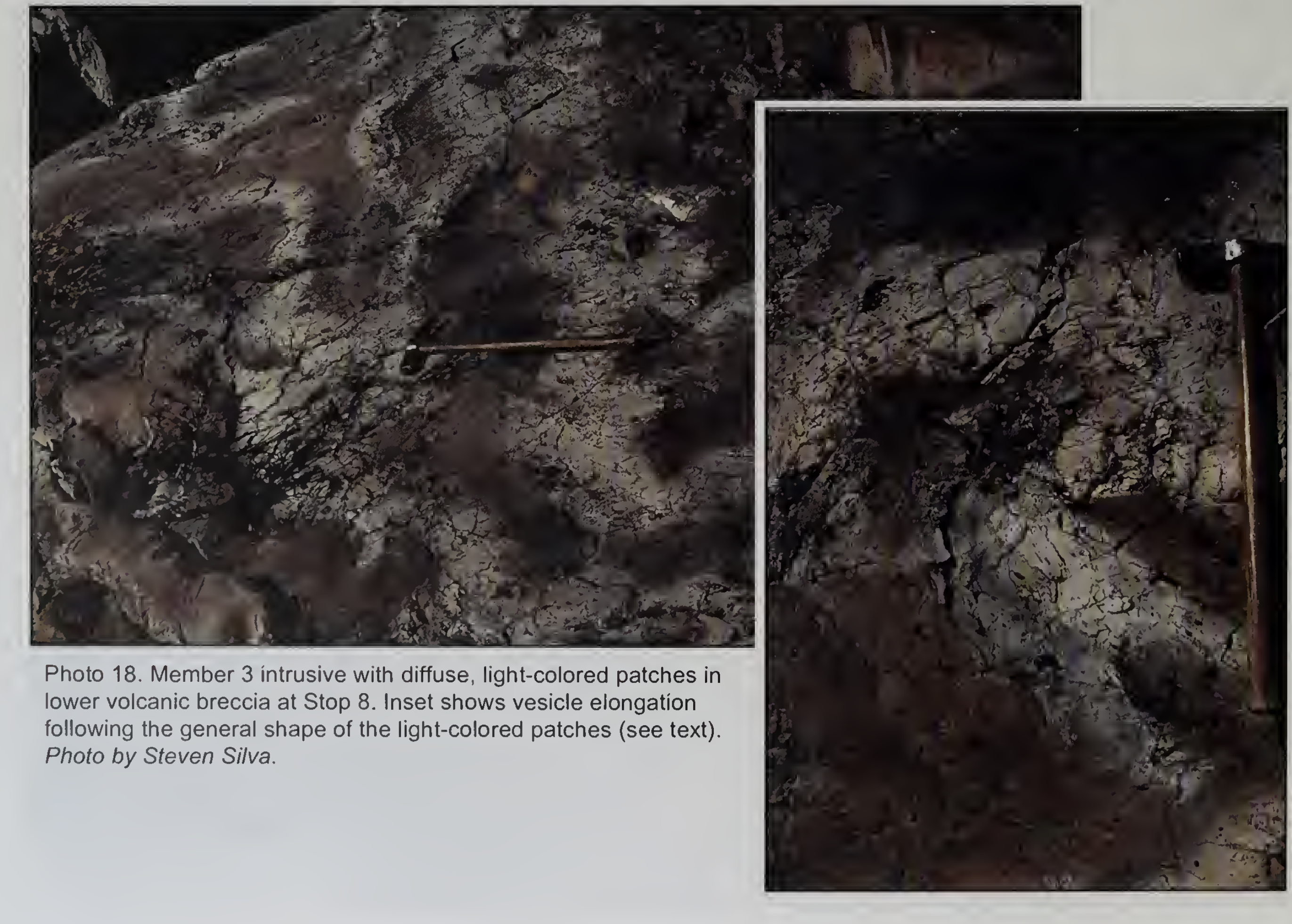

Photo 18. Member 3 intrusive with diffuse, light-colored patches in lower volcanic breccia at Stop 8. Inset shows vesicle elongation following the general shape of the light-colored patches (see text). *Photo by Steven Silva.*

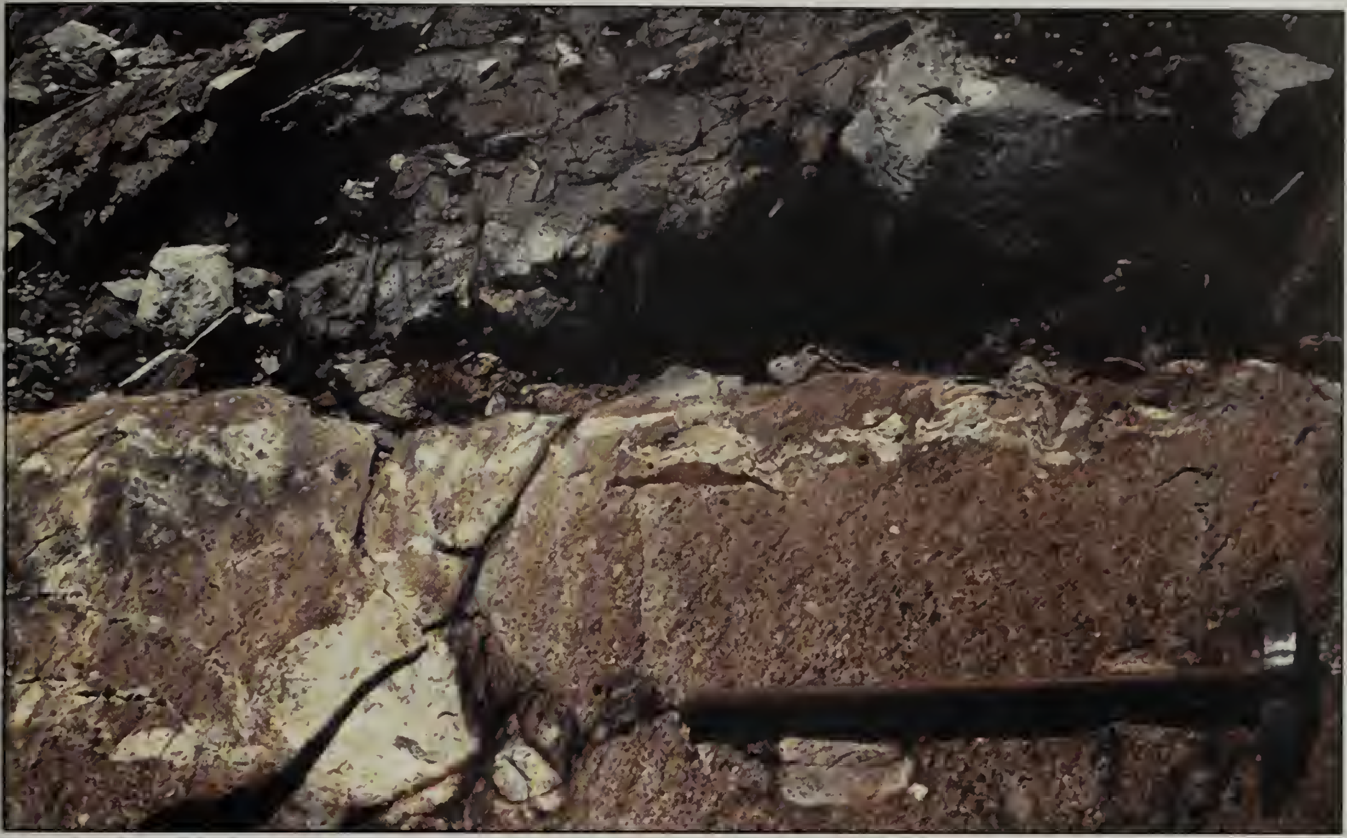

Photo 19. Top of sedimentary unit within Member 3 at Stop 8. Note disrupted phosphate band near top. *Photo by Steven Silva.*

The breccia described above has been intruded in a non-tabular fashion by a brown, aphanitic, sporadically vesicular body. The intrusive includes some diffuse, irregularly-shaped, light-colored patches (Photo 18). The direction of vesicle elongation parallels the boundaries of the light-colored patches, indicating the shape of the latter to be primary. The irregular contact of the intrusive, the lack of chilled margins, and the irregularly shaped diffuse patches all suggest that intrusion occurred shortly after deposition of the breccia, while it was still hot (lack of chilled margins) and plastic (irregular contacts and deformation of diffuse patches).

The breccia is overlain by a finely laminated, disrupted and discontinuous layer of phosphatic material up to 4 cm thick that in turn is overlain by a 1.8 to 3 m thick graded bed composed almost entirely of materials from the underlying unit (Photo 19). At the top of the sedimentary deposit are fragments of a second disrupted and discontinuous band of phosphatic material. Above the sedimentary sequence is a second breccia that has likewise been intruded by a dark, non-tabular, aphanitic body (Photo 20). Although the graded sediment may have been deposited over a very short time, the finely laminated phosphate probably represents a significant lapse in volcanism, indicating that Member 3 in this area was erupted in at least two pulses. The upper intrusive differs from the lower in that it lacks the diffuse light patches and is highly vesicular along its contacts. Despite the apparent chilling along its margins, an arm of the upper intrusive in the southwest corner of the outcrop has apparently dispersed fragments

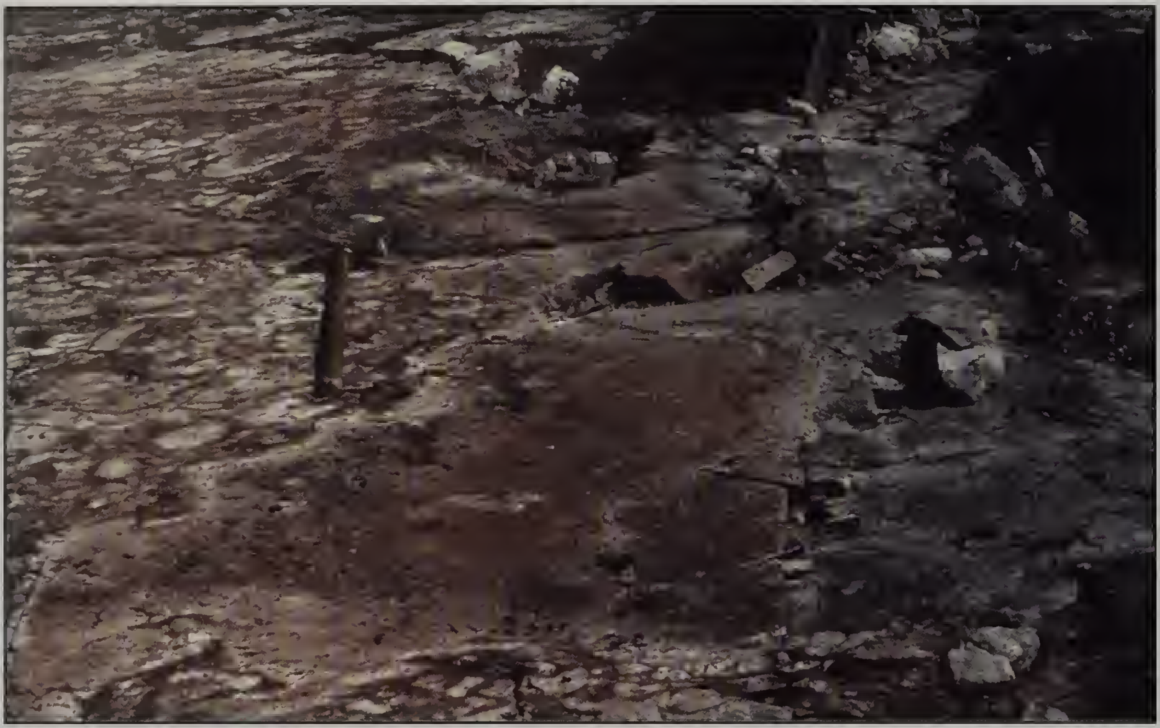

Photo 20. Member 3 intrusive in upper volcanic breccia showing vesicular margins and irregular contact with host breccia (Stop 8). *Photo by Steven Silva.*

into the host breccia, indicating that the breccia was not solidified during intrusion.

As illustrated at Stops 3, 6 and 8, the vesicular to pumiceous clasts in Member 3 occur in a spectrum of sizes and shapes and comprise varying proportions of the rock volume. These variations are probably related to changes in eruptive energy and volume within Member 3 in the Jamison Lake area and perhaps in the Tamarack tuff as a whole.

Back to the parking lot

Return to the flat area above the brush. Head uphill about S10°W through the saddle. Locate the dry pond in the saddle just beyond the prominent tall dead tree. Walk along the northeast edge of the pond and exit at the northwest corner. Continue in that direction to the top of the slope leading into the Wades Lake Basin. Follow the most obvious deer/people trail down (approx. N80°W) to the northeast shore of Wades Lake. Follow the trail at the lake's edge northwest until it crosses the Wades Lake branch of Jamison Creek and join the trail northeast, down toward Grass Lake and back to the parking lot (Figure 15).

ACKNOWLEDGMENTS

We would like to thank John Lull, Robin Bouse, Michael Clynne, David Harwood, Clark Johnson and Daniel Unruh for their thorough reviews and helpful suggestions. We would also like to thank John Fitzpatrick and Robin Bouse for the generous contribution of their time in producing the chemical analyses.

REFERENCES

Brooks, E.R. and Coles, D.G., 1980, Use of immobile trace elements to determine original tectonic setting of eruption of metabasalts, northern Sierra Nevada, California: Geologic Society of America Bulletin, v. 91, p. 665-671.

Brooks, E.R. and Legler, J.L., 1989, An unusual Devonian subaqueous pyroclastic-flow deposit in the northern Sierra Nevada, Sierra County, California: Geological Society of America Abstracts with Programs, v. 21, p. 59.

Brooks, E.R., Wood, M.M. and Garbutt, P.L., 1982, Origin and metamorphism of peperite and associated rocks in the Devonian Elwell Formation, northern Sierra Nevada, California: Geologic Society of America Bulletin, v. 93, p. 1208-1231.

Carlisle, D., 1963, Pillow breccias and their aquagene tuffs, Quadra Island, British Columbia: Journal of Geology, v. 71, p. 48-71.

Coles, K.S. and Varga, R. J., 1988, Early to middle Paleozoic phosphogenic province in terranes of the southern Cordillera, western United States: American Journal of Science, v. 288, p. 891-924.

Coney, P.J., Jones, D.L. and Monger, J.W.H., 1980, Cordilleran suspect terranes: Nature, v. 288, 329-333.

Crawford, A.J., Beccaluva, L. and Serri, G., 1981, Tectonomagmatic evolution of the West Philippine-Mariana region and the origin of boninites: Earth Planet. Sci. Letters, v. 54, p. 346-356.

Curtis, G.H., 1954, Mode of origin of pyroclastic debris in the Mehrten Formation of the Sierra Nevada. University of California Publications in Geological Sciences, v. 29, p. 453-502.

D'Allura, J.A., Moores, E.M. and Robinson, L., 1977, Paleozoic rocks of the northern Sierra Nevada: Their structural and paleogeographic implications *in* Stewart, J.H. and others, editors, Paleozoic paleogeography of the western United States: Society of Economic Paleontologists and Mineralogists, Pacific Section, Pacific Coast Paleogeography Symposium 1, p. 393-408.

DePaolo, D.J. and Wasserburg, G.J., 1979, Petrogenetic mixing models and Nd-Sr isotopic patterns: Geochimica et Cosmochimica Acta, v. 43, p. 615-627.

De Rosen-Spence, A.M., Provost, G., Dimroth, E., Gochnauer, K. and Owen, V., 1980, Archaean subaqueous felsic flows Rouyn-Noranda, Quebec, Canada, and their Quaternary equivalents: Precambrian Research, v. 12, p. 43-77.

Dickinson, W.R., 1977, Paleozoic plate tectonics and the evolution of the Cordilleran continental margin *in* Stewart, J.H., Stevens, C.H. and Fritsche, A.E., editors, Paleozoic paleography of the western United States: Society of Economic Paleontologists and Mineralogists, Pacific Section, Pacific Coast Paleogeography Symposium 1, p. 137-155.

Dickinson, W.R.,1981, Plate tectonics and the continental margin of California *in* Ernst, W.G., editor, The geotectonic development of California: Englewood Cliffs, New Jersey, Prentice Hall, p. 1-28.

Durrell, C. and D'Allura, J., 1977, Upper Paleozoic section in eastern Plumas and Sierra counties, Northern Sierra Nevada, California: Geological Society of America Bulletin, v. 88, p. 844-852

Durrell, C. and Proctor, P., 1948, Iron-ore deposits near Lake Hawley and Spencer Lakes, Sierra County, California: California Division of Mines and Geology Bulletin 129, p. 166-192.

Ewart, A., 1979, A review of the mineralogy and chemistry of Tertiary-Recent dacitic, latitic, rhyolitic, and related salic volcanic rocks *in* Barker, F., editor, Trondhjemites, dacites, and related rocks, p. 13-121.

Fisher, R.V. and Schmincke, H.-U., 1984, Pyroclastic rocks. Berlin, Springer-Verlag, 472 p.

Girty, G.H. and Wardlaw, M.S., 1985, Petrology and provenance of pre-Late Devonian sandstones in the Shoo Fly Complex, northern Sierra Nevada, California: Geological Society of America Bulletin, v. 96, p. 516-521.

Hamilton, W.B., 1988, Plate tectonics and island arcs: Geological Society of America Bulletin, v. 100, p. 1503-1527.

Hanson, G.N., 1980, Rare earth elements in petrogenetic studies of igneous systems. Annual Review Earth Planet. Science 8, p. 371-406.

Hanson, R.E., 1983, Volcanism, plutonism and sedimentation in a Late Devonian submarine island-arc setting, northern Sierra Nevada, California: New York, Columbia University, Ph.D. dissertation, 345 p.

Hanson, R.E., 1991, Quenching and hydroclastic disruption of andesitic to rhyolitic intrusions in a submarine island-arc sequence, northern Sierra Nevada, California: Geological Society of America Bulletin, v. 103, p. 804-816.

Hanson, R.E. and Schweickert, R.A., 1986, Stratigraphy of mid-Paleozoic island-arc rocks in part of the northern Sierra Nevada, Sierra and Nevada counties, California: Geological Society of America Bulletin, v. 97, p. 986-998.

Hanson, R.E., Saleeby, J.B. and Schweickert, R.A., 1988, Composite Devonian island-arc batholith in the northern Sierra Nevada, California: Geological Society of America Bulletin, v. 100, p. 446-457.

Harwood, D.S., 1983, Stratigraphy of upper Paleozoic volcanic rocks and regional unconformities in part of the northern Sierra terrane, California: Geological Society of America Bulletin, v. 94, p. 413-422.

Harwood, D.S., 1988, Tectonism and metamorphism in the northern Sierra terrane, northern California *in* Ernst, W.G., editor, Metamorphism and crustal evolution of the western United States; Rubey Volume 7: Englewood Cliffs, New Jersey, Prentice-Hall, p. 765-788.

Harwood, D.S. and Murchey, B.L. 1990, Biostratigraphic, tectonic, and paleogeographic ties between upper Paleozoic volcanic and basinal rocks in the northern Sierra terrane, California, and the Havallah sequence, Nevada *in* Harwood, D.S. and Miller, M.M., editors, Paleozoic and early Mesozoic paleogeographic relations; Sierra Nevada, Klamath Mountains, and related terranes: Boulder, Colorado, Geological Society of America Special Paper 255.

Kamp, P.J.J., 1984, Neogene and Quaternary extent and geometry of the subducted Pacific plate beneath North Island, New Zealand: Implications for Kaikoura tectonics: Tectonophysics, 108, p. 241-266.

Legler, J.L., Brooks, E.R. and Lull, J.S, 1991, Tamarack tuff: A Devonian submarine pyroclastic flow deposit in the northern Sierra Nevada, Plumas and Sierra counties: CALIFORNIA GEOLOGY, v. 44, p. 130-137.

Miller E.L., Holdsworth, B.K., Whiteford, W.B. and Rogers, D., 1984, Stratigraphy and structure of the Schoonover Sequence, northeastern Nevada: Implications for Paleozoic plate margin tectonics: Geological Society of America Bulletin, v. 95, p. 1063-1076.

Rouer, O., Lapierre, H., Coulon, C. and Michard, A., 1989b, New petrological and geochemical data on mid-Paleozoic island-arc volcanics of northern Sierra Nevada, California: Evidence for a continent-based island arc: Canadian Journal of Earth Science, v. 26, p. 2465-2478.

Rouer, O., Lapierre, H., Mascle, G., Coulon, C. and Albers, J., 1989a, Geodynamic implications of Devonian silicic arc magmatism in the Sierra Nevada and Klamath mountains, California: Geology, v. 17, p. 177-180.

Schweickert, R.A. and Snyder, W.S., 1981, Paleozoic plate tectonics of the Sierra Nevada and adjacent regions *in* Ernst, W.G., editor, The geotectonic development of California: Englewood Cliffs, New Jersey, Prentice Hall, p. 182-201.

Schweickert, R.A., Girty, G.H. and Hanson, R.E., 1984, Tectonic development of the northern Sierra terrane: An accreted Late Paleozoic island arc and its basement *in* Lintz, J., Jr., editor, Western Geological Excursions; v. 4, Geologic Society of America Guidebook, p. 1-65.

Schweickert, R.A., 1981, Tectonic evolution of the Sierra Nevada range *in* Ernst, W.G., editor, The geotectonic development of California: Englewood Cliffs, New Jersey, Prentice Hall, p. 87-131.

Silva, S.R., 1990, Geology of the Sierra Buttes Formation in the Jamison Lake area, Plumas County, California: Hayward, California, California State University, M.S. thesis, 151 p.

Snyder, W.S., 1977, Origin and exploration for ore deposits in upper Paleozoic chert-greenstone complexes of northern Nevada: Stanford, California, Stanford University, Ph.D. dissertation, 159 p.

Snyder, W.S. and Brueckner, H.K., 1983, Tectonic evolution of the Golconda allochthon, Nevada: Problems and perspectives *in* Stevens, C.H., editor, Pre-Jurassic rocks in western North America suspect terranes: Pacific Section, Society of Economic Paleontologists and Mineralogists Pacific Coast Paleogeography Symposium 1, p. 349-362.

Speed, R.C., 1979, Collided Paleozoic microplate in the western United States: Journal of Geology, v. 87, p. 279-292.

Speed, R.C. and Sleep, N.H., 1982, Antler orogeny and foreland basin; A model: Geological Society of America Bulletin, v. 93, p. 815-828.

Thompson, R.N., Morrison, R.A., Hendry, G.L. and Parry, S.J., 1984, An assessment of the relative roles of a crust and mantle in magma genesis: an elemental approach. Phil. Trans. R. Soc. Lond., A310, p. 549-590.

Varga, R. J., 1982, Implications of Paleozoic phosphorites in the northern Sierra Nevada range: Nature, v. 297, p. 217-220.

APPENDIX A

DESCRIPTION AND LOCATION OF THE SHOO FLY SAMPLES

Samples SFRF and SF963C are meta-quartz sandstones containing 95% quartz. Samples SF9610A, SF9614B, and SF9614C are meta-quartz sandstones each containing about 85% quartz. Plagioclase appears to be rare in all samples, but may have gone unrecognized to some extent. K-feldspar is absent as indicated by staining. Grain size varies from about 0.1 to 2 mm (up to 4mm in sample SF9614C) averaging between 0.2 and 0.5 mm. Principal secondary minerals occupying the matrix are white mica, chlorite, and actinolite? (Pale green, prismatic, relatively high relief, very slightly to non-pleochroic) in varying proportions. Carbonate comprises about 1% in samples SF963C, SF9614B, and SF9614C. Samples were collected at the following localities:

Sample	Latitude	Longitude	Location
SFRF	39°44'03"	120°45'13"	Renes Falls on Jamison Creek in Plumas Eureka State Park about 3.5 miles west of the campground, just past Ross Camp
SF963C	39°33'20"	120°47'25"	On Highway 49, 2.3 miles east of Downieville
SF9610A	39°59'08"	120°57'08"	On Highway 89, 5.1 miles north of Quincy
SF9614B and SF9614C	40°02'22"	120°58'57"	At the intersection of Highways 70 and 89 about 3.5 miles north of the turnoff for Keddie

APPENDIX B

ANALYTICAL PRECISION

Isotopes were analyzed with a Finnigan MAT 261 mass spectrometer. $^{87}Sr/^{86}Sr$ was normalized to $^{88}Sr/^{86}Sr = 8.37521$. Precision is 0.00002 at 95% confidence. $^{143}Nd/^{144}Nd$ was normalized to $^{146}Nd/^{144}Nd = 0.7219$. Precision is 0.000015 at 95% confidence.

Major and trace elements were analyzed on a Perkin Elmer ICPMS. The instrument was calibrated against USGS standards BCR, BHVO, AGV1, G2, QLO-1, and BIR-1. USGS JA1 was analyzed every six samples throughout the run. The 1ó precision on the five replicates of JA1 was better than ±4% for the major elements and better than ±3% for the trace elements except Nb at ±4.1% and Ta at ±7.7%.

APPENDIX C

CALCULATIONS FOR THE INVOLVEMENT OF SHOO FLY PARTIAL MELT IN SIERRA BUTTES MAGMA

Measured values

ε_{NdSF} = epsilon Nd of Shoo Fly rocks (average of Shoo Fly samples)

ε_{NdSB} = epsilon Nd of the Sierra Buttes rocks (average of Member 1 samples)

ε_{NdB} = epsilon Nd of the basalt (samples C11, assuming it to be representative of the mafic end member)

C_{SFO} = Concentration of Nd in the Shoo Fly rocks before partial melting (average of Shoo Fly samples)

C_B = Concentration of Nd in the basalt (samples C11, assuming it to be representative of the mafic endmember)

C_{SB} = Concentration of Nd in the Sierra Buttes magma (average concentration of Nd in Mem ber 1, assuming no fractional crystallization)

Estimated value

D = partition coefficient for Nd during partial melting of the Shoo Fly

Unknowns

X_{SF} = Fraction of Nd in the Sierra Buttes magma derived from the Shoo Fly melt

C_{SF} = Concentration of Nd in the Shoo Fly melt

F_{SF} = Fraction of Shoo Fly melt in Sierra Buttes magma before fractional crystallization

F_{PMSF} = Fraction of partial melting of Shoo Fly rocks

F_B = Fraction of basalt in the Sierra Buttes magma

Calculation of the fraction of Nd in the Sierra Buttes magma derived from the Shoo Fly melt (X_{SF})

The isotope mass balance equation below states that the fraction of Nd derived from the Shoo Fly melt times its isotopic composition ($X_{SF}\ \varepsilon_{NdSF}$) plus the fraction of Nd derived from the basalt times its isotopic composition ($(1-X_{SF})\varepsilon_{NdB}$) equals the isotopic composition of the Sierra Buttes magma (ε_{NdSB}).

(continued next page)

Appendix C Continued...

$$X_{SF}\,\varepsilon_{NdSF} + (1\text{-}X_{SF})\varepsilon_{NdB} = \varepsilon_{NdSB}$$

rearranged:

(1) $X_{SF} = (\varepsilon_{NdSB} - \varepsilon_{NdB}) / (\varepsilon_{NdSF} - \varepsilon_{NdB})$

Calculations of the fraction of Shoo Fly melt in the Sierra Buttes magma (F_{SF})

With the results from equation 1, two additional equations are needed to solve the two unknowns C_{SF} an F_{SF}. Equation 2 states that the mass of Nd in the Sierra Buttes magma derived from the Shoo Fly melt (C_{SF} F_{SF}) equals the fraction of Nd derived from the Shoo Fly melt (X_{SF}) times the total mass of Nd in the Sierra Buttes magma ($C_{SF}\,F_{SF}$ +(1- F_{SF})C_B).

2) $C_{SF}\,F_{SF} = X_{SF}\,(C_{SF}\,F_{SF} + (1\text{-}\,F_{SF})C_B)$

The next equation states that in a unit volume of Sierra Buttes melt, the mass of Nd derived from basalt ($C_{SF}\,F_{SF}$) plus the mass of Nd derived from the Shoo Fly ((1- F_{SF})C_B) equals the concentration of Nd in the Sierra Buttes magma (C_{SB}).

$$C_{SF}\,F_{SF} + (1\text{-}\,F_{SF})C_B = C_{SB}$$

rearranged:

3) $C_{SF} = (C_{SB} + F_{SF}C_B - C_B) / F_{SF}$

Substituting equation 3 into equation 2:

$$F_{SF}\,((C_{SB} + F_{SF}\,C_B - C_B) / F_{SF}) = X_{SF}\,(\,F_{SF}\,((C_{SB} + F_{SF}C_B - C_B) / F_{SF}) + (1\text{-}\,F_{SF})C_B$$

collecting terms:

$$C_{SB} + F_{SF}\,C_B - C_B = X_{SF}C_{SB}$$

rearranged:

4) $F_{SF} = ((C_{SB}\,(\,X_{SF} - 1)) / C_B) + 1$

Calculation of concentration of Nd in Shoo Fly melt

Results from equation 4 are used to solve equation 3:

Calculation of degree of partial melting of Shoo Fly rocks (batch melting equation from Hanson, 1980).

$$C_{SF} / C_{SFO} = 1 / (D\,(1\text{-}F_{PMSF}) + F_{PMSF})$$

rearranged:

$$F_{PMSF} = (D - (C_{SFO} / C_{SF})) / (D\text{-}1)$$

able. Sr-Nd Isotope and Major and Trace Element Analyses.

Samp. #	SC1	SC2	SC3	SC4	SC5	SC6	SC7	SC8	SC9	SC10	SC11
Member	M1	M1	M1	M1	M1	M1	M2	M3	M3	M3	M3
comp.	dacite	dacite	dacite	dacite	dacite	dacite	andesite	dacite	dacite	basalt	basalt
ppm											
Ti	335.8	432.0	298.0	384.8	330.0	341.5	1879.8	2830.2	5249.9	3438.2	2920.2
Rb	45.9	29.0	59.9	10.7	25.2	44.0	17.4	2.1	11.0	10.0	0.9
Sr	32.2	87.9	180.2	68.9	68.0	37.3	110.6	135.8	82.0	135.2	164.4
Y	17.6	48.1	20.6	31.7	15.8	16.5	15.1	17.3	19.6	10.5	13.4
Zr	75.1	82.6	71.4	77.0	73.1	87.0	49.5	37.1	48.7	54.3	39.9
Nb	5.0	6.6	5.3	6.8	6.2	7.0	2.3	2.2	2.4	2.8	1.8
Ba	1283.3	789.7	484.8	100.1	802.5	390.3	273.3	214.6	233.6	659.0	44.6
La	14.7	27.2	30.6	24.7	16.9	18.7	8.0	4.8	4.0	4.8	4.2
Ce	20.7	51.8	54.6	48.6	32.7	34.0	14.9	12.3	10.0	10.5	9.4
Nd	15.3	23.0	20.2	18.5	12.6	14.5	7.1	8.8	7.6	6.3	5.6
Sm	3.1	4.7	4.0	3.6	2.4	2.8	1.6	2.5	2.3	1.6	1.5
Eu	0.4	0.6	0.5	0.4	0.4	0.3	0.4	0.6	0.7	0.6	0.5
Tb	0.5	0.9	0.6	0.6	0.4	0.4	0.3	0.5	0.5	0.3	0.3
Gd	2.9	4.7	3.7	3.4	2.2	2.6	1.9	2.9	2.7	1.7	1.7
Dy	2.9	6.1	3.5	4.0	2.3	2.7	2.3	3.2	3.4	2.0	2.2
Ho	0.6	1.4	0.7	0.9	0.5	0.5	0.5	0.7	0.7	0.4	0.5
Er	1.9	4.5	1.9	2.7	1.6	1.6	1.6	1.7	2.1	1.2	1.3
Yb	2.0	4.7	2.0	2.8	1.9	1.8	1.7	1.5	2.0	1.2	1.3
Lu	0.3	0.7	0.3	0.4	0.3	0.3	0.3	0.2	0.3	0.2	0.2
Hf	2.7	3.1	2.5	2.8	2.8	3.3	1.5	1.1	1.5	1.3	1.0
Ta	4.8	4.8	3.4	3.6	4.7	2.3	1.1	2.0	1.3	0.7	0.5
Th	8.8	12.3	15.0	13.9	11.3	13.9	2.6	0.7	1.2	1.4	1.0
Samp. #	SC1	SC2	SC3	SC4	SC5	SC6	SC7	SC8	SC9	SC10	SC11
Member	M1	M1	M1	M1	M1	M1	M2	M3	M3	M3	M3
comp.	dacite	dacite	dacite	dacite	dacite	dacite	andesite	dacite	dacite	basalt	basalt
Wt. % **oxides**											
SiO_2	84.8	79.7	77.6	75.9	82.7	72.0	56.8	63.7	65.7	50.4	49.8
Na_2O	2.5	3.9	4.6	5.8	3.6	2.9	4.0	3.0	3.2	2.6	3.7
MgO	0.2	0.4	0.7	1.6	0.3	3.2	5.5	3.7	2.4	7.1	6.7
Al_2O_3	7.4	11.5	13.0	12.6	9.7	13.4	15.1	13.6	11.9	17.2	15.0
P_2O_5	0.0	0.0	0.0	0.0	0.0	0.0	0.1	0.1	0.1	0.0	0.1
K_2O	2.5	1.4	1.8	0.5	1.3	2.0	0.8	0.3	0.9	0.8	0.2
CaO	0.6	0.9	0.6	0.5	0.2	0.2	4.6	5.4	1.8	5.1	6.7
TiO_2	0.1	0.1	0.0	0.1	0.1	0.1	0.3	0.5	0.9	0.6	0.5
MnO	0.0	0.0	0.0	0.0	0.0	0.0	0.1	0.1	0.1	0.1	0.2
Fe_2O_3	0.7	0.6	0.7	1.5	1.0	3.5	6.0	6.1	9.0	11.5	8.6
LOI	1.2	1.5	1.0	1.5	1.1	2.6	6.7	3.5	4.1	4.5	8.6
Isotopes											
87/86Sr	0.73146	0.71983	0.71629	0.71898	0.71775	0.72361	0.71355	0.70968	0.70934	0.71034	0.71005
143/ 144Nd	0.511577	0.511598	0.511660	0.511571	0.511384	0.511566	0.511932	0.512310	0.512596	0.511983	0.512560
epsilon Nd	-17.1	-16.8	-15.3	-16.7	-19.6	-17.3	-11.2	-5.3	-0.3	-10.7	0.5

(continued next page)

Table. Sr-Nd Isotope and Major and Trace Element Analyses (continued).

Samp. #	SC12	SC13	SC14	SC15	SC16	SC17	SFRF	SF963C	SF9610A	SF9614B	SF9614
Member	M4	M4	M4	M4	M4	M4	Shoo Fly	Shoo Fly	Shoo Fly	Shoo Fly	Shoo F
comp.	dacite	dacite	dacite	dacite	dacite	dacite	meta-ss	meta-ss	meta-ss	meta-ss	meta-s
ppm											
Ti	1466.6	1588.0	1051.3	1470.1	1047.7	1522.5	1021.9	1631.0	3178.4	1443.3	2332.1
Rb	15.2	27.2	20.4	30.3	30.2	47.8	13.3	37.4	63.4	25.0	13.8
Sr	71.4	111.3	68.5	71.3	26.9	43.9	8.6	21.7	21.3	23.0	13.3
Y	34.7	40.3	35.6	36.9	41.6	29.1	9.4	10.6	14.9	10.0	16.4
Zr	159.6	169.6	155.2	143.8	98.4	62.5	324.9	188.7	252.4	198.3	361.7
Nb	6.3	7.2	8.3	7.0	4.3	2.4	2.4	5.8	11.1	3.0	7.6
Ba	406.2	239.5	427.1	450.3	358.5	1643.1	58.6	129.6	239.4	105.3	59.8
La	15.4	16.8	18.8	16.5	8.6	6.7	14.0	15.0	22.0	13.8	22.6
Ce	32.2	32.4	33.7	31.8	16.8	12.3	30.5	28.9	42.7	28.4	46.9
Nd	16.0	19.4	19.9	18.6	12.4	8.8	10.6	12.6	19.4	11.9	21.3
Sm	3.8	4.6	4.5	4.4	3.5	2.5	1.7	2.2	3.3	2.0	3.8
Eu	0.8	0.9	0.8	1.1	0.7	0.6	0.2	0.4	0.6	0.3	0.6
Tb	0.7	0.9	0.8	0.8	0.9	0.6	0.2	0.3	0.4	0.3	0.4
Gd	4.1	5.1	4.7	4.8	4.6	3.3	1.3	1.9	2.8	1.7	3.1
Dy	5.2	6.1	5.7	5.8	6.5	4.6	1.2	1.6	2.4	1.4	2.5
Ho	1.1	1.3	1.2	1.2	1.5	1.0	0.3	0.3	0.5	0.3	0.5
Er	3.5	4.0	3.7	3.7	4.4	3.1	0.9	0.9	1.3	0.8	1.4
Yb	3.6	4.3	4.0	3.8	4.7	3.4	1.0	1.0	1.3	0.8	1.4
Lu	0.6	0.7	0.6	0.6	0.7	0.5	0.2	0.2	0.2	0.1	0.2
Hf	4.3	4.8	4.4	4.1	3.0	2.2	7.8	4.7	6.0	4.8	8.1
Ta	2.8	2.3	2.1	1.8	1.7	1.4	3.4	3.1	2.5	3.1	3.3
Th	5.7	5.6	6.1	5.2	1.9	1.8	10.8	7.3	9.3	7.1	13.1

Samp. #	SC12	SC13	SC14	SC15	SC16	SC17	SFRF	SF963C	SF9610A	SF9614B	SF9614
Member	M4	M4	M4	M4	M4	M4	Shoo Fly	Shoo Fly	Shoo Fly	Shoo Fly	Shoo F
comp.	dacite	dacite	dacite	dacite	dacite	dacite	meta-ss	meta-ss	meta-ss		
Wt. % **oxides**											
SiO_2	73.3	73.1	76.3	73.9	80.6	76.0					
Na_2O	4.9	4.6	3.9	4.1	2.5	1.1	0.4	0.9	1.2	0.4	0.6
MgO	1.0	0.9	0.6	1.0	0.7	1.1	0.3	0.9	1.1	0.5	1.0
Al_2O_3	13.4	12.5	10.9	12.4	7.9	10.6	2.4	6.2	9.0	3.5	4.4
P_2O_5	0.1	0.1	0.0	0.1	0.0	0.1	0.0	0.0	0.1	0.1	0.1
K_2O	1.4	1.3	1.2	1.7	2.5	2.4	0.6	1.2	1.8	0.9	0.6
CaO	0.8	1.7	1.1	1.3	0.4	1.3	0.1	0.2	0.2	0.6	0.1
TiO_2	0.2	0.3	0.2	0.2	0.2	0.3	0.2	0.3	0.5	0.2	0.4
MnO	0.1	0.0	0.0	0.0	0.0	0.1	0.0	0.0	0.0	0.1	0.0
Fe_2O_3	3.3	3.3	3.8	3.0	3.1	4.0	0.6	2.4	3.8	2.0	3.9
LOI	1.5	2.1	2.0	2.2	2.1	3.3					
Isotopes											
87/86Sr	0.71278	0.71010	0.71147	0.71999	0.71184	0.71509					
143/144Nd	0.512244	0.512437	0.512439	0.512438	0.512302	0.512586	0.511238	0.511283	0.5113	0.511188	0.51
epsilon Nd	-5.5	-1.5	-1.5	-2.8	-4.0	-0.1	-22.6	-22.1	-21.7	-23.8	-24.6

GEOLOGY OF A LATE PALEOZOIC ISLAND ARC IN THE NORTHERN SIERRA TERRANE

Elwood R. Brooks[1]

GEOLOGIC SETTING

The Western Metamorphic Belt in the northern Sierra Nevada is divided into four fault-bounded tectonic belts (Moores and Day, 1984; Day and others, 1985). The easternmost of these, the Eastern Belt, is also known as the Northern Sierra terrane (Coney and others, 1980). It lies between the Feather River Peridotite Belt on the west and Mesozoic plutons to the east (Figure 1). The Eastern Belt consists mostly of the Early Paleozoic Shoo Fly Complex, on the west, and a series of three, superimposed, late Paleozoic and Jurassic volcanic-arc sequences.

The post-Cambrian, pre-Late Devonian, accretionary Shoo Fly Complex developed in a trench setting, and was assembled prior to Frasnian time by stacking of four, west-vergent, thrust slices (Girty and others, 1996; Hanson and others, 1996). The structurally highest of these is the Sierra City melange (Figure 1). The thrust slices are stitched by the 369+/-3 Ma Bowman Lake Batholith, which is considered the subvolcanic part of the mid-Famennian Sierra Buttes Formation (Hanson and others, 1996). The dacitic to andesitic Sierra Buttes Formation forms the basal part of the oldest, Devonian-Mississippian volcanic-arc sequence, and is separated from the Sierra City melange by a profound angular unconformity that truncates the imbricate thrust slices comprising the Shoo Fly Complex (Figure 1). This erosional unconformity is discontinuously blanketed by the epiclastic, Frasnian to mid-Famennian Grizzly Formation (Figure 2; Hanson and Schweickert, 1986). The dominant provenance of sediment in the Shoo Fly Complex evidently was ancient upper crust in the North American continental interior (Girty and others, 1996); this has important implications to the origin of the Sierra Buttes Formation.

The Sierra Buttes Formation passes upward, through the andesitic mid-Famennian Elwell Formation, to the more mafic, basaltic to basaltic andesitic Taylor Formation. Fossils have not been found in the Taylor Formation, but its age is closely bracketed by mid-Famennian and late Kinderhookian conodonts in underlying and overlying (lower Peale) formations (Harwood, 1992). Together, the Taylor, Elwell, and Sierra Buttes formations—the bulk of Harwood's (1992) Taylorsville sequence—make up a 4.5 kilometer (km)-thick succession of submarine, island-arc, volcanic and sedimentary rocks that perhaps was deposited in as few as 5 Ma at the close of the Devonian period.

Most rocks are volcanic or volcaniclastic; pelagic sediments (radiolarian cherts) are relatively rare. Andesitic to basaltic lava flows tend to be pillowed, appropriate for the submarine environment of deposition. Hypabyssal intrusives, some penecontemporaneous, are ubiquitous (dikes, sills, and more equant intrusive masses). The voluminous volcaniclastic rocks are every conceivable kind (autobrecciated lavas, pumiceous subaqueous pyroclastic-flow deposits, epiclastic turbidites and debris-flow deposits, peperites, etc.). Based on field relationships, petrography, and rock and mineral chemistry, these are classical island-arc rocks, and there exists only the most meager evidence that the island arc was ever emergent (D'Allura and others, 1977; Brooks and Coles, 1980; Brooks and others, 1982; Brooks and Schiffman, 1996).

---

[1] Department of Geological Sciences, California State University, Hayward

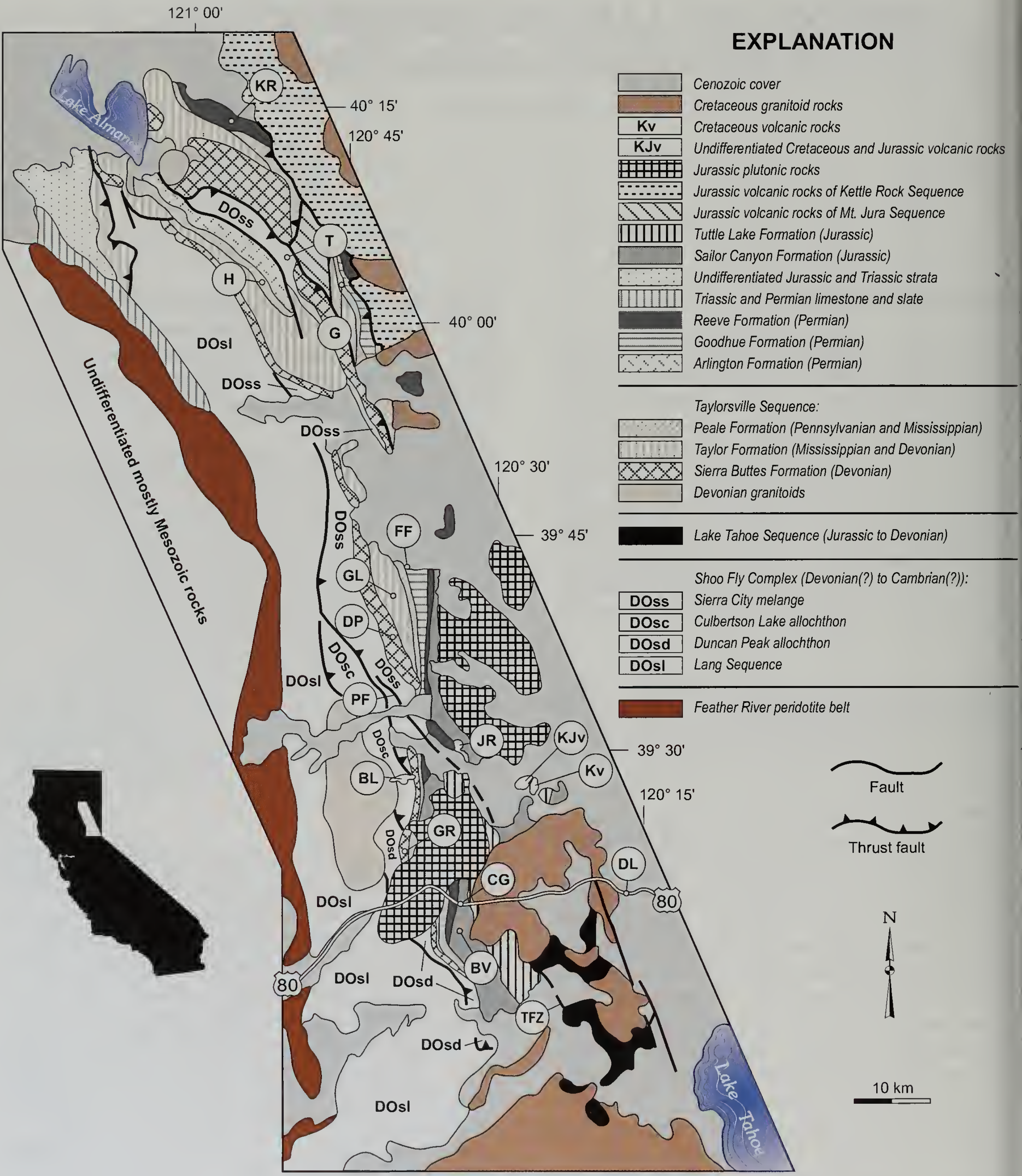
121° 00'
40° 15'
120° 45'
40° 00'
120° 30'
39° 45'
39° 30'
120° 15'
Lake Almanor
Lake Tahoe
KR
H
T
G
FF
GL
DP
PF
BL
GR
JR
KJv
Kv
CG
DL
BV
TFZ
80
DOss
DOsl
DOsc
DOsd
Undifferentiated mostly Mesozoic rocks
EXPLANATION
Cenozoic cover
Cretaceous granitoid rocks
Kv Cretaceous volcanic rocks
KJv Undifferentiated Cretaceous and Jurassic volcanic rocks
Jurassic plutonic rocks
Jurassic volcanic rocks of Kettle Rock Sequence
Jurassic volcanic rocks of Mt. Jura Sequence
Tuttle Lake Formation (Jurassic)
Sailor Canyon Formation (Jurassic)
Undifferentiated Jurassic and Triassic strata
Triassic and Permian limestone and slate
Reeve Formation (Permian)
Goodhue Formation (Permian)
Arlington Formation (Permian)
Taylorsville Sequence:
Peale Formation (Pennsylvanian and Mississippian)
Taylor Formation (Mississippian and Devonian)
Sierra Buttes Formation (Devonian)
Devonian granitoids
Lake Tahoe Sequence (Jurassic to Devonian)
Shoo Fly Complex (Devonian(?) to Cambrian(?)):
DOss Sierra City melange
DOsc Culbertson Lake allochthon
DOsd Duncan Peak allochthon
DOsl Lang Sequence
Feather River peridotite belt
Fault
Thrust fault
N
10 km

Figure 1. Geologic map of the Eastern Belt (Northern Sierra terrane). *From Hanson and others, 1996.* Circled letters pointing out localities relevant to this report are: KR (=Keddie Ridge), H (=Mt. Hough), G (=Genesee), FF (=Frazier Falls), GL (=Gold Lake), DP (=Dugan Pond), and BV (=Big Valley). Readers may consult Plate 1 in Harwood (1992) for additional detail.

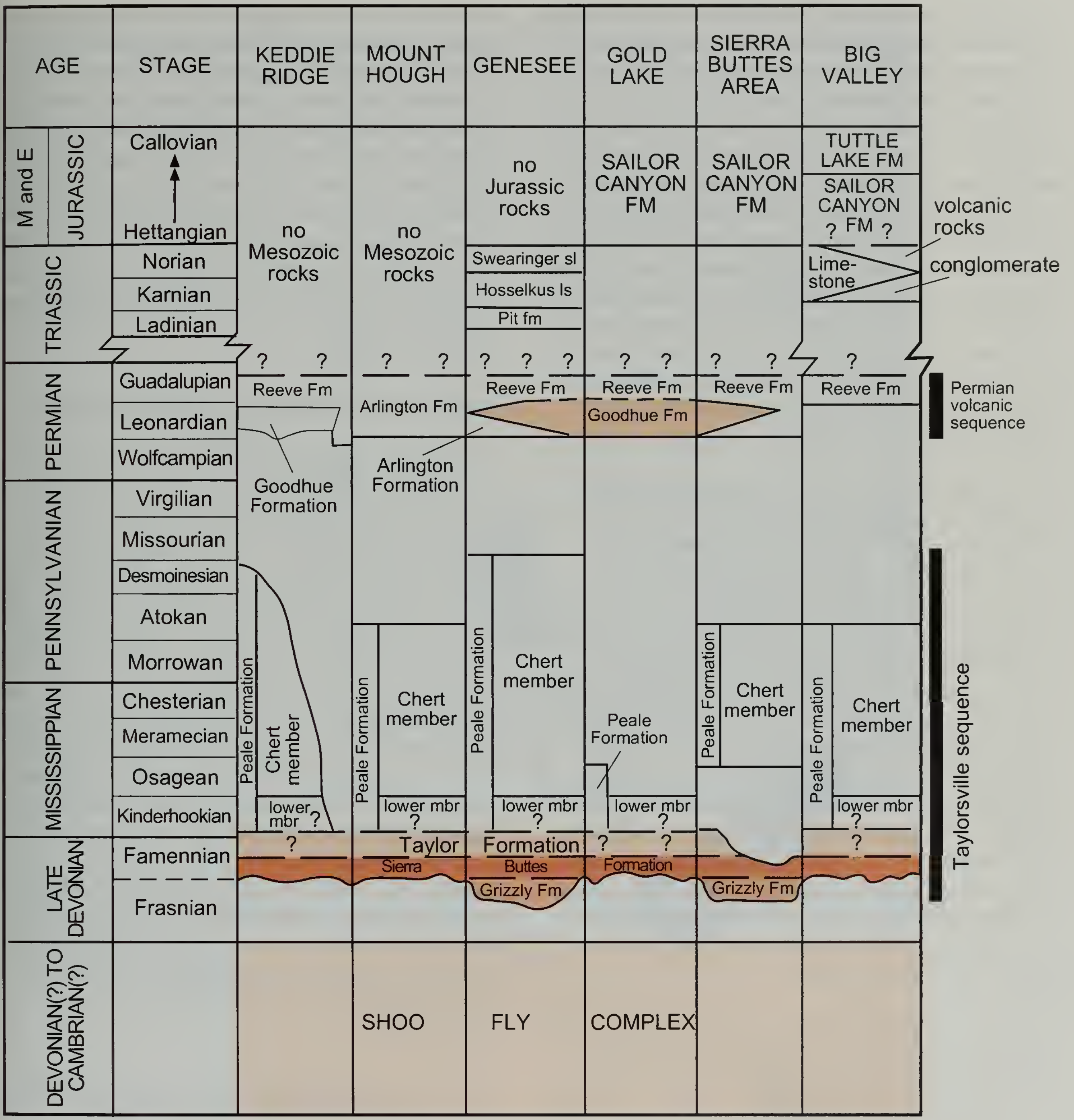

Figure 2. Stratigraphic columns in the Eastern Belt, arranged from northwest (Keddie Ridge) to southeast (Big Valley) along the strike; locations of columns are indicated by circled letters in Figure 1. Field trip is in the Gold Lake area. *From Hanson and others, 1996*; see also Harwood (1992).

Other major unconformities in the series of three, late Paleozoic and Jurassic, volcanic arcs were formed during late Pennsylvanian-early Permian time and during the late Permian and much of the Triassic (Figure 2). The latter probably represents the Sonoma orogeny, but the former, according to Harwood (1988), reflects uplift caused by crustal heating and extension related to early Permian basaltic volcanism (Goodhue Formation). This erosional unconformity developed on radiolarian cherts (chert member of the Peale Formation) that represent a long interval of volcanic quiescence and pelagic deposition (from early Mississippian to at least middle Pennsylvanian).

Estimates of relative abundance of volcanic rocks made by Harwood (1988) indicate that volcanism began with voluminous eruption of magmas of the Sierra Buttes Formation in the latest Devonian, continued at a high rate during accumulation of the Taylor Formation, but waned dramatically in the early Mississippian, with eruption of the lower, volcanic member of the Peale Formation. Permian volcanism produced only about half the amount of material recorded in either the Sierra Buttes or Taylor formation.

Neodymium isotopic ratios measured by Silva and others (this volume; initial epsilon Nd from -15 to -20) require substantial involvement of ancient continental crust in formation of the ini-tially erupted, dacitic Sierra Buttes magmas. Accordingly, it seems necessary to partially melt underlying Shoo Fly sedimentary rocks (sandstones, mudrocks)—largely derived from the North American craton, as noted above—to obtain the old continental crustal component. The basaltic magma required to pond beneath and partially melt the Shoo Fly rocks is obtained as upwelling asthenosphere initiates mantle melts consequent upon slab rollback (Silva and others, this volume). This mantle-derived component of the Devonian arc magma evidently became increasingly important with time, as involvement of the continental crustal component waned.

Andesite first appeared toward the close of Sierra Buttes volcanism, as subaqueous pyroclastic flows (Legler and others, 1991). Andesitic pillow lavas and penecontemporaneous sills in the Elwell Formation, and basaltic pillow lavas, crystal-lithic tuffs, and penecontemporaneous hypabyssal intrusions in the basal Taylor Formation soon followed (Brooks and others, 1982; Brooks, 1995). All rocks appear to be linked by high-level differentiation of previously mixed andesite (mixed mantle- and continental crust-derived melts). First, volatile-rich, essentially aphyric andesite erupted explosively from the top of the magma chamber (the pyroclastic flows); volatile-poor, aphyric andesite was next (Elwell Formation); and richly augite-phyric, cumulate basalt was last (basal Taylor Formation). Dacitic magma remained available at least until the close of Sierra Buttes volcanism, as one of the subaqueous pyroclastic flows (the Tamarack tuff, described later) is cut in many places by quartz-plagioclase porphyry. On the other hand, the early presence of basaltic magma is evidenced by abundant magmatic inclusions in many of the larger, dacitic, Sierra Buttes intrusions; disrupted mafic dikes occur in an intrusion near Snake Lake (Figure 3). Mixing of basaltic and dacitic magma was unavoidable.

METAMORPHISM AND DEFORMATION

Rocks of the Taylorsville sequence have undergone prehnite-pumpellyite- to low-greenschist-facies, regional metamorphism. Recrystallization was so thorough that, of the original crystalline constituents in basalts and basaltic andesites, only augite sometimes survived. Although grain boundaries in the finest rocks may be obliterated, much of the new mineral growth was mimetic—limited by original crystal and grain boundaries—so that rock textures tend to be faithfully preserved. Also, rock cleavage occurs only sporadically. For these reasons, the prefix "meta-" that should appear in rock names is omitted in this report. Accompanying metasomatism can be demonstrated on the mm- to dm-scale, at least. For example, relict plagioclase microlites occasionally consist of quartz instead of albite, and large epidote-rich patches (epidosite) in the interiors of andesitic pillows in the Elwell Formation can cause the whole-rock CaO content to rise to 17.5 wt.% (calculated volatile-free).

This regional metamorphism, and related deformation, has traditionally been attributed to a brief, late Jurassic (155+/-3 Ma), Nevadan orogeny (Schweickert and others, 1984). However, recent U-Pb zircon dating indicates that regional cleavage development actually occurred in middle Jurassic time (ca. 164-166 Ma) (Girty and others, 1995; Hanson and others, 1996). Further, Taylorsville sequence rocks in the area of this field trip (Figure 3) probably were thrice-metamorphosed. A large tract of andesitic to basaltic volcanic rocks in the Sierra Buttes, Elwell, and Taylor formations containing prehnite, pumpellyite, or both minerals extends southward from Deer Lake nearly 5 km to Young America Lake (Figure 3). Rocks north of Deer Lake were subjected to greenschist-facies metamorphism. The boundary between prehnite-pumpellyite- and greenschist-facies rocks is independent of formation contacts (indeed, it intersects contacts at a large angle), and cannot be related to granitic plutons. Since there exists at least scant textural evidence of sea-floor metamorphism in the prehnite-pumpellyite rocks (Brooks, 1992), I am inclined to agree with Howard Day (1992) that prehnite-pumpellyite metamorphism took place during late Devonian-early Mississippian construction and burial of the island arc. Day (1992) attributes the greenschist metamorphism to overprinting during the Nevadan orogeny. A small number of samples collected from the Sierra Buttes Formation south of Deer Lake and the Taylor Formation near Upper Salmon Lake (Figure 3) contains prehnite and actinolite, and may represent evidence of a transitional, prehnite-actinolite

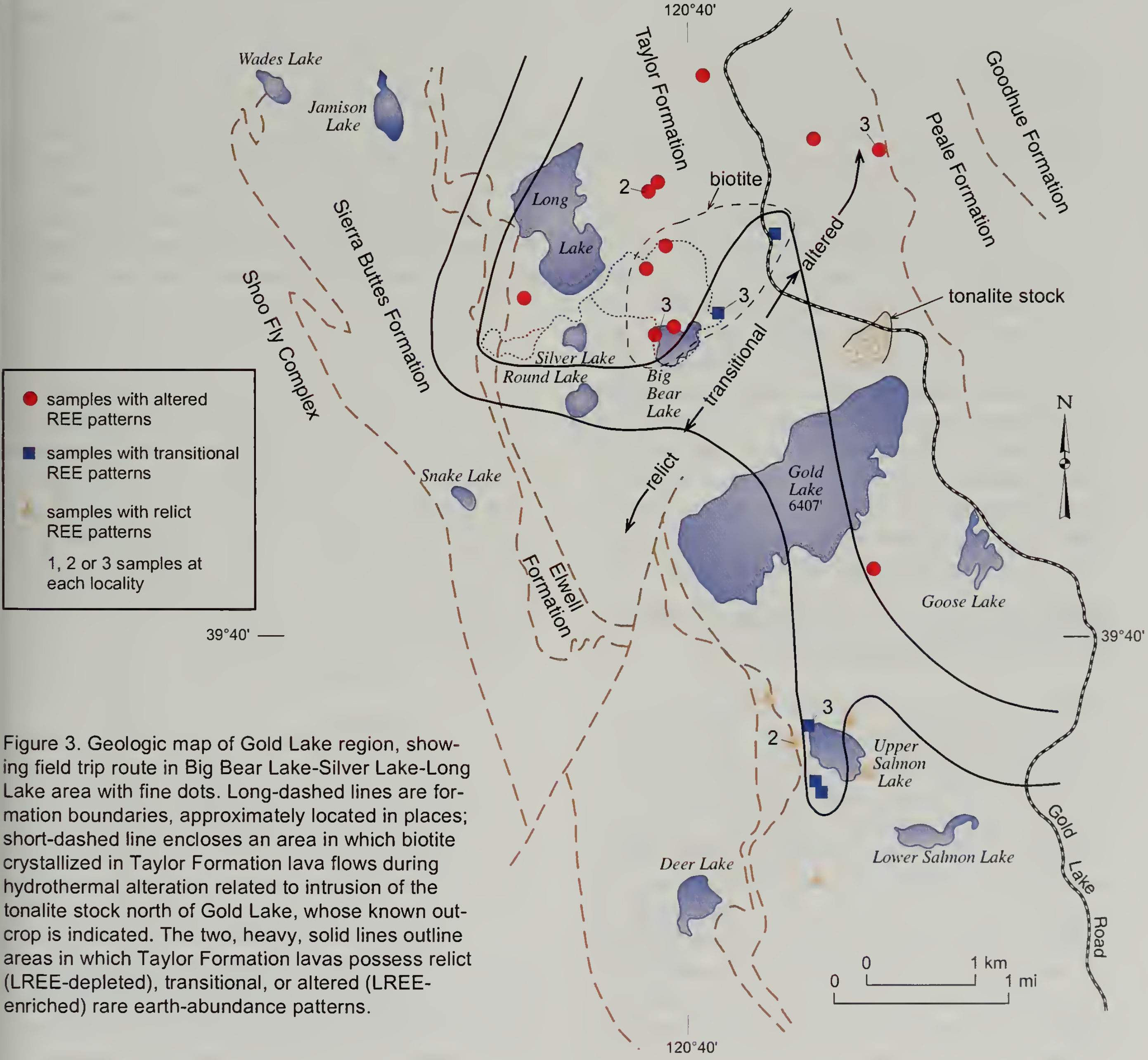

Figure 3. Geologic map of Gold Lake region, showing field trip route in Big Bear Lake-Silver Lake-Long Lake area with fine dots. Long-dashed lines are formation boundaries, approximately located in places; short-dashed line encloses an area in which biotite crystallized in Taylor Formation lava flows during hydrothermal alteration related to intrusion of the tonalite stock north of Gold Lake, whose known outcrop is indicated. The two, heavy, solid lines outline areas in which Taylor Formation lavas possess relict (LREE-depleted), transitional, or altered (LREE-enriched) rare earth-abundance patterns.

facies. The arrow in Figure 4 shows these facies relationships (the arrow is not meant to imply a facies series developed during a single metamorphic event). The presence of prehnite+actinolite-bearing mineral assemblages and absence of assemblages containing pumpellyite and actinolite suggest that metamorphism took place at relatively low pressures, below ca. 2.75 kbar (Figure 4). Lastly, rather impressive contact and hydrothermal metamorphism (described later) can be related to emplacement of a lower Cretaceous (120 Ma) tonalite stock north of Gold Lake (Figure 3; Lull, this volume).

Structural relationships in the Taylorsville sequence in the area of this field trip are quite simple. All rocks face easterly and nearly all dip fairly steeply in that direction, resulting in an upright homoclinal sequence apparently unbroken by large faults. This eastward tilting also took place in middle Jurassic time (Hanson and others, 1996). Macroscopic folds are present, but not prominent; mesoscopic folds in radiolarian cherts probably are in part the result of slumping of unlithified sediment. Steeply dipping cleavage, axial planar to some mesoscopic folds, is sporadically strongly developed, resulting in patchy distribution of phyllitic rocks in which original textures are difficult to discern. Clasts in relict beds intersected by the cleavage were reformed to become flattened in the plane of cleavage. These structures, except the synsedimentary folds, presumably are related to a middle Jurassic Nevadan orogeny.

PETROLOGY OF THE LATE DEVONIAN PART OF THE ISLAND ARC

I will now treat in more detail each of the three formations that together make up virtually all the volcanic part of the Taylorsville sequence. Most attention will be given to the Taylor Formation, since much of the field trip is devoted to it, and relatively little has been written about it in recent years (Durrell and D'Allura, 1977; Rouer and others, 1989). Little will be said about the Elwell Formation, as I previously have described it in detail (Brooks and others, 1982), and a measured section of it appears in Hanson and Schweickert (1986). The latter authors consider the Elwell Formation to be the upper member of the Sierra Buttes Formation north of the Middle Yuba River. However, I support Durrell and D'Allura (1977) in according it formation status. Little of the Sierra Buttes Formation will be seen on the field trip; Hanson (1991) provides a detailed description of it at the principal reference section in the Sierra Buttes arête north of Sierra City. Nevertheless, the Sierra Buttes Formation deserves more than passing mention because of the silicic composition of its lower part.

Many modern island arcs are compositionally zoned, both spatially and temporally. An early-formed, mostly basaltic, tholeiitic rock association, best developed nearest the trench, commonly is succeeded in mature island arcs by a largely andesitic, calcalkaline rock association, which forms over deeper parts of the subduction zone (Jakes and White, 1972). Volumetrically unimportant, alkalic, shoshonitic rocks may appear farthest from the trench. Attention was forcefully drawn to these relationships in a paper by Jakes and Gill (1970), in which the "island-arc tholeiitic series"

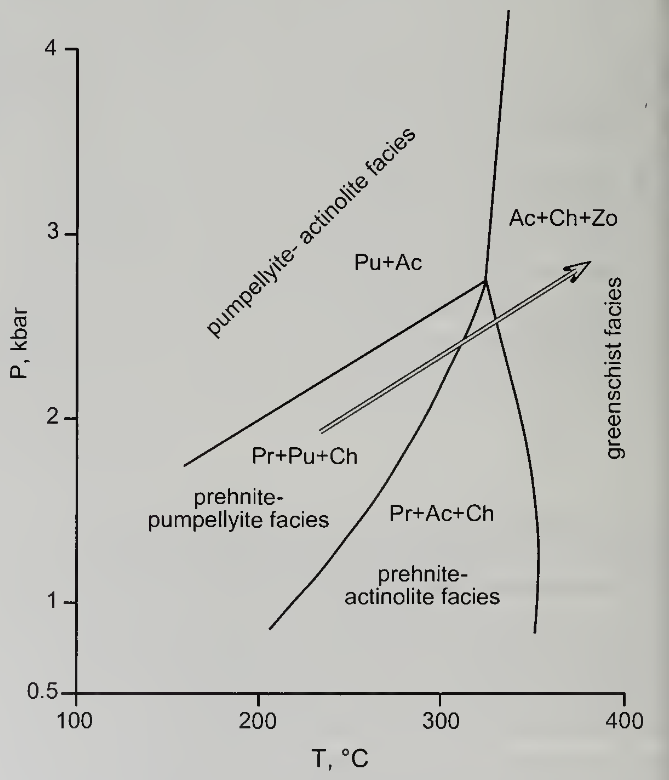

Figure 4. P-T conditions of regional metamorphism for iron-free minerals. *From Day, 1992, Figure 8.* Facies designations and P-T path for Taylorsville sequence in the Deer Lake area added by the writer. Pu=pumpellyite, Pr=prehnite, Ac=actinolite, Ch=chlorite, Zo=zoisite (Fe-poor epidote).

was named. The reader will discover below that, although lavas in the Elwell and Taylor formations were very largely tholeiitic, those comprising the lower part of the Sierra Buttes Formation—i.e., the basal part of the Devonian-Mississippian island arc —were calcalkaline. Of course, an explanation for this seeming anomaly has already been offered: the arc grew initially, not on oceanic crust, but upon oceanic sedimentary rocks derived from the ancient North American craton (then, as now, to the east).

Sierra Buttes Formation

Sierra Buttes Formation in the Sierra Buttes

According to Hanson (1991), the Sierra Buttes Formation in the high glaciated peaks of the Sierra Buttes largely comprises voluminous andesitic and silicic intrusive complexes. The former consists mostly of intrusive hydroclastic breccia, that is, unstratified, unsorted breccia resulting from injection of magma into wet sediment (silicic ash in this case). Large pillows are dispersed in the breccia. Also present are isolated-pillow breccias containing amoeboid pillows, and turbidites and debris-flow deposits representing redeposited intrusive hydroclastic breccia. The younger, silicic intrusive complex to the northwest comprises a number of coherent, massive to flow-banded, intrusive masses that grade into hydroclastic breccia at their margins; intrusive hydroclastic breccia containing large pillows; and isolated-pillow breccia bearing small amoeboid pillows equal to or less than 60 centimeters (cm) across. The andesites are plagioclase-phyric, the silicic lavas aphyric to quartz- and plagioclase-phyric dacite to rhyolite.

Tamarack Tuff

As noted by Hanson (1991), some of the silicic isolated-pillow breccia has been interpreted differently by Brooks and Legler (1989) and Legler and others (1991). They consider the isolated-pillow breccia to be the deposit of a subaqueous pyroclastic flow and the amoeboid pillows to be pumice lapilli and blocks in the deposit. They have mapped this distinctive deposit for 11 km along the strike, from Young America Lake northwesterly to a point overlooking Long Lake (Figure 3); the area mapped in common by both parties extends northerly for ca. 1.7 km from Young America Lake (compare Figure 2 in Hanson, 1991, and Figure 2 in Legler and others, 1991). Further comparison of Figure 11 in Hanson (1991) and Photo 1 in Legler and others (1991) will convince the reader that the two parties have examined the same rocks, informally named the Tamarack tuff for the exposures near the Tamarack Lakes (Legler and others, 1991).

The Tamarack tuff fulfills criteria for a subaqueous pyroclastic-flow deposit: 1) it was deposited subaqueously, in phosphatic radiolarian chert that probably accumulated in water <2 km deep; 2) it consists almost entirely of juvenile tephra (ca. 1/6 pumice blocks and coarse lapilli; ca. 5/6 less richly vesicular, fine lapilli and ash); 3) and it was emplaced by a mass flow (Brooks and Legler, 1989). The coarsest pumice blocks (>30 cm) are found among the southernmost outcrops near Young America and Tamarack Lakes, which are thought to be most proximal (Legler and others, 1991). Pumice blocks exhibit close-packed, spheroidal, relict microvesicles averaging ca. 0.07 mm across (51-68 vol.% vesicles in 8 point-counted blocks). Many blocks are equidimensional, but many others were drawn out into distinctive spindles conspicuously lineated parallel to their long axes (aspect ratio up to 16:1). Spindles commonly are deformed, even folded back on themselves isoclinally; such ductile behavior likely occurred during extrusion of pumice. As shown by truncated lineation, spindles were broken off at either end, and ends often are rounded, perhaps by abrasion during transport in the mass flow (Photo 1).

Pumice blocks are essentially aphyric, most thin sections intersecting only a few relict microphenocrysts of plagioclase, titanomagnetite, and embayed quartz; fresh clinopyroxene occurred in just three blocks. Relict plagioclase microlites and several millimeter (mm)-long elongated vesicles typically are strongly aligned, presumably by extrusion of viscous pumice. Original glass is evidenced by the perfectly round shape of many microvesicles, and occasional quench features of plagioclase microlites (notched ends of laths, rare hopper crystals). Pumice blocks are set in a tuffaceous matrix comprising nearly aphyric, richly microlitic, well-

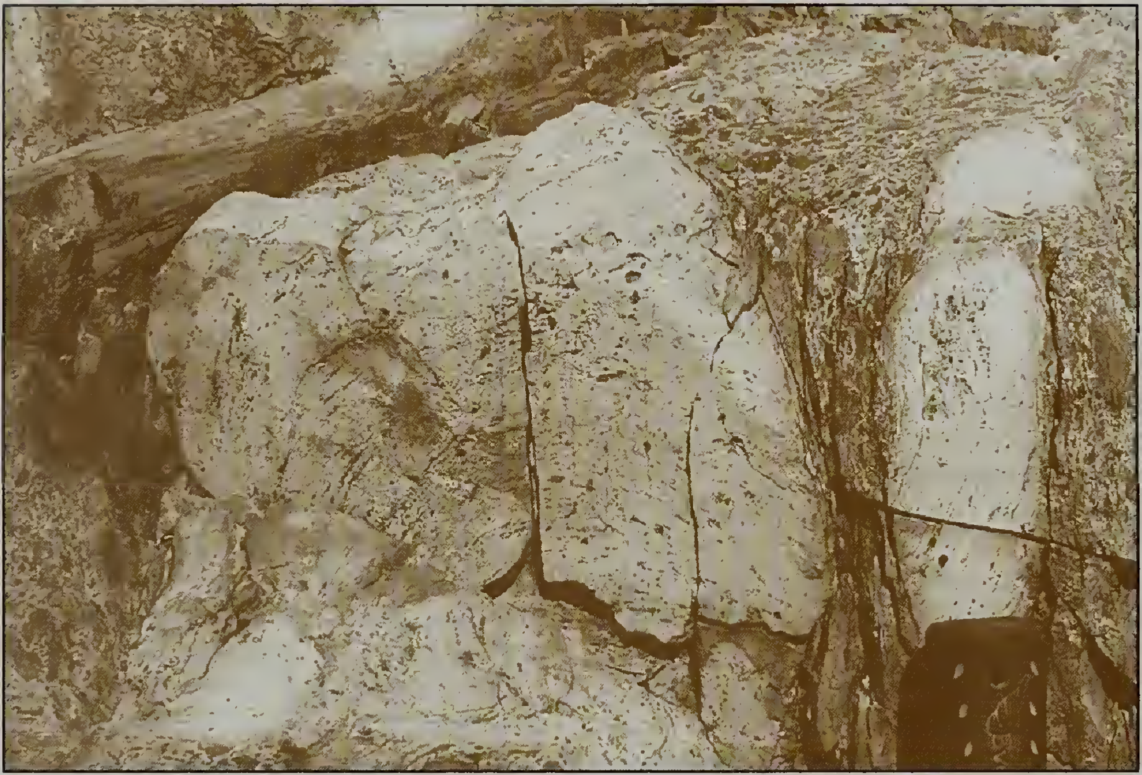

Photo 1. Pumice blocks in subaqueous pyroclastic-flow deposit (Tamarack tuff) east of Tamarack Lakes. Truncation of lineation at edges of blocks is particularly apparent in the smaller rounded block beneath the sledge handle. *Photo by E.R. Brooks.*

sorted, coarse ash and fine lapilli. The latter fragments are equant or elongated, and often blocky or three-cornered; subaqueous eruption of tephra is indicated.

Pumice blocks were selectively silicified and phosphatized. Microvesicles largely are filled with quartz, and 12 of 27 pumice blocks contain over 1 wt.% P_2O_5 (1.2-5.2 P_2O_5). (PO_4)-rich seawater evidently entered vesicles upon deposition of the mass flow; the phosphorus now resides in metamorphic apatite seen only in back-scattered electron images (P. Schiffman, written communication, 1991). The composition of the average tuffaceous matrix sample (Table 1) approximates that of the andesite originally erupted (Brooks and Legler, 1989).

Tamarack tuff mineral assemblages indicate metamorphism at the boundary between the prehnite-pumpellyite and greenschist facies. One-fifth of the samples examined petrographically, all from exposures south of Deer Lake, contain both prehnite and pumpellyite (quartz+albite+chlorite+epidote+ prehnite+pumpellyite+sphene+/-calcite+/-pyrite+/-white mica+/-apatite). Samples from the southernmost outcrop mapped, at Young America Lake, comprise the greenschist-facies assemblagequartz+albite+chlorite+epidote+actinolite+ sphene+pyrite+/-white mica+/-stilpnomelane, and, as noted earlier, a similar change from prehnite-pumpellyite- to greenschist-facies also occurs north Deer Lake.

Hanson (1991; p. 812, 813) argues that the pumice blocks must be pillows because "angular hyaloclastite shards between the pillows clearly were derived by in situ fragmentation of pillow margins...," and "...concomitant granulation of the chilled margins produces the hyaloclastite matrix between pillows." However, the tuffaceous matrix of the subaqueous pyroclastic-flow deposit, ca. 5/6 of the entire deposit, seems far too voluminous to have been produced only by granulation of pillow margins.

As pointed out above, the Tamarack tuff is of andesitic, not silicic composition. Hanson (1991; Table 1, sample S-108, and p. 812) implies that the chemical analysis of a coherent rhyolitic intrusive mass that "...contribut[ed] angular debris [and pillows] to the adjacent [isolated-pillow] breccia" also represents the composition of the breccia. Sample S-108 is surely rhyolitic (78.4 wt.% SiO_2), but as Hanson himself notes (1991, p. 812), "...is unusually phyric...," so that the intrusive mass could hardly have furnished the "pillows" (pumice blocks) in the adjacent deposit, which are essentially aphyric everywhere we have seen them. My interpretation of the relationships described by Hanson is straightforward intrusion of the phyric rhyolite body into already lithified Tamarack tuff, with autobrecciation of the margin of the former. Other such intrusions in the area display sharp contacts with the Tamarack tuff, and their margins exhibit both local autobrecciation and flow layering rigorously parallel to contacts.

Sierra Buttes Formation Northwest of the Sierra Buttes

As the Sierra Buttes Formation is followed northwesterly toward Jamison Lake from the Sierra Buttes (Figure 3), one continues to encounter

Table 1. Major-element, whole-rock chemical analyses of subqueous pyroclastic flows, lava flows, and hypabyssal intrusions in the Sierra Buttes Formation.

	Tamarack tuff[1]		Lithic-rich subaqueous pyroclastic flow[3]	
	Average of 19 samples of tuffaceous matrix	Average of 27 pumice blocks	Average of 2 samples of tuffaceous matrix	Average of 2 pumice blocks
SiO_2	59.76	71.76	61.60	82.82
Al_2O_3	16.39	11.64	16.19	9.00
TiO_2	0.71	0.47	0.71	0.21
$Fe_2O_3^T$	10.85	4.60	10.16	2.27
MgO	4.48	1.54	2.73	0.14
CaO	4.46	4.19	5.07	1.40
Na_2O	2.45	4.09	2.75	3.87
K_2O	0.61	0.42	0.57	0.18
P_2O_5	0.12	1.22	0.08	0.08
MnO	0.17	0.07	0.14	0.03
	Andesite	Dacite	Andesite	Rhyolite

	Average of core and rim of one pillow, Peck Mine[3]	Lava flow at Jamison Lake[3]		Average of 6 hypabyssal intrusions[2]
SiO_2	67.93	79.77	SiO_2	76.56
Al_2O_3	13.86	11.80	Al_2O_3	12.17
TiO_2	0.88	0.07	TiO_2	0.29
$Fe_2O_3^T$	8.20	1.57	Fe_2O_3	1.84
MgO	1.29	0.95	FeO	1.22
CaO	2.24	0.55	MgO	0.86
Na_2O	4.89	3.07	CaO	1.97
K_2O	0.34	2.17	Na_2O	3.48
P_2O_5	0.27	0.03	K_2O	1.57
MnO	0.10	0.02	MnO	0.04
	Dacite	Rhyolite		Rhyolite

All analyses recalculated to 100 wt.%, volatile-free; $Fe_2O_3^T$ = all Fe calculated as Fe_2O_3; rocks named using the TAS classification (Le Maitre and others, 1989).

1. XRF analyses by June Legler at Earth Sciences Board, U.C., Santa Cruz, 1982, and by X-ray Assay Laboratories Ltd., 1986.
2. $Fe_2O_3 = TiO_2 + 1.5$ (Irvine and Baragar, 1971). INAA and XRF analyses at Lawrence Livermore National Laboratory, 1978, except SiO_2 by XRF at X-ray Assay Laboratories Ltd., 1979.
3. ICP analyses by Activation Laboratories Ltd., 1998.

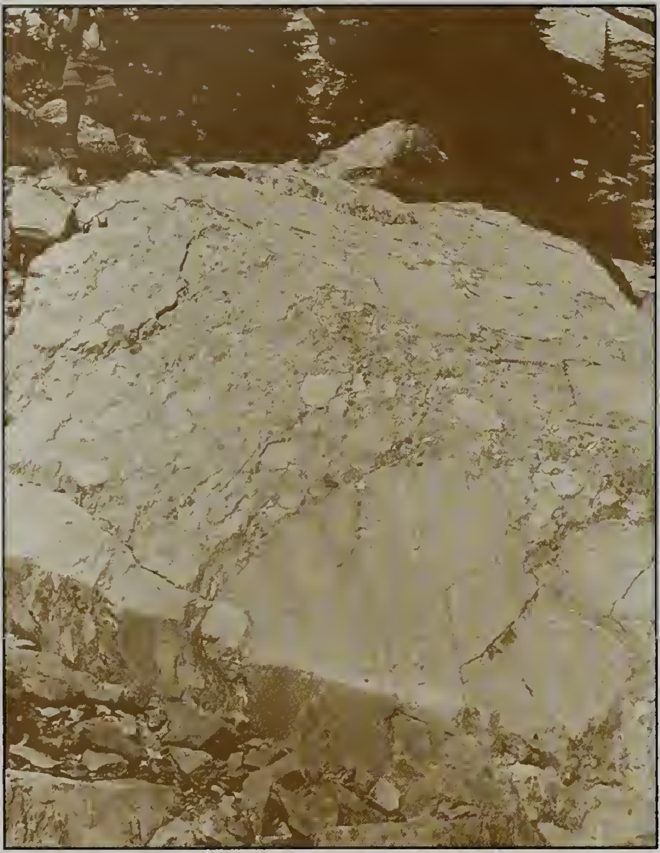

Photo 2. Silicic Sierra Buttes autobreccia west of Silver Lake. Large flow-layered clast in foreground is oriented differently from other such clasts, indicating flow of the breccia during formation. Field assistant in left background for scale. *Photo by E.R. Brooks.*

the relatively large, coherent, silicic, hypabyssal intrusions mapped by Hanson (1991). Indeed, they are known to occur at least as far north as Jamison Lake, where Silva and others (this volume) find they intrude rocks as young as the Elwell Formation. Where contacts with adjacent bedded rocks are exposed, as at Deer Lake, where a quartz-plagioclase porphyry cuts turbidites, they may be both concordant and discordant. so that the shapes of these intrusions frequently are unclear; a few are unambiguously thick columnar-jointed sills (Silva and others, this volume). Much of the Deer Lake intrusion is coarsely autobrecciated, producing monolithologic breccia often seen elsewhere. Photo 2, for example, illustrates such breccia west of Silver Lake (Figure 3), where occasionally flow-layered clasts like that in the foreground are differently oriented in the breccia. Size of the subangular to subrounded clasts shows remarkable variation, from a few centimeters to a meter or more. This breccia clearly experienced movement during formation.

Also present northwest of the Sierra Buttes, besides the Tamarack tuff, is one or more other subaqueous pyroclastic-flow deposits; flow-laminated, autobrecciated lava flows (and domes?), as at Jamison and Wades lakes (Silva and others, this volume); turbidites and debris-flow deposits; phosphatic chert; and rare pillow lava and related broken- and isolated-pillow breccia. The andesitic subaqueous pyroclastic-flow deposits are stratigraphically the highest units in the Sierra Buttes Formation (as narrowly defined, equating Member C of Hanson and Schweickert (1986) to the Elwell Formation).

I have examined geochemically and petrographically samples collected from several of the large silicic intrusions. The average of six chemical analyses appears in Table 1, and confirms the highly siliceous, rhyolitic nature of these intrusions. The magma from which they solidified was not very enriched in Shoo Fly partial melt, however, for Silva and others (this volume) show that the intrusions possess much less negative initial epsilon Nd values (0 to -5); indeed, they consider the magma to be a product of fractionation of mantle-derived mafic melt, previously mixed with silicic partial melt.

Most of the rhyolitic intrusions are prominently quartz- and plagioclase-phyric, relict quartz phenocrysts making up 6.6-23.2 vol.% of the porphyries, relict plagioclase phenocrysts 9.4-19.3 vol.%. Relict mafic phenocrysts occupy 0-3.2 vol.% of the rocks, relict titanomagnetite microphenocrysts 0-0.6 vol.%. The porphyry matrix (59.3-81.7 vol.%), sometimes so fine-grained as to appear cherty in hand sample, provides few clues to its original nature: the abundant plagioclase microlites characteristic of more mafic Sierra Buttes rocks are inconspicuous, and a single sample displayed relict spherulites up to 0.3 mm in diameter.

The relict quartz phenocrysts, which reach 1 cm or more in some intrusions, frequently are resorbed, exhibiting rounding and embayment of crystal margins. In sharp contrast, the plagioclase phenocrysts invariably are euhedral. Plagioclase microphenocrysts tend to cluster, with mafic and titanomagnetite microphenocrysts, as glomerocrysts. Plagioclase is replaced by albite (An_{0-7}), calcite, and several other minerals in various combinations and proportions. Square crystals of titanomagnetite up to ca. 0.4 mm across now consist of leucoxene. Some of the magnetite, at least, was of early generation, appearing as inclusions in plagioclase and quartz phenocrysts; in turn, the magnetite may enclose euhedral apatite crystals. Finally, four samples contained mafic phenocrysts completely replaced by aggregates of epidote, chlorite, white mica, calcite, sphene, and green stilpnomelane(?) in various combinations and proportions. The mafic phenocrysts, certainly pyroxene in one sample, contain inclusions of magnetite, apatite, and zircon.

Though potassium-feldspar phenocrysts might be expected to appear in these silica-rich rhyolites (73.9-80.3 wt.% SiO_2), and though Rouer and others (1989) claim that biotite was the only primary mafic phase in Sierra Buttes rhyolites, I have seen no evidence of either mineral. Wilson (1989) points out that, in calcalkaline rhyolites of island arcs, alkali feldspar is absent and biotite occurs only sporadically. In any case, some of these rocks seem impossibly silica-rich, and probably experienced silicification at some point in their history; the reader doubtless has noted that the more silicic Sierra Buttes rocks were referred to as dacites earlier in this report, based on the nearly ubiquitous co-occurrence of quartz and plagioclase phenocrysts.

The only occurrence of pillow lava north of the Sierra Buttes known to me is that at Peck Mine, west of Upper Salmon Lake (Figure 3). Large, close-packed, spheroidal, incipiently brecciated pillows are richly amygdaloidal, with quartz amygdules up to ca. 5 cm long distributed throughout them. Amygdules near pillow margins are strongly flattened parallel to the margins. Pillows are essentially aphyric; clusters of relict plagioclase and titanomagnetite microphenocrysts occur, but quartz phenocrysts are absent. Pillow matrices are charged with relict plagioclase microlites, aligned parallel to pillow margins; the original texture was hyalopilitic to pilotaxitic. The average analysis of samples collected from the core and rim of a single pillow appears in Table 1. The high Na_2O content probably reflects the abundance of plagioclase microlites. Although the pillow is dacitic according to the total alkalies-silica ("TAS") classification of volcanic rocks (Le Maitre and others, 1989), the SiO_2 content is elevated by the copious quartz amygdules, and the pillow lava doubtless was originally andesitic.

Finally, let's look at two units that represent the stratigraphically lowest and highest parts of the Sierra Buttes Formation. The basal member of the formation in the Jamison Lake-Wades Lake area comprises autobrecciated, flow-laminated, sparsely phyric lava flows (Silva and others, this volume). A chemical analysis appears in Table 1, and the reader will find that it is similar to the average of the silicic hypabyssal intrusions. Though rhyolitic in the TAS classification, Silva and others (this volume) refer to the flows as dacitic, for the same reason that I refer to the hypabyssal intrusions as dacitic, that is, the co-occurrence of quartz and plagioclase phenocrysts. The stratigraphically highest unit in the Sierra Buttes Formation northeast of Deer Lake is a lithic-rich subaqueous pyroclastic-flow deposit. The average analysis of two samples of the tuffaceous matrix of this deposit (Table 1) is similar to that of the lithic-poor Tamarack tuff. However, the pumice blocks are even more silicified than those in the Tamarack tuff, having more than 21 wt.% more silica than the matrix (Table 1)! This resulted in striking dilution of all the other oxides save Na_2O and P_2O_5. Compared to pumice blocks in the Tamarack tuff, however, P_2O_5 is extremely low; it is evident this subaqueous pyroclastic flow had little involvement with the (PO_4)-rich seawater. The accessory lithic blocks consist of various quartz-plagioclase porphyries (74.2-80.2 wt.% SiO_2). What was different about emplacement and diagenesis of this subaqueous pyroclastic flow?

How much of the Sierra Buttes Formation is calcalkaline? In previous papers (Brooks and Coles, 1980; Brooks and others, 1982), I have suggested, based on flimsy evidence, that the entire formation is calcalkaline. The results of recent, more complete rare earth element (REE) analyses are presented in Figure 5. Included in Figure 5 for comparison purposes are dashed-line envelopes enclosing chondrite-normalized rare earth-abundance patterns for modern, island-arc, tholeiitic andesites and dacites. Except near the tonalite stock at Gold Lake (Figure 3), the REEs remained immobile during metamorphic events affecting the Devonian-Mississippian arc (Brooks and others, 1982). It is clear from the upper half of Figure 5 that the silicic lava flows that rest directly upon the unconformity with the Shoo Fly Complex at Jamison and Wades lakes are calcalkaline, the light rare earth elements (LREEs) being strongly enriched relative to those in tholeiitic dacites. Indeed, for the elements from Sm to La, the abundance pattern for sample 3-97 is like those for active continental margin, Andean, calcalkaline dacites. This reinforces the hypothesis that the earliest, silicic Sierra Buttes magmas involved partial melts of continental crust-derived, Shoo Fly sedimentary rocks. Silva and others (this volume) provide additional, identical abundance patterns.

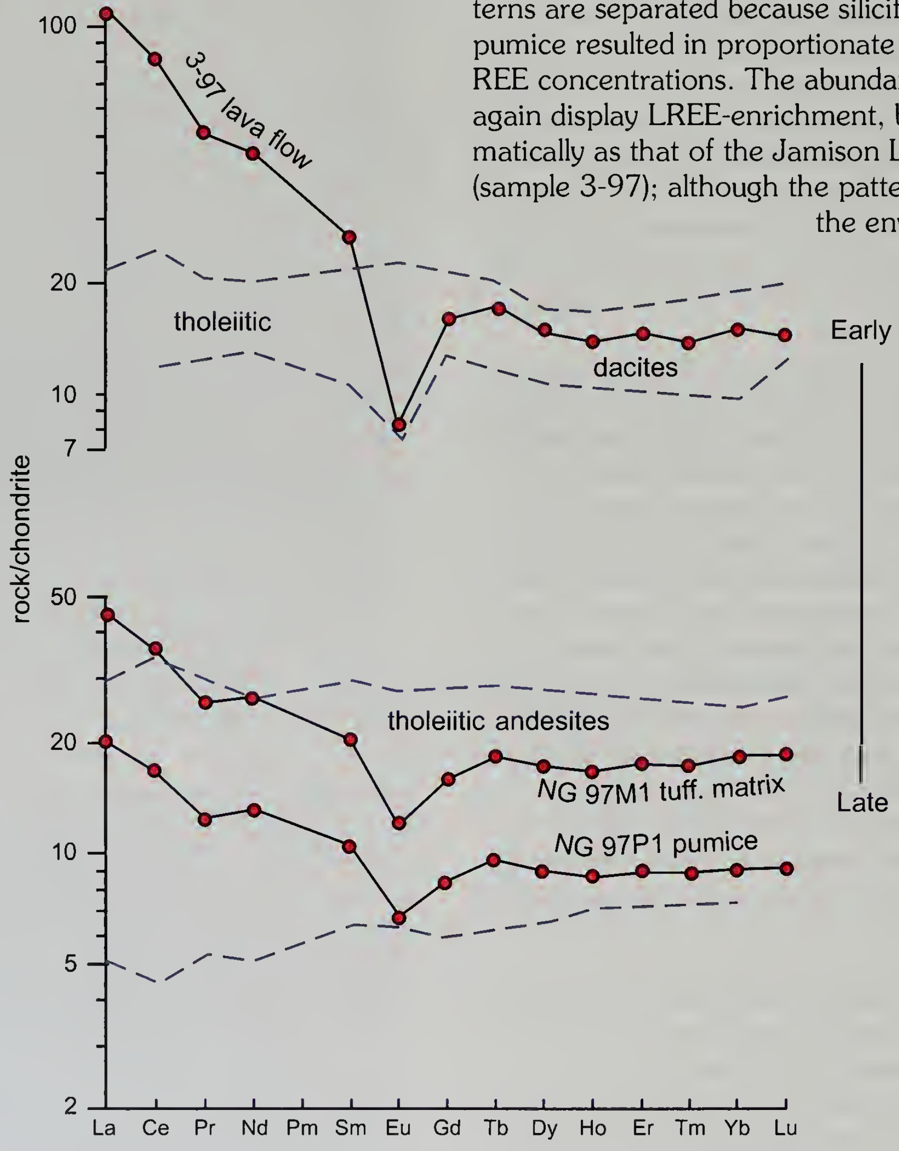

Figure 5. Chondrite-normalized rare earth-abundance patterns for early Sierra Buttes, calcalkaline, silicic lava flow at Jamison Lake (sample 3-97), and tuffaceous matrix and a pumice block in late Sierra Buttes, andesitic, lithic-rich, subaqueous pyroclastic-flow deposit northeast of Deer Lake (samples NG97M1 and NG97P1). Dashed-line envelopes enclose rare earth patterns for a number of modern, island-arc, tholeiitic dacites and andesites. *ICP-MS analyses by Activation Laboratories Ltd., 1998.* All REE concentrations in this report are normalized to the chondritic values of Boynton (1984).

Are the late Sierra Buttes andesites also calcalkaline? The lower half of Figure 5 shows abundance patterns for tuffaceous matrix and a pumice block in the lithic-rich subaqueous pyroclastic-flow deposit northeast of Deer Lake. The parallel patterns are separated because silicification of the pumice resulted in proportionate lowering of its REE concentrations. The abundance patterns again display LREE-enrichment, but not as dramatically as that of the Jamison Lake lava flow (sample 3-97); although the patterns remain within the envelope for tholeiitic andesites, the envelope is flat, like that for tholeiitic dacites. Legler (1983) thought that the Tamarack tuff might be tholeiitic, based on major-element oxide and petrographic features, but emphasized the inconclusiveness of her opinion. I was bolder in a recent abstract (Brooks and Schiffman, 1996), stating that the subaqueous pyroclastic flows are tholeiitic. Thus, although the REE patterns in Figure 5 suggest that the pyroclastic flows are mildly calcalkaline, mixing of calcalkaline, dacitic and tholeiitic, basaltic magmas to obtain andesitic magma having both calcalkaline and tholeiitic characteristics would be expected. However, by the time Elwell lavas were being erupted, any calcalkaline signature was absent. This is shown by their conspicuously LREE-depleted abundance patterns (Figure 6), and by Nd- and Sr-isotopic ratios that indicate little, if any, continental crustal involvement (Silva and others, this volume).

Elwell Formation

Following explosive eruption of the subaqueous pyroclastic flows comprising the uppermost Sierra Buttes Formation, effusive volcanism produced pillow lava and penecontemporaneous sills in the overlying Elwell Formation. The aphyric tholeiitic andesite in the Elwell Formation is somewhat less aluminous, and more Fe- and Ti-rich than the Sierra Buttes andesite (Brooks and others, 1982). Swarms of sills, individually up to ca. 85 m thick, occur throughout the 13-km length of Elwell Formation mapped, but the pillow lava is of limited extent, best viewed on the ridge northwest of Upper Salmon Lake. The spheroidal pillows, commonly 1 meter (m) across, are tightly molded to one another and cemented by radiolarian chert (Photo 3). A distinctive feature is closely spaced, thin shells of microvesicles concentric with the pillow margins (bottom right corner of Photo 3).

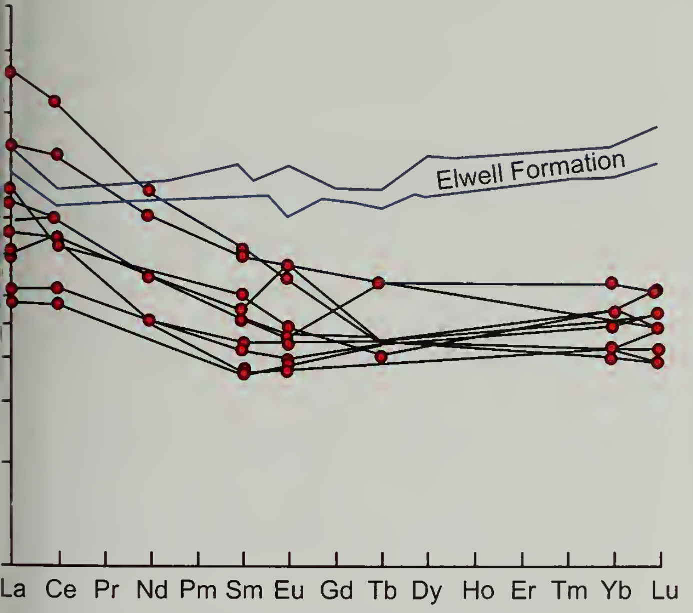

Figure 6. Chondrite-normalized rare earth-abundance patterns for ten samples of basalt and basaltic andesite collected from seven early Taylor, augite-phyric, hypabyssal intrusions. Envelope encloses abundance patterns for six tholeiitic pillow lavas and sills in the andesitic Elwell Formation. *INAA analyses by Activation Laboratories Ltd., 1994 (eight samples) and at Lawrence Livermore National Laboratory, 1978 (two samples, and the six Elwell samples).*

The Elwell Formation also is characterized by relatively abundant, phosphatic, carbonaceous, radiolarian chert, and interbedded turbidites and chert-matrixed debris-flow deposits rich in silicic detritus derived from the underlying Sierra Buttes Formation (Brooks and others, 1982). Some of the latter rocks may contain juvenile long-tube pumice, but I have been sure about the presence of pumice only in turbidites and debris-flow deposits near Mountain Mine in the Sierra Buttes. There Hanson and Schweickert (1986) measured the 360 m of section that comprise their Member C of the Sierra Buttes Formation (my Elwell Formation). Indeed, their estimates of the pumice content of the coarse-grained mass-flow deposits that make up most of the measured section range up to 100%, and pumice comprises the bulk of most such deposits. It seems certain that a pyroclastic component entered the Elwell Formation as the Sierra Buttes is approached from the north, lending credence to the notion that the Sierra Buttes peaks mark an important mid-Famennian vent area.

Finally, the Elwell Formation houses an unusual rock type, peperite, which formed when andesitic sills encountered still-moist, incompletely lithified chert not far beneath the sea floor (Brooks and others, 1982). I will describe the mode of formation when we visit an exposure at Stop 9 on the field trip.

I probably need to defend our continued use of the Elwell Formation (Durrell and D'Allura, 1977), which has been abandoned by other workers because of its alleged only local occurrence (Hanson and Schweickert, 1986; Harwood, 1992). We continue to use the formation for mapping purposes because it consists of such a distinctive, yet relatively thin assemblage of diverse rocks (not just black chert) that rather nicely separates the Sierra

Buttes Formation from the Taylor Formation. We find it ironic that the same workers who doubt its utility have championed use of the even more discontinuous Grizzly Formation.

Taylor Formation

The base of the Taylor Formation west of Upper Salmon Lake may be placed either at the bottom of a pebbly sandstone rich in silicic debris derived from the Sierra Buttes Formation or at the base of overlying, augite-phyric, pillow lava (Brooks, 1992). The epiclastic pebbly sandstone overlies the disrupted, pillowed top of a thick Elwell sill (Brooks and others, 1982). Fragile projections extend from decapitated pillows into the base of the pebbly sandstone, which contains fragments of the subjacent pillows, and displays reverse grading of the coarser, mostly dacitic clasts. Smoky-gray quartz and white feldspar grains derived from quartz and plagioclase phenocrysts choke the sand-size fraction of this high-density turbidite or debris-flow deposit. Since this deposit is so much like others rich in silicic detritus in the Elwell Formation, it may be best to place the contact with the Taylor Formation at the base of the immediately overlying, augite- phyric pillow lava (Photo 4), which marks the first appearance in the Devonian-Mississippian island arc of lavas rendered basaltic and basaltic andesitic by high contents of augite phenocrysts.

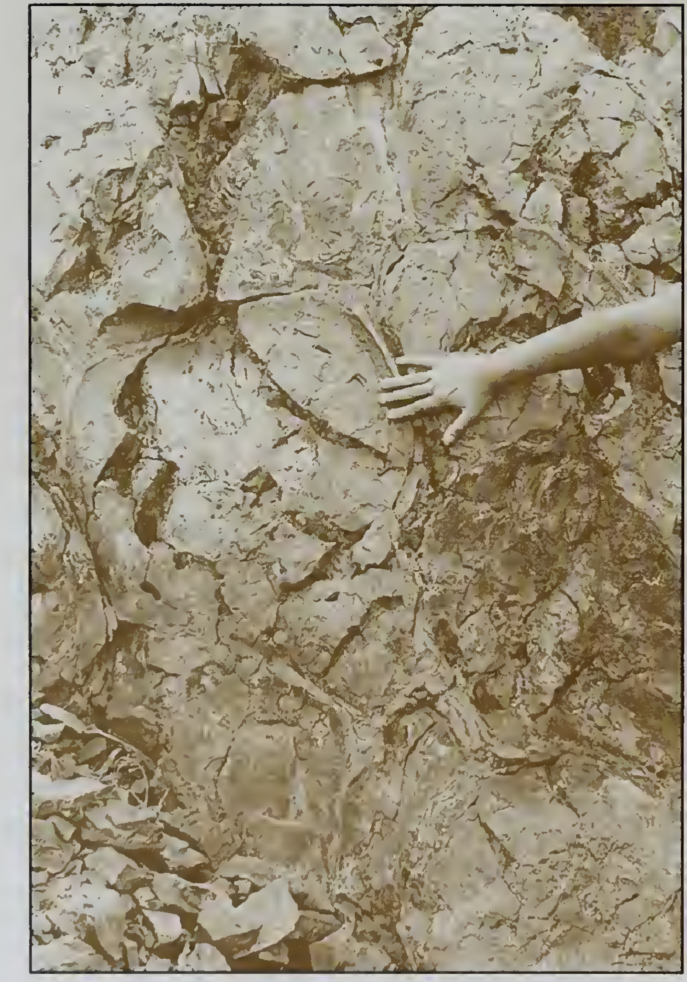

Photo 3. Pillow lava in the Elwell Formation northwest of Upper Salmon Lake. Scant amounts of chert cement the close-packed aphyric pillows. *Photo by E.R. Brooks.*

Richly augite-phyric sills and other hypabyssal intrusions (12-51 vol.% augite) also are present in the lower Taylor Formation, and in the underlying Elwell Formation, where they intrude the aphyric andesite sills and pillow lavas, and enclose xenoliths of them (Brooks and Schiffman, 1996). Farther northwest, near Silver Lake, the lower Taylor Formation is largely occupied by well-bedded, crystal-lithic tuffs and lapilli tuffs rich in augite and plagioclase, again deposited by turbidity currents and debris flows (Brooks, 1995). "Round-bubble" pumice is recognized in places. Peperite resulted where the tuffs were intruded by one of the hypabyssal intrusions, so the tuffs and intrusions are known to be broadly contemporaneous (Brooks, 1995; we will see the peperite at Stop 6 on the field trip). All of the augite-rich basaltic to basaltic andesitic rocks, then—hypabyssal intrusions, tuffs, and pillow lavas—appeared after cessation of Elwell andesitic volcanism. They are thought to represent the final draining, perhaps in two stages, of the differentiating, high-level magma chamber that had previously erupted Sierra Buttes subaqueous pyroclastic flows and Elwell sills and pillow lavas (Brooks and Schiffman, 1996). The augite phenocrysts represent crystals that had accumulated in the lower reaches of the magma chamber, probably following explosive eruption of the pyroclastic flows, when a precipitous drop in water pressure would have provoked crystallization.

Augite-phyric Hypabyssal Intrusions

Sills, dikes, and less easily characterized hypabyssal intrusions of strikingly augite-phyric

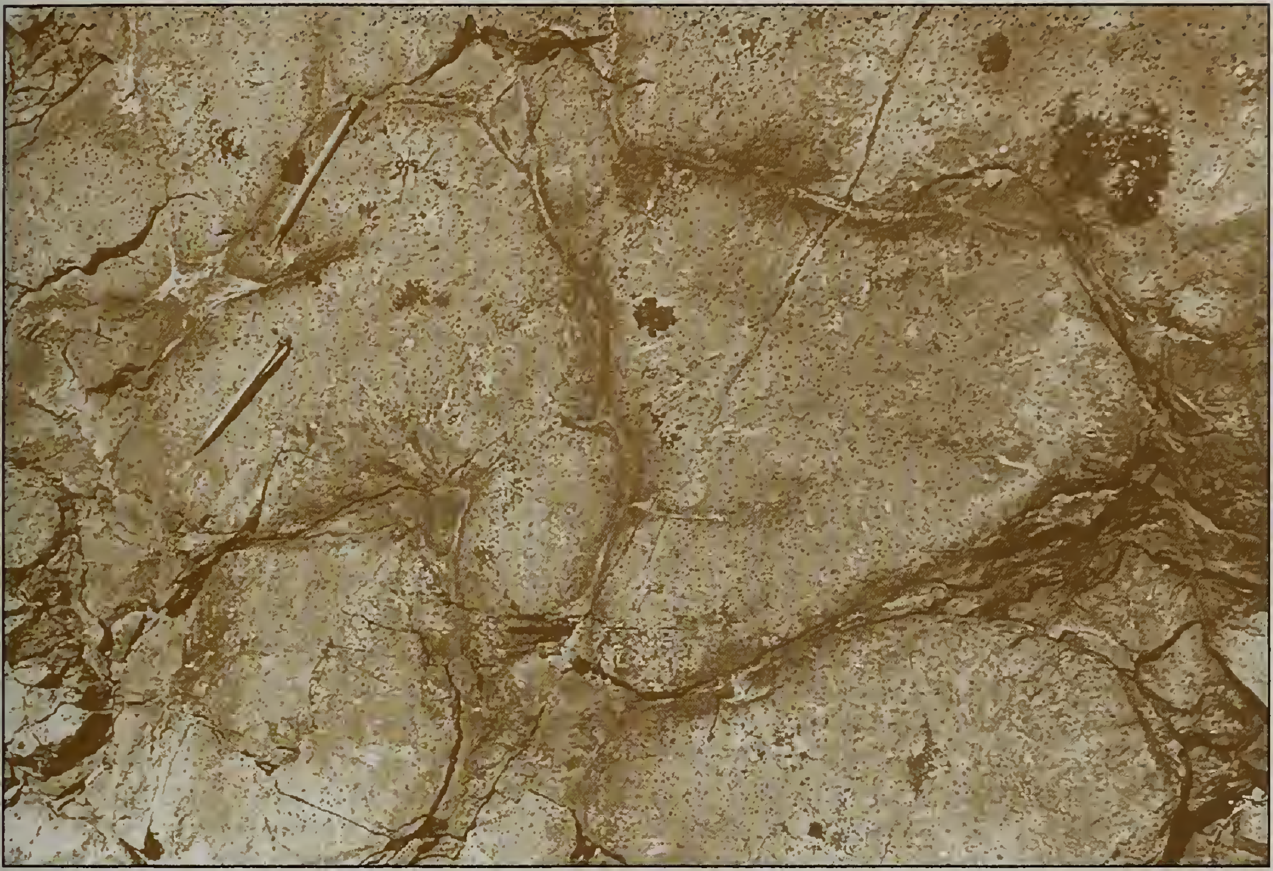

Photo 4. Closely-packed pillows at the base of the Taylor Formation west of Upper Salmon Lake. Note the distinctive elongated quartz amygdules around the outer parts of pillows. One of the pencils points out a portion of a pillow pressed back against itself. *Photo by E.R. Brooks.*

basalt and basaltic andesite intrude the island-arc sequence to as much as 300 m above the base of the Taylor Formation west of Silver Lake (the 300 m figure, however, must be reduced an unknown amount to account for inflation of the section by the intrusions). Intrusions in the Long Lake-Round Lake area are most strongly recrystallized (Figure 3), whereas those farther south, in the Upper Salmon Lake-Deer Lake area, where greenschist metamorphism gave way to prehnite-pumpellyite metamorphism, contain largely unreplaced, nearly pristine augite.

The augite phenocrysts are of greatest interest (see photomicrograph on page ii of this volume), and will be described in detail shortly, but first let's examine other petrographic and chem-ical features of these rocks. Modes of 11 samples reveal 12.1 to 51.1 vol.% of relict augite phenocrysts (average is 31.6 vol.%) and 0- 16.5 vol.% of relict plagioclase phenocrysts (average is 5.1 vol.%). Matrix makes up 44.7 -71.9 vol.%, and amygdules consisting of chlorite+/-quartz+/-calcite comprise 1.2 -6.1 vol.% of only three samples. The plagioclase phenocrysts, to ca. 2 mm long, were replaced, in various combinations and proportions, by epidote, white mica, calcite, and albite. Relict platy plagioclase microlites occur abundantly in the matrix of some samples, as do relict clinopyroxene microlites. Relict titanomagnetite microphenocrysts, replaced by sphene or leucoxene, are found in some samples. One sample had a relatively coarse (ca. 0.5 mm grains) intergranular matrix. Point-counting sometimes was made difficult by mysterious patches of actinolite+chlorite+/-epidote+/-calcite+/-quartz+/-sphene. These eventually were determined to have been augite glomerocrysts, nearly always completely replaced, even in samples containing pristine augite phenocrysts.

The average composition of seven of the augite-phyric hypabyssal intrusions appears in Table 2. When plotted in the TAS classification, the average analysis yields a basaltic andesite. The intrusions are found to be tholeiitic using major-element and norm criteria of Irvine and Baragar (1971). An island-arc tholeiite origin is indicated when concentrations of the immobile trace elements Ti, V, Y, and Zr are plotted in standard discrimination diagrams (although Zr is low—average of 21 ppm—due to accumulation of the augite phenocrysts, and the compatible element Cr is high—average of 458 ppm—for the same reason). Furthermore, as will be shown below, electron-microprobe analysis of unreplaced augite phenocrysts indicates the intrusions are island-arc tholeiites.

With such seemingly overwhelming evidence for an island-arc tholeiite origin, then, it will probably be a shock to view Figure 6, which shows the rare earth-abundance patterns for ten samples collected from the seven chemically analyzed intrusions. Surprisingly, they are LREE-enriched, suggesting injection of some more-silicic calcalkaline magma into the magma chamber. Upon accumulation of augite phenocrysts, one would expect all the REEs, like other incompatible elements (e.g., Zr), to have lower concentrations than those in the Elwell magma in which the phenocrysts nucleated and through which they settled. The envelope enclosing rare earth-abundance patterns for six Elwell lavas in Figure 6 shows that this is in fact the case, for all but two intrusions. However, one would expect LREE-depleted, not LREE-enriched patterns (Hanson, 1980). A plot of (Ce/Yb)n against volume % of augite phenocrysts reveals that the slope of the abundance patterns is independent of augite content. That is, no matter how much augite accumulates, there is still LREE-enrichment, and the latter therefore must be an artifact of magma mixing.

Table 2. Average major-element, whole-rock chemical analysis of 7 augite-phyric hypabyssal intrusions of early Taylor (Famennian) age.

SiO_2	51.6	(1.47)
Al_2O_3	12.65	(2.02)
TiO_2	0.45	(0.06)
Fe_2O_3	1.97	(0.06)
FeO	7.99	(0.43)
MgO	10.08	(1.52)
CaO	9.75	(1.87)
Na_2O	1.03	(0.62)
K_2O	0.64	(0.51)
MnO	0.20	(0.02)
P_2O_5	0.05	(0.01)
LOI	3.59	(1.18)

Fe_2O_3 = TiO_2 + 1.5; FeO = (0.8998) remaining $Fe_2O_3^T$; LOI = loss on ignition. Standard deviations in parentheses. Most analyses by Activation Laboratories Ltd., Fusion-ICP, 1994.

Interestingly, the rare earth-abundance patterns, shown later, for all four samples collected from pillow lavas at the very base of the Taylor Formation are strikingly LREE-depleted, and the pillow lavas are clearly tholeiitic. I therefore suggest that the first augite-phyric lavas erupted from the magma chamber were tholeiitic, like the Elwell magma from which the augite crystals had accumulated, but that, a little later, the next such lavas erupted were again affected by magma mixing, and accordingly display both tholeiitic and calcalkaline characteristics. The latter also occur as mildly LREE-enriched pillow lavas present a few hundred meters above the base of the Taylor Formation, especially at Upper Salmon Lake.

Several trace-element ratios also indicate involvement of partial melt obtained from continental crustal materials (Dostal, 1989). Th/La, a good indicator of crustal contamination, averages 0.26 in the seven hypabyssal intrusions, much higher than mantle values (ca. 0.12); Th/La averages 0.17 in nine Elwell lavas. Zr/Y averages 2.34 in the seven intrusions, but only 1.94 in the Elwell lavas. The Elwell lavas plot in the "primitive oceanic arc" field of a discrimination diagram devised by Crow and Condie (1987), but the hypabyssal intrusions, with higher La/Yb and Th/Yb ratios, fall in the field of "evolved island arcs."

So, it appears that there were two episodes of eruption of the augite-phyric lavas, first the strictly basal, tholeiitic pillow lavas. Next, after injection of some more-silicic magma into the bottom of the magma chamber, the hypabyssal intrusions and near-basal pillow lavas. Based on available sampling, the second episode represents the final participation of silicic, calkalkaline partial melt in magma genesis in the Devonian-Mississippian island arc. Highly LREE-enriched lavas, in fact, occur at the very top of the Taylor Formation east of Long Lake, but they will be explained in a very different way.

Augite Phenocrysts in the Hypabyssal Intrusions

Though subjected to one or more episodes of low-grade metamorphism, many augite phenocrysts escaped almost unscathed. They provide important information about the original nature of the rocks that contain them. These nearly pristine phenocrysts are recognized in outcrop by their light green color, a measure of their highly magnesian (and Fe-poor) character (Figure 7). Least-altered phenocrysts may have cores flecked by actinolite+/-chlorite+/-epidote, and edges fringed by actinolite needles. More advanced alteration resulted in veining of phenocrysts and replacement of phenocryst margins by actinolite and/or chlorite, producing ragged cores of augite (see photomicrograph on page ii of this volume). Finally, wholesale replacement often resulted in single-crystal pseudomorphs of actinolite, recognized in outcrop by their nearly black color. Though the augite was mostly replaced by actinolite and chlorite, in various proportions, these minerals may be joined by one or more of epidote, calcite, quartz, and sphene.

The typically euhedral to subhedral augite phenocrysts average ca. 3 mm long, rarely exceeding 2 cm; microphenocrysts range down to ca. 0.2 mm across. Modest clustering of augite crystals occurs, the glomerocrysts usually involving microphenocrysts. Edges of crystals may be rounded, and, in one sill, few phenocrysts are euhedral, most having been resorbed, some even reduced to kidney-shaped crystals. Compositional zoning of phenocrysts is common, usually expressed as broad, euhedral to resorbed, Mg-rich cores enclosed by very narrow, euhedral, relatively Fe-rich rims (average width about 0.1 mm). The extent of this normal zoning is documented by 146 electron-microprobe analyses of 20 augite phenocrysts in ten samples collected from seven of the Taylor hypabyssal intrusions (Brooks and Schiffman, 1996). The mean of the 41 most Fe-poor analyses ($Fs<6$), made in the cores of eight crystals, is $Wo_{43}En_{52}Fs_5$ (shown by the cross in Figure 7), whereas the mean composition of the outermost analyzed point ($Fs>15$) on the 12 most Fe-rich rims is $Wo_{37}En_{41}Fs_{22}$. The lines in Figure 7 join particularly Fe-rich ($Fs>15$) and/or Cr-poor (Cr equal to or less than 0.0025 ppm) points on the rims to the nearest analyzed point in the

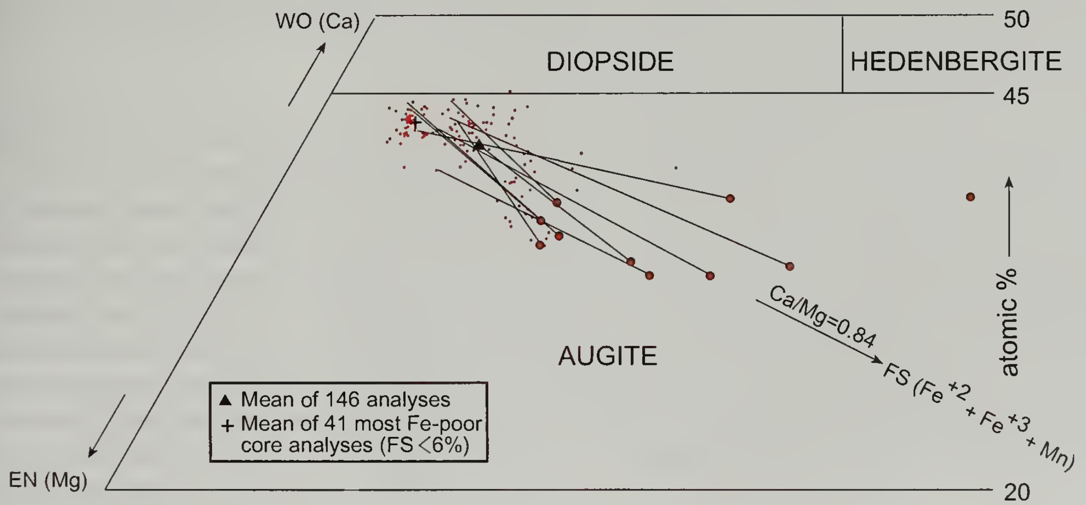

Figure 7. Composition of augite phenocrysts in seven early Taylor hypabyssal intrusions. Lines join core and rim (circled point) analyses of nine optically zoned phenocrysts; all phenocrysts are normally zoned. The arrow is drawn from the mean of the 41 most Fe-poor core analyses (marked by the cross) toward the Fs corner of the pyroxene quadrilateral. Wo=wollastonite, En=enstatite, Fs=ferrosilite.

cores of nine optically zoned phenocrysts, and reveal that the zoning may be quite impressive; in a couple phenocrysts, it is similar to the initial Skaergaard clinopyroxene fractionation trend.

Both Mg-rich cores and Fe-rich rims may exhibit oscillatory zoning, but most rims display only normal zoning, either continuous or discontinuous (Photo 5). Figure 8 illustrates the typical Al- and Ti-enrichment, and Cr depletion in the narrow Fe-rich rims. For the 41 most Fe-poor analyses made in phenocryst cores, mean TiO_2 is 0.04, Al_2O_3 0.66, and Cr_2O_3 0.51 wt.%. Since the Fe-rich rims clearly are of late (post-resorption) formation, I selected 104 microprobe analyses (Fs<13) that represent the broad, Mg-rich cores in order to determine the mean composition of the augite initially crystallized from the Elwell magma. Of particular interest are the values for TiO_2, Al_2O_3, and Na_2O, which are very low, even for island-arc tholeiites: TiO_2=0.08 (0.05), Al_2O_3=1.27 (0.76), and Na_2O=0.10 (0.05) wt.% (standard deviations in parentheses). Cr_2O_3 is of course high, 0.40 (0.17) wt.%, as is the Mg number, 91.9 (3.0). The latter, a sensitive indicator of zoning, varies from 82.2 to 97.4 in the Mg-rich cores, which frequently are oscillatory-zoned.

The Mg-rich cores also commonly display sieve texture, the relict glass inclusions uniformly distributed throughout cores, occurring in irregularly shaped patches within them, or occupying straight bands of variable width that parallel adjacent crystal margins. The latter inclusion bands doubtless follow certain zones in oscillatory-zoned cores, presumably the lower-melting, less Fe-poor ones. Relict glass inclusions, ranging from ca. 0.003 to 0.08 mm, display a great variety of shapes, from square or cuneiform to rounded or shapeless. The sieve texture, and accompanying resorption of Mg-rich phenocrysts, could have originated upon settling of phenocrysts into hotter or more mafic magma in deeper reaches of the magma reservoir; by "...influx of high-temperature or water-rich melt into [the] region of active crystallization" (Barsdell, 1988, p. 935); or upon decompression during uprise of the mafic magma. If the latter, the narrow Fe-rich rims of zoned phenocrysts would have to be a result of quenching during eruption of the magma.

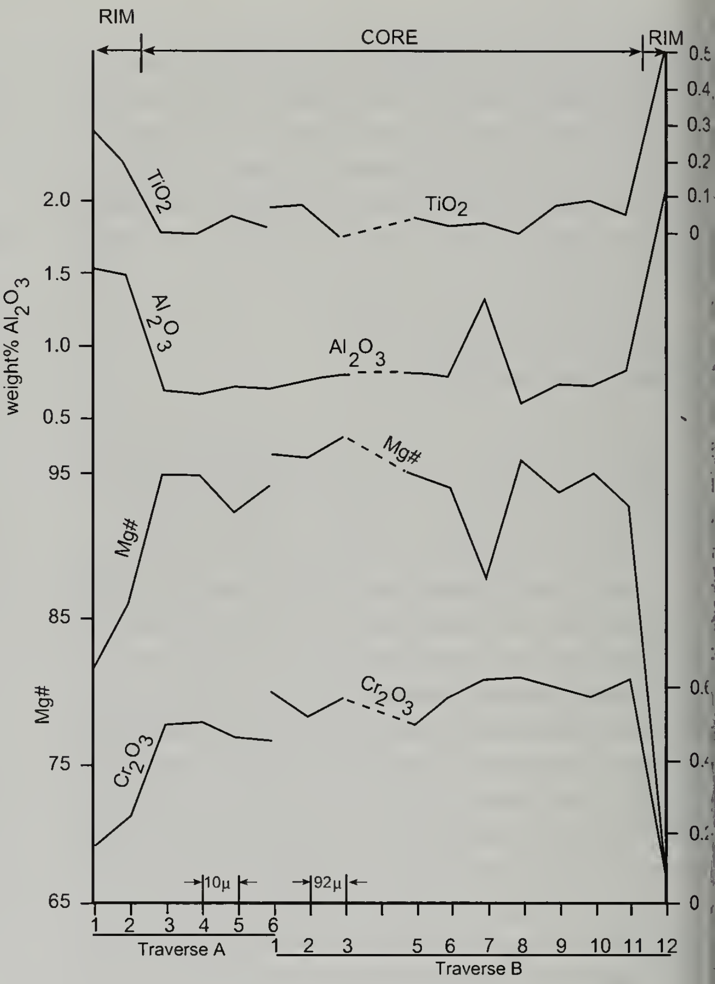

Figure 8. Plots of TiO_2, Al_2O_3, Cr_2O_3, and Mg number ($100[Mg/(Mg+Fe^{+2})]$) determined along rim-core traverses A and B in Photo 5. Diagram shows the typical Cr depletion and Al- and Ti-enrichment in narrow, post-resorption, Fe-rich rims of normally zoned phenocrysts. Note close reciprocal relationship between Mg number and Al_2O_3 (r = -0.96).

Several lines of evidence ensure that the highly magnesian cores were not mantle xenocrysts (Brooks and Schiffman, 1996). First, some of the most Mg-rich cores are found in strongly zoned, relatively small crystals that display only minor resorption and sieve texture (e.g., the phenocryst in Photo 5). Second, although relict glomerocrysts of augite+/-plagioclase are not uncommon, there are no mantle xenoliths, or even cumulate xenoliths, present. Third, as noted earlier, the Mg-rich cores generally are very poor in Al, unlike clinopyroxenes in mantle xenoliths, which contain 2-10 times more Al_2O_3. Further, lherzolitic clinopyroxenes also have higher Cr_2O_3 and TiO_2, and far higher Na_2O. Finally, and most telling, the first relatively mafic magma to appear in the island arc, the Sierra Buttes andesite, lacks large augite crystals.

The final goal of the electron-microprobe work was to use clinopyroxene phenocryst composition to identify the tectonic setting of volcanism. Brooks and Schiffman (1996) successfully employed the discrimination diagrams of Leterrier and others (1982) to determine that the phenocryst cores crystallized from magma that was subalkaline, orogenic, and tholeiitic, viz., from Elwell magma (Figures 9, 10 and 11). Step 1 in the method of Leterrier and others (1982) is separation of alkaline and subalkaline (calcalkaline and tholeiitic) lavas (Figure 9). If the lavas are subalkaline, as is the case here, one proceeds to step 2 (Figure 10), which distinguishes ridge- and rift-tholeiites from subduction-related basalts. In this case, we need to employ step 3 to further distinguish island-arc tholeiites from active-margin and island-arc calcalkaline basalts (Figure 11). It is interesting that four of the six zoned phenocrysts shown in Figure 11 exhibit trends toward the field of calcalkaline basalts. Since the narrow Fe-rich rims are demonstrably late, they probably crystallized from mixed magma having a calcalkaline component. Note that many core analyses are so low in Al that they plot outside the field of island-arc tholeiites.

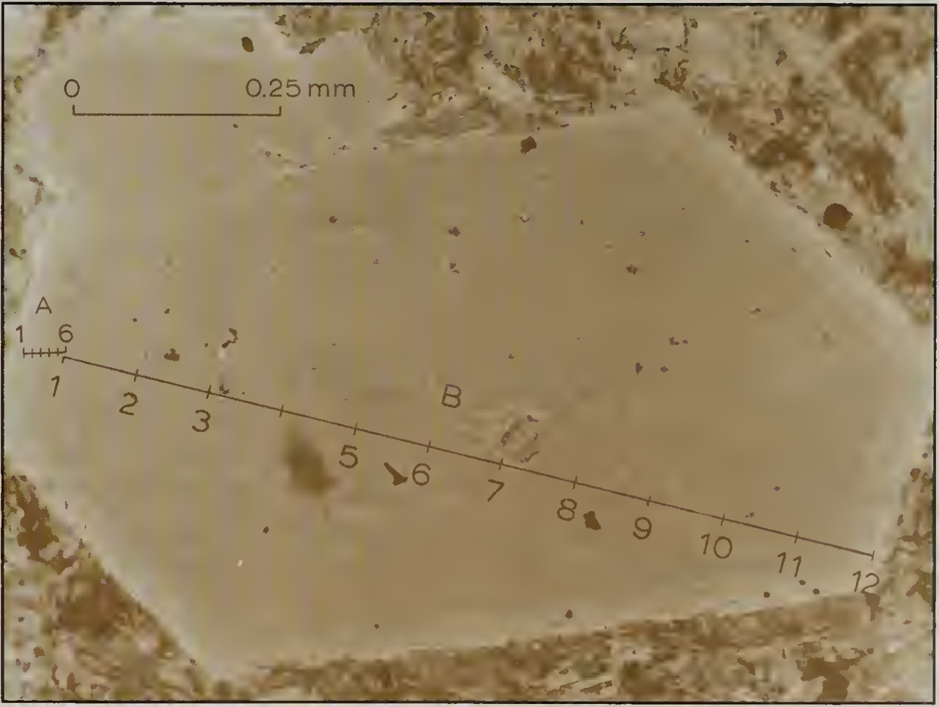

Photo 5. Rim-core electron-microprobe traverses A and B across small euhedral augite phenocryst in Taylor basaltic andesite intrusion. Narrow (0.03-0.05 mm) Fe-rich rim and broad, slightly resorbed, Mg-rich core; rim exhibits discontinuous normal zoning. Back-scattered electron image. *Back-scattered electron image by Peter Schiffman, U.C. Davis.*

Remainder of the Taylor Formation

According to Hanson and Schweickert (1986, p. 996), the Taylor Formation south of Dugan Pond (Figure 1) "...consists predominantly of fragmental andesitic debris in the form of grossly tabular units of massively bedded, very poorly sorted lapilli tuff and tuff-breccia intercalated with finer-grained andesitic tuffs." South of Interstate 80 (Figure 1), one finds "...andesitic tuff and crystal-lithic tuff turbidites..." that "...represent a distal part of the Taylor Formation" (Harwood, 1992, p. 16). In contrast, I find that north of Dugan Pond, in the area of Figure 3, the formation largely comprises pillow lava intercalated with varied, typically coarse-grained, volcaniclastic rocks, the whole stitched together by many hypabyssal intrusive bodies. Correspondingly, the Taylor Formation, only ca. 400 m thick south of Interstate 80 (Harwood, 1992), is 2.3 km thick east of Dugan Pond and ca. 3.1 km thick north of Gold Lake, in the area of our field trip. Coarsening and thickening of the formation northward, together with the appearance of abundant pillow lavas and hypabyssal intrusions, indicate that a vent is more closely approached in that direction.

Durrell and D'Allura (1977) provide a detailed description of the Taylor Formation in the Gold Lake-Long Lake area. In generalizing about the formation, they state that it "...is essentially volcaniclastic. Lavas, both massive and pillowed, form

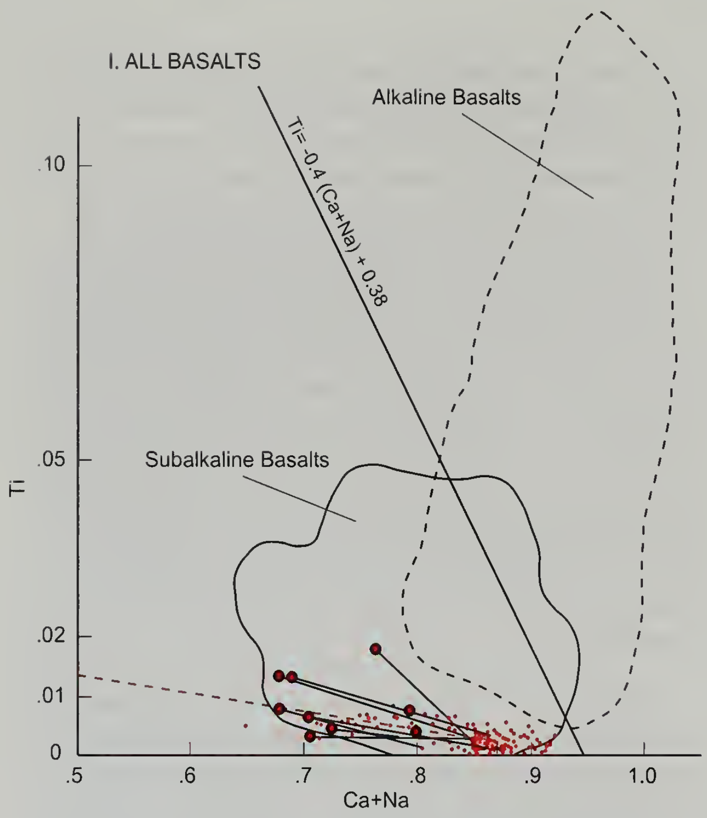

Figure 9. Discrimination of subalkaline from alkaline basalts using 146 electron-microprobe analyses. Method of Leterrier and others, 1982. The mean of the 41 most Fe-poor core analyses (Fs<6%) is marked by the cross (Ti=0.001, Ca+Na=0.87), whereas the nine most Cr-poor rim analyses (Cr equal to or less than 0.0025) are circled. For seven of the latter analyses, lines join points on rims (usually point nearest edge of crystal) to closest analyzed point in cores of optically zoned crystals. Dashed regression line reveals substantial negative correlation of cationic Ti and Ca+Na (r = -0.65). All contours in Figures 9, 10 and 11 represent a counting frequency of 5%; all electron-microprobe analyses by Peter Schiffman at U.C. Davis, 1992-93.

only a minor fraction of the section" (Durrell and D'Allura, 1977, p. 848). Yet their descriptions frequently mention pillow lavas, together with large volumes of crystal-lithic tuff, some well-bedded, and lapilli tuff and breccia, some coarse, with most clasts 3 to 45 cm across. A lithostratigraphic column presented by Rouer and others (1989, Figure 2) for the Salmon Lakes area shows that about 1/3 of the section there consists of pillowed flows, and another 20% or so of pillow breccia.

This report will focus on the Taylor pillow lavas, from which samples were first collected for chemical analysis in 1977; the petrography and chemistry of these will be discussed in the following section. Also, field and petrographic studies carried out on rocks near the base of the Taylor Formation at Upper Salmon Lake and west of Silver Lake shed light on the nature and origin of some of the voluminous volcaniclastic rocks.

West of Silver Lake, a hypabyssal intrusive body emplaced in still-wet unlithified ash resulted in formation of peperite to be viewed at Stop 6 on the field trip (Brooks, 1995). Well-bedded, crystal-lithic and crystal-lithic-vitric tuff and lapilli tuff serve as host for the intrusion. The tuffs comprise fining- and thinning-upward packages that display T_{a-c} Bouma sequences, and therefore are considered ash turbidites. Basal T_a divisions consist of several centimeters (cm) of structureless coarse tuff or lapilli tuff. T_b divisions are plane-parallel-laminated, and the uppermost, finest tuff comprising the T_c divisions displays asymmetric ripples having eroded crests (wavelength ca. 3 cm). Intercalated, relatively thick, structureless beds of lapilli tuff are interpreted as debris-flow deposits.

Brooks and Garbutt (1972) reported briefly on pillow lava, tuff, and broken-pillow breccia at Upper Salmon Lake; a fuller description appears in Brooks (1992). Pillow fragments in the thick-bedded breccias are distinctively plagioclase-glomerophyric and also are characterized by large quartz amygdules elongated perpendicular to original pillow margins. The broken pillows obviously were derived from the associated pillow lava, probably during slumping of oversteepened flanks of piles of pillows onto contemporaneously erupted tephra; the latter is represented by the crystal-lithic and lithic-vitric lapilli tuff matrix supporting the pillow fragments. The tuffaceous matrix may contain pumice lapilli exhibiting close-packed, round, quartz amygdules that usually do not exceed 1 mm in diameter. The broken-pillow breccias again are interpreted as the deposits of debris flows and/or high-density turbidity currents, and are interbedded with thinly stratified, crystal-lithic-vitric tuffs consisting of repeated, fining-upward packages displaying T_{a-c} Bouma sequences. Accordingly, the latter again are considered ash turbidites. Crests of T_c ripples commonly are truncated at the base of the next higher turbidite (ripple amplitudes are ca. 1-1.5 cm, wavelengths ca. 10 cm). We have never

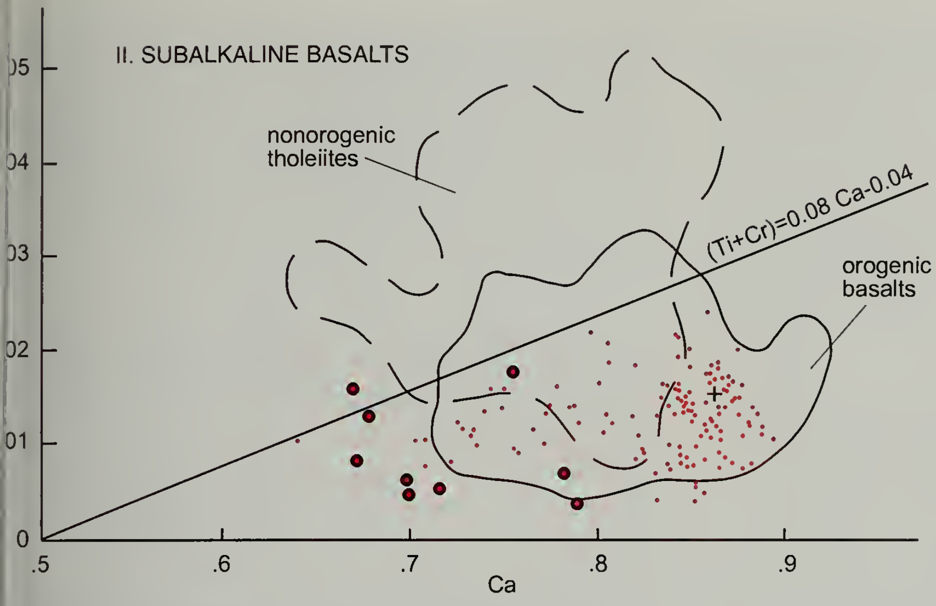

Figure 10. Discrimination of orogenic (subduction-related) basalts from nonorogenic tholeiites. *Method of Leterrier and others, 1982.* The mean of the 41 most Fe-poor core analyses is marked by the cross (Ca=0.86, Ti+Cr=0.016), whereas the nine most Cr-poor rim analyses are circled. In spite of the high Cr content of Mg-rich cores, the Ti content is so low that core analyses plot below the dividing line.

seen storm-wave ripples, so deposition must have occurred below storm-wave base (ca. 200 m). The trace fossils *Chondrites* and *Helminthopsis* occasionally appear in the T_c divisions.

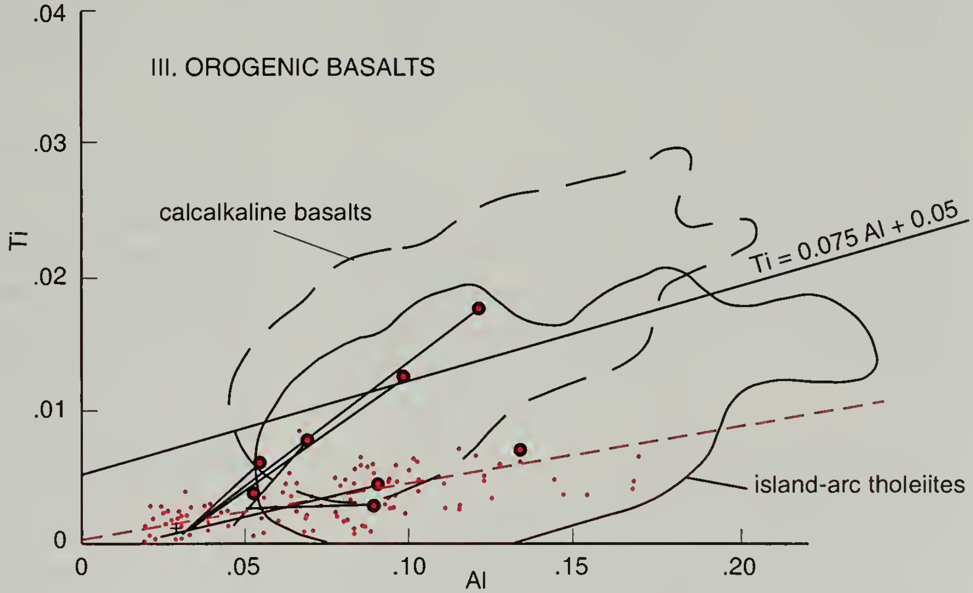

Figure 11. Discrimination of island-arc tholeiites from calcalkaline basalts. *Method of Leterrier and others, 1982.* The mean of the 41 most Fe-poor core analyses is marked by the cross (Ti=0.001, Al=0.028), whereas the eight most Cr-poor rim analyses are circled. For six of the latter analyses, lines join points on rims (usually point nearest edge of crystal) to closest analyzed point in cores of optically zoned crystals. Dashed regression line reveals substantial positive correlation of Al and Ti (r=0.61).

Finally, as we shall see at Stop 1 on our field trip, epiclastic rocks also are found in the Taylor Formation. At Stop 1, for example, we will view siltstones and pebbly sandstones consisting wholly of Sierra Buttes detritus; these occur ca. 1.8 km stratigraphically above the closest Sierra Buttes source rocks available at the present level of exposure! (Recall, however, that the section has been inflated by an unknown, but probably substantial amount by emplacement of hypabyssal intrusions.)

Pillow Lava in the Taylor Formation

Where it was possible to carefully map the boundaries of pillowed lava flows at Upper Salmon Lake, they were found to have flat bases, steep sides, and highly irregular upper surfaces diversified by hillocks and hollows having meter-scale relief (Brooks and Garbutt, 1972). The steepness of sides is at least partly due to post-depositional slumping of pillows. At Upper Salmon Lake, pillows often are embedded in relatively voluminous, locally subtly stratified, tuffaceous matrix; stratification parallels pillow surfaces known to have been the tops of pillows originally, so it is thought that the tuff was deposited synchronously with the pillows, perhaps from ash suspended in the water column. At other localities, the tuff separating pillows is well-graded and -stratified, and apparently is the product of periodic deposition from dilute turbidity currents. The tuffaceous matrix may contain angular brick-red fragments spalled from the originally glassy pillow rims.

In much of the Taylor Formation, the pillows are closely packed, with only minor tuffaceous matrix evident at pillow junctions; sometimes pillows are so tightly molded to one another that individuals are difficult to recognize. Pillows are almost always ellipsoidal, and little evidence exists for tubes or lobes. Pillows reach ca. 3 m in maximum dimension at Upper Salmon Lake, but are as little as 15 cm across elsewhere. Pillows may exhibit minor in situ fragmentation and veining by tuff; they are not prismatically jointed.

The pillow lavas tend to be quite richly amygdaloidal. The amygdule content of 11 point-counted thin sections ranged from 0 to 30 vol.% (the average amygdule content was 13 vol.%; only one sample contained no amygdules). These are minimum values, since I attempted to avoid obvious amygdules and veins while sampling. The abundance of amygdules suggests eruption in relatively shallow water (but deeper than ca. 200 m). Most striking in the field are large white quartz amygdules that usually occur just inside the relict glassy pillow rinds, and are elongated perpendicular to pillow margins. They often are present all the way around a pillow, like the spokes of a wagon wheel (Photo 4), but sometimes are confined to the original top of a pillow. The distribution of these elongated amygdules suggests nucleation and continuing growth of vesicles on a crystallization front as it moved toward the pillow center. Durrell and D'Allura (1977) mention quartz amygdules 2 cm in diameter and 8-15 cm long near the top of the Taylor Formation. McPhie and others (1993, Plate 17.2) illustrate very similar, radially distributed, "pipe" amygdules.

All pillow lavas are conspicuously phyric, containing a trace to 24.5 vol.% of relict augite phenocrysts (average of 5.0 vol.%) and 0-24.3 vol.% of relict plagioclase phenocrysts (average of 16.2 vol.%; only one sample had no plagioclase phenocrysts). The plagioclase phenocrysts are particularly characteristic of Taylor pillow lavas, typically forming small pink-weathering glomerocrysts. Though usually few and small, some pillows are choked with large augite phenocrysts.

Two samples were collected from highly distorted, amoeboid masses—probably pillows—that are found in a belt extending north at least 0.75 km from the northwest corner of Big Bear Lake (Stop 4 on the field trip; Figure 12). Some pillows are broken, and a large fraction of the voluminous matrix may consist of fragmented pillows. This unit has characteristics like those of intrusive, andesitic, isolated-pillow breccia described by Hanson (1991) within the Sierra Buttes Formation in the Sierra Buttes, including the dark red-brown pillow selvages (Photo 6). These are especially enigmatic rocks whose origin I still do not understand, but I tentatively interpret them as extrusive isolated-pillow breccia.

Microscopic Petrography of Taylor Formation Lava Flows

Nineteen samples of Taylor Formation lavas collected in 1977 were chemically analyzed (Brooks and Coles, 1980). These include the 11 point-counted pillow lavas just discussed, two others that are too recrystallized to count, three additional likely pillowed flows, two nonpillowed flows, and one brecciated, nonpillowed body that, in retrospect, may actually be a hypabyssal intrusion. All samples were examined petrographically, and a summary of results for the first 18 samples follows.

The 16 point-counts were recalculated to 100%, amygdule-free, in order to get a better idea of the proportions of magma and suspended phenocrysts prior to vesiculation. Assuming that most, or all, of the Cr present in these rocks (11-842 ppm) resides in the augite phenocrysts, there should be a good positive correlation of Cr with vol.% augite. Various linear-regression lines in fact have r=0.92-0.94, confirming this relationship, as well as the high quality of the point-counts (1500-1675 points counted per thin section). Using the vesicle-free modes, matrix (former magma) ranges from

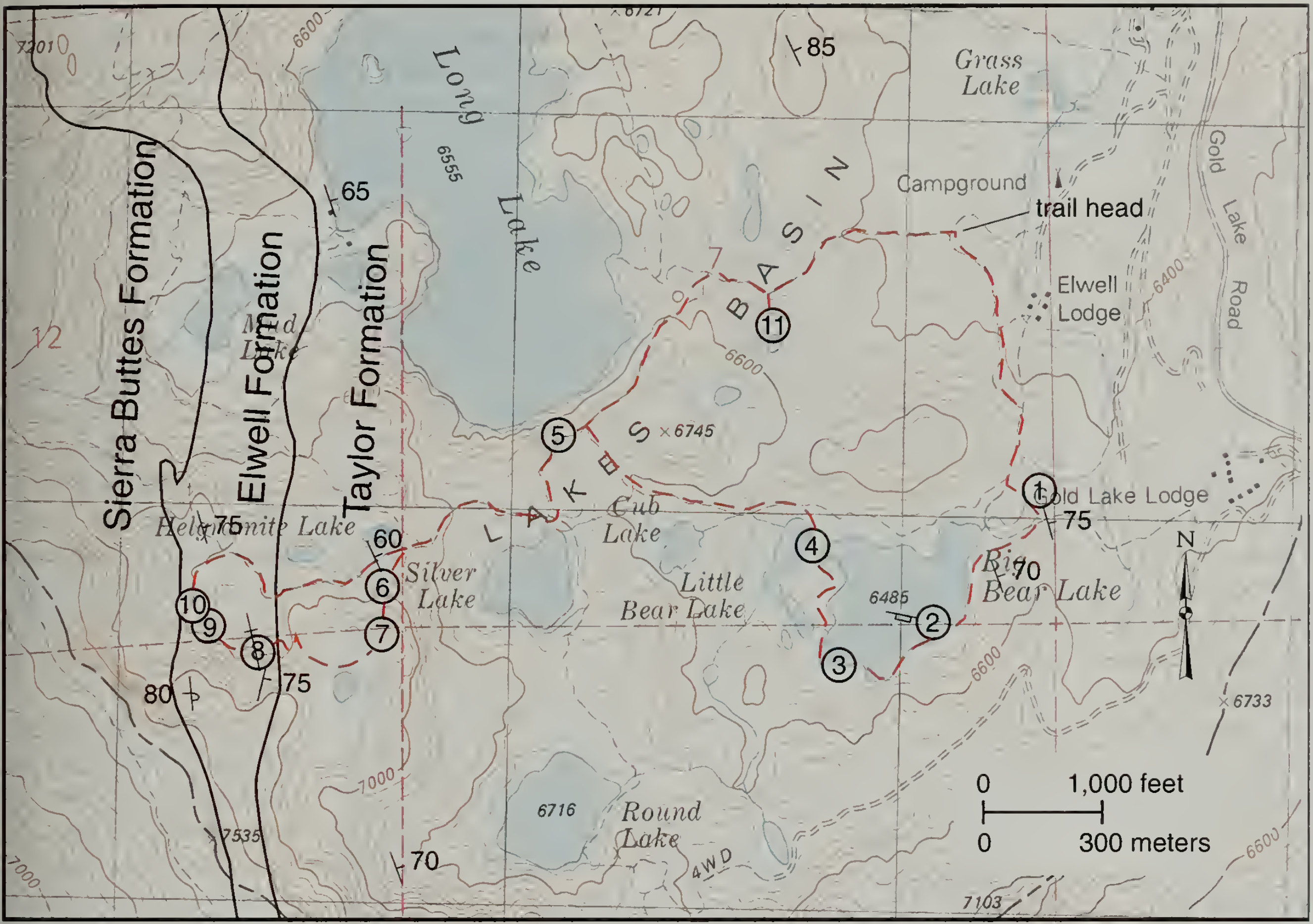

Base taken from U.S.G.S. 7.5 minute topographical map—Gold Lake Quadrangle

Figure 12. Geologic map of the Lakes Basin. Circled numbers locate stops on the field trip; route of trip is shown by the heavy dashed line. 40' contour interval.

62.1 to 86.9 vol.% (the average is 74.7 vol.%), plagioclase phenocrysts from 0 (2 samples) to 28.3 vol.% (average is 15.5 vol.%), and augite phenocrysts from 0.1 to 33.6 vol.% (average is 9.5 vol.%). One of the plagioclase phenocryst-free samples also is the one having 33.6 vol.% augite phenocrysts (669 ppm Cr); it also lacks plagioclase microlites, and has the lowest Na_2O content of all the samples, 0.86 wt.%. I have searched diligently for relict olivine phenocrysts in the Taylor lavas, and it is possible that a few of them (1.1 to 2.9 vol.%) occur in three of the samples.

Amygdules were found in all thin sections save one. They present a great variety of shapes—round, oval, egg-shaped, elongated, irregular; amygdules as small as 0.02 mm were recognized. They often are mineralogically zoned with, for example, cores and thin shells of chlorite in amygdules otherwise consisting largely of quartz. In addition to ubiquitous epidote, and nearly ubiquitous quartz and chlorite, many other minerals are found in the amygdules. Calcite and pyrite are frequently encountered; actinolite, albite, and biotite less so; and prehnite, sphene, white mica, and a black opaque mineral rarely.

The relict plagioclase phenocrysts and microphenocrysts, which range in size from ca. 0.2 to 4 mm, typically form small glomerocrysts, as already noted. Though usually euhedral, some rounding of phenocrysts is seen. Relict oscillatory zoning was recognized in two samples, epidote or chlorite occupying many narrow rows parallel to phenocryst margins. Plagioclase crystals were replaced by a bewildering array of metamorphic phases. As expected, albite (An_{0-7}) frequently is encountered, but it is not always present, resulting in relatively low whole-rock Na_2O contents. Epidote also occurs frequently, as does chlorite. Calcite, quartz, and white mica occur less frequently, and actinolite, biotite, and pumpellyite rarely. Pseudomorphs that consist only of quartz and chlorite, or of quartz alone, testify to extreme metasomatism.

The relict augite phenocrysts and microphenocrysts, conspicuously prismatic, range in size from ca. 0.25 to 8.5 mm, but usually not much over 2 mm. Like the plagioclase phenocrysts, they usually are euhedral, and display only modest resorption. They also may form glomerocrysts, and quite often are found in the plagioclase glomerocrysts. They, too, were replaced by a vast array of minerals. As anticipated, actinolite frequently is present, often as polysynthetically twinned single-crystal pseudomorphs; these may occur alone or be accompanied by chlorite, epidote, and quartz in various combinations. All three of the latter minerals are frequently encountered, and, indeed, one or more of them may be present to the exclusion of actinolite (five samples altogether were actinolite-free, and the augite in those was replaced by chlorite+/-epidote+/-quartz+/-calcite). Minerals seen less commonly are albite, biotite, calcite, sphene, and a black opaque mineral.

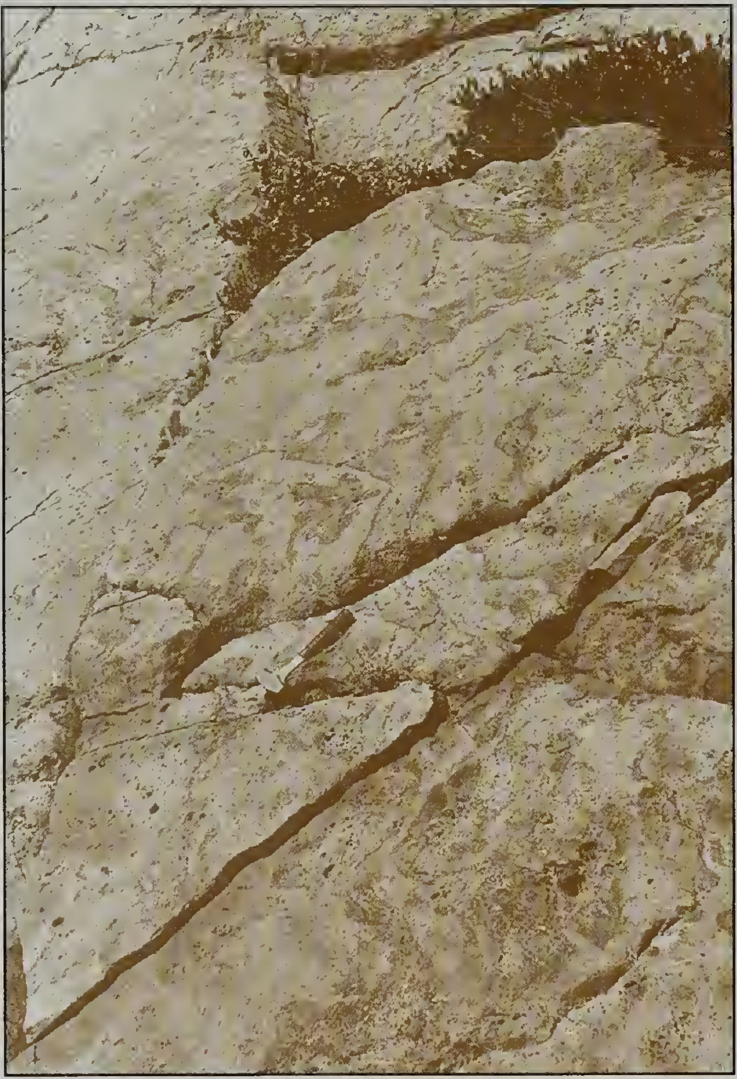

Photo 6. Probable isolated-pillow breccia in Taylor Formation north of Big Bear Lake. Bizarrely distorted pillows are outlined by the dark selvages. The sledge in this and subsequent photographs is 28 cm long. *Photo by E.R. Brooks.*

Pristine augite occurs in nearly half of the samples, but often only as ragged cores in otherwise replaced phenocrysts; wholly unaltered phenocrysts occur rarely. Optical properties of fresh augite include: colorless; simply- or polysynthetically-twinned; compositionally zoned; $2V_z$ ca. 60°-65°, r>v weak; Z^c at least 41°.

The possibility that olivine phenocrysts once were present is based simply on suggestive outlines of euhedral pseudomorphs. All the pseudomorphs consist largely or wholly of granular epidote, and actually may represent additional plagioclase phenocrysts. Relict titanomagnetite microphenocrysts—now leucoxene—were noticed in only two samples; some of the microphenocrysts were enclosed in plagioclase phenocrysts.

Relict, platy, plagioclase microlites—now almost always albite—are found in most samples, and are commonly plentiful. Microlites may be aligned around phenocrysts, but are otherwise unoriented. Some had forked terminations and some were hollow ("hopper" crystals) in a sample collected at Upper Salmon Lake. One might expect that such quench crystals would have been more frequently encountered, but an effort was made to collect samples from the cores of pillows, avoiding the likely more altered, originally glassy, pillow rims. Prismatic clinopyroxene microlites, sometimes little altered, also are present.

Finally, rock matrices also display a wide selection of metamorphic phases. Actinolite, albite, epidote, and sphene (some replaced by leucoxene) are most frequently encountered, biotite, calcite, chlorite, quartz, and one or more black opaque minerals much less so. The actinolite often forms bundles of fibers, but occasionally occurs as coarser prisms having ragged terminations. As will be explained later, the biotite in these rocks—originally misidentified as stilpnomelane—is a product of hydrothermal metamorphism associated with emplacement of the tonalite stock north of Gold Lake.

Augmented by additional rock samples collected to prepare this field trip, I now have metamorphic mineral assemblages for 21 localities in the Taylor Formation. Two of them indicate prehnite-pumpellyite-facies metamorphism, the remainder greenschist-facies metamorphism. The first two localities are, of course, in the area south of Deer Lake that was affected only by prehnite-pumpellyite metamorphism. All but one of the 19 greenschist localities are north of Deer Lake, in the area of Figure 3. The single outlier occurs ca. 2.5 km northeast of Sierra City. As mentioned when discussing metamorphism of the Tamarack tuff, it appears that the area of prehnite-pumpellyite-facies rocks south of Deer Lake passes to the south to greenschist-facies rocks approximately at the latitude of Young America Lake.

In terms of critical index minerals, three different, geographically unrelated mineral assemblages comprise the greenschists. An actinolite-free, chlorite-epidote-albite+/-calcite assemblage occurs at three localities; an albite-free, chlorite-epidote-actinolite-calcite assemblage at two localities; and an actinolite- and albite-bearing, chlorite-epidote-actinolite-albite+/-calcite assemblage at the remaining 14 localities. Unfortunately, the mineral chemistry of these metamorphic phases is not yet available.

Geochemistry of Taylor Formation Lava Flows

The 18 samples of Taylor Formation lava flows that I collected in 1977 (the "C-series," analyzed, except for SiO_2, by instrumental neutron activation analysis [INAA] and x-ray fluorescence [XRF] at the Lawrence Livermore National Laboratory [LLNL] in 1978) recently (1996-97) were augmented by 14 additional samples of pillow lavas, seven collected from pillow cores, seven from pillow rims. Nine separate pillows are represented by the latter analyses, five of them yielding samples of both core and rim (core and rim analyses of the five pillows are joined by lines in Figures 13 and 14). Most of these samples were collected from the C-series localities. They represent part of Mark Varney's CSU, Hayward, M.S.-thesis sampling project, designed to study the petrology of pillow lavas across the entire Devonian-Mississippian island arc, from Sierra Buttes to Peale formations. The samples were analyzed by inductively coupled plasma (ICP) at Activation Laboratories Ltd. in 1998. Although one might expect the ICP analyses to be superior to the INAA and XRF analyses made 20 years earlier, Table 3 shows that the average analysis of the 18 C-series samples (at least 13 of which represent pillow cores) is very similar to that of the seven pillow cores collected by Varney. The only significant differences are lower CaO and higher alkalies in Varney's pillow cores. However, when one uses the oxides SiO_2, Na_2O, and K_2O (Figure 13) to compare individual pillows collected at the same locality, the correspondence does not seem to be as good. The more recently analyzed pillows are almost always more alkalic than their counterparts analyzed in 1978, as also suggested by the average analyses of the two groups.

Precision of the 1978 LLNL analyses may be judged by examining the results for sample C-33 in Table 3. This sample was collected from the core of a pillow east of Deer Lake that was affected only by prehnite-pumpellyite metamorphism. Also, it was the only pillow point-counted that contained no amygdules (matrix 69.9 vol.%, plagioclase phenocrysts 24.4 vol.%, augite phenocrysts 5.7 vol.%). The coefficient of variation (standard deviation/arithmetic mean) of the three replicate analyses indicates that only TiO_2 and

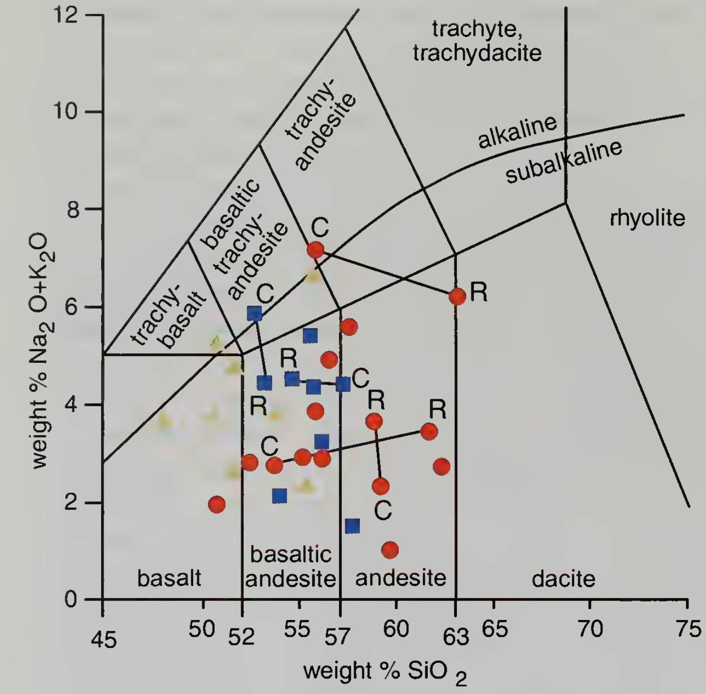

Figure 13. Total alkalies-silica diagram (*Le Maitre and others, 1989*) showing 32 analyses of Taylor Formation lava flows, all but two of them pillowed. Lines join core (C) and rim (R) analyses of five individual pillows. *The dividing line between alkaline and subalkaline lavas is from Irvine and Baragar (1971).* Triangles represent samples having "relict," LREE-depleted abundance patterns; circles "altered," LREE-enriched patterns; and squares "transitional," nearly flat patterns. The "shotgun" distribution of analyses probably largely reflects element mobility during the one or more metamorphic events that have affected these rocks.

K_2O were not well determined; both were near their respective detection limits (only one split was analyzed for SiO_2). Accuracy of the INAA results was confirmed by replicate analyses of U.S. Geological Survey basalt standard BCR-1; average % error from the standard values for the oxides of Al, Ti, Fe, Mg, Ca, Na, K, and Mn ranged from only 0.8 % for Ca to 5.3% for Mg.

Comparison of the coefficient of variation of the replicate analyses of C-33 with that of the average of the 18 C-series samples reveals large increases for all oxides but TiO_2 and SiO_2, up to 100% for K_2O. The coefficient of variation of the average of the seven pillow cores collected by Varney is similarly high for all oxides except SiO_2. Perhaps surprisingly, the coefficient of variation of the average of the seven pillow rims collected by Varney is no higher than that of the pillow cores for half the oxides and only marginally higher for another (Table 3). Though one might expect that glassy pillow rims would exhibit greater compositional variation than pillow cores following metamorphism, the average analyses are nearly the same.

This extensive variation in major-element oxide composition of the Taylor Formation lava flows is well illustrated graphically by the TAS diagram comprising Figure 13, in which all 32 chemical analyses are plotted. The "shotgun" scatter of analyses, though clearly centered on basaltic andesite, embraces several fields, even spilling into fields of alkaline lavas; four analyses, all representing pillow cores, lie above the line proposed by Irvine and Baragar (1971) to divide alkaline and subalkaline lavas. K_2O averages less than 0.4 wt.%, so that most of the considerable variation in alkalies is due to variation in Na_2O. The lower Na_2O contents correlate fairly well (r=0.65) with low plagioclase phenocryst contents; since much of the replacement of plagioclase was by albite, low phenocryst content should translate to low Na_2O content.

The use of triangles, squares, and circles to represent chemical analyses in Figure 13 requires brief explanation. The triangles represent samples exhibiting LREE-depleted abundance patterns, the circles LREE-enriched patterns, and the squares nearly flat patterns. The significance of the terms "relict," "altered," and "transitional," respectively, applied to these patterns will be explained later.

Some individual pillows, whose core and rim analyses are connected by lines in Figure 13, display rather extreme compositional variation, spanning a large fraction of the entire data set. Two of the five pillows seemingly possess strongly silicified rims, and three of them have rims relatively enriched in alkalies. Unfortunately, there is no consistent enrichment/depletion pattern among the pillows, and, furthermore, the pillows have yet to be examined petrographically. Pillows in the Betts Cove ophiolite have rims consistently depleted, in some cases dramatically, in both SiO_2 and Na_2O relative to cores (Coish, 1977). No Taylor pillow exhibits this pattern. The greenschist-facies

Table 3. Average major-element, whole-rock chemical analyses of lava flows, mostly pillowed, in the Taylor Formation

	Average of 3 replicate analyses of pillow lava C-33[1]			Average of 18 samples of lava flows collected in 1977 (C-series)[1]		
	arithmetic mean	standard deviation	coefficient of variation	arithmetic mean	standard deviation	coefficient of variation
SiO_2	50.6	—	—	55.3	3.1	0.06
Al_2O_3	17.81	1.43	0.08	16.49	3.73	0.23
TiO_2	0.51	0.11	0.22	0.48	0.10	0.21
$Fe_2O_3^T$	11.90	0.01	0.001	10.29	1.14	0.11
MgO	5.55	0.65	0.12	6.01	2.02	0.34
CaO	6.17	0.49	0.08	7.76	2.80	0.36
Na_2O	4.45	0.26	0.06	3.19	1.48	0.46
K_2O	0.18	0.03	0.17	0.28	0.28	1.00
MnO	0.19	0.01	0.05	0.19	0.05	0.26
	97.36			99.99		

Pillow lavas collected by Mark Varney in 1996-97[2]

	Average of cores of 7 pillows			Average of rims of 7 pillows		
	arithmetic mean	standard deviation	coefficient of variation	arithmetic mean	standard deviation	coefficient of variation
SiO_2	55.45	2.26	0.04	55.89	5.50	0.10
Al_2O_3	15.91	2.49	0.16	16.33	2.10	0.13
TiO_2	0.47	0.11	0.23	0.46	0.09	0.20
$Fe_2O_3^T$	10.70	1.64	0.15	10.50	2.68	0.26
MgO	6.46	2.74	0.42	5.88	2.09	0.36
CaO	6.24	2.15	0.34	6.53	1.88	0.29
Na_2O	4.01	1.77	0.44	3.46	1.14	0.33
K_2O	0.50	0.55	1.10	0.59	0.67	1.14
MnO	0.17	0.03	0.18	0.19	0.11	0.58
P_2O_5	0.09	0.08	0.89	0.19	0.28	1.47
	100.00			100.02		

All analyses except C-33 recalculated to 100 wt.%, volatile-free; $Fe_2O_3^T$ = all Fe calculated as Fe_2O_3.

1. SiO_2 by XRF at X-ray Assay Laboratories Ltd., 1979; other oxides by INAA and XRF at Lawrence Livermore National Laboratory, 1978.
2. ICP analyses by Activation Laboratories Ltd., 1998.

metamorphism that affected the Betts Cove ophiolite is attributed to hydrothermal circulation of heated seawater at a mid-ocean ridge (Coish, 1977).

I conclude that the extensive compositional variation indicated by large coefficients of variation of the average analyses in Table 3 and by scatter in the TAS diagram is the result of metamorphic mobilization of the major elements. Indeed, major-element mobility probably was too extensive for evidence of original igneous processes to survive. Interestingly, however, all the basalts, and the single trachybasalt, shown in Figure 13 occur at or near the base of the Taylor Formation.

Though two of the pillow rims seemingly were strongly silicified, and thin sections reveal striking examples of mm-scale silica metasomatism, relatively low coefficients of variation of SiO_2, coupled with very poor correlation (r=0.14) of SiO_2 content and vol.% amygdules, make it difficult to argue that most of the andesites in Figure 13 were produced by wholesale silicification of basalts and basaltic andesites. Nevertheless, 60% of the analyses falls in the fields of basalt and basaltic andesite, and the fiction that the Taylor Formation is andesitic (Diller, 1908; Durrell and D'Allura, 1977) unfortunately has persisted to the present day (Harwood, 1992).

In spite of the fact that four pillow cores plot above the dividing line separating alkaline from subalkaline lavas in Figure 13, we can safely conclude, in view of the large coefficients of variation of Na_2O, that the Taylor lava flows were subalkaline. Let's, then, revisit the question of whether the Taylor Formation was tholeiitic or calcalkaline, or, rather, the question of how much was tholeiitic and how much calcalkaline, as we already have learned that certain near-basal pillow lavas, as well as penecontemporaneous hypabyssal intrusions, exhibit both tholeiitic and calcalkaline characteristics. There are two widely employed approaches to this question using concentrations of major-element oxides, the AFM ternary diagram and Miyashiro's (1974) graph of SiO_2 against FeO*/MgO, where all Fe is calculated as FeO. The former diagram, not included here, suggests a transitional, tholeiitic to calcalkaline character, and also shows that there is no regular compositional variation of lavas from base to top of the Taylor Formation, as might be expected by fractional crystallization of a magnesian parent magma. It was, of course, predicted only two paragraphs earlier that evidence for such igneous processes would be masked by metamorphic mobilization of major elements. The Miyashiro diagram, Figure 14, suggests tholeiitic character, albeit very weakly. The symbols are the same as those in Figure 13, with the addition of sample numbers for the five pillows for which both core and rim analyses are available; as before, no consistent pattern of enrichment/depletion of pillow cores and rims can be discerned. The majority of samples, including three of the four basal pillow lavas with LREE-depleted abundance patterns mentioned earlier, lie above the line that separates the fields of calcalkaline and tholeiitic lavas. However, a careful reading of Miyashiro (1974) indicates that simple examination of the distribution of analyses may not suffice. The preferred criterion is the slope of the trend line through the analyses; if steeper than the line separating calcalkaline and tholeiitic lavas, the rock series is calcalkaline, if less steep, it is tholeiitic. The best-fit regression line for the Taylor lava flows—the gently sloping solid line in Figure 14—is much less steep than that separating the calcalkaline and tholeiitic fields, but r is only 0.07, so the regression line is essentially meaningless. Again, any evidence of the former existence of an igneous process is concealed by the scatter of analyses. Should the trend-line criterion fail, one next examines the distribution of analyses, but only those for which $2.0<\mathrm{FeO^*/MgO}<5.0$ (Miyashiro, 1974). In our

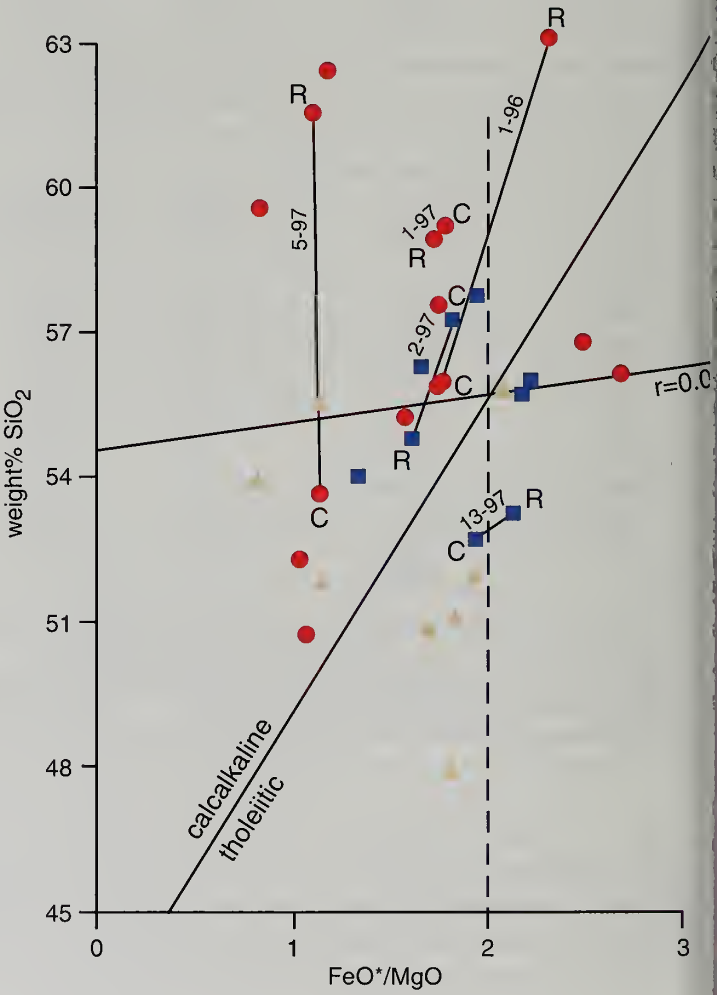

Figure 14. Graph of FeO*/MgO against wt.% SiO_2 (Miyashiro, 1974) showing 32 analyses of Taylor Formation lava flows. Symbols are the same as those in Figure 13, with the addition of sample numbers for the five individual pillows for which both core (C) and rim (R) analyses are available. The gently sloping solid line is the linear-regression line for the widely scattered analyses (r=0.07). The graph suggests that the lava flows were tholeiitic, not calcalkaline (see text for explanation).

case, only one of the seven samples having FeO*/MgO>2.0, a pillow rim, lies in the calcalkaline field. So, the major-element oxides suggest a tholeiitic or transitional, tholeiitic to calcalkaline character for the Taylor lavas. Do trace elements thought to be immobile during metamorphism do a better job of differentiating tholeiitic from calcalkaline lavas? The high-field strength elements Ti, Y, and Zr certainly seem to, and are featured in several discrimination diagrams devised by Julian Pearce and colleagues (Pearce and Cann, 1973; Pearce and Norry, 1979).

The Pearce and Cann (1973) series of discrimination diagrams has been widely used by those attempting to identify the paleotectonic setting of eruption of altered basalts. Indeed, they were employed successfully 2 decades ago by Brooks and Coles (1980) to determine that the C-series of samples originated in an island arc, and that the original basalts belong to the tholeiitic rock association of island arcs (Jakes and White, 1972). The two diagrams proposed by Pearce and Cann (1973) to distinguish among paleotectonic settings of altered basalts appear as Figures 15 and 16, the plotted data augmented by some of Mark Varney's samples. (Varney's samples are represented by open circles, the C-series samples by filled circles.) However, the sample set is reduced to 17 from the 32 plotted in Figures 13 and 14, mainly because I have used the chemical screen, 12 wt.%<(CaO+MgO)<20 wt.%, employed by Pearce and Cann (1973) to select basaltic rocks. Unfortunately, the large coefficients of variation of both CaO and MgO (Table 3) indicate that both of these oxides were readily mobilized during metamorphism, so that some samples passing the chemical screen probably were not originally basalts, while others failing the screen likely were, and should have been included. In spite of these problems, the Pearce and Cann screen probably is as useful as the TAS diagram in attempting to identify metabasalts.

The ternary diagram Ti/100-Zr-3Y is used first, to distinguish within-plate basalts from all other basalts (Figure 15). No Taylor Formation samples plot in the within-plate basalt field, and, according to Pearce and Cann (1973), separation of the remaining basalt types is best carried out using the Ti-Zr diagram (Figure 16). In spite of considerable scatter, the presence of low-K (island-arc) tholeiites is suggested by Figure 15, and is confirmed in Figure 16, where no analyses fall in the ocean-floor or calc-alkali basalt fields, or even in

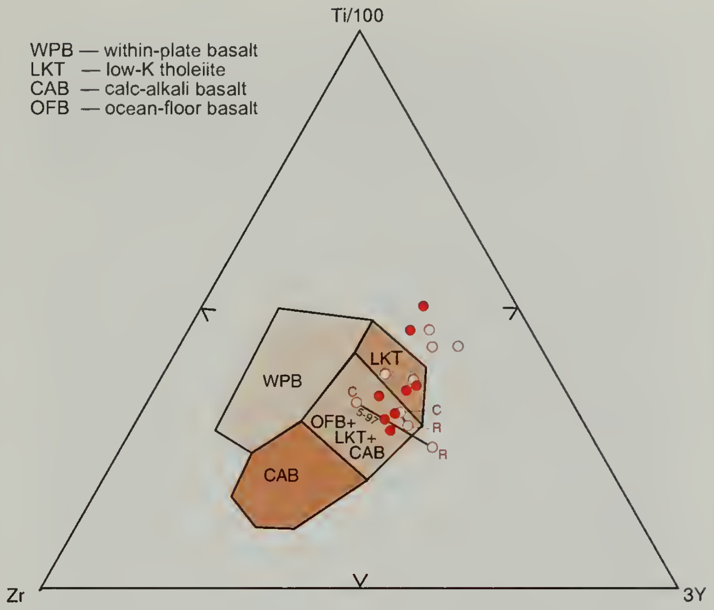

Figure 15. *Seventeen analyses of Taylor Formation metabasaltic lava flows plotted in the Ti/100-Zr-3Y discrimination diagram of Pearce and Cann (1973).* The former presence of low-K (island-arc) tholeiites is suggested. Open circles represent samples collected by Mark Varney, filled circles represent C-series samples. Pillow 5-97 has its rim relatively strongly enriched in Y.

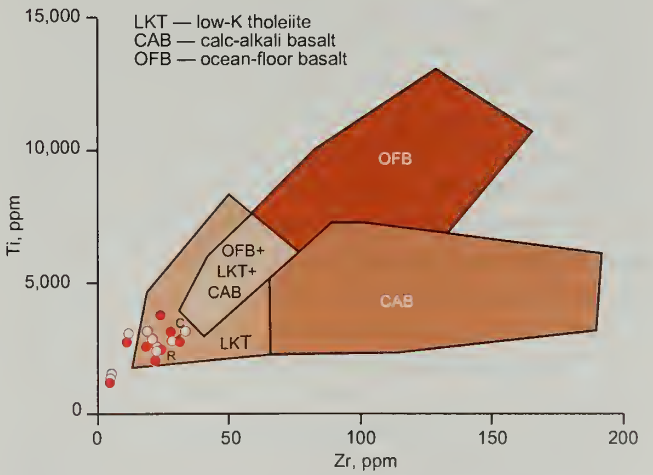

Figure 16. *Seventeen analyses of Taylor Formation metabasaltic lava flows plotted in the Ti-Zr discrimination diagram of Pearce and Cann (1973).* The former presence of low-K (island-arc) tholeiites is confirmed. Symbols as in Figure 15.

the field of overlap of all three types. Five samples, however, are so poor in Zr—and, in three cases, Ti as well—that they plot outside the field of low-K tholeiites in Figure 16. All these samples were collected in the Upper Salmon Lake area, three at the very base of the Taylor Formation (Figure 3). The latter three samples are rich in augite phenocrysts, thought to be of cumulate origin, and have correspondingly very high Cr contents (747-842 ppm). These are the same three samples that are depleted in both Zr and Ti (Figure 16), and the concentrations of these incompatible elements doubtless were reduced by dilution upon accumulation of the augite phenocrysts (which are particularly poor in Ti). The other two Zr-poor samples, collected a bit farther east, are Cr-poor (32-36 ppm), and the point-counted sample contains only a trace of phenocrystic augite, so that the low Zr content of these samples cannot be accounted for by accumulation of augite. The same five samples lie to the low-Zr side of the low-K tholeiite field in Figure 15.

As before, the compositional variation within a single pillow (sample 5-97, Figure 15) may equal that of the entire data set. The rim of pillow 5-97 is much richer in Y (18 ppm) than is the core (11 ppm).

Figure 17, a log-log graph again involving Zr and Y (Pearce and Norry, 1979), further confirms that the Taylor lava flows originated in an island arc. The same three augite-rich pillow lavas collected at the base of the Taylor Formation west of Upper Salmon Lake—C-42, 7-97C, and 10-97R—plot at low Zr (and Zr/Y) values well outside the island-arc basalt field because of augite accumulation. Also, the relative enrichment in Y of the rim of pillow 5-97 is again apparent. The outcrop from which sample C-42 was collected is shown in Photo 4.

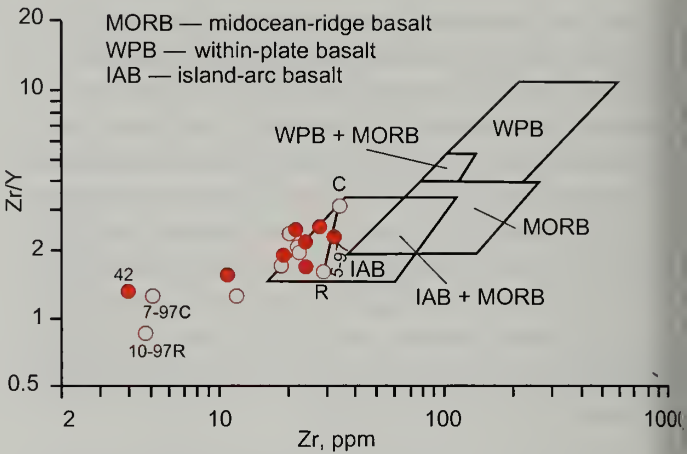

Figure 17. The former presence of island-arc basalts is indicated. Symbols as in Figure 15.

As we saw earlier, the tectonic setting of volcanism also can be ascertained using the composition of unaltered clinopyroxene phenocrysts (Leterrier and others, 1982). The electron-microprobe work on augite phenocrysts in the early Taylor hypabyssal intrusions described earlier also included analysis of phenocrysts in three of the Taylor lavas: the pillow lava at the base of the formation just mentioned (sample C-42), and isolated-pillow breccia and nonpillowed lava in the central part of the formation east of Long Lake (Figure 3). Eighteen analyses of seven phenocrysts in the three samples appear in the Leterrier and others (1982) discrimination diagrams comprising Figure 18. Like the magnesian augite phenocrysts in the early Taylor intrusions, those in the lava flows are remarkably Ti- and Al-poor, and Cr-rich (the mean composition is $Wo_{42}En_{50}Fs_{8}$). Indeed, though the Cr contents are about 2 1/2 times that of the mean island-arc tholeiite, the augite phenocrysts are so poor in Ti that one analysis plots below the 5% frequency contour for orogenic basalts. Also, they are so poor in Al that eight analyses plot outside the 5% contour for island-arc tholeiites. And, like the phenocrysts in the Taylor intrusions, the compositions of those in the lava flows indicate the lavas containing them were subalkaline, orogenic (subduction-related), and tholeiitic. This is especially important because the two samples collected east of Long Lake are in the area affected by hydrothermal alteration associated with intrusion of the tonalite stock (Figure 3), and possess LREE-enriched abundance patterns that conventionally would indicate the rocks are calcalkaline (samples C-24 and C-25 in Figure 19). As I argue below, however, these rocks were enriched in LREE, Th, and U during hydrothermal alteration, and the calcalkaline signature is not a primary one; the Leterrier and others (1982) diagrams correctly show that they originated as island-arc tholeiites.

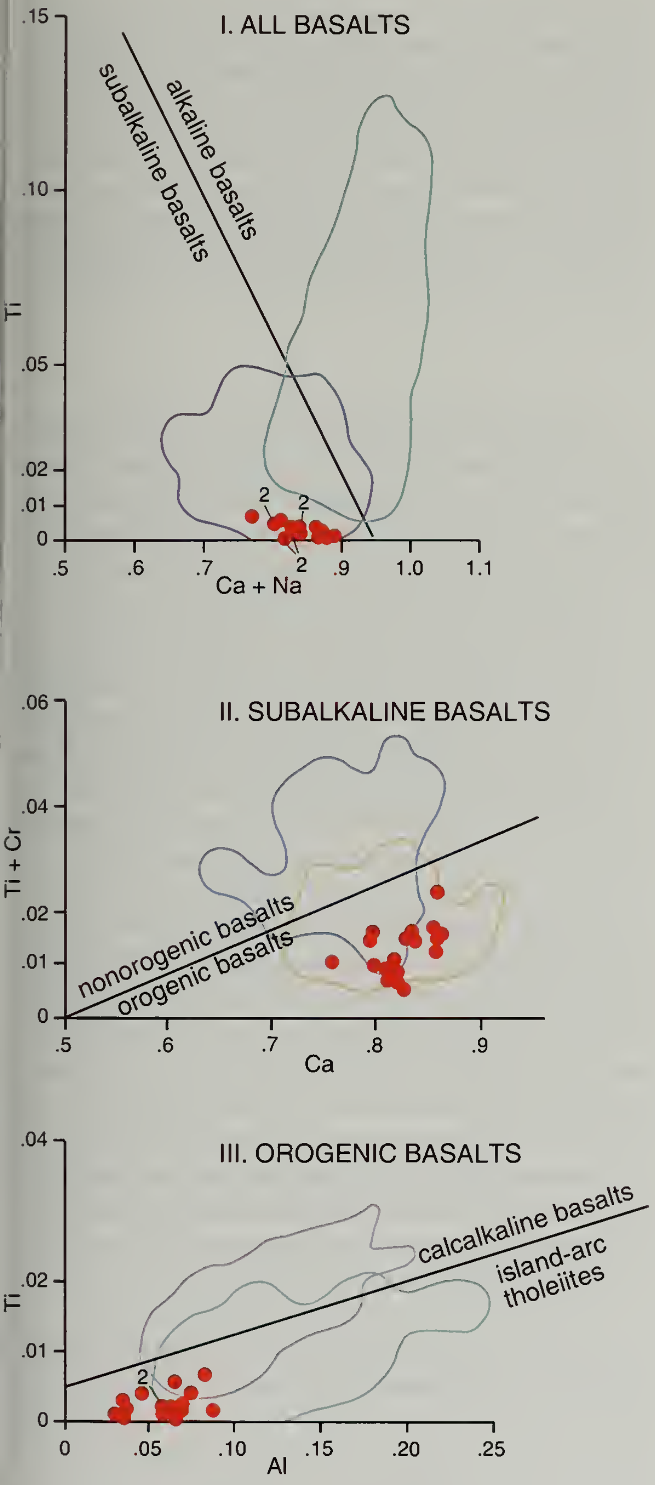

Figure 18. *Eighteen electron-microprobe analyses of seven augite phenocrysts in three Taylor Formation lava flows plotted in the discrimination diagrams of Leterrier and others, 1982.* Using all three diagrams in order from I to III, the lava flows are identified as island-arc tholeiites. All contours represent a counting frequency of 5%; equations of the dividing lines appear in Figures 9-11. *Electron-microprobe analysis by Peter Schiffman at U.C. Davis, 1992.*

CONTACT AND HYDROTHERMAL METAMORPHISM RELATED TO EMPLACEMENT OF THE TONALITE STOCK NORTH OF GOLD LAKE

An early Cretaceous (120 Ma) hornblende-biotite tonalite stock (or larger subjacent pluton) present north of Gold Lake (Figure 3) was the source of a swarm of hornblende andesite and biotite-hornblende dacite dikes (John Lull, this volume). It also was the source of hydrothermal fluids that altered the dikes and stock rather intensely, and that transported REE, Th, and U into the host Taylor Formation lavas. Lack of sufficient chemical data means the nature of the fluid can only be guessed by examination of the alteration-mineral assemblage and comparison with similar examples of REE-, Th-, and U-enrichment.

The alteration assemblage in dikes and stock is very much like that in granitic rocks of the Idaho Batholith that have been invaded by younger Eocene plutons (Criss and Taylor, 1983). It includes abundant white mica, chlorite, epidote, calcite, sphene, and pyrite. In the stock, both biotite and the calcic cores of plagioclase crystals are intensely altered, the former to white mica, chlorite, and pistacite, the latter to "saussurite" consisting dominantly of dark, microscopically indefinite material, probably an epidote mineral obscured by leucoxene. The effects of saussuritization are particularly evident in the dikes, where large plagioclase phenocrysts have a white, chalky appearance in outcrop (field trip Stop 2; Figure 12). Secondary biotite may occur abundantly in the dikes (Lull, 1984), and is rather widely distributed in the Taylor lavas northwest of the stock outcrop (Figure 3; the short-dashed line simply encircles those samples containing biotite, and, were samples available, the biotite-bearing area might extend to the stock). This hydrothermal biotite occurs in a much more limited area (not shown) on the east side of the stock.

Taylor Formation rocks that previously had been subjected to greenschist-facies metamorphism were converted to blastoporphyritic basic hornfelses where they adjoin the stock. The hornfels mineral assemblage—biotite-hornblende-quartz-calcic plagioclase-magnetite—indicates contact metamor-

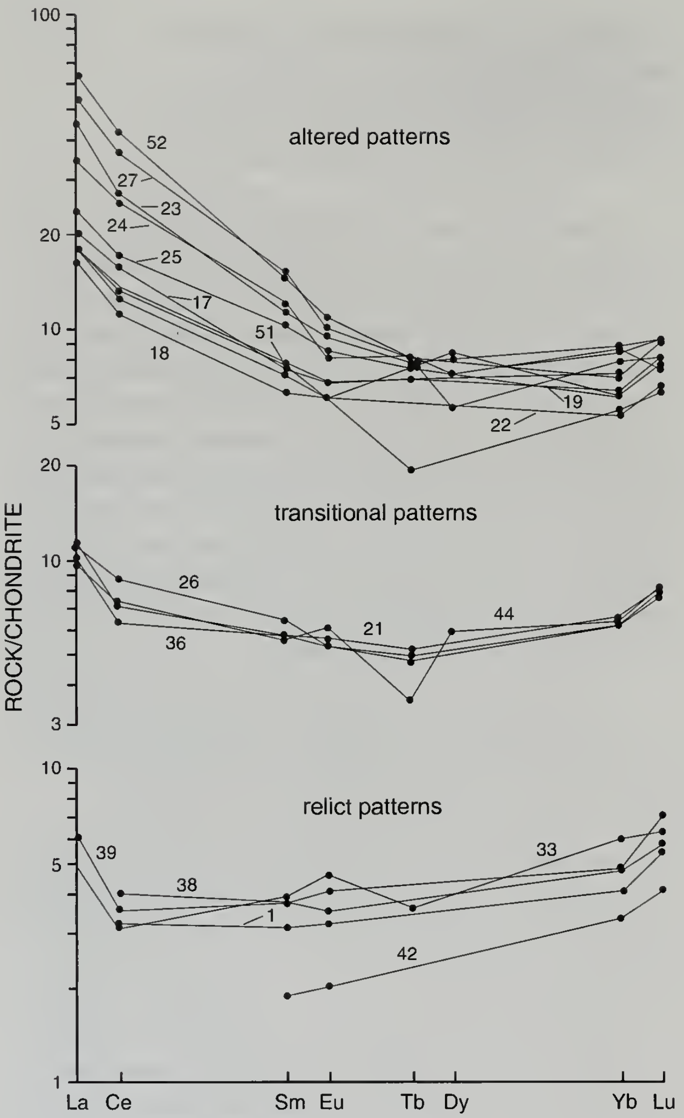

Figure 19. Chondrite-normalized rare earth-abundance patterns of 19 C-series samples collected from the Taylor Formation; at least 13 samples represent pillow lavas. Sample locations appear in Figure 3, except for C-1 and C-39, which were collected south of the area shown in the figure. The LREE-enriched, "altered" patterns, except for one, represent lava flows in the Big Bear Lake-Long Lake area northwest of the tonalite stock, and evidence addition of LREE from hydrothermal fluids leaving the cooling stock. *Analyses by INAA at the Lawrence Livermore National Laboratory in 1978.*

phism under conditions of the hornblende-hornfels facies. An outer albite-epidote hornfels facies would go unrecognized in the greenschists. Though relict plagioclase phenocrysts can be recognized, the original texture was essentially obliterated by a new granoblastic fabric. Poikiloblastic quartz and biotite are both abundant, but plagioclase (An_{52}) is surprisingly sparse, occupying very small, subidioblastic grains. Grain size of the subidioblastic hornblende (Z^c=21°) is extremely variable, from ca. 0.02 mm inclusions in quartz to ca. 4 mm porphyroblasts (or augite pseudomorphs?). Subidioblastic to idioblastic magnetite is abundant, and pyrite also is present.

Turning now to REE behavior in the Taylor Formation, Figures 19 and 20 show chondrite-normalized rare earth-abundance patterns for 33 samples. Figure 19 contains the patterns for 19 C-series samples analyzed by INAA at the LLNL in 1978, and Figure 20 the patterns for 14 more samples collected by Mark Varney and analyzed by ICP at Activation Laboratories Ltd. in 1998. As explained earlier, nearly all samples were collected from pillow lavas; five samples represent lava flows that are nonpillowed or indefinitely pillowed, one (C-19) possibly a hypabyssal intrusion. Twelve of Varney's samples were collected at or near seven of the C-series localities, and the 1978 analyses are in surprisingly good agreement with the 1998 analyses. Compare, for example, C-52 and 1-96, from the same locality at the top of the Taylor Formation. All 14 REE were analyzed by ICP, but only nine (including Gd) by INAA. Only those analyses with standard deviation/abundance<20% are included in Figure 19, and in a few cases, abundances were below the detection limit altogether (e.g., La, Tb, and Dy in C-42); analytical method, accuracy, and precision are discussed in Brooks and Coles (1980).

The abundance patterns are arranged in three groups in both figures. The "relict" patterns are LREE-depleted, the "altered" patterns LREE-enriched, the "transitional" patterns nearly flat. Distribution of the three groups of samples is shown in Figure 3. All of the samples having LREE-depleted patterns were collected in the vicinity of Upper Salmon Lake or south of the area shown in the figure (C-1 was collected 3.6 km south of Lower Salmon Lake, C-39 from the base of the Taylor Formation 7.75 km south-southeast of Lower Salmon Lake). In striking

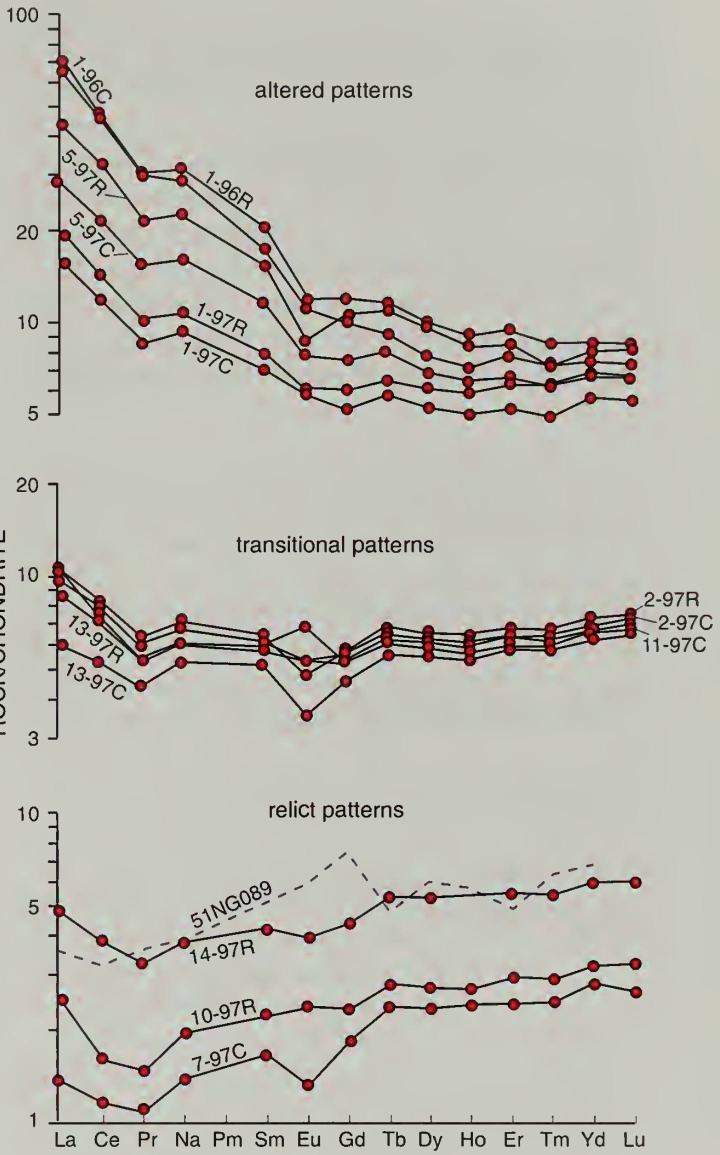

Figure 20. Chondrite-normalized rare earth-abundance patterns of 14 additional Taylor pillow lavas. Sample locations in Figure 3. Samples were collected from both core (C) and rim (R) of five pillows. The LREE-enriched, “altered” patterns are for samples collected in the Big Bear Lake-Long Lake area northwest of the tonalite stock, and reflect introduction of LREE by hydrothermal fluids emanating from the cooling stock. Sample 51NG089 is a Recent island-arc tholeiite from Ulawan volcano, New Britain (Jakes and Gill, 1970). *Analyses by ICP at Activation Laboratories Ltd. in 1998.*

contrast, all the “altered” samples, save one, were collected north of Gold Lake, in the Big Bear Lake-Long Lake area. The single sample collected south of Gold Lake is C-19, and, should it prove to represent a hypabyssal intrusion, its abundance pattern may be LREE-enriched for that reason. Furthermore, the five “transitional” samples at Upper Salmon Lake represent the near-basal pillow lavas mentioned earlier that appear to display mixed, relict tholeiitic and calcalkaline characteristics. The remaining 19 altered and transitional samples are all confined to the Big Bear Lake-Long Lake area.

The three samples having the lowest REE concentrations—C-42, 7-97C, and 10-97R—all were collected from augite-rich pillow lavas at the base of the Taylor Formation west of Upper Salmon Lake. They are the three samples discussed earlier that also are depleted in Zr and Ti. They are quite clearly tholeiitic, based on concentrations of the immobile trace elements Zr, Ti, and Y; composition of the augite phenocrysts; and the REE concentrations. For comparative purposes, the rare earth-abundance pattern of sample 51NG089, from Ulawan olcano, New Britain, is included in Figure 20; this sample typifies a modern island-arc tholeiite with very low REE concentrations (Jakes and Gill, 1970).

Are, then, the Taylor lavas north of Gold Lake having LREE-enriched abundance patterns calcalkaline? No. There is no stratigraphic control of patterns, as seems to be the case for basal and near-basal pillow lavas near Upper Salmon Lake; indeed, there is no relationship—other than a completely random one—between stratigraphic position of lava flows and level of LREE enrichment. Nor does any consistent relationship with silica content exist, as would be expected to result from fractional crystallization or partial melting processes. The change from south to north from LREE-depleted patterns to LREE-enriched ones that span nearly the entire width of the Taylor Formation, seems much too abrupt to be a primary feature of the island arc.

How, then, are the LREE-enriched patterns to be explained? Augite phenocryst composition and Ti, Zr, and Y concentrations indicate these rocks also were originally tholeiitic. Your attention again is directed to the hydrothermally altered tonalite stock north of Gold Lake. It is thought that LREE were introduced into the Taylor lava flows by fluids emanating from the cooling stock. Unfortunately, the tonalite outcrop is covered on its southwest side by glacial moraine (Figure 3), and, possibly, little of the stock is exposed. On the other hand, the exposed part may just represent a cupola atop a larger body extending to the northwest in the subsurface. This is suggested by the large area of rocks containing hydrothermal biotite and the clustering of LREE-enriched samples in that direction (Figure 3).

Many workers have now shown that the REE, as well as Th and U, may be readily mobilized by hydrothermal fluids bearing appropriate complexing anions such as Cl^-, F^-, SO_4^{-2}, PO_4^{-3}, and CO_3^{-2}. Wendlandt and Harrison (1979) found that a CO_2-rich vapor in equilibrium with a silicate melt will be enriched in REE, especially the LREE, and that this is consistent with the formation of REE-carbonate complexes in the vapor. Caruso and Simmons (1981) found that abundant CO_2 in hydrothermal fluids mobilized the LREE and U as carbonate complexes in the Sherman granite, Wyoming; microcracks thought to represent pathways for the fluids are sealed in part by calcite. Since calcite also is a common product of hydrothermal alteration of the Gold Lake stock and dikes, it is likely that the LREE were transported as carbonate complexes in the northern Sierra. What was the source of the CO_3^{-2}? Let me suggest, very speculatively, that the rising tonalite stock intersected easterly dipping carbonaceous cherts in the Elwell Formation at depth.

Figure 21, which compares the most LREE-depleted (sample 7-97C) and most LREE-enriched (sample 1-96C) abundance patterns available, shows that the Taylor lavas north of Gold Lake were enriched in all the REE, but particularly so in the LREE. A linear-regression correlation matrix was prepared using the concentrations of 26 trace elements in the 11 C-series samples collected north of Gold Lake. The strongest correlations generally were found among only U, Th, and the LREE. Correlations among La, Ce, Sm, Eu, Th, and U all had r greater than 0.85; only two correlations, U with Sm and Eu, had r below 0.9. La/Yb, a measure of the relative enrichment in LREE, also correlates strongly with Th (r=0.96), as would be expected, but, interestingly, correlates equally well with Th (r=0.97) when all 18 C-series samples containing detectable Th are used. When La/Yb and Th are correlated using all 14 of Varney's pillow lava samples, r= 0.98; the correlation of La/Yb with U has r=0.96. It is clear that U, Th, and the LREE behaved very coherently during the hydrothermal alteration process.

Figure 21 includes a chondrite-normalized rare earth-abundance pattern for the nearly equigranular, low-color index (ca. 12), eastern part of the Gold Lake tonalite stock; no Eu anomaly is evident. The Th content of sample GL-4 is 4.37 ppm, the U content 1.89 ppm.

It only can be surmised where the REE now reside in the Taylor lava flows. The only mineral so far identified in the lavas that could accommodate the REE in its lattice is sphene. Indeed, the relative enrichment

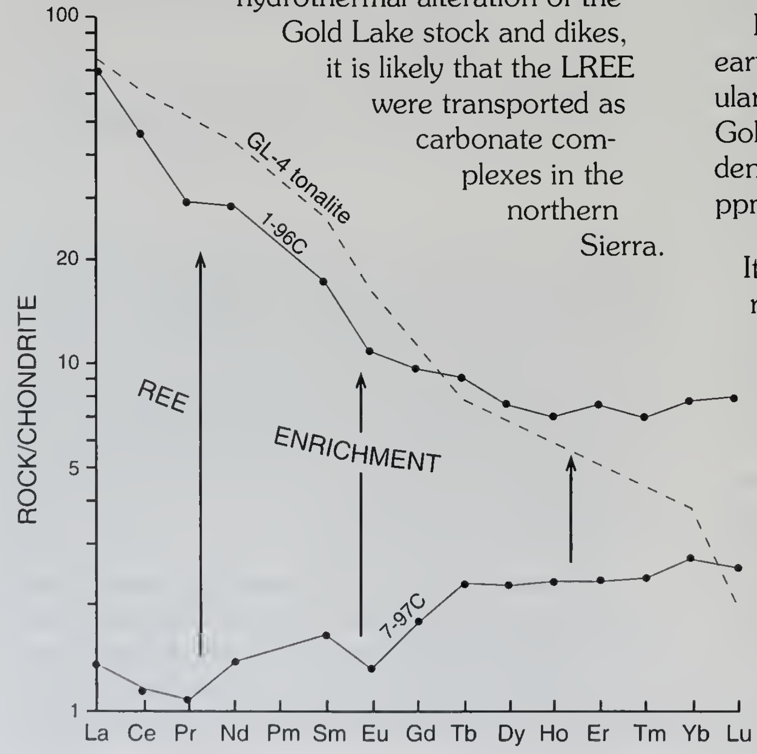

Figure 21. Chondrite-normalized rare earth-abundance patterns for the most LREE-depleted (7-97C) and enriched (1-96C) Taylor samples, showing the magnitude of REE enrichment caused by hydrothermal addition of the REE. Also shown is an abundance pattern (GL-4) for the early Cretaceous tonalite intrusion responsible for the REE addition.

of the REE in the rims of the five pillows for which both rim and core analyses are available (Figure 20) may reflect the fact that the outermost, originally very glass-rich rims of pillows present at Upper Salmon Lake (where they have been carefully studied) now consist largely of chlorite charged with sphene granules (Brooks, 1992). On the other hand, these very narrow outermost rims usually fractured and were lost to the pillow matrix during deposition. It is unlikely they would contribute very much, if at all, to a rim sample. Nevertheless, sphene and/or leucoxene appears to be present in all of the C-series samples examined petrographically, and the sample with the highest REE content, C-52 (Figure 19), has its matrix riddled with granular brown sphene. Also, all the samples contain chlorite, and it is known that the REE may be strongly accumulated by surface adsorption on such phyllosilicates (Roaldset, 1975).

Finally, let's look at one last discrimination diagram that did not work. Although useful because more silicic rocks, not just basalts, can be used, the Wood (1980) diagram (Figure 22) incorporates one flaw, the mobility of Th during hydrothermal alteration processes. Analyses of the ten C-series samples having altered rare earth-abundance patterns and four of the five samples having relict patterns (Figure 19) are plotted in Figure 22 (neither Th, Ta, nor Hf was detected in C-42). We again see the strong correlation of Th with La/Yb, as the four samples with the highest Th content (C-52, C-27, C-23, and C-24; 3.1-5.5 ppm), crowded into the Th corner of Wood's diagram, also are those having the highest La/Yb. The least altered samples, those four with relict REE patterns, have a mean Th content of 0.34 ppm, just above the norm for fresh island-arc tholeiites (0.25 ppm; Wilson, 1989). Although the analyses of these Ta-poor samples all fall neatly in the field of volcanic-arc basalts (Figure 22), they clearly are not calcalkaline, except possibly for C-19, as we have just seen. Even that portion of the volcanic-arc basalt field containing nine analyses of Elwell Formation sills and pillow lavas (Brooks and others, 1982), also clearly tholeiitic, falls well below the Hf/Th=3 division between calcalkaline basalts and island-arc tholeiites. I suspect that Wood (1980) set this dividing line too high, and that it should be shifted toward the Th corner, to about Hf/Th=1; samples C-1 and C-33, and all but one of the Elwell samples would then be classified as island-arc tholeiites. In any case, the Wood diagram provides additional evidence of the great mobility of Th during hydrothermal alteration processes.

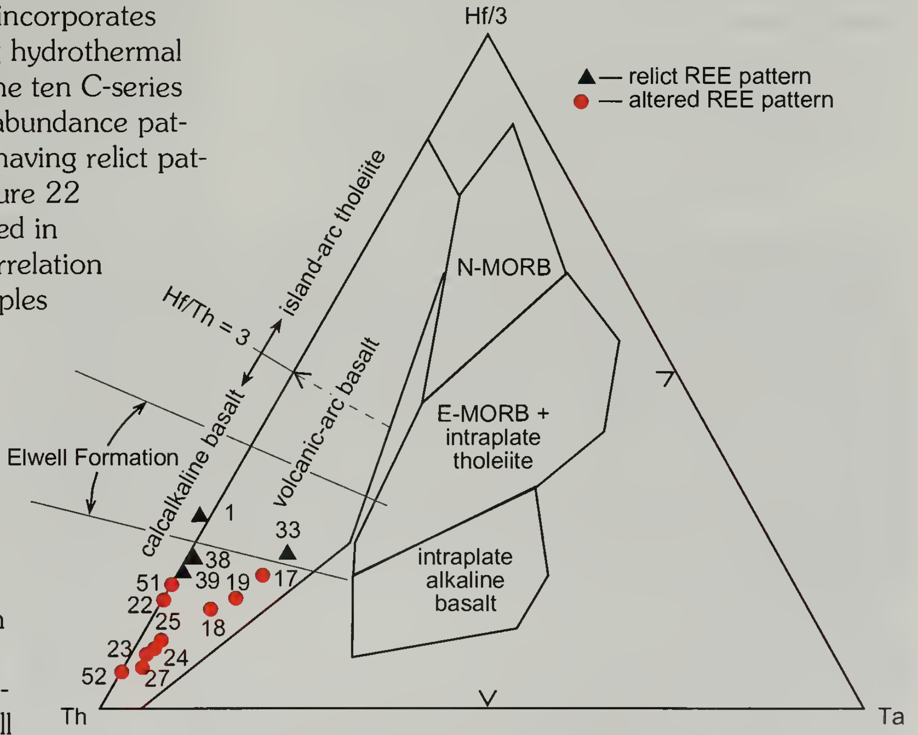

Figure 22. Analyses of 14 Taylor Formation lavas having relict (N=4) and altered (N=10) rare earth-abundance patterns plotted in the discrimination diagram of Wood (1980), demonstrating the striking mobility of Th during hydrothermal alteration of originally tholeiitic Taylor lavas. Ta concentrations were below the detection limit in samples whose analyses fall along the Th-Hf/3 side of the triangle.

FIELD TRIP IN THE LAKES BASIN

Driving Directions to the Lakes Basin

Where the entrance road to the Feather River Inn intersects California Highway 70/89, turn left and drive 0.5 miles (mi.) to the junction with California Highway 89. Turn right on Highway 89 and drive 2.7 mi. through Graeagle to the junction with Plumas National Forest Road 24 (Gold Lake Road). Turn right and drive 6.7 mi. up the east face of the Sierra Nevada across magnificent recessional moraines to the paved road to the Plumas National Forest Lakes Basin campground. Turn right and drive 0.3 mi. to the junction with the road entering the campground on your right. Proceed straight ahead 0.6 mi. to the end of the road at the Bear-Silver Lake trailhead (Figure 12).

Eleven stops have been planned along a clockwise circuit through the Lakes Basin (Figure 12). Stops 1 through 7, and 11, are in the lower half of the Taylor Formation, Stops 8 and 9 are in the Elwell Formation, and Stop 10 will permit a peek at silicic autobreccia quarried by a glacier from the Sierra Buttes Formation to the west. We will start approximately in the middle of the Taylor Formation (Stop 1), and proceed *down-section* all the way to Stop 9. All of the Devonian rocks we visit have been affected by Jurassic greenschist-facies metamorphism, and by early Cretaceous hydrothermal metamorphism as well (Figure 3).

From the parking area at the trailhead, take the Bear Lake trail toward Big Bear Lake, 0.5 mi. away. Patchy ground moraine associated with a late post-Sangamon glacial advance is encountered along the way (Mathieson, 1981). Leave the Bear Lake trail just after it first becomes tangent to a stream on your left (Big Bear Lake outlet), cross the stream, and proceed uphill to Stop 1 on the ridge-forming outcrops.

Stop 1. Taylor Formation Pillow Lava Overlain by Sandy and Silty Turbidites

The pillows here are for the most part so large and closely-packed that they are revealed only by occasional elongated, white, quartz amygdules arranged radially about pillow centers, like the spokes of a wagon wheel. However, as one walks easterly across the outcrop, epidote-rich, tuffaceous(?), pillow matrix increases sufficiently in amount that pillow "triple junctions" are seen; also, margins of pillows weather brick red. Pillow triple junctions, dark pillow selvages, and elongated quartz amygdules near pillow margins all are well shown in Photo 7; the view is southeast, so that the facing direction (NE) is toward the left edge of the photograph. Many roundish, yellow-green, epidote-rich patches occur in the pillow lava nearby. Abundant, small, relict, plagioclase phenocrysts typically form glomerocrysts; relict augite phenocrysts are inconspicuous. Tiny (1-2 mm), round, green, chlorite amygdules accompany the large quartz amygdules, and epidote may be found in amygdules as well.

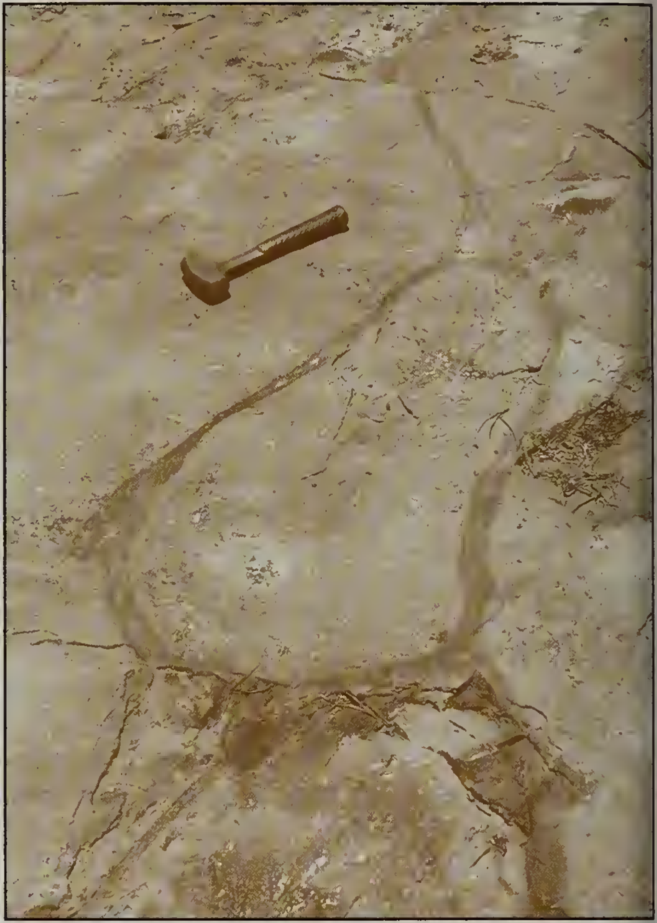

Photo 7. Taylor Formation pillow lava at field trip Stop 1. Dark brick-red selvages outline individual closely-packed pillows. Scant tuffaceous(?) matrix is present at pillow triple junctions, and white quartz amygdules are elongated perpendicular to some pillow margins. *Photo by E.R. Brooks.*

Thin sections show that the plagioclase phenocrysts now consist of albite (ca. An_5) and the rare augite phenocrysts of actinolite. Copious amounts of relatively coarse and deeply colored actinolite occur in the rock matrix, which probably originally was hyalopilitic, glass dominating slender plagioclase microlites. The subidioblastic actinolite prisms (Z^c ca. 15°; birefringence ca. 0.029) are conspicuously pleochroic and relatively Fe-rich (X=yellow, Y=olive, Z=blue-green; Z>Y>X). Tiny black opaque laths, probably of ilmenite, also are ubiquitous.

Table 4 presents the average chemical analysis of two pillow cores collected at this locality (samples C-21 and 2-97C); the analysis may be compared to the averages of Taylor lava flows in Table 3. The TAS classification yields a silicic basaltic andesite.

Table 4. Average of major-element, whole-rock chemical analyses of two Taylor Formation pillow cores collected at Stop 1.

SiO_2	56.75
Al_2O_3	15.25
TiO_2	0.42
$Fe_2O_3{}^T$	10.53
MgO	5.40
CaO	7.60
Na_2O	3.67
K_2O	0.14
P_2O_5	0.05
MnO	0.18
	99.99

$Fe_2O_3{}^T$ = all Fe calculated as Fe_2O_3

To the southeast along the outcrop are fine exposures of the overlying turbidites. The basal unit, comprising three, amalgamated, fining upward turbidites, occupies a channel in very closely-packed pillows. Strata are buttressed against the steep north side of the channel. The lower two of the three turbidites, each about 85 cm thick, have structureless bases of sandstone and pebbly sandstone that pass upward to finer, well-stratified sandstone; the uppermost turbidite, ca. 55 cm thick, is capped by siltstone (lower half of Photo 8). Surprisingly, these Taylor Formation rocks consist of materials derived from the Sierra Buttes Formation, ca. 1.8 km down-section from here! Subrounded to subangular pebbles to ca. 3 cm long consist of plagioclase-phyric andesite and quartz- and plagioclase-phyric dacite, and smoky gray quartz phenocrysts freed by erosion make up much of the sand-size detritus in places. Photo 9 shows a relatively angular, 28 mm-long pebble of quartz-phyric dacite present in the stratified top of the lowest turbidite; the facing direction (NE) is toward the top of the photograph. The thin bed containing the pebble is inversely graded. Is it a traction-carpet layer in a high-density turbidite?

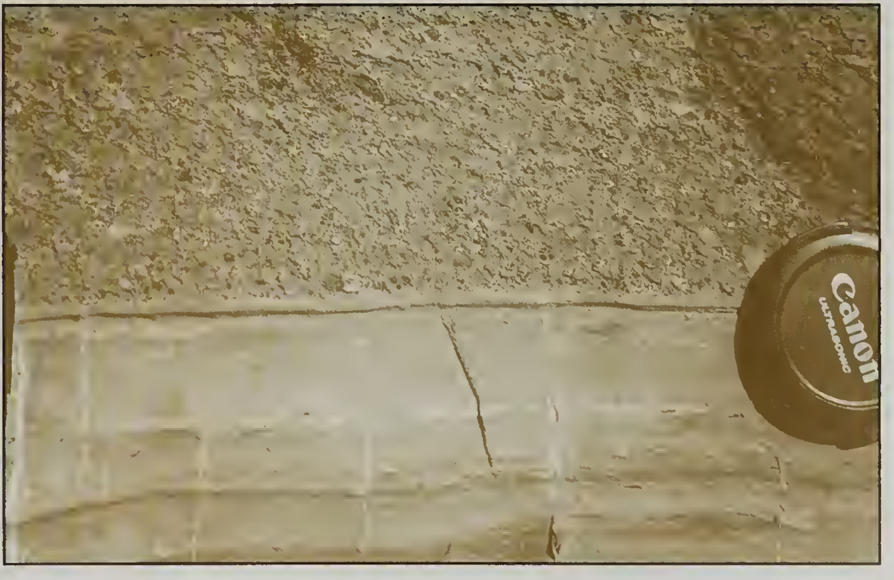

Photo 8. Mafic turbidite of local derivation overlying the silty top of a more silicic turbidite having a more distant source in the Sierra Buttes Formation. Stop 1 in the Taylor Formation. Facing direction is toward the top of the photograph. *Photo by E.R. Brooks.*

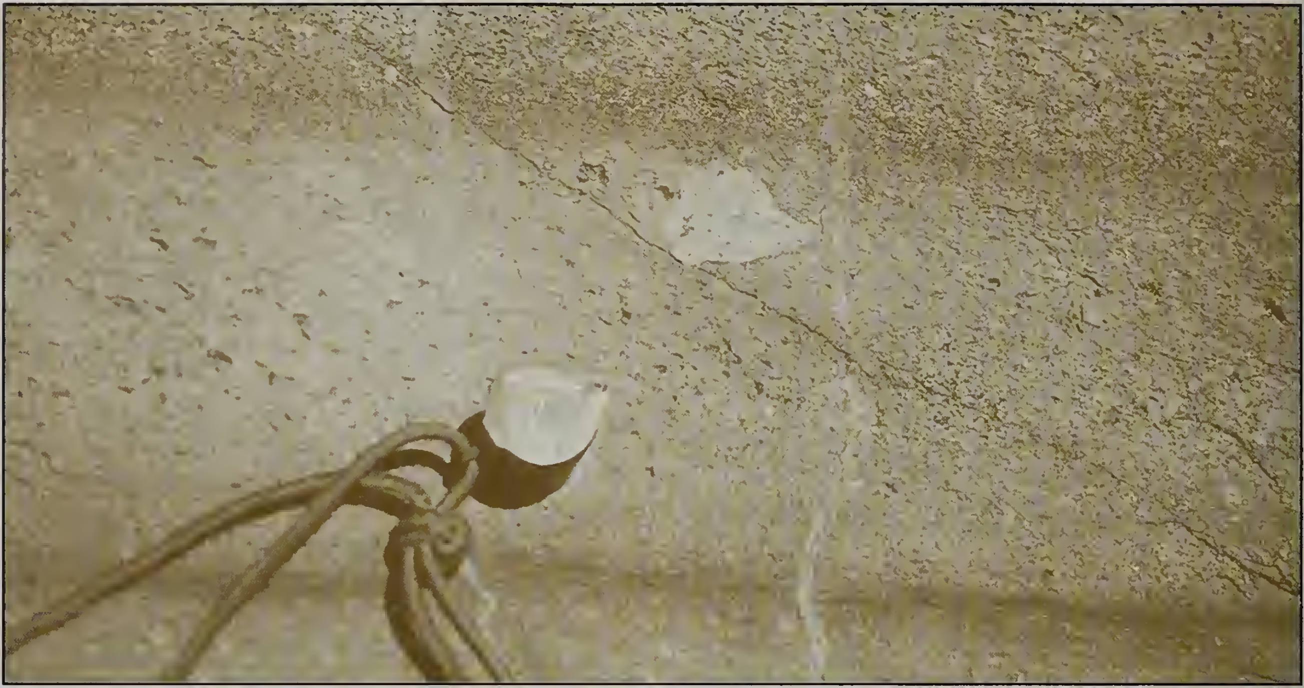

Photo 9. Stratified top of an epiclastic turbidite consisting of sediment derived from the Sierra Buttes Formation. Stop 1 in the Taylor Formation. The subangular dacitic pebble in the center of the photograph occurs at the top of an inversely graded bed (facing direction is toward the top of the photograph). *Photo by E.R. Brooks.*

Abruptly overlying the silstone is another pebbly sandstone of very different composition (Photo 8). It is rich in augite phenocrysts to 8 mm long and smaller plagioclase phenocrysts eroded from Taylor lava, and also contains plagioclase-phyric pebbles to 6 cm long. Occasional quartz-phyric dacite pebbles nevertheless still occur, and a single phosphate nodule is present, perhaps reflecting the (PO_4)-rich ocean water in which the turbidites accumulated (Brooks and others, 1982). The top of this 38 cm-thick bed contains rip-up clasts derived from the underlying siltstone. Photo 8 shows the exceedingly sharp conformable contact between dark augite-rich sandstone and underlying, more silicic siltstone. Many bleached fractures cut across the bedding, perhaps former pathways for hydrothermal fluids leaving the Gold Lake tonalite stock or subjacent pluton.

So, in only a little more than 2.5 m of section, we see evidence of turbidity currents transporting detritus from very different sources, one local (Taylor Formation), one distant (Sierra Buttes Formation). Also, the turbidites at this locality are plainly of the epiclastic, not pyroclastic, kind, since Sierra Buttes volcanoes were long extinct when these turbidites were deposited.

Thin sections of pebbly sandstone of Sierra Buttes derivation disclose a strong foliation determined by dimensional preferred orientation (DPO) of chlorite and biotite. Though some of the biotite, considerably coarser than the chlorite, lies rigorously in the foliation, some biotite plates lie directly across the foliation, and the biotite crystallized during emplacement of the nearby early Cretaceous tonalite stock (Figure 3). Relict lithic clasts tend to be aphyric or sparsely plagioclase-phyric; one clast contained a quartz phenocryst. Clast matrices range from those rich in plagioclase microlites to those that are microlite-free; the former often are pilotaxitic. Other grains, of coarse sand- to granule-size, represent plagioclase and quartz phenocrysts freed from their matrices by erosion. Surprisingly well-formed plagioclase grains, suggesting little abrasion during erosion and transport, are particularly abundant. The metamorphic mineral assemblage of the pebbly sandstone is albite-chlorite-quartz-epidote-biotite-pyrite-black opaque mineral.

A thin section of the siltstone reveals strong foliation parallel to the relict stratification, thin laminae being alternately rich and poor in biotite; epidote forms ellipsoidal patches that parallel the foliation (Photo 8). The larger relict grains, of fine sand-size, are mostly of quartz, some conspicuously angular.

Relict lithic clasts (fine to medium pebbles) in the augite-rich pebbly sandstone are aphyric or plagioclase- and augite-phyric. They may be richly amygdaloidal, the vesicles filled with chlorite, biotite, quartz, epidote, and actinolite in widely variable proportions. Lithic-clast matrices, typically containing few plagioclase microlites, are rich in fibrous actinolite in decussate arrangement; biotite also may be abundantly present. Very coarse sand- and granule-size grains of plagioclase and augite now largely consist, respectively, of albite (ca. An_6) and actinolite, chlorite, epidote, quartz, and biotite in endlessly varying combinations and proportions. Not all is Taylor debris, however. Several quartz grains were located; one was very angular, but others retained original crystal faces. With addition of the Fe-rich actinolite, the mineral assemblage is the same as that in the pebbly sandstone of Sierra Buttes derivation.

Upon leaving the turbidite exposures, walk south to a prominent trail. Turn right and follow the trail west to Big Bear Lake. Then follow a well-worn fisherman's path south along the east shore of Big Bear Lake to the first prominent point of land in the lake; Stop 2 is at the end of the point (Figure 12). The summit of Mt. Elwell is seen N40W of Stop 2.

Stop 2. Early Cretaceous Andesite Dike

The Taylor Formation here is inconspicuously brecciated; we will see much better examples of breccia at Stop 3. The attraction at Stop 2 is not the Taylor Formation, but the narrow, gray, hornblende andesite dike choked with large, chalky, white, plagioclase phenocrysts. The rectangular (actually tabular) phenocrysts are so conspicuous because they have been hydrothermally altered to very fine-grained epidote and white mica; cleavages have been dulled by the alteration. The generally smaller, black, lustrous phenocrysts are of hornblende (and, rarely, biotite). Though quite severely altered, this is the only rock you will see today that has escaped greenschist-facies regional metamorphism. This is so because the dike is early Cretaceous (122 Ma), originating in the tonalite stock (or subjacent pluton) at the northeast end of Gold Lake (Lull, this volume). The 120-122 Ma ages of the dike and stock place an upper limit on the age of regional metamorphism, traditionally attributed to a late Jurassic, Nevadan orogeny.

The tabular andesite dike obviously followed a pre-existing planar fracture, which actually is exposed where the dike briefly left it to exploit other fractures having different orientations. Careful examination of the dike at this point will reveal miniature apophyses choked with plagioclase phenocrysts, one curved and seemingly detached from the dike (near the pencil eraser in Photo 10). Photo 10 suggests that the dike was confused at this point about which set of fractures to follow. The dike stops abruptly at times, only to reappear farther along the master fracture. Interesting right-angle offsets (not fault

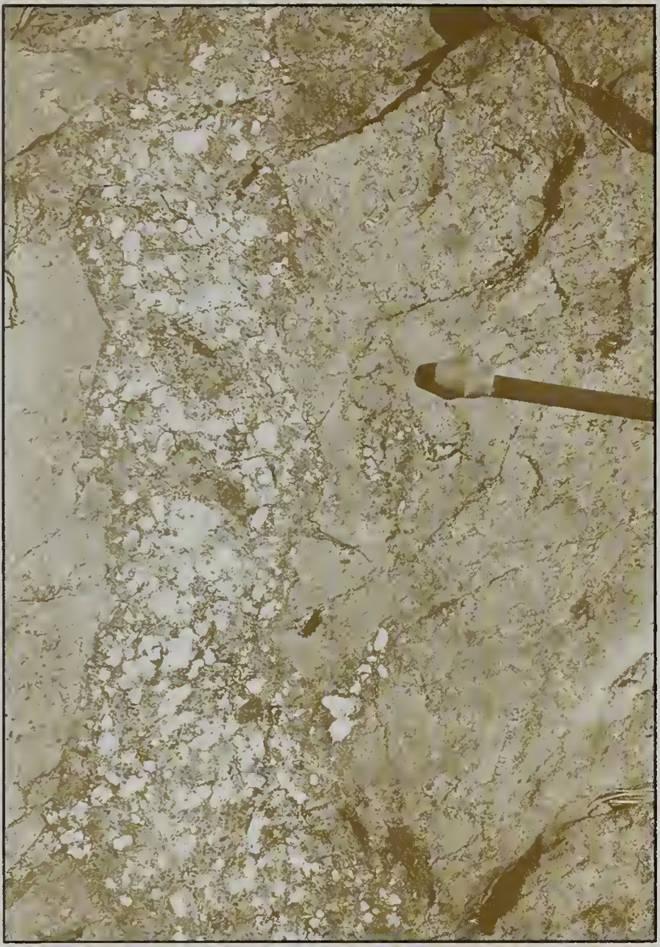

Photo 10. Early Cretaceous hornblende andesite dike intruding the Taylor Formation at Stop 2. The numerous white plagioclase phenocrysts have been hydrothermally altered to epidote and white mica. The dike evidently was intruded into two sets of fractures at this point. *Photo by E.R. Brooks.*

offsets) of the dike occur where the master fracture intersected fractures oriented at right angles to it. The master fracture strikes N78W and dips steeply southward, so that projection of the dike to the southeast will cause it to intersect the tonalite stock just south of the stock's outcrop, where it is covered by moraine (Figure 3).

Microscopic study discloses that the large (to 1 cm) plagioclase phenocrysts display considerable rounding (resorption), and that, though they largely were replaced by epidote and white mica, untwinned plagioclase still is apparent in places. Numerous strongly zoned and polysynthetically twinned, platy plagioclase microlites hid-den in the aphanitic rock matrix, however, essentially escaped alteration. Were the phenocrysts altered while still in the magma? The rest of the matrix now consists of extremely fine-grained quartz and biotite. The numerous prismatic phenocrysts of hornblende, to ca. 3 mm, are accompanied by equally abundant, sometimes clustered microphenocrysts, as well as micro- lites. The phenocrysts are color-zoned, with brown rims and green interiors (=Z'); the smaller microphenocrysts may be completely brown, sometimes quite reddish. Other properties include Z^c ca. 18°, birefringence ca. 0.03, and polysynthetic twinning on {100}. The hornblende is not entirely pristine: patches of chlorite and epidote formed at the expense of the hornblende adjoin rounded, altered, plagioclase inclusions in one phenocryst. Also present in the andesite are pyrite cubes and apatite microphenocrysts 0.3 mm in diameter.

When you have finished admiring this spectacular dike, continue west along the lakeshore past the *faux* petroglyphs. The path soon becomes brushy and less trodden, so follow your leader closely. We will have to negotiate a rock ledge above the lakeshore at one point, but no one ever has fallen into the water. We will see more andesitic dike rock and a lot more Taylor breccia, some containing augite-phyric fragments, on the way to Stop 3.

Stop 3. A Debris-flow Deposit in the Taylor Formation: Epiclastic or Pyroclastic?

Though clearly not in place, but representative of glacially excavated rock upslope from us, this beautiful slab allows us to discuss the terminology of fragmental volcanic rocks ("volcaniclastic" rocks) in subaqueous island arcs. Some such rocks, of course, must be pyroclastic, but many are in fact epiclastic, like those at Stop 1, where sedimentary terms ("pebbly sandstone," "siltstone") were used even though the rocks consisted entirely of volcanic materials (i.e., were "volcanogenic"). Still other volcaniclastic rocks—doubtless many of them—consist of pyroclasts resedimented shortly after deposition by sediment gravity flows—turbidity currents and debris flows. These may be difficult to recognize, since epiclastic sediments also are deposited by turbidity currents and debris flows, as at Stop 1. To identify rocks consisting of pyroclasts, or resedimented pyroclasts, one must search for pumice. As Fiske (1969, p. 2) pointed out long ago, "It is...unlikely that large volumes of pumiceous debris can be eroded from lithified source rocks...,"so that abundant pumice is not expected to be found in epiclastic rocks. Fiske (1969, p. 2) also noted "...that rocks rich in pumice have enormous surface areas of unstable volcanic glass, and this material is highly susceptible to diagenesis and low-grade metamorphism." Indeed, confirmation of the former presence of pumice in these thrice-metamorphosed rocks rarely is easy; an exception will be seen at Stop 7. When in doubt about the origin of a rock, whether pyroclastic, epiclastic, or a product of that gray area between the two, I have tended to use Fisher's (1966) classification of pyroclastic fragments, *provisionally* arriving at rock names such as "lapilli tuff" and "tuff-breccia." Autoclastic and hydroclastic volcaniclastic rocks also occur in subaqueous island arcs, as we will see at Stops 6, 9, and 10.

Consider now the slab of volcaniclastic rock made available to us by a late post-Sangamon glacier. How would the rock be named using Fisher's (1966) classification? (sixty blocks are supported by 40% ash, leading to the name "tuff-breccia.") At first glance, this tuff-breccia—if that's what it is—appears heterolithologic, since block colors range from very light to quite dark. However, most, if not all, blocks contain the same, small (up to ca. 2.5 mm), relict, augite phenocrysts, often as glomerocrysts (Photo 11). Proportions of phenocrysts do vary greatly from block to block, but all blocks doubtless are broadly of the same composition, likely basalt or basaltic andesite. Although the overall sorting of this matrix-supported tuff-breccia(?) is of course poor, the two size modes (block and ash) are individually remarkably well-sorted. The tuff-breccia(?) probably is a debris-flow deposit, but how did the fragments originate? As pyroclasts, eroded from lava flows, etc.? Photo 11 shows parts of four subangular blocks present at the upper left

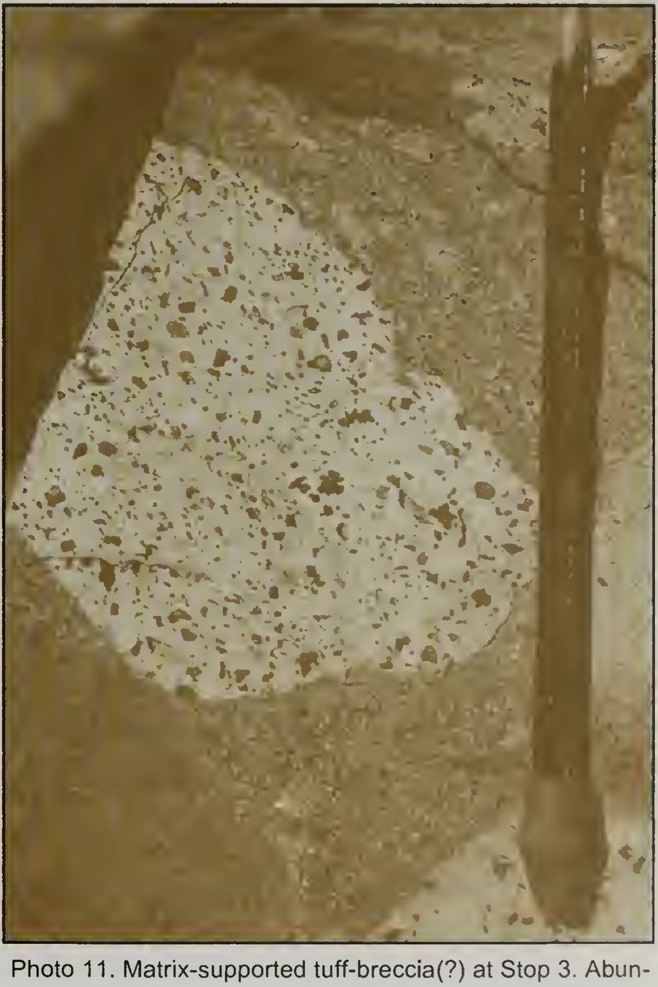

Photo 11. Matrix-supported tuff-breccia(?) at Stop 3. Abundant relict augite phenocrysts and glomerocrysts (black crystals) confirm a Taylor Formation source for the blocks. Blocks and tuffaceous(?) matrix are individually remarkably well sorted. *Photo by E.R. Brooks.*

corner of the slab; note the highly varied colors and augite phenocryst proportions. A nice augite glomerocryst appears in the center of the photograph.

A thin section of one of the blocks shows it to be both richly augite-phyric and richly amygdaloidal. Plagioclase phenocrysts also were once present, but were rendered nearly invisible when replaced by granular epidote+/-calcite+/-biotite. The augite phenocrysts were replaced by actinolite and biotite+/-calcite+/-epidote. Sphene is concentrated in the very fine-grained rock matrix, and calcite, epidote, and biotite can be identified there, as well. Biotite is most conspicuous in amygdules, where it occurs with chlorite, epidote, and actinolite; coarse idioblastic epidote nucleated on vesicle walls, and penetrates extremely fine-grained chlorite in amygdule interiors. In marked contrast, occasional amygdules consist very largely of calcite. The biotite, evidently formed during early Cretaceous hydrothermal metamorphism, previously was misidentified as stilpnomelane, a mineral often found in mafic greenschists.

Upon leaving Stop 3, continue on the rough fisherman's path along the west side of Big Bear Lake, crossing the stream issuing from the lake on your left. The high knob we pass on your right consists of additional closely-packed Taylor pillows. Just before reaching Big Bear Lake again, an outcrop exhibiting bizarrely deformed masses embedded in voluminous matrix is encountered at Stop 4 (Figure 12). Here is one of the least understood rocks in the entire island arc.

Stop 4. Possible Isolated-pillow Breccia in the Taylor Formation

I have interpreted these distorted masses—quite possibly incorrectly—as deformed pillows incorporated into slumping lapilli tuff immediately upon deposition, while still plastic. They share many features with andesitic pillows described by Hanson (1991) in rocks that he considers to be intrusive isolated-pillow breccias. Shared characteristics include the highly irregular, sometimes amoeboid shapes (Photo 6); dark red-brown, originally glassy selvages; and incorporation of granulated glassy selvages into the pillow matrix (Photo 12). Accordingly, I tentatively interpret the rocks at Stop 4 as extrusive isolated-pillow breccia. Hanson (1991, p. 813) feels that the amoeboid shapes of pillows "...develop when chilled pillow rinds are repeatedly punctured by protruding fingers of magma during quenching." Hanson and I at least agree that these highly distorted masses are pillows.

Other features of the pillows at Stop 4 are their plagioclase-phyric and amygdaloidal character. Epidote, chlorite, and quartz amygdules are so abundant in some pillows that I entertained the possibility that the pillows really were deformed pumice blocks in a subaqueous pyroclastic flow. However, the pillows are not microvesicular, as are the pumice blocks in the Tamarack tuff, an andesitic subaqueous pyroclastic-flow deposit in the upper part of the Sierra Buttes Formation (Legler and others, 1991). Photo 12 shows twisted pillows at Stop 4 that exhibit dark red-brown, originally glassy rinds that apparently were fragmented in places and incorporated into adjacent pillow matrix.

Microscopic examination of a pillow reveals that relict subhedral plagioclase phenocrysts and glomerocrysts are very abundant, but that few relict augite phenocrysts are present. All phenocrysts have been replaced by appropriate metamorphic phases, and the mineral assemblage is one characteristic of the greenschist facies for mafic protoliths: epidote-albite (ca. An_6)-actinolite-chlorite-quartz- sphene-pyrite. (Note that the hydrothermal biotite is not present here.) Mineralogy of the amydules is interesting. Most consist largely of epidote, the others mostly of chlorite or quartz. The former possess narrow rims of quartz+/-chlorite, and are otherwise filled by coarse idioblastic epidote—the prisms oriented perpendicular to vesicle walls—followed abruptly inward by much finer grained epidote and pyrite. The narrow rims of microgranular quartz persist in the chlorite-rich amygdules, whose central parts consist of relatively coarse platy chlorite and fine sphene, and occasional coarse epidote idioblasts. The few amygdules consisting mostly of quartz have the same very fine-grained quartz rim, followed inward by a second thin shell of chlorite and sphene, and, finally, by quartz whose grain size increases inward, opposite the behavior of epidote noted above. Most amygdules have round or oval, undistorted shapes.

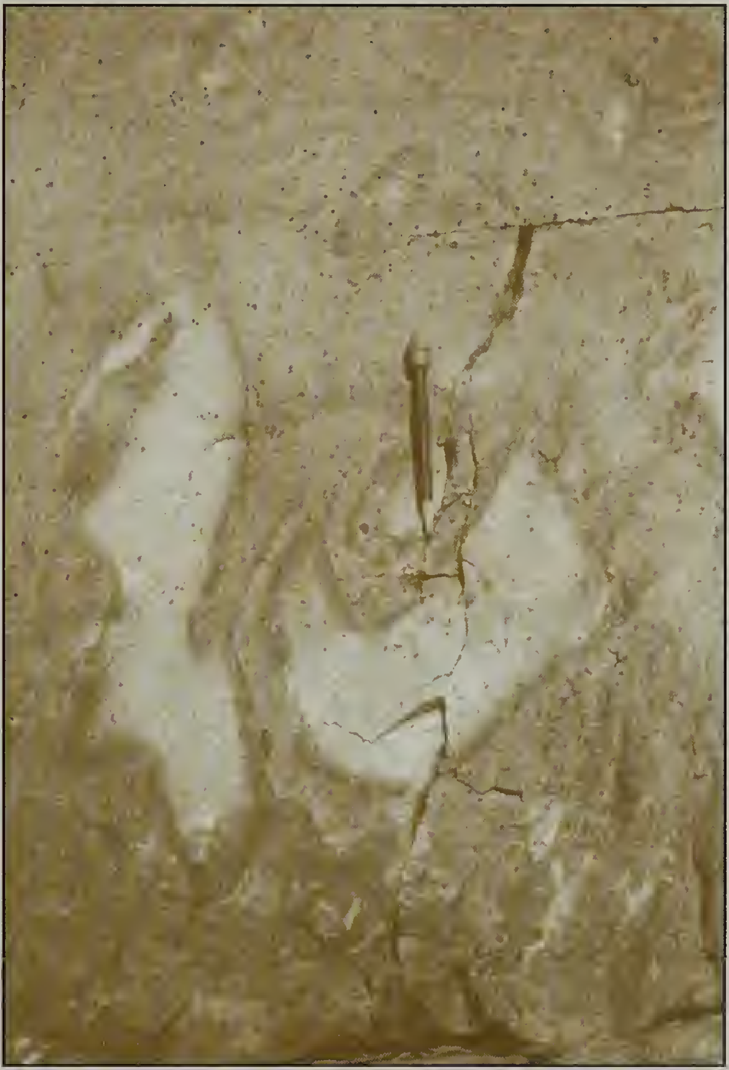

Photo 12. Possible isolated-pillow breccia in the Taylor Formation at Stop 4. Small deformed pillows are partially bounded by dark red-brown selvages representing original glassy margins. Granulation of the glassy margins probably contributed material to the voluminous pillow matrix. *Photo by E.R. Brooks.*

Upon leaving Stop 4, continue north on the path past Little Bear Lake to the Bear Lake trail. Turn left (west) toward Long Lake, first passing Cub Lake, one of the series of paternoster lakes that began with Big Bear Lake. Cub Lake rests on a glacial tread ca. 20 m above that hosting Big and Little Bear lakes. As you leave the Cub Lake signpost, large, white, glacial erratics will be encountered on both sides of the trail. These consist of quartz- and plagioclase-phyric dacite, and we will view this material at Stop 10, nearer its source in the Sierra Buttes Formation. Climb one more glacial riser, and, when the trail junction is reached at the recessional moraine above Long Lake, turn left (southwest) toward Silver Lake. We will pause for a view of Mt. Elwell and the glacially carved Long Lake basin at Stop 5 (Figure 12).

Stop 5. Overview of Stratigraphy

Photo 13, a view northwesterly to the south shoulder of Mt. Elwell and the ridge separating the Jamison and Long Lake basins, shows, from right to left, the bottom of the Taylor Formation, the thin Elwell Formation, and the top of the Sierra Buttes Formation. All the reddish gray rocks enclosing Long Lake belong to the Taylor Formation; the apparent dip of the tabular units underlying Mt. Elwell is ca. 30° E. Much of the Elwell Formation consists of easily broken radiolarian chert, so that it is poorly exposed and heavily forested; a 15 m-thick andesite sill forms a bump on the skyline, however. The contact between gray-weathered Elwell chert and brown, oxidized, Sierra Buttes Formation is seen at the lowest point in the saddle. Sierra Buttes rocks are often exceptionally pyritic and strongly oxidized immediately beneath the Elwell chert.

After you have enjoyed the view, walk up the trail to Silver Lake. Continue straight ahead at the trail junction, toward Mt. Elwell and the Pacific Crest Trail. At the next trail junction, several switchbacks above Silver Lake, take the left fork, but soon leave it and proceed southerly to Stop 6 at the base of the large bedrock knob (Figure 12).

Stop 6. Peperite Near the Base of the Taylor Formation

This spectacular exposure of peperite recently was described by Brooks (1995; Photo 14). Well-bedded crystal-lithic tuff and lapilli tuff serve as host for a hypabyssal intrusion having sill-like top and discordant base. Augite- and plagioclase-phyric tuffs and intrusion are petrographically alike, and thought to be basaltic. The lapilli tuff forms relatively thick structureless beds considered to be deposits of debris flows. Interbedded with these are thinning- and fining-upward sequences of tuff thought to

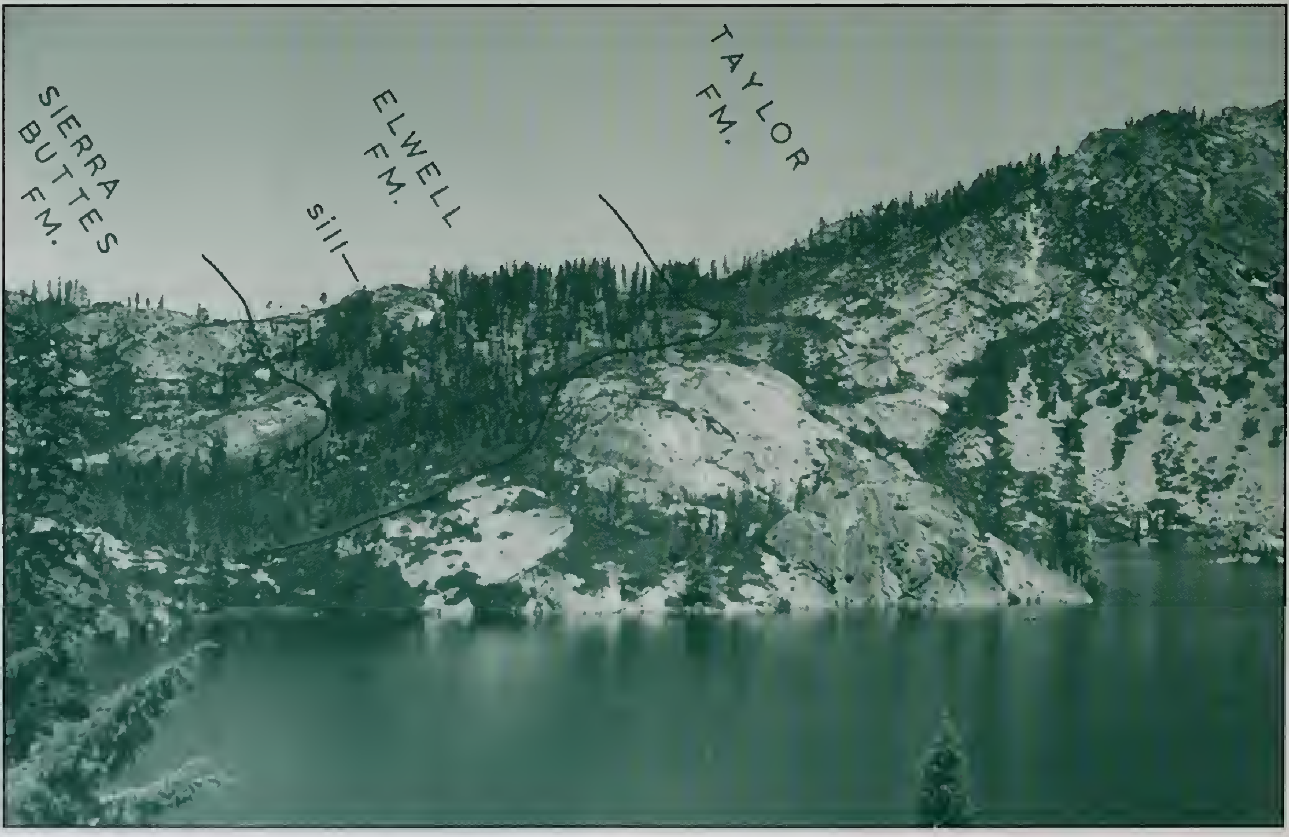

Photo 13. Easterly dipping Taylor Formation is underlain successively by the Elwell and Sierra Buttes formations. View northwesterly across Long Lake from Stop 5. Summit of Mt. Elwell (7,818', 2,383 m) is at the right edge of the photograph. *Photo by E.R. Brooks.*

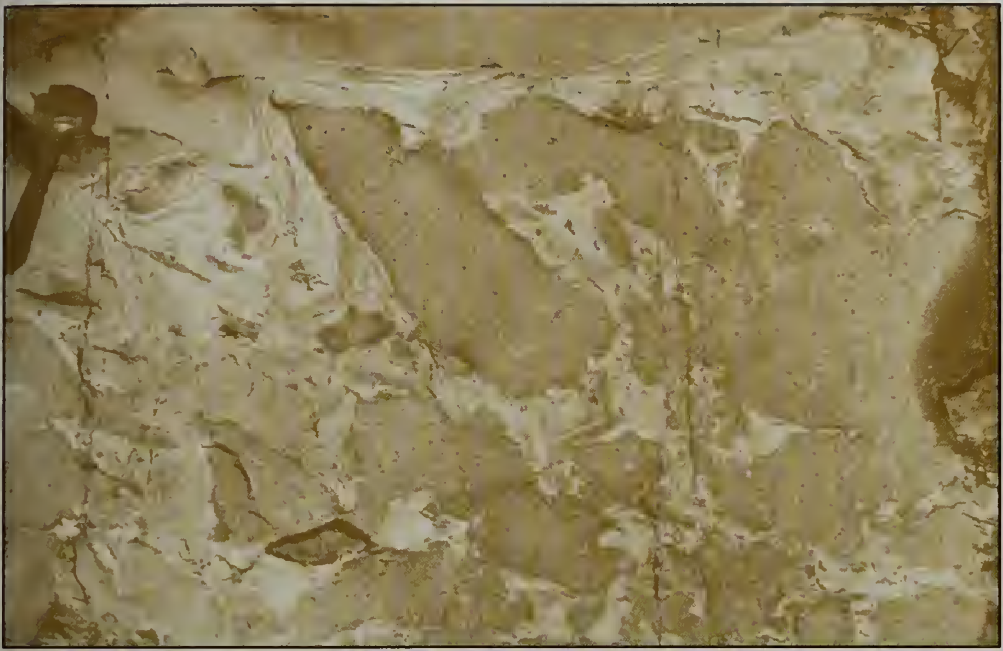

Photo 14. Peperite composed of irregular, block- and lapilli-size, augite-phyric, basalt fragments embedded in fine tuff. Facing direction (NE) is toward the top of the photograph. Note the fragment-cored anticlines in overlying thinly laminated tuff, and the progressive destruction of lamination downward into the intrusion caused by fluidization of ash. *Photo by E.R. Brooks.*

be ash turbidites. A thin horizon up to ca. 70 cm thick adjoining the generally concordant top of the intrusion contains especially fine-grained, thinly laminated tuff that was evidently water-saturated and unlithified at the time of emplacement of the intrusion (Photos 14 and 15).

The water-saturated ash initially was heated by the intrusion at approximately constant, essentially hydrostatic pressure. Concurrently, the top of the intrusion was quenched and divided by shrinkage fractures. Pressure momentarily approached zero as the shrinkage fractures opened abruptly, causing vaporization of the pore water and substantial, but *not* explosive, expansion and fluidizing flow of the resulting steam. The ash was swept into the shrinkage fractures, and, where the downward-propagating fractures intersected one another, basalt fragments were detached to form in situ peperite (Photo 14). (Justification of the rather dogmatic assertions in this paragraph appears in Brooks, 1995.)

Mesoscopic folds are associated with the row of basalt blocks in coarse peperite marking the fractured top of the intrusion (Photos 14 and 15). Each anticline has a basalt block in its core, whereas the spaces between blocks are occupied by synclines surmounting tuff-filled shrinkage fractures. In fold profiles, individual tuff laminae commonly thin—even terminate—against the upper surfaces of basalt blocks in anticlinal crests and thicken greatly in adjoining synclinal troughs (Photo 15). However, the marked thickening of tuff laminae in synclinal troughs decreases rapidly upward, so folds quickly become more open up-section before dying out completely in overlying laminated tuff (Photo 15). Were the anticlines produced by lifting of detached basalt blocks into plastic tuff, by stuffing tuff into shrinkage fractures between blocks to form the synclines and pulling it over their upper surfaces to produce the anticlines, or by both processes? Whatever the cause of folding, forcible intrusion of magma may be ruled out; indeed, the basalt intrusion largely was emplaced *passively*, by fluidization of tephra along its margins (Kokelaar, 1982).

Upon leaving Stop 6, clamber up the west edge of the outcrop, climbing over some nicely rippled ash turbidite (Bouma T_c division) at one point. Planar-bedded turbidites and debris-flow deposits, interrupted only by dikes and sills, occur all the way to the top of the bedrock knob at Stop 7.

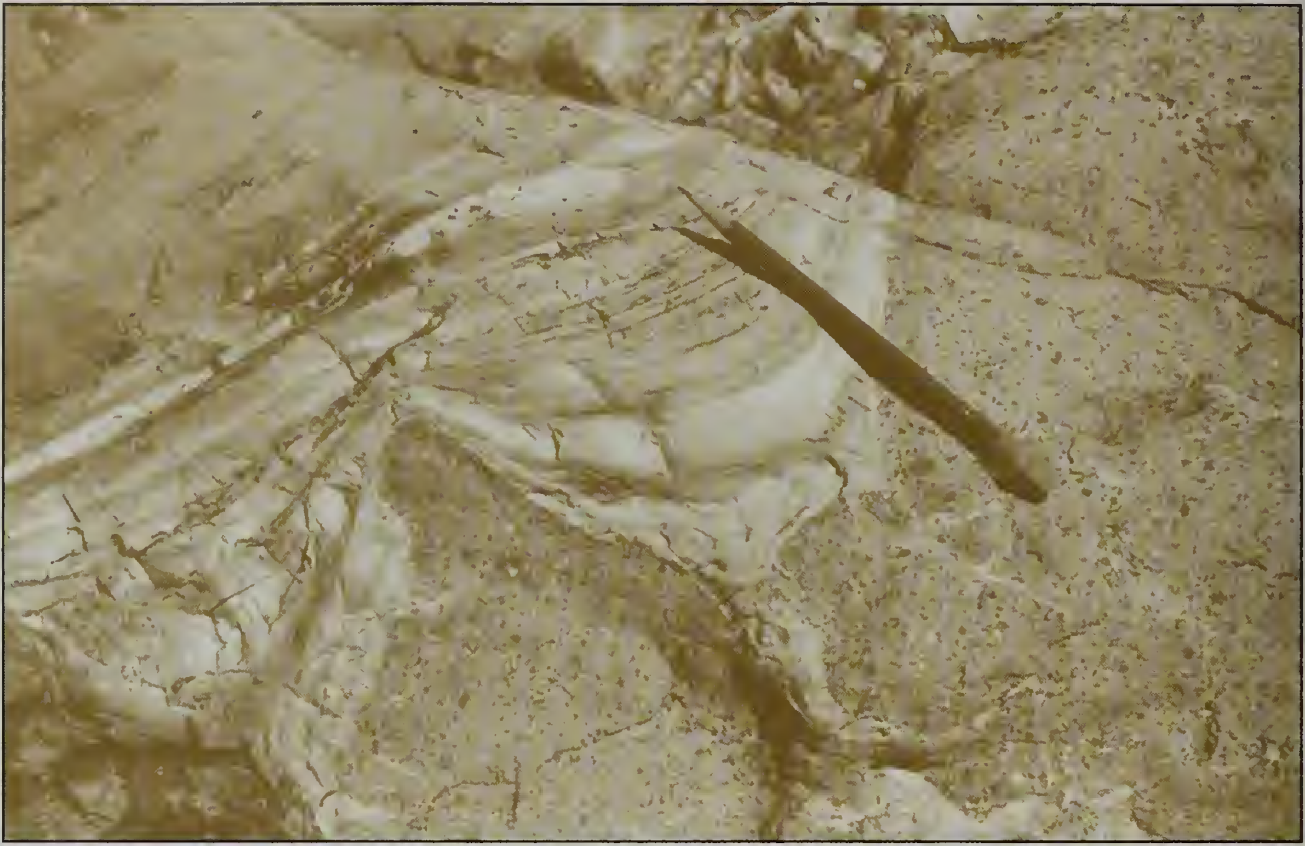

Photo 15. Block-cored anticline in thinly laminated tuff flanked by disharmonic synclines; the right-hand syncline can be seen to pass downward into a tuff vein filling an irregular shrinkage fracture. Pencil points up-section. Dark crystals in the basalt are relict augite phenocrysts. *Photo by E.R. Brooks.*

Stop 7. Pumice in the Taylor Formation

Here is the elusive pumice. Pick a round "lump" (technically, a lapillus), get your nose down on the outcrop, and, with your hand lens, you should see tiny, round, gray, quartz amygdules. If not, try another lump—some pumice is microvesicular, and some lumps are not pumice at all, but instead sparsely vesicular lithic fragments. These are "round-bubble" pumices, rather than the more familiar "long-tube" variety found in subaerial ash-flow tuffs (ignimbrites). The presence of relict pumice indicates that this structureless lapilli tuff originated either as a pyroclastic flow or as resedimented pumiceous tephra (a debris flow).

Thin sections show that many of the larger (ca. 2.5 cm) lapilli indeed are poorly vesicular lithic fragments. The lithic lapilli contain augite and/or plagioclase phenocrysts, are weakly to richly microlitic (plagioclase microlites), and are only locally microvesicular or possess only scattered larger vesicles (up to ca. 1 mm). Recrystallization of these lapilli resulted in such varied products as plagioclase phenocrysts replaced by quartz or by albite, epidote, and chlorite, and augite phenocrysts replaced largely by quartz and actinolite, with some epidote, or by actinolite, chlorite, epidote, and minor quartz. Generalizations are almost impossible; suffice it to say that the common mafic greenschist assemblage, albite-epidote-actinolite-chlorite-sphene-quartz, is very well developed. Most amygdules consist of quartz+/-epidote.

Much of the pumice is microvesicular, the close-packed vesicles averaging ca. 0.05 mm across, but easily recognized down to 0.015 mm. Otherwise round microvesicles are elongated and aligned where the pumice was stretched and/or squeezed. In some pumice, the glass between vesicles now consists largely of chlorite sprinkled with sphene granules; patches of quartz and epidote also are present. Cloudy leucoxene marks the former walls of microvesicles, which are filled with the same chlorite that replaced the glass. Other pumices are replaced largely by epidote and actinolite; microvesicles again are filled with chlorite, or are overgrown by epidote crystals that nucleated in adjacent glass. Some of the most vesicular pumice (microvesicles touching one another) is completely replaced by granular epidote. Pumice fragments may contain relict plagioclase microphenocrysts.

Stop 8 in the upper part of the Elwell Formation is reached by carefully following your leader down the bedrock knob, past a meltwater pond (dry in September), over a lateral moraine, and steeply downhill to the highest of a series of three tiny glacially excavated basins now occupied by two ponds and a marsh (in the highest basin). As you cross the lateral moraine, you will see a variety of lithologies derived from the Elwell and Sierra Buttes formations upstream. According to Mathieson (1981), all the glacial debris in the Lakes Basin was left by one of the larger of the late post-Sangamon valley glaciers; its terminal moraine may be found at 5,200 feet elevation in Gray Eagle Creek just northwest of the Gold Lake Road.

Stop 8. Traverse of the Upper Part of the Elwell Formation, Greatly Expanded by Mafic Sills

The contact between Elwell and Taylor formations is unexposed here, but there is no evidence of the augite-rich pillow lava that marks the base of the Taylor Formation west of Upper Salmon Lake (Photo 4). Instead, it appears that the interbedded tuffs and lapilli tuffs we have just seen at Stops 6 and 7 continue to the base of the Taylor Formation in this area.

At Stop 8, we will traverse, from east to west, a nearly unbroken, approximately vertical section of the upper part of the Elwell Formation expanded to nearly twice the actual stratigraphic thickness (ca. 43 m) by four mafic sills ranging from 0.7 to ca. 33 m thick. One of the sills is a penecontemporaneous, aphanitic, andesite sill belonging to the Elwell Formation. Two are richly augite-phyric sills of early Taylor age, and the other, plagioclase-phyric sill containing only a few augite phenocrysts could be a Taylor feeder. The main goal of the traverse is to attempt to determine how much of the volcaniclastic part of the upper Elwell Formation, if any, is pyroclastic, how much epiclastic. In the Sierra Buttes to the south, Hanson and Schweickert (1986) estimated that the pumice content of coarse-grained mass-flow deposits that make up most of the Elwell Formation there ranges up to 100%. Quartz- and plagioclase-phyric clasts, and quartz and plagioclase sand grains obviously derived from the underlying Sierra Buttes Formation are abundant at Stop 8, but a pyroclastic component has proved impossible to verify. Dark, apparently relatively mafic, lenticular masses that resemble pumice lapilli are commonplace, but they also often contain quartz and/or plagioclase crystals, unlike typically aphyric Elwell lavas. Another complication is the strong foliation (parallel to relict bedding) in these volcaniclastic rocks. The delicate fabric of long-tube pumice may have been destroyed during development of the foliation and/or the anastomosing foliation may have produced lenticular masses that masquerade as pumice lapilli. Possible long-tube pumice was noted in only one thin section that otherwise consisted of quartzofeldspathic sandstone. The pumice(?) grains were coarse ash-size and displayed parallel streaks of albite and chlorite (and/or an epidote mineral); some grains seemed to be molded to undeformed quartz and plagioclase sand grains.

Most of the first 29 m of the ca. 78 m-thick section comprises strongly foliated, otherwise structureless material containing prominent, white to light gray, aphanitic to quartz-phyric, lenticular to tabular clasts oriented parallel to the foliation. Also present are red-weathered, dark greenish gray, plagioclase-phyric lentils and filaments, some of which also contain scarce quartz phenocrysts. I initially thought that these might be andesitic pumices, but no pumice is apparent in thin section. Occasionally one finds tabular, chert-like, rip-up clasts that rigorously parallel the foliation. If bedded intervals exist in this monotonous section, they are not conspicuous. Interbedded in the lowermost 2 m of the section, however, is fine-grained well-stratified material, probably sand- to clay-size sediment derived from the Sierra Buttes Formation. Very thin beds of chert-like material may have been the source of the tabular rip-up clasts found higher in the section.

Thin sections of the non-bedded, structureless material (probably a debris flow or flows) show that all the detritus probably was Sierra Buttes-derived. Larger, granule- and pebble-size fragments are sparsely phyric (quartz+/-plagioclase microphenocrysts) and microlitic (plagioclase); relict felsitic matrices may contain spherulites up to 0.17 mm in diameter that now consist largely or wholly of quartz. Though quartz and plagioclase microphenocrysts in the larger fragments are well-formed, grains up to 1.9 mm across clearly broken from quartz and plagioclase phenocrysts also are present. The fabric of the mafic lentils seen in outcrop is dominated by anastomosing epidote+/-chlorite films that enclose very fine-grained lenses containing the broken phenocrysts; the very fine-grained material evidently represents the finest, silt- and clay-size grains in the original epiclastic sediment. Finally, several larger fragments consist mostly of chlorite, epidote, and quartz, but even these enclose a few relict quartz and plagioclase microphenocrysts.

Following a 1.2 m-gap in the outcrop, where the eastern margin of a remarkably thick sill unfortunately is not exposed, the next ca. 33 m of section consist, without a break, of richly augite-phyric basalt. The well-exposed western edge of the sill is perfectly concordant, except for minor dike-like behavior at one point, to well stratified, north-striking, vertically dipping chert and other sedimentary rocks. The sill displays no chilled margin, no columnar joints, and only a few quartz-chlorite amygdules. Its most prominent characteristic is the large, euhedral, augite phenocrysts. A number of phenocrysts reach 2 cm in length. Eight- and six-sided sections of stubby prismatic phenocrysts are rimmed and veined by black actinolite, islands of unreplaced pale green augite remaining. The relict mode of sample C-16 (Table 5) is: 29.5 vol.% augite, 6.3 vol.% plagioclase, 2.4 vol.% vesicles, and 61.8 vol.% matrix.

Table 5 provides whole-rock chemical analyses of two samples of the basalt, C-16 collected in 1977, PP-5 collected in 1984. Except for rather large differences in TiO_2 and the alkalies, the analyses are remarkably similar considering the variety of analytical procedures employed over the years (Table 5). Comparison may be made to the average analysis of seven such intrusions in Table 2. Table 6 provides average compositions of unzoned augite pheno-

Table 5. Major-element, whole-rock chemical analyses of two samples of augite-phyric basalt collected from the thick sill of early Taylor age at Stop 8.

	C-16	PP-5
SiO_2	51.49	51.12
Al_2O_3	14.32	15.11
TiO_2	0.46	0.35
Fe_2O_3	1.56	1.87
FeO	8.42	8.27
MgO	10.85	9.36
CaO	11.32	11.83
Na_2O	0.89	1.13
K_2O	0.45	0.73
MnO	0.20	0.20
P_2O_5	0.04	0.03

Analyses recalculated to 100 wt.%, volatile-free. PP-5 analysed by Fusion-ICP at Activation Laboratories Ltd. in 1994; $Fe_2O_3 = TiO_2 + 1.5$, FeO = (0.8998) remaining Fe_2O_3. C-16 analysed by INAA at Lawrence Livermore National Laboratory in 1978, except that SiO_2 was analyzed by XRF at X-ray Assay Laboratories Ltd. in 1979, and FeO and P_2O_5 were analyzed at the Branch of Analytical Chemistry, U.S. Geological Survey, Menlo Park, in 1983.

crysts in the two samples. The augite in sample C-16 is a little more magnesian and Fe-poor than that in PP-5; both samples were collected from the central part of the sill, but not from the same point. Reference to Figure 6 indicates the Fe-poor nature of these phenocrysts, also revealed by their pale green in hand specimen.

Thin sections of these and other samples of the sill show that subhedral to euhedral augite phenocrysts and microphenocrysts are partly to wholly replaced by nearly colorless, Fe-poor actinolite single crystals, from phenocryst margins inward. Such marginal replacement results in highly irregular remnants of augite in the central parts of phenocrysts; the remnants are veined by actinolite. Augite and actinolite share polysynthetic-twin composition planes exactly ({100} in the actinolite); were these inherited from the augite, or was all twinning post-metamorphic? The photomicrograph on page ii of this volume shows a phenocryst in sample C-16 with a single twin lamella running down its middle, through both augite and actinolite. The actinolite may be accompanied by considerable chlorite, often, when replacement of augite is complete, in centrally located, irregular patches that mimic in size, shape, and distribution of the augite remnants in other, partially replaced phenocrysts. Also, ragged augite cores may have thin films of chlorite intervening between augite and marginal actinolite. Did chlorite precede actinolite during the augite-replacement process? Actinolite rims may have fringing "whiskers" of actinolite growing into the rock matrix. The nearly colorless actinolite reflects the Fe-poor nature of the replaced augite (Table 6). Augite phenocrysts are unzoned, but do exhibit patchy sieve texture.

Some samples are too recrystallized to point-count, with matrix actinolite crystals sometimes so coarse that they cannot be distinguished from augite microphenocrysts

Table 6. Electron-microprobe analyses of 4 unzoned augite phenocrysts in 2 samples of basalt collected from the thick sill of early Taylor age at Stop 8.

	Average of 5 analyses of 2 phenocrysts in C-16	Average of 8 analyses of 2 phenocrysts in PP-5
SiO_2	53.44	52.40
TiO_2	0.07	0.08
Al_2O_3	1.48	2.15
Cr_2O_3	0.33	0.20
Fe_2O_3	1.25	2.39
FeO	3.69	3.56
MgO	18.29	17.34
CaO	21.22	21.64
Na_2O	0.08	0.08
MnO	0.15	0.16
	$Wo_{42.0}En_{50.4}Fs_{7.6}$	$Wo_{43.0}En_{47.9}Fs_{9.1}$

Analyses by Peter Schiffman; U.C., Davis; 1992 (C-16) and 1993 (PP-5).

replaced by actinolite. Also, relict, euhedral, plagioclase microlites and microphenocrysts completely replaced by epidote+/-white mica are almost impossible to see. Titanomagnetite microphenocrysts have been replaced by sphene. The few former vesicles mostly are filled with chlorite and a little colloform chalcedony (now finely granular quartz) at vesicle margins.

Adjoining the western edge of the thick sill are 70 cm of well stratified, fine-grained, volcanogenic sedimentary rocks interbedded with carbonaceous radiolarian chert. Microscopic examination reveals that the radiolarians now consist of microgranular quartz exhibiting many, sharp, straight or curved grain boundaries. Large radiolarians are ca. 0.2 mm long, and those as small as 0.03 mm can be recognized. The radiolarians have been flattened to ellipsoids in the foliation, which is marked by graphite films. Several angular grains of quartz sand to 0.5 mm across testify to continued deposition of Sierra Buttes-derived detritus even during intervals of pelagic deposition represented by the chert.

Still farther west is another perfectly concordant sill, this one only 70 cm thick and pinching out in both directions along the strike. It contains small plagioclase phenocrysts and only a few augite phenocrysts, and is amygdaloidal. Between this sill and the next, augite-phyric sill to the west is a very interesting, 3.85 m-thick section consisting mostly of volcanogenic sedimentary rocks.

The uppermost bed in this section is a relatively coarse, especially quartz-rich, epiclastic turbidite 1.15 m thick. The subtly stratified pebbly sandstone base (45 cm thick) is so charged with very coarse grains of vitreous gray quartz sand that it sparkles in the sun. The turbidite fines upward to well stratified coarse sandstone. Some very fine-grained laminae occur at the top of the bed, adjacent to the plagioclase-phyric sill. Thin sections reveal that the quartz sand is immature, most grains being sharply pointed and extremely angular. Among obvious sand grains, quartz dominates plagioclase at least 2 to 1. Locally voluminous, microgranular, quartzofeldspathic material represents either recrystallized, silt- and clay-size, matrix grains or additional sand grains comprising the porphyry matrix from which quartz and plagioclase phenocrysts were eroded. Chlorite and epidote are concentrated in darker laminae in the sandstone. The metamorphic mineral assemblage is albite (An_7)-chlorite-epidote-sphene-quartz-white mica.

The next lower bed in the 3.85 m-thick interval contains the coarsest and greatest variety of clasts that we will see at Stop 8. The very coarse, essentially structureless base of the bed, 1.3 m thick, passes upward to 0.6 m of very fine-grained, streaky material. The microscope discloses that the streaky material is very strongly foliated due to DPO of iron oxide-stained white mica and sinuous lenticular masses free of white mica (hence white in hand sample). The latter are extremely fine-grained, but a few microlites and a couple, possible, relict spherulites suggest that they originally were glassy. Very strongly rounded (resorbed) quartz phenocrysts occur both in the lenticular masses—probably highly deformed dacite fragments—and in the white mica-rich areas between fragments. Some phenocrysts are almost circular, some are embayed; they range in size from ca. 1.5 to 0.13 mm. Since the contained quartz phenocrysts are unbroken, were the white mica-rich areas also fragments, the fragment boundaries obscured by the strong foliation? Less common plagioclase phenocrysts, up to ca. 2 mm long, tend not to be so resorbed.

The very coarse base of this bed—probably another turbidite—contains tabular rip-up clasts of phosphatic chert up to 5 cm thick (Photo 16, left of the pencil), and large (e.g., 30 cm-long), plagioclase- and quartz-phyric, dacite clasts—some flow-banded—of obvious Sierra Buttes derivation (Photo 17). The latter may be equant and well rounded (Photo 17), but most are subangular to subrounded and elongated in the plane of relict bedding together with slabs of phosphatic chert. A number of light-colored, subangular, quartz-phyric, flow-banded pebbles appear in Photo 16. Dark, richly plagioclase- and quartz-phyric, lenticular masses still are present, strongly flattened in the foliation (several occur to the right of the pencil in Photo 16). A round phosphate nodule is present, either freed by erosion from the chert or having grown in the turbidite diagenetically. A flattened phosphate nodule appears in Photo 17 above the rounded dacite cobble (light gray lens-shaped body ca. 4 cm long; the darker gray lenticular mass to the right is chert). The pebbly matrix supporting these varied coarse clasts again is rich in quartz sand and quartz-phyric pebbles.

Finally, the lowermost of the three beds sandwiched between the two sills is a turbidite much like the uppermost one. It is 0.75 m thick, and is separated from the overlying very coarse bed by a 5 cm-thick, gray, chert bed. This turbidite also contains a 1 cm-thick, light gray, chert bed within its pebbly base, so, unless the chert bed actually is an especially long rip-up clast, two turbidites must be present.

The underlying augite-phyric sill is 2 m thick, and contains a tabular chert xenolith 3 cm thick and at least 35 cm long. Beneath the sill are 8 m more of pebbly to sandy quartz-phyric debris thinly interbedded with gray phosphatic chert. Some of the chert at the west edge of the exposure is repeated by nearly isoclinal folds, so something less than 8 m of sedimentary rocks actually are exposed. A sample collected from one of these few-cm-thick, quartz-rich, sandstone beds had a little black chert attached. Sinuous, anastomosing films of graphite pass about relict radiolarians in the chert, making them more apparent in thin section. The radiolarians are very elusive, however, consisting of relatively coarse (but still very fine-grained) quartz. White mica is plentiful, and occasional angular

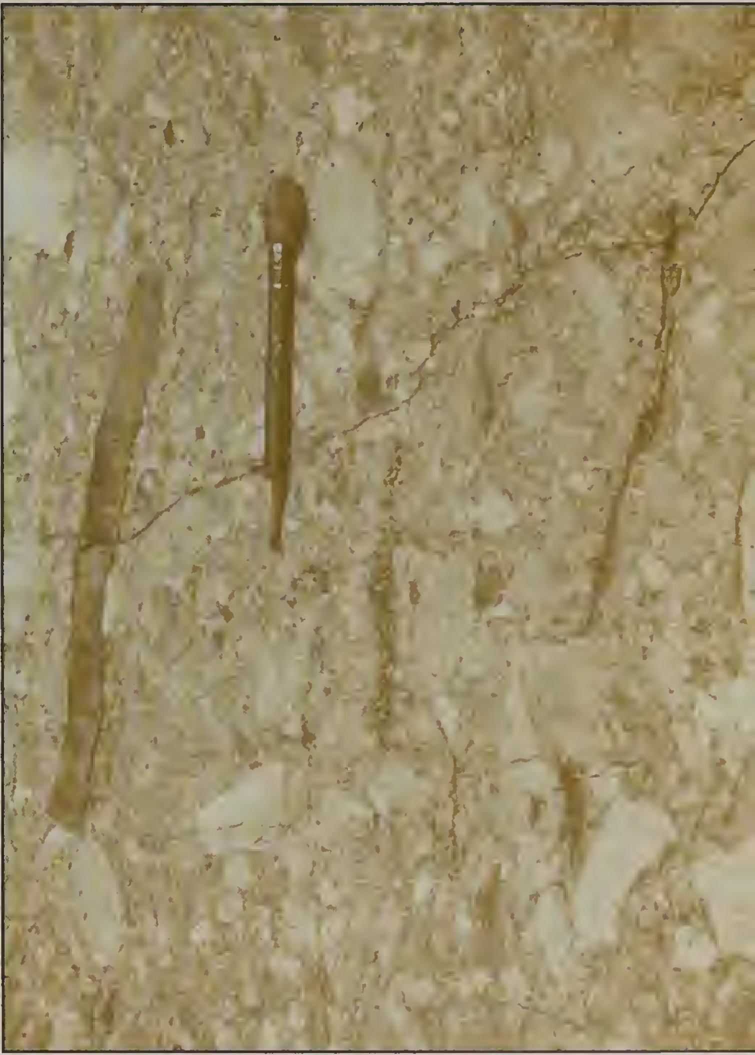

Photo 16. Dark gray, tabular, rip-up clast of graphitic chert (left of pencil) in foliated (parallel to pencil), but otherwise structureless pebbly sandstone base of a relatively very coarse epiclastic turbidite in the Elwell Formation at Stop 8. Dark phyric films to right of pencil masquerade as pumice fragments. Note also the flow-banded dacite pebbles in the lower right-hand corner of the photograph. The pencil is ca. 12 cm long. *Photo by E.R. Brooks.*

grains of detrital quartz are present. The quartz-rich sandstone (technically, a lithic arenite or wacke) is well foliated, with DPO of white mica and graphite. Fragments derived from Sierra Buttes porphyries having voluminous fine-grained matrices are abundant, as are the usual eroded phenocrysts. The former are microlite-free, display obvious relict spherulites ca. 0.1 mm in diameter, and contain very few, rounded, quartz phenocrysts, sometimes embayed. Many quartz phenocrysts must have been broken from their matrices, however, as they now appear as angular sand grains. The latter were somehow concentrated prior to or during transport, as they are present greatly out of proportion to the few phenocrysts seen in the porphyry fragments. Plagioclase phenocrysts are not present.

As we walk northerly down the west edge of the outcrop, the thinly interbedded sandstone and chert are much deformed. Tight similar folds having axial-plane cleavage are present, and, near the foot of the slope, these folds become more open, the cleavage intersecting bedding at a high angle. Photo 18 shows a refolded antiform nicely outlined by a single bedding surface in the chert (inked in the photograph for emphasis). The ealier, F_1-fold axis changes orientation from ca. N@15° to ca. N45E@60° from one side of the open F_2 fold to the other. F_2 cleavage strikes ca. N20W. F_1 may be penecontemporaneous, the result of slumping of unlithified chert on the sea floor. F_2 would be attributed to the Nevadan orogeny by most workers.

As we leave Stop 8 and walk westerly toward Stop 9, additional open folds are encountered in the bedded chert. Lens-shaped, white, phosphate nodules, which weather recessively, accentuate the bedding of the chert, which weathers light- to dark-gray. Nodules in some samples consist almost entirely of fluorapatite, but those in most samples have generous admixtures of quartz. Phosphate nodules are thought to have formed by direct inorganic precipitation of fluorapatite from pore water within decaying radiolarians at the sediment-water interface (Brooks and others, 1982). The presence of phosphate is important in determining the maximum depth of water at the time of deposition of the chert and interbedded turbidites, as Coles and Varga

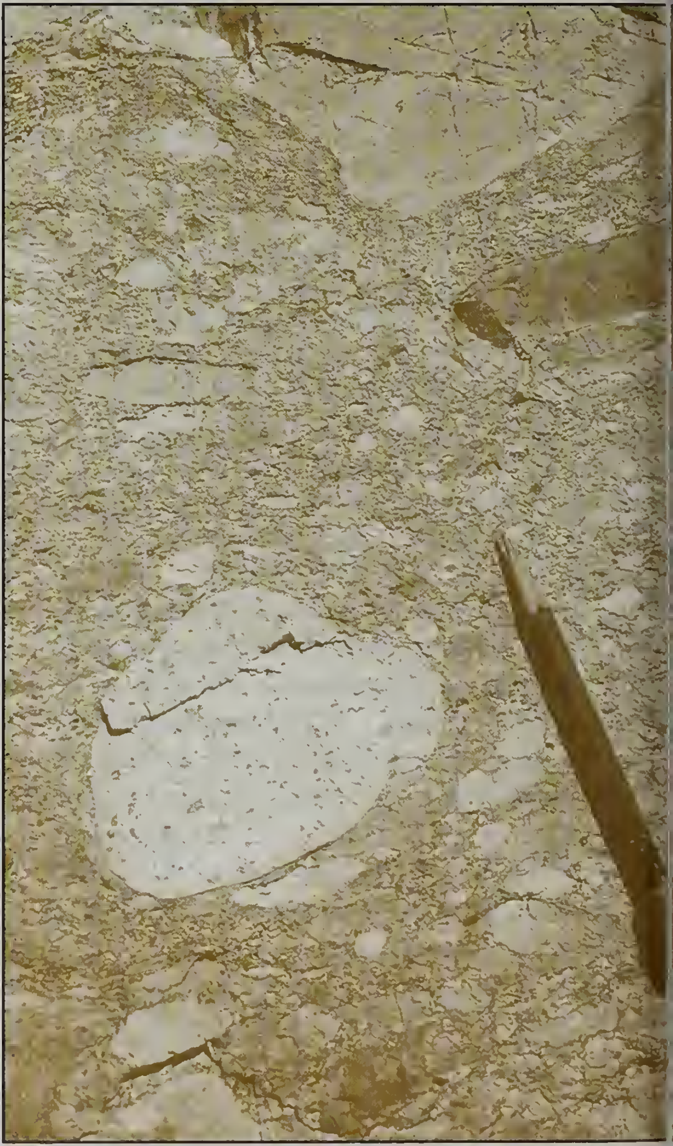

Photo 17. Rounded cobble of Sierra Buttes quartz-plagioclase porphyry in the pebbly sandstone base of an epiclastic turbidite in the Elwell Formation at Stop 8. The light gray lens-shaped body above the cobble is a phosphate nodule, the dark gray lenticular mass to its right graphitic chert. The pencil is ca. 12 cm long; photograph taken 2-3 m south of Photo 16. *Photo by E.R. Brooks.*

(1988) report that phosphatic cherts such as this accumulate at depths probably no greater than 2 km. Growth of the phosphate nodules was complete before pore water was eliminated from the chert, for they were transported as rigid bodies—sometimes being broken—in the fluid chert matrix of peperite like that at Stop 9.

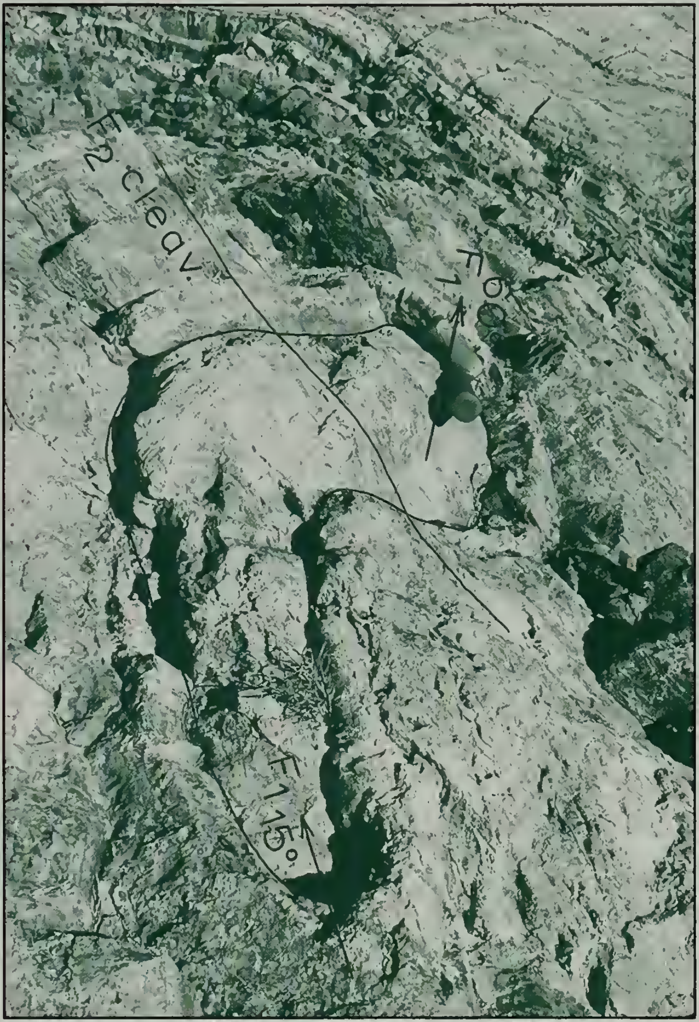

Photo 18. Refolded antiform in bedded chert in the Elwell Formation at Stop 8. Direction of view approx. NNE; F_2 cleavage strikes ca. N20W. The more open F_2 fold probably is Jurassic, the F_1 fold possibly synsedimentary (Famennian). 28 cm-long sledge for scale. *Photo by E.R. Brooks.*

Stop 9. Peperite in the Elwell Formation

Peperite occurring in the Elwell Formation was exhaustively described by Brooks and others (1982). It differs considerably from that seen in the Taylor Formation at Stop 6. The host sediment is radiolarian chert instead of tuff, and the volcanic component consists of aphanitic andesite rather than augite- and plagioclase-phyric basalt. Also, much of the Elwell peperite has been well stirred ("dispersed") by steam explosions, unlike the in situ Taylor peperite. This is not a good place to study the interaction of intrusive andesitic magma and still-moist incompletely lithified chert documented by Brooks and others (1982), but it is a good place to view the resulting peperite, which litters the ground all about this locality. Help yourself to anything that is loose!

Photo 19 of peperite at Stop 9 shows sharply angular, irregular, lapilli-size fragments of andesite supported by a relatively voluminous chert matrix. Notice that some of the fragments possess incredibly sharply pointed, fragile corners. These, together with quench microlites of plagioclase, testify to the formerly glassy character of the fragments; such fragments formed by thermal-contraction cracking of andesitic magma quenched to richly microlitic glass during intrusion of the magma into cold, wet chert not far below the sea floor. A vesicular andesite fragment appears in the upper left-hand corner of Photo 19, and a small black chert fragment is seen just to the left of the pencil eraser. The lack of closely fitting "puzzle" fragments, and the presence of the voluminous chert matrix and of fragments derived from chert sufficiently lithified to sustain brittle fracture, evidence wide dispersal of this peperite by steam explosions. Although good examples of "jigsaw-fit" fragments do not occur, a few andesite fragments are cut by narrow, sinuous, chert veins. The peperite is poorly

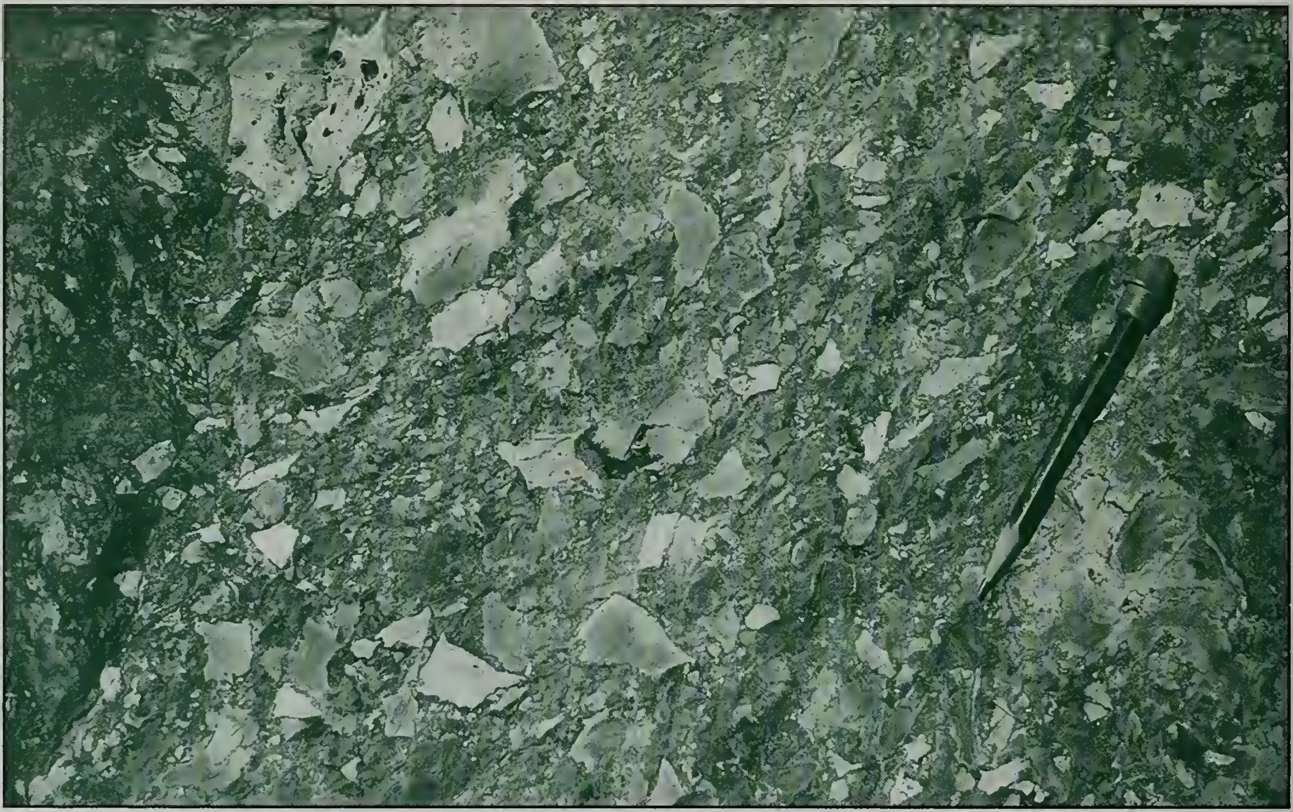

Photo 19. Dispersed, matrix-supported peperite in the Elwell Formation at Stop 9. Sharply angular lapilli-size fragments of aphyric andesite are set in a radiolarian chert matrix. Note the tiny black chert clast left of the pencil eraser, and the vesicular andesite fragment in the upper left-hand corner of the photograph. *Photo by E.R. Brooks.*

sorted, and blocks up to at least 0.8 m long are found here.

Stop 10. Monolithologic Breccia in the Sierra Buttes Formation

We will not have time or energy to climb the high ridge to the west to view the Sierra Buttes Formation cropping out there (Elwell peperite is still underfoot at Stop 10), but a glacier has done the work for us, bringing down these cabin-size pieces of monolithologic breccia. On the ridge are large varicolored bodies of monolithologic breccia representing autobrecciated, dacitic, hypabyssal intrusions (and domes?).

Dacite blocks in the autobreccia are rich in gray quartz and pink, white, and tan plagioclase phenocrysts. The quartz phenocrysts are equant, reflecting their origin as beta-quartz crystals. Matrices of the dacite blocks are extremely fine-grained, even chert-like. The blocks are compositionally so similar to one another, and to the comminuted breccia matrix, that they are not always easily distinguished from the latter. Occasional dacite blocks are subtly flow-banded. The coarser fraction of the autobreccia exhibits a very wide range of clast sizes, and the finer matrix is sufficiently abundant that the breccia can be considered matrix-supported.

The relict mode of a meter-size block in a similar (the same?) breccia at the foot of the steep cirque headwall just southwest of us (Photo 2) is 15.6 vol.% quartz phenocrysts, 9.4 vol.% plagioclase phenocrysts, 0.4 vol.% titanomagnetite microphenocrysts, and 74.6 vol.% matrix. Thin sections disclose anhedral to euhedral quartz phenocrysts up to ca. 4 mm in greatest dimension that are fairly extensively embayed and rounded. Quartz phenocrysts typically are shattered, the sometimes misoriented fragments separated slightly by calcite-chlorite veins. Euhedral plagioclase phenocrysts and glomerocrysts are much less apparent, having been darkened and rendered opaque upon replacement by albite (An_7), calcite, white mica, quartz, leucoxene, epidote, and chlorite! Microphenocrysts of both quartz and plagioclase are present, as are euhedral titanomagnetite microphenocrysts up to 0.3 mm across, now completely replaced by leucoxene. The latter may be associated with apatite, and some occur as inclusions in quartz and plagioclase phenocrysts, presumably having crystallized very early. The extremely fine-grained porphyry matrix is nearly free of plagioclase microlites, and tiny (e.g., 0.1 mm), round, quartz single crystals that probably represent completely recrystallized spherulites are only occasionally encountered.

Upon leaving Stop 10, follow the contour northeasterly to a trail that returns us to Silver Lake (Figure 12). When again reaching the junction with the Bear Lake trail below Silver Lake, proceed straight ahead toward Long Lake and the Lakes Basin campground. Magnificent effects of mountain glaciation are apparent along this trail. A recessional moraine encloses Long Lake on your left, and, farther down the trail, striated and grooved bedrock surfaces littered with erratics appear (the glacier moved almost due east here). Below the next junction, with the trail to Long Lake, you will see on your right, where the trail begins to flatten, a bedrock knob with a large erratic perched atop it. Take a sharp right turn off the trail and climb up to the erratic, where you will be rewarded by seeing unusual stellate glomerocrysts of augite at Stop 11 (Figure 12).

Stop 11. Stellate Augite Glomerocrysts in a Taylor Formation Breccia

We are back in the Taylor Formation, in yet another breccia consisting of light gray amygdaloidal blocks set in a dark reddish matrix. Most blocks are choked with large (e.g., 2 cm-long), relict, augite phenocrysts, many of which are arranged in star-shaped clusters ("stellate" glomerocrysts). The phenocrysts largely have been replaced by black actinolite single crystals having cleavages with vitreous luster. Should you see any light green material with your hand lens, especially in the central parts of phenocrysts, it is unreplaced augite. The euhedral augite phenocrysts have an unusual habit in that they are tabular parallel to {100}. The broad waxy-lustered surfaces you see are partings that developed parallel to {100} polysynthetic twins in the actinolite. Inconspicuous euhedral plagioclase phenocrysts also are present.

The main attraction here is the stellate glomerocrysts, several of which appear in Photo 20, one just to the right of the coin. Also shown are the broad waxy-lustered sections of phenocrysts that have cleaved parallel to the {100} parting; the largest, below and to the right of the coin, is 9 x 19 mm.

Thin sections show that the plagioclase phenocrysts originally were compositionally zoned; they now consist of albite single crystals flecked by xenoblastic epidote. The rock matrix is charged with sphene granules and unoriented actinolite fibers; epidote and albite also are found. Large irregularly shaped amygdules are mineralogically complex, with rims of fine-grained quartz and cores of calcite or of chlorite+/-epidote+/-calcite+/-biotite. Also, tiny (e.g., 0.1 mm) amygdules of fine-grained quartz pervade the rock.

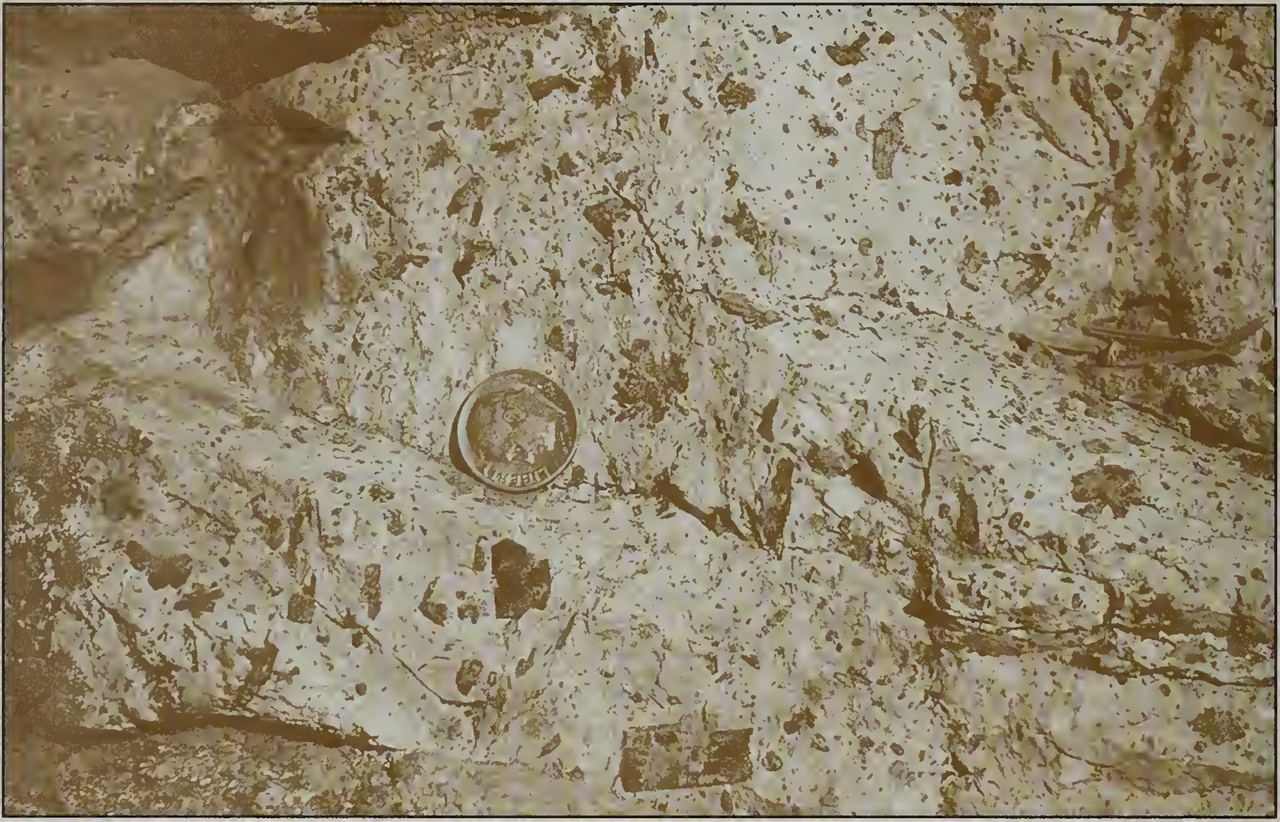

Photo 20. Augite-phyric block in Taylor Formation breccia at Stop 11. The augite phenocrysts largely have been replaced by black actinolite single crystals that frequently cleave parallel to a {100} parting, producing the broad sections of phenocrysts seen below the center of the photograph. Also present are unusual stellate glomerocrysts of augite, one just to the right of the coin. *Photo by E.R. Brooks.*

Upon leaving Stop 11, return to the trail and continue down to the Bear-Silver Lake trailhead. I hope you enjoyed the trip!

ACKNOWLEDGMENTS

I wish to pay tribute to the more than 450 students who completed the California State University, Hayward, (CSUH) summer field geology course during the 25 years (1970-1994) that it was taught in the northern Sierra Nevada. They, together with numerous teaching assistants and, especially, my colleagues Mike Wood and Phil Garbutt, have influenced in many ways my ideas about these often enigmatic rocks. For the same reason, I am greatly indebted to June Legler, John Lull, Barry Marcus, Bruce Pauly and Steve Silva, CSUH students whose M.S. theses I supervised in the Northern Sierra terrane. Susan Schultz and Mary Lou Swisher helped me collect pillow lavas in 1977, and Mark Varney collected them in 1996-97. Richard Hanson kindly gave permission to use Figures 1 and 2. The generosity of Peter Schiffman in conducting mostly unremunerated SEM and electron-microprobe work over the years has known no bounds.

Many of the chemical data appearing here were obtained while I held an Associated Western Universities-Department of Energy faculty participation appointment at the Lawrence Livermore National Laboratory (LLNL) in 1978; analytical costs were borne by the Earth Sciences Division, LLNL. Acquisition of additional chemical data in 1979, 1986, 1994, and 1998 was funded by various grants received from CSUH.

REFERENCES

Barsdell, M., 1988, Petrology and petrogenesis of clinopyroxene-rich tholeiitic lavas, Merelava volcano, Vanuatu: Journal of Petrology, v. 29, part 5, p. 927-964.

Boynton, W.V., 1984, Geochemistry of the rare earth elements: Meteorite studies *in* Henderson, P., editor, Rare earth element geochemistry: Elsevier, p. 63-114.

Brooks, E.R., 1992, Geology of the Eastern Belt of the northern Sierra Nevada *in* Schiffman, P. and Wagner, D.L., editors, Field guide to the geology and metamorphism of the Franciscan Complex and Western Metamorphic Belt of northern California: California Division of Mines and Geology Special Publication 114, p. 54-78.

Brooks, E.R., 1995, Paleozoic fluidization, folding, and peperite formation, northern Sierra Nevada, California: Canadian Journal of Earth Sciences, v. 32, p. 314-324.

Brooks, E.R. and Garbutt, P.L., 1972, Broken-pillow breccia in the northern Sierra Nevada, Sierra County, California: Geological Society of America Abstracts with Programs, v. 4, p. 131-132.

Brooks, E.R. and Coles, D.G., 1980, Use of immobile trace elements to determine original tectonic setting of eruption of metabasalts, northern Sierra Nevada, California: Geological Society of America Bulletin, Part I, v. 91, p. 665-671.

Brooks, E.R. and Legler, J.L., 1989, An unusual Devonian subaqueous pyroclastic-flow deposit in the northern Sierra Nevada, Sierra County, California: Geological Society of America Abstracts with Programs, v. 21, p. 59.

Brooks, E.R. and Schiffman, P., 1996, Al- and Ti-poor calcic pyroxenes in Devonian tholeiitic metabasalts, northern Sierra Nevada: Phenocrysts or xenocrysts?: abstract, Eos, Transactions, American Geophysical Union, v. 77, no. 46, p. F789.

Brooks, E.R., Wood, M.M. and Garbutt, P.L., 1982, Origin and metamorphism of peperite and associated rocks in the Devonian Elwell Formation, northern Sierra Nevada, California: Geological Society of America Bulletin, v. 93, p. 1208-1231.

Caruso, L. and Simmons, G., 1981, Uranium and REE migration in the Sherman Granite, SE Wyoming: abstract, Eos, Transactions, American Geophysical Union, v. 62, no. 45, p. 1064.

Coish, R.A., 1977, Ocean floor metamorphism in the Betts Cove ophiolite, Newfoundland: Contributions to Mineralogy and Petrology, v. 60, p. 255-270.

Coles, K.S. and Varga, R.J., 1988, Early to middle Paleozoic phosphogenic province in terranes of the southern Cordillera, western United States: American Journal of Science, v. 288, p. 891-924.

Coney, P.J., Jones, D.L. and Monger, J.W.H., 1980, Cordilleran suspect terranes: Nature, v. 288, no. 5789, p. 329-333.

Criss, R.E. and Taylor, H.P., Jr., 1983, An $^{18}O/^{16}O$ and D/H study of Tertiary hydrothermal systems in the southern half of the Idaho batholith: Geological Society of America Bulletin, v. 94, p. 640-663.

Crow, C. and Condie, K.C., 1987, Geochemistry and origin of late Archean volcanic rocks from the Rhenosterhoek Formation, Dominion Group, South Africa: Precambrian Research, v. 37, p. 217-229.

D'Allura, J.A., Moores, E.M. and Robinson, L., 1977, Paleozoic rocks of the northern Sierra Nevada: Their structural and paleogeographic implications *in* Stewart, J.H., and others, editors, Paleozoic paleogeography of the western United States: Society of Economic Paleontologists and Mineralogists Pacific Coast Paleogeography Symposium 1, p. 395-408.

Day, H.W., 1992, Tectonic setting and metamorphism of the Sierra Nevada, California *in* Schiffman, P. and Wagner, D.L., editors, Field guide to the geology and metamorphism of the Franciscan Complex and Western Metamorphic Belt of northern California: California Division of Mines and Geology Special Publication 114, p. 12-28.

Day, H.W., Moores, E.M. and Tuminas, A.C., 1985, Structure and tectonics of the northern Sierra Nevada: Geological Society of America Bulletin, v. 96, p. 436-450.

Diller, J.S., 1908, Geology of the Taylorsville region, California: U.S. Geological Survey Bulletin 353, 128 p.

Dostal, J., 1989, Geochemistry of Ordovician volcanic rocks of the Tetagouche Group of southwestern New Brunswick: Atlantic Geology, v. 25, p. 199-209.

Durrell, C. and D'Allura, J., 1977, Upper Paleozoic section in eastern Plumas and Sierra counties, northern Sierra Nevada, California: Geological Society of America Bulletin, v. 88, p. 844-852.

Fisher, R.V., 1966, Rocks composed of volcanic fragments: Earth-Science Reviews, v. 1, p. 287-298.

Fiske, R.S., 1969, Recognition and significance of pumice in marine pyroclastic rocks: Geological Society of America Bulletin, v. 80, p. 1-8.

Girty, G.H., Hanson, R.E., Girty, M.S., Schweickert, R.A., Harwood, D.S., Yoshinobu, A.S., Bryan, K.A., Skinner, J.E. and Hill, C.A., 1995, Timing of emplacement of the Haypress Creek and Emigrant Gap plutons: Implications for the timing and controls of Jurassic orogenesis, northern Sierra Nevada, California *in* Miller, D.M. and Busby, C., Jurassic magmatism and tectonics of the North American Cordillera: Geological Society of America Special Paper 299, p. 191-201.

Girty, G.H., Lawrence, J., Burke, T., Fortin, A., Gallarano, C.S., Wirths, T.A., Lewis, J.G., Peterson, M.M., Ridge, D.L., Knaack, C. and Johnson, D., 1996, The Shoo Fly Complex: Its origin and tectonic significance *in* Girty, G.H., Hanson, R.E., Schweickert, R.A. and Harwood, D.S., editors, The Northern Sierra terrane and associated Mesozoic magmatic units: Implications for the tectonic history of the western Cordillera: Society of Economic Paleontologists and Mineralogists, Pacific Section, Book 81, p. 1-23.

Hanson, G.N., 1980, Rare earth elements in petrogenetic studies of igneous systems: Annual Reviews of Earth and Planetary Science, v. 8, p. 371-406.

Hanson, R.E., 1991, Quenching and hydroclastic disruption of andesitic to rhyolitic intrusions in a submarine island-arc sequence, northern Sierra Nevada, California: Geological Society of America Bulletin, v. 103, p. 804-816.

Hanson, R.E. and Schweickert, R.A., 1986, Stratigraphy of mid-Paleozoic island-arc rocks in part of the northern Sierra Nevada, Sierra and Nevada counties, California: Geological Society of America Bulletin, v. 97, p. 986-998.

Hanson, R.E., Girty, G.H., Girty, M.S., Hargrove, U.S., Harwood, D.S., Kulow, M.J., Mielke, K.L., Phillipson, S.E., Schweickert, R.A. and Templeton, J.H., 1996, Paleozoic and Mesozoic arc rocks in the Northern Sierra terrane *in* Girty, G.H., Hanson, R.E., Schweickert, R.A., and Harwood, D.S., editors, the Northern Sierra terrane and associated Mesozoic magmatic units: Implications for the tectonic history of the western Cordillera: Society of Economic Paleontologists and Mineralogists, Pacific Section, Book 81, p. 25-55.

Harwood, D.S., 1988, Tectonism and metamorphism in the northern Sierra terrane, northern California *in* Ernst, W.G., editor, Metamorphism and crustal evolution of the western United States, Rubey Volume 7: Englewood Cliffs, N.J., Prentice-Hall, p. 764-788.

Harwood, D.S., 1992, Stratigraphy of Paleozoic and lower Mesozoic rocks in the northern Sierra terrane, California: U.S. Geological Survey Bulletin 1957, 78 p.

Irvine, T.N. and Baragar, W.R.A., 1971, A guide to the chemical classification of the common volcanic rocks: Canadian Journal of Earth Sciences, v. 8, p. 523-548.

Jakes, P. and Gill, J., 1970, Rare earth elements and the island arc tholeiitic series: Earth and Planetary Science Letters, v. 9, p. 17-28.

Jakes, P. and White, A.J.R., 1972, Major and trace element abundances in volcanic rocks of orogenic areas: Geological Society of America Bulletin, v. 83, p. 29-40.

Kokelaar, B.P., 1982, Fluidization of wet sediments during the emplacement and cooling of various igneous bodies: Journal of the Geological Society (London), v. 139, p. 21-33.

Legler, J.L., 1983, A submarine pyroclastic flow deposit in the Sierra Buttes Formation, northern Sierra Nevada, California [M.S. thesis]: Hayward, California State University, 149 p.

Legler, J.L., Brooks, E.R. and Lull, J.S., 1991, Tamarack tuff: A Devonian submarine pyroclastic flow deposit in the northern Sierra Nevada, Plumas and Sierra counties: CALIFORNIA GEOLOGY, v. 44, p. 130-137.

Le Maitre, R.W., editor, Bateman, P., Dudek, A., Keller, J., Lameyre, J., Le Bas, M.J., Sabine, P.A., Schmid, R., Sorensen, H., Streckeisen, A., Woolley, A.R. and Zanettin, B., 1989, A classification of igneous rocks and glossary of terms: Recommendations of the International Union of Geological Sciences Subcommission on the Systematics of Igneous Rocks: Oxford, Blackwell Scientific Publications, 193 p.

Leterrier, J., Maury, R.C., Thonon, P., Girard, D. and Marchal, M., 1982, Clinopyroxene composition as a method of identification of the magmatic affinities of paleo-volcanic series: Earth and Planetary Science Letters, v. 59, p. 139-154.

Lull, J.S., 1984, Petrology and structure of an early Cretaceous dike swarm, northern Sierra Nevada, California [M.S. thesis]: Hayward, California State University, 146 p.

McPhie, J., Doyle, M. and Allen, R., 1993, Volcanic textures: A guide to the interpretation of textures in volcanic rocks: Hobart, University of Tasmania, Centre for Ore Deposit and Exploration Studies, 196 p.

Mathieson, S.A., 1981, Pre- and post-Sangamon glacial history of a portion of Sierra and Plumas counties, California [M.S. thesis]: Hayward, California State University, 258 p.

Miyashiro, A., 1974, Volcanic rock series in island arcs and active continental margins: American Journal of Science, v. 274, p. 321-355.

Moores, E.M. and Day, H.W., 1984, An overthrust model for the Sierra Nevada: Geology, v. 12, p. 416-419.

Pearce, J.A. and Cann, J.R., 1973, Tectonic setting of basic volcanic rocks determined using trace element analyses: Earth and Planetary Science Letters, v. 19, p. 290-300.

Pearce, J.A. and Norry, M.J., 1979, Petrogenetic implications of Ti, Zr, Y, and Nb variations in volcanic rocks: Contributions to Mineralogy and Petrology, v. 69, p. 33-47.

Roaldset, E., 1975, Rare earth element distributions in some Precambrian rocks and their phyllosilicates, Numedal, Norway: Geochimica et Cosmochimica Acta, v. 39, p. 455-469.

Rouer, O., LaPierre, H., Coulon, C. and Michard, A., 1989, New petrological and geochemical data on mid-Paleozoic island-arc volcanics of northern Sierra Nevada, California: Evidence for a continent-based island arc: Canadian Journal of Earth Science, v. 26, p. 2465-2478.

Schweickert, R.A., Bogen, N.L., Girty, G.H., Hanson, R.E. and Merguerian, C., 1984, Timing and structural expression of the Nevadan orogeny, Sierra Nevada, California: Geological Society of America Bulletin, v. 95, p. 967-979.

Wendlandt, R.F. and Harrison, W.J., 1979, Rare earth partitioning between immiscible carbonate and silicate liquids and CO2 vapor: Results and implications for the liquids formation of light rare earth-enriched rocks: Contributions to Mineralogy and Petrology, v. 69, p. 409-419.

Wilson, M., 1989, Igneous petrogenesis: London, Unwin Hyman, 466 p.

Wood, D.A., 1980, The application of a Th-Hf-Ta diagram to problems of tectonomagmatic classification and to establishing the nature of crustal contamination of basaltic lavas of the British Tertiary Volcanic Province: Earth and Planetary Science Letters, v. 50, p. 11-30.

THE BEACON POINT FORMATION, SIERRA COUNTY, CALIFORNIA: A JURASSIC TECTONIC BOUNDARY

Bruce D. Pauly[1]

INTRODUCTION

The Beacon Point formation is 30 kilometers (km) north of Lake Tahoe and 5 km west of the California-Nevada border in southeastern Sierra County, California (Figure 1). It underlies the northern Verdi Range, and is between the northern Sierra Nevada geologic province to the west and the Basin and Range province to the east. The portion of the northern Sierra Nevada to the west of the northern Verdi Range is a region of metamorphosed Mesozoic and Paleozoic island-arc and related rocks known collectively as the Western Metamorphic Belt (Schiffman and Wagner, 1992). Mesozoic and Paleozoic granitic plutons (Saucedo and Wagner, 1992) have intruded these rocks. The Basin and Range province is highly extended and covered primarily by Tertiary volcanic rocks.

Saucedo prepared a reconnaissance map of the northern Verdi Range during compilation of the Chico Quadrangle geologic map (Saucedo and Wagner, 1992). Garside (1998) included a description of the Verdi Range in a study of Mesozoic rocks of the Reno-Carson City area. The author studied the field trip area for his MS thesis project (Pauly, 2000).

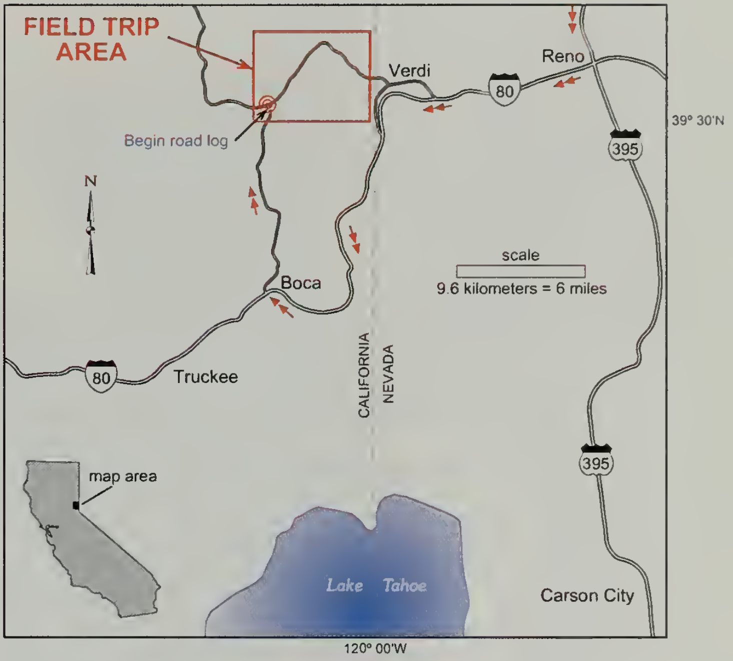

Figure 1. Location map.

ROCK UNITS AND AGES

Jurassic (?) Beacon Point formation (Map unit: J(?)bp)

The metamorphosed, mafic volcanic and volcaniclastic rocks in the field trip area (Figure 2) were informally designated the Jurassic (?) Beacon Point formation by Pauly (2000). These rocks are the main focus of this field trip. No direct evidence has been located, such as fossils, for the age of these rocks. The Jurassic (?) age is based on correlation (discussed below; Pauly, 2000) with the Middle Jurassic Tuttle Lake Formation (Templeton, 1991), exposed approximately 40 km southwest of the Verdi Range. The Beacon Point formation lithology and mineralogy are discussed in detail below, and during the field trip.

Cretaceous-Jurassic granitic rocks: (Map unit: KJgr)

Granitic rocks occur in sharp contact with the Beacon Point formation at three localities (Figure 2), and will be seen at Stops 1 and 6. These rocks are gray, medium-grained, and phaneritic. They

---

[1] Department of Geological Sciences, California State University,Hayward, CA 94542
email: brucepauly@yahoo.com

Rock Units

Qal Quaternary alluvium

MPv Miocene-Pliocene volcanic rocks
Gray, and/or brown (weathered) andesitic lava flows and lahars. Vesicular; porphyritic with abundant plagioclase phenocrysts.

KJgr Cretaceous-Jurassic granitic rocks
Gray, medium-grained hornblende and biotite-rich granite and granodiorite. Typically not deeply weathered. Local mafic inclusions.

J(?)bp Jurassic (?) Beacon Point formation Dark gray-green, metabasaltic, altered breccia/conglomerate, volcanogenic sandstone/siltstone, and mafic intrusives (undifferentiated). Breccia/conglomerate and volcanogenic sandstone/siltstone locally bedded.

GEOLOGIC MAP OF THE NORTHERN VERDI RANGE, SIERRA COUNTY, CA

BRUCE PAULY
DEPT. OF GEOLOGICAL SCIENCES
CALIFORNIA STATE UNIVERSITY, HAYWARD
1998 - 99

CS Columnar section locality

CM Contact metamorphism study locality

Geologic Symbols

\ Bed strike

38 Bed strike and dip

— Contact, located ± 200'

— — — Contact, approximately located

— ? — ? — Contact, location uncertain

• • • • • • Contact, concealed

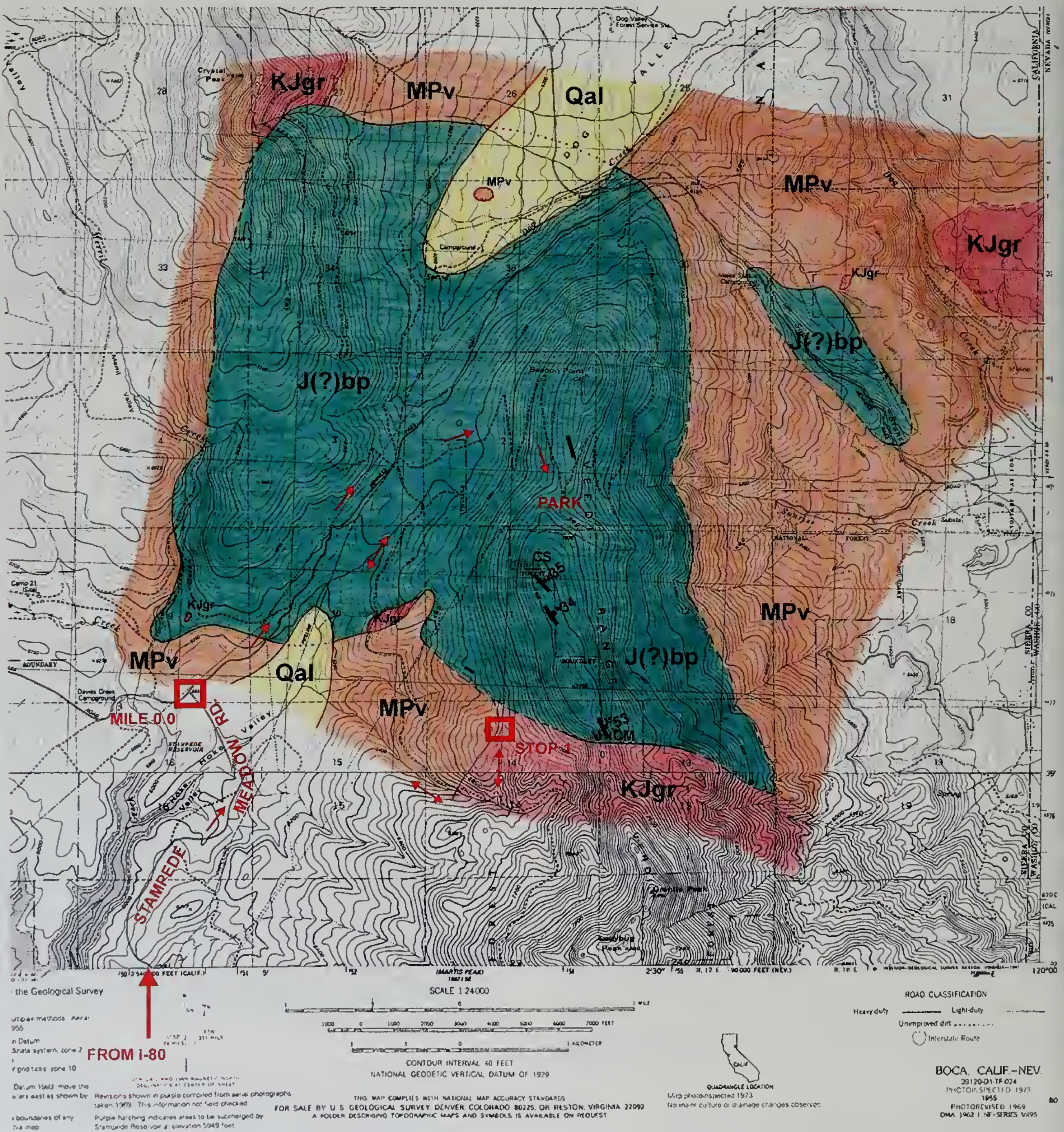

Figure 2

are typically not deeply weathered. Saucedo and Wagner (1992) characterize them as hornblende and/or biotite-rich granite and granodiorite. Garside and others (1992) obtained a K-Ar biotite age of 90.7 Ma for the granitic rocks in contact with the northwest Beacon Point formation near Crystal Peak (Figure 2). Evernden and Kistler (1970) obtained K-Ar biotite ages of 99.6 and 101.5 Ma for the Haypress Creek pluton, 40 km northwest of the Verdi Range near Sattley. Phillipson (1995) obtained a U-Pb zircon age of 164 ± 2 to 168 ± 7 Ma (Middle Jurassic) for the same pluton, and interpreted Cretaceous plutonism to the east as having disturbed the K-Ar system in the Haypress Creek pluton. Thus, it is likely that K-Ar ages obtained for plutons in the study area represent reset ages, and that these rocks are actually of Middle Jurassic age.

Miocene-Pliocene volcanic rocks: (Map unit: MPv)

Miocene and Pliocene andesitic lava flows and lahars also occur in the field trip area, surrounding much of and at lower elevation than the Beacon Point formation (Figure 2). These rocks will be seen at Stop 1. They contain pyroxene, hornblende and plagioclase phenocrysts. Plagioclase phenocrysts vary in length from 1 to 5 millimeters (mm). The Miocene-Pliocene volcanic rocks are similar in appearance and mineralogy to the 16.0 Ma (Bell and Garside, 1987) Kate Peak Formation described throughout western Nevada (Axelrod, 1959), and the Tertiary volcanic rocks mapped south, west (Latham, 1985) and east (Bell and Garside, 1987) of the field trip area.

STRUCTURE AND DEFORMATION

Well-bedded exposures of volcanogenic sandstone within the Beacon Point formation are confined to the northern Verdi Range ridge south of Beacon Point. The bedding strike ranges between N15W and N40W, and the dip ranges from 34NE to 53NE (Figures 2 and 3). Therefore, post-depositional tilting took place. The beds face upright. Other than easterly tilting, the Beacon Point formation is structurally undeformed. There is no obvious penetrative cleavage or foliation. Weak schistosity is developed at a few localities along plutonic contacts. No folds were observed, however bedded outcrops of sufficient size to observe mesoscopic folds are restricted to only a few localities (Pauly, 2000).

LITHOLOGY

Three different lithofacies of the Beacon Point formation were recognized along the Verdi Range ridge (Figure 3) by Pauly (2000).

Volcanogenic breccia/ conglomerate (60%)

Breccia and conglomerate are prominent in the Beacon Point formation (Photo 1). Both types of rocks are greenish-gray. Clasts display a wide range of size (granules to boulders) and rounding (angular to well-rounded). The larger clasts tend to be well-rounded. Approximately 50% of the clasts appears to be completely altered to greenish minerals, while the remainder appears to have retained some or all of its original gray (Photo 1). Most of the clasts appear to be mafic, based on their dark color, and volcanic, based on common porphyritic texture. Vesicles are poorly-developed. Visible phenocrysts are either plagioclase (75%) or dark mafic minerals (25%). Rare plutonic cobbles occur in the breccia/conglomerate (Photo 2); they are subrounded to rounded. The breccia/ conglomerate matrix is fine grained and ranges from greenish-gray to brown. Locally, the matrix material is distinctively green and similar in color to the selectively altered green clasts within the breccia/conglomerate (Photo 1). The breccia/conglomerate rocks were deposited in beds, which are described and interpreted in the Emplacement Processes section below.

Volcanogenic sandstone/ siltstone (30%)

Fine- to medium-grained, gray, brown, and greenish sandstone (and less common siltstone) occurs locally as thin (sub-meter) interbeds within the breccia/conglomerate (Photo 3). At other localities the sandstone is massive and up to 5 meters (m) thick. Petrographic analysis (Pauly, 2000) reveals that gain mineralogy and textures match those of the clasts of the breccia/conglom-

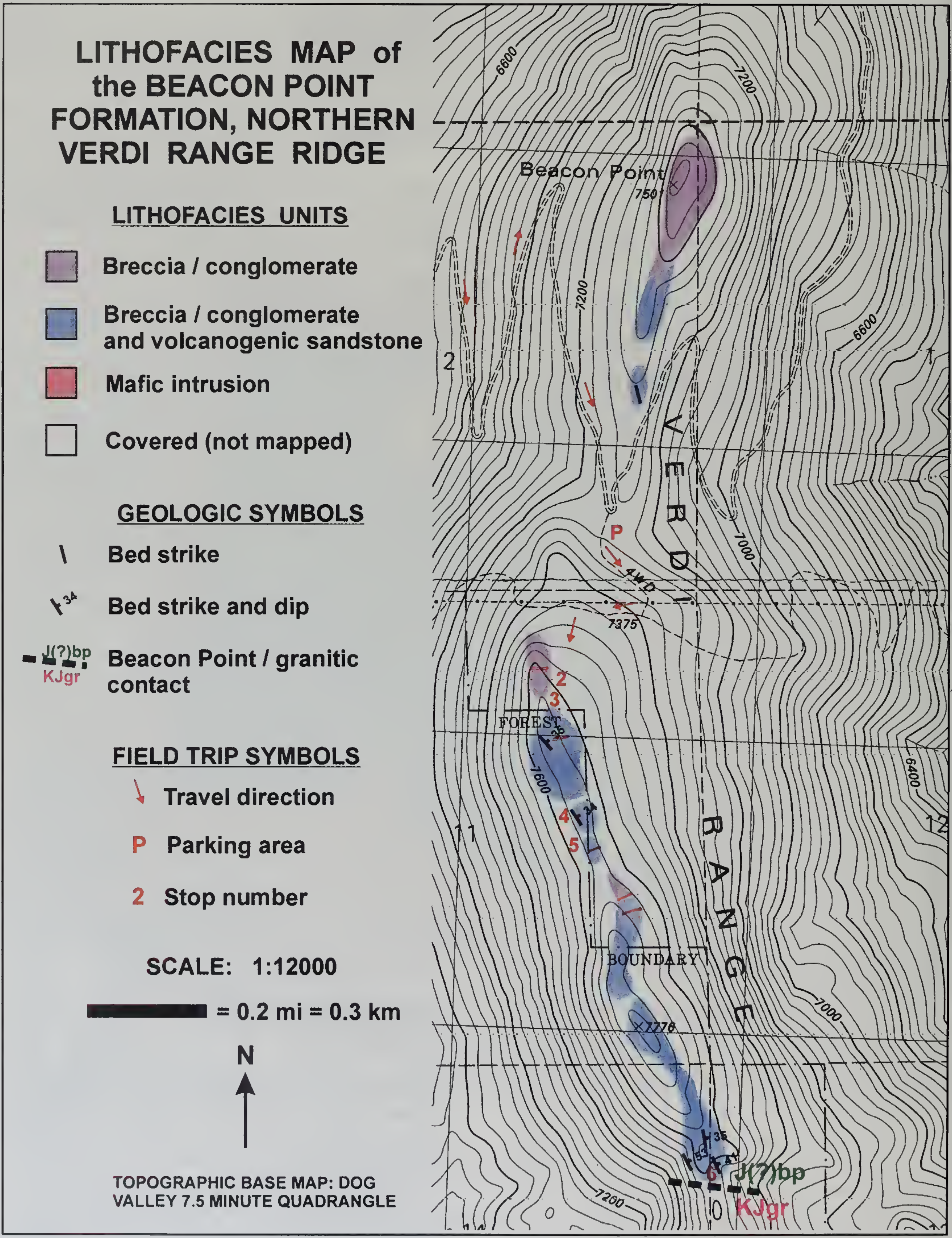
LITHOFACIES MAP of the BEACON POINT FORMATION, NORTHERN VERDI RANGE RIDGE
LITHOFACIES UNITS
Breccia / conglomerate
Breccia / conglomerate and volcanogenic sandstone
Mafic intrusion
Covered (not mapped)
GEOLOGIC SYMBOLS
Bed strike
34
Bed strike and dip
J(?)bp
KJgr
Beacon Point / granitic contact
FIELD TRIP SYMBOLS
Travel direction
P
Parking area
2
Stop number
SCALE: 1:12000
= 0.2 mi = 0.3 km
N
TOPOGRAPHIC BASE MAP: DOG VALLEY 7.5 MINUTE QUADRANGLE
6600
7200
Beacon Point
7501
7200
6600
2
VERDI
P
7000
4WD
7375
2
3
FOREST
36
7600
6400
11
4
34
5
RANGE
12
BOUNDARY
7000
7776
35
53
41
6
J(?)bp
KJgr
7200

Figure 3.

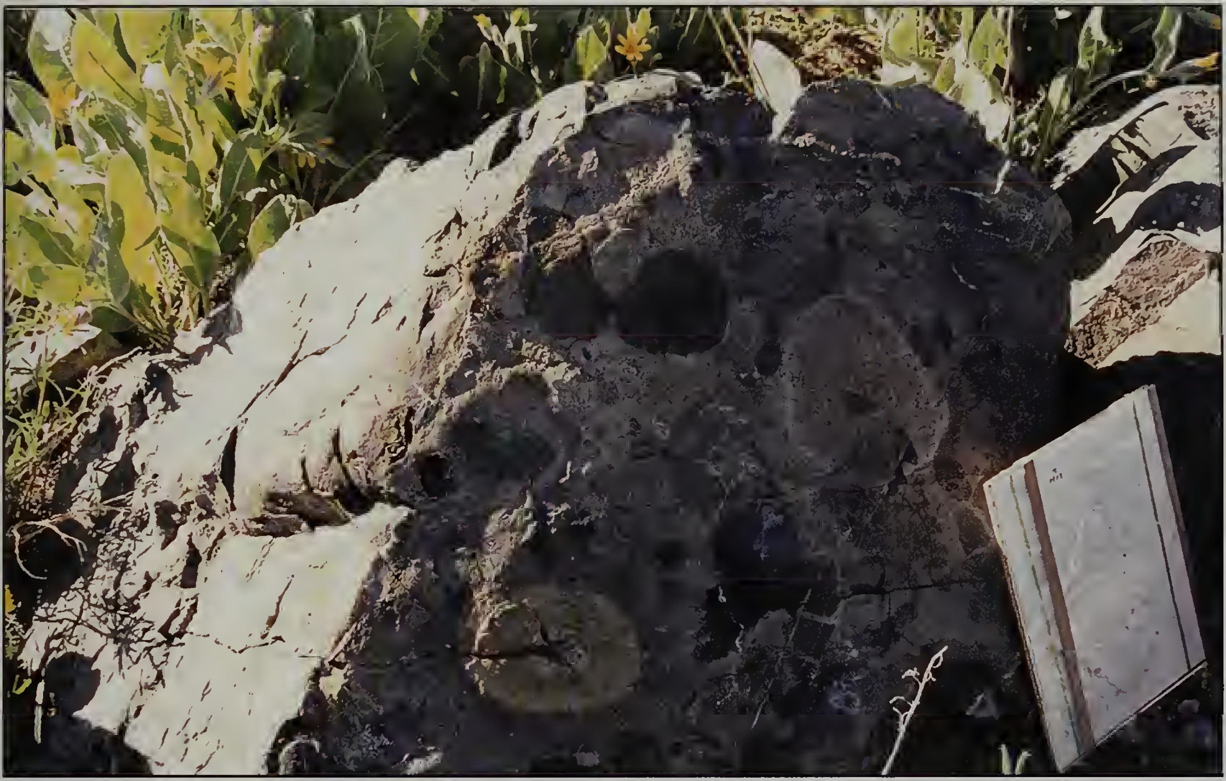

Photo 1. (Stop 2) Float chunk of breccia/conglomerate. Wide variations in clast coloration and rounding are evident. Two large clasts (center) have apparently been selectively and completely altered to greenish minerals. Map case is approximately 23 x 30 cm. *Photo by Bruce Pauly.*

erate. At a few localities, bedding is preserved well enough for attitude measurement (Figures 2 and 3). Sedimentary structures such as scours and cross-stratification are present. These structures were used to determine that the beds face upright (Pauly, 2000). The sandstone/siltstone typically is interbedded in the breccia/conglomerate. In these beds, porphyritic and aphanitic clasts, identical to those observed in the breccia/conglomerate, are locally present. The clast size ranges from coarse sand to medium pebbles.

Mafic intrusives (10%)

At several locations in the study area, dark gray-green, porphyritic rocks occur in linear (NE trending), 1 to 10 m wide bands (Photo 4). These rocks also occur in larger irregularly-shaped lenses or pods. The rocks are in sharp contact with the breccia/conglomerate, and thus appear to have intruded fully-lithified rocks. The porphyritic rocks consist of 10% phenocrysts and 90% groundmass (visual estimate). Abundant white plagioclase crystals (up to 10 mm) and dark mafic phenocrysts are visible to the naked eye in some of these rocks. Other mafic intrusive rocks are aphanitic (only a few phenocrysts visible to the naked eye) and typically contain amygdules. The intrusive rocks are homogeneous. The field relations, lithology, and texture suggest these rocks represent hypabyssal intrusions, likely dikes.

Greenish metamorphic minerals (especially actinolite and epidote) are prominent throughout the Beacon Point formation and impart an overall greenish cast to the rocks and associated surficial debris and soil. Thus the Beacon Point formation appears to have been completely metamorphosed.

MINERALOGY

The Beacon Point mafic intrusive rocks are 70% porphyritic and 30% aphanitic. Mircophenocrysts (20%) consist of calcic (An_{75-85}) plagioclase (90%) and partial to complete actinolite pseudomorphs after augite (10%). Groundmass (80%) minerals

Photo 2 (Stop 6). Subrounded to subangular plutonic clast (above and to right of hammer handle) in breccia/conglomerate. *Photo by Bruce Pauly.*

include microcrystalline actinolite, calcic plagioclase, biotite, epidote, quartz, potassium feldspar, and magnetite (Figure 4). The plagioclase microphenocrysts display crystal zoning (Photo 5). Unmetamorphosed augite cores of actinolite pseudomorphs are also zoned (Photo 6). Beacon Point formation volcanogenic breccia/conglomerate and sandstone/siltstone mineralogies are similar to the mafic intrusives. The breccia/conglomerate clasts and the mafic intrusive rocks are also geochemically very similar (discussed below). The observed lithology and mineralogy suggest that the Beacon Point formation consists of metamorphosed basalt and possibly andesite.

METAMORPHISM

The rocks of the interior of the Beacon Point formation now consist of calcic plagioclase, augite, actinolite, epidote, quartz, biotite, potassium feldspar, and magnetite. There are also prominent epidosites (rocks consisting entirely of recrystallized quartz and epidote), especially in the fine-grained layers and matrix of the breccia/conglomerate. The calcic plagioclase is interpreted to be a relict igneous phase, based on the relict igneous features (Photo 5) and high Ca content. The augite crystals are interpreted to be a relict igneous phase as well (Photo 6). Epidosites form as a result of seafloor hydrothermal alteration of basalts at 300-350°C (Schiffman and others, 1990). The abundance of actinolite suggests greenschist-facies metamorphism of a basic protolith. However, recrystallized albite and chlorite, which would normally be expected to accompany the actinolite, are absent in these rocks. Metamorphism of the Beacon Point formation will be discussed further at Stop 6.

EMPLACEMENT PROCESSES

The Beacon Point breccia/conglomerate rocks are bedded and consist of porphyritic and aphanitic volcanic clasts (origin discussed below) supported by a fine-grained matrix (Figure 5). The majority of the clasts show evidence of reworking

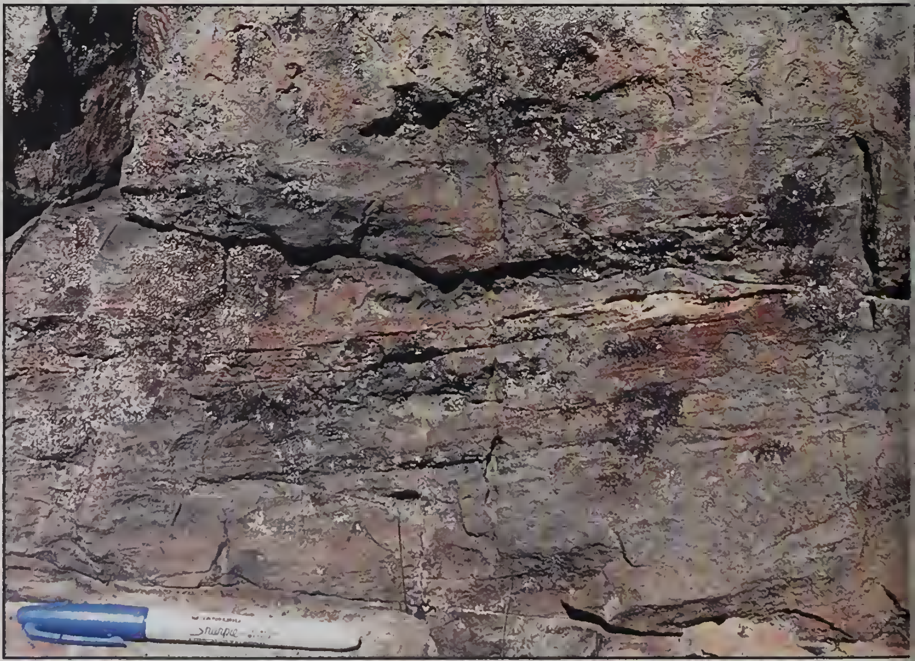

Photo 3 (Stop 4). Sandstone interbed (center) within breccia/conglomerate (upper and lower portions of photo). Thin bedding is visible in the sandstone. *Photo by Bruce Pauly.*

(particularly rounding), suggesting erosion and transportation. Flow characteristics such as reverse grading, isolated boulders, and vertically oriented clasts protruding into the fine-grained cap layers (Figure 5; Photos 7 and 8) suggest that the breccia/conglomerate rocks were deposited by subaqueous, high-density, cohesive debris flows. The debris-flow deposits are discussed in detail at Stop 3.

Volcanogenic sandstone interbeds (Stop 4) occur within the breccia/conglomerate deposits, possibly representing the distal portions of the debris flows. Mafic intrusives cut sharply through the breccia/conglomerate, and appear to be hypabyssal dikes (Stop 5). The field occurrences of these lithofacies (Figure 3) are discussed below and at Stop 5.

Many of the Beacon Point rocks, especially the breccia/conglomerate, display evidence of alteration. In some cases, clasts that are completely altered to greenish epidote are immediately adjacent to clasts that appear relatively unaltered (Photo 1). This selective alteration suggests that some clasts may have been altered prior to incorporation into the debris-flow deposits. Electron microprobe analysis of mineralogy and textures (recrystallized epidote with quartz) indicates that epidosite-like alteration has occurred (Pauly, 2000). Alteration of the Beacon Point formation will be discussed in more detail below and at Stop 3.

GEOCHEMISTRY AND TECTONIC SETTING

The weight percent of SiO_2 within the Beacon Point formation varies in the breccia/conglomerate clasts from 48.6 to 57.7, and from 48.4 to 59.0 in the intrusive rocks (Pauly, 2000). Therefore, nomenclature for these basic to intermediate rocks, (based simply on weight percent SiO_2), ranges from basalt to andesite. A plot of total alkalies ($Na_2O + K_2O$) vs. SiO_2 weight percent (LeBas and others, 1986) shows that total alkali content varies from about 4.5 to 8.5 weight percent, with five of the six samples greater than 6% (Figure 6). The resulting chemical classifications are basalt, trachy-basalt, basaltic trachy-andesite, and trachy-andesite. The average weight percent of K_2O is 3.0, which indicates these are fairly high-K basalts and andesites. Further classification into the alkaline or subalkaline basaltic magma series based on total alkali content is not possible due to the large variation of alkali abundance (Figure 6), likely caused by mobilization of alkalies and/or SiO_2 during alkali-metasomatism, alteration and/or metamorphism. However, Figure 6 certainly indicates the rocks are quite alkalic. Several samples have fairly high (6-8%) MgO levels, almost reaching boninitic (Wilson, 1989) magma series levels.

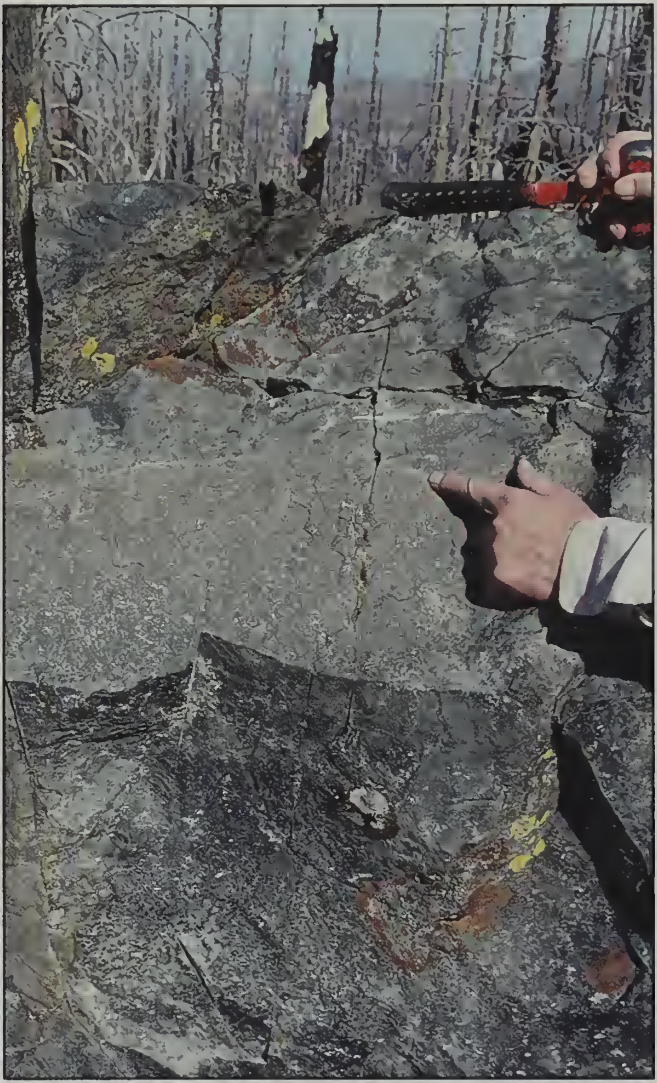
Photo 4 (Stop 5). Mafic intrusive (below finger). Dark gray groundmass and prominent white plagioclase phenocrysts (up to 10 mm) impart porphyritic texture. The mafic intrusive is in sharp contact with breccia/conglomerate (above finger). Lower intrusive contact not shown. *Photo by Bruce Pauly.*

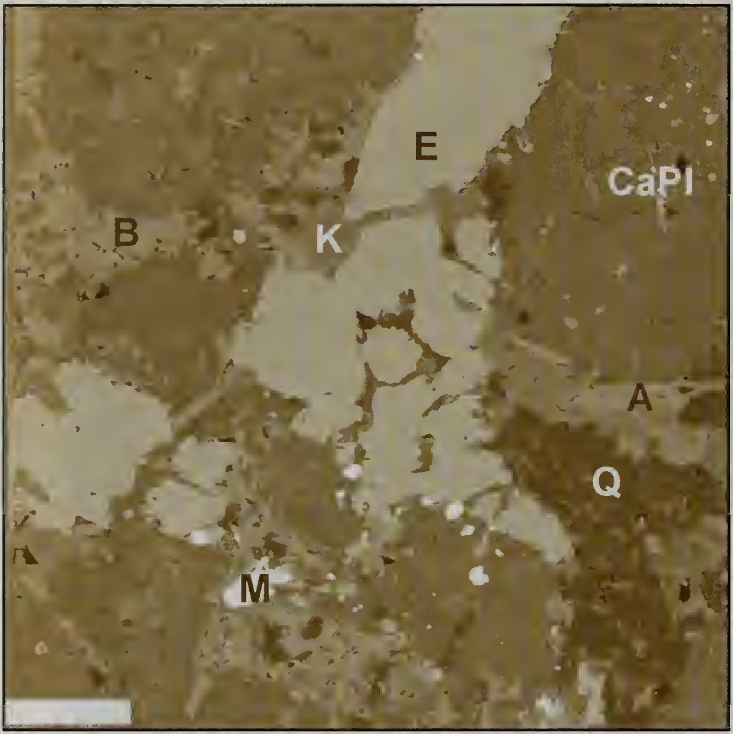

Figure 4. Back-scattered electron image showing the mineral assemblage in the groundmass of Beacon Point porphyritic, mafic intrusive rocks. Labeled minerals: CaPl—calcic plagioclase; A—actinolite; Q—quartz; B—biotite; K—potassium feldspar; E—epidote; M—magnetite. Scale bar equals 0.167 mm. *Photo by Peter Schiffman and Bruce Pauly.*

Trace-element abundance patterns are useful for distinguishing basaltic magma series and tectonic settings. This is particularly true for rocks that have been metamorphosed or altered, because certain trace-elements are less mobile than, for example, alkali ions and can therefore be used as a basis for discrimination (Rollinson, 1993). A chondrite-normalized (Nakamura, 1974) rare-earth element (REE) abundance diagram for Beacon Point samples displays light REE (LREE) enrichment, with relatively flat middle and heavy REE (HREE) abundances (Figure 7). This pattern is characteristic of subalkaline magmas (Wilson, 1989). LREE enrichment is approximately three to four times the HREE levels, characteristic of calc-alkaline magmas (Wilson, 1989). Tholeiitic magmas characteristically have flatter REE patterns that lack the distinctive LREE enrichment. This diagram also shows that the breccia/conglomerate clast pattern is nearly identical to that of the intrusive rocks. The Th/Yb vs. Ta/Yb discrimination diagram (Pearce, 1982) distinguishes calc-alkaline, shoshonitic, and tholeiitic magma (Figure 8). The Beacon Point data plot in a fairly tight cluster within the calc-alkaline field.

Figure 9 is a MORB (mid-ocean ridge basalt)-normalized (Pearce, 1983) multi-element diagram (spidergram). Trace-elements are ordered in terms of their mobility in an aqueous fluid phase and their relative incompatibility in melts. The low field strength (LFS) elements Sr, K, Rb, and Ba are classed as mobile and plot to the left in the diagram. The high field strength (HFS) elements (Th through Yb) are considered immobile and plot

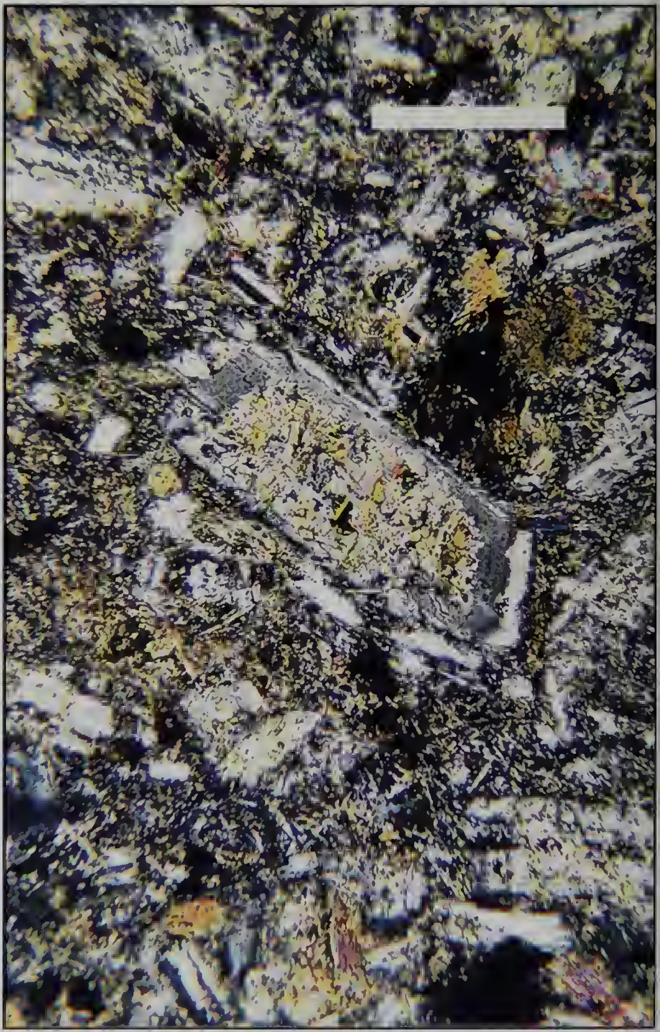

Photo 5. Subhedral plagioclase microphenocryst (center) in porpyritic, mafic intrusive rock. Oscillatory compositional zoning and polysynthetic twin lamellae are visible in the rim. The microphenocryst's core has been replaced by epidote and actinolite. XPL. Scale bar equals 0.25 mm. *Photo by Bruce Pauly.*

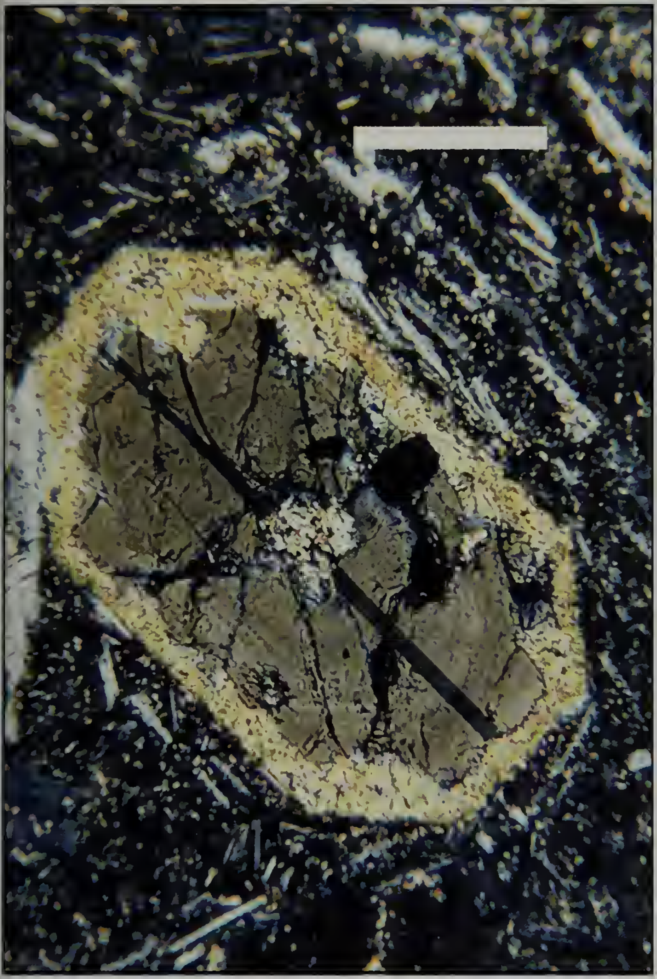

Photo 6. A euhedral clinopyroxene microphenocryst displaying marginal pseudomorphic replacement by actinolite in mafic intrusive rock. Compositional zoning and twin lamellae (relict igneous textures) are prominent. Pilotaxitic texture shown by plagioclase microlites surrounding the clinopyroxene crystal suggests flow within the intrusive magma. XPL. Scale bar equals 0.25 mm. *Photo by Bruce Pauly.*

to the right. Incompatibility increases inwards from both edges to the center of the diagram. One of the intrusive samples is omitted from Figure 9 due to anomalous Zr and Hf measurements. The LFS elements are all relatively enriched. The HFS elements Ta and Nb show pronounced depletion. LFS elements have been shown to be relatively enriched in the upper crust (Wilson, 1989). The pattern therefore indicates magma contamination by the upper crust, suggesting a subduction-related arc setting. Ta and Nb depletion is also characteristic of arc-related magmas. The overall pattern of Figure 9 is indicative of oceanic island-arc high-K calc-alkaline basalt (Wilson, 1989), and suggests that the tectonic setting of the Beacon Point formation was an oceanic island arc.

Figure 9 also shows Zr and Hf enrichment for breccia/conglomerate clasts and intrusive samples of the Beacon Point formation. The selective enrichment of Zr and Hf has been observed in some (particularly boninitic) volcanic arcs (Murton, 1989). Most authors attribute Zr and Hf enrichment to metasomatism of a depleted mantle source by fluids from a subducting slab (Murton and others, 1992). This evidence supports the conclusion that the tectonic setting for the Beacon Point formation was an oceanic island arc.

The observed mineralogy and depositional characteristics of the Beacon Point formation also support the inferred oceanic, island-arc setting. Continental calc-alkaline arcs display a greater abundance of dacites and rhyolites than oceanic arcs. Much of the additional volume of acid rock in continental arcs consists of pyroclastic flows and ignimbrites (Wilson, 1989), which were not observed in the Beacon Point formation (Pauly, 2000). The observed submarine debris-flow deposits are more consistent with an oceanic island-arc setting.

Alkali-metasomatism and epidosite alteration, observed in the Beacon Point formation (Pauly, 2000), are also documented in the Jurassic Ritter Range pendant (Hanson, R.B. and others, 1993), approximately 220 km southeast of the Verdi Range in the eastern Sierra Nevada. The Ritter Range pendant represents an oceanic volcanic arc (Sorensen and others, 1998). Alkali-metasomatism and epidosite alteration occur in many environments. Though not diagnostic of, these processes are consistent with an oceanic island-arc setting for the Beacon Point formation.

PALEOVOLCANOLOGY

Clast Generation

Based on the mineralogical and geochemical similarity of the intrusive and clastic rocks of the Beacon Point formation, it appears that fragmentation of erupting basaltic lava or erosion of lava deposits generated the volcanic clasts. Lava

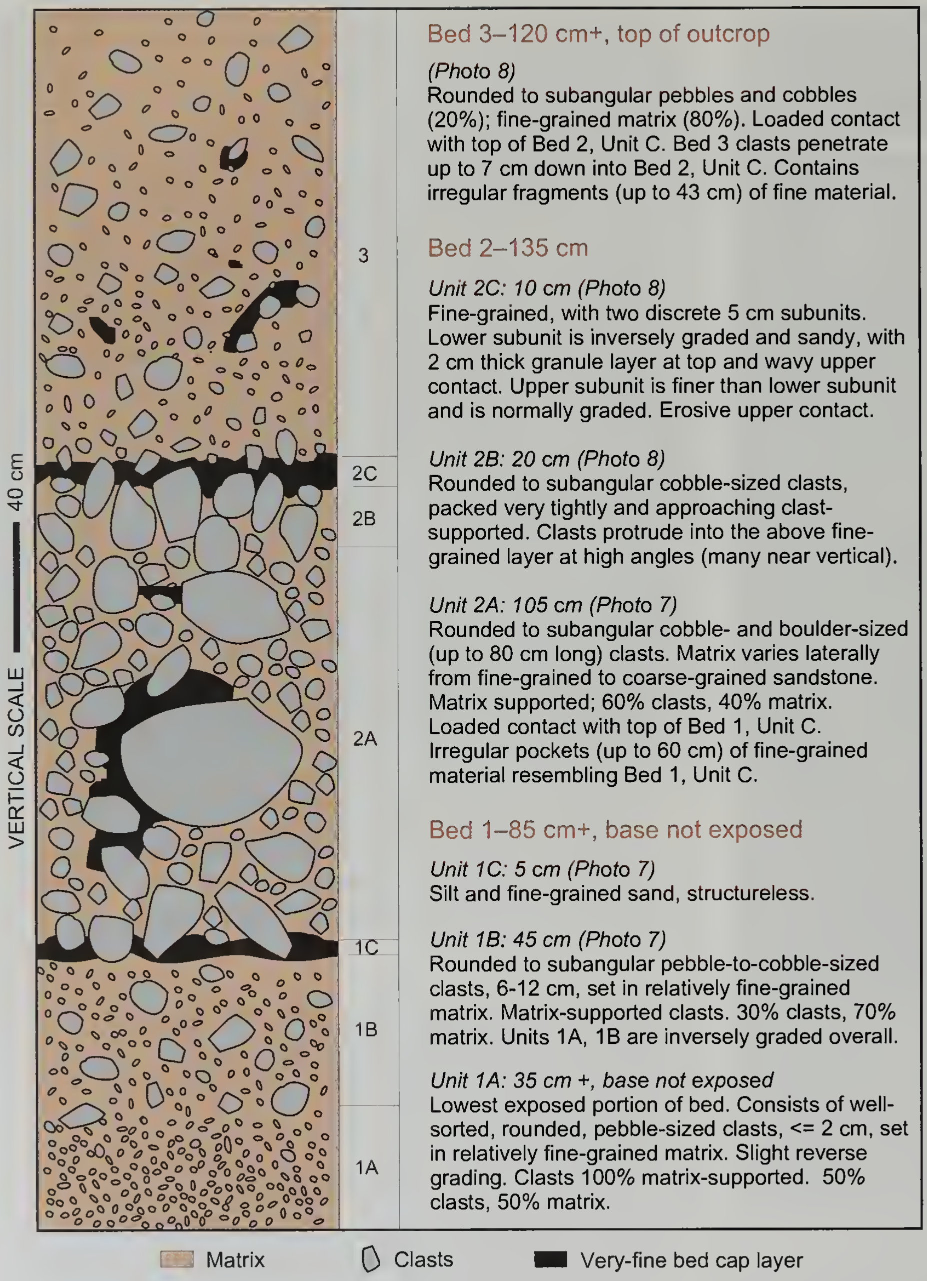

Bed 3–120 cm+, top of outcrop

(Photo 8)
Rounded to subangular pebbles and cobbles (20%); fine-grained matrix (80%). Loaded contact with top of Bed 2, Unit C. Bed 3 clasts penetrate up to 7 cm down into Bed 2, Unit C. Contains irregular fragments (up to 43 cm) of fine material.

Bed 2–135 cm

Unit 2C: 10 cm (Photo 8)
Fine-grained, with two discrete 5 cm subunits. Lower subunit is inversely graded and sandy, with 2 cm thick granule layer at top and wavy upper contact. Upper subunit is finer than lower subunit and is normally graded. Erosive upper contact.

Unit 2B: 20 cm (Photo 8)
Rounded to subangular cobble-sized clasts, packed very tightly and approaching clast-supported. Clasts protrude into the above fine-grained layer at high angles (many near vertical).

Unit 2A: 105 cm (Photo 7)
Rounded to subangular cobble- and boulder-sized (up to 80 cm long) clasts. Matrix varies laterally from fine-grained to coarse-grained sandstone. Matrix supported; 60% clasts, 40% matrix. Loaded contact with top of Bed 1, Unit C. Irregular pockets (up to 60 cm) of fine-grained material resembling Bed 1, Unit C.

Bed 1–85 cm+, base not exposed

Unit 1C: 5 cm (Photo 7)
Silt and fine-grained sand, structureless.

Unit 1B: 45 cm (Photo 7)
Rounded to subangular pebble-to-cobble-sized clasts, 6-12 cm, set in relatively fine-grained matrix. Matrix-supported clasts. 30% clasts, 70% matrix. Units 1A, 1B are inversely graded overall.

Unit 1A: 35 cm +, base not exposed
Lowest exposed portion of bed. Consists of well-sorted, rounded, pebble-sized clasts, <= 2 cm, set in relatively fine-grained matrix. Slight reverse grading. Clasts 100% matrix-supported. 50% clasts, 50% matrix.

Figure 5. Columnar section.

fragmentation may have occurred subaerially (producing pyroclasts) and/or subaqueously (producing hydroclasts). Direct evidence of subaerial eruption (such as tuffaceous matrices) and/or subaqueous eruption (such as chilled clast margins) is absent, so either or both environments are possible. The lack of prominent, well-developed vesicularity favors fairly deep subaqueous fragmentation. Clasts may also have been produced secondarily by erosion of subaqueous and/or subaerial lava deposits (epiclasts). These clast production processes and end products are consistent with those observed in modern, oceanic, island-arc settings (Carey, 2000).

Depositional Environment

Pauly (2000) prepared a litho facies map of the Beacon Point formation along the northern Verdi Range ridge crest (Figure 3). It shows the exposed extent of the breccia/conglomerate, mixed breccia/conglomerate and volcanogenic sandstone, and mafic intrusives. From north to south along the ridge, the map shows three repeating patterns of lithofacies variation, from breccia/conglomerate to mixed breccia/conglomerate and volcanogenic sandstone. These repeating patterns, along with the wide grain size range (silt to small boulders), suggest that a volcaniclastic apron is a possible depositional environment. The observed range of volcaniclastic grain sizes also suggests that the Beacon Point formation may have been deposited in a mid-apron area. In modern island-arc settings, the volcaniclastic apron, at the base of the volcanic flank, progrades into the basin similarly (but not identically) to growth of a submarine fan (Carey and Sigurdsson, 1984).

Transportation Processes

The observed subaqueous debris-flow deposits and prominent clast rounding are evidence of subaqueous transportation and deposition. This suggests that at least the lower portion of the inferred apron's slope must have been submerged. Carey and Sigurdsson (1984) suggest that the typical causes of clast remobilization in island-arc settings are slope instability, seismic activity, and/or current or storm activity.

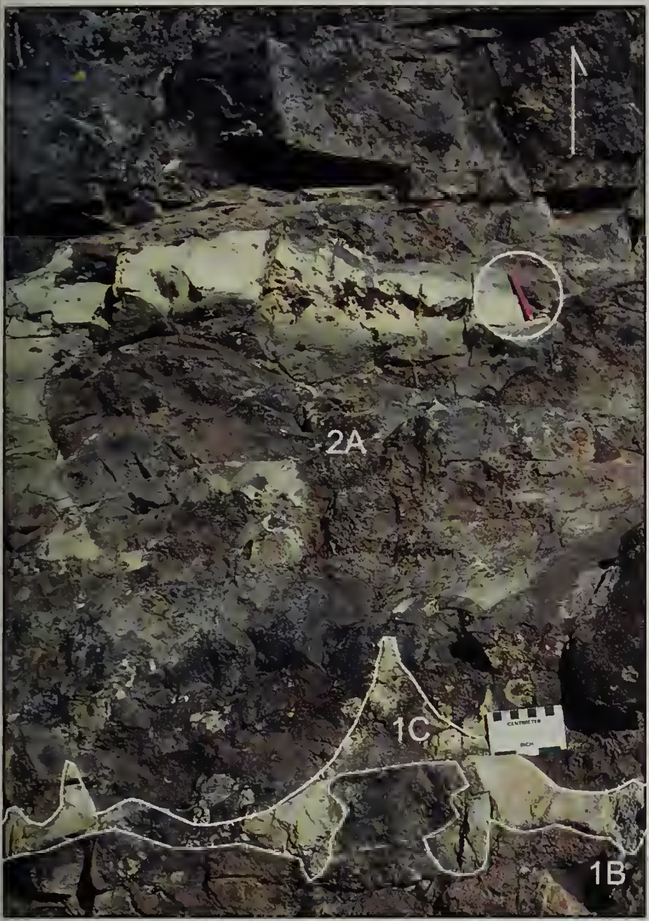

Photo 7. Stratigraphic up is toward top of photo (arrow). Centimeter scale is at contact of Bed 1, Unit C (whitish, fine-grained) and Bed 2, Unit A. Note the loaded contact at top of Bed 1, Unit C. Pencil (circle) rests on an irregular fragment of fine-grained material, similar to that comprising Bed 1, Unit C. *Photo by Bruce Pauly.*

REGIONAL CORRELATIONS

In order to improve age control and establish possible tectonically significant correlations, Pauly (2000) compared the Beacon Point formation to other documented Jurassic terranes in the region.

Tuttle Lake Formation

Templeton (1991) studied the Tuttle Lake Formation at English Mountain, 40 km southwest of the Verdi Range. The type locality of the Tuttle Lake Formation is approximately 15 km south (along strike) of English Mountain. Templeton (1991) documented metamorphosed andesitic tuff-breccias cut by metamorphosed mafic hypabyssal intrusions. He interpreted the tectonic setting to be an oceanic island arc, based on the mineralogy and voluminous, coarse, subaqueous debris-flow deposits.

Age control of the Tuttle Lake Formation is given by its stratigraphic position conformably above the Early to Middle Jurassic Sailor Canyon Formation (Templeton, 1991), and its intrusion by Middle Jurassic plutons with U-Pb zircon ages of approximately 165 Ma (Hanson, R.E. and others, 1993). Templeton (1991) also reported the occurrence of Early to Middle Jurassic marine pelecypod fossils (*Posidonia*) in the Tuttle Lake Formation.

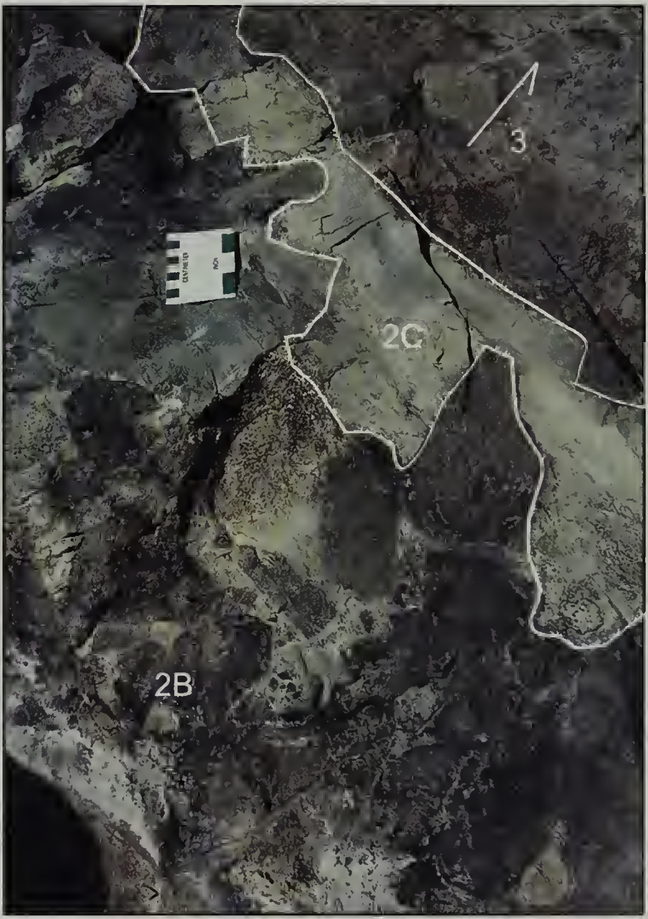

Photo 8. Stratagraphic up is toward upper right of photo (arrow). Centimeter scale rests on Bed 2, Unit B, just below contact (outlined in white) with Bed 2, Unit C. Note matrix-supported Bed 2, Unit B clasts protruding nearly vertically into fine-grained Bed 2, Unit C. Oblique view, so bed thickness is exaggerated. *Photo by Bruce Pauly.*

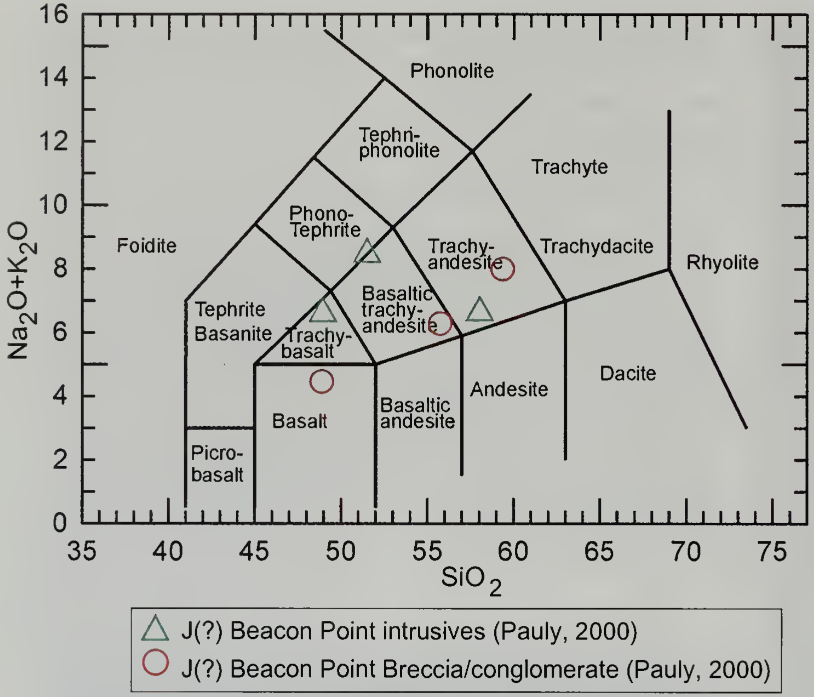

Figure 6. Total alkalies vs. silica diagram (LeBas and others, 1986) of intrusives and breccia/conglomerate from the Beacon Point formation. Spread of plotted points is likely due to alkali and/or SiO_2 mobilization during alteration and/or metamorphism.

Subsequent to Templeton's work (1991), the Tuttle Lake Formation was studied near Snow Mountain (Hargrove, 1995), 50 km southwest of the Verdi Range, and in the Webber Peak/Meadow Lake area (Mielke, 1996), 35 km west of the Verdi Range. The mineralogy reported by Templeton (1991), Hargrove (1995) and Mielke (1996) is similar to that of the Beacon Point formation. Hargrove (1995) and Mielke (1996) reported trace-element abundances for the Tuttle Lake Formation. These data support Templeton's inferred oceanic island-arc setting. Pauly (2000) compared Tuttle Lake and Beacon Point trace-element data. A multi-element spidergram (Figure 10) shows that, except for a distinct difference in Zr and Hf abundances, there is close correspondence between the Tuttle Lake and Beacon Point patterns.

The relative enrichment of Zr and Hf in the Beacon Point formation may be the result of differing degrees of alteration and/or metasomatism.

The debris-flow deposits described in the Tuttle Lake Formation (Templeton, 1991) are similar in appearance to those found in the Beacon Point formation. As in the Beacon Point formation, beds are commonly reverse-graded, with pebble- to boulder-sized rounded and angular clasts suspended in the matrix. Bedding attitude is also similar to that of the Beacon Point formation (generally N/S strike and east dip). Pauly (2000) observed important textural differences in the debris-flow deposits of the Tuttle Lake and Beacon Point formations. The Tuttle Lake Formation deposits are thicker and coarser-grained. Individual debris-flow deposits in the Tuttle Lake Formation are up to 17 m thick (Templeton, 1991), as opposed to the maximum thickness of 3.0 m observed in the Beacon Point formation. The Tuttle Lake Formation clasts are larger (up to 1.7 m, with a higher percentage of cobbles and boulders) and more angular.

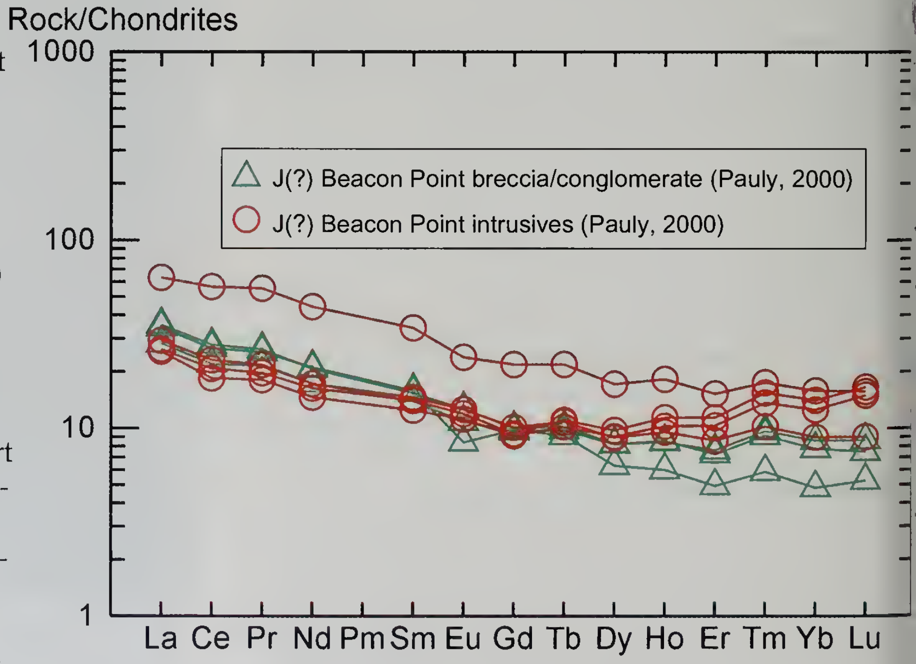

Figure 7. Chondrite-normalized (Nakamura, 1974) REE abundance patterns of intrusives and breccia/conglomerate from the Beacon Point formation. Subalkaline, calc-alkaline magma is indicated. Intrusives and breccia/conglomerate show similar patterns.

The volcanogenic sandstone is medium-grained, as opposed to fine to medium-grained in the Beacon Point formation. These textural differences suggest that the Beacon Point formation was deposited relatively source-distal compared to the Tuttle Lake Formation. The paleogeographic implications of this inference are discussed below.

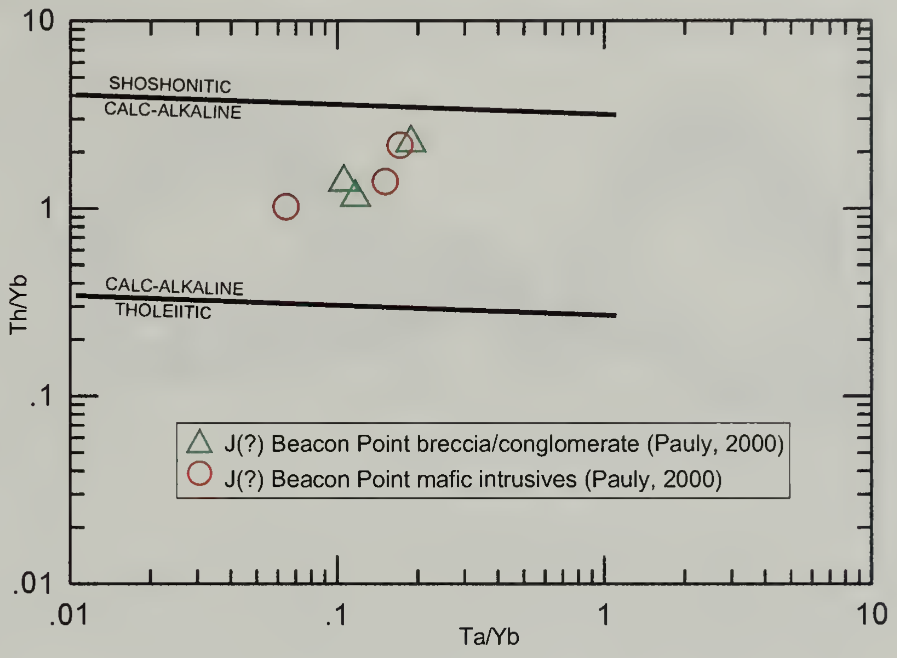

Figure 8. Th/Yb vs. Ta/Yb diagram (Pearce, 1982) distinguishes calc-alkaline Beacon Point from shoshonitic and tholeiitic magmas.

Pauly (2000) tentatively documented a likely correlation between the Beacon Point and Tuttle Lake formations based on the mineralogical, geochemical, and field comparisons described above. These formations could have originated from the same magmatic system. If plutonism near the Beacon Point formation is correlative to the Haypress Creek plutonism near Sattley, then both the Beacon Point and Tuttle Lake formations appear to have been intruded by similarly-aged (approximately 165 Ma) plutons. Thus, Tuttle Lake-Beacon Point volcanism, if correlative, may have been restricted to a fairly short (few-million year) time span.

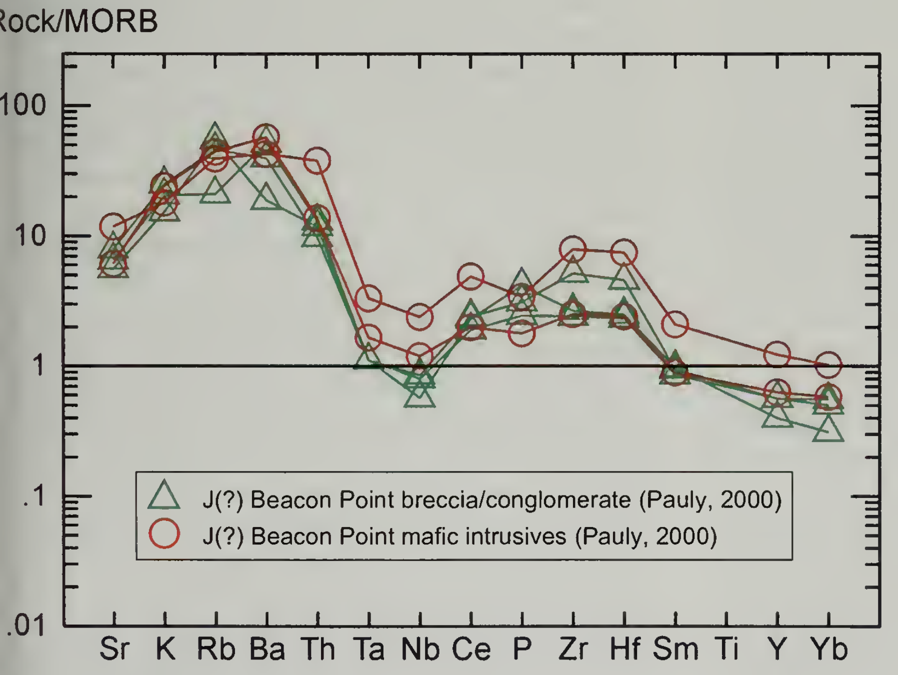

Figure 9. MORB-normalized (Pearce, 1983) multi-element spidergram. Overall pattern, with Sr, K, Rb, Ba enrichment and Ta, Nb depletion is characteristic of oceanic island-arc high-K calc-alkaline basalt. Zr and Hf enrichment may be due to metasomatism (see text).

Peavine/Kettle Rock Sequences

The metavolcanic and metavolcaniclastic Peavine sequence is exposed 12 km northeast of the northern Verdi Range at Peavine Peak (Godwin, 1958; Bonham, 1969; Garside, 1998). Axelrod (in Godwin, 1958) reported that fossil flora from a black shale in the Peavine sequence appeared to be Jurassic in age. Garside (1998) documented nonmarine rhyolitic to basaltic lava flows, lahars, flow domes, ignimbrites, and minor volcaniclastic rocks. The Kettle Rock sequence is exposed near

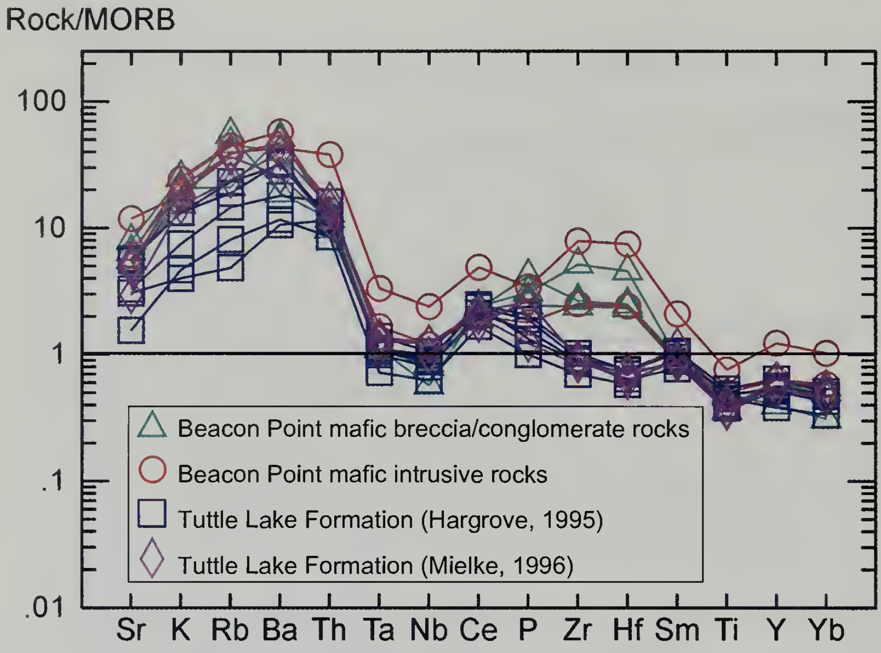

Figure 10. MORB-normalized (Pearce, 1983) spidergram shows close correspondence between the Beacon Point and Tuttle Lake patterns, except for relative Zr and Hf enrichment in the Beacon Point samples.

Taylorsville, 80 km northwest of the Verdi Range. Christe (1993) reported a paleontological age of Middle Jurassic or younger for these rocks. These metamorphosed rocks record at least four intervals of subaerial, andesitic to dacitic volcanism, along with intervals of clastic deposition. Christe and Hannah (1990) suggest a correlation of the Kettle Rock sequence to the Peavine sequence based on similar mineralogy, lithology, and inferred tectonic setting. Weight percent SiO_2 ranges from approximately 55 to 70% in the Peavine and Kettle Rock sequences (Christe and Hannah, 1990; Garside, 1998), as opposed to 49 to 58% in the Beacon Point formation (Pauly, 2000). Deposition in the Peavine and Kettle Rock sequences is interpreted to have been predominantly subaerial (Christe and Hannah, 1990; Garside, 1998) as opposed to subaqueous in the Beacon Point formation (Pauly, 2000). The inferred tectonic setting of the Peavine and Kettle Rock sequences is a continental volcanic arc (Christe and Hannah, 1990; Garside, 1998), as opposed to an oceanic island arc for the Beacon Point formation (Pauly, 2000). Thus the Beacon Point formation and the Peavine-Kettle Rock sequences appear to be time correlative, but represent different styles of volcanism and tectonic settings.

Regional Paleoenvironmental Configuration

Summarizing the above discussion, Middle Jurassic paleoenvironments in the Beacon Point region appear to be represented by the Tuttle Lake Formation (source-proximal, oceanic island arc), Beacon Point formation (source-distal, oceanic island arc), and the Peavine-Kettle Rock sequences (continental arc). Assuming that present-day positions are indicative of relative Middle Jurassic positions, it appears the Beacon Point formation was near a tectonic boundary separating oceanic island-arc and continental-arc settings during the Middle Jurassic.

Ritter Range Pendant

Sorensen and others (1998) discussed the paleoalteration of a northwest- to southeast-trending Jurassic volcanic arc in the eastern Sierra Nevada, approximately 220 km southeast of the Beacon Point formation. The arc is exposed in the Ritter Range, Alabama Hills, and the White-Inyo Mountains. Ages reported for the arc range from 202 to 150 Ma (Sorensen and others, 1998). The metavolcanic rocks of the Ritter Range pendant are interpreted to represent oceanic arc volcanism, with the Alabama Hills and White-Inyo Mountains farther east representing continental arc volcanism (Sorensen and others, 1998). As in the Beacon Point formation, the Ritter Range mafic protoliths are calc-alkaline, and epidosites and alkali-metasomatism are observed (Hanson, R.B. and others, 1993; Sorensen and others, 1998). MORB-normalized spidergram patterns for Ritter Range samples correspond closely to Beacon Point patterns (Figure 11). The patterns for both pendants show similar Zr and Hf enrichment. Pauly (2000) proposed that the Beacon Point and Ritter Range pendants may be sections of the same Jurassic arc, based on trace-element, paleoalteration, and (very) approximate age similarities. The tectonic implications of this possibility are discussed below.

TECTONIC IMPLICATIONS AND SPECULATIONS

Relative Paleolocation of the Beacon Point Formation

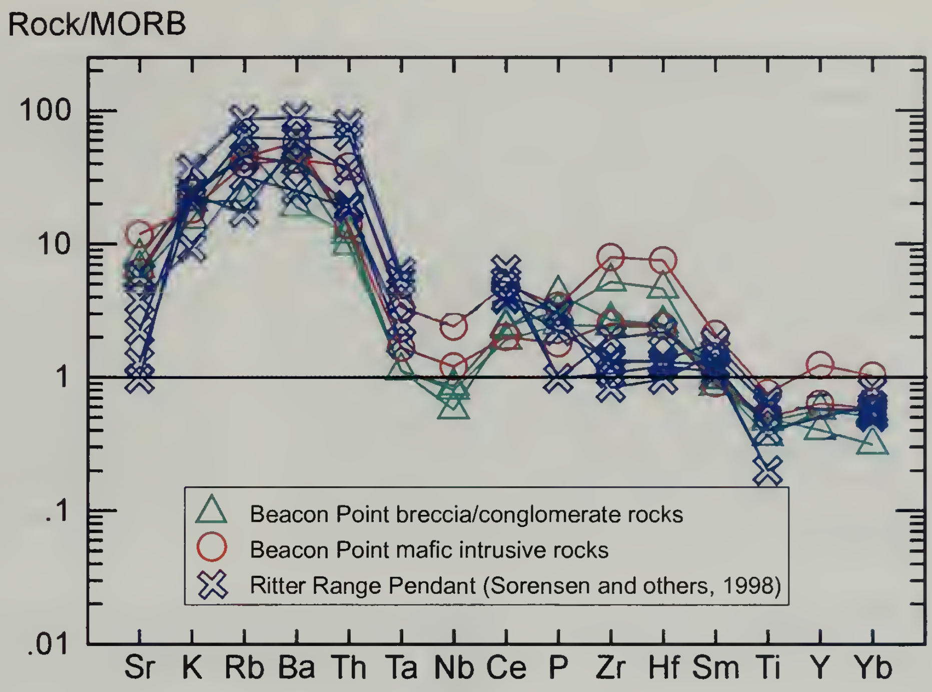

Figure 11. MORB-normalized (Pearce, 1983) spidergram shows close correspondence between Beacon Point formation and Ritter Range pendant patterns. Note Zr and Hf enrichment shown by both patterns.

In the Beacon Point formation, mafic intrusions (geochemically identical to the breccia/conglomerate clasts) are common. The depositional environment appears to have been a volcaniclastic apron, and continentally-derived sediments are rare (if represented by the plutonic clasts) or absent. Where marine stratovolcanoes (modern analogues to the Beacon Point formation) are near a significant landmass, the volcanogenic sedimentation mixes with continentally-derived sediment (Cas and Wright, 1987). If the Beacon Point formation was deposited between an island arc and a continental arc, it appears the Beacon Point formation was emplaced nearer to the island arc than to the continental arc.

Tectonic Scenarios

The simplest scenario fitting the inferred Middle Jurassic regional paleoenvironmental configuration (see above) would be to assume that the Beacon Point formation is the source-distal equivalent of the Tuttle Lake Formation. In Figure 12a (Scenario 1), an oceanic slab, being subducted by another oceanic slab, is responsible for the oceanic island-arc volcanic activity. The Tuttle Lake and Beacon Point formations do not contain accretionary wedge rocks, so both formations are shown on the back-arc side of the island arc. The Tuttle Lake Formation (submarine) is at or near the western edge of the marginal back-arc basin. The Beacon Point formation (submarine) is downslope and farther east in the marginal back-arc basin. A continental mass, represented by the Peavine sequence, is at the eastern edge of the marginal basin.

More complex models are required to fit the paleogeography if the island arc and continental arc were simultaneously active. Two theoretically possible tectonic scenarios (Figure 12b) explain this situation (Moores and Twiss, 1995). Scenario 2 shows two parallel, east-dipping subduction zones, with the Beacon Point formation representing a back-arc basin. In Scenario 3, two subduction zones dip in opposite directions under the active arcs, and the Beacon Point formation represents a forearc basin. In the syn-collisional time frames of both Scenarios 2 and 3, the Tuttle Lake Formation is near the active island arc to the west, the Beacon Point formation is in an inter-arc position, and the continental arc to the east is active.

Scenarios 2 and 3 show the island arc and the continental arc to be converging. At the time of collision, a suture may form, juxtaposing island-arc rocks to the west (Tuttle Lake and Beacon Point formations) and continental-arc rocks to the east (Peavine sequence). The post-collisional tectonic situation is shown for Scenarios 2 and 3 in Figure 12b. Because these convergent scenarios place the Tuttle Lake, Beacon Point and Peavine rocks closer (resembling the present locations) than Scenario 1, Pauly (2000) favors Scenario 2 or 3 as more likely to have occurred.

In all three scenarios of Figure 12, continentally-derived xenoliths could have been transported to the Beacon Point depositional area. Xenoliths would not be expected to occur in the Tuttle Lake Formation in any of the scenarios, as this would have required upslope transportation in Scenario 1. In Scenarios 2 and 3, the island arc would have blocked xenolith transportation westward to the Tuttle Lake Formation.

Implications

The Beacon Point formation appears to have been between an oceanic island arc to the southwest and a continental mass to the northeast during the Middle Jurassic. The lithological, geochemical, and tectonic setting similarities between the Beacon Point and Tuttle Lake formations, and the inferred tectonic boundary

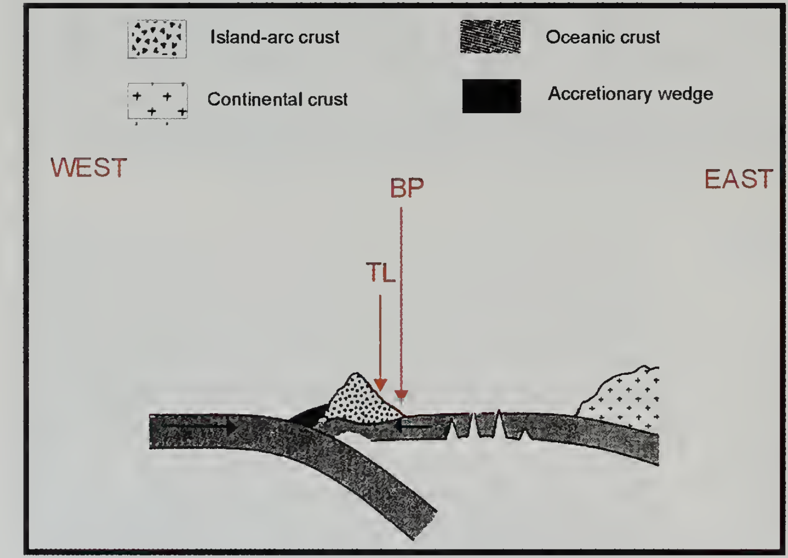

Figures 12a and 12b. Speculative tectonic cross sections for the Beacon Point region in Middle Jurassic time. Cross sectional view north, no scale implied. TL—Tuttle Lake Formation; BP—Beacon Point formation.

12a. Tectonic diagram is adapted from Wilson (1989); superimposed paleogeography (red) is from Pauly (2000). The Beacon Point formation is located in a marginal back-arc basin between an active oceanic island arc and an inactive continental mass.

12b. Tectonic diagrams are from Morres and Twiss (1995); superimposed paleogeography (red) is from Pauly (2000). Left diagram of each scenario is pre-collisional, right diagram is post-collisional. The Beacon Point formation is located between a converging active oceanic island arc to the west and an active continental arc to the east in both pre-collisional diagrams. See text for discussion.

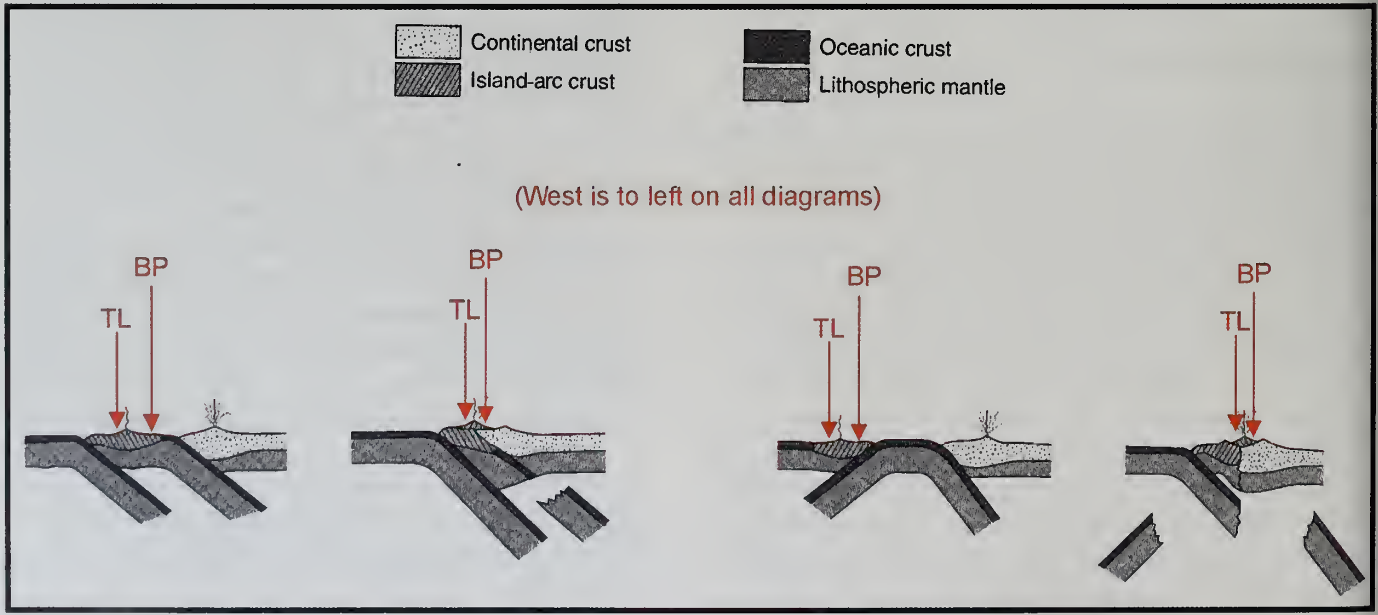

adjacent to and northeast of the Beacon Point formation, suggest the Beacon Point formation is part of the northern Sierra Nevada geologic province. Thus it appears that the Middle Jurassic regional boundary of the northern Sierra Nevada geologic province was northeast of the Beacon Point formation.

ACKNOWLEDGMENTS

I thank the many individuals who helped with the MS thesis project on which this field trip is based, including: Elwood (Woody) Brooks, Scott Hassler, Phil Garbutt, Anna Buising, and Jeff Seitz (all at California State University, Hayward), George Saucedo (Division of Mines and Geology), Michael Carr (Rutgers University), Peter Schiffman (University of California, Davis), Larry Garside (Nevada Bureau of Mines), Richard Hanson (Texas Christian University), Ken Wohletz (Los Alamos National Laboratory), and Sorena Sorensen (Smithsonian Institute). I thank the editor, Woody Brooks, for inviting my contribution to this volume. Scott Hassler and Eldridge Moores (University of California, Davis) provided draft reviews that were very helpful. The staff at California Department of Conservation's Division of Mines and Geology publications patiently accepted manuscript revisions.

ROAD LOG

FIELD TRIP

Four-wheel drive vehicles and sturdy hiking boots are recommended for this field trip. All stops are on Toiyabe National Forest land. Driving time from Blairsden to Stop 1 is approximately 2 hours and 20 minutes. From Blairsden, follow CA-70 34 miles east, over Beckwourth Pass, to Hallelujah Junction. Turn south and follow US-395 for 24 miles to I-80 in Reno. Travel west on I-80 toward Truckee and Donner Pass (Figure 1).

The Verdi Range is visible looking west from I-80 near the Verdi exit (9.5 miles west of the US-395 / I-80 junction, Figure 1). The range runs from Verdi Peak (communications building at summit) on the left (south) to Beacon Point on the right (north). Light gray, granitic rocks (Cretaceous-Jurassic) are visible on Verdi Peak and nearby peaks of the southern part of the ridge. Dark gray outcrops of Jurassic (?) Beacon Point metavolcaniclastic rocks are visible along the ridge crest north to Beacon Point. The sharp contact is visible in a saddle. Brown, Miocene-Pliocene volcanic rocks blanket the hills in the foreground.

Leave I-80 at the Boca/Hirschdale exit, 28.5 miles west of the US-395 / I-80 junction in Reno (Figure 1). Cross the railroad tracks just north of the highway, and follow Stampede Meadow Road north (Figure 2). The road passes just east of Boca and Stampede reservoirs, and through outcrops of Tertiary lava flows, lahars, and tuffs. After 10 miles, Henness Pass Road is reached at a T intersection (marked as mile 0.0 on Figure 2). Set the trip odometer to 0.0 miles. Cumulative miles traveled are listed in the left column of the road log below. Follow the red arrows on Figure 2.

0.0 Intersection of Stampede Meadow and Henness Pass roads. Turn right onto Henness Pass Road (dirt). The intersection is in Miocene-Pliocene volcanic rocks (Figure 2). Travel 0.6 miles to the next log point.

0.6 Watch for the contact with the Beacon Point formation under the second set of utility wires. Soil changes from light brown to dark gray-green, and a few large chunks of metavolcaniclastic float are visible near the road edge. Travel 1.3 miles to the next log point.

1.9 Intersection of Henness Pass and Verdi Peak roads. Take the first, hard right (southeast) onto Verdi Peak Road (dirt, signed for Verdi Peak). Travel 1.0 miles to next log point.

2.9 Contact. Leave Beacon Point rocks, enter Miocene-Pliocene volcanic rocks. A few Cretaceous-Jurassic granitic outcrops occur here as well. Travel 1.4 miles to the next log point.

4.3 Contact. Leave Miocene-Pliocene volcanic rocks, enter Cretaceous-Jurassic granitic rocks. Travel 0.2 miles to the next log point.

4.5 Watch for sharp bend (left, then right) of the road. At this bend, turn left (north) onto the dirt logging road (not shown on Figure 2). Travel 0.5 miles to the next log point.

5.0 Park in the clearing at the end of the road (marked as Stop 1 on Figure 2).

STOP 1 (OVERVIEW)

Stop 1 is near a three-way intersection of the Jurassic (?) Beacon Point, Cretaceous-Jurassic granitic, and Miocene-Pliocene volcanic rocks (Figure 2), and thus provides an overview of the field relations in the area (Photo 9). Good outcrops of the granitic rocks occur at the east edge of the clearing. These medium-grained, light-gray rocks are hornblende- and biotite-rich granite and granodiorite (Saucedo and Wagner, 1992). They are not deeply weathered. Miocene-Pliocene volcanic rocks cap the short hill just west of the clearing. These rocks are andesitic lava flows and lahars (Latham, 1985; Bell and Garside, 1987; Saucedo and Wagner, 1992). The rocks are commonly weathered dark brown. Porphyritic texture is well developed, with pyroxene, hornblende and

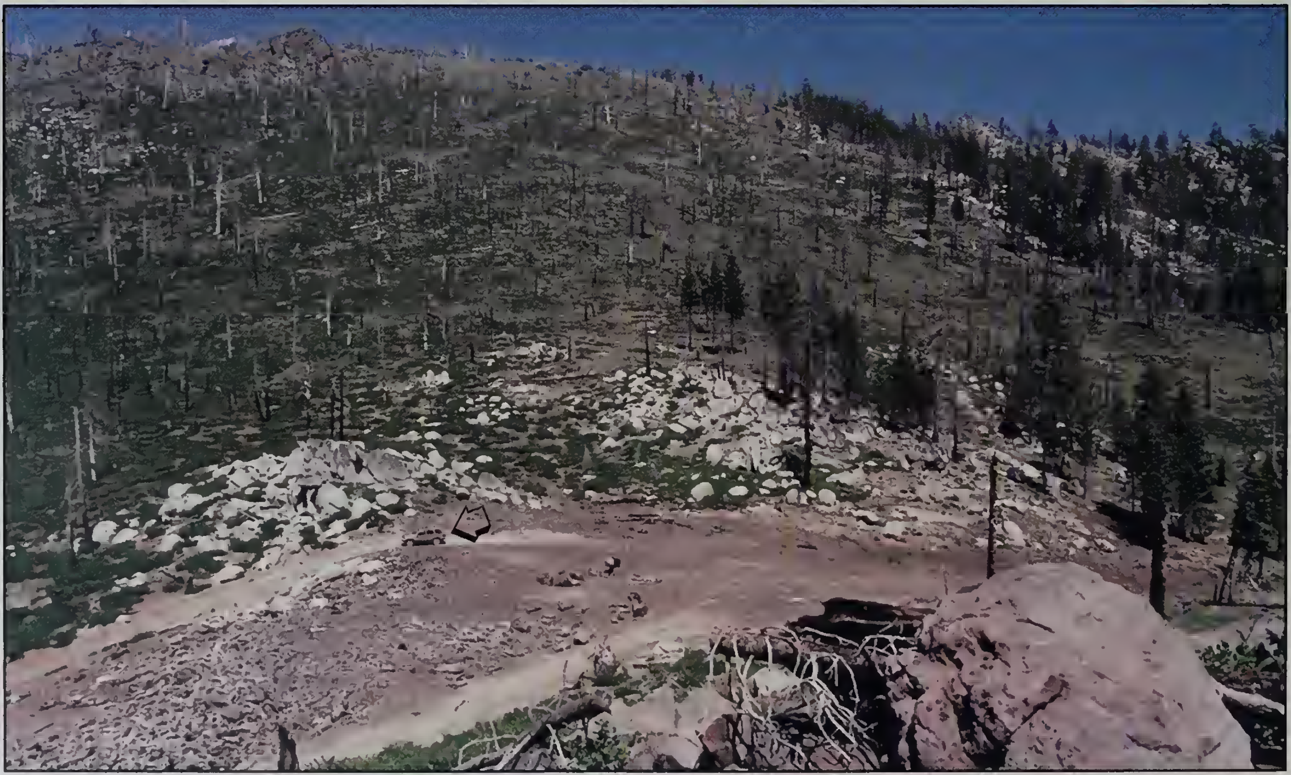

Photo 9. View looking east to the Verdi Range ridge crest, running approximately north/south, in the background. The dark gray, Jurrasic (?) Beacon Point formation crops out along the ridge crest. Light gray, Cretaceous-Jurassic granitic rocks crop out along the ridge at the right edge of photo, and in middleground. Light brown, Miocene-Pliocene volcanic rocks are exposed in the foreground. Vehicle in left center for scale (arrow). *Photo by Bruce Pauly.*

plagioclase phenocrysts. Plagioclase phenocrysts are commonly prominent and vary from 1 to 5 mm in length.

The contact between the granitic and Beacon Point rocks (Stop 6) is clearly visible on the northern Verdi Range ridge, east of the clearing. Outcrops of the Beacon Point formation comprise the ridge crest north of the contact, toward Beacon Point. The Beacon Point formation is the main focus of the trip, and will be examined in detail at Stops 2-6 along the ridge. Due north lies Dog Valley, which is covered by Quaternary alluvium (Figure 2). To the northwest is the Crystal Peak area, where granitic rocks crop out. The ridge running south from Crystal Peak is capped by Miocene-Pliocene volcanic rocks to the north and Beacon Point rocks to the south. Miocene-Pliocene volcanic rocks cover the area west of this ridge. Saucedo and Wagner (1992) show the possible location of the Dog Valley Fault along Henness Pass Rd., visible in the western foreground. Pauly (2000) did not find field evidence for this fault. Cretaceous-Jurassic granitic rocks crop out south of the clearing.

5.0 Return to vehicles. Backtrack 3.1 miles to the intersection of Henness Pass and Verdi Peak roads.

8.1 Intersection of Henness Pass and Verdi Peak roads. Momentarily rejoin Henness Pass Road, then take the next right turn (east) onto the unsigned, dirt road near the information post. Travel 2.6 miles to the next log point, traversing upslope via 3 switchbacks (Figures 2 and 3).

10.7 Saddle (end of road log). Bear right (south), and park on the left in the clearing 50 yards beyond saddle. The parking area and Stops 2-6 are marked on Figure 3.

Hike southeast up the road, past boulders of Beacon Point volcaniclastic float. After 0.2 miles, the road switches back west, under a set of utility wires. Approximately 100 yards beyond the switchback, watch on your left for a clearing in the brush (just short of the highest point on the road, which continues downslope toward Stop 1; see Figure 3). At this spot, turn left, and hike southwest approximately 0.15 mile toward the tall, dark outcrops that are visible through the trees. Stop 2 is at the northeast tip of the outcrops.

STOP 2 (BRECCIA/CONGLOMERATE, ALTERATION)

This stop provides an opportunity to examine the volcaniclastic breccia/conglomerate unit of the Beacon Point formation, exposed in the abundant chunks of float (Photo 1). These rocks consist of volcanic, pebble to boulder-sized clasts surrounded by a fine-grained matrix. The clasts consist of actinolite and epidote pseudomorphs after augite microphenocrysts, relict calcic plagioclase microphenocrysts, and fine-grained biotite and epidote. The fine-grained matrix is composed of very fine-grained epidote, actinolite, biotite, and quartz, in sub-equal amounts. Two textural clast populations are present. Some of the clasts are well-rounded (conglomerate), and others are angular to sub-angular (breccia). This suggests at least two source environments. Some of the rocks are sorted by clast size, some are sorted by degree of rounding, and a few are sorted based on both characteristics. Clast-preferred orientation is visible in some of the rocks. The sorting and organization of the clasts, along with the clast-preferred orientation, is evidence for deposition via some type of flow process. This will be discussed more at Stop 3.

The clasts and matrix show tremendous color variety (Photo 1). Some of the clasts are entirely green or yellowish-green, in sharp contrast to the surrounding matrix.

Other clasts are colored similarly to the adjacent matrix. Because of the wide color and texture variations of the clasts, petrographic and/or chemical analysis is necessary to determine if they are similar or dissimilar mineralogy. Geochemical and electron microprobe analyses indicate the clasts are nearly identical in composition. Some of the clasts appear to be selectively colored, so we can infer that a variety of degrees of alteration of the clast material occurred prior to deposition. The fine-grained matrix also varies in color, from light green to brown. The color variation is due to alteration and/or weathering.

Climb up and to your right (facing the outcrop), heading northwest. Stop 3 is at the top of the outcrop.

STOP 3 (DEBRIS-FLOW DEPOSITS, ALTERATION)

This is the location of the greatest vertical, continuous extent of the breccia/conglomerate (approximately 3.5 m). Meter-scale beds are apparent when the outcrop is viewed from a few meters back. Thin (cm-scale) layers of greenish silt and fine-sand grained material separate the beds. A columnar section measured at this point (Pauly, 2000) is shown in Figure 5 (locality indicated on Figure 2).

To view the upper portion of Beds 2 and 3, climb up and to the right (facing the rocks) to the top of the outcrop.

Bed 1 (Figure 5) contains well-sorted pebbles at its exposed base. It is reverse-graded, with clast size increasing from pebbles to cobbles. Bed 2 (Figure 5) is poorly sorted (pebbles, cobbles, and boulders) and contains isolated pieces of greenish fine-grained material, similar to the material between the beds. Bed 2 clasts have pushed down into Bed 1C, deforming it (Photo 7). At the top of Bed 2B, matrix-supported cobbles protrude nearly vertically into fine-grained Bed 2C (Photo 8). Bed 3 is in erosive, loaded contact with the top of Bed 2C. At this contact, Bed 3 clasts push down into Bed 2C. Clasts in all beds are matrix supported, and Beds 1 and 3 show an upward increase in matrix content.

The isolated fragments of bed-capping material found within Beds 2 and 3 (Figure 5) suggest the depositional event had sufficient energy to rip these pieces up from the top of the previous bed. Another indicator of event energy is the erosive contact between Beds 1 and 2, and Beds 2 and 3. Substantial matrix strength is suggested by the predominance of matrix-supported clasts, the occurrence of boulders apparently suspended in Bed 2 (Figure 5), and particularly by the relatively large matrix-supported clasts protruding into the overlying fine layer with their long axes nearly vertical (Figure 5). The deformation of the fine grained cap layers (Beds 1C and 2C) by clasts from the overlying beds (soft-sediment deformation) indicates the underlying beds were not completely lithified prior to the subsequent depositional event, possibly suggesting frequent and perhaps nearly continuous deposition.

The breccia/conglomerate deposits appear to represent subaqueous, cohesive debris flows in that the observed flow characteristics (reverse grading, isolated boulders, vertically protruding clasts, and increasing upward matrix percentage) all indicate a strong, cohesive sediment-water matrix. Silt and fine-sand bed caps of the type observed here are far more common in subaqueous than in subaerial debris flows (Nemec and Steel, 1984). In a cohesive debris flow, the matrix, although comprising as little as 5% of the flow by volume, can provide buoyancy (Lowe, 1982). The strength of the matrix, whether moving or stationary, retards the sinking of boulders and smaller clasts and therefore aides in the transportation of materials (Fisher, 1971).

The debris-flow beds here are thinner (meters rather than tens of meters) and more fine-grained compared to those in the Tuttle Lake Formation to the west. The Tuttle Lake Formation is interpreted to represent subaqueous, proximal volcaniclastic sedimentation (Templeton, 1991; Hanson, R.E. and others, 1993). It appears that the Beacon Point formation was deposited relatively source-distal.

Many of the Beacon Point rocks show evidence of alteration. Some breccia/conglomerate clasts are selectively altered to epidote minerals (Photo 1), and the fine-grained material capping the debris-flow beds is also of similar, white green color (Photo 7). The greenish, fine-grained material was analyzed using an electron microprobe (Pauly, 2000). It is completely recrystallized and consists of 80% epidote, 15% quartz and 5% actinolite. This mineral assemblage, and the recrystallized texture suggest that epidosite-like alteration has occurred. Epidosite forms at 300-350°C by recrystallization of basalt in submarine hydrothermal solutions (Schiffman and others, 1990). It appears that the fine-grained layers were originally basaltic silt and clay. Epidosite in the Beacon Point formation is prominent, except at plutonic contacts.

Climb off the outcrop, heading southeast. Walk south along the ridge, crossing a short, grassy clearing. Bear right (west) and pass around the next outcrop just downslope from the ridge. Climb back up (east) toward the ridge as soon as this outcrop is passed. Stop 4 is just beyond this outcrop, slightly below (west of) the ridge.

STOP 4 (VOLCANOGENIC SANDSTONE/SILTSTONE)

Volcanogenic sandstone/siltstone beds at Stop 4, interbedded in a debris-flow deposit (Photo 3), consist of individual plagioclase, actinolite, epidote, biotite, quartz and magnetite grains that range from silt to fine-sand sized. This mineralogy is similar to the breccia/conglomerate and mafic intrusive rocks. At this outcrop, truncated bedding and scours indicate the rocks are facing upright, and the bedding attitude is N33W, 34NE. Relatively thin (centimeters to meter) volcanogenic sandstone/siltstone interbeds within the debris-flow deposits (as observed here) may be sandy caps to debris flows, or they may represent distal portions of relatively fine-grained flows. Thicker (meter scale), more extensive volcanogenic sandstone deposits, mixed with breccia/conglomerate, likely represent distal debris flow deposition.

Continue hiking south along the ridge and/ or just downslope (west) of the ridge as necessary. Watch for the lithology change (breccia/conglomerate to mafic intrusive) at Stop 5. The large, grassy clearing is about 100 m south of (beyond) Stop 5.

STOP 5 (MAFIC INTRUSIVE, LITHOFACIES VARIATION)

At this stop, mafic intrusive rocks cut through the breccia/conglomerate (Photo 4). The intrusion crosscuts bedding, and appears to be a (hypabyssal) dike. The contact is sharp, indicating complete lithification of the debris-flow deposit prior to intrusion. Here, the intrusive rocks contain large, readily visible plagioclase phenocrysts (Photo 4). At other localities, the plagioclase phenocrysts are not visible, but small amygdules can be seen. Electron microprobe analysis indicates that the plagioclase is calcic (An_{75-85}). Clinopyroxene (augite) phenocrysts have been partially to completely pseudomorphed by actinolite (Photo 6). Pilotaxitic plagioclase microlites imply flow within the intrusion. The intrusive and breccia/conglomerate rocks have similar REE abundance (Figure 7) and multi-element spidergram (Figure 9) patterns.

The breccia/conglomerate rocks, prominent at Stops 2 and 3, are less prominent here, and complemented by volcanogenic sandstone interbeds. This pattern of lithofacies variation, from breccia/conglomerate to volcanogenic sandstone, repeats three times along the northern Verdi Range ridge crest (Figure 3), and suggests the depositional environment may have been a volcaniclastic apron. Observed volcaniclastic grain sizes in the Beacon Point formation range from silt to small boulders, perhaps suggesting deposition in a mid-apron area.

Continue hiking south along the ridge. Cross a wide grassy clearing, and continue either on the ridge or just downslope to the west as appropriate. Stop 6 is at the granitic contact.

STOP 6 (RELATIVE AGES, METAMORPHISM, PLUTONIC CLASTS)

Here, an outcrop of the Beacon Point formation just north of the contact hosts a pegmatite vein, and the granitic rocks just south of the contact contain dark mafic xenoliths, comprised presumably of Beacon Point country rock. These observations suggest that the Beacon Point rocks are relatively older than the granitic rocks.

A detailed study of the metamorphic mineralogy at the southern plutonic contact (Stop 6) was performed by Pauly (2000). Thin sections from a series of mixed breccia/conglomerate and volcanogenic sandstone/siltstone samples taken progressively closer to the plutonic contact show an increasing occurrence of recrystallized quartz, hornblende and clinopyroxene closer to the contact. This mineral assemblage, along with the development of granoblastic quartz texture (Photo 10), indicates hornblende-hornfels (contact) metamorphic conditions. There is no actinolite, calcic plagioclase, or epidote at this plutonic contact. The hornblende-hornfels aureole here is fewer than 20 m wide (Pauly, 2000).

The presence of pyroxene and calcic plagioclase in the Beacon Point formation interior, along with the absence of chlorite and albite, indicates that albitization, a common low-T greenschist- or sub-greenschist-facies reaction represented by pyroxene + Ca-plagioclase + H_2O = epidote + chlorite + albite (Hibbard, 1995) has not occurred in these rocks. The above reaction consumes water and generates the richly hydrous (10-13% water) phase chlorite (Deer and others, 1992). Chlorite is absent in these rocks, and relatively anhydrous phases actinolite (1-2% water) and

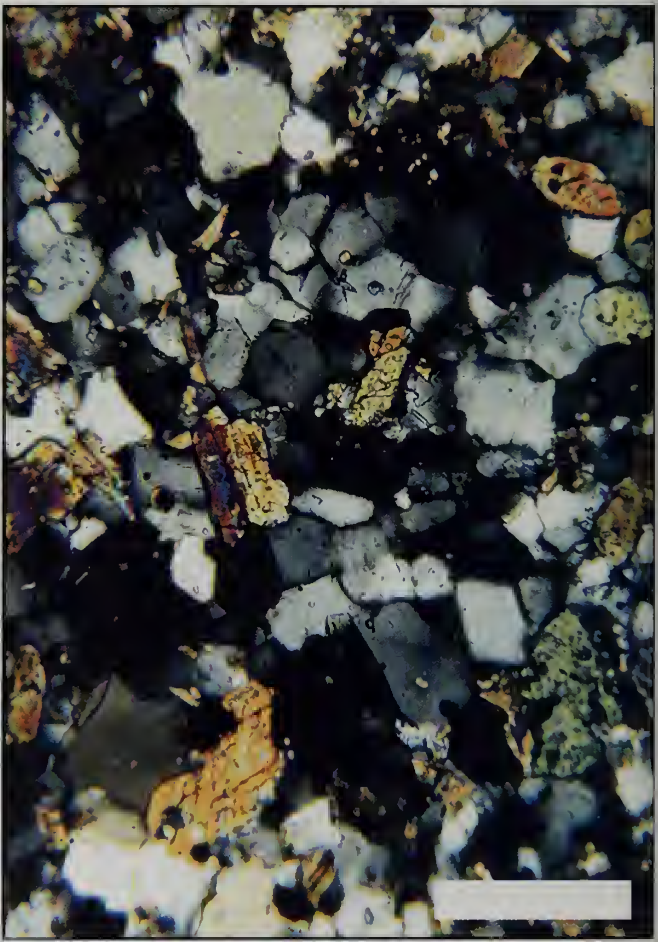

Photo 10 (Stop 6). Thin section of Beacon Point formation at plutonic contact. Well-developed granoblastic texture displayed by quartz, occurring with hornblende and clinopyroxene indicate hornblende-hornfels (contact) metamorphism. XPL. Scale bar = 0.25 mm. *Photo by Bruce Pauly.*

epidote (1-2% water) are abundant. This suggests that the environment was relatively dry, perhaps due to lack of fluids and/or inability of fluids to circulate in these undeformed rocks. It is also possible that recrystallization was limited by reaction kinetics. Evidently, metamorphism of the interior of the Beacon Point formation occurred at low- to sub-greenschist conditions.

In island-arc settings, hydrothermal fluids are abundant and have immediate access to subaqueous volcanic and volcaniclastic deposits. Thus, epidosite formation can begin relatively soon after initial subaqueous deposition. Epidosites formed at the time of or shortly after initial volcanism in the Ritter Range pendant (Hanson, R.B. and others, 1993).

One possible scenario for the metamor-phic history of the Beacon Point formation is that a single sub- to lower-greenschist facies metamorphic episode (likely seafloor hydrothermal alteration at 300-350°C) produced the prominent epidosites, actinolite and epidote. This event was then followed by a hornblende-hornfels facies metamorphic event (450-575°C) that was restricted to the narrow plutonic contact aureole. Previously-formed epidosites, actinolite and epidote would have been recrystallized to higher-temperature hornblende-hornfels facies minerals within the contact aureole.

A second possible metamorphic scenario begins with epidosite formation, but was followed by a second, separate episode of sub- to low-greenschist facies metamorphism that generated the actinolite and epidote. Albitization must not have occurred during the second metamorphic episode, since albite and chlorite are absent. Finally, a contact-metamorphism event (hornblende-hornfels facies) occurred and generated the narrow contact aureole.

The relative ages and field relations (Figure 2) between the Beacon Point formation and the granitic rocks suggest a roof pendant relationship. Further evidence is the contact metamorphic episode mentioned above. The Beacon Point roof pendant was informally documented by Pauly (2000).

Rare plutonic clasts occur in the debris-flow deposits (Photo 2). Petrographic analysis (Photo 11) shows that the clasts are metamorphosed, so they are not from the

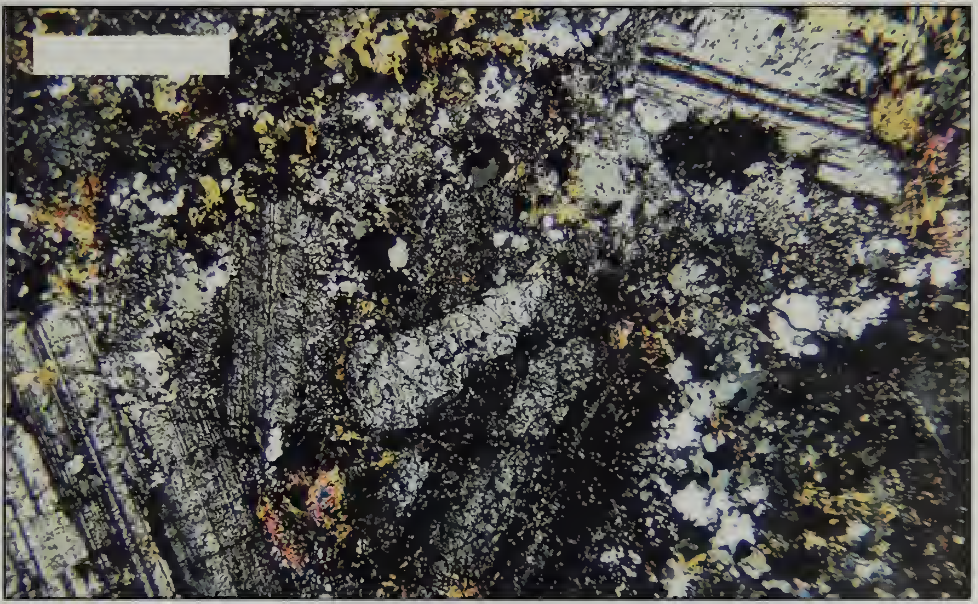

Photo 11 (Stop 6). Thin section of the plutonic clast shown in Photo 2. Clast boundary runs through upper left corner of photo. Clast contains relatively large, twinned plagioclase crystals that are all that remain of the original igneous crystals. The plagioclase crystals have distorted twin lamellae due to metamorphism. Biotite, epidote, actinolite, and granoblastic quartz (lower right) now comprise the fine-grained areas. XPL. Scale bar = 0.25 mm. *Photo by Bruce Pauly.*

Cretaceous-Jurassic granitic rocks. One possibility is that these clasts are cognate xenoliths, related to the volcanic source area. Another possibility is that these clasts are true xenoliths, perhaps from a granitic source area that was shedding sediments into the basin in which the Beacon Point debris-flow deposits were accumulating. Perhaps a continental mass was nearby (Figure 12).

Backtrack north along the ridge, passing Stops 5, 4 and 3. At Stop 2, leave the ridge and hike through the brush to the clearing at the dirt road. The location of the dirt road can be seen from a distance as it runs east/west under the utility wires. Turn right and follow the road back down to the vehicles. Backtrack to I-80.

REFERENCES

Axelrod, D.I., 1959, The Pliocene Verdi flora of western Nevada: University of California Publications in Geological Sciences, v. 34, p. 91-160.

Bell, J.W. and Garside, L.J., 1987, Geology of the Verdi Quadrangle: Nevada Bureau of Mines and Geology, 1:24,000.

Bonham, H.F., Jr., 1969, Geology and mineral deposits of Washoe and Storey counties, Nevada: Nevada Bureau of Mines and Geology Bulletin no. 70, 140 p.

Carey, S. and Sigurdsson, H., 1984, A model of volcanogenic sedimentation in marginal basins *in* Kokelaar, B.P. and Howells, M.F., editors, Marginal basin geology, volcanic and associated sedimentary and tectonic processes in modern and ancient marginal basins: Geological Society of London Special Publication no. 16, p. 37-58.

Carey, S., 2000, Volcaniclastic sedimentation around island arcs *in* Sigurdsson, H., editor, Encyclopedia of Volcanoes: Academic Press, 1417 p.

Cas, R.A.F. and Wright, J.V., 1987, Volcanic successions: London, Allen and Urwin, 528 p.

Christe, G., 1993, The stratigraphy and depositional environments of Jurassic volcanic and volcaniclastic rocks of the Kettle Rock sequence north of 40°N latitude, northern Sierra Nevada, California *in* Dunn, G. and McDougall, K., editors, Mesozoic Paleogeography of the Western United States-II: Pacific Section SEPM, book no. 71, p. 275-288.

Christe, G. and Hannah, J.L., 1990, High-K, continental-arc volcanism in the Kettle Rock sequence of the Eastern Mesozoic belt, northern Sierra Nevada, California: Implications for early Mesozoic Cordilleran tectonics *in* Anderson, J.L., editor, The nature and origin of Cordilleran magmatism: Boulder, Colorado, Geological Society of America Memoir 174, p. 315-325.

Deer, W.A., Howie, R.A. and Zussman, J., 1992, An introduction to the rock forming minerals: Longman Group, 696 p.

Evernden, J.F. and Kistler, R.W., 1970, Chronology of emplacement of Mesozoic batholitic complexes in California and western Nevada: U.S. Geological Survey Professional Paper no. 6232, 42 p.

Fisher, R.V., 1971, Features of coarse-grained, high-concentration fluids and their deposits: Journal of Sedimentary Petrology, v. 41, no. 4, p. 916-927.

Garside, L.J., Bonham, H.F., Jr. and McKee, E.H., 1992, Potassium-argon ages of plutonic rocks and associated vein and alteration minerals, northeast Sierra Nevada, California and Nevada: Isochron/West, no. 58, p. 13-15.

Garside, L.J., 1998, Mesozoic metavolcanic and metasedimentary rocks of the Reno-Carson City area, Nevada and adjacent California: Nevada Bureau of Mines and Geology Report no. 49, 30 p.

Godwin, L.H., 1958, Geology of the west side of Peavine Mountain, Washoe County, Nevada [M.S. Thesis]: University of Nevada, Reno, 59 p.

Hanson, R.E., Girty, G.H., Harwood, D.S., Schweickert, R.A., Templeton, J.H., Yoshinobu, A.S., Wracher, M.D. and Girty, M.S., 1993, Devonian and Jurassic volcano-plutonic associations in the Northern Sierra Terrane: Implications for arc evolution and Mesozoic deformation *in* Lahren, M.M., Trexler, J.H. and Spinosa, C., editors, Crustal Evolution of the Great Basin and Sierra Nevada: Cordilleran/Rocky Mountain Section, Geological Society of America Guidebook, Dept. of Geological Sciences, University of Nevada, Reno, p. 97-128.

Hanson, R.B., Sorensen, S.S., Barton, M.D. and Fiske, R.S., 1993, Long-term evolution of fluid-rock interactions in magmatic arcs: evidence from the Ritter Range pendant, Sierra Nevada, California, and numerical modeling: Journal of Petrology, v. 34, part 1, p. 23-62.

Hargrove, U.S., 1995, Geology of the Huntley Mill sill complex: a multiphase peperitic sill intruded into wet sediments, Jurassic, northern Sierra Nevada, California [B.S. Thesis]: Fort Worth, Texas Christian University, 80 p.

Hibbard, M.J., 1995, Petrography to petrogenesis: Englewood Cliffs, Prentice Hall, 587 p.

Latham, T.S., 1985, Stratigraphy, structure, and geochemistry of the Plio-Pleistocene volcanic rocks of the western Basin and Range province near Truckee, California [Ph.D. dissertation]: University of California, Davis, 341 p.

LeBas, M.J., LeMaitre, R.W., Streckeisen, A. and Zanettin, B., 1986, A chemical classification of volcanic rocks based on the total alkali silica diagram: Journal of Petrology, v. 27, p. 745-750.

Lowe, D.R., 1982, Sediment gravity flows II: Depositional models with special reference to the deposits of high-density turbidity currents: Journal of Sedimentary Petrology, v. 52, no. 1, p. 279-297.

Mielke, K.L., 1996, Paleovolcanology, petrology, stratigraphy, and structure of Jurassic and Cretaceous island-arc rocks in the Webber Peak and Meadow Lake areas, Nevada and Sierra counties, northern Sierra Terrane, California [M.S. Thesis]: Fort Worth, Texas Christian University, 110 p.

Moores, E.M. and Twiss, R.J., 1995, Tectonics: New York, Freeman, 425 p.

Murton, B.J., 1989, Tectonic controls on boninite genesis *in* Saunders, A.D. and Norry, M.J., editors, Magmatism in the ocean basins: Geological Society of London Special Publication no. 42, p. 347-377.

Murton, B.J., Peate, D.D., Arculus, R.J., Pearce, J.A. and Van der Laan, S.R., 1992, Trace element geochemistry of volcanic rocks from Site 786, Izu-Bonin forearc region: Proceedings of the Ocean Drilling Program, Scientific Results, v. 125, p. 211-236.

Nakamura, N., 1974, Determination of REE, Ba, Fe, Mg, Na, and K in carbonaceous and ordinary chondrites: Geochimica Cosmochimica Acta, v. 38, p. 757-775.

Nemec, W. and Steel, R.J., 1984, Alluvial and coastal conglomerates: their significant features and some comments on gravelly mass-flow deposits *in* Koster, E.H. and Steel, R.J., editors, 1984, Sedimentology of Gravels and Conglomerates: Canadian Society of Petroleum Geologists, Memoir no. 10, p. 1-32.

Pauly, B.D., 2000, Geology of the Beacon Point formation, Sierra County, California [M.S. Thesis]: California State University, Hayward, 132 p.

Pearce, J.A., 1982, Trace element characteristics of lavas from destructive plate boundaries *in* Thorpe, R.S., editor, Andesites: orogenic andesites and related rocks: New York, John Wiley and Sons, p. 525-548.

Pearce, J.A., 1983, The role of sub-continental lithosphere in magma genesis at destructive plate margins *in* Hackesworth, C.J. and Norry, M.J., editors, Continental basalts and mantle xenoliths: Shiva, Nantwich, p. 230-249.

Phillipson, S.E., 1995, Petrology, age, and structural relations of the composite Middle Jurassic Haypress Creek pluton, northern Sierra Terrane, California [M.S. Thesis]: Fort Worth, Texas Christian University, 89 p.

Rollinson, H.R., 1993, Using geochemical data: New York, John Wiley and Sons, 352 p.

Saucedo, G.J. and Wagner, D.L., 1992, Geologic map of the Chico Quadrangle: California Division of Mines and Geology Map no. 7A, 1:250,000.

Schiffman, P., Bettison, L.A. and Smith, B.M., 1990, Mineralogy and geochemistry of epidosites from the Solea graben, Troodos ophiolite, Cyprus *in* Malpas, J. and others, editors, Ophiolites: oceanic crustal analogues: Proceedings of the Symposium Troodos 1987, Nicosia, Cyprus, Geological Survey Department, p. 673-683.

Schiffman, P. and Wagner, D.L., editors, 1992, Field guide to the geology and metamorphism of the Franciscan Complex and Western Metamorphic Belt of northern California: California Division of Mines and Geology, Special Publication no. 114, 78 p.

Sorensen, S.S., Dunne, G.C., Hanson, R.B., Barton, M.D., Becker, J., Tobisch, O.T. and Fiske, R.S., 1998, From Jurassic shores to Cretaceous plutons: Geochemical evidence for paleoalteration environments of metavolcanic rocks, eastern California: Geological Society of America Bulletin, v. 110, no. 3, p. 326-343.

Templeton, J.H., 1991, Submarine volcanism and volcaniclastic sedimentation in a Jurassic island-arc environment, northern Sierra Nevada, California [M.S. Thesis]: Fort Worth, Texas Christian University, 134 p.

Wilson, M., 1989, Igneous Petrogenesis: A Global Tectonic Approach: London, Chapman and Hall, 466 p.

CHARACTERISTICS AND EMPLACEMENT OF AN EARLY CRETACEOUS DIKE SWARM AND STOCK IN THE LAKES BASIN, NORTHERN SIERRA NEVADA

John S. Lull[1]

INTRODUCTION

Early Cretaceous andesitic to dacitic dikes and an associated tonalite stock (Gold Lake Stock) intrude Late Paleozoic island-arc metavolcanic and metasedimentary rocks in the Lakes Basin region of the Northern Sierra Nevada (Figure 1). These Early Cretaceous hypabyssal rocks are related to the voluminous Sierra Nevada Batholith, composed of numerous individual plutons emplaced mainly during the Cretaceous period (Hamilton, 1969). They are the only representatives of Cretaceous plutonism in the Lakes Basin region; Middle Jurassic plutons are exposed to the east.

Although these dikes are conspicuous and widespread throughout the area, they were not studied in any detail by early workers. Turner (1895) briefly referred to a dike of “hornblende porphyrite,” and Durrell and D’Allura (1977) mentioned “light gray, porphyritic hornblende diorite dikes” that cut the entire sequence. No further description was given in either case.

Lull (1984) undertook a thorough investigation of the dikes, describing their distribution, structure, chemistry, age and petrology. The distribution and structure of the dikes can be used to infer the location of an intrusive center and make deductions regarding emplacement mechanism. Petrographic studies of the dikes led to interesting conjecture on deuteric alteration processes in shallow intrusive rocks.

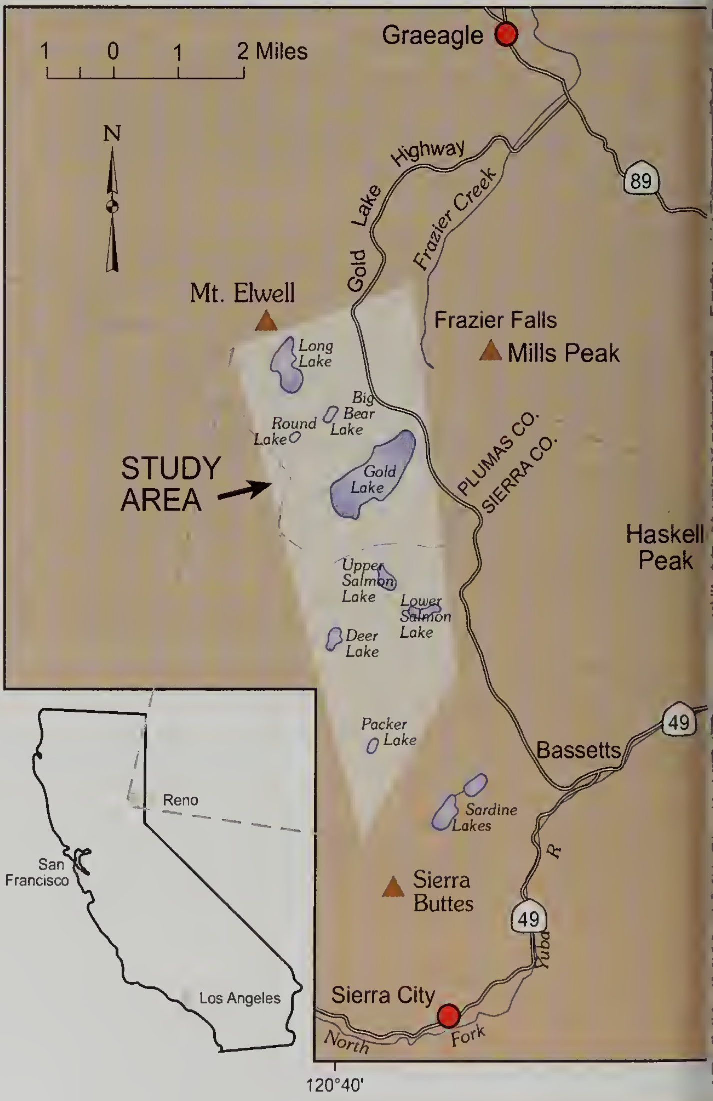

Figure 1. Location of Lakes Basin.

---

[1] e-mail: wavestalker@coastside.net

AGE AND GEOLOGIC SETTING

Field evidence indicates the dikes and stock are post-Late Jurassic and pre-Tertiary. They intrude Late Paleozoic metavolcanic rocks that were regionally metamorphosed and deformed during the Late Jurassic Nevadan Orogeny (Schweickert and others, 1983), yet the dikes are not metamorphosed and are undeformed, even where they cut strongly foliated rocks. The dikes also cut Middle Jurassic (Hanson and others, 1996) granitic rocks in the area northeast of Haskell Peak, but do not intrude local Tertiary volcanic rocks. The tonalite stock near Gold Lake cuts one of the dikes and K-Ar dates indicate the dikes and stock to be close in age.

Hornblende K-Ar dates were determined by Ronald W. Kistler (U.S. Geological Survey, Menlo Park) for the hornblende tonalite phase of the stock and one of the dikes. The stock dated 120.1 Ma (+/- 1.4 Ma) and the dike yielded an age of 122.3 Ma (+/- 0.9 Ma). These Early Cretaceous dates accord well with the field evidence and indicate the stock and dikes are broadly contemporaneous. They also appear to be the youngest pre-Tertiary intrusive rocks in the Lakes Basin region. Other local granitic rocks of the Sierra Nevada Batholith, exposed to the east near Yuba Pass and in the Haskell Peak area, are Middle Jurassic in age (Hanson and others, 1996).

The dikes intrude the entire sequence of Late Paleozoic island arc rocks in the Lakes Basin area. Three formations comprise this metavolcanic sequence: 1) The Sierra Buttes Formation is an assemblage of andesitic to dacitic intrusives, breccias, flows, and tuffs (Bond and others, 1977); 2) The Elwell Formation conformably overlies the Sierra Buttes Formation and is composed largely of black phosphatic chert with local accumulations of pillow lava and sills (Brooks and others, 1982); 3) The Taylor Formation conformably overlies the Elwell Formation and is composed of basaltic to andesitic breccias, tuffs, pillow lavas, and flows (Bond and others, 1977). These volcanic rocks have been regionally metamorphosed to greenschist facies during the Late Jurassic Nevadan Orogeny, and locally exhibit a penetrative slaty cleavage. The Cretaceous dikes are most abundant in the area between Long Lake and Gold Lake where they intrude the Taylor Formation. The Gold Lake Stock is exposed in a roadcut just northeast of Gold Lake where it intrudes the Taylor Formation.

East of Lakes Basin, near Frazier Falls, the dikes also intrude the Early Mississippian to Middle Pennsylvanian Peale Formation (Harwood, 1992), which conformably overlies the Taylor Formation. The Peale is composed of radiolarian chert with minor bedded breccia and keratophyre tuff (Durrell and D'Allura, 1977).

The Early Cretaceous dikes and stock are a product of the extensive plutonism that took place throughout most of the Mesozoic and Early Tertiary in response to subduction along the western margin of North America. The greater part of this plutonism took place during the Cretaceous Period when an active Andean-type margin existed along the west coast of California (Hamilton, 1969). The continental volcanic arc associated with this margin has been largely eroded away, exposing its plutonic roots that make up most of the Sierra Nevada Batholith.

DESCRIPTION OF DIKES

General Field Appearance

The dikes average about 1.5 meters (m) thick and occur as conspicuous, light-gray plagioclase-hornblende porphyries in sharp contact with the country rock. They have not been deformed or metamorphosed, although they have been subjected to varying degrees of deuteric alteration. The abundant large (up to 3 centimenters [cm]) chalky-white plagioclase phenocrysts and light–gray groundmass give the dikes a striking appearance that contrasts strongly with the country rock. This also helps distinguish them from Paleozoic dikes in the area, which are generally darker, metamorphosed to greenschist facies, and difficult to distinguish from the rest of the metavolcanic rocks.

In most cases the Cretaceous dikes eroded at about the same rate as the country rock, but in some cases they stand out in relief, forming low walls (Photo 1), or are recessed, forming trenches. This can be attributed to variations in resistance to

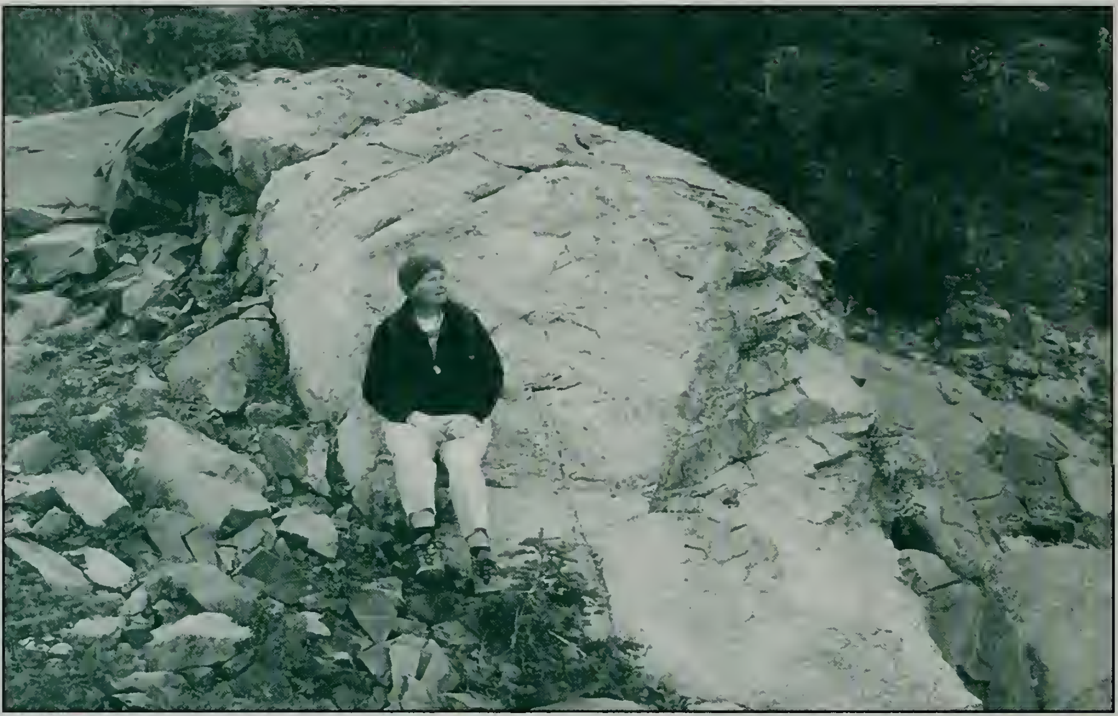

Photo 1. Three m-thick Cretaceous andesite dike (looking west) (Stop 2). Dike intrudes darker-colored metavolcanic rocks of the Taylor Formation and stands out in relief as a result of differential weathering. *Photo by J. Lull.*

erosion of the country rock. For example, the dikes commonly form trenches in the highly resistant quartz porphyry unit of the Sierra Buttes Formation. The dikes are discontinuous in outcrop due to partial coverage by glacial debris and vegetation, but can usually be traced from one outcrop to the next (Figure 2). Exposed segments range from a few meters to 100 m long. Most dikes maintain a fairly consistent trend. However, in a few cases they pinch out, sidestep 1 or 2 m in en echelon fashion, and continue on a parallel course. This is a common phenomenon for dike swarms elsewhere (Bailey, 1924).

Dimensions and Distribution

Ninety separate dikes were mapped in the Lakes Basin and surrounding area in order to determine their concentration, regional trend, and distribution. Although outcrops are discontinuous, individual dikes can be correlated by following the dike trend, and by textural and lithologic similarity. In the few cases where correlation of dike segments was uncertain, they were mapped as separate dikes.

Dike thickness ranges from 0.2 to 4.6 m, but most are 0.5 to 2.5 m. Only a few exceed 3 m. Total thickness of all mapped dikes is 140.3 m, representing the minimum amount of distention resulting from dike emplacement. Individual dikes maintain a fairly consistent thickness except where they pinch out. Where terminations are exposed, the dikes gradually narrow for up to several meters along their trend until pinching out. A few of the dikes pinch out in long tongues up to 3 m long and only 3-4 cm wide (Photo 2).

Accurate total dike lengths cannot be determined due to incomplete exposure. None of the mapped dikes have both terminations exposed, although several pinch out at one end with no apparent continuation. Some dikes pinch out and start again within 2 to 3 m along the same trend. Although most of the dikes are only partially exposed, with both terminations covered, some limits on dike length can be inferred from the field data. In well exposed areas, the dikes can usually be traced for 100 m or more; it is reasonable to assume that most of them exceed 100 m. It is

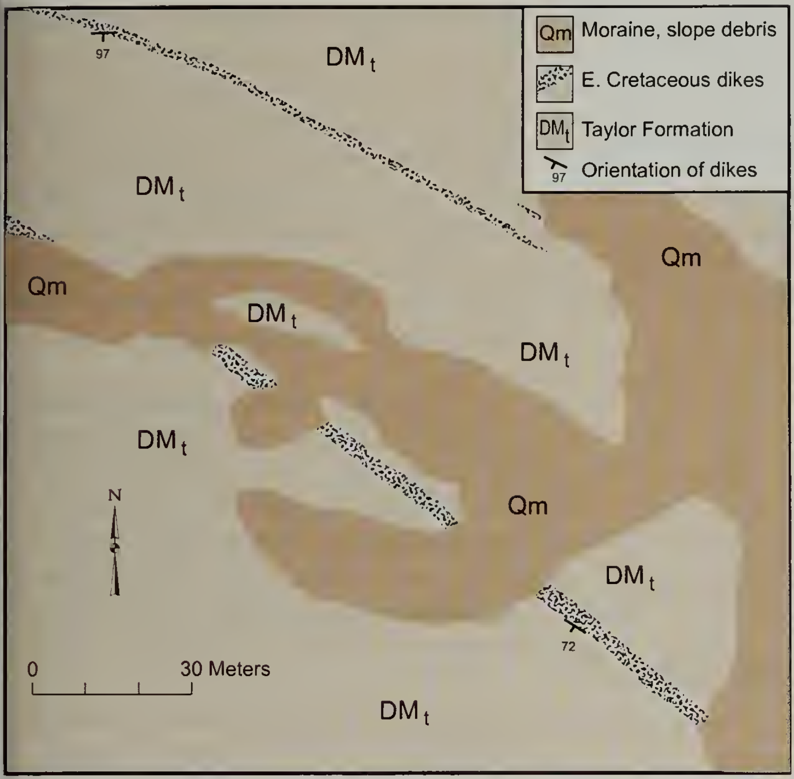

Figure 2. Map of two dikes on slope northwest of Long Lake. The southern dike shows the typical discontinuous outcrop pattern, resulting from partial coverage by moraine deposits. Also note pinch-out and side-step of northern dike.

more difficult to place an upper limit on length, but the fact that the dikes are localized in a relatively small area (approximately 50 square kilometers [km]) suggests that they are not many kilometers long.

An upper limit on length is suggested by a dike near Tamarack Lakes, about 8 km south of Gold Lake. Assuming all the dikes originated from an intrusive center near Gold Lake (see Orientation and Intrusive Mechanism, below), this dike must be close to 8 km long. The dike dips at a relatively low angle and appears to be a subhorizontal sheet. It contains well-defined flow laminations along the contact, indicating high viscosity, possibly resulting from loss of volatiles over a relatively great travel distance. Since no other dikes were found farther from the probable intrusive center, most of the dikes appear to be fewer than 8 km long.

Overall concentration of the Cretaceous dikes in Lakes Basin is relatively low, but does show a significant trend. In a well-exposed area between Round Lake and Gold Lake, where the dikes are most abundant, dike concentration is at least 1% and locally reaches 6%. These figures are based on total thickness and length of mapped dikes and represent estimated volume percent of dikes to country rock. For the entire area in which the dikes occur, dike concentration is considerably less than 1%. Dike concentration appears to increase in the area northwest of Gold Lake and decrease to the south of Gold Lake. This trend lends support to an intrusive center subjacent to the area north of Gold Lake.

Orientation and Intrusive Mechanism

The dikes exhibit a subradial trend focused on an area just north of Gold Lake near the Cretaceous tonalite stock (Figures 3 and 4). Figure 4 shows the average orientation of dikes in different locations as determined by stereonet

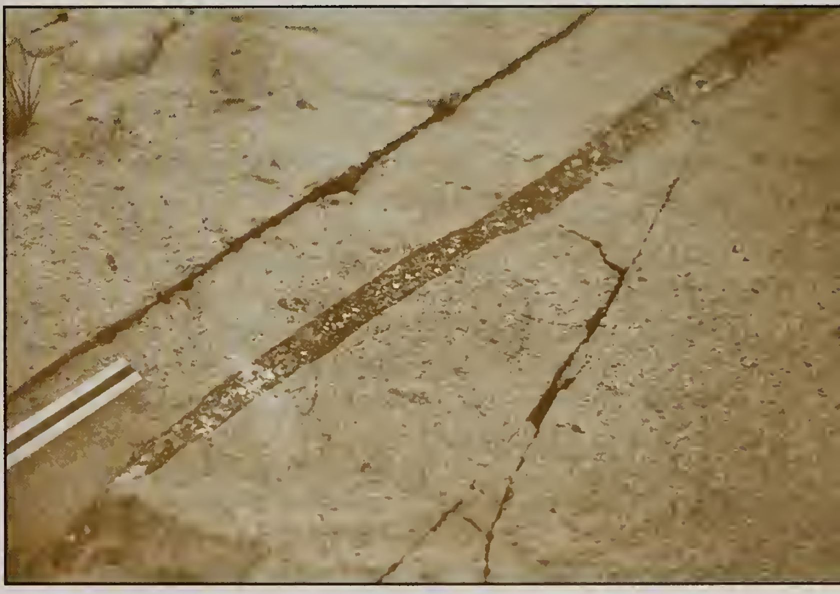

Photo 2. Dike termination. Dike has narrowed to about 4 cm thick and pinches out at lower left. *Photo by J. Lull.*

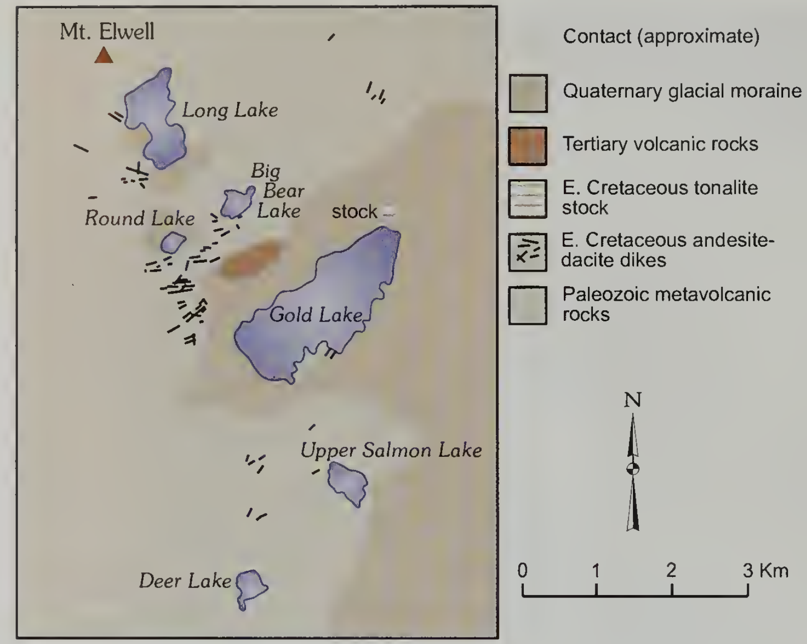

Figure 3. Map of Cretaceous andesite/dacite dikes and tonalite stock in Lakes Basin.

plots. Dikes trend nearly north-south in the Frazier Falls area, east-west in the Long Lake area, and northeasterly in the areas west and south of Gold Lake. The complete radial swarm is not apparent due to lack of exposure east of Gold Lake. Several other radial dike swarms have been described in the literature (Harker, 1904; Bailey, 1924; Parsons, 1939; Johnson, 1961; Smith, 1975; Shelley, 1988). In these cases, the dikes appear to radiate around intrusive centers. Therefore, the presence of an intrusive center for the dikes in Lakes Basin is inferred near the focus of the radial swarm, in the region just north of Gold Lake.

Dip directions of the dikes also suggest an intrusive center near Gold Lake. Dikes north of Gold Lake are vertical or dip southward and dikes south of the lake are vertical or dip northward. Most of the dikes dip steeply (70-90 degrees); only a few dip less the 65 degrees.

Radial fault and fracture patterns have long been recognized in association with intrusive centers and salt domes where vertical tectonism and roof stretching have been important (Badgley, 1965). Theoretical studies on the formation of fracture systems around magmatic intrusions predict that radial fractures form around a prolate, near spherical pluton when magmatic pressure slightly exceeds lithostatic stress (Koide and Bhattachargi, 1975). Such conditions also favor the intrusion of radial dikes (Robson and Barr, 1964). Where magmatic pressure greatly exceeds lithostatic stress, concentric fractures predominate.

The strength of the overlying country rock is the major factor in determining lithostatic stress. The thick package of recrystallized metavolcanic rocks in the Lakes Basin is relatively strong and would be expected to provide high lithostatic stress, resulting in a radial fracture pattern in response to magmatic stress.

In cross section, the forceful upward intrusion of a pluton creates marginal joint fans in the roof rocks that dip toward the intrusion. If the overlying

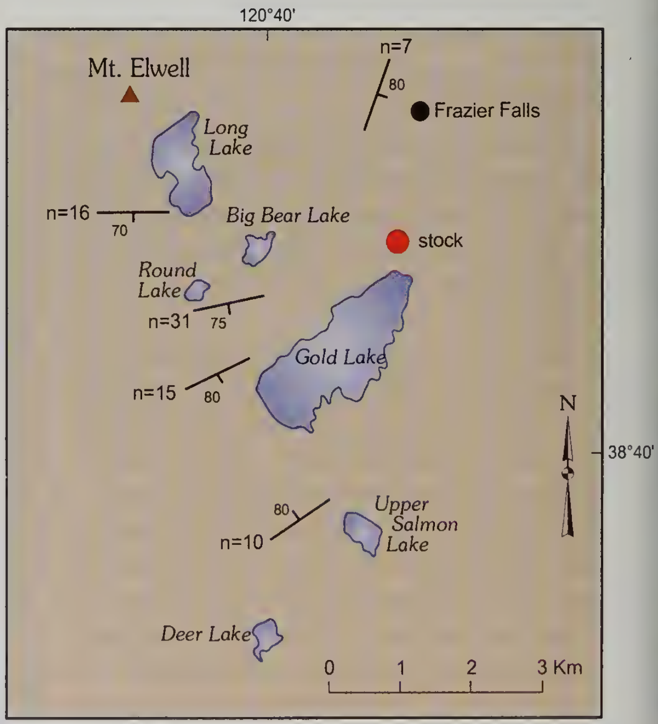

Figure 4. Map showing average orientation of Cretaceous dikes as determined from stereonet plots. n = number of dikes; strike and dip symbols = average orientation of dikes in the surrounding area.

country rock is relatively strong, a broad fan of steeply-dipping joints will develop as the expression of arching in a rigid medium (Balk, 1937). Weak overlying materials yield more readily, resulting in a zone of low-angle joints. Figure 5 shows these relationships diagrammatically. The situation shown in "C" of Figure 5 closely resembles the geometry of the dikes in Lakes Basin and lends support to a "broadly arched-roof" mechanism for dike emplacement.

Contacts and Cross-Cutting Relationships

Contacts between the dikes and country rock are discordant and very sharp. Mechanical interactions along contacts were minor and limited to slight fracturing and partial incorporation of fragments of wall rocks into the dikes. Cross-cut dikes and sills match across opposing dike walls, indicating forceful dilation of incipient fractures during dike emplacement. Most dike contacts maintain a fairly consistent trend overall, but in detail the contacts can show considerable variation in shape. Apophyses are the most spectacular variations along contacts. These are irregular offshoots from the main dike that vary from a few centimeters to several meters long (Photo 3). They probably represent short, irregular fractures that deviated from the main zone of weakness during dike emplacement. Although most apophyses are irregular, in some cases they branch from the main dike and partly fill a fracture that is parallel to the dike (Photo 4). These parallel fractures in the country rock are probably the result of the same tensional stresses responsible for emplacement of the dikes. A few of the dikes, especially those less than 1 m thick, change trend abruptly, possibly in response to conjugate fractures or the influence of older dike contacts (Figure 6).

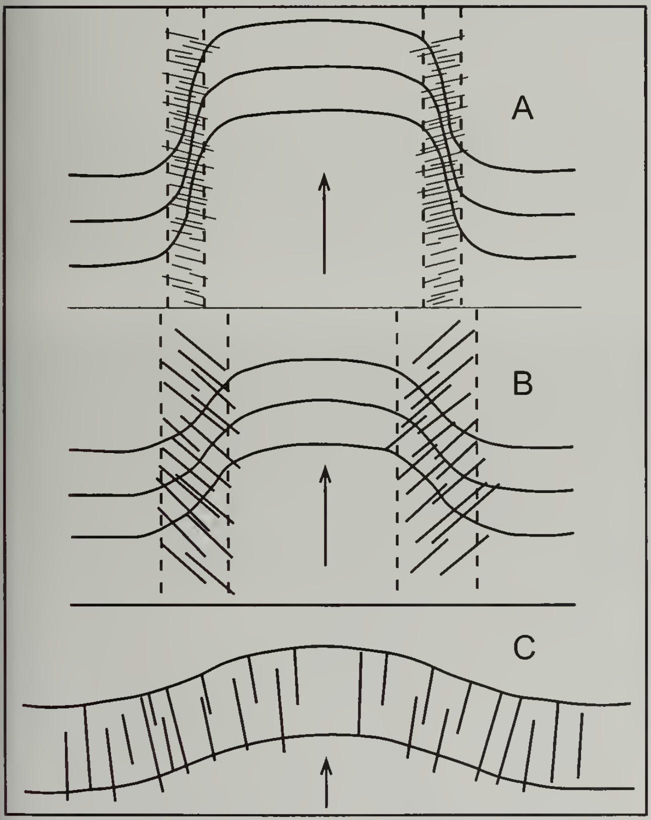

Figure 5. Development of marginal fractures and joint fans. Arrows indicate vertical emplacement of subjacent pluton. A = Weak country rock. B = Stronger material; fractures dip more steeply and are wider-spaced than in A. C = Strong roof rock; a broad arch with steeply-dipping tension fractures is developed. The fractures in C mimic the orientation of the Cretaceous dikes in Lakes Basin. *From Balk (1937).*

Several of the Cretaceous dikes cut one another. Although cross-cutting dikes are obviously younger than the dikes they cut, compositional and textural similarities indicate the dikes clearly belong to the same intrusive suite; the age difference is not significant. Contacts between dikes are sharp but chilled margins are lacking. This suggests the older dikes had solidified but were not cold at the time later dikes were intruded. The only consistent difference between the younger and older dikes is that the older dikes are thicker (Figure 6). This may represent a diminishing magma supply during the later stages of the intrusive event.

Internal Structure

Internal structures in the dikes are defined primarily by the distribution and orientation of phenocrysts and joint sets. These structures can be used to interpret flow direction, flow differentiation, and possible variations in viscosity within the dikes.

Flow alignment of phenocrysts is common along the dike margins. The most common flow alignment is shown by hornblende phenocrysts, which

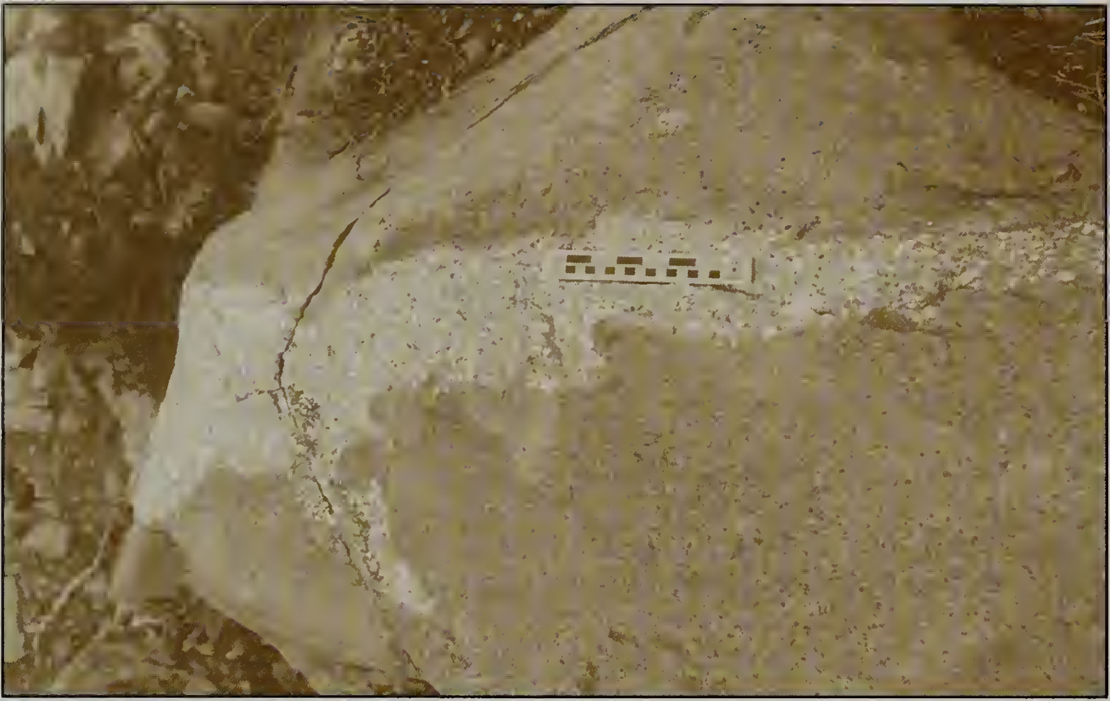

Photo 3. Apophysis from dike at Stop 2. Small divisions on scale are in centimeters. *Photo by J. Lull.*

tend to be aligned parallel to dike walls and define a lineation parallel to the dip direction of the dike (i.e., vertical in vertical dikes). In many dikes, tabular plagioclase phenocrysts define a flow foliation parallel to dike walls. The alignment of hornblende and plagioclase phenocrysts is restricted to the dike margins, extending from a few millimeters to a maximum of 40 cm inward from the dike walls. Therefore, the flow alignment of phenocrysts is probably due to viscous flow along contacts where cooling rates and viscosity are relatively high. In thin section, flow-aligned hornblende phenocrysts show signs of strain, presumably from stress due to viscous flow. The near-vertical lineation of hornblende also suggests that flow of magma in the dikes was mainly in a vertical direction. This is in contrast to near-surface radial dikes fed by a central volcanic vent where flow direction has a strong horizontal component (Shelley, 1988).

Distribution of phenocrysts is more or less uniform in most of the dikes, but in some cases variations occur in the concentration of plagioclase phenocrysts. The most common type of variation is a clustering toward the center of a dike, leaving the margins nearly free of plagioclase phenocrysts (Photo 5). Phenocryst-free margins vary widely from 3 to 20 cm. In some cases a narrow zone of phenocrysts occurs along the contract and is sepa-

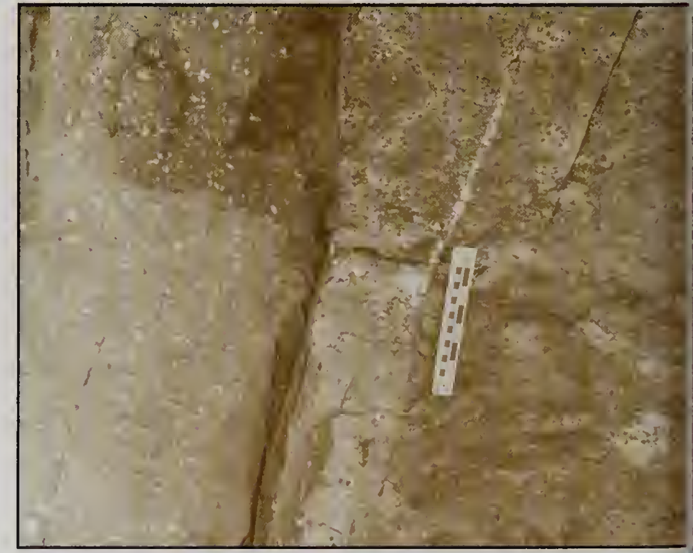

Photo 4. Thin offshoot of dike (just below cm scale) partly filling country rock fracture parallel to dike (dike is to the right in photo; Stop 3). Note second parallel, closed fracture in country rock to the left of the filled fracture. *Photo by J. Lull.*

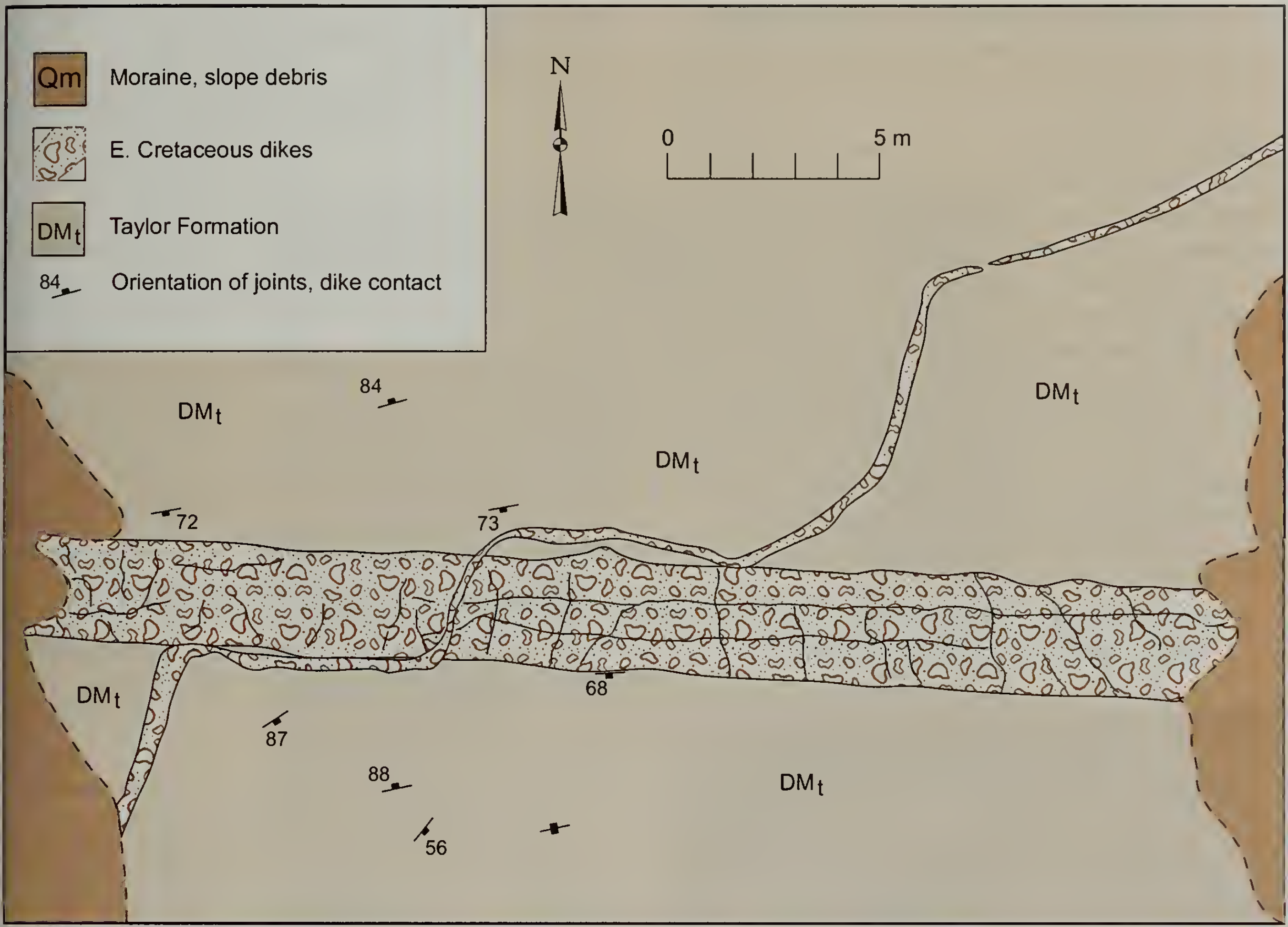

Figure 6. Map of cross-cutting dikes on slope southwest of Big Bear Lake. Note that the younger, cross-cutting dike partly follows the contact of the older dike.

rated by a phenocryst-free zone from the main concentration in the center of the dike.

Flow differentiation and clustering of phenocrysts have been observed in dikes and sills elsewhere. For example, in picrite dikes on the Isle of Skye, Scotland, olivine phenocrysts show variations in distribution similar to those noted above (Gibb, 1968). Komar (1972) ascribed the movement of phenocrysts away from walls to the center of a dike to grain dispersive pressure, combined with the increase in velocity gradient and fluid viscosity toward dike walls.

The plagioclase phenocrysts also show another kind of clustering that seems to be the result of a different process. They are commonly concentrated in apophyses and irregularities along dike

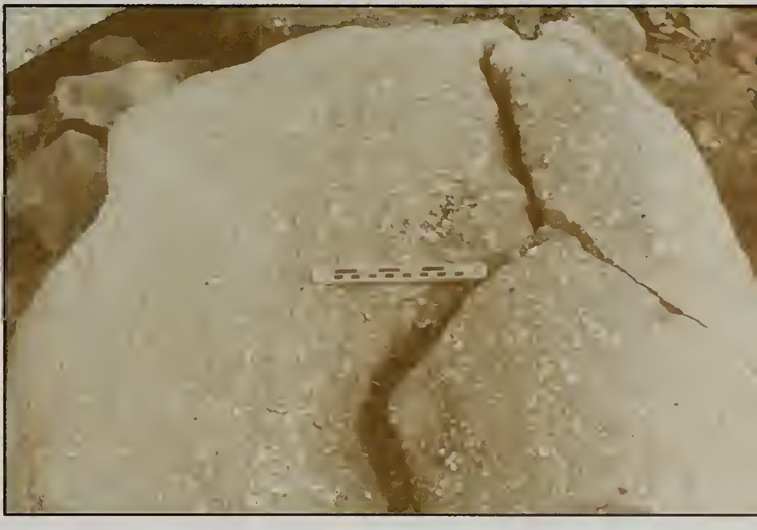

Photo 5. Flow differentiation of plagioclase phenocrysts toward center of dike (Stop 5). Note paucity of phenocrysts along dike margins. *Photo by J. Lull.*

margins (Photo 6), where they appear to have been entrapped in a confined space, similar to a log jam on a river.

Three distinct joint sets are present in the dikes (Figure 7). Longitudinal and diagonal joints are steeply-dipping, poorly developed, and usually discontinuous, although in some cases they pass into the country rock. The longitudinal joints may represent further extension after dike emplacement. Cross joints are subhorizontal and well-developed in some of the dikes (Photo 7). They do not pass into the country rock and appear to be normal to flow lineation. Therefore, the cross joints may be tensional in origin and could represent final elongation through rupture of the congealing melt (Balk, 1937).

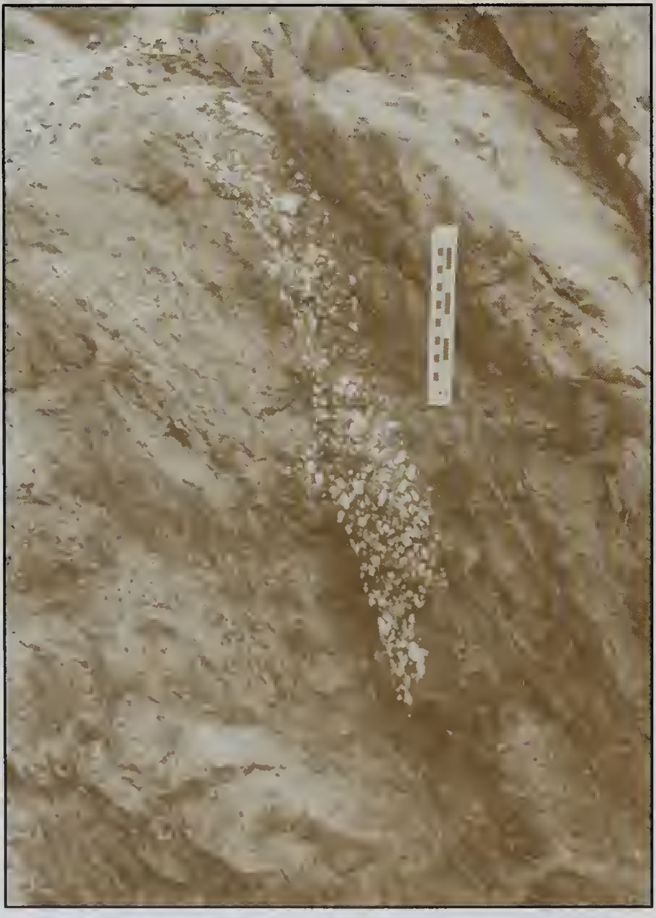

Photo 6. Concentration of plagioclase phenocrysts in apophysis near termination of dike (Stop 4). *Photo by J. Lull.*

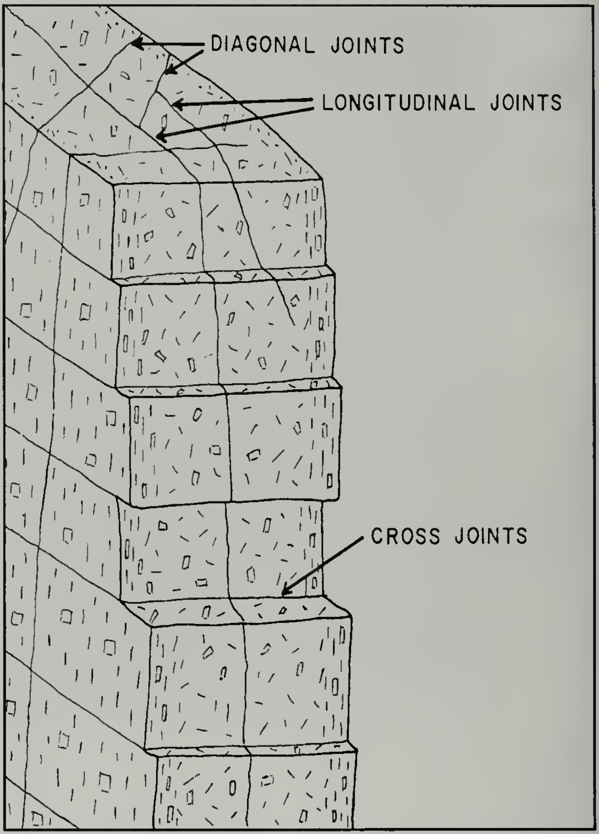

Figure 7. Schematic of joint system in a vertical dike. Longitudinal and diagonal joints dip steeply. Cross joints are subhorizontal and normal to flow direction in dike. Predominantly vertical flow direction is inferred by vertical lineation of hornblende phenocrysts along dike walls.

Lithology

The dike rocks vary in composition from high silica andesite to dacite. They are porphyritic with large (1 cm, average) plagioclase phenocrysts and smaller hornblende phenocrysts set in a gray, fine-grained to aphanitic felsic groundmass. Quartz and biotite phenocrysts are present in about half of the dikes. Chemical analysis (see Chemistry) suggests that dikes containing quartz phenocrysts are dacites and those lacking quartz phenocrysts are andesites.

The plagioclase phenocrysts range from 1 millimeter (mm) to 3 cm in diameter, are subhedral to euhedral, tabular, and vary in abundance from < 1 to 25% rock volume. Although a few dikes are relatively free of plagioclase phenocrysts, most contain at least 10% by volume. The plagioclase phenocrysts are usually extensively replaced by fine-grained epidote and sericite. The few relatively fresh crystals are strongly zoned with altered calcic cores. The plagioclase varies in composition from calcic oligoclase to andesine.

Hornblende phenocrysts occur as euhedral prisms, range from 1 to 9 mm long, and from 5 to 20% rock volume. They are ubiquitous in the dikes and unaltered to partially replaced by chlorite, epidote, sphene and biotite. In a few cases the hornblende has been completely replaced by sheaf-like aggregates of chlorite or biotite. In thin section, many of the hornblende phenocrysts show strong color zoning, with olive-green cores and straw-yellow rims. The hornblende often shows a preferred orientation with bent and broken crystals, probably resulting from magmatic stress related to viscous flow during dike emplacement.

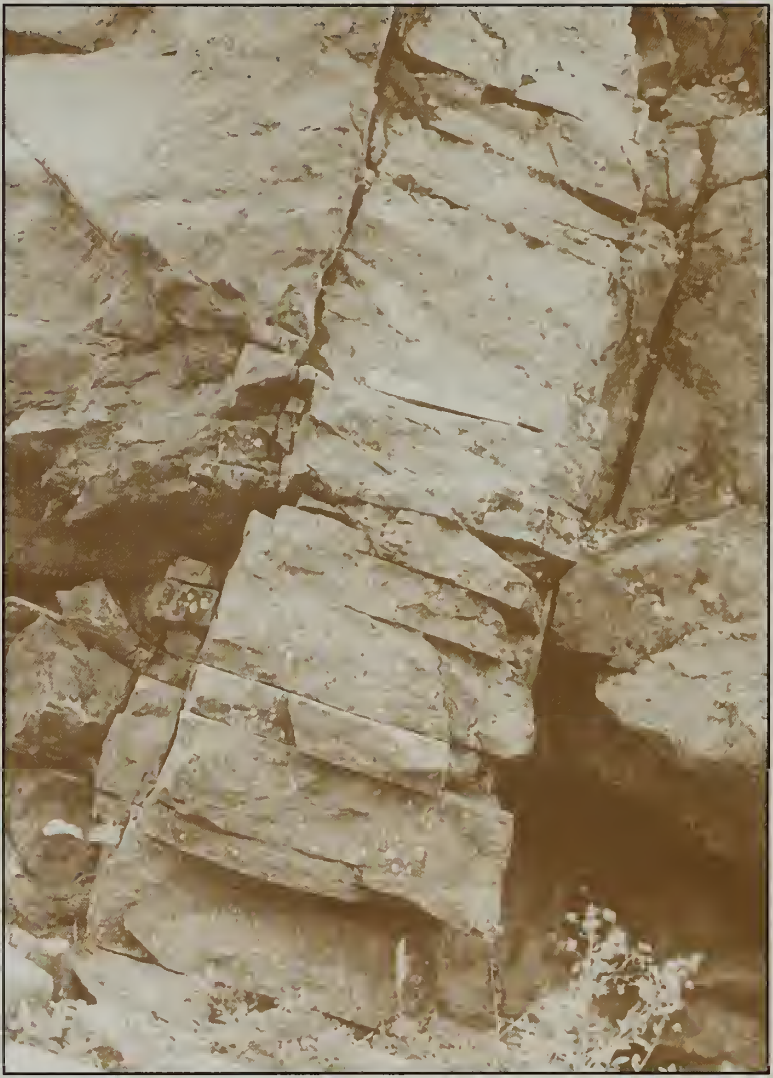

Photo 7. Dike (0.6 m thick) with well-developed cross joints. Note that cross joints are subhorizontal, normal to dip direction of dike, and do not pass into the country rock. *Photo by J. Lull.*

Many of the dikes contain abundant hornblende microphenocrysts (0.5 mm long), resulting in a distinct bimodal size distribution of phenocrysts. The microphenocrysts appear to represent a second generation of hornblende crystallization at the onset of accelerated cooling during dike emplacement. They probably crystallized during the initial consolidation of the groundmass.

Biotite phenocrysts (0-4% rock volume) are euhedral to subhedral and range from 1 to 8 mm in diameter. Most biotite crystals are partly to completely replaced by chlorite, epidote and sphene. The alteration took place preferentially along cleavage planes. The biotite commonly shows signs of strain, presumably due to magmatic stress.

Quartz phenocrysts (0-3% rock volume) range from 1 mm to 1 cm in diameter and are usually anhedral, rounded, and embayed, probably due to partial resorption by hydrous fluids during final consolidation of the melt. However, occasional euhedral crystals with square or hexagonal outlines also occur. The quartz is unaltered, but in at least one case, actinolite needles nucleated around a quartz phenocryst, forming a rim of prisms oriented normal to the surface of the quartz crystal.

The groundmass (60-90% rock volume) is essentially composed of very fine-grained plagioclase and quartz. Plagioclase is predominant, less altered than the phenocrysts, and occurs as subhedral to euhedral zoned microlites ranging in composition from oligoclase to andesine. Groundmass quartz is anhedral and largely interstitial to the plagioclase. Alteration minerals (see Deuteric Alteration) comprise up to 30% of the groundmass. There is a rough positive correlation between grain size of the groundmass (0.02-0.17 mm) and dike thickness. Grain size generally increases with increasing dike thickness, indicating a slower cooling rate for thicker dikes.

Accessory minerals include apatite, pyrite and iron oxide. These minerals are generally very fine-grained and occur in minor amounts in most of the dikes. In a few dikes, pyrite crystals range up to 1 cm in diameter.

Deuteric Alteration

Late-stage, hydrous alteration minerals are present in all the dikes and include white mica, chlorite, epidote, sphene, biotite and calcite. Very fine-grained actinolite is present in the groundmass of a few dikes. These alteration minerals extensively replace phenocrysts (see above) and are scattered in varying proportions throughout the groundmass. The alteration is pervasive and not restricted to fractures in the dikes.

This late-stage, deuteric alteration appears to be the result of reactions between crystals and a fluid-rich volatile phase during the final stages of crystallization. The fluids responsible for deuteric alteration are the final differentiates of the magma (Tyson and others, 1979); the active agents are primarily water and carbon dioxide.

Since fluid-rich volatiles are responsible for the alteration, their retention in the magma is an important factor. If the volatiles escape, deuteric alteration will be minimal or absent. Diabase dikes and sills in southern Death Valley and Arizona show a direct correlation between degree of alteration and impermeability of the country rock (Janet Hammond, personal communication, 1982). Where the diabase intruded permeable and fractured country rock, the volatiles escaped (as evidenced by pegmatites), and there is little or no deuteric alteration. Where the diabase dikes intruded impermeable strata or gneissic basement, volatile fluids were sealed in, and the diabase shows pervasive deuteric alteration.

The Cretaceous dikes in Lakes Basin intrude relatively impermeable, recrystallized metavolcanic rocks that would have effectively sealed volatiles in the dikes. There is no evidence of escape of a fluid phase; no pegmatites or felsic veins are associated with the dikes. Therefore the residual fluid phase was mostly sealed in and reacted with previously formed crystals, resulting in fairly extensive late-stage alteration.

Inclusions

At least three different types of inclusions occur in the dikes: 1) angular fragments of country rock; 2) subangular medium- to coarse-grained granitic rocks; and 3) rounded, fine-grained inclusions of mafic to intermediate composition. The angular country rock inclusions are xenoliths that were clearly derived from the enclosing rock during intrusion of the dikes. Most are only a few centimeters in diameter and generally occur along dike contacts. The granitic inclusions are rare; only two or three were observed in the mapped dikes. They range up to 15 cm in diameter and were probably derived from deeper-seated plutonic rocks. The mafic/intermediate inclusions are composed essentially of hornblende and plagioclase, +/- minor amounts of quartz. Grain size averages 0.5 to 1.0 mm, usually with an equigranular texture, but some are porphyritic and nearly identical to the enclosing dike rock. These inclusions range to almost 50 cm in diameter and are usually rounded or oblate (Photo 8). They occur in several dikes and comprise <1% rock volume.

The origin of the mafic/intermediate inclusions is uncertain, but they may be the result of magma mingling prior to intrusion of the dikes. Evidence of mafic and felsic magma mixing and mingling has been documented in many parts of the Sierra Nevada Batholith (Ingersoll and others, 1999) and mafic enclaves are abundant in granodiorite east of Yuba Pass.

Chemistry

Five separate dike samples were analyzed for major elements by X-ray fluorescence. The dike samples were chosen to represent the range in composition based on lithologic characteristics, such as the presence or absence of quartz phenocrysts, and color index. The chemical analyses

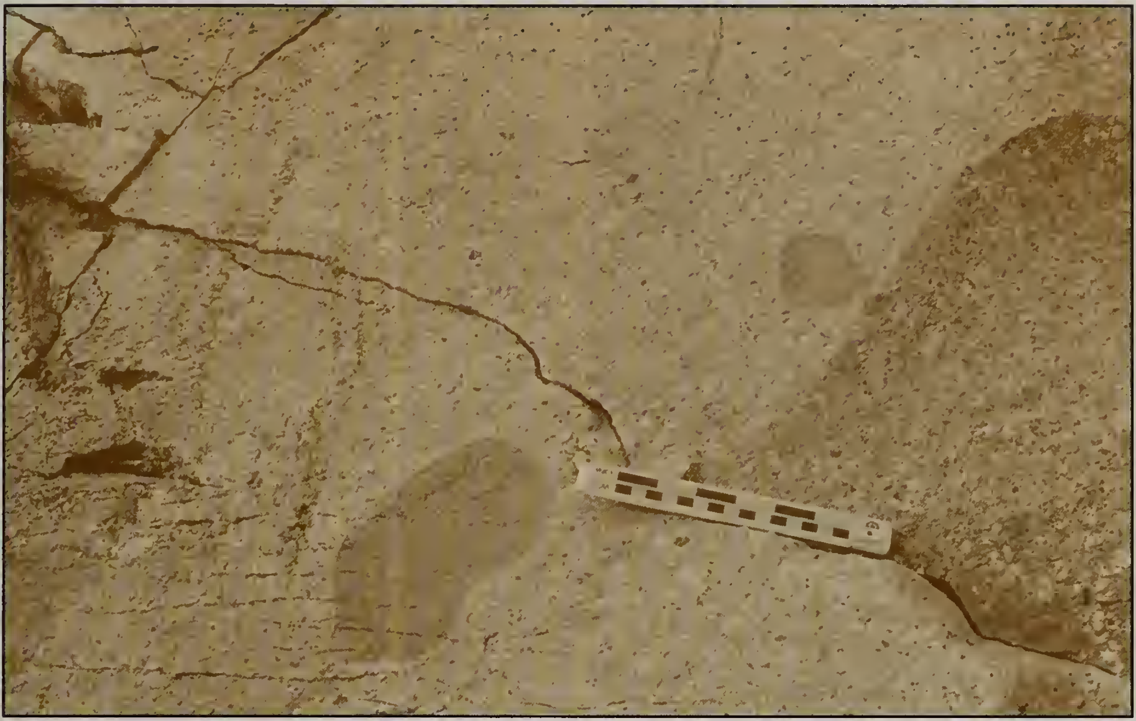

Photo 8. Rounded mafic inclusions in dike (Stop 5). *Photo by J. Lull.*

show a range in SiO_2 from 60.38% to 67.7% (Table). The two more mafic samples lack quartz phenocrysts, contain less than 63% SiO_2, and plot as medium-K "acid" andesite on a K_2O-SiO_2 diagram (Figure 8). The other three samples contain more than 63% SiO_2, have quartz phenocrysts, and plot as medium-K dacite. Based on these data, the dikes grade in composition from andesite to dacite. Assuming the presence of quartz phenocrysts indicates >63% SiO_2, approximately half the dikes are dacites.

Table. Analyses, normalized to 100% (weight %), of five dike samples and one sample of the hornblende tonalite from the Gold Lake Stock (GLS). Determined by XRF analysis at the University of California, Santa Cruz. Dike samples 76 and 12-3 are andesites and lack quartz phenocrysts. Samples 87-2, 36-1 and 82-2 are dacites and contain quartz phenocrysts.

Sample #	76	12-3	87-2	36-1	82-2	87-1 GLS
SiO_2	60.38	60.38	63.33	64.11	67.70	67.00
Al_2O_3	17.05	17.04	17.20	16.27	16.56	15.97
Fe_2O_3	2.32	2.20	2.09	2.06	2.04	2.00
FeO	4.05	3.45	3.06	3.08	1.43	1.79
MgO	4.25	4.47	3.11	3.72	2.04	2.74
CaO	6.68	5.54	5.74	5.35	4.56	4.60
Na_2O	2.98	2.38	2.71	3.08	2.78	3.38
K_2O	1.36	1.46	2.01	1.60	2.36	1.85
TiO_2	0.79	0.64	0.57	0.56	0.48	0.48
P_2O_5	0.15	0.19	0.18	0.17	0.16	0.17

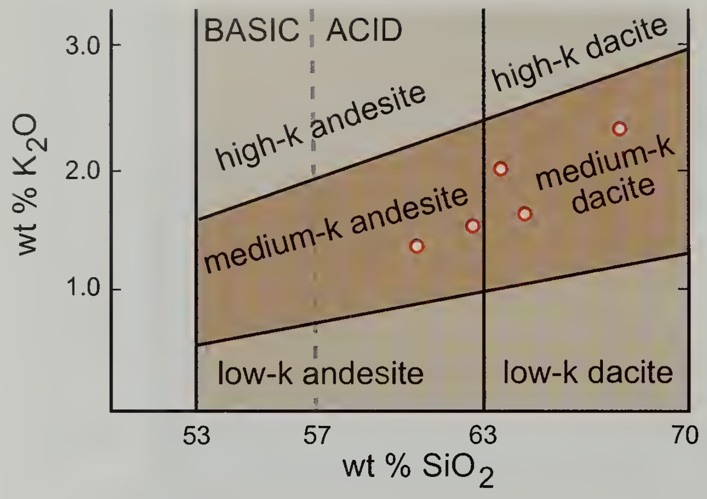

Figure 8. Classification of andesites and dacites using K_2O and SiO_2 content (after Gill, 1981). The five analyzed dike samples are plotted.

Based on SiO_2 vs. FeO*/MgO (Miyashiro, 1974), the chemistry shows a clear calc-alkalic trend (Figure 9). This supports a direct relationship of the dikes to Mesozoic subduction and continental arc volcanism. Oxide variation trends are fairly consistent, suggesting the dikes represent a single intrusive suite derived from the same parent magma.

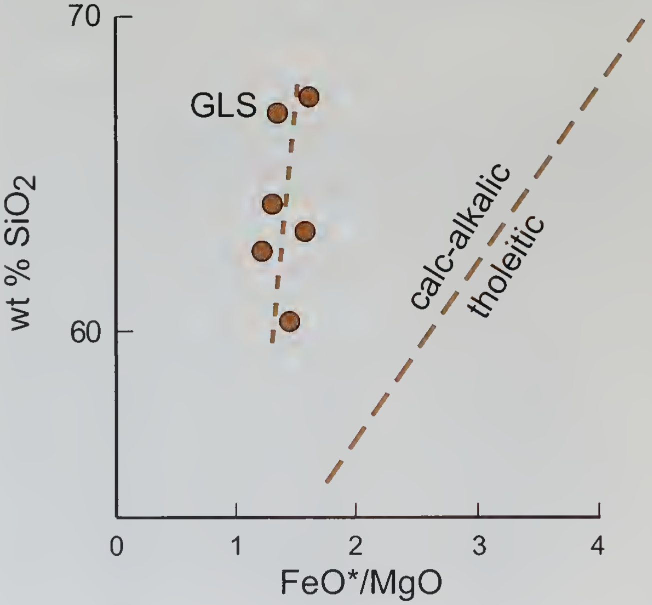

Figure 9. SiO_2 vs. FeO*/MgO in wt. % (after Miyashiro, 1974). Dike samples and Gold Lake Stock (GLS) are plotted. A clear calc-alkalic trend is indicated.

GOLD LAKE STOCK

The Gold Lake Stock is exposed in a roadcut just northeast of Gold Lake. In outcrop, the stock is approximately 100 m wide. It is composed of two distinct but compositionally similar phases, which differ mainly in color index and quartz content. Both phases are tonalites, based on the IUGS classification. The lighter phase (leuco-tonalite) has a color index of 8% or less. The darker phase (hornblende tonalite) has a color index of 15 to 20% (higher color index is due to the presence of hornblende) and contains slightly less quartz than the leucocratic phase. The contact between the two phases is not exposed, but the lack of any intrusive relationships between them, such as apophyses or xenoliths, suggests they comprise a single, zoned stock.

The leuco-tonalite is well-exposed in the roadcut and in sharp vertical contact with the metavolcanic rocks of the Taylor Formation (Figure 10). It also cuts one of the dacite dikes. Three other dikes in the roadcut are identical in lithology to the tonalite and appear to be direct offshoots of the stock. The leuco-tonalite has a medium-grained, hypidiomorphic equigranular texture, with 50% plagioclase, 35% quartz, 8% biotite, 3% potassium feldspar, 3% pyrite, and <1% hornblende. The plagioclase (An_{30}-An_{35}) is strongly zoned and partly replaced by white mica and epidote. Biotite is also partly altered to chlorite and epidote.

The hornblende tonalite is poorly exposed just west of the roadcut. It is slightly porphyritic, with zoned plagioclase phenocrysts to 1 cm in diameter set in a medium-grained hypidiomorphic granular groundmass. The mode is 53% total plagioclase (9% phenocrysts), 26% quartz, 10% biotite, 8% hornblende, 3% potassium feldspar, and <1% pyrite. Plagioclase and biotite are partly altered as in the leucocratic phase, and the hornblende is partly replaced by chlorite, epidote and sphene. Major element XRF analysis of the hornblende tonalite indicates a silica content of 67% (Table) and a strong chemical affinity between the dacite dikes and the stock (see Dike-Stock Affinity). The chemical analysis of the stock is very similar to the average tonalite analysis published by Nockolds (1954).

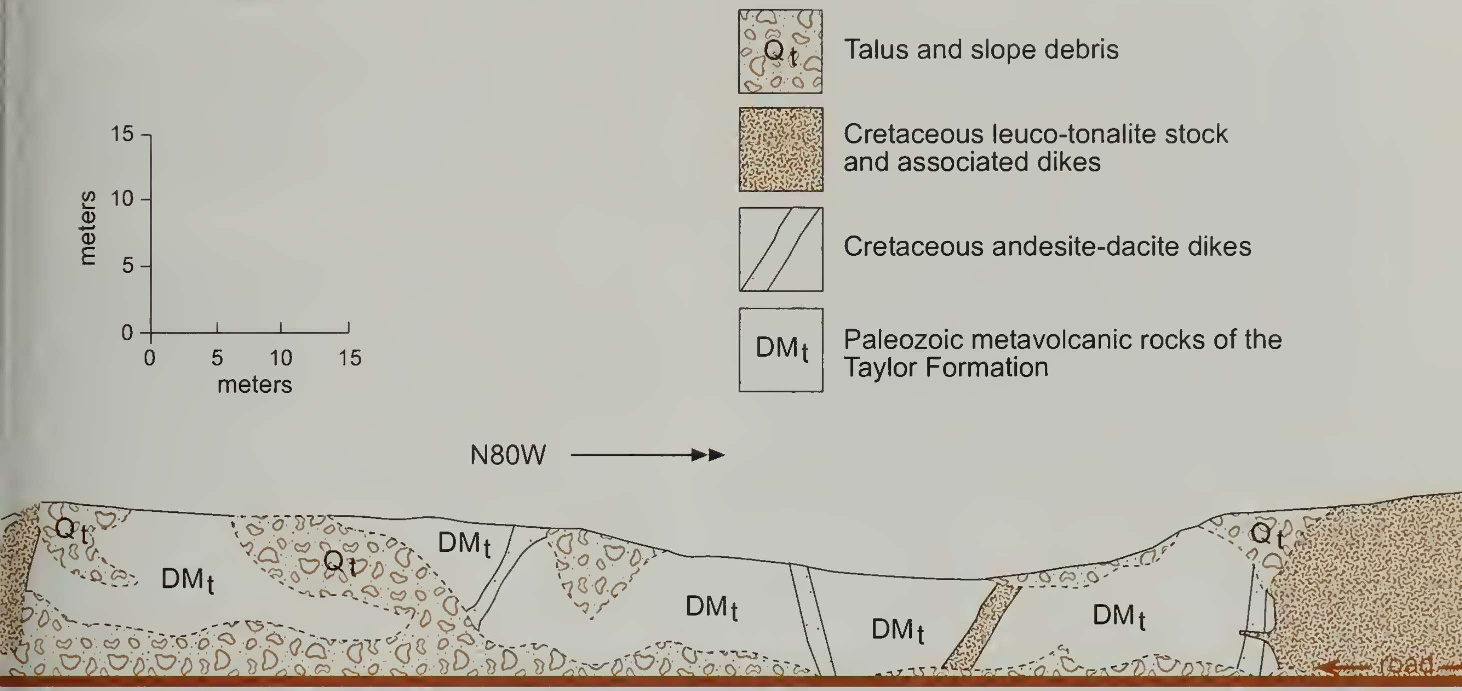
Qt
Talus and slope debris
Cretaceous leuco-tonalite stock and associated dikes
Cretaceous andesite-dacite dikes
DMt
Paleozoic metavolcanic rocks of the Taylor Formation
15
10
5
0
meters
0
5
10
15
meters
N80W
Qt
DMt
Qt
DMt
DMt
DMt
DMt
Qt
road

Figure 10. Roadcut on south side of Gold Lake Road (Stop 6). The leuco-tonalite (Gold Lake Stock) is in contact with the Taylor Formation near the west end of the roadcut. Several Cretaceous dikes cut the Taylor Formation; the three thickest dikes (two at the east end of the roadcut, one closer to the stock) appear to be direct offshoots of the stock, based on composition.

DIKE-STOCK AFFINITY

The Early Cretaceous dikes and Gold Lake Stock show a close affinity based on age and spatial relationships. K-Ar dates of hornblende indicate that the stock and dikes are essentially coeval (120-122 Ma). The K-Ar age for the stock is about 2 Ma younger than the date for the dike, but this is relatively insignificant considering the 1.4 Ma margin of error in the K-Ar dates. The dikes also appear to be structurally related to the stock. The dikes show a radial trend focused on the stock, are most abundant in the area directly northwest of the stock, and decrease in abundance to the north and south of that area (Figures 3 and 4)

Dikes and stock also show a magmatic affinity based on compositional similarity. The tonalite stock represents the plutonic equivalent of the high-silica andesite and dacite dikes. Dikes and stock contain the same mineral assemblage and show similar deuteric alteration. The main lithologic difference is textural; the stock is coarser-grained and more equigranular, due to the slower cooling rate of a larger volume intrusive. Based on major-element chemistry, the stock is nearly identical to the higher-silica dacite dikes. It also fits well on oxide variation curves with the dikes, and fits the calc-alkalic trend of the dikes (Figure 9).

The close affinity of dikes and stock suggests they are comagmatic and part of the same intrusive event. However, because the stock is a relatively small intrusive body and is slightly younger than at least some of the dikes, it is unlikely that the majority of the dikes are direct offshoots of the stock. It is more likely that both dikes and stock are tied to a larger, subjacent pluton.

CONCLUSIONS

Based on age, lithology and structural relationships, the Early Cretaceous andesitic to dacitic dikes and tonalite stock appear to be co-genetic and to represent hypabyssal members of an unexposed, subjacent pluton of unknown dimensions. The dikes were emplaced as a result of tensional stresses, due to doming and fracturing of the roof rocks during forceful emplacement of the subjacent pluton (Lull and Brooks, 1983; Lull, 1984). Magmatic stress slightly exceeded lithostatic stress of the overlying rocks, resulting in a broad fan of radial fractures in the country rock. The distribution of the dikes expresses this fracture pattern. The pluton is estimated to be somewhere beneath the area between Gold Lake, Round Lake and Long Lake, where the dikes are most abundant.

Magma feeding the dikes and stock was rich in late stage volatiles (probably mostly carbon dioxide and water). The volatiles were largely sealed in, resulting in extensive deuteric alteration of the dikes.

It is unknown whether the dikes were vented to the surface, but these Cretaceous hypabyssal rocks are associated with the rest of the Sierra Nevada Batholith. The batholith represents the roots of an extensive, Andean-type volcanic arc that existed along the western continental margin of North America during most of the Mesozoic (Hamilton, 1969).

FIELD TRIP GUIDE

The field trip starts at the Round Lake trailhead, just off Gold Lake Highway, 7.6 miles south of the intersection of Gold Lake Highway and Highway 89, or 7.9 miles north of the intersection with Highway 49 at Bassetts. See Figure 11 for locations of field trip stops.

Hike up the trail toward Round Lake. At the first fork, about 300 meters up the trail, keep to the left. The trail continues through a wooded area for about 0.5 miles, then turns northward and begins to climb into the open. Just up the hill, approximately 0.6 miles from the trailhead, the trail takes a sharp bend to the left. At this turn there is a clear view of Mt. Elwell to the north. Stop at the turn.

Stop 1. (elevation 6,640 feet) Just north of the trail is a partly-buried boulder (about 1.5 m in diameter) of plagioclase-hornblende porphyry. This is a glacial erratic from one of the Cretaceous dikes. Note the abundant large chalky-white plagioclase, black hornblende and sparse biotite phenocrysts. This is a typical phenocryst assemblage for the high-silica andesite dikes (the dacite dikes contain quartz phenocrysts). The groundmass consists mainly of very fine-grained plagioclase and quartz.

The white of the plagioclase and greenish tint of the groundmass indicate alteration minerals, including sericite, epidote and chlorite. This is the result of late-stage (deuteric) alteration.

Continue up the trail for about 0.5 miles where it passes a small pond. The hill to your left (south) is capped with columnar basalt of Tertiary age. Just past the pond, the trail climbs up a hill. After a broad left turn, the trail turns sharply to the right. Just before the sharp turn, pull off the trail to the left (east).

Stop 2. (elevation 6,760 feet) Look for the dike on a rocky knoll about 15 m east of the trail (Photo 1). This dike is nearly 3 m

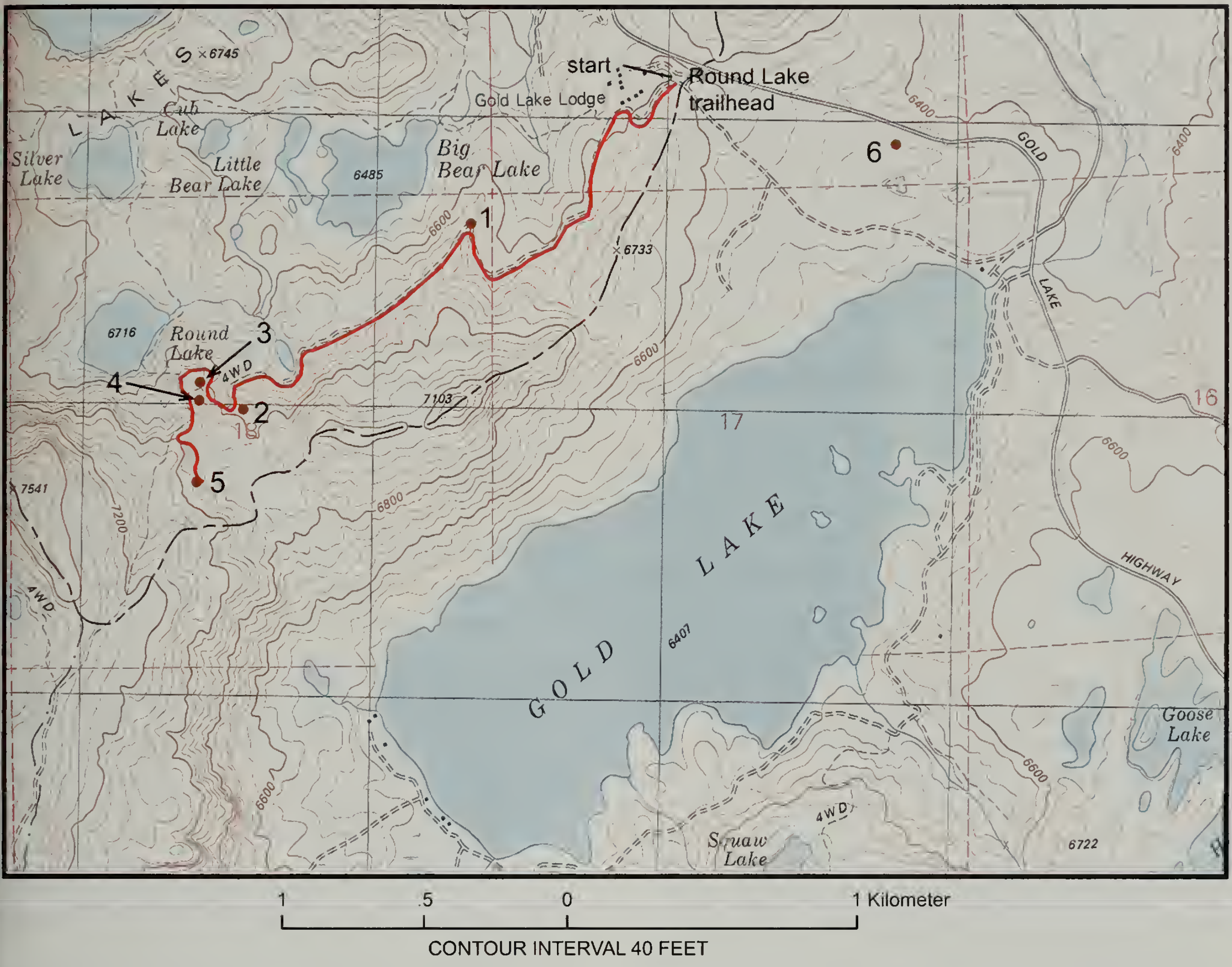

Figure 11. Field trip map. Numbered stops are indicated. Base map is from the 7 1/2' Gold Lake Quadrangle, 1981. *U.S. Geological Survey.*

thick, trends approximately east-west, and dips steeply to the south. It can be traced for over 100 m to the east. Lithology of this dike is very similar to the boulder at Stop 1. Note the plagioclase phenocrysts stand out in relief on weathered surfaces.

There are several apophyses (offshoots of the dike, Photo 3) along dike contacts, ranging from a few centimeters to several meters long. Some are highly irregular in shape and contain high concentrations of plagioclase phenocrysts that were trapped during intrusion. Also note partial incorporation of country rock fragments along some of the contacts.

The country rock here is meta-andesite tuffs and tuff breccias of the Late Paleozoic Taylor Formation. Most of the original texture has been preserved and graded bedding can be observed in places.

Continue up the trail and turn right at the fork. Near the top of the hill, look for a dike on the left side just before the trail takes a sharp bend to the left.

Stop 3. (elevation 6,840 feet) This dike is 1 m thick, trends northwest, and dips steeply south. Note that it contains quartz phenocrysts up to 5 mm in diameter. Most are rounded and partly resorbed, but a few show euhedral, hexagonal outlines. Chemical analysis of selected dike samples suggests those with quartz phenocrysts are dacites (>63% SiO_2) and those lacking quartz phenocrysts are andesites.

This dike cuts sharply across Nevadan cleavage in the Taylor Formation metavolcanic rocks. The cleavage does not pass into the dike, clearly indicating that these Early Cretaceous dikes post-date the Nevadan Orogeny. Also, note fractures in the country rock that parallel the dike. One of the fractures is partially filled with an apophysis from the dike (Photo 4). These fractures may be related to the forceful intrusion of a subjacent pluton responsible for the injection of the dikes.

On the backside (from the trail) of the outcrop, the dike shows flow foliation of plagioclase and lineation of hornblende phenocrysts. The flow direction is clearly parallel to dike walls and hornblende lineation suggests vertical flow.

Continue on the trail around the knoll (passing the cutoff down to Round Lake) to a fork in the trail on the south side of the knoll. Climb on the outcrop about 30 m southeast of the trail intersection and locate two east-west trending dikes.

Stop 4. (elevation 6,840 feet) The higher (southerly) dike is up to 3 m thick and cuts sharply across the Nevadan cleavage of the Taylor Formation metavolcanic rocks. This dike is right on trend with the dike seen at Stop 2, with similar lithology, thickness, and orientation; it is probably the same dike. At this location, it pinches out to the west in a long anastomosing apophysis, then appears to be offset to the north, on a parallel trend, where it is cut by a light-colored, northeast-trending dike with <1% plagioclase phenocrysts. The cross-cutting dike is about 1.5 m thick and except for the lack of plagioclase phenocrysts, is similar to the rest of the Cretaceous dikes.

Proceed on the trail that heads uphill to the southwest. About 150 m up the trail at approximately 6,920 feet elevation, the trail levels out between two large pine trees with bare trunks, then turns to the right around a large rocky knoll. Leave the trail just before the turn, heading left of the knoll, due south. Continue south for about 250 m; maintain approximately the same elevation.

Stop 5. (elevation 6,960 feet) There are several east-west trending dikes in this area. They can be traced fairly easily from one outcrop to the next. Look for a dike showing a concentration of plagioclase phenocrysts toward the center of the dike. This flow differentiation probably results from a combination of grain dispersive pressure between phenocrysts and increased fluid viscosity toward dike walls. On weathered surfaces the plagioclase and quartz phenocrysts stand out in relief.

Another dike just to the south contains abundant (up to about 1% by volume) rounded mafic enclaves (Photo 8) ranging from 1 to 50 cm in diameter. They are ovoid to amoeboide. Most are fine-grained equigranular but a few have porphyritic texture. They are composed of plagioclase, quartz, and an altered mafic mineral, probably hornblende. The porphyritic inclusions contain plagioclase and hornblende phenocrysts and are remarkably similar to the enclosing dike rock. Some of the enclaves may represent magmatic inclusions resulting from magma mingling prior to dike injection.

Hike back down the trail to the trailhead. Drive out to the Gold Lake Highway and turn right (southeast). Drive 0.5 miles to a large roadcut on the south side of the road. Park in the pullout on the north side of the road just past (east of) the roadcut. Hike up to the west end of the roadcut.

Stop 6. The light-colored leuco-tonalite of the Gold Lake Stock is well-exposed at the west end of the roadcut. It is in sharp vertical contact with the Taylor Formation. At the contact an apophysis of the stock also cuts one of the Cretaceous dikes. The tonalite is a medium-grained, hypidiomorphic granular rock composed primarily of plagioclase and quartz, with approximately 10% biotite, 3% pyrite, 3% potassium feldspar and <1% hornblende. A darker, hornblende-rich phase of the tonalite is poorly exposed just west of the roadcut. It is best exposed on the north side of the road and is similar to the leuco-tonalite but contains more hornblende and less quartz. It is slightly porphyritic with zoned plagioclase phenocrysts up to 1 cm in diameter. Contact relationships between the leuco-tonalite and hornblende tonalite are not apparent, but the two phases are interpreted to represent a single, zoned stock or pluton.

Several Cretaceous dikes cut the metavolcanic rocks of the Taylor Formation in the roadcut east of the stock. At least three of these dikes appear to be direct offshoots of the stock; they have a fine-to medium-grained phaneritic groundmass, contain abundant pyrite, and are mineralogically identical to the stock. One of these dikes occurs about 25 m east of the stock contact. The other two can be found at the far east end of the roadcut (look for rusty-weathered surfaces, due to weathering of pyrite).

The Gold Lake Stock appears to be closely related to the Early Cretaceous dike swarm, based on age, composition, and spatial relationships. Hornblende K-Ar dates reveal an age of 120.1 Ma for the stock and 122.3 Ma for one of the dikes. The stock and dikes have similar lithology and chemistry. Also, the dikes exhibit a radial trend focused on the stock. Therefore, the Cretaceous dikes and Gold Lake Stock are interpreted to be co-magmatic offshoots of a subjacent pluton, beneath the Gold Lake basin.

ACKNOWLEDGMENTS

I thank June Legler and Steve Silva for their helpful reviews, which greatly improved this field trip.

REFERENCES

Badgley, P.C., 1965, Structural and tectonic principles: New York, Harper and Row, Inc. 521 p.

Bailey, E.B., 1924, The Tertiary and post-Tertiary geology of mull, Loch Aline, and Oban: Memoirs of the Geological Survey of Scotland: London, E. Stanford, Ltd., 449 p.

Balk, R., 1937, Structural behavior of igneous rocks: Geological Society of America Memoir No. 5, 177 p.

Bond, G.C., Menzies, M. and Moores, E.M., 1977, Paleozoic-Mesozoic rocks of the northern Sierra Nevada: Field Guide, Geological Society of America Cordilleran Section Annual Meeting, Sacramento, California, 31 p.

Brooks, E.R., Wood, M.M. and Garbutt, P.L., 1982, Origin and metamorphism of peperite and Associated rocks in the Devonian Elwell Formation, northern Sierra Nevada, California: Geological Society of America Bulletin, v. 93, p. 1208-1231.

Durrell, C. and D'Allura, J.A., 1977, Upper Paleozoic section in eastern Plumas and Sierra counties, northern Sierra Nevada, California: Geological Society of American Bulletin, v. 88, p. 844-852.

Gibb, F.G.F., 1968, Flow differentiation in the xenolithic ultrabasic dikes of the Buillins and the Strathaird Peninsula, Isle of Skye, Scotland: Journal of Petrology, v. 9, p. 411-443.

Gill, J.B., 1981, Orogenic andesites and plate tectonics: Heidelberg, Springer-Verlag, 390 p.

Hamilton, W., 1969, Mesozoic California and the underflow of Pacific mantle: Geological Society of America Bulletin, v. 80, p. 2409-2430.

Hanson, R.E., Girty, G.H., Girty, M.S., Hargrove, U.S., Harwood, D.S., Kulow, M.J., Mielke, K.L., Phillipson, S.E., Schweickert, R.A. and Templeton, J.H., 1996, Paleozonic and Mesozoic arc rocks in the northern Sierra terrane *in* Girty, G.H., Hanson, R.E., Schweickert, R.A., and Harwood, D.C., editors, The Northern Sierra terrane and associated Mesozoic magmatic units: Implications for the tectonic history of the western Cordillera: SEPM Pacific Section, Book 81, p. 25-55.

Harker, A., 1904, The Tertiary igneous rocks of Skye: Memoirs of the Geological Survey, Scotland, 481 p.

Harwood, D.S., 1992, Stratigraphy of Paleozoic and Lower Mesozoic rocks in the northern Sierra terrane: U.S. Geological Survey Bulletin 1957, 78 p.

Ingersoll, R.V., Ratajeski, K., Glazner, A.F. and Cloos, M., 1999, Mesozoic convergent margin of central California: Geologic field trips in northern California, centennial meeting of the Cordilleran section of the Geological Society of America, Department of Conservation, Division of Mines and Geology Special Publication 119, p. 101-135.

Johnson, R.B., 1961, Patterns and origin of radial dike swarms associated with West Spanish Peak and Dike Mountain, south-central Colorado: Geological Society of America Bulletin, v. 72, p. 579-596.

Koide, H. and Bhattacharji, S., 1975, Formation of fractures around magmatic intrusions and their role in ore localization: Economic Geology, v. 70, p. 781-799.

Komar, P.D., 1972, Mechanical interactions of phenocrysts and the flow differentiation of Igneous dikes and sills: Geological Society of America Bulletin, v. 83, p. 973-988.

Lull, J.S., 1984, Petrology and structure of an Early Cretaceous dike swarm, northern Sierra Nevada, California: M.S. thesis, California State University, Hayward, 146 p.

Lull, J.S. and Brooks E.R., 1983, Petrology and structure of an Early Cretaceous dike swarm, northern Sierra Nevada, California: Geological Society of America Abstracts with Programs, v. 15, no. 5, p. 411.

Miyashiro, A., 1974, Volcanic series in island arcs and active continental margins: American Journal of Science, v. 274, p. 321-355.

Parsons, W.H., 1939, Volcanic centers of the Sunlight area, Park County, Wyoming: Journal of Geology, v. 47, p. 1-26.

Robson, G.R. and Barr, K.G., 1964, The effect of stress on faulting and minor intrusions in the vicinity of a magma body: Bulletin Volcanologique, v. 27, p. 315-330.

Schweickert, R.A., Bogen, M.L., Girty, G.H., Hanson, R.E. and Merguerian, C., 1983, Timing and structural expression of the Nevadan orogeny, Sierra Nevada, California: Geological Society of America Abstracts with Programs, v. 15, no. 5, p. 293.

Shelley, D., 1988, Radial dikes of Lyttelton volcano—their structure, form, and petrography: New Zealand Journal of Geology and Geophysics, v. 31, p. 65-75.

Smith, R.P., 1975, Structure and petrology of Spanish Peaks dikes, south-central Colorado: Ph.D. dissertation, Boulder, University of Colorado, 185 p.

Turner, H.W., 1895, The age and succession of the igneous rocks of the Sierra Nevada: Journal of geology, v. 3, p. 385-414.

Tyson, R.M., Mollins, P.A. and Chans, L.L., 1979, Deuteric alteration in the Partridge River troctolite, Duluth Complex, Minnesota: Geological Society of America Abstracts with Programs, v. 11, no. 5, p. 258.

TERTIARY VOLCANIC ROCKS OF THE BLAIRSDEN AREA, NORTHERN SIERRA NEVADA, CALIFORNIA

David L. Wagner[1], George J. Saucedo[1], Thomas L.T. Grose[2]

INTRODUCTION

Large accumulations of Tertiary volcanic rocks overlie pre-Cenozoic bedrock in the central and northern Sierra Nevada. Most of the volcanic rocks are Miocene and Pliocene, subduction-related, calc-alkaline andesites that erupted from volcanoes along and east of the Sierra Nevada (Figure 1). This volcanism was part of a Miocene magmatic arc that extended from the Pacific Northwest through the Sierra Nevada southward to the Death Valley region and southern Nevada (Brem, 1977; Christiansen and Yeats, 1992). Andesitic flows, breccia, tuff-breccia, and lahars (mudflows) flowed westward initially following and eventually inundating the paleo-drainages. An estimated 1,000 to 2,000 cubic miles of andesitic rock was deposited on the Tertiary Sierran landscape north of the Tuolumne River (Curtis, 1954). Near the crest of the Sierra Nevada, proximal brecciated andesite flows are the predominant rock type. Lahars and some flows traveled westward down the paleo-slope of the Sierra, some even reaching the Great Valley. Erosion between eruptive episodes produced copious amounts of the andesitic sand and gravel that is intercalated with the lahars and flows. New drainages were cut through the volcanic cover into pre-Cenozoic bedrock forming new canyons, leaving volcanic cap rock on many ridges.

This field trip will examine exposures of the northernmost Sierran volcanic rocks in the Grizzly and Diamond mountains between Blairsden and Honey Lake. These mountains make up the northeasternmost part of the Sierra Nevada Geomorphic Province. The Diamond and Grizzly mountains are fault-bounded blocks down-dropped from the main part of the Sierra along northwest-trending faults of the Walker Lane belt of Stewart (1988). Cordell Durrell (1959a) established the stratigraphy of the Blairsden Quadrangle and later (Durrell, 1966, 1987) extended his formations to include the volcanic rocks of the Grizzly and Diamond mountains. New geologic mapping by the authors and radiometric dating reveal that substantial revision is necessary in the age assignments of the rocks, as well as the stratigraphic framework described by Durrell (1959a).

Previous work and nomenclature of Sierran volcanic rocks

A wealth of information on the Cenozoic volcanic rocks of the Sierra Nevada is available in the earlier papers on Sierran geology (Whitney, 1865; Turner, 1894, 1896; Ransome, 1898; Diller, 1908; Lindgren, 1911). These papers, together with the U.S. Geological Survey folios (Gold Belt Folios) by Lindgren, Turner and Ransome published between 1894 and 1900, established the Cenozoic stratigraphic framework of the Sierra Nevada.

Lindgren (1911, p. 31) summarized the Cenozoic volcanic sequence as follows:

a. Quaternary basalt: Primarily exposed in the Lassen, Susanville and Truckee areas.

b. Doleritic basalt: This was called Warner Basalt by Durrell (1959a) where it occurs in the Blairsden Quadrangle.

c. Andesite breccia, tuff and some flows: Andesitic rocks erupted from vents along the crest of the Sierra and are widespread throughout the central and northern Sierra Nevada. These are the Ingalls, Bonta and Penman formations of Durrell (1959a) on the Blairsden Quadrangle and the Mehrten Formation of Piper and others (1939) in the central Sierran foothills.

---

[1] California Department of Conservation, Division of Mines and Geology

[2] Colorado School of Mines

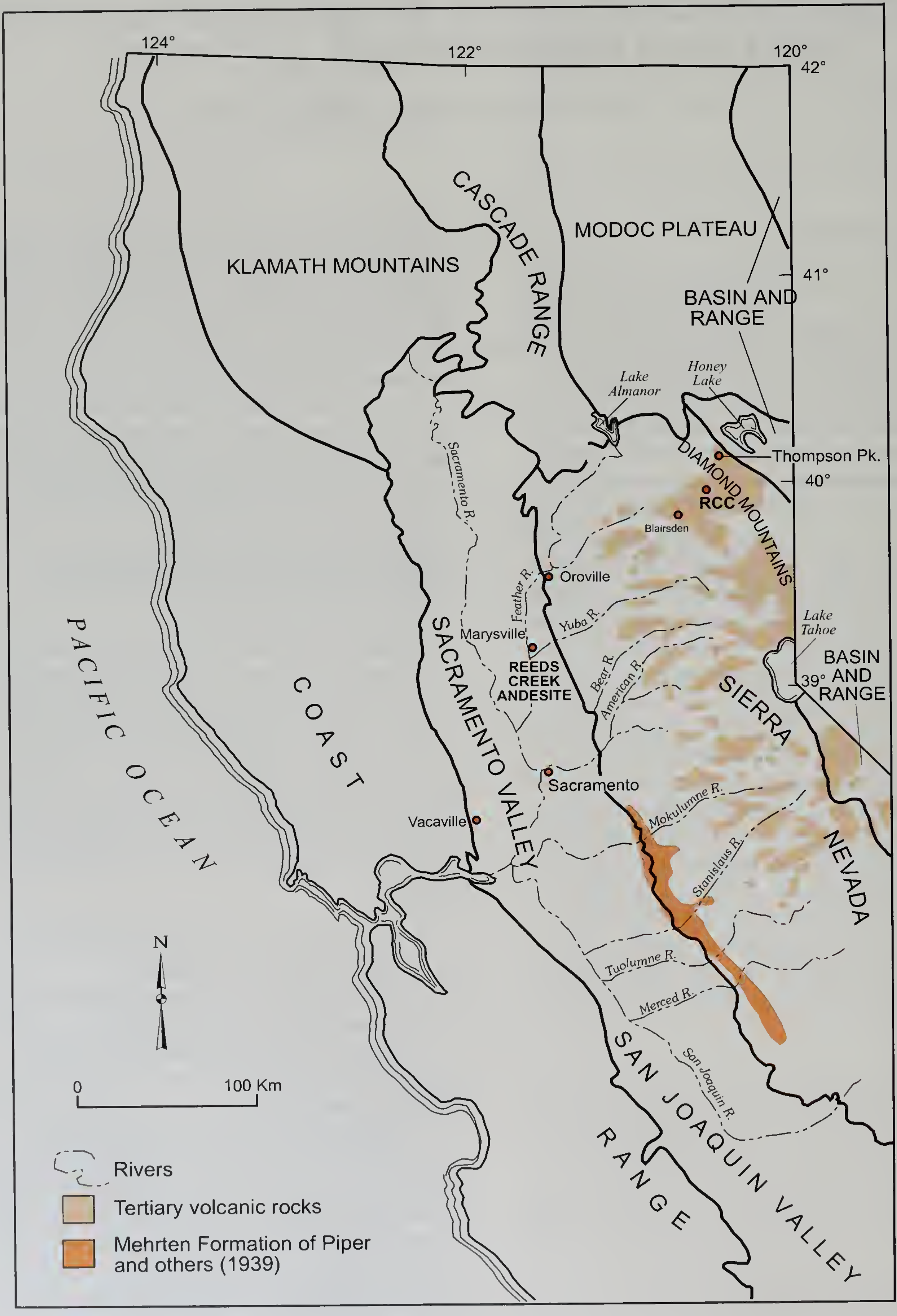

Figure 1. Map showing features and localities mentioned in text.

d. Older basalt: This was named the Lovejoy Formation by Durrell (1959a,b) and is the cap rock of Oroville Table Mountain.

e. Rhyolite tuff and associated sedimentary rocks: This rhyolitic unit was named the Valley Springs Formation by Piper and others (1939) in the central Sierran foothills and the Delleker Formation by Durrell (1959a) in the northern Sierra.

This sequence of volcanic rocks rests variously on pre-Cenozoic bedrock, "auriferous gravels" of Eocene age, or the Ione Formation of Eocene age. No formal formation names were proposed by Lindgren (1911) and the Cenozoic volcanic rocks of the central and northern Sierra were simply referred to as Tertiary or "Neocene" [*sic*] volcanics in the Gold Belt Folios.

Clark and Anderson (1938) argued that at least some of the andesite in the northern Sierra is as old as Eocene to Oligocene. Their contention was based on andesite pebbles, which they believed to be correlative with the Tertiary andesites of the Sierra Nevada, that were found in the Wheatland Formation along with Eocene fossils. Their paper was important because it exerted a major influence on later workers, such as Creely (1955, 1965) and Durrell (1959a,b, 1966). Durrell (1959a) indicated his Ingalls Formation could be correlative with the Wheatland Formation. However, Wagner and Saucedo (1990a) showed the andesite at Reeds Creek, the purported source of andesite pebbles in the Wheatland Formation, ranges in age from 18.0 to 8.4 Ma and concluded that andesitic rocks in the northern Sierra are younger than the Wheatland Formation.

Piper and others (1939) introduced the name Mehrten Formation for the well-bedded andesitic volcanic and volcaniclastic rocks exposed in the Mokelumne River area (Figure 1). They did not restrict the name to the Mokelumne area, stating that similar rocks are widespread on the west slope of the Sierra Nevada. Curtis (1954, p. 457) greatly expanded the term Mehrten Formation to include "...all the deposits of clastic and pyroclastic material of predominantly andesitic composition deposited on the Sierra Nevada and contiguous terrain during this volcanic epoch." Although the term Mehrten was never formally expanded as suggested by Curtis (1954), many geologists informally apply the name to all the Tertiary andesitic rocks of the Sierra Nevada. In the Oroville area, Creely (1955, 1965) provisionally mapped andesitic tuff, tuff-breccia and sedimentary andesitic rocks as Mehrten Formation.

Durrell (1959a) divided the Tertiary volcanic rocks of the Blairsden Quadrangle into six formations. Durrell (1959a, p. 165) argued these formations extend beyond the Blairsden Quadrangle and are separated by unconformities. The oldest formation, according to Durrell (1959a), is the Lovejoy Formation. In a companion paper, Durrell (1959b) correlated the Lovejoy Formation with basalt that is present in the subsurface beneath much of the Sacramento Valley and with the Putnam Peak Basalt of Weaver (1949) exposed near Vacaville (Figure 1). Although later work (Grommé, 1963; Siegel, 1988) has supported Durrell's (1959b) correlation, the age of the Lovejoy Formation remains controversial. Durrell (1959a,b) maintained that the Lovejoy Formation is Eocene.

Dalrymple (1964) questioned the Eocene age for the Lovejoy Formation because he obtained a 24.4±0.6 Ma (K/Ar dates reported prior to 1977 were recalculated, using new constants, by Saucedo and others, 1992) potassium-argon date on dacite tuff beneath the Lovejoy Formation at Oroville Table Mountain. Dalrymple (1964) also obtained a 22.8±0.4 Ma potassium-argon date on the Delleker Formation on the Blairsden Quadrangle, which according to Durrell (1959a) overlies the Lovejoy Formation. Dalrymple (1964) concluded the age of the Lovejoy Basalt must be between 22.8 and 24.4 Ma, or early Miocene. Roberts (1985) reported a 16.3 Ma date from rocks that may be Lovejoy Basalt at Thompson Peak near Susanville. Page and others (1995) dated three specimens collected from widely-spaced Lovejoy localities using Ar/Ar step-heating and concluded the basalt is 16 Ma.

As Dalrymple (1964) pointed out, the age assignments made by Durrell (1959a) for the volcanic formations in the Blairsden Quadrangle imply the Tertiary volcanic history of the northern Sierra Nevada is different from that of the central Sierra Nevada.

Stratigraphy of the Blairsden Quadrangle

Durrell (1959a) divided the Tertiary rocks of the Blairsden Quadrangle into eight formations (Figure 2). Only the six volcanic formations are pertinent to this discussion. Durrell (1959a) made some important departures from Lindgren's (1911) ideas of the geologic history of the Sierra, which profoundly affected the stratigraphic interpretations he made in the Blairsden area. Lindgren (1911) believed the Tertiary drainages of the Sierra had headwaters within an ancestral Sierra and that uplift of the present range began just after emplacement of the Miocene rhyolitic rocks. Uplift continued during and after the Miocene-Pliocene volcanism that produced andesitic rocks from volcanoes along the crest of the range. On the other hand, Durrell (1959a,b, 1966, 1987) believed the headwaters of the Tertiary rivers were east of the present range and that uplift of the Sierra did not begin until after the Pliocene. Moreover, he believed that of the volcanic formations, only the Lovejoy Formation was restricted to a valley; the Ingalls, Bonta and Penman formations were deposited as sheets on a nearly flat topographic surface. Workers in the central Sierra (Piper and others, 1939; Curtis, 1951, 1954; Slemmons, 1966; Brem, 1977; Wagner 1981), agreed with Lindgren (1911) that the andesites were emplaced over a pre-existing topography of significant relief.

Lovejoy Formation The Lovejoy Formation (also formally known as the Lovejoy Basalt; the usage preferred in this paper) consists of as many as 15 flows of olivine basalt (Photo 1). It is a distinctive, unusually hard basalt that is black on fresh surfaces and chocolate-brown when weathered and has characteristic fracturing yielding curved-sided blocks. It usually forms flat-topped ridges devoid of soil and vegetation save brightly colored lichens. The Lovejoy extends northeast from the Blairsden Quadrangle to an abrupt termination at the escarpment above Honey Lake in the Thomp-

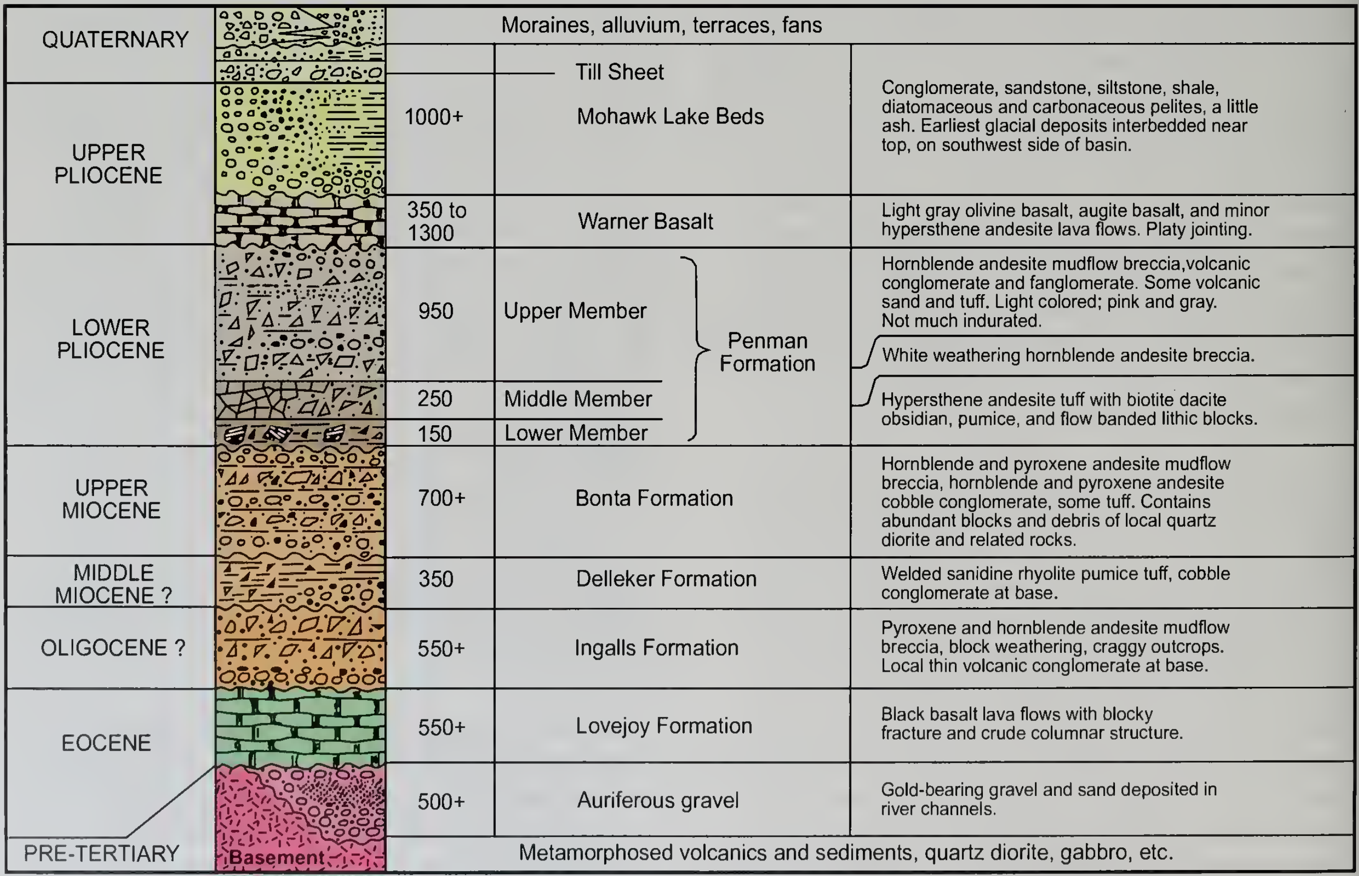

QUATERNARY		Moraines, alluvium, terraces, fans		
UPPER PLIOCENE		Till Sheet		Conglomerate, sandstone, siltstone, shale, diatomaceous and carbonaceous pelites, a little ash. Earliest glacial deposits interbedded near top, on southwest side of basin.
	1000+	Mohawk Lake Beds		
	350 to 1300	Warner Basalt		Light gray olivine basalt, augite basalt, and minor hypersthene andesite lava flows. Platy jointing.
LOWER PLIOCENE	950	Upper Member	Penman Formation	Hornblende andesite mudflow breccia,volcanic conglomerate and fanglomerate. Some volcanic sand and tuff. Light colored; pink and gray. Not much indurated.
	250	Middle Member		White weathering hornblende andesite breccia.
	150	Lower Member		Hypersthene andesite tuff with biotite dacite obsidian, pumice, and flow banded lithic blocks.
UPPER MIOCENE	700+	Bonta Formation		Hornblende and pyroxene andesite mudflow breccia, hornblende and pyroxene andesite cobble conglomerate, some tuff. Contains abundant blocks and debris of local quartz diorite and related rocks.
MIDDLE MIOCENE ?	350	Delleker Formation		Welded sanidine rhyolite pumice tuff, cobble conglomerate at base.
OLIGOCENE ?	550+	Ingalls Formation		Pyroxene and hornblende andesite mudflow breccia, block weathering, craggy outcrops. Local thin volcanic conglomerate at base.
EOCENE	550+	Lovejoy Formation		Black basalt lava flows with blocky fracture and crude columnar structure.
	500+	Auriferous gravel		Gold-bearing gravel and sand deposited in river channels.
PRE-TERTIARY		Metamorphosed volcanics and sediments, quartz diorite, gabbro, etc.		

Figure 2. Stratigraphy of the Blairsden Quadrangle established by Durrell (1959a).

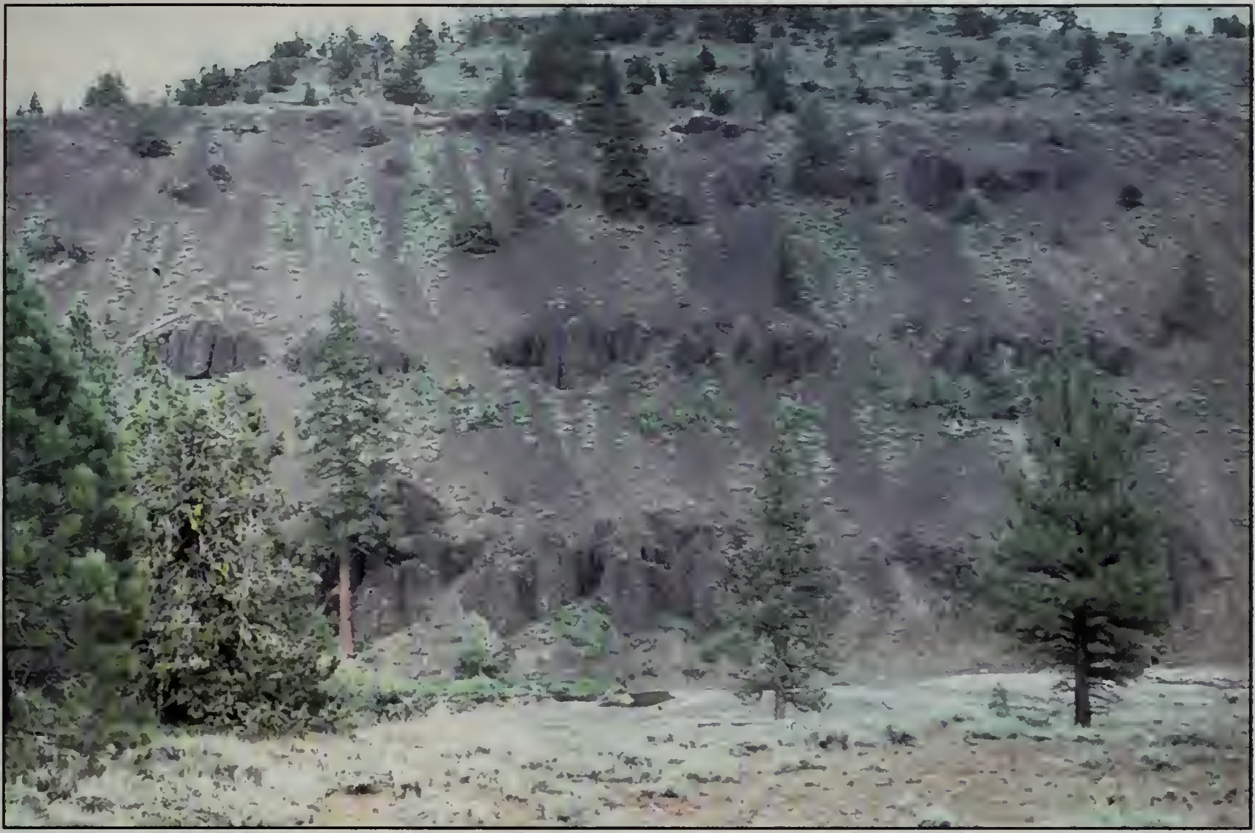

Photo 1. Lovejoy Basalt exposed along Red Clover Creek designated as the type locality by Durrell (1959b). According to Durrell (1959b) there are nine flows varying from 10 to 50 feet thick. *Photo by David L. Wagner.*

son Peak area. Durrell (1959a,b) believed the source of the Lovejoy Basalt lay east of the escarpment, but mapping by Roberts (1985) and Wagner and Saucedo (1990b) suggests the source of the Lovejoy is along the Honey Lake escarpment. Fluid Lovejoy Basalt flowed south from Thompson Peak, turned westward and flowed across the Sierra, flooding much of the Tertiary Sacramento Valley (Figure 3) to near Vacaville where it is exposed as the Putnam Peak Basalt of Weaver (1949). Durrell (1987) estimated that the volume of Lovejoy Basalt erupted was 37 cubic miles, covering an area of 50,000 square miles.

The age of the Lovejoy has been controversial for years. Durrell (1959a,b, 1966, 1987) steadfastly believed in an Eocene age. Radiometric data on the other hand, suggest a Miocene age (Dalrymple, 1964; Roberts, 1985; Wagner and Saucedo, 1990a; Page and others, 1995). Argon retention problems have hampered dating the Lovejoy Basalt by K/Ar method (Dalrymple, 1964). Of the 15 K/Ar dates on the Lovejoy we are aware of, nine fall within the 14 to 17 Ma age range. Recently, Page and others (1995) reported dates for the Lovejoy using the Ar/Ar step-heating method and concluded the Lovejoy is 16 Ma. Thus, the presently accepted interpretation of the available data indicates the Lovejoy Basalt is approximately 16 million years old. This means the Lovejoy is broadly coeval with the Columbia River Basalt Group and the Steens Basalt of southeast Oregon (Carlson and Hart, 1988), as well as the basalts erupted from the northern Nevada rift (Zoback and Thompson, 1978; Zoback and others, 1994). The significance of this will be described in more detail below.

Ingalls, Bonta, Penman formations Durrell (1959a,b) formally defined these three formations, all composed of andesitic mudflows, breccia, conglomerate, sandstone and some lava flows. Grose (in preparation), mapping on the Blairsden and the adjacent quadrangles, as well as Grose and others

(1991) in the Diamond Mountains to the north have been unable to recognize Durrell's formations as mappable units. Durrell (1959a) argued that the Ingalls is probably Oligocene, the Bonta is Miocene and the Penman is Pliocene. Saucedo and Wagner (1992) obtained radiometric dates from localities designated by Durrell (written communication to DMG) as characteristic Ingalls and Penman. The Ingalls date is 11.3±0.7 Ma and Penman dates are 13.6±0.7 Ma and 6.8±0.7 Ma. Durrell (personal communication, 1984; reported in Saucedo and others, 1992) obtained a date of 19.7±2.3 Ma for the Bonta Formation. Page and others (1995) summarized available radiometric data and concluded that rocks considered Ingalls are 11 to 14 Ma, rocks considered Bonta are 11 to 19.7 Ma and those considered to be Penman are 7 to 14 Ma. Durrell (1966, p. 191) believed that only the Bonta and Penman formations could be equivalent to the Mehrten Formation of the central Sierra. It appears to us that the bulk of the Tertiary andesites of the northern Sierra are equivalent to the Mehrten Formation as defined by Curtis in 1954.

Warner Basalt Durrell (1959a) correlated the Doleritic basalt of Turner (1896) on the Blairsden Quadrangle with the Warner Basalt of the Warner Mountains of northeastern California. However, according to Hannah (1977) the term "Warner Basalt" is a collective term for similar looking basalts

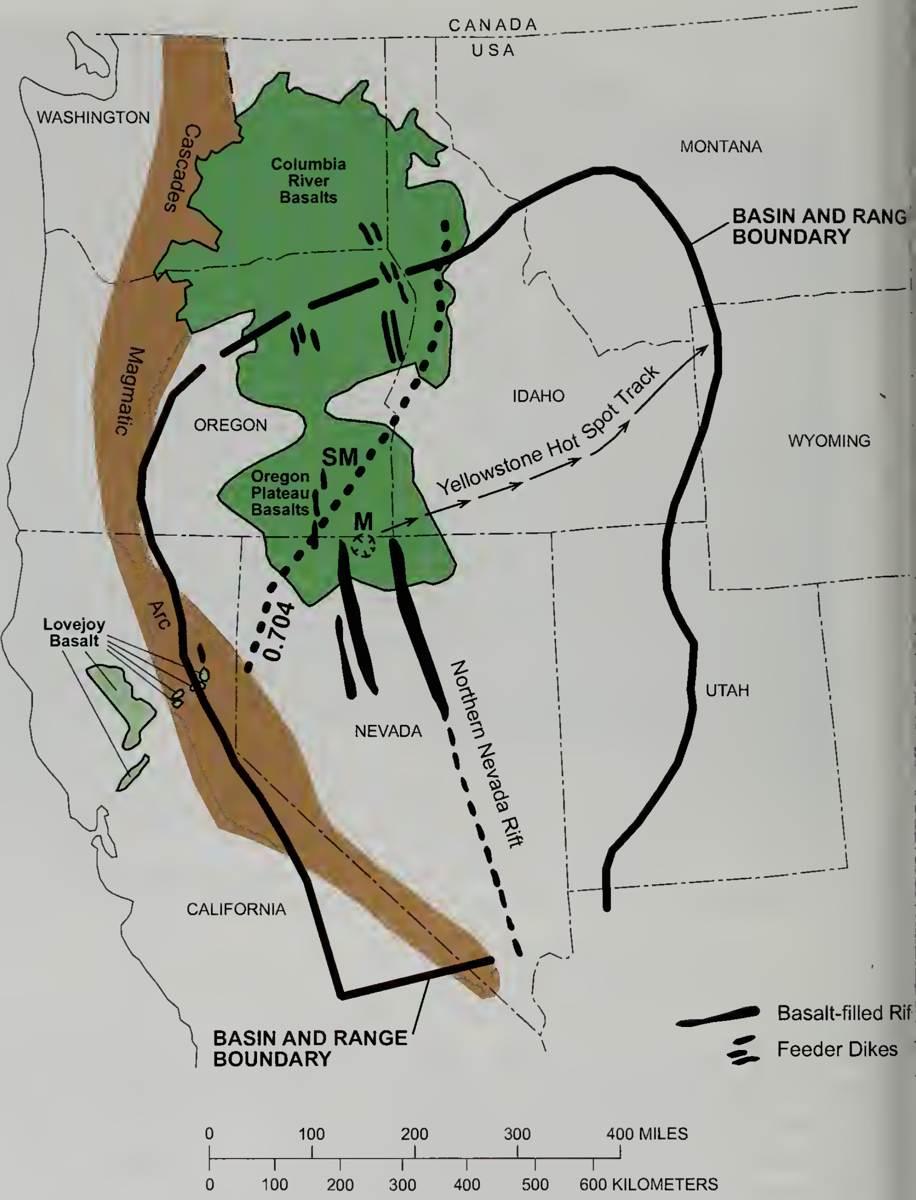

Figure 3. Major volcano-tectonic features of the western United States about 16 Ma. Revised from Durrell (1959b), Pierce and Morgan (1992), Christiansen and Yeats (1992), and Dickinson (1997). **SM**—Steens Mountain. **M**—McDermitt caldera. The Lovejoy Basalt erupted along the western boundary of the Basin and Range Province approximately the same time as the eruption of the Columbia River and Oregon Plateau basalts, as well as basalts along the northern Nevada and associated rifts. The Lovejoy Basalt erupted from vents along the incipient boundary of the Basin and Range at 16 Ma and flowed westward to the Great Valley of California where it is now largely buried by late Cenozoic valley fill. According to Pierce and Morgan (1992), a mantle plume rose and encountered thin, rifted crust near the present location of McDermitt. The plume intercepted the base of the crust and spread laterally, providing magma to feeder vents along the northern Nevada rift, at Steens Mountain, and in the Columbia Plateau. We speculate that effects of the plume may have extended to the west boundary of the Basin and Range, and provided magma to feeder vents from which the Lovejoy Basalt erupted. The ^{87}Sr/^{86}Sr=0.704 line is the eastern boundary of Mesozoic oceanic accreted terranes.

throughout northeastern California and does not imply contemporaneity. Duffield and McKee (1986) reviewed regional correlations of the Warner Basalt and concluded it was not a meaningful lithostratigraphic unit. Saucedo and others (1992) reported a radiometric date of 11.4±0.7 Ma for the rocks mapped as intrusive Warner Basalt near Red Clover Creek. Grose (in preparation) mapped the Warner Basalt of Durrell (1959a) on the Blairsden Quadrangle as unnamed mafic andesite and basalt.

DISCUSSION

Volcanism lasted from the Oligocene to the Pleistocene in the northern Sierra. The amounts of gravel and sand in the volcanic section attest to long periods of erosion sufficient to carve new canyons and valleys. Younger lahars, flows and tuffs followed and often filled drainages cut into older volcanic rocks. Subsequent erosion produced still newer drainages cut into older volcaniclastic deposits creating confusing outcrop patterns. Without radiometric dating and detailed geologic mapping, it is difficult if not impossible, to sort out stratigraphic relationships and reconstruct stratigraphic sequences. Durrell's age assignments were made prior to the development of radiometric dating and were based on sparse and imprecise plant fossils as well as superposition. Determining relative age of units based on superposition of units is especially difficult in volcanic terranes where standard stratigraphic techniques are often not applicable (Williams and McBirney, 1979, p. 310-16).

Red Clover Creek (Figure 1), in the northeast corner of the Blairsden Quadrangle, is the best locality to observe the stratigraphy established by Durrell (1959a,b, 1966, 1987) and examine the problems of working in volcanic terranes. Although contacts between units are difficult to observe, there is an apparent sequence of units conforming to the stratigraphy of Durrell. Radiometric dating by Siegel (1988) shows that andesite assigned to the Ingalls Formation at Red Clover Creek is mid-Miocene, while dates by Siegel (1988) and Dalrymple (1964) on rhyolitic tuff of the Delleker Formation topographically higher to be earliest Miocene to (Siegel, 1988). This is the reverse of Durrell's sequence.

Thompson Peak, overlooking Honey Lake is the eastern terminus of Lovejoy Basalt. In the past, the source of the Lovejoy has been presumed to lie to the east because of the abrupt termination of the basalt along the Honey Lake escarpment. Our mapping across Honey Lake Basin shows there are no similar rocks exposed as far east as the Nevada border or northward to at least 41° latitude. As mentioned earlier, the Lovejoy is probably 16 million years old, making it approximately the same age as an intense 14 to 17 Ma volcano-tectonic episode marked by widespread basalt magmatism in the northern Great Basin and the Pacific Northwest to the east of the Cascade volcanic arc (Figure 3). The Lovejoy Basalt is chemically similar to the Columbia River Basalt Group (Doukas, 1983; Siegel, 1988), but the previously uncertain age assignment of the Lovejoy prevented meaningful temporal correlation. Outpouring of basalts in the Columbia Plateau, the Oregon Plateau and northern Nevada immediately followed the inception of Basin and Range faulting at about 17 Ma (Noble, 1972; Christiansen and McKee, 1978; McKee and Noble, 1986; Zoback and others, 1994). We speculate the Lovejoy Basalt erupted from a fissure associated with a major crustal fracture zone that would later become the Honey Lake escarpment, and flowed west down the paleoslope of the Sierra around the same time. Honey Lake Basin had not yet formed or it would have filled with basalt. A well drilled to granitic basement in the basin did not penetrate basalt nor does gravity modeling of the basin suggest the presence of large amounts of basalt in the subsurface (Ceron, 1992). Lovejoy Basalt on Thompson Peak forms a linear belt along the northwest-trending Honey Lake escarpment suggesting the feeder vents were also trending northwest, parallel to the feeder dikes of the Columbia River and the Oregon Plateau basalts, and the northern Nevada rift. This suggests all these fissures developed in response to same stress regime. The cause of this stress pattern is thought to be shearing due to development of the San Andreas Fault System (Christiansen and McKee, 1978; McKee and Noble, 1986; Dickinson, 1997).

The major current hypotheses for the flood basalts in the Pacific Northwest are: 1) they are associated with back-arc rifting or spreading (Christainsen and McKee, 1978); 2) they are associated with a mantle plume that was a precursor to the Yellowstone hot spot (Pierce and Morgan, 1992); and 3) they are the result of a meteorite impact (Alt and others, 1990). Our interpretation is consistent with either of the first two hypotheses. The 14 to 17 Ma flood basalts of the Great Basin have been linked to the mantle plume that evolved into the Yellowstone Hot Spot (Pierce and Morgan, 1992; Dickinson, 1997). Pierce and Morgan (1992) hypothesized that a mantle plume intercepted the base of the crust at 16 Ma, marked by the McDermitt caldera on the Oregon-Nevada border (Figure 3). During ascent, decompression melting produced large volumes of basaltic magma that vented through rifts as flood basalts. According to Pierce and Morgan (1992) the plume was 600 kilometers (km) in diameter when it encountered the base of the lithosphere, so it could have vented basaltic magma through fissures along the future Honey Lake escarpment.

Acknowledgments

We appreciate the careful reviews by Jim Smith of the U.S. Geological Survey and Alan Deino of the Berkeley Geochronology Center, both of whom greatly improved the manuscript. Peggy Walker, Ed Foster, Jim Williams, Dinah Maldonado and Frances Rubish of the Department of Conservation's Division of Mines and Geology prepared the graphics.

ROAD LOG (Figure 4)

The trip begins at the Feather River Inn, on Hwy 70, immediately north of the intersection with Hwy 89. If you are taking a self-guided tour, we recommend a U.S. Forest Service (USFS) map of the Plumas National Forest; some of the roads described here may not show on highway road maps.

Mileage

0.0 Feather River Inn (east side of Hwy 70 immediately north of the Hwy 89 junction). Here we are on the so-called "Mohawk Lake beds" of Turner (1891). Turner (1891) and (Durrell, 1959a, 1987) thought these deposits accumulated in a deep-water lake but more recent studies by Yount and others (1993) indicate most of the deposits are fluvial, marsh, and glacial sediments that accumulated in valleys similar to Sierra Valley today. Therefore, these sediments will be referred to informally here as the Mohawk beds. There are good exposures of the Mohawk beds in roadcuts along Hwy 70 for the first few miles of the trip. The Feather River Inn is in the drainage of Bonta Creek. Durrell's (1959a) Bonta Formation is named for Bonta Creek, but there is no designated type locality for the Bonta. Bonta Creek drains the western slope of Penman Peak, the namesake for the Penman Formation of Durrell (1959a). Head east on Hwy 70.

1.7 Good exposures of the Bonta Formation of Durrell (1959a,b) can be seen in the roadcuts to the left (north).

2.2 On the left (north) is a contact mapped by Durrell (unpublished map) between the Bonta and Penman formations. The Penman is overlapped by the Mohawk beds in the upper part of the roadcut.

2.5 In the roadcut to the left (north), Mohawk beds overlie rhyolitic tuffs of the Delleker Formation of Durrell (1959a).

2.8 Rocks of the Penman Formation considered by Durrell (1959a) to be Pliocene are exposed in the roadcut to the left. Saucedo and others (1992) reported a date of 13.6±0.7 Ma for andesite from this locality indicating a mid-Miocene age for these rocks.

3.7 Straight ahead, south of the highway is Beckwourth Peak. Its slopes are of Miocene-Pliocene andesite breccia and it is capped by Miocene andesite flows (9.23±0.08 Ma, Grose, in preparation).

3.8 Coarse gravels of the Mohawk beds.

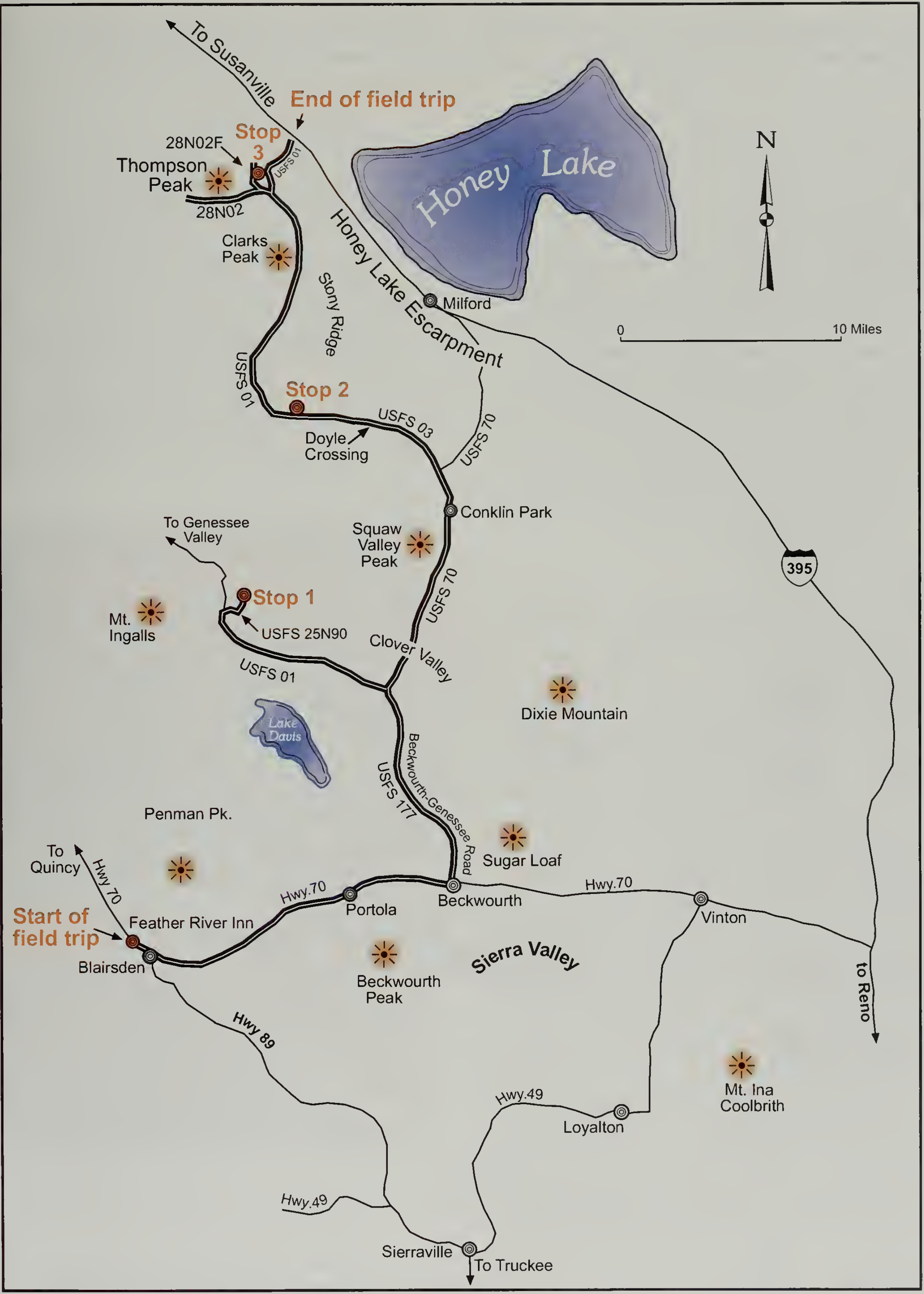

Figure 4. Road map of the field trip and locations of some features mentioned in the text.

4.9 We are crossing granitic rocks of the Sierran Batholith overlain by Mohawk beds that are exposed as we enter Humbug Valley.

8.1 Delleker, the namesake for Durrell's (1959a) Delleker Formation.

9.0 Entering Portola. To the left is Delleker Formation overlain by river gravels.

11.4 Ridge of Sierran granitic rock is exposed in the pass leading to the Sierra Valley. On the right (south) the Feather River has cut a deep gorge through granitic rock and an altered andesite intrusive dated at 12.25±0.20 Ma (Grose, 1999c). Once we are through the pass and into Sierra Valley, the headwaters of the Middle Fork of the Feather River are to the right (south) in a maze of waterways known as the "Channels of Sierra Valley."

15.1 Turn left (north) at the town of Beckwourth on the Beckwourth-Genesee Road (USFS Primary Road 177; county road 111). Beckwourth, Beckwourth Peak and Beckwourth Pass to the east are named for Jim Beckwourth, a "black mountain man, war chief of the Crows, trader, trapper, explorer, frontiersman, guide, scout, interpreter, adventurer, and gaudy liar" (Wilson, 1972). In 1850 or 1851, Beckwourth discovered the pass that bears his name and blazed an emigrant trail across the Sierra to Marysville. The highest peak to the southeast across Sierra Valley is Mt. Ina Coolbrith, named for the first poet laureate of California who, as a young girl, came with her family to California in 1851. Her family was in the lead wagon of the first wagon train to use the trail in 1851, guided by Jim Beckwourth. To the right is Sugar Loaf, an andesitic intrusive that is probably related to a volcanic center on the southeast side of Sierra Valley near Loyalton that is 13.3±0.5 million years old (Saucedo and others, 1992).

20.1 Ahead is an andesitic volcanic neck also associated with the Dixie Mountain volcano. Note the vertical and recumbent columnar jointing.

23.5 Entering Clover Valley. Looking southeast across Clover Valley you can see Dixie Mountain, an eroded remnant of a 10 million-year old volcano that was comparable in size to Mt. Shasta (Grose, 2000).

24.5 Intersection with USFS Primary Road 70. Keep heading northwest along Beckwourth-Genesee Road. The high mountain on the northwest skyline is Mt. Ingalls, dated at 4.7±0.1 Ma (Grose, in preparation). It is the youngest and biggest volcano in this general area.

30.5 Intersection with USFS road 25N05. Remain on Beckwourth-Genesee Road.

31.2 Intersection with USFS road from Lake Davis via Bagley Pass. According to Durrell (1987) there are good exposures of his Bonta Formation near Bagely Pass. Keep heading toward Genesee.

33.4 Turn right on USFS road 25N90. This road has a steep section that usually requires 4WD to make the return trip. If you do not have 4WD you should park at the drop-off and walk to the parking place 0.8 mi. from the intersection.

Stop 1. (Figures 4 and 5)

This is Red Clover Creek, the type locality of the Lovejoy Basalt and the best place to observe the stratigraphic succession of Durrell (1959a). Dalrymple (1964), Seigel (1988), Abrams (1991), Grose (in preparation), and the authors have investigated this locality. The purpose of this stop is to demonstrate complex relationships between the volcanic units and to see how different investigators reached conflicting conclusions. Durrell (1959a) mapped a succession of Lovejoy overlain by Ingalls Formation andesitic breccia, overlain by Delleker Formation rhyolite tuff, which is in turn overlain by Bonta andesitic breccia (Figure 5). Dalrymple (1964) reported an age of 22.8±0.4 Ma for the Delleker Formation here and Siegel (1988) obtained an average age of 30 Ma for the Delleker at this locality, consistent with the age range of rhyolitic tuffs elsewhere in the Sierra Nevada and the northern Great Basin (Deino, 1985). If one accepts the most recent dating of Page and others (1995), the Lovejoy Basalt is 16 Ma. However, Siegel (1988) obtained a date of 14.35 Ma for the Ingalls here. Clearly, the radiometric ages do not substantiate the sequence as mapped by Durrell (1959a), though in the absence of radiometric data, the sequence does indeed seem to be as Durrell described it.

Figure 5 is a geologic map modified from Durrell (1959b) showing the traverse at this stop. Proceed to the southeast along the creek (Site 1, Figure 5) where a contact between Lovejoy Basalt and Ingalls Formation andesite breccia is exposed. Here the andesite mapped as Ingalls Formation appears to overlie the Lovejoy Basalt. Proceed downstream (northwest) to Site 2 (Figure 5). Here is a small body of andesite breccia (Photo 2) mapped by Durrell

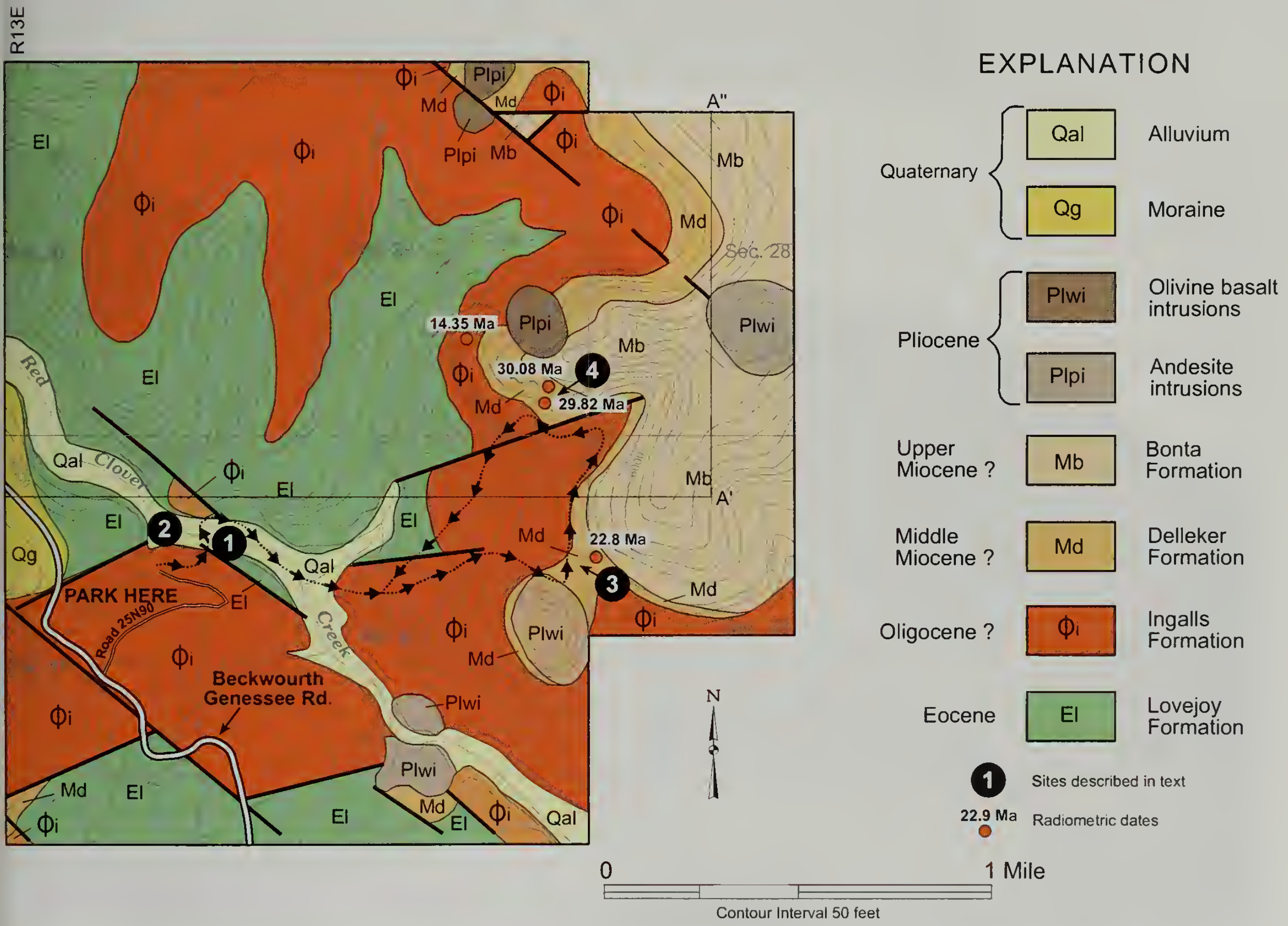

Geology - Cordell Durrell (1959a,b)

Figure 5. Geologic map of the Red Clover Creek locality modified from Durrell (1959b). The numbered points of interest are described in the road log. A schematic block diagram along line A – A' – A" on Figure 6 shows our intrepretation of this area.

(1959b) as Ingalls Formation in fault contact with the Lovejoy Basalt, whereas Abrams (1991) contended the andesite breccia rests depositionally upon the Lovejoy. There are two exposures here, one upslope above the andesite and another in the streambed, that we think show that this andesite breccia actually underlies the basalt (Photos 2 and 3). Andesite breccia mapped as Ingalls Formation (Durrell, 1959b; Abrams, 1991) caps the ridge. It appears to us that andesite breccia mapped as Ingalls Formation occurs both above and below the Lovejoy Basalt at this locality.

Return upstream (southeast) along the east side of the creek, cross a willow thicket and head uphill. After passing two large granitic blocks (you may want to try to determine whether these are bedrock exposures or large accidental clasts in mudflow) proceed up the slope. This is typical andesitic mudflow breccia of the Ingalls Formation. Continue east-southeast upslope to the logging road and proceed east to the saddle where light colored tuff of the Delleker Formation is exposed (Site 3, Figure 5). This is where Dalrymple (1964) obtained a date of 22.8±0.4 Ma. This date, along with a date on a dacite tuff beneath the Lovejoy Basalt at Oroville Table Mountain, led Dalrymple to bracket the age of the Lovejoy between 22.2 and 23.8 Ma.

Head north along the logging road to Site 4 (Figure 5). Siegel (1988) reported $^{40}Ar/^{39}Ar$ dates of 30.08±0.6 Ma and 29.82±0.17 Ma on the rhyolite of the Delleker Formation. In addition, Siegel

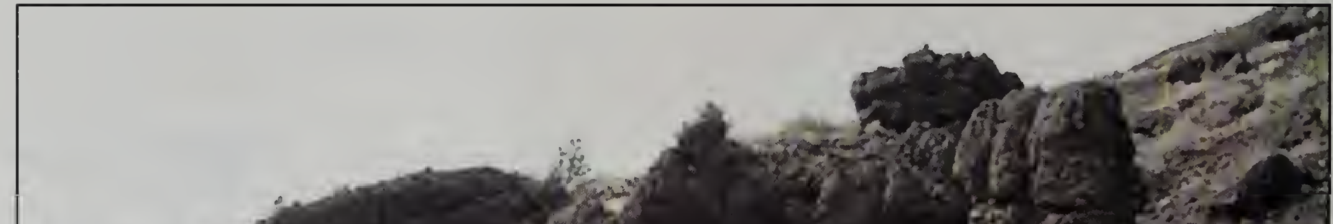

Photo 2. Andesitic mudflow along Red Clover Creek. This is Site 2 on Figure 5. This patch was mapped as Ingalls Formation in fault contact with Lovejoy Basalt by Durrell (1959b) and shown by Abrams (1991) as overlying Lovejoy. However, there are two exposures of the contact here (one is shown on Photo 3) indicating the Lovejoy Basalt flowed over the andesite, and therefore cannot be the oldest volcanic unit here. *Photo by David L. Wagner.*

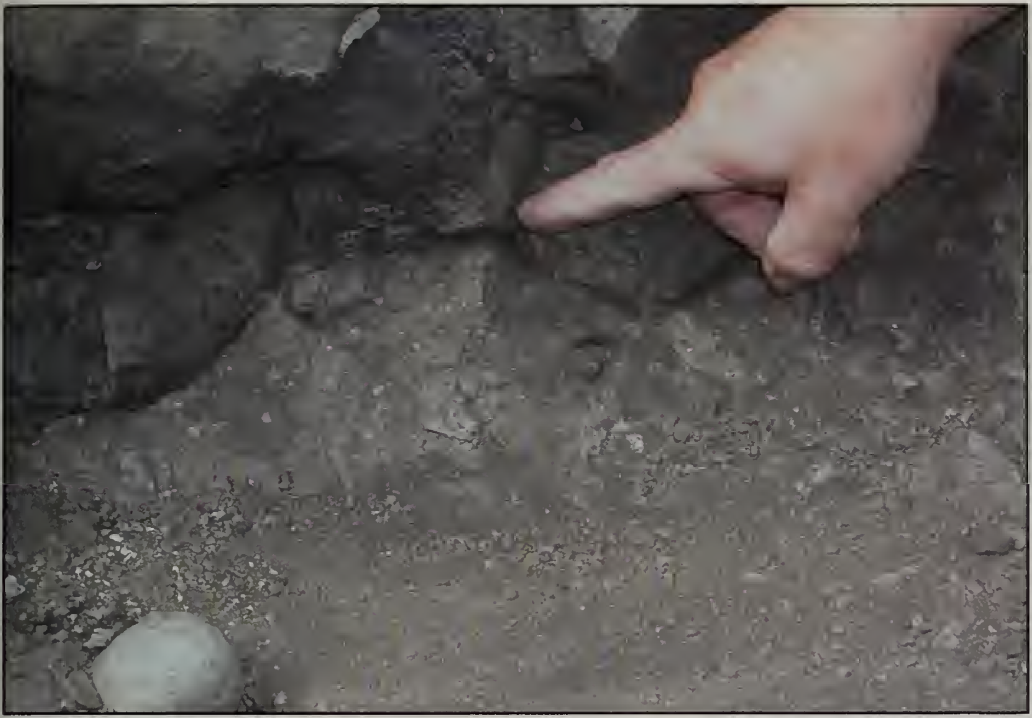

Photo 3. Contact between the Lovejoy Basalt (upper part of photo) and andesitic mudflow. This exposure is upslope from the creek. There is a second exposure in the creek bed where Lovejoy Basalt appears to overlie andesite breccia. *Photo by David L. Wagner.*

(1988) reported an $^{40}Ar/^{39}Ar$ date of 14.35 ±0.66 on andesite that seems to underlie the Delleker tuff. Although Siegel's date was analytically sound, he felt it was incorrect because he was convinced the sequence mapped here by Durrell was correct. Our interpretation of the geologic history at this locality is summarized on Figure 6. Radiometric data here and elsewhere, however, indicate the Delleker rhyolite is the oldest Tertiary volcanic unit in the region and ranges in age from late Oligocene to early Miocene. Erosion followed deposition of the rhyolite. The next unit to be deposited was the andesite breccia of unknown age that underlies the Lovejoy at Site 2. The oldest known andesite in the Blairsden area is dated at 19.7 Ma (by Durrell, 1984, reported in Saucedo and others, 1992). Another episode of erosion ensued and at 16 Ma the fluid Lovejoy Basalt flowed from the northeast down a channel cut into the older units. Another erosional episode was followed by deposition of the 14.35 million year-old andesite mudflow breccia. Volcanism continued through the Miocene and into the Pliocene. Return to the Beckwourth-Genesee Road and backtrack to the intersection with USFS road 70.

42.3 Head north across Clover Valley. To the southeast is the Dixie Mountain volcanic center. It is the source of much of the andesite in this area.

46.8 Ahead is Squaw Valley Peak, an andesite flow from the Dixie Mountain volcano that flowed nearly east-west across older northwest flowing andesitic mudflows, also from Dixie Mountain volcano.

48.8 Passing through granitic basement unconformably underlying the volcanic rocks in this area.

51.5 Entrance to Conklin Park Campground. Restrooms available.

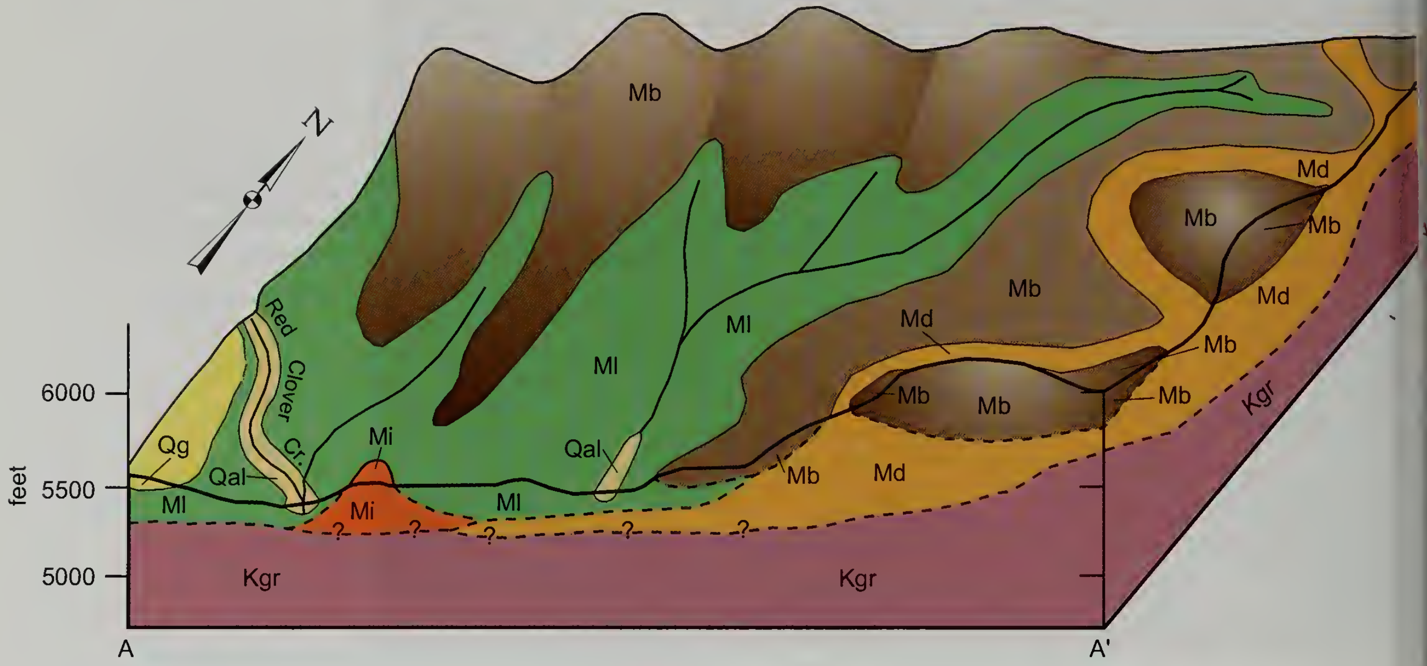

Figure 6. Schematic block diagram modified from Figure 5 based on radiometric dates and our interpretation of the Red Clover Creek locality. Younger intrusive rocks are not shown for simplicity. The Tertiary volcanic section rests on Cretaceous granitic rocks (Kgr). The oldest Tertiary volcanic rocks are the rhyolitic tuffs of the Delleker Formation (Md) ranging from 30.8 to 22.8 Ma erupted from sources to the east. After a period of erosion that left a topographic high underlain by Delleker rhyolite tuff, the oldest andesites were emplaced, presumably between 19.7 and 16 Ma, shown as Mi on this diagram and at site 2 on Figure 5. Most of this older andesite breccia was removed prior to the emplacement of the Lovejoy Basalt at 16 Ma. Lovejoy Basalt flowed over the existing topography underlain by granitic rock (Kgr), Delleker Formation (Md) and the older andesite breccia (Mi). Andesitic volcanism continued after 16 Ma and lasted until at least 6.8 Ma in this area. Andesitic rocks mapped by Durrell (1959a,b) as Penman formations, and Warner Basalt are shown on this diagram as Mb. Erosion since the Pliocene resulted in the exposure we see now.

54.0 Intersection with the road to Milford. Head north on road 03 toward Doyle Crossing. Here we are at the contact between andesite breccia considered by Durrell (unpublished data) to be Ingalls Formation and granitic bedrock. The ridge to the north is granitic rock that also is exposed in the valley bottom. Thus, there is approximately 870 feet of relief in the bedrock in this region. This, plus the outcrop pattern of the granitic rock, indicates there is significant paleotopography in this region.

59.8 To the north across the valley light-colored granitic rock is exposed in the burned area. This is a paleoridge with andesite mudflows on both sides.

61.6 Cross the bridge and keep to the left on road 03. This is the south end of Stony Ridge, one of the largest masses of Lovejoy Basalt. It extends northward to an abrupt termination at the Honey Lake escarpment. Proceed 0.7 mi. and park.

Stop 2 (62.3 miles)

Here andesite mudflow breccia is exposed. A blasted outcrop provides an excellent opportunity to examine an andesitic mudflow (Photo 4). Wagner and Saucedo (1990b) reported a date of 9.6±0.24 Ma for a mafic andesite clast from this outcrop and 8.94±0.17 Ma for an andesite dike that intrudes the andesite breccia. The dike can be observed a few hundred feet west of this outcrop. Initially, we thought this andesite breccia underlies the Lovejoy Basalt; the dates indicate that it is younger, so it must have been deposited on or buttressed against the Lovejoy Basalt. The base of the Lovejoy is not exposed here, but at the north end of Stony Ridge the Lovejoy is underlain by arkosic sand containing abundant andesite cobbles. Return to the vehicles and proceed west on road 03.

65.8 Intersection with USFS road 01 near Murdocks Crossing. Proceed north on 01. We will be crossing rolling topography underlain by deeply weathered granitic rock.

69.6 Ahead is Clarks Peak, composed of granite and capped by an andesite flow. This indicates the amount of erosional lowering of the granitic surface since the deposition of the andesite, which is undated, but likely of mid-Miocene age. To the east is Stony Ridge capped by Lovejoy Basalt.

77.9 Turn left on the road to Thompson Lookout (28N02). Proceed 2.1 miles and turn right on 28N02F; proceed 1.4 miles and park in the quarry.

Stop 3 (81.4 miles)

Roberts (1985), who obtained a date of 16.3 Ma on basalt from this locality, described the basalt exposed on this ridge. Cordell Durrell was cited by Roberts as saying this basalt is identical to the Lovejoy Basalt but apparently he would not agree to a correlation because of the mid-Miocene date. Lovejoy Basalt is exposed at the north end of Stony Ridge only 4 miles to the southeast. A distinctive, 10 million-year old diktytaxitic basalt, the Basalt of Thompson Peak, overlies this basalt and also overlies the Lovejoy at Stony Ridge. Roberts (1985) suggested the presence of agglutinate, scoria, and fragments of volcanic bombs indicate this area could be a vent source for the Lovejoy Basalt. Durrell (1959a,b, 1966, 1987) argued the source of the Lovejoy is to the east and it is truncated by the Honey Lake Fault zone. The only Lovejoy Basalt east of the Honey Lake escarpment we are aware of is a fault-bounded, highly altered block of basalt in a roadcut along Hwy 395 a few miles northeast of Thompson Peak (Roberts, 1985). We consider this block to

Photo 4. Exposure of fresh andesite mudflow at Doyle Crossing (Stop 2). Wagner and Saucedo (1990b) reported a date of 9.6 Ma on a clast from this exposure and date of 8.94 on a dike that intrudes this mudflow. *Photo by David L. Wagner.*

be a sliver in the Honey Lake Fault zone and not indicative of an eastern source for the Lovejoy.

Our mapping (Grose and others, 1991 and references therein) and mapping of Roberts (1985) suggest the Lovejoy Basalt was erupted from vents along fissures that were precursors to the faults that resulted in the Honey Lake escarpment. Olivine-bearing mafic andesite, that in outcrop resembles the Lovejoy Basalt, was also intruded along faults in the same region but is younger, 9.60±0.24 Ma (Grose and others, 1990). Because the Lovejoy Basalt has not been found in the subsurface in the Honey Lake Basin and because it flowed to the south and then west in a paleovalley, the Honey Lake Basin probably had not yet formed. Nearly all of the cooling units of the Oligocene to Miocene silicic eruptions (34 to 20 Ma) in Nevada can be matched on both sides of the present Honey Lake basin (Alan Deino, personal communication). We speculate that the Lovejoy magma was intruded along newly initiated faults that mark the beginning of northern Basin and Range faulting at 16 to17 Ma (Noble, 1972; Christiansen and McKee, 1978).

The Lovejoy is a flood basalt as indicated by its wide extent, chemical similarity between flows and large volume. Doukas (1983) and Siegel (1988) compared the chemistry to the Columbia River basalts and found similarities that led them to suggest the Lovejoy Basalt formed in a tectono-magmatic setting similar to the Columbia River Basalt Group. The 16.3 Ma date of Roberts (1985) and 16 Ma of Page and others (1995) for the Lovejoy Basalt makes a compelling argument that they did form in the same tectono-magmatic episode. Lovejoy volcanism coincided with the intense 14 to 17 Ma magmatism in the Columbia Plateau, Steens Mountain, Oregon and northern Nevada. In addition, the vent and feeder dike we propose to be the source of the Lovejoy would trend northwest, parallel to major magmatic feeder dikes of the Columbia River Basalt Group (Figure 3). In northern Nevada, a zone of fissures filled with 14 to 17 Ma basalt, the northern Nevada rift of Zoback and others (1994), marked initiation of Basin and Range extension. There is no evidence that flood basalts flowed into this area from Washington, Oregon or Nevada. We feel there is a strong argument that the Lovejoy Basalt erupted 16 million years ago along one or more northwest-trending fissure vents as Basin and Range faulting began in this region. As discussed earlier, we feel an attractive hypothesis is that decompression melting of a mantle plume head at the base of the crust as suggested by Pierce and Morgan (1992) caused venting of flood basalts over widely separated areas of the northern Great Basin about 16 Ma.

Return to vehicles and retrace the 3.5 mile route to USFS road 01.

81.4 Turn left and head down Janesville Grade.

86.1 Junction with Hwy 395. End of field trip.

REFERENCES

Abrams, R.H.,1991, New evidence for the age of the Lovejoy Formation at its type locality, Red Clover Creek, northern Sierra Nevada, California: San Francisco State University senior thesis, 32 p.

Alt, David, Hyndman, D.W. and Sears, J.W., 1990, Impact origin of late Miocene volcanism, Pacific Northwest: Geological Society of America Abstracts with Programs, v. 22, p. 2.

Bateman, P.C. and Wahrhaftig, Clyde, 1966, Geology of the Sierra Nevada *in* Bailey, E.H., editor, Geology of Northern California: California Division of Mines and Geology Bulletin 190, p. 107-172.

Brem, G.F., 1977, Petrogenesis of Late Tertiary potassic volcanic rocks of the Sierra Nevada and the western Great Basin: University of California, Riverside Ph.D. dissertation, 361 p.

Carlson, R.W. and Hart, W.K., 1988, Flood basalt volcanism in the northwestern United States *in* Macdougall, J.D., editor, Continental flood basalts: Dordrecht, The Netherlands, Kluwer Acedemis Publishers, p. 36-61.

Ceron, J.F., 1992, Gravity modeling of the Honey Lake Basin, California: Colorado School of Mines M.S. thesis, 145 p.

Christiansen, R.L. and Yeats, R.S., 1992, Post-Laramide geology of the U.S. Cordilleran region *in* Burchfiel, B.C., Lipman, P.W. and Zoback, M.L., editors, The Cordilleran Orogen: Conterminus U.S.: Boulder, Colorado, Geological Society of America, The Geology of North America, v. G3, p. 261-406.

Christiansen, R.L. and McKee, E.H., 1978, Late Cenozoic volcanic and tectonic evolution of the Great Basin and Columbia intermountane regions *in* Smith, R.B. and Eaton, G.P., editors, Cenozoic tectonics and geophysics of the western Cordillera: Geological Society of America Memoir 152, p. 283-311.

Clark, B.L. and Anderson, C.A., 1938, Wheatland Formation and its relation to early Tertiary andesites in the Sierra Nevada: Geological Society of America Bulletin, v. 49, p. 931-955.

Creely, R.S., 1955, Geology of the Oroville Quadrangle, California: University of California, Berkeley Ph.D. dissertation, 269 p.

Creely, R.S., 1965, Geology of the Oroville Quadrangle, California: California Division of Mines and Geology Bulletin 184, 86 p.

Curtis, G.H., 1951, The geology of the Topaz Lake Quadrangle and the eastern half of the Ebbets Pass Quadrangle, California: University of California, Berkeley Ph.D. dissertation, 310 p.

Curtis, G.H., 1954, Mode of origin of the pyroclastic debris in the Mehrten Formation of the Sierra Nevada, California: University of California Publications in Geological Sciences, v. 29, p. 253-502.

Dalrymple, G.B., 1964, Cenozoic chronology of the Sierra Nevada, California: University of California Publications in Geological Sciences, v. 47, 41 p.

Deino, A.L., 1985, Stratigraphy, chemistry, K-Ar dating and paleomagnetism of the Nine Hill Tuff, California-Nevada: University of California, Berkeley Ph.D. dissertation, part 1, p. 1-338.

Dickinson, W.R., 1997, Tectonic implications of Cenozoic volcanism in coastal California: Geological Society of America Bulletin, v. 109, p. 936-954.

Diller, J.S., 1908, Geology of the Taylorsville region, California: U.S. Geological Survey Bulletin 353, 128 p.

Doukas, M.P., 1983, Volcanic geology of the Big Chico Creek area, Butte County, California: San Jose State University M.S. thesis, 157 p.

Duffield, W.A. and McKee, E.H., 1986, Geochronology, structure, and basin-range tectonism of the Warner Range, northeastern California: Geological Society of America Bulletin, v. 97, p. 142-146.

Durrell, Cordell, 1959a, Tertiary stratigraphy of the Blairsden Quadrangle, Plumas County, California: University of California Publications in Geological Sciences, v. 34, p. 161-192.

Durrell, Cordell, 1959b, The Lovejoy Formation of northern California: University of California Publications in Geological Sciences, v. 34, p. 193-220.

Durrell, Cordell, 1966, Tertiary and Quaternary geology of the northern Sierra Nevada *in* Bailey, E.H., editor, Geology of Northern California: California Division of Mines and Geology Bulletin 190, p. 185-197.

Durrell, Cordell, 1987, Geologic history of the Feather River country, California: Berkeley and Los Angeles, University of California Press, 337 p.

Grommé, C.S., 1963, Remanent magnetization of igneous rocks from the Franciscan and Lovejoy formations, northern California: University of California, Berkeley Ph.D. dissertation, 225 p.

Grose, T.L.T., 2000, Volcanoes in the Susanville region, Lassen, Modoc, Plumas counties, northeastern California: CALIFORNIA GEOLOGY, September/October, 2000 p. 4-27.

Grose, T.L.T., in preparation, Geologic map of the Blairsden 15-minute Quadrangle, Plumas County, California: California Division of Mines and Geology Open-File Report, scale 1:62,500, in preparation.

Grose, T.L.T., in preparation, Geologic map of the Portola 15-minute Quadrangle, Plumas County, California: California Division of Mines and Geology Open-File Report, scale 1:62,500.

Grose, T.L.T., Wagner, D.L., Saucedo, G.J. and Medrano, M.D., 1989, Geologic map of the Doyle 15-minute Quadrangle, Lassen and Plumas counties, California: California Department of Conservation, Division of Mines and Geology Open-File Report 89-31, scale 1:62,500.

Grose, T.L.T., Saucedo, G.J. and Wagner, D.L., 1991, Geologic map of the Susanville Quadrangle, Lassen County, California: California Department of Conservation, Division of Mines and Geology Open-File Report 91-01, scale 1:100,000.

Hannah, J.L., 1977, Tectonic setting of the Modoc region, northeastern California *in* Short Contributions to California Geology: California Division of Mines and Geology Special Report 129, p. 35-39.

Lindgren, Waldemar, 1911, The Tertiary gravels of the Sierra Nevada of California: U.S. Geological Survey Professional Paper 73, 226 p.

Lindgren, Waldemar, Turner, H.W. and Ransome, F.L., 1894-1900, The Gold Belt Folios: U.S. Geological Survey Atlas Folios 3, 5, 11, 17, 18, 29, 31, 37, 41, 43, 51, 63, 66 (individually and as co-authors), scale 1:125,000.

McKee, E.H. and Noble, D.C., 1986, Tectonic and magmatic development of the Great Basin of the western United States during late Cenozoic time: Modern Geology, v. 10, p. 39-49.

Noble, D.C., 1972, Some observations on the Cenozoic volcano-tectonic evolution of the Great Basin, western

United States: Earth and Planetary Sciences, v. 17, p. 142-150.

Page, W.D., Sawyer, T.L. and Renne, P.R., 1995, Tectonic deformation of the Lovejoy Basalt, a late Cenozoic strain gage across the northern Sierra Nevada and Diamond mountains, California *in* Quaternary geology along the boundary between the Modoc Plateau, southern Cascades and northern Sierra Nevada, Friends of the Pleistocene Pacific Cell Field Trip, William D. Page, leader.

Pierce, K.L. and Morgan, L.A., 1992, The track of the Yellowstone hot spot: Volcanism, faulting and uplift *in* Link, P.K., Kuntz, M.A. and Platt, L.B., editors, Regional Geology of Eastern Idaho and Western Wyoming: Geological Society of America Memoir 170, p. 1-53.

Piper, A.M., Gale, H.S., Thomas, H.E. and Robinson, T.W., 1939, Geology and ground-water hydrology of the Mokelumne area, California: U.S. Geological Survey Water Supply Paper 780, p. 14-101.

Ransome, F.L. 1898, Some lava flows of the western slope of the Sierra Nevada, California: U.S. Geological Survey Bulletin 89, 89 p.

Roberts, C.T., 1985, Cenozoic evolution of northwestern Honey Lake Basin, Lassen County, California: Colorado School of Mines Quarterly, v. 80, no. 1, 63 p.

Saucedo, G.J. and Wagner, D.L., 1992, Geologic map of the Chico Quadrangle: California Department of Conservation, Division of Mines and Geology Regional Geologic Series, Map No. 7A, scale 1:250,000.

Saucedo, G.J., Fulford, M.M., Mata-Sol, R.A. and Lindquist, T.A., 1992, Radiometric ages of rocks in the Chico Quadrangle, California: California Department of Conservation, Division of Mines and Geology Regional Geologic Map Series, Map No. 7A, Sheet 4, 21 p.

Siegel, David, 1988, Stratigraphy of the Putnam Peak Basalt and correlation to the Lovejoy Formation, California: California State University, Hayward M.S. thesis, 119 p.

Slemmons, D.B., 1966, Cenozoic volcanism of the central Sierra Nevada, California *in* Bailey, E.H., editor, Geology of Northern California: California Division of Mines and Geology Bulletin 190, p. 199-214.

Stewart, J.H., 1988, Tectonics of the Walker Lane belt, western Great Basin; Mesozoic and Cenozoic deformation in a zone of shear *in* Ernst, W.G., editor, Metamorphism and crustal evolution of the western United States, Rubey Volume VII: Englewood Cliffs, New Jersey, Prentice Hall, p. 683-713.

Turner, H.W., 1891, Mohawk Lake Beds: Philosophical Society of Washington Bulletin, v. 11, no. 4, p. 385-409.

Turner, H.W., 1894, The rocks of the Sierra Nevada: U.S. Geological Survey, Seventeenth Annual Report, part II, p. 435-495.

Turner, H.W., 1896, Further contributions to the geology of the Sierra Nevada, U.S. Geological Survey, Seventeenth Annual Report, p. 521-762.

Wagner, D.L. and Saucedo, G.J., 1990a, Age and stratigraphic relationships of Miocene volcanic rocks along the eastern margin of the Sacramento Valley, California *in* Ingersoll, R.V. and Nilsen, T.H., Sacramento Valley Symposium and Guidebook: Pacific Section S.E.P.M., v. 65, p.143-151.

Wagner, D.L. and Saucedo, G.J., 1990b, Reconnaissance geologic map of the Milford 15′ Quadrangle, Lassen and Plumas counties, California: Department of Conservation, Division of Mines and Geology Open-File Report 90-08, scale 1:62,500.

Wagner, H.M., 1981, Geochronology of the Mehrten Formation in Stanislaus County, California: University of California, Riverside Ph.D. dissertation, 342 p.

Weaver, C.E., 1949, Geology of the Coast Ranges immediately north of San Francisco Bay Region, California: Geological Society of America Memoir 35, 242 p.

Whitney, J.D., 1865, Geology, reports of progress and synopsis of the field work from 1860 to 1864: Geological Survey of California, v. 1, 498 p.

Wilson, Elinor, 1972, Jim Beckwourth: Norman, University of Oklahoma Press, 248 p.

Williams, Howel and McBirney, A.R., 1979, Volcanology: San Francisco, Freeman Cooper, 397 p.

Yount, J.C., Harwood, D.S. and Bradbury, J.P., 1993, Mohawk Lake or Mohawk Meadow? Sedimentary facies and stratigraphy in Mohawk Valley, upper middle fork of the Feather River, California: Geological Society of America Abstracts with Programs, Cordilleran and Rocky Mountain sections, Reno, Nevada, v. 25, no. 5, p. 168.

Zoback, M.L. and Thompson, G.A., 1978, Basin and Range rifting in northern Nevada: Clues from a mid-Miocene rift and its subsequent offsets: Geology, v. 6, p. 111-116.

Zoback, M.L., McKee, E.H., Blakely, R.J. and Thompson, G.A., 1994, The northern Nevada rift: Regional tectono-magmatic relations and middle Miocene stress direction: Geological Society of America Bulletin, v. 106, p. 371-382.

NEOTECTONICS OF THE SIERRA NEVADA AND THE SIERRA NEVADA-BASIN AND RANGE TRANSITION, CALIFORNIA, WITH FIELD TRIP STOP DESCRIPTIONS FOR THE NORTHEASTERN SIERRA NEVADA

John Wakabayashi[1], Thomas L. Sawyer[2]

INTRODUCTION

The 600 kilometer (km)-long Sierra Nevada is the most prominent mountain range in California. Considerable research has been published on the basement (pre-Cenozoic) geology of the Sierra Nevada. (See other papers in this volume and their references.) Literature on the neotectonic development of the Sierra Nevada is comparatively scarce, however. Since the classic work of Bateman and Wahrhaftig (1966), little has been published on the neotectonics of the Sierra Nevada, with the notable exception of Unruh's (1991) study of late Cenozoic tilting of the Sierra, and Huber's (1981) and (1990) studies on the ancestral San Joaquin and Tuolumne River drainages. The general view of the Sierra Nevada as a westward-tilted block with major faulting on its east side and comparatively little internal deformation (Lindgren, 1911; Bateman and Wahrhaftig, 1966; Christensen, 1966) still appears to be valid.

The Sierra Nevada and the Central Valley are part of the Sierra Nevada microplate, an element of the broad Pacific-North American plate boundary (Argus and Gordon, 1991; Figure 1). The dextral movement of the Sierra Nevada microplate relative to stable North America is 9 to 11 millimeter (mm)/yr at an orientation varying from about N28°W in the southern part of the range near Lone Pine to about N50°W at the northernmost part of the range near Quincy (Argus and Gordon, 1991). The motion of the Sierra Nevada microplate relative to stable North America is thus approximately parallel to the strike of the San Andreas Fault system that is oriented from N35°W to N40°W in central and northern California. Internal deformation of the microplate, which includes the Central Valley and the Sierra Nevada range, is relatively minor. In contrast, the microplate is bounded on the west by a significant fold and thrust belt that marks the eastern margin of the Coast Range province (Wentworth and Zoback, 1989), and on the east by a prominent east-facing escarpment, that marks the Sierra Nevada Frontal Fault system (referred to here informally as the "Frontal Fault system"), a zone of prominent normal, normal-dextral and dextral faulting (Clark and others, 1984; Beanland and Clark, 1995).

Prior to becoming part of the transform plate margin, the Sierra Nevada was the site of a Cenozoic volcanic arc. The southernmost active volcano of the active Cascades arc is Mt. Lassen (Figure 1), but earlier late Cenozoic volcanic arc activity extended much farther south before shutting off as the Mendocino triple junction migrated northward and the convergent plate margin was replaced by a transform one (Atwater and Stock, 1998). Cenozoic volcanic deposits related to the volcanic arc are draped over pre-Cenozoic metamorphic and plutonic rocks (Figure 1). These volcanic deposits provide critical constraints on the nature of late Cenozoic faulting and deformation in, and along the eastern boundary of, the Sierra Nevada (distribution of late Cenozoic volcanic rocks in Figure 1, faults in Figure 2).

In a general sense, the Sierra Nevada slopes gently westward and abruptly eastward from its crest. The general asymmetry of the Sierra Nevada reflects uplift and gentle westward tilting. This

---

[1] 1329 Sheridan Lane, Hayward, CA 94544; wako@tdl.com; www.tdl.com/~wako/
[2] Piedmont Geosciences, Inc., 10235 Blackhawk Drive, Reno, NV 89506; piedmont@USA.com

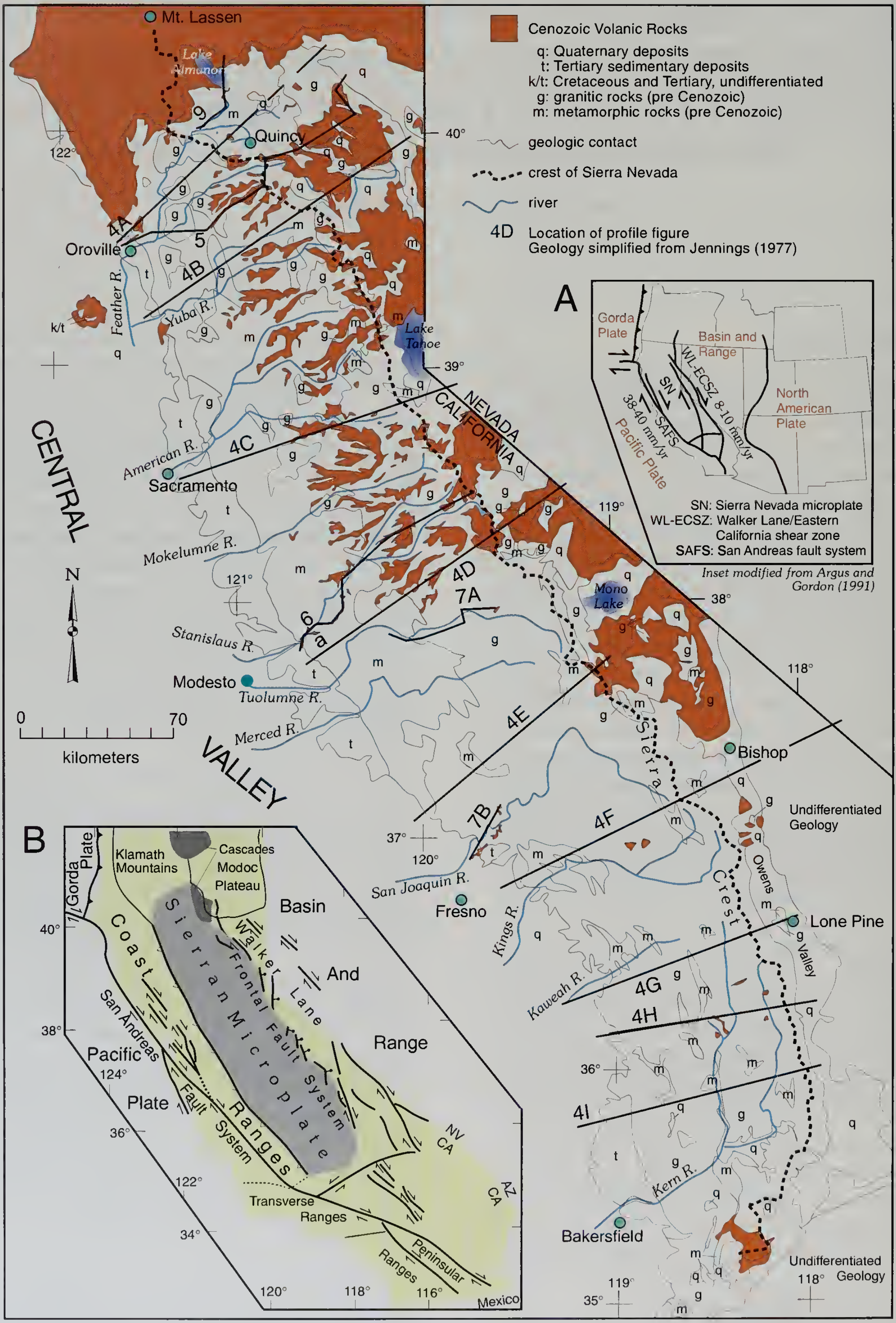

Figure 1. Generalized geologic map of the Sierra Nevada, showing Quaternary alluvium, Cenozoic volcanic rocks (shaded), granitic rocks and metamorphic rocks.

tilting and associated uplift is associated with significant vertical deformation along the Frontal Fault system, and other faults to the east of this fault system. The Frontal Fault system represents the Sierra Nevada-Basin and Range boundary or transition zone, the westernmost element of the Walker Lane belt (Figure 1). In contrast to the Frontal Fault system, vertical deformation within the range is minor and cumulative vertical separations and/or slip rates of individual faults are one to three order of magnitude lower than faults along the eastern boundary (Figure 2).

This paper is divided into two parts: a synthesis of neotectonics of the Sierra Nevada, followed by a field trip guide to neotectonics along the northernmost Sierra Nevada-Basin and Range boundary zone. In synthesis we will review published research on late Cenozoic Sierra Nevada uplift, stream incision, and neotectonics, and present new data on these subjects. The synthesis will conclude with a discussion of recent studies that have suggested that late Cenozoic uplift of the Sierra Nevada did not occur.

PRESENT DAY TOPOGRAPHY AND THE LATE CENOZOIC TILTING AND UPLIFT OF THE SIERRA NEVADA

Present Day Topography

There are significant differences in the topographic expression of the Sierra Nevada along strike (Christensen, 1966; Bateman and Wahrhaftig, 1966). In the northern part of the range the westward slope is relatively constant from the crest, whereas in the southern part of the range, it has a very gradual gradient west of the crest that steepens in the western foothills (Figures 3 and 4). On an exceptionally clear day the crest of the range is visible from Sacramento, whereas from Fresno only the top of the steep western slope can be seen. The crestal elevations also vary from 2,100-2,700 meters (m) in the northern part of the range to 4,200-4,400 m in the central to southern part of the range. The height of the eastern escarpment varies from about 1,000 m in the northernmost part of the range to nearly 3,300 m at Lone Pine (Figure 4; Photos 1 and 2). In the following sections we will discuss these differences in topographic expression in the context of various episodes of uplift of the mountain range.

Uplift and Cenozoic Stratigraphy

Uplift for different time periods have been estimated by several methods, including: differential tilt of Cenozoic strata on the eastern margin of the Central Valley (Bateman and Wahrhaftig, 1966; Grant and others, 1977; Unruh, 1991), comparison of gradients of Tertiary stream deposits perpendicular and parallel to the range axis (Lindgren, 1911; Christensen, 1966), reconstruction of old drainages from deposits that are preserved in Tertiary paleo channels (Huber, 1981, 1990), and paleobotanical studies (Axelrod, 1957; Axelrod and Ting, 1960; Axelrod, 1980). Specific uplift estimates discussed here are summarized in Table 1.

The best-constrained estimates are those that involve datable deposits. These methods can only be applied where Cenozoic strata cover Sierran basement rocks and are exposed along the eastern margin of the Central Valley. The oldest of the Cenozoic cover strata are the Eocene gold-bearing gravels, commonly referred to as the “auriferous” gravels, and their equivalents along the eastern Central Valley margin, the Ione Formation. Overlying the Eocene deposits are 20-34 Ma rhyolite tuffs, including the Valley Springs and Delleker formations (Wagner and others, 1981; Saucedo and Wagner, 1992). These Oligocene to early Miocene rhyolites are overlain by 4-14 Ma andesites, andesitic mudflows, and associated volcanic sedimentary rocks, including the Mehrten and related formations (Bartow, 1979; Wagner and others, 1981; Saucedo and Wagner, 1992). The term “Mehrten Formation” will be used to describe these rocks, following the broad definition of Curtis (1954). Northward younging of youngest late Cenozoic volcanic rocks may be expected because of the northward migration of the Mendocino triple junction and associated shut off of subduction and arc volcanism. However, the age data do not reflect such a pattern. Either a time transgressive pattern does not exist, or the uncertainties in the existing geochronologic dataset are too large. The “stalling” of the southern edge of the subducted Juan de Fuca plate at approximately the same latitude during the last 4 Ma (Atwater and Stock,

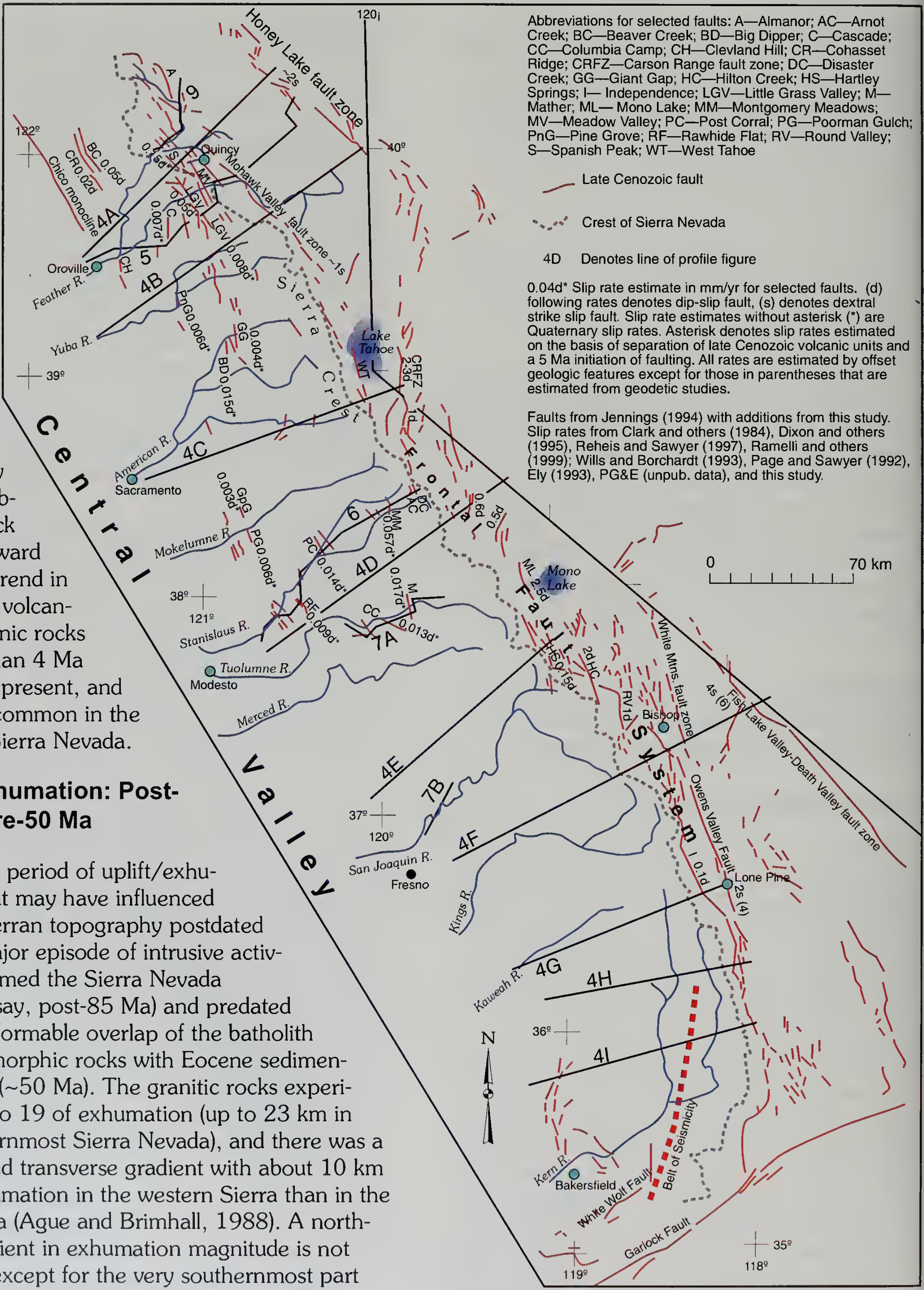

Abbreviations for selected faults: A—Almanor; AC—Arnot Creek; BC—Beaver Creek; BD—Big Dipper; C—Cascade; CC—Columbia Camp; CH—Clevland Hill; CR—Cohasset Ridge; CRFZ—Carson Range fault zone; DC—Disaster Creek; GG—Giant Gap; HC—Hilton Creek; HS—Hartley Springs; I— Independence; LGV—Little Grass Valley; M—Mather; ML— Mono Lake; MM—Montgomery Meadows; MV—Meadow Valley; PC—Post Corral; PG—Poorman Gulch; PnG—Pine Grove; RF—Rawhide Flat; RV—Round Valley; S—Spanish Peak; WT—West Tahoe

Late Cenozoic fault

Crest of Sierra Nevada

4D Denotes line of profile figure

0.04d* Slip rate estimate in mm/yr for selected faults. (d) following rates denotes dip-slip fault, (s) denotes dextral strike slip fault. Slip rate estimates without asterisk (*) are Quaternary slip rates. Asterisk denotes slip rates estimated on the basis of separation of late Cenozoic volcanic units and a 5 Ma initiation of faulting. All rates are estimated by offset geologic features except for those in parentheses that are estimated from geodetic studies.

Faults from Jennings (1994) with additions from this study. Slip rates from Clark and others (1984), Dixon and others (1995), Reheis and Sawyer (1997), Ramelli and others (1999); Wills and Borchardt (1993), Page and Sawyer (1992), Ely (1993), PG&E (unpub. data), and this study.

Figure 2. Generalized late Cenozoic fault map of the Sierra Nevada.

1998) may also contribute to a lack of a northward younging trend in shut off of volcanism. Volcanic rocks younger than 4 Ma are locally present, and are more common in the northern Sierra Nevada.

Early Exhumation: Post-85 Ma, pre-50 Ma

The first period of uplift/exhumation that may have influenced current Sierran topography postdated the last major episode of intrusive activity that formed the Sierra Nevada batholith (say, post-85 Ma) and predated the unconformable overlap of the batholith and metamorphic rocks with Eocene sedimentary rocks (~50 Ma). The granitic rocks experienced up to 19 of exhumation (up to 23 km in the southernmost Sierra Nevada), and there was a pronounced transverse gradient with about 10 km more exhumation in the western Sierra than in the crestal area (Ague and Brimhall, 1988). A north-south gradient in exhumation magnitude is not apparent except for the very southernmost part of the range that has experienced a very large amount of exhumation. Considerable erosion

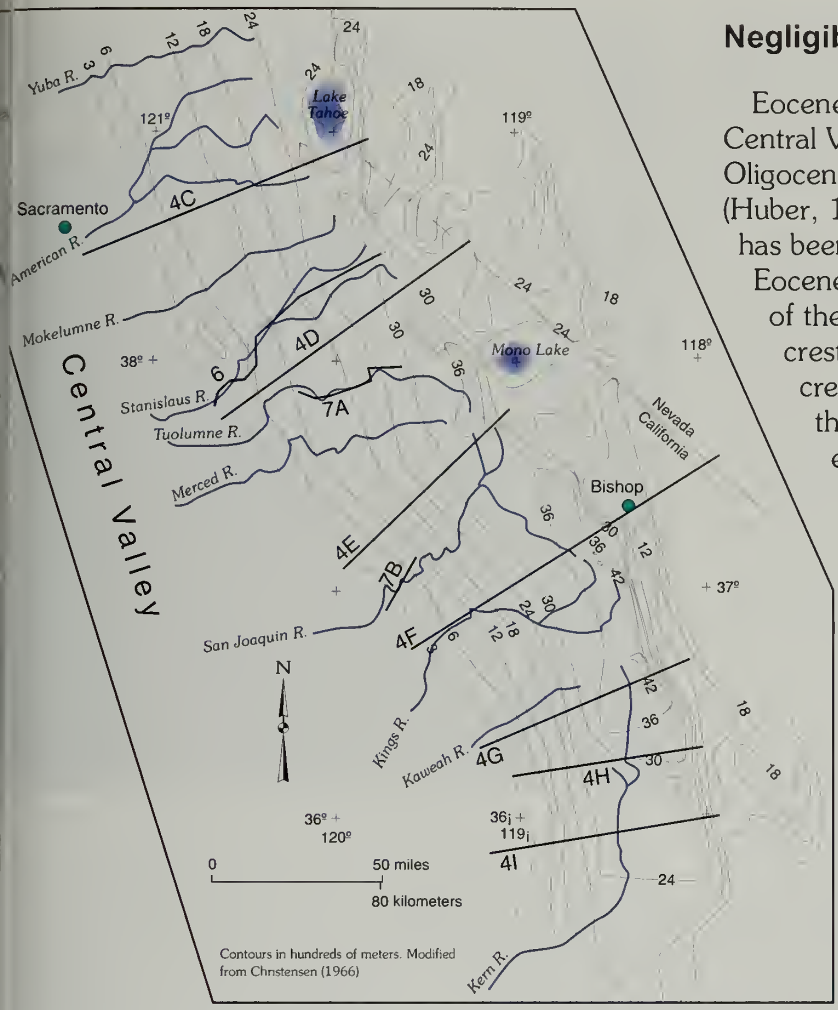

Figure 3. Generalized topography of the central and southern Sierra Nevada.

was associated with this exhumation event, but how much uplift was associated with the exhumation is unclear, because no indicators of elevation relative to sea level are preserved. The magnitude and duration of the 85-50 Ma exhumation event is about an order of magnitude higher than late Cenozoic exhumation. The large magnitude of exhumation during this period suggests that uplift may have been significant during this period as well. The pattern of post 85 Ma, pre-50 Ma exhumation is much different than the westward tilting in the late Cenozoic, which has led to greater exhumation in the east, near the crest (Ague and Brimhall, 1988), as reflected in the pattern of late Cenozoic stream incision (see subsequent discussion on stream incision).

Negligible Eocene-Miocene Uplift

Eocene rocks along the eastern margin of the Central Valley are tilted more steeply than the Oligocene and Miocene rocks that overlie them (Huber, 1981; Unruh, 1991). The difference in tilt has been interpreted as evidence for significant Eocene to Miocene uplift, because projection of the more steeply tilted Eocene strata to the crest predict elevations of Eocene strata at the crest that are more than 1,000 m higher than Miocene strata (Huber, 1981). However, Eocene strata directly underlie Miocene and Oligocene strata everywhere in the range, including areas near the Sierra crest (Lindgren, 1911; Bateman and Wahrhaftig, 1966). Thus minor warping of the Eocene strata occurred near the Central Valley margin prior to deposition of the Oligocene and Miocene strata, but warping was restricted to the valley margin, and the overall uplift of the range related to warping was negligible. Some incision of streams occurred between Eocene and Miocene time, but the amount of incision of Miocene and Oligocene channels into the Eocene deposits is less than 60 m (Lindgren, 1911; Yeend, 1974). This indicates that the topographic relief of the Sierra had been reduced to fairly low levels by Eocene time in the central and northern Sierra (Lindgren, 1911; Bateman and Wahrhaftig, 1966; Christensen, 1966; Durrell, 1966; and many others).

Late Cenozoic (Post-late Miocene) Uplift

The late Cenozoic uplift of the Sierra may be approximately reflected by the topographic expression of the range. Uplift is greatest directly west of the Frontal Fault system, which is reflected in the position of the range crest relative to the eastern escarpment. As a consequence of this pattern of uplift, the Sierran block has been gently tilted westward. In the northern and central Sierra, the gentle west slope consists of a series of regionally concordant upland surfaces on late Cenozoic strata capping basement interfluves between the west-flowing drainages in this part of the range

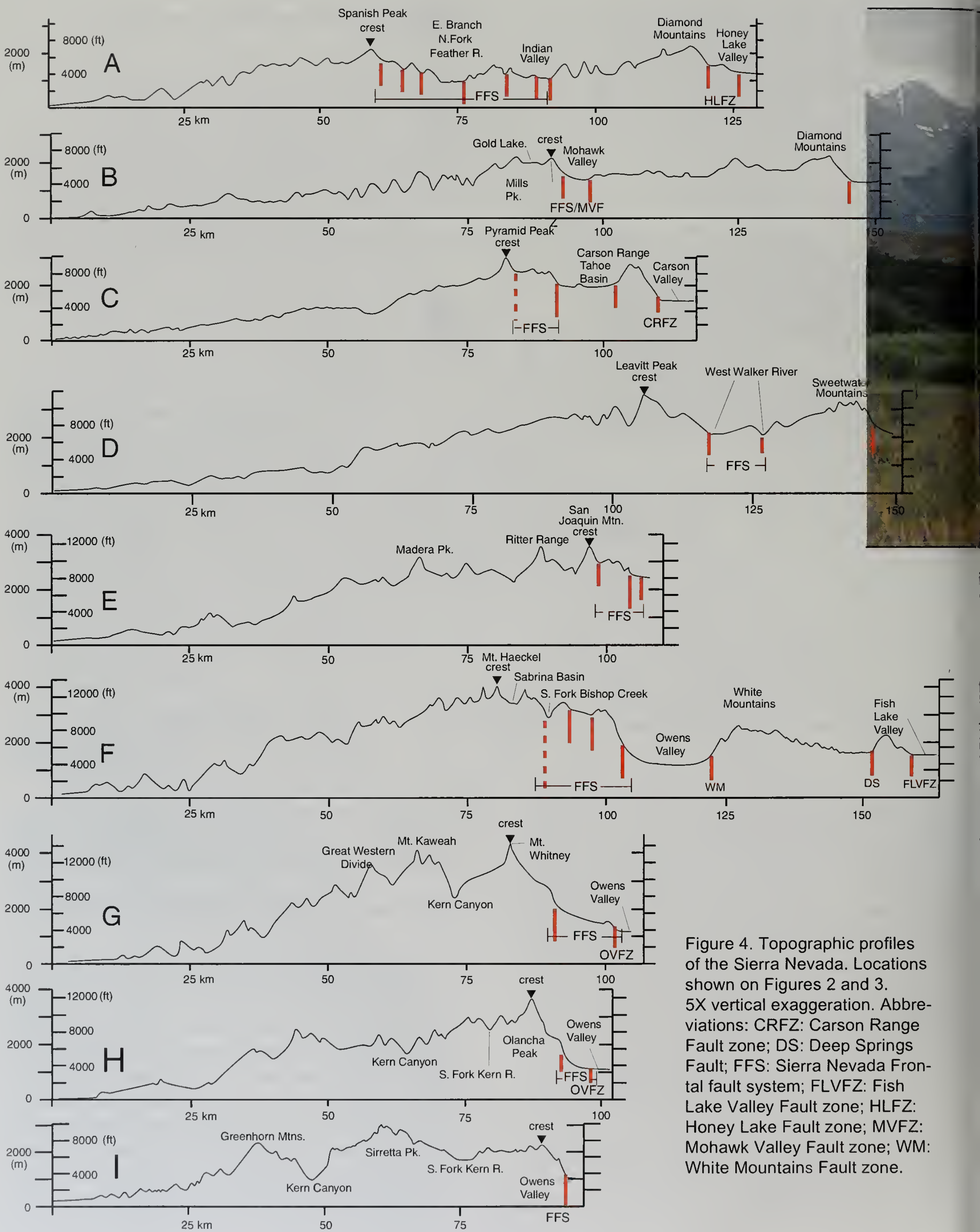

Figure 4. Topographic profiles of the Sierra Nevada. Locations shown on Figures 2 and 3. 5X vertical exaggeration. Abbreviations: CRFZ: Carson Range Fault zone; DS: Deep Springs Fault; FFS: Sierra Nevada Frontal fault system; FLVFZ: Fish Lake Valley Fault zone; HLFZ: Honey Lake Fault zone; MVFZ: Mohawk Valley Fault zone; WM: White Mountains Fault zone.

Photo 1. The highest part of the eastern Sierran escarpment looking west from Lone Pine in Owens Valley. The difference in elevation between this point and the highest peak (Mt. Whitney, 4,419 m above sea level, the highest peak in the Sierra Nevada, on the right skyline) is 3,280 m. Mt. Whitney is on the crest of the range. *Photo by Joseph Wakabayashi.*

(Bateman and Wahrhaftig, 1966). The capping of basement interfluves with late Cenozoic deposits indicates significant stream incision since deposition (see subsequent discussion on stream incision).

Uplift estimates have been made on the basis of tilt of late Cenozoic strata along the eastern margin of the Central Valley (Unruh, 1991) or westernmost Sierra (Huber, 1981), based on a rigid tilt block model. The rigid tilt block model assumes that tilt occurs with a hinge line near the western margin of the range, with the maximum uplift at the Sierra crest, major east-down faulting along the eastern side of the Sierran block, and no internal deformation (i.e., the amount of tilt is constant across and along strike). Such estimates are dependent on the paleogradient of the Cenozoic drainages in their westernmost reaches, but independent of original gradient changes within the range. This is because the uplift is calculated as the difference between the paleoprofile of the deposit and the present reconstructed (tilted) profile, which adds a constant amount of tilt to the paleoprofile. This method predicts the elevations of late Cenozoic deposits or channels in the interior of the range. In addition to the sensitivity of this method to paleogradients, the method is also sensitive to the validity of the rigid tilt block model.

Photo 2. Eastern Sierran escarpment looking west from Quincy in American Valley. The bare granite escarpment is the glaciated eastern face of Spanish Peak (2,139 m above sea level). Total elevation difference between Spanish Peak and American Valley is 1,090 m. *Photo by John Wakabayashi.*

Table 1. Late cenozoic uplift estimates.

BASIS OF ESTIMATE	UPLIFT (M)	INITIATION OF UPLIFT (MA)	NOTES
differential tilt of late Cenozoic strata, easternmost Central Valley (Unruh, 1991)	1950	~5 (3.8 - 8.4)	for 80 km-wide range; assumes zero paleogradient before tilting and rigid tilt block model
as above	2440	as above	as above except 100 km-wide range (Unruh, 1991)
as above	1870	as above	for 80 km wide range with 1 m/km paleogradient on western margin of range and rigid tilt block model
as above	2340	as above	as above except 100 km-wide range
as above	1950-2330		100 km-wide range with paleogradient limits of 1.1-4.9 m/km from data of Christensen (1966)
reconstruction of Lovejoy basalt (this study)	1860	~5	assumes 1 m/km paleogradient
as above	1530-1660	as above	uses paleogradient range of 3.8-5.7 m/km similar to paleogradient limits estimate from Yuba River of Christensen (1966)
differential tilt, northern Sierra Nevada (Lindgren, 1911)	1190-1490	<35	tilt estimate from difference between range parallel and perpendicular gradients of Tertiary stream deposits
uplift, Donner Summit (American River drainage) (Axelrod, 1957)	1620	<5?	based on interpretation of paleobotanical data
tilts of Tertiary deposits, Stanislaus drainage (Christensen, 1966)	1160-1620	~5	tilt estimate from gradients of part of ancestral stream course with range of paleogradients from modern alluviated stream data
reconstruction of Stanislaus Table Mountain latite and related rocks (this study)	1940	~5	assumes 1 m/km paleogradient for western reach and 11 m/km for eastern reach
as above	1670-1930	as above	assumes 1.1-4.9 m/km range of western paleogradients from Christensen (1966) and 10 m/km gradient difference between western and eastern reaches
reconstruction of ancestral Tuolumne River channel (Huber, 1990)	1480	<10	based on differing gradients of ancestral channel parallel and perpendicular to tilt axis, rigid tilt block model
uplift, headwaters of San Joaquin (Axelrod and Ting, 1960)	2000	<3	based on interpretation of paleobotanical data
as above, adjusted by Huber (1981)	1000	as above	
reconstruction of ancestral San Joaquin River channel (Huber, 1981)	2150	<10	based on present gradient of Kennedy Table Mountain trachyte, a 1 m/km paleogradient for the western reach of the ancestral drainage, and rigid tilt block model

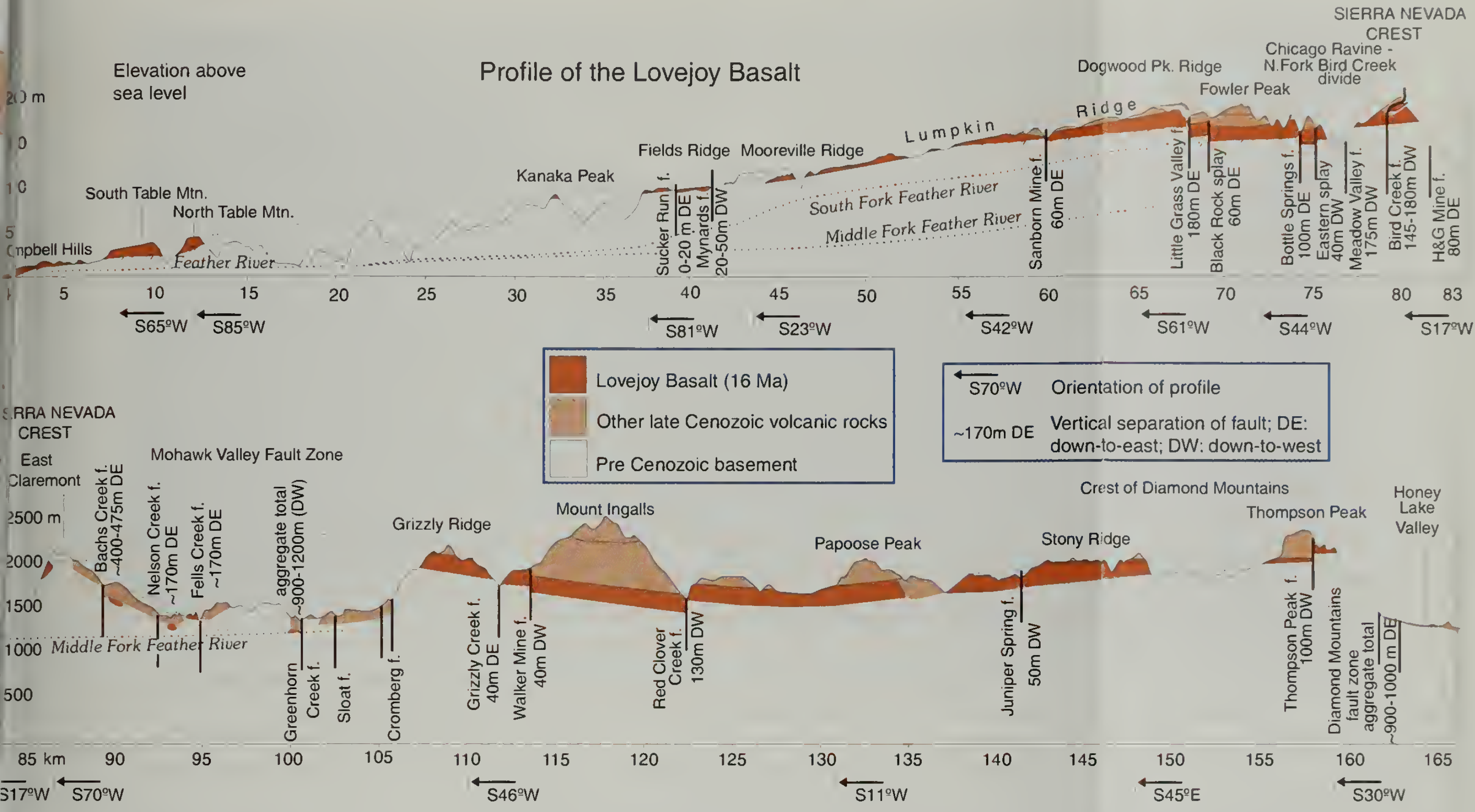

Figure 5. Profile of the Lovejoy basalt (location shown on Figures 2, 3 and 4). This profile extends from the eastern margin of the Central Valley to the Honey Lake basin, well east of the present Sierra Nevada crest. *Sources of data are Page and Sawyer (1992) and PG&E unpublished data. 5X vertical exaggeration.*

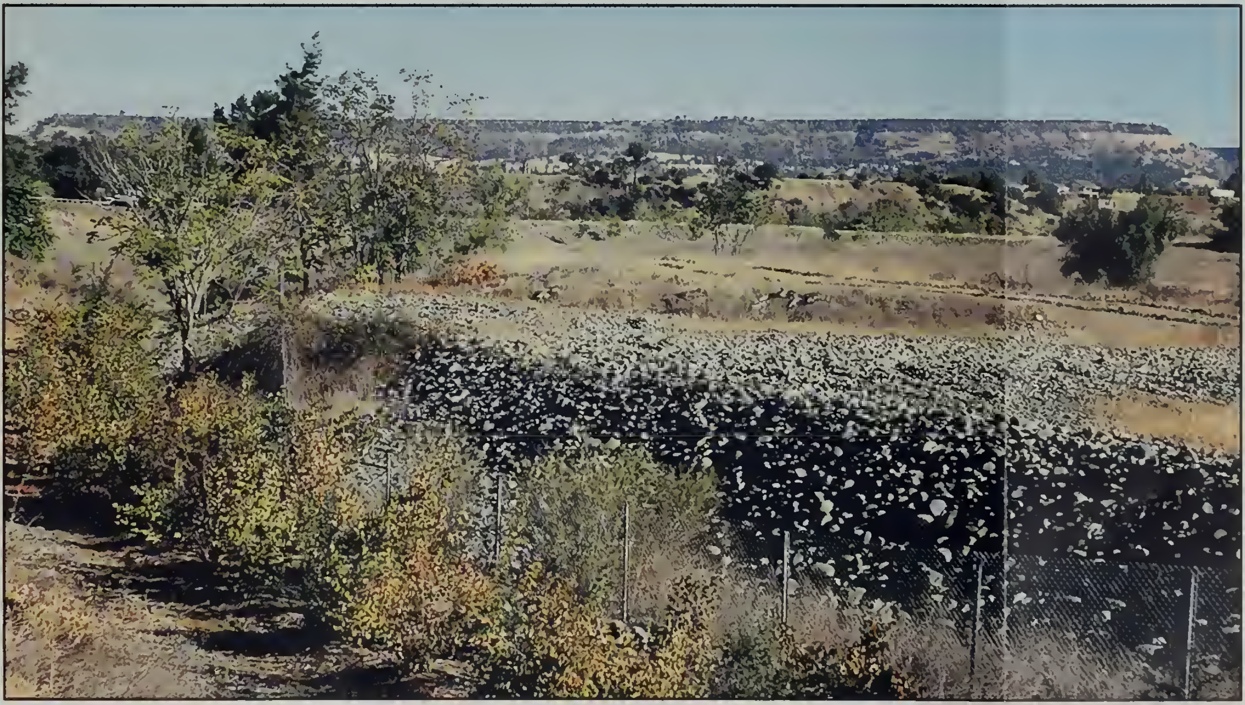

Photo 3. Lovejoy basalt (caps flat topped bluff) looking north from Oroville. *Photo by John Wakabayashi.*

Topographic profiles of late Cenozoic deposits such as the ~10 Ma deposits of the ancestral Tuolumne River channel (Huber, 1990), 16 Ma Lovejoy basalt (age from multiple Ar/Ar ages of Renne [unpublished data] see also Page and Sawyer, 1992; Figure 5; Photo 3), and 9 Ma Table Mountain Latite (Ely, 1992; Figure 6; Photo 4), can be used to test the rigid tilt block model because the altitude of late Cenozoic strata is known within the interior and at the crest of the range. Uplift estimates derived from these strata are subject to uncertainty of the paleogradients of the Cenozoic drainages, including any internal changes in paleogradient.

Derivation of crestal uplift from tilt for both methods also depends on the lack of absolute subsidence of the site of deposition of the eastern Central Valley flood plain deposits relative to sea level during the late Cenozoic. Based on the similarity of Miocene deposits to modern day flood plain deposits, Huber (1981) and Unruh (1991) concluded that the environment of deposition of the paleo flood plain deposits and modern ones are not different, indicating little absolute subsidence of this depositional environment relative to sea level.

Based on the similarity of channel deposits beneath the ~9 Ma Kennedy Table Mountain trachyte and present-day fluvial deposits on the flood plain of the eastern San Joaquin Valley, and field evidence that suggests that the Kennedy Table Mountain flow was planar across a very broad valley, Huber (1981) estimated an initial gradient of the western part of the ancestral (~10 Ma) stream drainage as 1 m/km. He suggested this gradient may have increased upstream to about 6 m/km on the basis of an abrupt change in the gradient of the preserved trachyte flow and its underlying

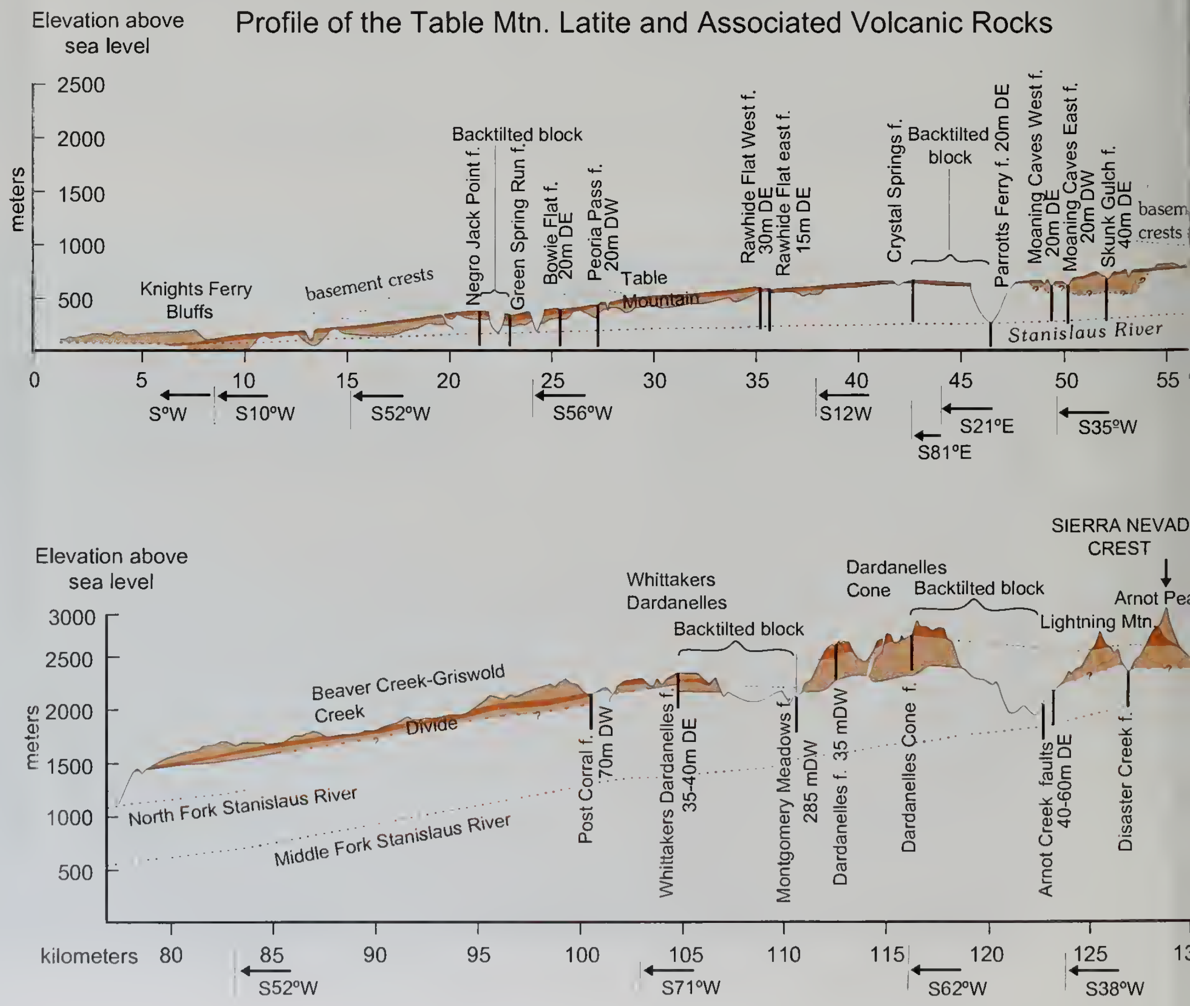

Figure 6. Profile of the Table Mountain Latite and related volcanic rocks (locations shown on Figures 2, 3 and 4). 5x vertical exaggeration. Sources of data are Ely (1992) and PG&E unpublished data.

Photo 4. Table Mtn. Latite (main resistant unit capping the peaks) looking toward the Dardanelles and Dardanelles Cone (see Figure 6 for location of these features) looking northeast from State Highway 108 at the Donnell Lake overlook. This section is part of a zone of significant deformation directly west of the crest. *Photo by John Wakabayashi.*

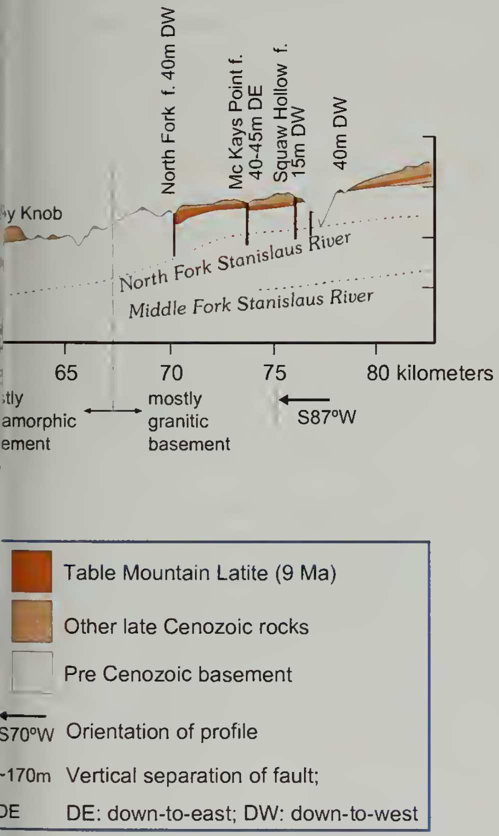
North Fork f. 40m DW
Mc Kays Point f. 40-45m DE
Squaw Hollow f. 15m DW
40m DW
y Knob
North Fork Stanislaus River
Middle Fork Stanislaus River
65
70
75
80 kilometers
tly amorphic ement
mostly granitic basement
S87°W
Table Mountain Latite (9 Ma)
Other late Cenozoic rocks
Pre Cenozoic basement
S70°W Orientation of profile
-170m Vertical separation of fault;
DE DE: down-to-east; DW: down-to-west

deposits, and further increased upstream to 8.6 m/km so the paleochannel elevation would be high enough to pass through a bedrock notch at the present crest. Huber (1981) estimated a post- 10 Ma crestal uplift of 2,150 m for the ancestral San Joaquin River drainage based on the 1 m/km paleogradient for the westernmost reach of the ancestral channel and the present tilt of the 9 Ma Kennedy Table Mountain trachyte, which is preserved only in the western part of the drainage (Figure 7). Based on ~10 Ma paleochannel deposits of the ancestral Tuolumne River, and assuming that a reach of the paleochannel parallel to the range axis reflects the original stream gradient (with adjustment of the original paleogradient to keep the paleo elevation of the stream at or below the elevation of the current drainage), Huber (1990) estimated 1,480 m of post-10 Ma crestal uplift at Tower Peak in the Tuolumne River drainage.

Based on a rigid tilt block model and assuming negligible initial stream gradient, Unruh (1991) estimated 1950 m of post ~5 Ma crestal uplift (5 Ma is preferred approximate onset of tilting; 3.8 to 8.4 Ma is full range) for a range width of 80 km and 2,440 m for a 100 km wide range based on the tilt of unconformities in that age range. If a 1 m/km initial gradient, used by Huber (1981) is applied to Unruh's estimates, the uplift estimates become 1,870 m for a 80 km wide range and 2,340 km for a 100 km wide range.

Christensen (1966) estimated a upper and lower limit of paleogradients of Tertiary streams based on their alluviated nature and data on modern stream gradients related to drainage area from alluviated

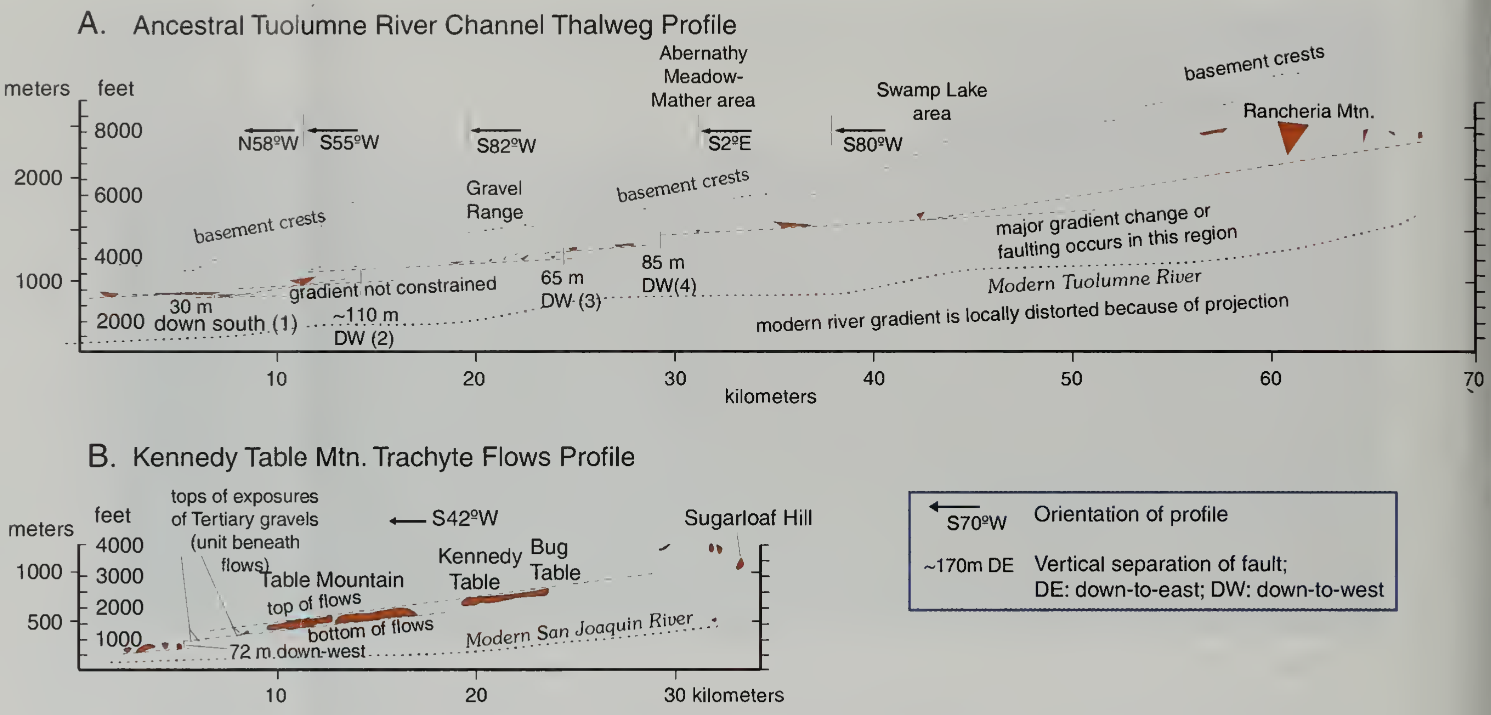

Figure 7. Profile of the (A) thalweg of the ancestral Tuolumne River channel, late Cenozoic gravel and volcanic deposits filling the channel shown in orange. Notes: 1) down-to-upstream side fault constrained by nearly continuous outcrop (Smith Station Fault); also coincides with linear down-south topographic escarpment; down-west faulting or gradient change directly east; 2) possible down-west separation coincides with significant down-west topographic escarpment; 3) possible down-west separation coincides with linear NW-striking drainages, aligned saddles, and linear west-down topographic escarpment (Columbia Camp Fault); 4) possible down-west separation coincides with possible down-west steps in glacial deposits, aligned along a NNW-striking trend over a distance of 10 km (Mather Fault). (B) Profile of the Kennedy Table Mountain trachyte (orange). Locations on Figures 2, 3 and 4. 5x vertical exaggeration for both profiles. *Sources for (A): Huber (1990), Dodge and Calk (1987), Kistler (1973), Turner and Ransome (1897). Sources for (B): Bateman and Busacca (1982), Marchand and Allwardt (1978).*

streams from many different climates and areas of the world. He used the range of paleogradients subtracted from the gradients in certain reaches of interpreted Tertiary streams and a rigid tilt model to estimate uplift. For at least two of his drainages, he did not use late Cenozoic deposits to estimate the tilt of Tertiary stream profiles, leading to erroneous relationships when compared to Tertiary stream deposits (discussed in Huber, 1981). In other drainages, the selection by Christensen (1966) of the reaches of Tertiary streams profiled is not explicit, so it is difficult to directly compare his estimates to those of others, but the magnitude of the estimates is similar to other estimates summarized here (Table 1). The limits of paleogradients of Christensen (1966) can be locally applied to other uplift estimates, where data on paleogradients are lacking.

The 16 Ma Lovejoy basalt erupted in Honey Lake Valley, east of the present Sierran crest and flowed westward across what is now the western margin of the Central Valley (Durrell, 1966). The 9 Ma Table Mountain Latite erupted near and east of the present Sierra Nevada crest, and flowed westward to the Central Valley (Slemmons, 1966). Both of these deposits form well-preserved and topographically inverted remnants distributed along transects crossing much or all of the Sierra Nevada. Thus, these units can be used to test the rigid tilt block model and estimate late Cenozoic uplift (Figures 5 and 6).

A rigid tilt block model based on the gradient of the western part of the Lovejoy basalt predicts 2,340 m of uplift at the crest, whereas the actual amount cannot exceed 1,926 m. This is the difference in elevation between the top of the lowest outcrop on the eastern flank of the Central Valley and the highest outcrop at the crest. The rigid tilt block model overestimates uplift by 21% or more because it does not account for significant east-side down faulting in the region directly west of the crest (Little Grass Valley, Bottle Springs and related faults (Photo 1).

A rigid tilt block model, based on the gradient of the western part of the Table Mountain Latite, predicts 2,507 m of crestal uplift, whereas the actual uplift is 2,730 m or less based on the difference between the top of the lowest latite outcrops and the elevation of the latite at the crest. Hence, the rigid tilt block model may underestimate uplift by about 8%. However the significant gradient change of about 10 m/km between the western and eastern remnants (eastern, upstream segment is the steeper) may reflect changes in the paleogradient of the drainage down where the latite flowed, instead of post-latite deformation. This gradient change approximately coincides with the basement transition from primarily metamorphic on the west to granitic on the east, so the gradient change may reflect an erosional resistance contrast that influenced the paleo stream gradient. In this case, the rigid block model predicts 2,715 m of uplift, which is close to the difference in elevation between crestal and lowest remnants. Note that, similar to the Lovejoy basalt, significant deformation of the Table Mountain occurs in the area directly west of the crest, one of the consequences of which is the highest latite outcrops are west of the crest (Photo 2).

If an initial gradient of 1 m/km is assumed for the Lovejoy basalt, then 1,860 m of crestal uplift has occurred since 16 Ma. There is little change of the gradient of the Lovejoy basalt between the eastern margin of the Central Valley and the Little Grass Valley Fault, the western border of the deformed region west of the crest. If a paleogradient of 3.8-5.7 m/km is used for the Lovejoy basalt, based on a paleogradient range similar to that of Yuba River estimated by Christensen (1966) (and comparable to the present-day gradient of the western part of the Feather River), then the estimated crestal uplift is 1,530-1,660 m.

For the Table Mountain Latite, estimated post-9 Ma uplift is 1,940 m, assuming a paleogradient of 1 m/km on the western portion of the latite and an 11 m/km paleogradient for the eastern part (Photo 2). If paleogradient limits of 1.1-4.9 m/km estimated by Christensen (1966) for the western part of the drainage are used, then the uplift is 1,670-1,930 m.

Based on the above, there is some variation in late Cenozoic uplift along strike in the Sierra Nevada, but it does not appear to vary systematically. Estimates based on different methods appear to yield estimates within the same approximate range: about 1,400-2,400 m. Uplift estimates south of the San Joaquin drainage are difficult to test owing to the lack of late Cenozoic cover. However, the study of Unruh (1991) indicates that magnitude of uplift may be comparable to the above estimates at least as far south as the Kings River drainage. The amounts of late Cenozoic uplift are similar to that estimated from paleobotanical studies (Axelrod, 1957; Axelrod and Ting, 1960; Axelrod, 1980).

Timing of the initiation of uplift is somewhat imprecise because of uncertainty in dating of key stratigraphic horizons. Unruh (1991) interpreted the initiation of uplift to be marked by a regional unconformity between late Cenozoic strata in the eastern Central Valley, dated at 3.8 to 8.4 Ma, with a preferred age of ~5 Ma. However, uncertainties (in accuracy, more than precision) in conventional K/Ar dating of Cenozoic rocks may introduce greater uncertainties in this range (particularly in the older age limit). Huber (1981) suggested that late Cenozoic uplift accelerated after 10 Ma, but the precise start up age is rather widely bracketed (younger age limit is similar to that applied by Unruh). Unruh (1991) also noted that late Cenozoic uplift appeared to begin at the same time along the strike of the range. Estimates on the timing of initiation of tilt based on the incision history of the North Fork Feather River of Ar-Ar dated Plio-Pleistocene lava flows suggest an approximate 4.3 to 6 Ma start up time for late Cenozoic tilting (see subsequent discussion of stream incision; earlier estimate given by Wakabayashi and others, 1994).

STREAM INCISION RATES

The uplift and deformation of the Sierra Nevada have been accompanied by erosion and incision by streams. In the northern Sierra, the lack of large scale channeling of Oligocene and Miocene volcanic rocks and sediments into or through Eocene strata suggests little incision between Eocene and Miocene time (Table 2, bottom). In the southern Sierra (Tuolumne River drainage and south), Eocene deposits are lacking and younger Cenozoic deposits are rare, so estimates of Cenozoic incision rates are difficult.

Long-term average late Cenozoic incision rates can be estimated by dividing the elevation difference between the present channel and the tops of late Cenozoic deposits capping the interfluves by the age of the youngest of these deposits (Table 2). Most of the uppermost late Cenozoic deposits are mudflows of the Mehrten Formation and related rocks. Based on the age of the uppermost Mehrten Formation, the incision since deposition of the Mehrten Formation is estimated to be post-5 Ma. Stream incision would likely follow deposition of these volcanic rocks because of their deposition, whether or not tectonic tilting occurred. Thus, incision rates have also been estimated on the basis of the elevation difference between the bottom of late Cenozoic volcanic deposits and the present channel divided by the age of the youngest volcanic deposits (Table 2). Such rates are minimal because time required for the stream to cut through the volcanic rocks is not accounted for. The uncertainty introduced by the time required to downcut through the volcanic deposits is greatest where the volcanic deposits are thick relative to the total amount of incision and, especially, where the volcanic deposits are young (Quaternary). In the San Joaquin River drainage, incision can be measured with respect to the reconstructed position of the 10 Ma ancestral channel, as well as 3.5 Ma volcanic rocks that apparently erupted into the canyon (Huber, 1981). Little data are available on younger (latest Pliocene and Quaternary) rates of incision except in the northernmost Sierra Nevada, where volcanic rocks of 2.8, 2.1, ~1 Ma, and ~600 ka are found within the canyon walls of the North Fork Feather River (Figures 8 and 9).

Post-Mehrten incision ranges up to 1,340 m of total incision and 1,190 m of incision below late Cenozoic volcanic deposits (Table 2). For the major drainages, late Cenozoic long-term incision rates associated with the deepest parts of the canyons range from 0.10 to 0.24 mm/yr for incision below late Cenozoic volcanic deposits and 0.10 to 0.27 mm/yr for incision including downcutting through late Cenozoic volcanic deposits (Table 2). Rates estimated for the San Joaquin River are somewhat lower than those estimated for other drainages, but Huber (1981) notes evidence for acceleration of uplift during the post-10 Ma time frame. If significant late Cenozoic incision in the San Joaquin drainage did not begin until about 5 Ma, then post-5 Ma averaged incision rates of the San Joaquin River may be as high as 0.19 mm/yr. Incision and associated rates decrease progressively westward (downstream) toward the Central Valley margin, with some local variation related to late Cenozoic faulting (Photo 1; Figures 6 and 9).

In the North Fork Feather River upstream of its confluence with the East Branch North Fork, a succession of volcanic rocks was deposited into the ancestral canyon (Figures 6 and 9). These deposits are now preserved as bench or terrace-like remnants on the walls of the canyon, and river gravels are present locally along the bases of the remnants (Figures 6 and 9). Two volcanic units are relatively continuous in the canyon and are the remnants of basalt lava flows that flowed down the ancestral canyon from upstream in what is now Lake Almanor (Figures 8 and 9). The volcanic remnants record a cyclic history of lava flowing down the ancestral North Fork canyon, followed by river incision through the flow, another flood of lava down the canyon, and renewed incision (Figure 10). Thus, the oldest flows are preserved as the highest remnants above the present stream bottom, and the youngest flows are preserved as the lowest remnants. This relationship has been confirmed by Ar/Ar dating of the volcanic units (Wakabayashi and others, 1994).

Incision rates between deposition of different volcanic units can be estimated from the difference in elevation from the top of one unit to the bottom of the next younger one divided by the difference in age between the two units (Table 3).

able 2. Cenozoic incision rates.

Reach of stream	Minimum Incision (m); incision below volcanic rocks in parentheses	Incision rate, 5 Ma to present (mm/yr) Minimum basement incision rate in parentheses
	North Fork Feather River	
Serpentine Canyon (on East Branch)	820 (700)	0.16 (0.14)
At Sierra Crest near Belden	1340 (1190)	0.27 (0.24)
	Middle Fork Feather River	
At Sierra Crest	880 (610)	0.18 (0.12)
Hartman Bar area	950 (830)	0.19 (0.17)
Kanaka Peak	670 (620)	0.13 (0.12)
	North Yuba River	
Sierra Buttes area	880 (640)	0.18 (0.12)
Near Downieville	915 (640)	0.18 (0.12)
Cherokee Creek confluence	640 (460)	0.13 (0.092)
	North Fork American River	
Royal Gorge	1130 (700)	0.23 (0.14)
Moody Ridge	700 (620)	0.14 (0.12)
Near Indian Creek confluence	520 (430)	0.10 (0.086)
Near Auburn	240 (140)	0.049 (0.028)
	North Mokelumne River	
Near Mokelumne Peak	1190 (980)	0.24 (0.19)
Near (upstream of) Bear River confluence	880 (700)	0.18 (0.14)
Near (upstream of) Tiger Creek reservoir	370 (240)	0.073 (0.049)
Upstream of confluence, other forks	450 (420)	0.095 (0.084)
Mokelumne Hill (main river)	270 (210)	0.054 (0.042)
	Stanislaus River	
Lightning Mtn.	810 (400)	0.16 (0.080)
Dardanelles Cone	1185 (630)	0.24 (0.13)
Dardanelles E of Dardanelles fault	1075 (710)	0.22 (0.14)
Whittaker Dardanelles E of Whitaker Dardanelles fault	965 (610)	0.19 (0.18)
1.5 km downstream of Post Corral fault	1065 (670)	0.21 (0.15)
N. Fork-Middle Fork confluence	710 (520)	0.14 (0.10)
Directly E of Parrotts Ferry fault	395 (370)	0.079 (0.074)
Directly W of Rawhide Flat W fault	375 (270)	0.075 (0.054)
Directly E of Peoria Pass fault	275 (130)	0.055 (0.026)
	San Joaquin River (Huber, 1981)	
Fish Creek confluence	554 (10-3.5 Ma)	0.085
	372 (3.5-0 Ma)	0.11
N. Fork San Joaquin confluence	580 (10-3.5 Ma)	0.089
	390 (3.5-0 Ma)	0.11
Pine Flat (78 km E of hingeline)	675 (10-3.5 Ma)	0.10
	277 (3.5-0 Ma)	0.079
Mammoth Pool Dam	762 (10-0 Ma)	0.076
West end, Kennedy Table Mountain	533 (457) (10-0 Ma)	0.053 (0.046)
West end, Table Mountain	347 (268) (10-0 Ma)	0.035 (0.027)
	Post-Eocene to Miocene Incision (~35 to 15 Ma)	
Reach of stream	Incision (m)	rates (mm/yr)
Yuba River drainage	≤60	<0.003
American River drainage	≤60	<0.003

Note: For each river, rates are listed from upstream to downstream.

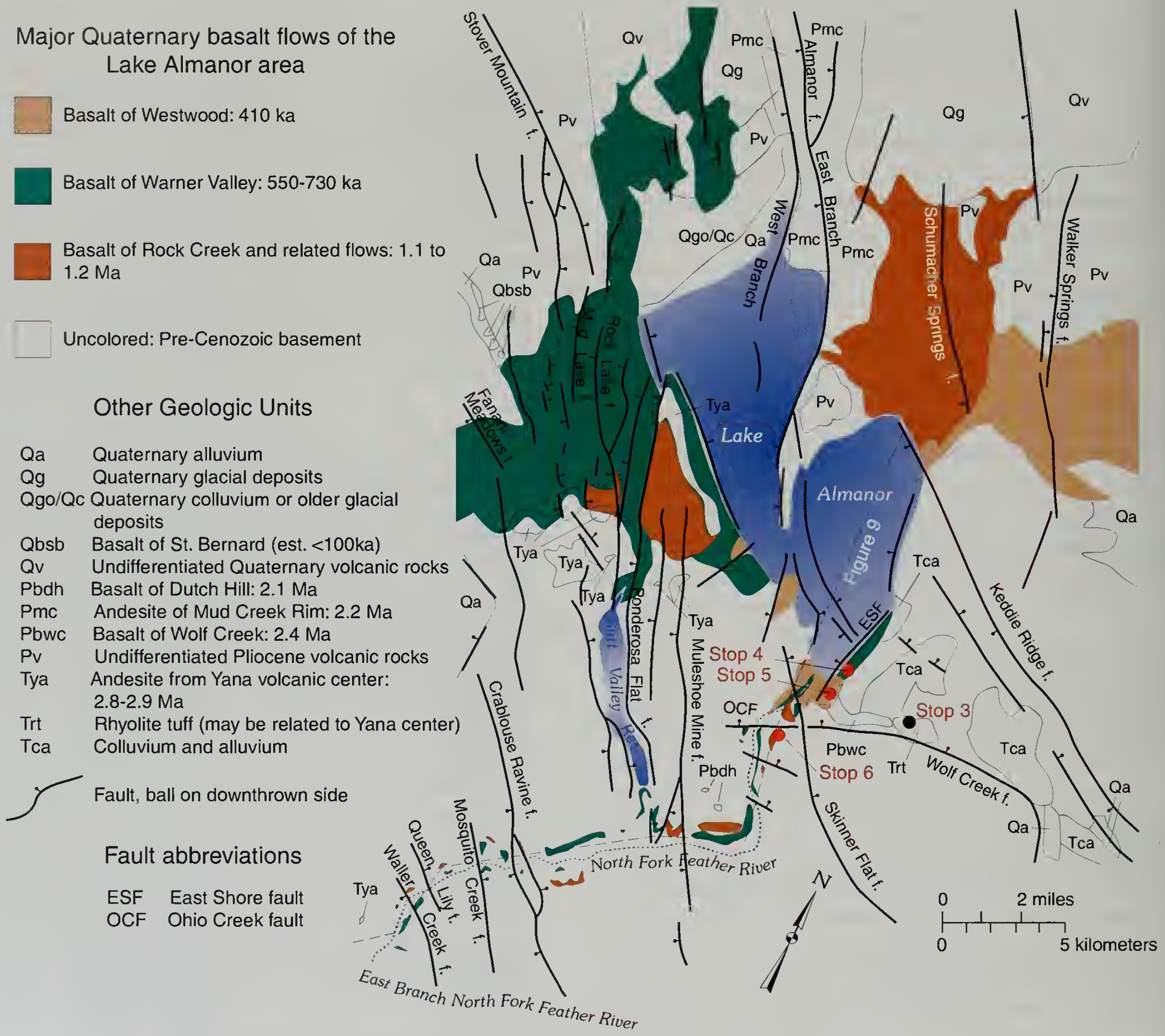
Major Quaternary basalt flows of the Lake Almanor area
Basalt of Westwood: 410 ka
Basalt of Warner Valley: 550-730 ka
Basalt of Rock Creek and related flows: 1.1 to 1.2 Ma
Uncolored: Pre-Cenozoic basement
Other Geologic Units
Qa Quaternary alluvium
Qg Quaternary glacial deposits
Qgo/Qc Quaternary colluvium or older glacial deposits
Qbsb Basalt of St. Bernard (est. <100ka)
Qv Undifferentiated Quaternary volcanic rocks
Pbdh Basalt of Dutch Hill: 2.1 Ma
Pmc Andesite of Mud Creek Rim: 2.2 Ma
Pbwc Basalt of Wolf Creek: 2.4 Ma
Pv Undifferentiated Pliocene volcanic rocks
Tya Andesite from Yana volcanic center: 2.8-2.9 Ma
Trt Rhyolite tuff (may be related to Yana center)
Tca Colluvium and alluvium
Fault, ball on downthrown side
Fault abbreviations
ESF East Shore fault
OCF Ohio Creek fault
Stover Mountain f.
Almanor f.
East Branch
West Branch
Schumacher Springs f.
Walker Springs f.
Fanani Meadows f.
Mud Lake f.
Rock Lake f.
Lake Almanor
Figure 9
Butt Valley Re
Ponderosa Flat f.
Muleshoe Mine f.
Crablouse Ravine f.
Keddie Ridge f.
Wolf Creek f.
Skinner Flat f.
Mosquito Creek f.
Queen Lily f.
Waller Creek f.
North Fork Feather River
East Branch North Fork Feather River
Stop 3
Stop 4
Stop 5
Stop 6
N
0 2 miles
0 5 kilometers

Figure 8. Major late Cenozoic volcanic units of the Lake Almanor area.

As discussed previously, this method may include incision driven solely by the deposition of the volcanic rocks. Alternatively, incision has been estimated based on the difference in elevation between the base of one unit to the base on the next youngest unit (Table 3). This method may significantly underestimate the incision rate because the amount of time required for the stream to cut through the volcanic deposits may be significant relative to the time interval between volcanic units. Examination of incision rates based on volcanic units in the North Fork Feather River canyon varies with time and proximity to late Cenozoic faults (Table 3; Figure 9). The data appear to show that incision rates from ~1 Ma to ~0.6 Ma and from 1 Ma to present were higher than incision rates from 2.1 to 1 Ma or 2.8 to 1 Ma by a factor of two to three or more. The data indicate that incision rates between ~1 Ma and ~0.6 Ma were either indistinguishable or faster than post-~0.6 Ma incision rates.

The possible decrease noted in the post ~0.6 Ma incision rates of the North Fork Feather River may be due to several factors. Some factors include: 1) incision has "caught up" with tilting and uplift so the stream gradient is constant with time; 2) regional climatic variations may have resulted in decreased flow of the North Fork Feather River in the past 0.6 Ma; 3) drainage rearrangement has decreased the flow in the North Fork Feather River in the past 0.6 Ma; and 4) acceleration of, or initiation of east-down (upstream-down) faulting in this reach of the river in the last 0.6 Ma may have lowered the effective local stream gradient. Movement histories of the two most significant faults crossing this reach of the North Fork Feather River, the Butt Valley Fault zone (Sawyer and others, 1996; Muleshoe Mine and China Bar faults on Figure 9) and the Skinner Flat Fault, support the premise that significant east-down faulting started after approximately 600 ka or so. Movement on these faults deposed the ~0.6 Ma basalt flows, based on identical separation of the ~1 Ma and ~0.6 Ma basalt flow units. However, there is too much uncertainty in fault separation estimates to determine whether movement began as recently on other faults in the region. In addition, data are insufficient to evaluate the relative role that Quaternary faulting had (compared to other factors) in the deceleration of incision rates.

The onset of incision of the North Fork Feather River canyon may be estimated by extrapolating the earliest constrained incision rate from the base of the oldest volcanic unit to the paleo canyon rim (Figure 11). This estimate is subject to three large uncertainties. First, the elevation of the paleo canyon rim is difficult to estimate. The second significant uncertainty comes from assuming that the incision rate between 2.8 Ma to ~1 Ma was constant and equal to the average rate in this period. The major increase in incision rate after 1 Ma compared to the rate between 2.8 Ma and 1 Ma rate may indicate that incision rate progressively increased from 2.8 to 1 Ma period and that incision rates from the onset of incision to 2.8 Ma should be less than the 2.8 Ma to 1 Ma average rate, which would lead to a significant underestimate in the age of onset of incision. The third source of uncertainty is in the method of determining incision rates. Incision rates based on the elevation difference between the top of a volcanic unit and bottom of the next youngest unit will overestimate the incision rate due to tectonic and other factors. Incision rates based on the elevation difference between the base of a volcanic unit and the base on the next youngest unit may underestimate incision rates because the time the river took to cut through the volcanic unit is not accounted for.

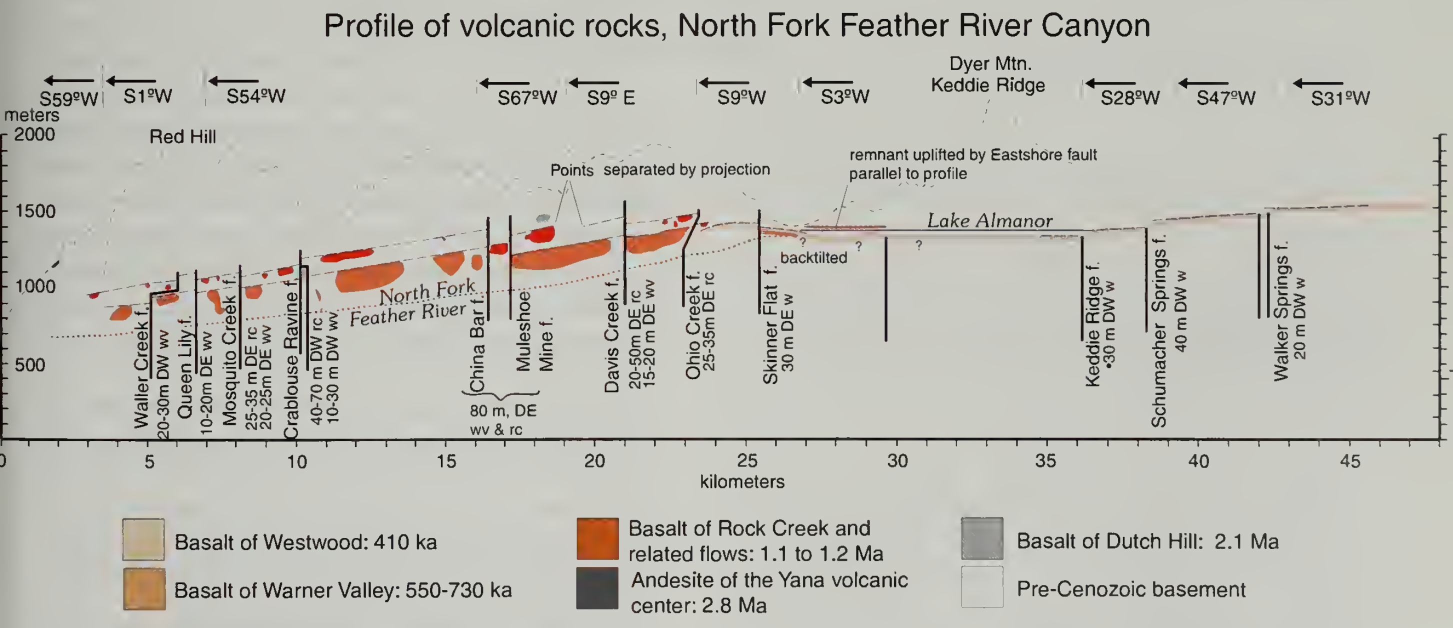

Figure 9. Profile of late Cenozoic basalt flows, North Fork Feather River canyon. 5x vertical exaggeration.

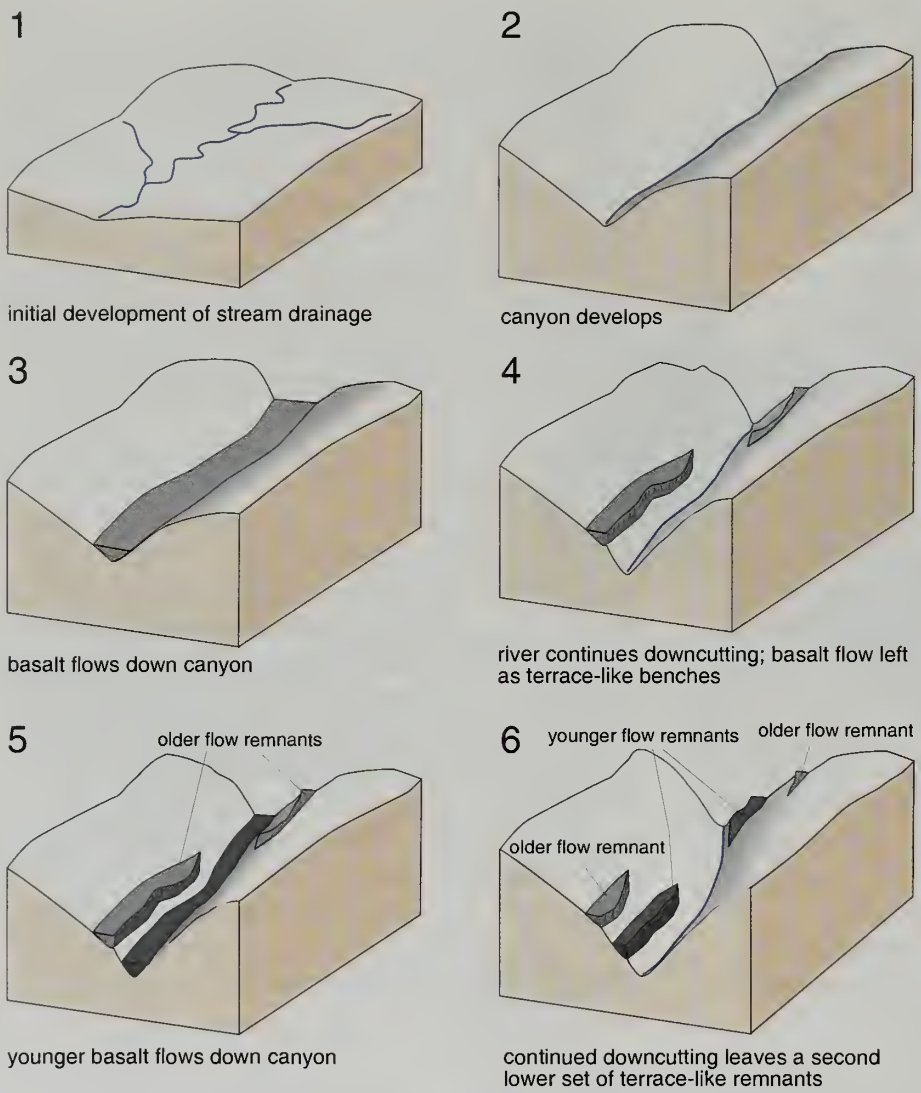
1
initial development of stream drainage
2
canyon develops
3
basalt flows down canyon
4
river continues downcutting; basalt flow left as terrace-like benches
5
older flow remnants
younger basalt flows down canyon
6
younger flow remnants
older flow remnant
older flow remnant
continued downcutting leaves a second lower set of terrace-like remnants

Figure 10. Block diagram illustrating development of basalt flow remnants in the North Fork Feather River canyon.

The estimated age of onset of incision of the North Fork Feather River based on the above assumptions is 4.3 to 6.0 Ma. (Figure 11), and a larger range of age is implicit, but difficult to quantify based on the uncertainties discussed above. The estimate for onset of incision is similar to estimate of the onset of late Cenozoic uplift of Unruh (1991).

The data appear to show significant temporal variations in incision rate in the North Fork Feather River since 2.8 Ma, with higher Quaternary rates than the late Cenozoic average. There are no data to indicate whether other Sierra Nevada drainages experienced higher incision rates in the Quaternary. The increase in Quaternary incision rates of the North Fork Feather River may be a response to late Cenozoic tilting of the Sierra. If a rigid block model applies to Sierra Nevada deformation, then it is likely that other Sierra Nevada drainages experienced an acceleration of incision rates during the Quaternary. In such a model, stream gradients and related stream power available for channel downcutting were low prior to the onset of late Cenozoic uplift but increased progressively as uplift and tilting of the Sierra Nevada began.

PRESERVED PRE-CENOZOIC TOPOGRAPHY: INFLUENCE ON ALONG STRIKE VARIATION IN SIERRAN TOPOGRAPHY

If the magnitude of late Cenozoic uplift does not systematically increase southward within the range, why does the crestal elevation increase southward, and why do the southern and northern Sierra Nevada have different cross sectional topography? Evaluation of topography that predates late Cenozoic uplift may give some insight into this problem. Such an evaluation indicates that along strike variations in present Sierran topography reflect pre-Cenozoic topography.

The minimum topographic relief that existed at the time of the deposition of Cenozoic deposits, here referred to as paleo relief, can be estimated by comparing the elevation of basement (pre-Cenozoic granitic and metamorphic rocks) topographic highs relative to the elevation of Cenozoic strata at the base of paleo drainage channels. The elevation difference is a minimum estimate of relief that

Table 3. Incision rate of the North Fork Feather River.

Fault block or reach of river	Elevation, top/ bottom of volcanic remnants above river (m)	Age, volcanic remnants (Ma)	Incision rate (mm/yr) parentheses denote minimum basement incision rate
Ohio Creek to Salmon Creek	150/7 267/186	0.57-0.73 0 1.11-1.20	0.57-0.73 Ma to present: 0.21-0.26 (0.096-0.12)1.11-1.20 to 0.57-0.73 Ma: 0.31-0.52 (0.18-0.31)
Davis Creek to Meeker Bar	219/76 344/283 407/332	0.57-0.73 1.11-1.20 2.05	0.57-0.73 Ma to present: 0.30-0.38 (0.10-0.13) 1.11-1.20 to 0.57-0.73 Ma: 0.43-0.71 (0.33-0.54) 2.05 to 1.11-1.20 Ma: 0.13-0.15 (0.052-0.058)
Butt Creek to Crablouse Ravine	271/107 381/302	0.57-0.73 1.11-1.20	0.57-0.73 Ma to present: 0.37-0.48 (0.15-0.19) 1.11-1.20 to 0.57-0.73 Ma: 0.43-0.72 (0.31-0.51)
Crablouse Ravine to Mosquito Creek	204/101 305/235	0.57-0.73 1.11-1.20	0.57-0.73 Ma to present: 0.28-0.36 (0.14-0.18) 1.11-1.20 to 0.57-0.73 Ma: 0.32-0.54 (0.21-0.35)
Mosquito Creek to Queen Lily	213/49 293/244	0.57-0.73 1.11-1.20	0.57-0.73 Ma to present: 0.29-0.37 (0.067-0.086) 1.11-1.20 to 0.57-0.73 Ma: 0.39-0.64 (0.31-0.51)
Waller Creek Fault to East Branch confluence	165/85 302/238 470/378	0.57-0.73 1.11-1.20 2.81	0.57-0.73 Ma to present: 0.23-0.29 (0.12-0.15) 1.11-1.20 to 0.57-0.73 Ma: 0.34-0.57 (0.24-0.40) 2.81 to 1.11-1.20 Ma: 0.14 (0.082-0.086) 2.81 Ma to present: 0.17 (0.13)

predated late Cenozoic uplift, because some erosional lowering of these basement topographic highs has occurred during the late Cenozoic. Erosion rates of upland areas in the Stanislaus River drainage have been estimated at 0.008-0.018 mm/yr averaged over the last 9 Ma (Page and Noryko, 1977). Erosion rates for several upland sites in the northern Sierra Nevada have been estimated as 0.015 to 0.075 mm/yr for the last several thousand years (Riebe and others, in review). Thus, the amount of erosional lowering of basement highlands in the late Cenozoic is probably small compared to the total amount of preserved paleo relief that ranges up to a kilometer or more.

In general, paleo relief increases progressively southward from the northernmost Sierra to the

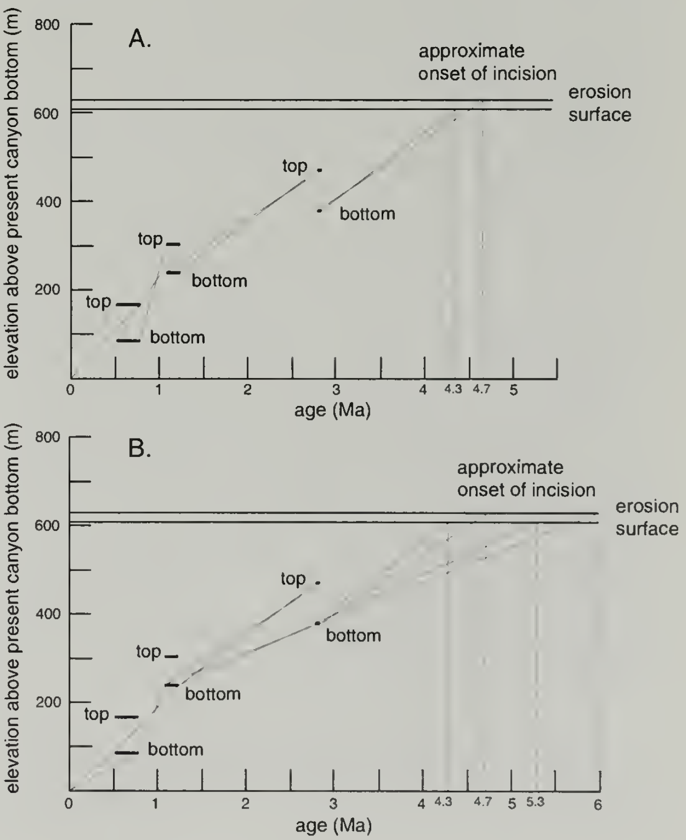

Figure 11. Diagram showing the downcutting of the North Fork Feather River through time, as constrained by dated inset volcanic rocks, and estimates of the onset of incision. A) shows downcutting history including incision through the volcanic rocks, whereas B) shows only incision through basement.

San Joaquin River drainage. Paleo relief in drainages is discussed below for drainages from north to south. The Lovejoy basalt, in the Feather River region, underlying gravels (where present) and overlying mudflows are higher than adjacent basement exposures, except for a granitic knob near the west end of Mooreville Ridge that crests about 200 m higher than the base of the basalt (Figure 5). Elsewhere in the Feather River drainage, the bases of Mehrten or Eocene gravel channels are generally fewer than 200 m below basement crests, with the highest amounts of paleo relief in the western (downstream) reaches of the southern part of the drainage and the western Feather River-Yuba River divide. In the Yuba River drainage, the region within 25 km west of the crest includes several basement highs with paleo relief of more than 400 m, the highest of which is the Sierra Buttes, 790 m above the base of the ancestral Yuba River. The American River drainage is similar to the Yuba, except that in the southern part of the drainage the region with local paleo relief of over 400 m extends up to 35 km southwest from the crest. The Mokelumne River drainage has several ridges of 250 to 520 m of paleo relief in the western part of the drainage, where the paleo rivers cut through resistant units of metavolcanic rocks. In the middle elevation reaches paleo relief is generally fewer than 250 m, except for Blue Mountain, which has local paleo relief of 690 m. In the higher elevations of the Mokelumne River drainage, paleo relief is mostly below 350 m except for isolated highs, such as Mokelumne Peak with a local paleo relief of 680 m. The Stanislaus drainage (Figure 6) is somewhat similar to the Mokelumne, with relatively high paleo relief in the lower elevation parts of the drainage (up to 380 m), and relatively subdued paleo relief in the middle and higher elevations of the drainage (mostly fewer than 300 m except for isolated highs up to 700 m). (These occur mostly in the middle-elevation reaches.) In the Stanislaus and Mokelumne River drainages, most of the highest peaks in the crestal region are capped with several hundred meters of Cenozoic volcanic rocks.

The Tuolumne River drainage is in the transition area from the northern Sierra type topography (constant westward slope) to the southern Sierra type topography (steep western front) (Figures 3 and 4). The elevation of the basement above the base of the ~10 Ma ancestral Tuolumne River channel ranges from 400 m in the west to about 900 m in central Yosemite National Park (Rancheria Mountain in Figure 7A). The high paleo relief is much more continuous than to the north where the highest areas of paleo relief are discrete ridges and peaks. Similarly, incision of the ~10 Ma San Joaquin River channel increases eastward from fewer than 300 m to over 700 m across the major west-facing topographic step, and is up to 1,280 m farther east, with many ridges with peaks over 1,000 m of paleo relief (Huber, 1981). South of the San Joaquin River, late Cenozoic deposits are too scattered to allow reconstruction of Cenozoic drainages, so it is difficult to evaluate paleo relief.

Based on the distribution and elevation of pre-late Cenozoic basement highlands, it appears that much of the difference in topographic expression between the northern and southern Sierra Nevada is a consequence of greater paleo topography in the southern part of the range. Thus, much of the higher crestal elevations in the southern part of the range may be a result of pre-late Cenozoic topography rather than larger magnitudes of late Cenozoic uplift. The large contrast in pre-late Cenozoic topography across the major west-facing topographic step in the San Joaquin drainage suggests that much of this escarpment represents pre-late Cenozoic topography rather than major late Cenozoic west-down faulting or warping. This supports the hypothesis of Wahrhaftig (1965) who argued that the west-facing topographic escarpments were erosional in origin and not fault scarps. However, the ancestral Tuolumne River profile (Figure 7A) suggests that west-down faulting associated with the topographic steps may be present, although the contribution of this faulting to the topography is subordinate to that of the paleo relief.

Because uplift between the Eocene and Miocene was apparently negligible, as noted previously, the paleo relief is probably a consequence of an earlier period of uplift that was likely associated with major exhumation between late Cretaceous and Eocene time. This is consistent with thermochronologic evidence (House and others, 1997, 1998).

Why more pre-late Cenozoic topography is preserved in the southern part of the range is not clear. Thermobarometric studies indicate that the depth of crystallization of plutons does not systematically vary along strike across the regions of differing preserved topography (Ague and Brimhall, 1988), so the amount of pre-Eocene, post-batholithic uplift is relatively constant along strike. Within the rather large permissible age range for the pre-Eocene uplift event, some 35 million years, it is possible the uplift occurred earlier in the northern part of the range, so there was more time for erosion to reduce relief prior to the deposition of the Eocene gravels. Alternatively, the reduction of Eocene paleo relief in the northern Sierra Nevada may be a consequence of the larger number of major river systems that traversed that region. The ancestral Feather, Yuba, American and Stanislaus rivers all had sources well east of the present crest, whereas there is no major paleo drainage south of the San Joaquin River that is known to headed east of the present crest.

It is interesting to consider what proportion of the present elevation of the Sierra Nevada is a result of late Cenozoic uplift and what proportion is a result of pre-Eocene uplift. Because late Cenozoic rocks make up the highest elevations from the Stanislaus northward, late Cenozoic uplift is responsible for most of the crestal elevation. Thus, for the Feather River drainage, crestal elevations are about 2,000 m and the estimated late Cenozoic uplift is 1,500 to 1,900 m; some of the difference in elevation is a consequence of the capping of crestal ridgetops with 200 to 250 m of late Cenozoic volcanic rocks. For the Stanislaus drainage, the estimated late Cenozoic uplift is 1,700-1,900 m and the crestal elevations are as high as 3,500 m (several hundred meters of this elevation come from late Cenozoic volcanic rocks that overlie the Table Mountain Latite and correlative rocks).

In the Tuolumne drainage, the estimated late Cenozoic uplift is 1,480 m and the crestal elevations are as high as 4,000 m. In the San Joaquin drainage, the estimated late Cenozoic uplift is 2,150 m and crestal elevations are as high as 4,000 m. Thus, residual topography from pre-Eocene uplift contributes significantly to the elevation of the southern, but not the northern, Sierra Nevada.

LATE CENOZOIC FAULTING

Late Cenozoic Vertical Separation along the Frontal Fault System

The eastern escarpment of the Sierra is higher in the southern part of the range, but relationship between the height of this escarpment and amounts of late Cenozoic east-down separation along the Frontal Fault system is unclear. This is because correlative late Cenozoic deposits are present on both sides of the Frontal Fault system south of the headwaters of the San Joaquin River.

In the northernmost Sierra Nevada (Feather River drainage), the vertical separation of ~5 Ma volcanic mudflows and 16 Ma Lovejoy basalt across faults of the Frontal Fault system in the northernmost Sierra (Feather River drainage) is approximately 600-1,000 m. In the vicinity of Sonora Pass (Stanislaus River drainage), the vertical separation of the ~9 Ma Eureka Valley tuff that overlies the Table Mountain Latite is about 1,100 m (positions of units from Noble and others, 1974 and Slemmons, 1966). At the headwaters of the San Joaquin River a 2.2 to 3.6 Ma volcanic unit is vertically separated about 980 m across the Frontal faults (Bailey, 1989). The aggregate vertical separation of these volcanic rocks between crestal exposures and their buried correlatives in the Long Valley caldera may be as much as 2,100 m (Bailey, 1989); much of this separation may be partly a consequence of caldera collapse instead of entirely Frontal faulting. Gravity data have been interpreted as indicating 2.1 km of downdropping and filling of Owens Valley with late Cenozoic sediments (Pakiser and others, 1964). Bachman (1978) using different estimates for the density of valley fill with the same data estimated 1.1 km of downdropping. The part of the height of the eastern escarpment above Owens Valley that is a product of late Cenozoic faulting would add to the downdropping (below Owens Valley) estimate for the total late Cenozoic vertical separation across the escarpment. This amount is difficult to estimate owing to the lack of late Cenozoic deposits near the crest.

Late Cenozoic vertical separation along the highest part of the eastern Sierra escarpment in Owens Valley is probably at least comparable to reaches of the escarpment to the north (~1 km). Such an estimate would yield a total late Cenozoic vertical separation for the escarpment in Owens Valley of 2.1 km using Bachman's (1978) interpretation of the gravity and 3.1 km using the original interpretation of Pakiser and others (1964). If late Cenozoic above-valley vertical separation along the eastern escarpment of Owens Valley is similar to the post-2.4 Ma uplift of the White Mountains (bounding the Owens Valley on the east and attaining similar maximum crest elevation at White Mountain peak), estimated from the tilt of the Waucobi Lake beds (Bachman, 1978), then the late Cenozoic vertical separation along the eastern Sierra Nevada escarpment of Owens Valley is 2.3 km with Bachman's interpretation of Owens Valley gravity data and 3.4 km with the original gravity interpretation of Pakiser and others (1964).

Late Cenozoic vertical separation across the Frontal Fault system does not seem to vary systematically from the northernmost Sierra to the headwaters of the San Joaquin River. Vertical separation along the Frontal Fault system may be higher south of the San Joaquin River headwaters, based on the above discussion, but this is difficult to confirm with available data. If vertical separation along the Frontal Fault system is indeed higher in Owens Valley than to the north, then it contrasts with the lack of systematic variation of late Cenozoic uplift. This contrast may be partly because late Cenozoic tilting and uplift of the Sierra Nevada was associated not only with east-down separation along the present Frontal Fault system, but also with older fault systems to the east, as will be discussed below.

Timing of Late Cenozoic Vertical Separation along the Frontal Fault System: Evidence for Westward Migration of the Sierra Nevada-Basin and Range Boundary

Faulting along much of the Frontal Fault system postdated the initiation of late Cenozoic tilting and uplift of the Sierra Nevada. Many of the tilted Cenozoic deposits that record this deformation have sources east of the present range crest, and the ancestral drainages in which these deposits occur could not have flowed "uphill." Some of the major paleo drainages in the range, such as the San Joaquin (Huber, 1981) Stanislaus, American and Yuba river (Lindgren, 1911) drainages, have been beheaded by movement along the Frontal faults. Most of the late Cenozoic volcanic rocks of the Sierra erupted from sources east of the present crest (Durrell, 1966; Slemmons, 1966). Some Frontal faults, such as the Spanish Peak-Little Grass Valley fault zone, and the Carson Range-Disaster Creek fault zone, continue southward into the range with diminished vertical separation that results in local downdropping of the crest of the range (discussed below). These faults, volcanic rocks, and beheaded drainages indicate that the Sierra Nevada-Basin and Range boundary and associated Frontal faulting have migrated westward in the late Cenozoic.

In the Feather River area, the 16 Ma Lovejoy basalt and overlying mudflow deposits (Mehrten Formation or equivalents), have the same separation across faults of the Frontal Fault system indicating that faulting did not commence until after the deposition of these mudflows (Page and Sawyer, 1992; PG&E unpublished data). The age of the youngest mudflow deposits is poorly constrained. The youngest age for these deposits in the area is 6.8 Ma (Saucedo and Wagner, 1992), but it is not clear whether this age is from the stratigraphically highest part of these deposits. The stratigraphically highest parts of similar deposits to the south may be as young as 4 Ma (Unruh, 1991). Some andesitic deposits in the vicinity of and south of Donner Summit (headwaters of the North Fork American River) have ages of 3.3 to 5.4 Ma (Harwood, 1986; data cited in Saucedo and Wagner, 1992) and may be proximal equivalents of some of the mudflows in the northern Sierra. However no evidence has been presented that directly links these deposits to mudflow deposits to the west or links them temporally with andesitic rocks to the north. Accordingly, Frontal faulting in the Feather River area probably began sometime after 6.8 Ma.

Prior to the establishment of the present Frontal Fault system, the northern Sierran block may have extended to the east-facing escarpment along the Honey Lake Fault zone, east of the crest of the Diamond Mountains (Figures 2 and 5). Movement on the Honey Lake fault zone postdates the 10 Ma Thompson Peak Basalt, that has a source east of the escarpment and is faulted across it (Roberts, 1985). Mehrten Formation and equivalent andesitic rocks are common west of the Diamond Mountains crest, but are rare or absent east of it. This indicates that significant dip slip faulting along the Honey Lake escarpment may have begun between 10 Ma and 6.8 Ma (younger age limit is dependent on the age of the youngest Mehrten Formation as discussed above).

Movement on some of the most significant faults of the Frontal Fault system in the North Fork Feather River canyon probably did not begin until after 600 ka. Thus, the northern Sierra Nevada-Basin and Range boundary appears to have migrated 50 km westward, from the Honey Lake area to the present eastern escarpment of the northern Sierra Nevada within the last 6.8 Ma. It has encroached into the northernmost part of the range since the mid to late Quaternary.

The Sierra Nevada-Basin and Range boundary to the south also appears to have migrated westward during the late Cenozoic. The western edge of the central Walker Lane belt (i.e., the Sierra Nevada-Basin and Range boundary) from 38°N to 39°N migrated 100 km westward from 15 to 7 Ma, based on detailed structural, stratigraphic and geochronologic studies (Dilles and Gans, 1995). East of the Lake Tahoe area, Sierran Frontal faulting began after 10 Ma based on syntectonic sediments in the Verdi Basin (Trexler and others, 1999) and began at 7 Ma based on syntectonic basal sediments in the Gardnerville Basin (Muntean and others, 1999). The data from these basins fit the overall progression of deformation noted by Dilles and Gans (1995). Slemmons and others (1979) also suggested westward encroachment of the Walker Lane into the Sierran block, based on somewhat broader age constraints.

In the Mammoth area (headwaters of the San Joaquin River), the major faults of Frontal Fault system did not begin vertical movement until after about 3 Ma, otherwise the flow of a 2.2 to 3.6 Ma volcanic unit across the faults would have been blocked (Bailey, 1989). This is supported by the calculated 3 Ma elevation of the headwaters of the ancestral San Joaquin River (Huber, 1981)

Bachman (1978) suggested that Sierran escarpment in the Owens Valley area did not form until 2.3 to 3.4 Ma, consistent with the timing of Frontal faulting in the headwaters of the San Joaquin River. If his conclusions are correct, then the height of the eastern escarpment plus the depth of late Cenozoic valley fill may be entirely a consequence of late Cenozoic faulting, unlike crestal elevations that are partly inherited from pre-Eocene uplift. Although Bachman's (1978) data and observations constrain timing of the uplift of the White Mountains (the range east of Owens Valley), they do not necessarily preclude the earlier existence of a Sierran escarpment associated with prior Frontal faulting.

In the southern Sierra, a belt of seismicity (Figure 2) characterized by east-side-down normal fault focal mechanisms, has been interpreted as an incipient westward jump of the Sierra Nevada-Basin and Range boundary (Jones and Dollar, 1986). The topography across this zone (Figure 4I) is consistent with major faulting along this zone, but there are no late Cenozoic deposits to verify that the topography indeed reflects late Cenozoic vertical separation.

Along Strike Variation in the Character of the Frontal Fault System

South of Bishop, the eastern front of the Sierra is bounded by a major dextral fault, the Owens Valley Fault, and by normal faults along the base of the main topographic escarpment, principally the Independence Fault. This escarpment is continuous far to the south. North of Bishop, where much of the dextral slip diverges eastward (Figure 1), the rangefront is composed of a series of left stepping en-echelon escarpments that reflect normal or oblique faulting. This geometry persists as far north as the Tahoe Basin. North of the Tahoe

Basin, a zone of dextral faulting, the Mohawk Valley Fault zone marks the eastern boundary of the Sierra. In the vicinity of Quincy the Frontal Fault system broadens so faulting is distributed on many strands in a zone 30-40 km wide (Figures 2, 4A and 12; Photo 5).

North of Bishop several of the en echelon Frontal faults can be traced southward across the crest of the range because late Cenozoic deposits exist to identify faulting (Figures 1, 2 and 12). Cumulative separation decreases abruptly from east to west across the range crest (PG&E,

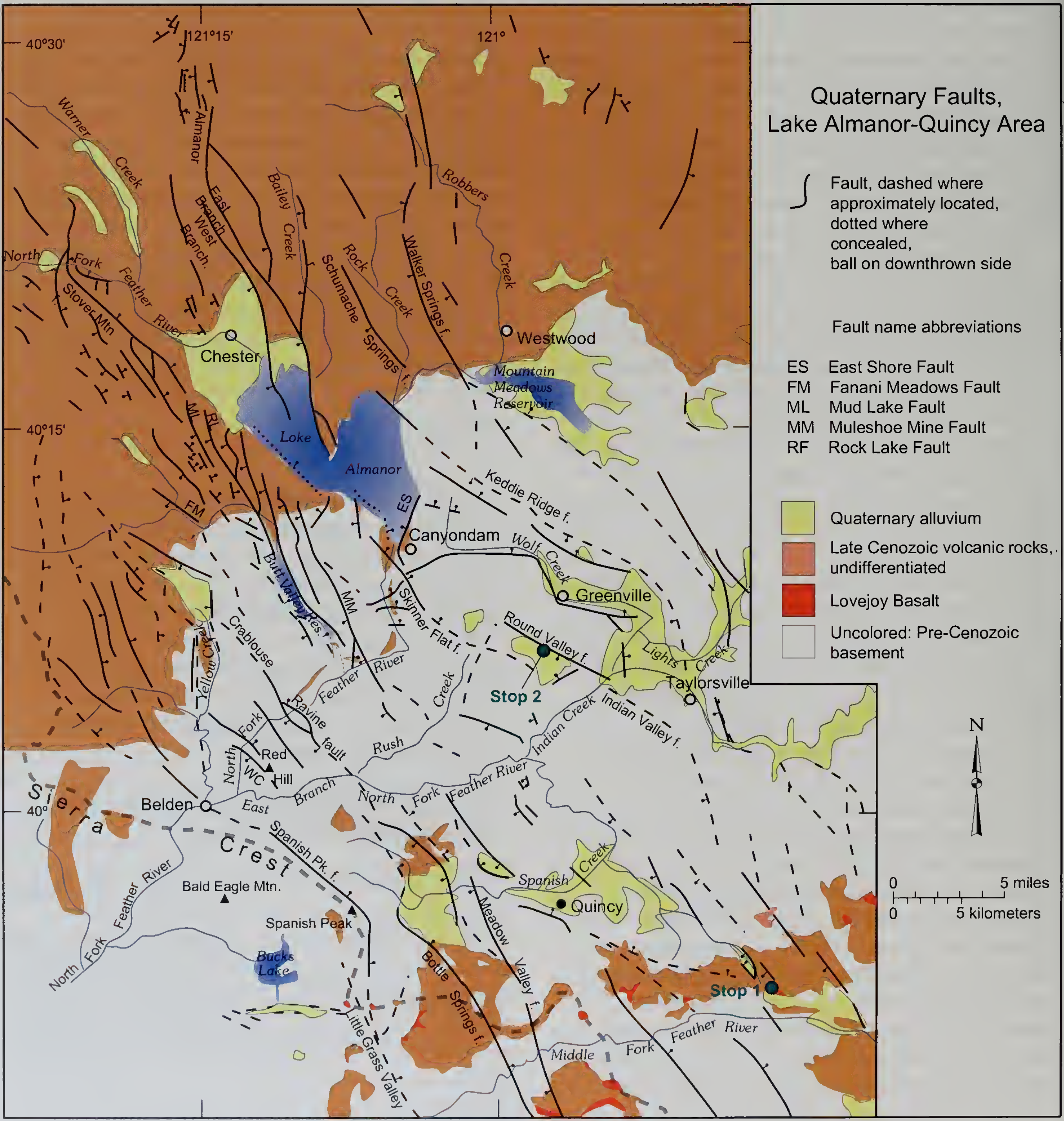

Figure 12. Late Cenozoic (most Quaternary) faults in the Lake Almanor-Quincy area and distribution of late Cenozoic deposits.

Photo 5. Mohawk Valley north-northwestward from the summit of Haskell Peak, a peak on the top of the escarpment. Difference in elevation between Haskell Peak and the valley floor is about 1,100 m. *Photo by John Wakabayashi.*

unpublished data; Figure 2). For example, the Spanish Peak Fault, the main Frontal Fault west of Quincy, extends from the base of the eastern escarpment southward across the range crest and into the northern Sierra Nevada as the Little Grass Valley Fault. The Spanish Peak Fault vertically separates the Mehrten Formation by about 600 m down-to-the east, whereas the Little Grass Valley Fault zone separates correlative mudflows and the underlying Lovejoy basalt about a third as much (180-240 m) (PG&E, unpublished data; Photo 1). Other Frontal faults that cross the crest have been identified in the upper Stanislaus drainage where the Disaster Creek and Arnot Creek faults are the southern continuation of the Carson Range Fault zone (Figures 2 and 6), and in the headwaters of the San Joaquin River, where faulting along the Hartley Springs Fault zone crosses the crest (Huber, 1981; Bryant, 1984; Bailey, 1989). The geometry of faults along much of the Sierra Nevada north of the Bishop suggests that other Frontal faults probably extend southward across the crest in a similar manner, but late Cenozoic deposits are lacking to confirm their presence. These faults provide a structural tie between faults of the Frontal Fault system and lesser, but apparently related, late Cenozoic faults in the eastern part of the Sierran block.

Internal Deformation of the Sierra Nevada

Internal deformation within the Sierra Nevada, which is recorded by faulting and local tilting of late Cenozoic deposits, is minor compared with major faulting along the Frontal Fault system (Lindgren, 1911; Bateman and Wahrhaftig, 1966; Christensen, 1966). The 1975 M5.7 Oroville earthquake (Hart and Rapp, 1975) led to many studies of faulting in the foothills region of the Sierra, most of which were consultants' studies that resulted in unpublished reports. Partly as a result of the concentration of studies in the foothills region, the concept of a "Foothills Fault system" was developed, which postulated that late Cenozoic internal deformation in the Sierra Nevada is concentrated in the foothills region (WCC, 1977; 1978; Bartow, 1990). According to this model, late Cenozoic faulting reactivated parts of pre-Cenozoic faults within the metamorphic rocks of the Sierra (Schwartz and others, 1977).

However, analysis of the deformation of the Lovejoy basalt and Table Mountain Latite (Ely, 1992; Sawyer and Page, 1992), as well as evidence from other areas of the Sierra, indicate that internal deformation and faulting is not preferentially concentrated along the Foothills Fault system nor within the metamorphic rocks (Sawyer and others, 1993a; PG&E, unpublished data; Figures 2, 5 and 6). Where constraints from late Cenozoic deposits exist (north of the San Joaquin River drainage), internal deformation appears to be distributed relatively evenly across the Sierra without regard to the type of basement (Figures 1 and 2; Photo 2). Cumulative late Cenozoic displacements systematically increase eastward toward the Frontal Fault system (Figures 2, 5 and 6). This pattern is consistent with the studies of the en echelon Frontal faults that cross the crest, because cumulative displacement on these strands decreases systematically west of the crest (Figure 2).

The internal faults shown in Figure 2 do not capture all of the internal faulting within the range. Fault lengths shown reflect only the length along which likely late Cenozoic faulting can be supported by stratigraphic or strong geomorphic evidence (following criteria reviewed in Jennings, 1994, based on PG&E, unpublished data). Because of the scattered nature of suitable outcrops necessary to confirm late Cenozoic offset, the fault lengths shown likely represent minimum lengths. In addition, late Cenozoic faults have not been identified in regions lacking late Cenozoic deposits. This explains the lack of internal faults south of the Tuolumne River drainage on Figure 2. The pattern of internal faulting within the granitic terrain (Figures 2, 6 and 7A) indicates that internal faulting may continue southward into the region lacking in Cenozoic cover. Significant tilting (dip steeper than 40°) of an isolated late Cenozoic volcanic deposit along the West Fork Granite Creek (a tributary to the San Joaquin River) is almost certainly of tectonic origin, and is evidence of late Cenozoic internal faulting south of the southernmost internal fault shown in Figure 2.

The northernmost and southernmost Sierra exhibit different a somewhat different distribution of internal deformation that may be transitional to tectonic provinces to the north and south of the Sierra, respectively. In the southernmost Sierra, the western margin of the range is bordered by several Quaternary faults, some of which moved during the 1952 M 7.5 Kern County earthquake (Jennings, 1994; Figure 2). In the northernmost Sierra, north of the Feather River, the western margin of the range is marked by a prominent west-down flexure, the Chico Monocline, which warps or displaces Pliocene volcanic rocks. North of the Feather River, a pair of internal faults, the Beaver Creek and Cohasset Ridge faults, has a aggregate down-to-the-east vertical separation rate of 0.07 mm/yr, higher than any other identified internal faults (Figure 2).

Similar to faulting along the Frontal Fault system, many of the late Cenozoic internal faults may have initiated movement after late Cenozoic uplift and tilting began. Mehrten Formation and related mudflow deposits are offset the same amount as older Cenozoic strata across most of the internal faults (PG&E, unpublished data; WCC 1977, 1978). Based on estimates for ages of the youngest mudflow deposits the initiation of movement on these internal faults was approximately 4 to 5 Ma (see earlier discussion on uncertainties in the ages of these deposits, however). There are a few faults in the foothills region that display greater vertical separations of older late Cenozoic units (PG&E, unpublished data), indicating that some internal faults were active at least as long ago as 20 Ma. It is possible these older faults may have been associated with the localized deformation in the westernmost part of the range between the Eocene and Miocene noted earlier.

Based on an initiation of faulting around 5 Ma, vertical separation rates of faults can be estimated, allowing comparisons to other faults within the Sierra and the Frontal Fault system. These estimates show that vertical separation rates increase eastward toward the crest from thousandths of a mm/yr in the Sierra Nevada foothills region to hundredths of a mm/yr directly west of the crest. These rates are minor compared with vertical separation or dip slip rates of tenths of a mm/yr to several mm/yr for faults of the Frontal Fault system (Figure 2). Thus, although the distribution of internal deformation of the Sierra Nevada may be somewhat different than was previously perceived, the general conclusion that this internal deformation is small in scale compared to deformation along the Frontal Fault system is still supported.

Late Quaternary Faulting Within the Sierra Nevada and Along the Frontal Fault System

Although late Quaternary faults were recognized along the eastern escarpment of the Sierra Nevada more than a century ago (Gilbert, 1883; Russell, 1887), they have only been recognized within the Sierra Nevada since the 1975 Oroville earthquake. Most of the more than 30 significant faults of the Frontal Fault system have demonstrated late Quaternary offsets and these faults range from 25 km to more than 100 km long (Clark and others, 1984; Jennings, 1994). Among these faults is a nearly continuous zone of overlapping Holocene and historical faults that bound nearly 400 km of the Sierran front from southernmost Owens Valley northward to Reno.

Two of the more significant Frontal faults are the Carson Range Fault zone and the Owens Valley Fault zone at either end of the zone of Holocene faulting. The Carson Range Fault zone, which includes the Genoa Fault, near the north end of the zone, is marked by a prominent, fresh scarp. This scarp is a consequence of late Holocene fault ruptures, the two most recent of which were 2,000-2,200 and 500-600 years ago. These ruptures are associated with 3 to 5.5 m of single-event normal fault displacement along much of the length of the zone, and suggest M 7.2 to 7.5 earthquakes on the basis on comparison to historic earthquake ruptures in the Basin and Range (Ramelli and others, 1999). In 1872 a M~7.8 earthquake ruptured the Owens Valley Fault zone and also produced several meters of surface offset, in a right-lateral to right-oblique sense (Beanland and Clark, 1995). The Carson Range Fault zone has a recurrence interval of 1.5 to 4.5 ka for individual segments (Ramelli and others, 1994), which is comparable to the recurrence interval for the Owens Valley Fault zone of 3.3 to 5 ka (Beanland and Clark, 1995). These and other prominent faults of the Frontal Fault system have dip-slip rates of several tenths of a mm/yr to 2.5 mm/yr (Clark and others, 1984; Petersen and others, 1996; Figure 2).

In contrast, evidence for latest Pleistocene to Holocene movement has been found on only eight faults within the Sierra Nevada (Page, 1999), which in part may be due to additional difficulties of identifying Quaternary faults in a mountainous region like the Sierra Nevada (Page and Sawyer, in press). The Cleveland Hill Fault is the only fault in the Sierra Nevada to have ruptured historically. In 1975 a ML5.7 Oroville earthquake produced minor oblique-right surface rupture along the Cleveland Hill Fault (Hart and Rapp, 1975; Clarke and others, 1976). Trenching investigations on this and other late Quaternary faults provide evidence for recurrent movement during the mid to late Quaternary. Single-event displacements appear to be minor (5 to 50 cm) suggesting relatively small earthquakes, and recurrence intervals are on the order of tens of thousands to possibly hundreds of thousands of years for faults in the western part of the Sierra (Page and Sawyer, in press).

Paleoseismic trenching studies of the Little Grass Valley Fault at Dogwood Peak revealed evidence for three to four late Pleistocene events associated with colluvial wedges 25 to 75 cm thick (Page and Sawyer, in press). Vertical single-event displacement likely exceeded the colluvial wedge thickness. In addition, low angle slickensides and stratigraphic relationships suggest a significant, if not dominant component of strike-slip on the fault, so net displacement is greater than the vertical displacement. Thus, the single-event displacement on the Little Grass Valley Fault is apparently greater than that of faults that have been trenched in the western Sierra. The Little Grass Valley Fault may be representative of faults in the eastern part of the Sierran block that are related to Frontal faults crossing the crest of the range.

RELATIONSHIP OF STREAM INCISION, UPLIFT, TOPOGRAPHY AND THERMOCHRONOLOGY

Incision through late Cenozoic deposits is up to 1,340 m (up to 1,190 m through basement below these deposits) along parts of major river drainages of the Sierra Nevada. This amount is considerably less than the late Cenozoic uplift estimates that range up to 2,400 m. The magnitude of late Cenozoic uplift and incision may be different for areas south of the limit of late Cenozoic cover strata. However, the similarity of tilt for late Cenozoic strata of the same age along the length of the eastern Central Valley margin (Unruh, 1991), as well as the uniformity of uplift and incision across areas of different topographic expression described above, suggest that similar magnitudes of late Cenozoic uplift and incision are valid south of the limit of late Cenozoic deposits.

The canyon bottoms in the most deeply incised streams represent the deepest exposure of rock that was buried prior to late Cenozoic erosion in the Sierra. The late Cenozoic basement incision of ~1 km is probably too small to have been recorded by either (U-Th)/He apatite dating (45-85°C range of partial retention of He in apatite [Wolfe and others, 1998]), or apatite fission track dating (60-125°C is the partial annealing zone for apatite fission tracks [Dumitru, 1991]). It is not surprising, therefore, that (U-Th)/He ages from the Sierra record cooling and exhumation immediately following emplacement of the youngest Sierran plutons (mean ages of 45-85 Ma) and show no evidence of the late Cenozoic uplift event (House and others, 1997; 1998). Similarly, fission track data show cooling below 95°C around 67 Ma for samples from Kings River canyon and Yosemite Valley, and no evidence of late Cenozoic uplift (Dumitru, 1990).

House and others (1998) suggested the data indicate that peak elevation of the Sierra Nevada was attained in the Cretaceous and that elevations and topographic relief have been steadily decreasing since then, with no uplift in the late Cenozoic. To support their model, House and others (1998) cited: 1) the lack of evidence for late Cenozoic exhumation in (U-Th)/He ages; 2) differences in (U-Th)/He ages approaching the Kings River canyon; 3) and the approximate correspondence of constant 0.1 mm/yr incision rates, calculated as 10 Ma to 0 Ma average rates for the deepest part of the San Joaquin River canyon by Huber (1981), with the total amount of basement exhumation since the Cretaceous. If their model is correct, the progressively steeper westward gradients of progressively older late Cenozoic strata reflect the original stream gradients, not progressive late Cenozoic tilting and uplift. If this is so, stream gradients and stream power, and hence, stream incision rates, would be expected to have progressively decreased since the Cretaceous. This hypothesis is inconsistent with stream incision data, discussed previously (Table 2), which indicate negligible incision from the Eocene to Miocene, and major incision in the last 5 Ma.

As previously discussed, late Cenozoic basement incision is probably too small to be recorded by (U-Th)/He ages. The difference in (U-Th)/He approaching the Kings River canyon may be a consequence of: 1) Early canyon development as interpreted by House and others (1998). There is good evidence of large amounts of preserved paleo relief, as noted previously, and this relief may have been greater in the Eocene if some lowering of the highland areas since then is accounted for. The samples in the House and others (1998) study were taken at an approximate elevation of 2,000 m, well above the canyon floor, and probably above the part of the canyon deepened by late Cenozoic incision. This interpretation suggests large relief across the canyon in late Cretaceous to Eocene time, but does not preclude late Cenozoic uplift and incision of the magnitude reported herein; 2) The difference in (U-Th)/He ages approaching Kings River canyon is an artifact of crossing a major basement deformation zone with greater exhumation. This interpretation is consistent with the pattern of differential exhumation reported by Ague and Brimhall (1988). Although there is a spike of older (U-Th)/He ages in the vicinity of the Kings River canyon, the pattern does not hold for the other basement canyons crossed. However, the older ages may to correspond to areas of deeper exhumation shown by Ague and Brimhall (1988). These more deeply exhumed zones do not show a close correspondence with the major river canyons. Extrapolation of 0.1 mm/yr incision rates (the post-10 Ma rates of Huber [1981] from the San Joaquin River) to the Cretaceous to explain basement exhumation is inconsistent with incision data, discussed previously. This indicates high rates (tenths of a mm/yr) in the late Cenozoic and negligible incision (thousandths of a mm/yr or less) between the end of the Eocene and Miocene time. The proposed relationship between river incision and basement exhumation is also not in accord with the pattern of differential exhumation that does not show a correspondence between deepest exhumation and canyon development (Ague and Brimhall, 1988). The boundaries between zones of different levels of exhumation are subparallel to the range axis and cut across the major canyons. Moreover, the incision rate used for the San Joaquin only applies to the reach of largest amount of incision of the stream below the reconstructed 10 Ma channel. Incision rates decrease downstream from this reach, and this decrease occurs within the part of the stream traversing granitic rocks (Table 2).

In summary, data support two periods of uplift in the Sierra Nevada that have influenced the present elevation and relief of the range: an earlier period bracketed between about 85 and 50 Ma, and a recent and apparently ongoing period of uplift beginning sometime after 5 to 10 Ma. Topographic relief from the earlier stage of uplift was greatly reduced by Eocene time, as reflected by the surfaces of low relief that are overlain by Eocene to Miocene deposits of the Sierra. Deep late Cenozoic incision, tilting of late Cenozoic strata, and the prominent eastern escarpment, reflect late Cenozoic uplift that has significantly elevated the range. Residual topography from the earlier uplift pulse accounts for as much as half of the elevation and relief of the central and southern Sierra (Tuolumne River drainage and south), but accounts for less of the elevation in the northern part of the range.

FIELD TRIP GUIDE TO LOCALITIES ALONG THE NORTHERN PART OF THE SIERRA BASIN AND RANGE BOUNDARY ZONE

Neotectonics of the Northern Sierra Nevada-Basin and Range Boundary Zone

The Sierra Nevada-Basin and Range boundary in the Feather River area south of Quincy occupies a relatively narrow zone (the Mohawk Valley Fault zone) fewer than 10 km wide (Figures 2 and 4B). This fault zone has the appearance of a graben from Blairsden to near Quincy (Photos 1 and 6). Northward from the vicinity of Quincy, the zone broadens, and is 30 to 40 km wide where it crosses the North Fork Feather River (Photos 3 and 5). The zone of distributed faulting continues northward into the southern Cascades. In addition to Mohawk Valley, there are many Quaternary basins that may be fault controlled, including American Valley, Indian Valley, Humbug Valley, and the Lake Almanor basin (formerly Big Meadow, Photo 3).

Normal displacement across the Mohawk Valley Fault zone is constrained by vertical separations of late Cenozoic volcanic rocks (Photo 1), but strike-slip displacement is presently unconstrained. However, the regional fault geometry is consistent with a right-oblique fault zone. Oblique slip is supported by paleoseismic trenching studies that have revealed obliquely oriented slickensides (15°SE) on primary fault planes, suggesting a predominant strike-slip component, with subordinate dip slip (Sawyer and others, 1993b). This is consistent with the pull-apart like geometry of many of the Quaternary basins in the area as well as inversions of seismic strain data (WLA, 1996), and with regional kinematic models (Argus and Gordon, 1991; Pezzopane and Weldon, 1993; Dixon and others, 1995).

The distributed nature of Quaternary faulting north of Quincy may be a consequence of the recency of initiation of faulting in this region, reflecting insufficient time to develop a mature through-going fault system. As noted previously, there is evidence from the North Fork Feather River canyon of initiation of significant faulting after ~0.6 Ma. This region may record a westward jump of the Sierra Nevada-Basin and Range boundary that is ongoing or has recently taken place.

Additional discussion of geology and neotectonics is included for specific field trip stops described below.

Field Trip Stops Along the Northern Sierra Nevada-Basin and Range Boundary Zone.

Starting point in Blairsden. Mileage 0.0 at Junction of Highways 89 and 70.

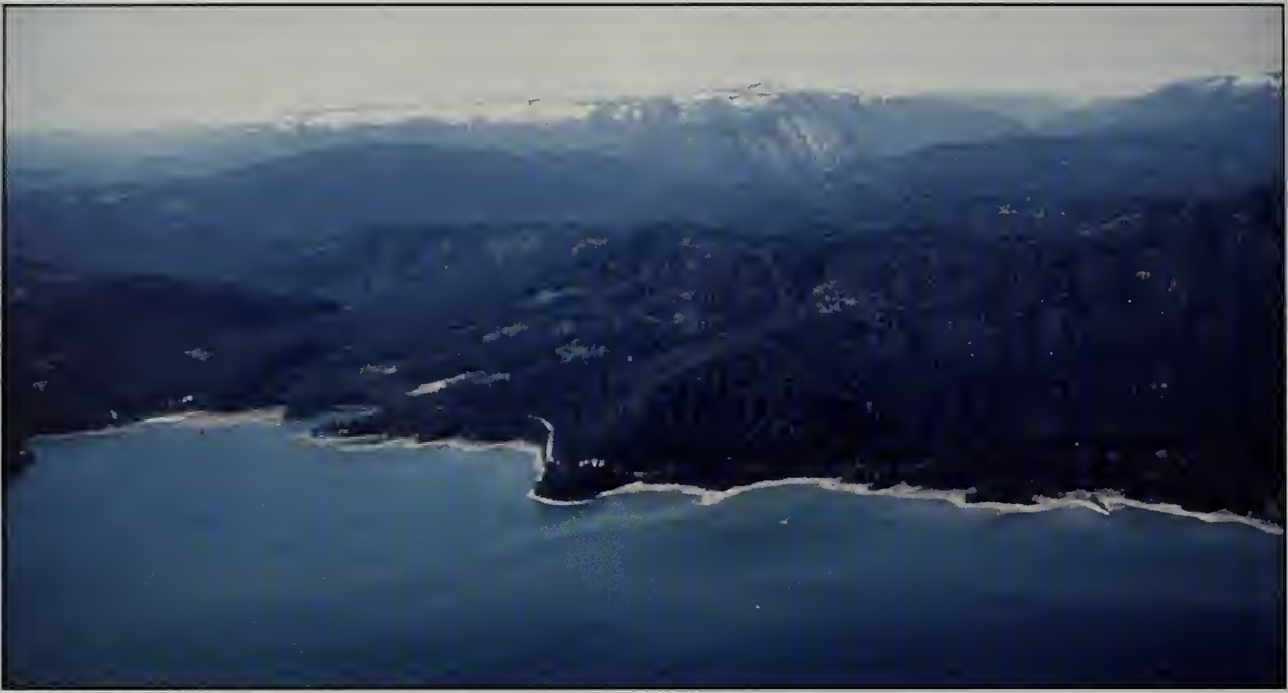

Photo 6. Over Lake Almanor looking southwest toward the Sierra Nevada crest (snow-capped ridge). Spanish Peak is on the left end of the high ridge. The North Fork Feather River flows away from the viewer from near the lefthand margin of the shoreline and flows toward the right-center of the photograph. This view gives an impression of the distributed nature of faulting along the Frontal Fault system at this latitude. This faulting is distributed over a zone about 35 km from the west shore of Lake Almanor in the foreground to the base of the snow covered escarpment in the background. Note the gentle upland surfaces, such as those atop the snow covered escarpment in the distance and some of the wooded ridges in the middle ground. These are remnants of the gentle topography that pre-dates late Cenozoic uplift. *Photo by John Wakabayashi.*

Our starting point in Blairsden is near the southern end of Mohawk Valley, a graben-like feature along the eastern escarpment of the Sierra Nevada that gives the Mohawk Valley Fault zone its name (Photo 6). The valley is filled with fine-grained sediments that reflect an environment of deposition similar to the present one for more than 400 ka (Yount, 1995), and also may reflect lowering of westward-flowing drainage gradients as a result of down-to-the-east faulting along the Mohawk Valley Fault zone. There has been 600-1,200 m (west of our present location) of down-to-the-east vertical separation post-deposition of the late Miocene to early Pliocene Mehrten Formation across the western traces of the Mohawk Valley Fault zone, which has produced the abrupt eastern escarpment during the late Cenozoic (Page and Sawyer, 1992). Hence the long-term average vertical separation rate is about 0.1 to 0.24 mm/yr on a fault that probably has a dominant right-slip component.

As part of a regional seismic hazards study conducted by PG&E, the activity of the Mohawk Valley Fault zone was evaluated in two trenches about 20 km to the south near the town of Calpine. One trench was excavated across a small graben at the range front, but did not expose the main range-front fault. The second trench was excavated across a subparallel splay fault delineated by a 3.7 m-high scarp. Stratigraphic relations, soil development, and radiocarbon dates from the trenches provided evidence of recurrent late Quaternary surface-rupturing events. Single-event displacements of 1.6-2.6 m or more on the splay fault indicate these probably represent large paleo earthquakes. A Holocene event is suggested by youthful scarplets and small closed depressions along this part of the fault (Sawyer and others, 1993b).

Drive northwest on Highway 70/89 from the Highway 70/89 junction near Blairsden. About 5 miles from the starting point the valley narrows and we drive through a steep canyon cut into andesitic mudflow deposits of the Mehrten Formation. At 11.3 miles, there is a very large flat dirt turnout on the left (west) side of the road. Pull into this turnout and park.

Stop 1. Lovejoy basalt along Highway 70/89. It was all downhill to the west at 16 Ma! The Lovejoy basalt exposed as a knob on the west side of the road (Photo 7) provides one of the two best late Cenozoic strain gauges across the Sierra Nevada (Sawyer and Page, 1992; Figure 5). This basalt originally erupted east of the Honey Lake escarpment and flowed westward all the way to what is now the western margin of the Sacramento Valley (Photos 1 and 3). Needless to say, at 16 Ma, there was no Sierran escarpment to impede the basalt flow. The Lovejoy basalt crops out near the tops of the mountains to the east of us, as well as near the top of some of the mountains to our west (600 m higher). This gives one an idea of the post-16 Ma vertical displacement on the faults bounding the Mohawk Valley graben. As discussed previously, most of the slip on this fault system is strike-slip, rather than dip-slip. The Lovejoy basalt at this location and at the crest is overlain by Mehrten Formation and/or correlatives and the offset of both units is the same, indicating that vertical separation along the Frontal Fault system in this area did not begin until after Mehrten deposition.

From Stop 1 continue driving northwest on Highway 70/89. At mile 22.7 we are at the junction of the Bucks Lake Road on the western edge of the town of Quincy. Quincy is in a basin filled with Quaternary alluvium, one of several basins that may be pull apart basins along the Frontal Fault system in this area. As we drive beyond this road junction we can look to the west and see a bare granitic, glaciated escarpment (Photo 2). The summit of this escarpment is Spanish Peak, which marks the crest of the range. Mehrten Formation

Photo 7. The Lovejoy basalt at Stop 1 along Highway 70 near Spring Garden. *Photo by John Wakabayashi.*

correlatives are present near the summit of Spanish Peak on its gentle western flank. The vertical offset between these deposits and equivalent deposits to the east in the Meadow Valley area is 600-790 m depending on the original flow direction of the mudflow deposits. Additional down-to-the-east displacement may be accommodated between Meadow Valley and Quincy, so the difference in elevation of Spanish Peak compared to Quincy (1,090 m) may approximate the amount of late Cenozoic east-down displacement on the Frontal Fault system in this area. At this latitude, the Frontal Fault system has broadened into a zone of distributed faulting 15 km wide; northward it widens to 35-40 km.

Optional Stop O-1 (mileage not added to main road log). From Quincy take the Bucks Lake Road 5.8 miles to Meadow Valley. Meadow Valley is a graben filled with Quaternary alluvium of Spanish Creek, which accumulated as a result of the drainage being dammed by down-to-the west faulting along the Meadow Valley Fault. To the south this fault crosses the Sierra Nevada crest and displaces the Lovejoy basalt (Figure 5). If we were to continue an additional 5.7 miles along the Bucks Lake Road we would cross the Spanish Peak Fault (which bounds the west side of the graben and extends along the base of the Spanish Peak escarpment) before reaching Bucks Summit at the crest of the range (Figure 12).

Main road log resumes. Continuing northwest of Highway 70, we soon leave American Valley. At mileage 32.9 we turn right onto Highway 89 and drive toward Crescent Mills and Indian Valley. At mile 39.9 we enter Crescent Mills in Indian Valley, another basin filled with Quaternary alluvium that has formed along the Frontal Fault system in this area. At mile 44.5 in the town of Greenville, we reach an intersection with the road to Round Valley. Turn onto this road and drive 3 miles to Round Valley reservoir. When you reach the intersection with the perimeter road around the lake, park in a parking area to your left.

Stop 2. Round Valley. The reservoir fills a basin that formed by down-to-the-west faulting that has dammed an east-flowing drainage. The small dam raises the water level above the natural bedrock sill at the outlet, flooding this small basin. One can see that the bedrock is serpentinite, which is part of one of the major basement (pre-Cenozoic) fault zones in the area. This locality illustrates how late Cenozoic faulting has locally reactivated pre-Cenozoic fault zones. However, this fault zone, as do most late Cenozoic faults in the Sierra, only locally track the basement fault; this fault appears to diverge westward from the basement fault zone to the north. This is one of the reasons for following the convention established by Woodward-Clyde Consultants (WCC, 1977, 1978) of giving late Cenozoic faults names that are distinct from the pre-Cenozoic fault zones they locally reactivate. For example, the late Cenozoic Little Grass Valley Fault locally follows the older basement Dogwood Peak Fault but deviates significantly from the basement fault over much of its length. In addition, as discussed previously, many late Cenozoic faults occur within areas of the Sierra Nevada batholith in which no major pre-Cenozoic shear zones have been mapped. Thus, not all late Cenozoic faults follow pre-existing basement faults.

From Round Valley reservoir, drive 3 miles back to Highway 89 in Greenville (mileage at this junction is now 50.5 miles). Drive west on Highway 89 toward Lake Almanor. At mile 57.1, just before reaching a railroad crossing (the only one along this stretch of road), park in a small dirt turnout on your right. Hike up the slope to the cuts along the railroad tracks north of the highway.

Stop 3. Old colluvium and alluvium east of Lake Almanor along Highway 89. In the railroad cut we see iron-stained colluvium and alluvium (Photo 8). Stratification in these deposits can be seen; note the layers of coarse and fine material. At the top of this exposure we find overlying rhyolite tuff. Farther west, closer to Lake Almanor, this tuff is overlain by 2.4 Ma basalt, and the contact is well exposed in the railroad cuts. If you have the energy you can hike along the tracks to this point; make sure to walk the tracks to the north from the road rather than recrossing the road. This tuff may correlate to ~2.8 Ma volcanic rocks of the Yana volcanic center that are common to the west (M.A. Clynne, oral communica-

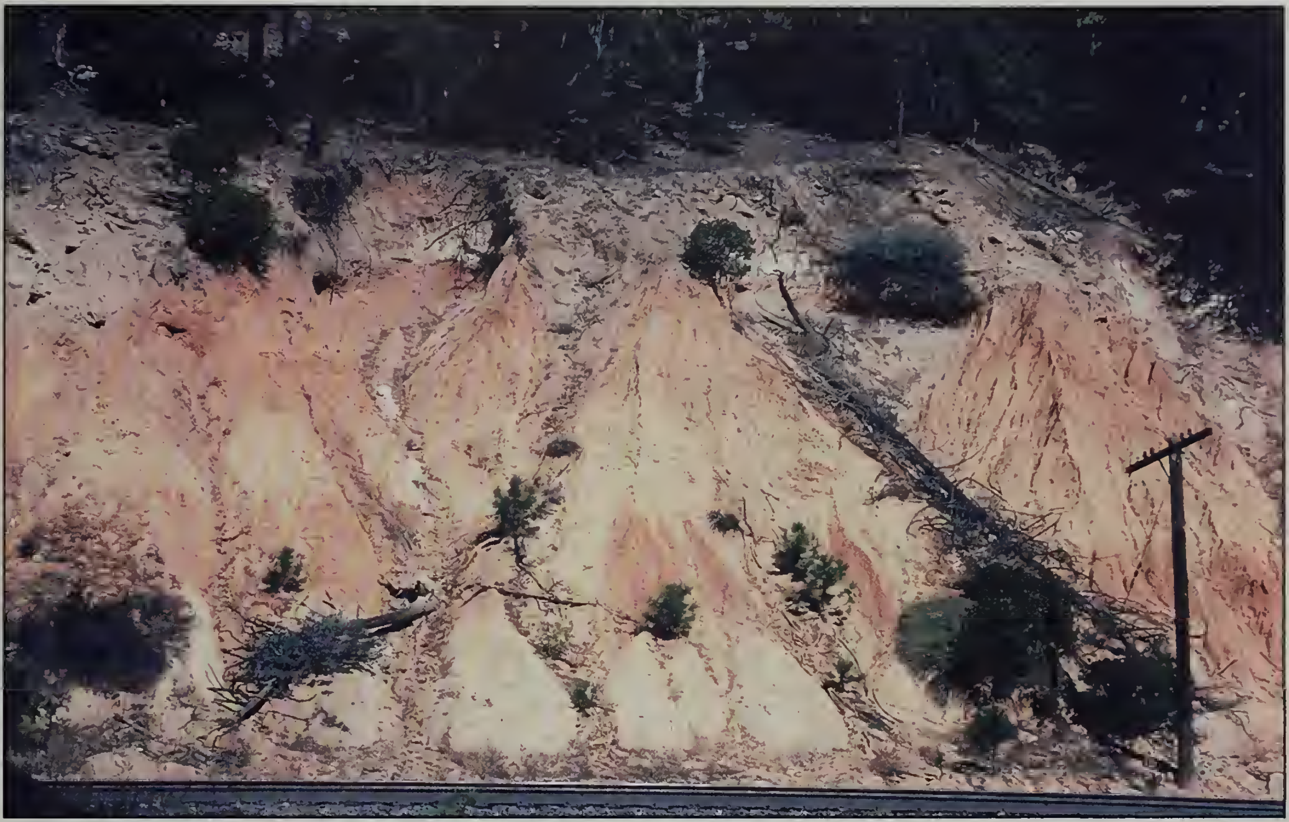

Photo 8. Alluvium and colluvium capped by rhyolite ashflow tuff (uppermost light layer) at Stop 2 along Highway 89 west of Greenville. *Photo by John Wakabayashi.*

tion, 1995). The colluvium and alluvium are thus minimally several million years old. The relative lack of incision of Wolf Creek relative to these deposits indicates that little erosion has taken place in this area. These deposits may be examples of types of surficial deposits that cover low relief upland surfaces that predate late Cenozoic uplift of the Sierra (some of these low relief upland surfaces can be seen in Photo 5).

From this stop continue driving westward on Highway 89 toward Lake Almanor. At mile 57.8-58.0 we pass through roadcuts in basalt that has been dated (Ar/Ar) at 2.4 Ma and overlies the ashflow tuff seen at the previous stop. At mile 59.3, having just passed through the town of Canyondam, we reach the intersection with Highway 147 where we turn right (north) and drive north 0.4 miles to a large paved parking area along the left (west) side of the road where we will park.

Stop 4. Eastside overlook. This is a good viewpoint for the Lake Almanor basin. Lake Almanor is a reservoir that floods another fault-bounded basin along the Frontal Fault system. At this point we are at the northern limit of what is generally defined as the Sierra Nevada, as deposits of Plio-Pleistocene volcanic rocks cover essentially all older rocks to the north (the southern part of the Modoc plateau) (Photo 3; Figure 8). In spite of the difference in rock types exposed at the surface, faulting along the Frontal Fault system continues northward across the "transition," part of a fault system that has been termed the Tahoe-Medicine Lake trough (Page and others, 1993). The Hat Creek Fault, which forms the spectacular escarpment of the Hat Creek Rim north of this area (just north of the north edge of Figure 12), is part of the northern continuation of this fault system (Wills, 1990; Muffler and others, 1994). The Sierran-Modoc Plateau transition is thus more a transition in rock types at the surface than a tectonic transition. If the weather is good we should be able to see Mt. Lassen, the southernmost active Cascade volcano to the west across the lake. The relatively steep slope from the overlook down to the Lake Almanor shoreline is a fault scarp of the Eastside Fault in ~0.6 Ma Basalt of Westwood. The Eastside Fault strikes approximately north-south and forms a prominent shoreline escarpment on the east shore of Lake Almanor; it is one of the faults that bounds this basin. Looking northward across the lake we observe a type of "inverted topography" in which older volcanic rocks have been uplifted and younger volcanic rocks have flowed down channels cut into the older rocks. Across Lake Almanor the highest areas are underlain by 2.2 Ma andesites. Younger basalt flows, the ~1 Ma Basalt of Rock Creek, ~0.6 Ma Basalt of Warner Valley, and ~0.4 Ma Basalt of Westwood, flowed down channels cut into older rocks (in the case of the 0.4 Ma basalts the rocks fill a channel cut into the 1 Ma rocks) (Figure 8). On the floor of the Almanor basin itself, beneath the lake and basin sediments, the volcanic flows likely overlie one another in stratigraphic sequence.

From this stop drive back southward on Highway 147 to Highway 89 (mile 60.1 at intersection), turn right (west) proceed 0.1 miles to the intersection with the Seneca Road and turn left (south).

Optional Stop O-2 (mileage not added to main road log). Instead of turning south onto the Seneca Road, continue 0.1-0.2 miles and find parking along the Highway 89. Almanor dam and the canyon of the North Fork Feather River should be visible. Hike to the rim of the canyon. The rim is capped with the ~0.4 Ma Basalt of Westwood. Identical in appearance, but underlying by about 10 m of this basalt, is the ~0.6 Ma Basalt of Warner Valley. The Basalt of Westwood flowed into and the Almanor basin from its northeast corner, whereas the Basalt of Warner Valley flowed into the basin from the northwest (Figure 8).

Main road log resumes. From the Highway 89/Seneca Road intersection (mile 60.2) head south of the Seneca Road for 0.2 of a mile, then park.

Stop 5. Eastside Fault on Seneca Road. The rocky outcrop on the east side of the road is the scarp of the Eastshore Fault cutting ~0.4 Ma Basalt of Westwood. This is the southern continuation of the Eastside Fault scarp that was standing on top of at the last stop.

Leaving this stop, we continue south on Seneca Road. At 1.8 miles from Stop 5 (mile 62.2), park along the right (canyon) side of the road.

Stop 6. Highest elevation remnant of ~1 Ma basalt. At this viewpoint we are "downstream" of the Almanor basin from the standpoint of the direction that the basaltic lavas flowed, yet we are significantly higher than the Almanor basin; because we are "downstream" of the Almanor basin the elevation difference we see must be a consequence of faulting. The top of the basalt outcrop in the roadcut is 113 m higher than the high water level of Lake Almanor. The outcrop we see in the roadcut is ~1 Ma basalt, slightly younger in age than the Basalt of Rock Creek, but virtually indistinguishable in stratigraphic position (because so little time elapsed between the eruption of this flow and the Basalt of Rock Creek). Note the preserved channel margin, the steeply-dipping baked zone beneath the flow remnant (Photo 9). Below the basalt flow is a thin deposit of colluvium overlying basement metamorphic rocks. The canyon that the basalt flowed down must have had fairly steep sides based on the inclination of the basal baked zone. The elevation difference between this remnant and the basin demonstrates the vertical component of the faulting bounding the Almanor basin (water depth is about 30 m). Note that the surface of this basalt in the Almanor basin is considerably lower than the bottom of the lake. In the basin, this basalt would be expected to be overlain successively by flows of the ~0.6 Ma Basalt of Warner Valley, the ~0.4 Ma Basalt of Westwood, and late Quaternary alluvial deposits that overlie these basalts in the basin. Across the deep canyon on the North Fork Feather River, we see a flat bench. The canyon walls reveal that the bench is underlain by Basalt of Westwood that overlies Basalt of Warner Valley. The Basalt of Westwood may not have made it much farther downstream than the downstream limit of the bench, for it has not been found downstream of this point.

Across the canyon from the flat bench is a wooded knob (NE of our viewpoint and lower than us).

Photo 9. Basalt exposed at Stop 6. This ~1 Ma flow shows a lower contact over colluvium that mantled the former canyon wall. The basalt exhibits spheroidal weathering at this locality, but most roadcuts in this and the other Quaternary basalt remnants in the North Fork Feather River canyon are fresher. *Photo by John Wakabayashi.*

This knob is capped with the Basalt of Warner Valley that overlies the Basalt of Rock Creek. These relationships and those across the canyon on the bench suggest the Skinner Flat Fault, which passes east of this knob and uplifts these exposures relative to Lake Almanor, became active after deposition of the Basalt of Warner Valley; it has increases in displacement from north to south (Figure 9). These relationships and the faulting of the Basalt of Westwood on the bench on the northwest (opposite) side of the river also suggest either: 1) the Skinner Flat Fault may not have started significant movement until after the deposition of the Basalt of Westwood; or 2) or the northern tip of faulting has propagated progressively northward since Basalt of Westwood time.

On the above-described wooded knob and the bench across the river basaltic units still overlie each other in normal stratigraphic fashion. Downstream of these outcrops, starting with the outcrops where we are stopped, an 'inverted' topographic series of basalt benches is seen, a consequence of successive river incision with periods of basalt flowing down the canyon (Figure 9). The 'cross over' point is marked by the Ohio Creek Fault that passes between the 'normal' stratigraphic sequences to our north and the outcrop that we are standing next to (Figure 9).

If we turn and look downstream (it is most convenient to hike southeast up a dirt road onto the knoll on the east side of the main road) we can see the river bend around a hill that has two prominent flat surfaces at different elevations (Photo 10). The upper flat is underlain by ~1 Ma basalt (the same basalt unit we are standing next to). The lower flat is underlain by the ~0.6 Ma Basalt of Warner Valley. Similar bench-like remnants exhibiting 'inverted' topographic relationships (oldest benches are highest) are present along the walls of the North Fork Feather River canyon as far downstream as the confluence of the North Fork with the East Branch North Fork (Photo 4; Figure 11).

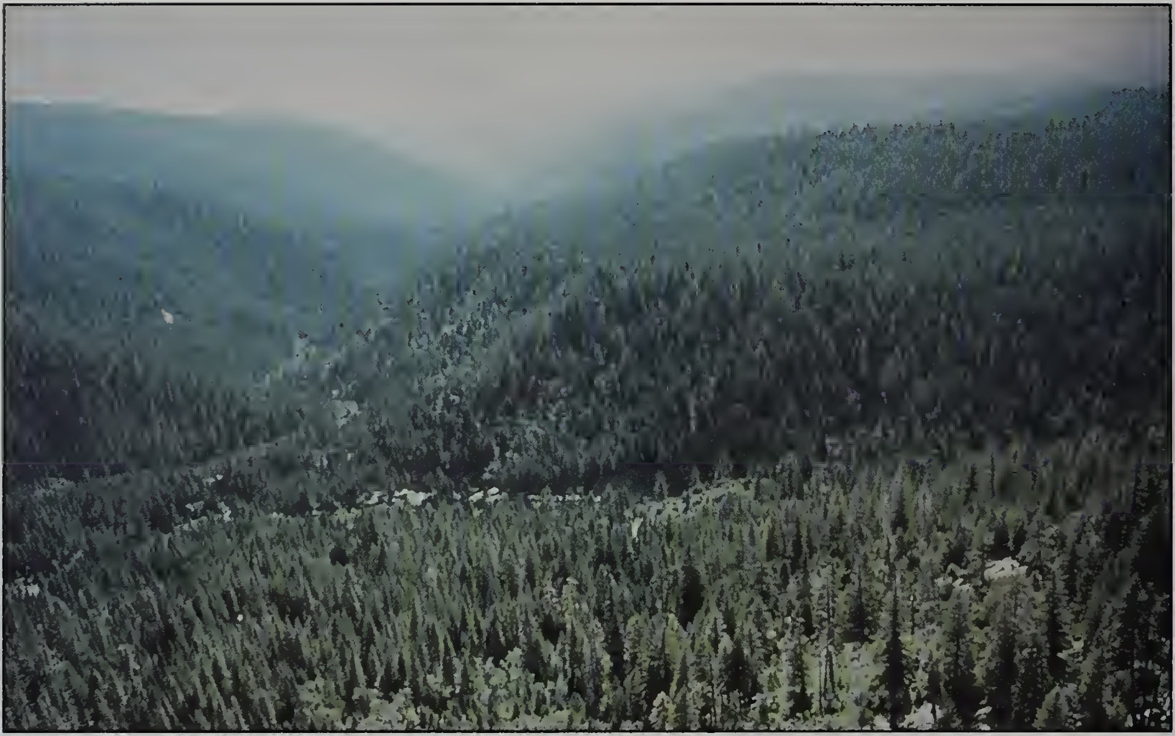

Photo 10. Downstream from Stop 6 toward the stacked basalt benches on the opposite side of the canyon above Seneca. The lower flat is ~0.6 Ma basalt, and the upper flat is ~1 Ma basalt. *Photo by John Wakabayashi.*

A canyon followed approximately the same course since at least 2.8 Ma, based on the oldest inset volcanic unit. The depth of the canyon at 2.8 Ma can be estimated by noting the position of the inset volcanic remnant of this age relative to erosion surfaces or basement topographic highs above it.

As noted earlier these volcanic remnants permit analysis of the incision history of the North Fork Feather River and an estimate for the onset of incision. Our drive will proceed down the canyon, time permitting.

Road log back to Blairsden. From Stop 6 (mile 62.2) we continue on the Seneca Road dropping in elevation. We will pass several outcrops of basalt in the roadcuts during our descent. These are outcrops of the Basalt of Warner Valley that make up a fairly large remnant (Figure 9). After reaching the bottom of the canyon the road crosses the river and heads through the hamlet of Seneca. Some of the high cuts above the road expose river gravels below the Basalt of Warner Valley. These gravels have been mined for placer gold. After passing through Seneca the road starts to ascend again and the basalt is exposed in many of the roadcuts. This is also the Basalt of Warner Valley and is the lower remnant of the 'double stack' we viewed when looking downstream from Stop 6. Several spur roads veer off to the left to mines at the base of the gravels that are at the base of this basalt remnant. This is the largest remnant in the canyon. Note that we pass in and out of basaltic and basement metamorphic outcrops in the roadcuts. This is because of the irregular contact between the basalt and basement caused by erosion of the steep basalt contact of the basalt against the former canyon wall. Locally baked zones between individual flows may be seen. At mile 68.1 continue straight at an intersection with the Dutch Flat Road. At mile 69.8 continue straight at the intersection of the Ohio Valley road. Shortly thereafter, at mile 69.9 we make a left turn onto the Caribou Road that leads toward Highway 70.

Optional Stop O-3 (mileage not added to main road log). Instead of turning left onto the Caribou Road, continue on the road and reach Butt Valley Reservoir within a few tenths of a mile. This reservoir fills a valley that is a fault-bounded graben. Based on the studies of the faulting in North Fork Feather River canyon (see earlier discussion), and studies along the northward continuation of these faults, these faults did not begin moving until after deposition of the Basalt of Warner Valley (~0.6 Ma). However, a stream drainage did exist here as early as 1 Ma because Basalt of Rock Creek (~1 Ma) and the Basalt of Warner Valley both flowed down this drainage from Lake Almanor. Outcrops of both of these units are found in nearly continuous exposures in the fault-dissected upland upstream of the reservoir, and a tongue of Basalt of Warner Valley extends down the Butt Creek drainage to the upstream end of the reservoir (Figure 8).

Main road log resumes. Having made the left turn onto the Caribou Road (mile 69.9) we descend and pass over a small bridge over the spillway from Butt Valley dam. Just below the road are outcrops of the Basalt of Warner Valley that is present as a bench on both sides of Butt Creek. After passing below the dam to the other side of the Butt Creek canyon, we continue straight through an intersection, then reach a point where our road splits into two one-way roads (keep right as the sign indicates). After the roads rejoins we round two switchbacks and see outcrops of Basalt of Warner Valley, part of another large remnant (Figure 9). After two sharp switchbacks (first right then left) we come to a third switchback where we see (on the left, for the passengers to look, not the driver!) a good contact of Basalt of Warner Valley over colluvium of the former canyon wall. This is a very similar type of contact to that seen at Stop 6. Continuing our steep descent we soon reach the bottom of the canyon at Belden Forebay. As we drive down the canyon, we can see several bench-like remnants of basalt on the canyon walls. Note that most of these remnants are covered with a thick wedge of colluvium. One of the best examples of one of these piles of colluvium can be seen above a remnant of the Basalt of Warner Valley that underlies the Belden Siphon, an inverted siphon (a very large pipe in this case), that crosses above the road.

Optional Stop O-4 (mileage not added to main road log). A good place to view this remnant, colluvial pile can be reached by turning onto a road that crosses the river just downstream of the North Fork campground (this is upstream of the remnant). After crossing the river, the road ascends steadily. At a point where one is almost at the same elevation as the top of the basalt remnant (on the opposite side of the canyon), take a spur road that diverges left from the road you've been driving on to a flat parking area just short of the Belden Siphon. From here we get a good view across to the basalt remnant and the large pile of colluvium atop it.

Main road log resumes. We reach the intersection with Highway 70 at mile 72.3 (this is the confluence of the East Branch North Fork and North Fork Feather River) and turn left onto Highway 70. At mile 88.3 we have reached the intersection with Highway 89 at the confluence of Indian and Spanish creeks where we turn right and follow Highway 70/89. From here it is 32.9 additional miles to the Highway 70/89 junction near Blairsden (total mileage 121.2).

ACKNOWLEDGMENTS

Much of the data in this paper is derived from studies that the authors participated in as consultants to PG&E, under the direction of W.D. Page of the Geosciences Department of PG&E. Participants in these studies who contributed to these data include W.D. Page, S.C Thompson, R.W. Ely, P.R. Renne, D.E. Champion, M.A. Clynne, and L.P.J. Muffler. We are thankful for the permission to use these data. This research has benefited from stimulating discussions with W.D. Page, J.R. Unruh, S.C. Thompson, M.A. Clynne, D.E. Champion, R.W. Ely, C.S. Riebe, and Jon Stock. This paper has benefited from reviews by Cliff Riebe and Craig DePolo.

REFERENCES

Ague, J.J. and Brimhall, G.H., 1988, Magmatic arc asymmetry and distribution of anomalous plutonic belts in the batholiths of California: Effects of assimilation, crustal thickness, and depth of crystallization: Geological Society of America Bulletin, v. 100, p. 912-927.

Argus, D.F. and Gordon, R.G., 1991, Current Sierra Nevada-North America motion from very long baseline interferometry: Implications for the kinematics of the western United States: Geology, v. 19, p. 1085-1088.

Atwater, T., Stock, J., 1998, Pacific-North America plate tectonics of the Neogene southwestern United States: An update: International Geology Review, v. 40, p. 375-402.

Axelrod, D.I., 1980, Contributions to the Neogene paleobotany of central California: University of California Publications in Geological Sciences, v. 121, p. 1-212.

Axelrod, D.I. and Ting, W.S., 1960, Late Pliocene floras east of the Sierra Nevada: University of California Publications in Geological Sciences, v. 39, no. 1, p. 1-117.

Bailey, R.A., 1989, Geologic map of the Long Valley Caldera, Mono-Inyo Craters volcanic chain, and vicinity, eastern California: U.S. Geological Survey Miscellaneous Investigations Series Map I-1933, scale 1:62,500.

Bachman, S.B., 1978, Pliocene-Pleistocene break-up of the Sierra Nevada-White-Inyo Mountains block and the formation of Owens Valley: Geology, v. 6, p. 461-463.

Bateman, P.C. and Busacca, A.J., 1982, Geologic map of the Millerton Lake Quadrangle, west-central Sierra Nevada, California: U.S. Geological Survey geologic quadrangle map GQ-1548, scale 1:62,500.

Bateman, P.C. and Wahrhaftig, C., 1966, Geology of the Sierra Nevada *in* Bailey, E.H., editor, Geology of Northern California, California Division of Mines and Geology Bulletin 190, p. 107-172.

Bartow, J.A., 1979, Age control for the latest movements on the Melones Fault zone in the Sierra foothills belt from K-Ar dates for late Tertiary intrusions: U.S. Geological Survey Open-File Report 79-582, 12 p.

Bartow, J.A., 1990, The late Cenozoic evolution of the San Joaquin Valley, California: U.S. Geological Survey Professional Paper 1501, 40 p.

Beanland, S. and Clark, M.M., 1995, The Owens Valley Fault zone, eastern California, and surface rupture associated with the 1872 earthquake: U.S. Geological Survey Bulletin 1982.

Becker, T., Sharp, W. and Renne, P., 1994, 40Ar/39Ar dating of young, low-K tholeiites: Examples from northeast California, U.S.A. *in* Lanphere, M.A., Dalrymple, G.B., and Turrin, B.D., editors, Abstracts of the Eight International Congress on Geochronology, Cosmochronology, and Isotope Geology: U.S Geological Survey Circular 1107, p. 24.

Bryant, W.A., 1984, Hartley Springs Fault zone, Mono County, California: California Division of Mines and Geology Fault Evaluation Report 157, scale 1:62,500.

Christensen, M.N., 1966, Late crustal movements in the Sierra Nevada of California: Geological Society of America Bulletin, v. 77, p. 163-182.

Clark, M.M., Sharp, R.V., Castle, R.O. and Harsh, P.W., 1976, Surface faulting near Lake Oroville, California, in August 1975: Seismological Society of America Bulletin, v. 66, p. 1101-1110.

Clark, M.M., Harms, K.K., Lienkaemper, J.J., Harwood, D.S., Lajoie, K.R., Matti, J.C., Perkins, J.A., Rymer, M.J., Sarna-Wojcicki, A.M., Sharp, R.V., Sims, J.D., Tinsley, J.C., III. and Ziony, J.I., 1984, Preliminary slip rate table and map of late Quaternary faults of California: U.S. Geological Survey Open-File Report 84-106.

Curtis, G.H., 1954, Mode of origin of the pyroclastic debris in the Mehrten Formation of the Sierra Nevada: University of California Department of Geological Sciences Bulletin, v. 29, no. 9, p. 453-502.

Dilles, J.H. and Gans, P.B., 1995, The chronology of Cenozoic volcanism and deformation in the Yerington area, western Basin and Range and Walker Lane: Geological Society of America Bulletin, v. 107, p. 474-486.

Dixon, T.H., Robaudo, S., Lee, J. and Reheis, M., 1995, Constraints on present-day Basin and Range deformation from space geodesy: Tectonics, v. 14, p. 755-772.

Dodge, F.C.W. and Calk, L.C., 1987, Geologic map of the Lake Eleanor Quadrangle, central Sierra Nevada, California: U.S. Geological Survey Map GQ-1639, scale 1: 62,500.

Dumitru, T.A., 1990, Subnormal Cenozoic geothermal gradients in the extinct Sierra Nevada magmatic arc: consequences of Laramide and post-Laramide shallow-angle subduction: Journal of Geophysical Research, v. 95, p. 4925-4941.

Dumitru, T.A., 1991, Major Quaternary uplift along the northernmost San Andreas Fault, King Range, northwestern California: Geology, v. 19, p. 526-529.

Durrell, C., 1966, Tertiary and Quaternary geology of the northern Sierra Nevada *in* Bailey, E.H., editor, Geology of Northern California, California Division of Mines and Geology Bulletin 190, p. 185-197.

Ely, R.W., 1992, Late Cenozoic uplift and faulting of the Sierra Nevada in the vicinity of Stanislaus Table Mountain, California: Geological Society of America, Abstracts with Programs, v. 24, no. 5, p. 22.

Gilbert, G.K., 1883, A theory of the earthquakes of the Great Basin, with a practical application: American Journal of Science, Third Series, v. XXVII, no. 157, p. 49-53.

Grant, T.A., McCleary, J.R. and Blum, R.L., 1977, Correlation and dating of geomorphic and bedding surfaces on the east side of the San Joaquin Valley using dip *in* Singer, M.J., editor, Soil Development, Geomorphology and Cenozoic History of the Northeastern San Joaquin Valley and Adjacent Areas, California; Davis, California, University of California Press, Guidebook for joint field session (ASA, SSSA, GSA), p. 312-318.

Guffanti, M., Clynne, M.A., Smith, J.G., Muffler, L.J.P. and Bullen, T.D., 1990, Late Cenozoic volcanism, subduction, and extension in the Lassen region of California, southern Cascade range: Journal Geophysical Research, v. 95, p. 19453-19464.

Hart, E.W. and Rapp, J.S., 1975, Ground rupture along the Cleveland Hill Fault *in* Sherburne, R.W. and Hauge, C.J., editors, Oroville, California, earthquake 1 August 1975: California Division of Mines and Geology Special Report 124, p. 61-72.

House, M.A., Wernicke, B.P., Farley, K.A. and Dumitru, T.A., 1997, Cenozoic thermal evolution of the central Sierra Nevada, from (U-Th)/He thermochronometry: Earth and Planetary Science Letters, v. 151, p. 167-179.

House, M.A., Wernicke, B.P. and Farley, K.A., 1998, Dating topography of the Sierra Nevada, California, using apatite (U-Th)/He ages: Nature, v. 396, p. 66-69.

Huber, N.K., 1981, Amount and timing of late Cenozoic uplift and tilt of the central Sierra Nevada, California-evidence from the upper San Joaquin river basin: U.S. Geological Survey Professional Paper 1197, 28 p.

Huber, N.K., 1990, The late Cenozoic evolution of the Tuolumne River, central Sierra Nevada, California: Geological Society of America Bulletin, v. 102, p. 102-115.

Jennings, C., 1977, Geologic map of California: California Division of Mines and Geology, Geologic Data Map 2, Scale 1: 750,000.

Jennings, C.W., 1994, Fault activity map of California and adjacent areas: California Division of Mines and Geology, scale 1:750,000.

Jones, L.M. and Dollar, R.S., 1986, Evidence of Basin-and-Range extensional tectonics in the Sierra Nevada: The Durrwood Meadows swarm, Tulare County, California (1983-1984): Seismological Society of America Bulletin, v. 76, p. 439-461.

Kistler, R.W., 1973, Geologic map of the Hetch Hetchy Quadrangle, Yosemite National Park, California: U.S. Geological Survey Map GQ-1112, scale 1:62,500.

Lindgren, W., 1911, The Tertiary gravels of the Sierra Nevada of California: U.S. Geological Survey Professional Paper 73, 226 p.

Marchand, D.E. and Allwardt, A., 1978, Preliminary geologic map showing Quaternary deposits of the northeastern San Joaquin valley, California: U.S. Geological Survey, Miscellaneous Field Studies Map MF-945, scale 1:125,000.

Muntean, T.W., Cashman, P. and Trexler, J., 1999, Tectonic evolution of the Neogene Gardnerville sedimentary basin, western Nevada: Geological Society of America Abstracts with Programs, v. 31, no. 6, p. A81.

Muffler, L.J.P., Clynne, M.A. and Champion, D.E., 1994, Late Quaternary normal faulting of the Hat Creek basalt, northern California: Geological Society of America Bulletin, v. 106, p. 195-200.

Noble, D.C., Slemmons, D.B., Korringa, M.K., Dickinson, W.R., Al-Rawi, Y. and McKee, E., 1974, Eureka Valley Tuff, east-central California and adjacent Nevada: Geology, v. 2, p. 139-142.

Page, W.D., 1999, Quaternary faulting on strands of the Foothills Fault system and other faults within the Sierra Nevada, California: Geological Society of America Abstracts with Programs, v. 31, no. 6, p. A-84.

Page, W.D. and Noryko, W.R., 1977, Erosion rates in the Sierra Nevada foothills near Sonora, California: Geological Society of America Abstracts with Programs, v. 9, no. 4, p. 479.

Page, W.D. and Sawyer, T.S., 1992, Tectonic deformation of the Lovejoy basalt, a late Cenozoic strain gauge across the northern Sierra Nevada, California; EOS, v. 73, p. 590.

Page, W.D. and Sawyer, T.S., in press, Identifying Quaternary faulting within the northern and central Sierra Nevada, California: in Association of Engineering Geologists, Engineering Geology Practice in Northern California.

Page, W.D., Sawyer, T.S., McLaren, M., Savage, W.U. and Wakabayashi, J., 1993, The Quaternary Tahoe-Medicine Lake trough: the western margin of the Basin and Range transition, NE California: Geological Society of America, Abstracts with Programs v. 25, p. 131.

Pakiser, L.C., Kane, M.F. and Jackson, W.H., 1964, Structural geology and volcanism of the Owens Valley region, California-a geophysical study: U.S. Geological Survey Professional Paper 438, 68 p.

Petersen, M.D., Bryant, W.A., Cramer, C.H., Cao, T.C., Reichle, M.S., Frankle, A.D., Lienkaemper, J.J., McCrory, P.A. and Schwartz, D.P., 1996, Probabilistic seismic hazard assessment for the state of California: both—California Division of Mines and Geology Open-File Report 96-08 and U.S. Geological Survey Open-File Report 96-706, 31 p.

Pezzopane, S.K. and Weldon, R.J. II, 1993, Tectonic role of active faulting in central Oregon: Tectonics, v. 12, p. 1140-1169.

Ramelli, A.R., Bell, J.W., de Polo, C.M. and Yount, J.C., 1999, Large-magnitude, late Holocene earthquakes on the Genoa Fault, west-central Nevada and eastern California: Bulletin of the Seismological Society of America, v. 89, p. 1458-1472.

Ramelli, A.R., de Polo, C.M. and Bell, J.W., 1994, Synthesis of data and exploratory trenching along the northern Sierra Nevada Fault zone: Final technical report, U.S. Geological Survey, 65 p.

Reheis, M.C. and Sawyer, T.L., 1997, Late Cenozoic history and slip rates of the Fish Lake Valley, Emigrant Peak, and Deep Springs fault zones, Nevada and California: Geological Society of America Bulletin, v. 109, p. 280-299.

Renne, P.R., Tobisch, O.T. and Saleeby, J.B., 1993, Thermochronologic record of pluton emplacement, deformation, and exhumation at Courtright shear zone, central Sierra Nevada, California: Geology, v. 21, p. 331-334.

Riebe, C.S., Kirchner, J.W., Granger, D.E. and Finkel, R.C., in review, Erosional equilibrium and disequilibrium in the Sierra Nevada mountains, inferred from cosmogenic ^{26}Al and ^{10}Be in alluvial sediment: submitted to Geology.

Roberts, C.T., 1985, Cenozoic evolution of the northwestern Honey Lake basin, Lassen County, California: Colorado School of Mines Quarterly, v. 80, no. 1, 73 p.

Russell, I.C., 1887, Notes on the faults of the Great Basin and of the eastern base of the Sierra Nevada: Bulletin of the Philosophical Society of Washington, v. 9, p. 5-7.

Saucedo, G.J. and Wagner, D.L., 1992, Geologic map of the Chico Quadrangle: Geologic map of the Sacramento Quadrangle: California Division of Mines and Geology Regional Geologic Map Series, Map No. 7A, scale 1: 250,000.

Sawyer, T.L., Hitchcock, C.S., Knudsen, K.L., Sowers, J.M., Crampton, T., Sawyer, J.E., Wakabayashi, J., Lettis, W.R. and Caskey, S.J., 1996, Middle to late Quaternary strike-slip faulting on the Muleshoe Mine Fault, Butt Valley Fault Zone (BVFZ), NE California: Geological Society of America, Abstracts with Programs, v. 28, no. 5, p. 108-109.

Sawyer, T.L., Wakabayashi, J., Page, W.D., Thompson, S.C. and Ely, R.W., 1993a, Late Cenozoic internal deformation of the northern and central Sierra Nevada, California: A new perspective: EOS, Transactions American Geophysical Union, v. 74, no. 44, p. 609

Sawyer, T.L., Page, W.D. and Hemphill-Haley, M.A., 1993b, Recurrent late Quaternary surface faulting along the southern Mohawk Valley Fault zone, NE California: Geological Society of America Abstracts with Programs, v. 25, no. 5, p. 142.

Schwartz, D.P., Alt, J.N. and Packer, D.R., 1977, Relationship of Paleozoic and Mesozoic structures to late Cenozoic faulting in the northern and western Sierra Nevada, California: Geological Society of America, Abstracts with Programs, v. 9, p. 1165.

Slemmons, D.B., 1966, Cenozoic volcanism of the central Sierra Nevada, California *in* Bailey, E.H., editor, Geology of Northern California, California Division of Mines and Geology Bulletin 190, p. 199-208.

Slemmons, D.B., Van Wormer, D., Bell, E.J. and Silberman, M.L., 1979, Recent crustal movements in the Sierra Nevada-Walker Lane region of California-Nevada: Part I, rate and style of deformation: Tectonophysics, v. 52, p. 561-570.

Trexler, J.H., Jr., Cashman, P.H. and Henry, C.D., 1999, The Verdi Basin: a syntectonic Neogene basin in western Nevada: Geological Society of America Abstracts with Programs, v. 31, no. 6, p. A103.

Turner, H.W. and Ransome, F.L., 1897, Sonora folio, California: U.S. Geological Survey Geologic Atlas of the United States, folio 41, scale 1: 125,000.

Unruh, J.R., 1991, The uplift of the Sierra Nevada and implications for late Cenozoic epeirogeny in the western Cordillera: Geological Society of America Bulletin, v. 103, p. 1395-1404.

Wagner, D.L., Jennings, C.W., Bedrossian, T.L. and Bortugno, E.J., 1981, Geologic map of the Sacramento Quadrangle: California Division of Mines and Geology Regional Geologic Map Series, Map No. 1A, scale 1: 250,000.

Wakabayashi, J., Page, W.D., Renne, P.R., Sharp, W.D. and Becker, T.A., 1994, Plio Pleistocene volcanic rocks and incision of the North Fork Feather River, California: tectonic implications: Abstracts for the 8th International Conference on Geochronology, Cosmochronology and Isotope Geology, U.S. Geological Survey Circular 1107, p. 345.

Wentworth, C.M. and Zoback M.D., 1989, The style of later Cenozoic deformation at the eastern front of the California Coast Ranges: Tectonics v. 8, p. 237-246.

Wills, C. J., 1990, Active faults north of Lassen Volcanic National Park, northern California: CALIFORNIA GEOLOGY, v. 44, p. 51-58.

Wills, C.J. and Borchardt, G., 1993, Holocene slip rate and earthquake recurrence on the Honey Lake Fault zone, northeastern California: CALIFORNIA GEOLOGY, v. 21, p. 853-856.

WCC (Woodward-Clyde Consultants), 1977, Earthquake evaluation study, Auburn Dam, Volume 3, Regional geology and tectonics: report to the U.S. Bureau of Reclamation.

WCC (Woodward-Clyde Consultants), 1978, Stanislaus Nuclear Project, Site Suitability, Appendix C.4 of Volume 6: Foothills Fault system study: report to Pacific Gas and Electric Company.

WLA (William Lettis and Associates), 1996, Lake Almanor and Butt Valley dams Seismic Stability Assessment, Volume 1: Seismic Source Characterization and Estimated Ground Motions: report to Pacific Gas and Electric Company.

Wolf, R.A., Farley, K.A. and Kass, D.M., 1998, Modeling of the temperature sensitivity of the apatite (U-Th)/He thermochronometer: Chemical Geology, v. 148, p. 105-114.

Yeend, W.H., 1974, Gold bearing gravel of the ancestral Yuba River, California: U.S. Geological Survey Professional Paper 722.

Yount, J., 1995, Stratigraphy of Quaternary deposits in Mohawk Valley *in* Quaternary geology along the boundary between the Modoc Plateau, southern Cascade Mountains, and the northern Sierra Nevada, Friends of the Pleistocene, Pacific Cell, 1995 Field Trip Guide, Road Log, Day 3, p. 11-12.

THIS BOOK IS DUE ON THE LAST DATE
STAMPED BELOW

BOOKS REQUESTED BY ANOTHER BORROWER
ARE SUBJECT TO IMMEDIATE RECALL

RECEIVED
APR 1 7 2006
PSL

LIBRARY, UNIVERSITY OF CALIFORNIA, DAVIS

D4613-1 (5/02)M

UNIVERSITY OF CALIFORNIA, DAVIS
3 1175 02627 0879